Intersecting *doublesex* neurons underlying sexual behaviours in *Drosophila melanogaster*



A thesis submitted for the degree of

Doctor of Philosophy at the University of Oxford

by

Hania Jamil Pavlou

Graduate Fellow of Magdalen College

Department of Physiology, Anatomy and Genetics

Sherrington Building, Parks Road

University of Oxford

Oxford, OX1 3PT

UK

Hilary 2014

To the quiet strength of my mother

Abstract

In *Drosophila,* the functionally conserved transcription factor, *doublesex* (*dsx*), is pivotal to the specification of sexual identity in both males and females. One of its key dedicated roles involves regulating the development of a sexually dimorphic nervous system (NS) that underlies both male and female reproductive behaviours. Specific inhibition of the function of *dsx*-expressing neurons in males and females results in a global disruption of these sex-specific behavioural outputs. However, little is known about the functional organisation of this *dsx* circuit that encodes the potential to display these behaviours.

Such investigations require the generation of a novel transgenic tool, capable of separating the function of *dsx* in the NS from that of the body. To achieve this, I generated a novel split-GAL4 $dsx^{GAL4\text{-}DBD}$ hemidriver by ends in homologous recombination. Coupling the novel tool with the pan-neuronal $elav^{VP16\text{-}AD}$ hemidriver, revealed spatial restriction of $dsx^{GAL4\text{-}DBD}/elav^{VP16\text{-}AD}$ expression to *dsx* neurons only; enabling the realisation of novel patterns of *dsx*-expression in the peripheral NS.

Next, the ability to elicit male-specific behavioural outputs upon activation of all *dsx* neurons formed the basis of a large behavioural screen aimed at parsing *dsx* circuitry into functionally distinct clusters. I utilised the novel $dsx^{GAL4\text{-}DBD}$ hemidriver to screen a large collection of extant enhancer trap lines ($ET^{VP16\text{-}AD}$), for the elicitation of distinct sub-behaviours of male courtship. Here, I show that the activity of *dsx*-expressing clusters in:

i) the brain (*dsx*-pC1, -pC2 and -pC3 collectively) regulate the early steps of male courtship (initiation, orientation and wing extension),
ii) the pro- and mesothoracic ganglia (*dsx*-TN1 and -TN2) regulate the middle steps of male courtship (wing extension and possibly courtship song) and
iii) the abdominal ganglia (*dsx*-Abg) regulate the late steps of male courtship (abdominal curling, attempted copulation and copulation).

These data establish functional correlations between *dsx* clusters in distinct neuroanatomical foci and specific sub-behaviours of the courtship repertoire.

Furthermore, the novel intersectional tool primed a collaborative study on female post-copulatory behaviours. We identified key sensory neurons in the female reproductive tract involved in initiating post-mating behaviours. Subsequent functional interrogations of *dsx* circuitry in the central NS revealed a subset of *dsx*-expressing neurons in the Abg that mediate changes in the female behavioural repertoire after mating.

Characterisation of this relatively simple neural circuitry sheds light on the organisation of the fly brain. Ultimately, future studies will define principles of neural circuit operation, which may be similarly conserved in the nervous systems of higher animals.

Table of contents

Abstract **3**

Table of contents **4**

List of accompanying materials **12**

Acknowledgements **13**

Author's declaration **15**

Glossary **16**

1 Introduction **22**

1.1 Behaviour 24

1.2 Behaviour genetics 25

1.3 Neurogenetics of behaviour in *D. melanogaster* 26

1.4 Prevalent genetic tools in *D. melanogaster* 27

1.4.1 Binary expression systems 28

1.4.2 Ternary expression systems 30

1.4.2.1 Realisation of neural morphology and connectivity 34

1.4.2.2 Neural ablation or inhibition 35

1.4.2.3 Manipulating neural activity 36

1.4.2.4 Realising neural activity 37

1.5 Courtship behaviours in *D. melanogaster* 38

1.5.1 Male courtship behaviours 38

1.5.2 Female courtship behaviours 41

1.6 Sex determination in *D.melanogaster* 42

1.7 Genetic correlates of courtship behaviour 45

1.7.1 Fruitless 45

1.7.2 Fruitless and courtship 48

1.7.3 Doublesex 50

1.7.4 Doublesex and courtship 51

1.8 Neural correlates of courtship behaviour 53

1.8.1 Organisation of the adult CNS 54

1.8.1.1 The brain 56
1.8.1.2 The ventral nerve cord 58
1.8.2 CNS foci necessary for courtship behaviour 58
1.8.3 Spatiotemporal distribution of Fru^M expressing neurons 61
1.8.4 Spatiotemporal distribution of $Dsx^{M/F}$ expressing neurons 62
1.8.5 Co-expression of Dsx^M- and Fru^M-expressing neurons 64
1.8.6 Sexual dimorphism in the fly brain 66
1.9 Assigning function to elements of the courtship circuitry 70
1.9.1 Relaying sensory information 70
1.9.2 Deciding to court 77
1.10 Other somatic correlates of behaviour 80
1.11 Aims and objectives 83
2 Materials and Methods 85
2.1 Drosophila 86
2.1.1 Drosophila melanogaster stocks 86
2.1.2 Wild-type strain 92
2.1.3 Sex determination mutant genotypes 92
2.1.4 Fly husbandry 92
2.1.5 Drosophila microinjection 93
2.1.5.1 DNA preparation 93
2.1.5.2 Microinjection 93
2.1.5.3 Selecting *P*-element transformants 93
2.1.5.4 Determining chromosomal insertion 93
2.1.5.5 Outcrossing of transgenic strains into an isogenised wild-type background 94
2.1.6 Dissection techniques 95
2.1.6.1 Whole-mount dissection of adult CNS and/or other somatic tissues 95
2.1.6.2 Whole-mount pupal CNS 96
2.1.6.3 Whole-mount larval CNS and/or other somatic tissues 97
2.1.6.4 Embryo collection 97

2.2 Visualisation techniques 98
2.2.1 Immunofluorescence 98
2.2.1.1 Incubations for larval, pupal and adult tissues. 98
2.2.1.2 Embryonic incubations 98
2.2.1.3 Phalloidin muscle preparations 99
2.2.1.4 Primary and secondary antibodies utilised in immunofluorescent characterisations 99
2.2.2 Confocal microscopy 101
2.2.3 Image processing 101
2.2.4 Cell counts 102
2.3 Bacterial protocols 103
2.3.1 Strains and plasmids 103
2.3.2 Culture Media 104
2.3.3 Antibiotics and Indicators 105
2.3.4 *E. coli* Transformation Techniques 105
2.3.4.1 Chemical transformation 105
2.3.4.2 Electroporation 105
2.3.5 Isolation of plasmid DNA from *E. coli* 106
2.3.5.1 Small-Scale isolation of plasmid DNA 106
2.3.5.2 Large-Scale Isolation of ultra-pure plasmid DNA 106
2.4 General molecular biology protocols 106
2.4.1 Polymerase chain reaction (PCR) 106
2.4.1.1 Primer design 106
2.4.1.2 Cloning PCR Products 107
2.4.2 Restriction digest of DNA 107
2.4.3 DNA gel electrophoresis 108
2.4.4 Visualization and photography of gels 108
2.4.5 Gel extraction of DNA fragments 108
2.4.6 Subcloning DNA Fragments into plasmid vectors 108

2.4.7 Ligation 109
2.4.8 Purification of genomic DNA 109
2.4.9 Quantification of nucleic acids 110
2.4.10 DNA sequencing 110
2.5 Behavioural analyses 110
2.5.1 Equipment 110
2.5.1.1 Chambers 110
2.5.1.2 Cameras 110
2.5.2 Behavioural assays 111
2.5.2.1 Male courtship behaviour 111
2.5.2.2 Female courtship behaviour 112
2.6 Statistics 113
3 Generation of Intersectional Tools 115
3.1 Introduction 116
3.2 Intersectional strategies 117
3.3 Gene targeting by homologous recombination 120
3.3.1 Ends-out homologous recombination 122
3.3.2 Ends-in homologous recombination 124
3.3.3 Chosen strategy 126
3.4 Generation of gene targeted GAL4 and QF 'donor' constructs 127
3.4.1 QF donor construct 127
3.4.1.1 Parent vector 127
3.4.1.2 Cloning strategy 128
3.4.2 GAL4-DBD donor construct 131
3.4.2.1 Parent vector 131
3.4.2.2 Cloning strategy 132
3.4.3 *P*-element transformation of donor constructs 133
3.5 Generation of dsx^{QF} and $dsx^{GAL4\text{-}DBD}$ via genetic crosses 134
3.5.1 Integration 134

3.5.1.1 Crossing scheme for *dsx*^{QF} 134

3.5.1.2 Relative frequency of episomal integration for *dsx*^{QF} 138

3.5.1.3 Crossing scheme for *dsx*$^{GAL4\text{-}DBD}$ 138

3.5.1.4 Relative frequency of episomal integration for *dsx*$^{GAL4\text{-}DBD}$ 140

3.5.1.5 Verification of *dsx*$^{GAL4\text{-}DBD}$ integration by PCR 141

3.5.1.6 Phenotype of independent integrant fly lines 142

3.5.2 Resolution 144

3.6 Discussion 145

3.6.1 Approach 145

3.6.2 Modifications 146

3.6.3 Ends-in vs. Ends-out 148

3.6.4 Frequency of integration 149

3.7 Conclusion 150

4 Characterisation of the novel *dsx*$^{GAL4\text{-}DBD}$ allele 151

4.1 Introduction 152

4.2 Testing the fidelity of the novel *dsx*$^{GAL4\text{-}DBD}$ allele 153

4.2.1 Pairing *dsx*$^{GAL4\text{-}DBD}$ with *elav*$^{VP16\text{-}AD}$ faithfully recapitulates *dsx*^{GAL4} expression in the adult CNS 154

4.2.2 Pairing *dsx*$^{GAL4\text{-}DBD}$ with *elav*$^{VP16\text{-}AD}$ faithfully recapitulates *dsx*^{GAL4} neural architecture in the adult CNS 155

4.2.3 *dsx*$^{GAL4\text{-}DBD}$/*elav*$^{VP16\text{-}AD}$ vs. *dsx*^{GAL4} expression in other somatic tissues 159

4.2.3.1 An overall view of expression in the mature adult 160

4.2.3.2 Fat body, Oenocytes and the Alimentary tract 162

4.2.3.3 Reproductive system 162

4.3 Characterisation of *dsx*$^{GAL4\text{-}DBD}$/*elav*$^{VP16\text{-}AD}$ neural circuitry both within, and outwith, the CNS….. 165

4.3.1 Spatiotemporal expression of *dsx*$^{GAL4\text{-}DBD}$/*elav*$^{VP16\text{-}AD}$ in the central nervous system of males and females 166

4.3.2 Spatial expression patterning of *dsx*$^{GAL4\text{-}DBD}$/*elav*$^{VP16\text{-}AD}$ in the peripheral nervous system of adult males and females 173

4.3.2.1 *dsx*$^{GAL4\text{-}DBD}$/*elav*$^{VP16\text{-}AD}$ is expressed in gustatory neurons of the labellum .. 173

4.3.2.2 *dsx*$^{GAL4\text{-}DBD}$/*elav*$^{VP16\text{-}AD}$ is expressed in gustatory neurons of the forelegs .. 175

4.3.2.3 *dsx*$^{GAL4\text{-}DBD}$/*elav*$^{VP16\text{-}AD}$ is expressed in the alimentary tract 177

4.3.2.4 *dsx*$^{GAL4\text{-}DBD}$/*elav*$^{VP16\text{-}AD}$ is expressed in the genitalia of male and females .. 180

4.3.2.5 *dsx*$^{GAL4\text{-}DBD}$/*elav*$^{VP16\text{-}AD}$ is expressed in sensory neurons of the terminalia of 5 day old adult males and females..... 185

4.3.3 Innervations of *dsx*$^{GAL4\text{-}DBD}$/*elav*$^{VP16\text{-}AD}$-expressing neurons in adult males and females 188

4.3.3.1 *dsx*$^{GAL4\text{-}DBD}$/*elav*$^{VP16\text{-}AD}$-expressing neurons innervate adult male and female reproductive systems 189

4.3.3.2 *dsx*$^{GAL4\text{-}DBD}$/*elav*$^{VP16\text{-}AD}$-expressing motoneurons innervate longitudinal muscles of the dorsal abdomen in adult males and females 192

4.3.4 *dsx*$^{GAL4\text{-}DBD}$/*elav*$^{VP16\text{-}AD}$-expressing neurons and their role in reproductive behaviours 195

4.3.4.1 *dsx*$^{GAL4\text{-}DBD}$/*elav*$^{VP16\text{-}AD}$ neurons are necessary for male sexual behaviour . 195

4.3.4.2 *dsx*$^{GAL4\text{-}DBD}$ neurons are critical for female sexual behaviour..... 196

4.4 Discussion 200

4.4.1 Expression dictated by *dsx*$^{GAL4\text{-}DBD}$/*elav*$^{VP16\text{-}AD}$ in the CNS 200

4.4.2 Expression dictated by *dsx*$^{GAL4\text{-}DBD}$/*elav*$^{VP16\text{-}AD}$ in the PNS 202

4.4.3 *dsx*$^{GAL4\text{-}DBD}$/*elav*$^{VP16\text{-}AD}$ motor control..... 208

4.4.4 *dsx*$^{GAL4\text{-}DBD}$/*elav*$^{VP16\text{-}AD}$-expressing neurons are necessary for male and female reproductive behaviours 209

4.5 Conclusions 212

5 Enhancer-Trap Screen..... 213

5.1 Introduction..... 214

5.2 Activation of all *dsx*$^{GAL4\text{-}DBD}$/*elav*$^{VP16\text{-}AD}$ neurons is sufficient to elicit male courtship 216

5.3 Strategy to utilise the *ET*$^{VP16\text{-}AD}$ enhancer trap collection 219

5.4 *ET*$^{VP16\text{-}AD}$ collection..... 220

5.5 Phase 1 - Enhancer trap thermogenetic screen..... 221

5.5.1 Method..... 221

5.5.2 Results..... 224

5.5.2.1 Wing extension candidates 225

5.5.2.2 Abdominal curling candidates 225

5.5.2.3 Candidates displaying 'partial' behaviours 228

5.6 Phase 2 - Neuroanatomical characterisation of $ET^{VP16\text{-}AD}$ candidate lines 230

5.6.1 Method 230

5.6.2 Results 231

5.6.2.1 Omitting candidate lines with ectopic patterns of reporter expression 231

5.6.2.2 Omitting candidate lines with extensive patterns of reporter expression ... 234

5.6.2.3 Candidate lines with restricted patterns of reporter expression 245

5.7 Phase 3 – Silencing intersected neurons using $ET^{VP16\text{-}AD}$ candidate lines 257

5.7.1 Method 257

5.7.2 Results 257

5.7.2.1 Behavioural similarities and differences between candidate lines 260

5.8 Correlating neuroanatomy with behaviour 263

5.8.1 Functionally assigned *fru* neurons involved in courtship initiation, wing extension and courtship song 264

5.8.2 Correlating *dsx* circuit elements with courtship initiation and wing extension... 267

5.8.3 Previously identified neurons involved in copulation 268

5.8.4 Correlating *dsx* circuit elements with attempting copulation and copulation..... 270

5.9 Discussion 272

5.9.1 The approach 272

5.9.2 Prospective avenues and experiments 275

5.10 Conclusion 278

6 Parsing *dsx* neural circuitry underlying female post-mating behavioural responses……280

6.1 Introduction 281

6.2 Results 283

6.2.1 Targeted expression of membrane-bound SP in *doublesex*-expressing neurons triggers post-mating behaviours 283

6.2.2 Knocking down SPR function specifically in *dsx*-expressing neurons abolishes post-mating behavioural responses 288

6.2.3 *dsx* neurons are part of the fru^{+}/ppk^{+} circuitry involved in sensing SP 292

6.2.4 *dsx* sensory neurons in the female reproductive system appear cholinergic ... 294

6.2.5 Intersecting *dsx* neurons critical for mediating post-mating behavioural responses 296

6.2.6 *dsx*-Abg neurons involved in post-mating responses target the brain and reproductive system 300

6.3 Discussion 303

6.3.1 SP-responsive sensory neurons regulate different aspects of the post-mating response 304

6.3.2 Co-expression of SPR and *dsx* in the female reproductive organs and potential functions in directing post-mating responses 305

6.3.3 How does the female's CNS integrate information about reproductive status to switch behaviour and physiology post-copulation? 306

6.3.4 Integrating Sensory Inputs 307

6.4 Conclusions 308

7 Summary Discussion 309

7.1 Investigative summary 310

7.2 Future experiments 317

7.2.1 The *dsx* 'connectome' 320

Appendix 322

Bibliography 331

Accompanying Materials 348

List of accompanying materials

Pavlou, H.J. and Goodwin, S.F. (2013). Courtship behavior in *Drosophila melanogaster:* towards a courtship 'connectome'. Current Opinions in Neurobiology, 23(1): 76-83.

Rezával, C., Pavlou, H.J., Dornan, A.J., Chan, Y.B., Kravitz, E.A., Goodwin, S.F. (2012). Neural circuitry underlying *Drosophila* female postmating behavioral responses. Current Biology, 22(13): 1155-1165.

Acknowledgements

Throughout my career, I have approached every undertaking with courage, perseverance, tenacity and integrity. I have three brilliant minds, Professors A.S. Fleming, J.D. Levine and M.B Sokolowski, to thank for having left this positively deep imprint on me, and for always encouraging me to be critical of the orthodoxies that surround us. I hope this thesis is a testament to this philosophy that I so vigorously try to attain.

As the poem goes, "*no man is an island*" and I am certainly no exception. I have been extremely fortunate to have supportive family, friends and colleagues that have all, in their own right, played an integral part to the completion of this thesis.

First and foremost, I extend my deep and cordial gratitude to my supervisor, Stephen F. Goodwin, for giving me the opportunity to succeed. His intellectual input, continuous support, encouragement, generosity and friendship were instrumental to the completion of this thesis. We both know that this D.Phil. was a source of great joy and incessant frustration. However, when weighed against one another, joy always prevailed.

I thank the present and past members of the Goodwin lab for all their help during the most trying of times. As the 'oracle' of the lab, Megan Neville has always been a source of guidance and inspiration. I thank her for her patience, intellectual support, infinite wisdom, and enthusiasm throughout the years. I also thank her for being my partner in crime and for the many funny moments we have shared at Stephen's expense. I thank Carolina Rezával for always being dependable in my hour of need and for being as big a Brandi Carlile fan as I am. I have always appreciated her intellectual input and enjoyed our chats and fits of laughter that made the laborious task of dissecting so much more enjoyable. I will always be grateful to Tony Dornan for his friendship and abiding support throughout my studies. Interacting with Tony was always effortless and fruitful, and I found his counsel to be invaluable. I thank him for always making time to discuss my project, provide intellectual and technical advice, and for burning the candle at both ends to review and comment on draft chapters. I also thank Tony for enduring my endless monologues with good grace; but to be fair, I believe I've paid my dues by listening to the countless exaggerated renditions of the handful of stories he claims are his own. I thank Jean-Christophe Billeter (a.k.a. pissed-oeuf) for sewing the seed to pursue a D.Phil. in the Goodwin lab. I value our friendship, and find his knack for putting things into perspective and for always providing sound advice indispensable. I thank Tetsuya Nojima for scouting out the culinary gems of Oxford and for our many gastronomic experiences that entailed discussing the views of his favourite philosophers. I thank Suzanne for a fantastic year in Glasgow even though it came at the expense of pickling my liver, and Elizabeth Ashley for paving the way to completing a D.Phil. at Oxford. I also thank my internal examiners, Professors Gero Meisenböck and Scott

Waddell for taking the time to discuss my project at length and provide constructive feedback. This has been an honour and invaluable experience.

I am extremely grateful to have met the most incredible people during my time at Oxford. I thank the FTC members of Magdalen College (Mike DiMattia 'Mike n Ike', Christopher Lee 'Vinnie', Eric Ball 'Ballz', Simon Franklin 'Stanklin', Jean Choi 'Genie', Nadia Galinier 'Nadz' and Sarah Clarke 'Sclarkey'), for their friendship and for always being a source of inspiration. They have all gone on to do great things, and I don't have a doubt in my mind that they will all become key players in their respective fields. I also thank all my friends that were simultaneously undertaking a D.Phil. at Oxford. Knowing that there were others that were suffering the calamities of research (Mike, José Lourenço, Clara Ferreira, and Ahmed Al-Dailami) made it ever the more comforting. I am particularly grateful to Mike and José for being my unwavering pillars from day one; I couldn't have done this without them.

I thank all my friends from across the pond that cheered for me from the side-lines. A big thanks to Emis and Alex Akbari, Daniela Palombo, and Samantha King for their constant banter that always put a smile on my face. I thank Jon and Janice Schneider, and Jade and Joey Atallah for being my surrogate siblings and for always touching base. I thank Jiye/Julie/Julienne Bai (who should pick a name and stick with it) and Hitomi Kobayashi for their long-standing friendship. I have come to embrace their incessant winging about 'life', as this made me realise that there are at least two other people on this planet that are more cynical than I am.

I am eternally grateful to my parents, Jamil and Yvette, for their adoration, infinite wisdom, endless support and constant encouragement and belief from the day I was born. They shaped and nurtured me and taught me the power of love and forgiveness. I thank them for letting me stand on my own two feet and for teaching me to never fear the unknown. I can only hope to have done them proud. I thank my sisters, Tania and Nataly, for their friendship, unwearied support and humour. My 'endless student' phase is finally over! I know that they both feel that they have vicariously undertaken a D.Phil., having selflessly endured my endless rants and bouts of stress. It's a shame that only one of us bears the title. Last, but not least, a very special thank you to my partner and best friend, Natasha Georgiou, for her humility, boundless love, inexhaustible patience, dedication, and humour that made this journey remarkable. I look forward to spending the next chapter of my life with you.

Some of my fondest memories are of my time at Oxford. I will miss it beyond measure.

Author’s declaration

I hereby declare that all the work reported in this thesis is my own unless stated otherwise in the text. None of the work has been previously submitted for any other degree at any other institution. All sources of information used in the preparation of this thesis are indicated by reference.

Hania Jamil Pavlou

Glossary

Anatomical Terms

Abdominal Ganglion	Abg
Abdominal nerve trunk	AbNvTk
Accessory Gland	Acg
Antennal lobe	AL
Antennal mechano-sensory and motor centres	AMMC
Apodeme	Apo
Calyx	Ca
Cell body rind	CBR
Central complex	CC or CX
Central nervous system	CNS
Cervical connexion	CvCn
Common oviduct	OvdC
Direct flight muscles	DFM
Ejaculatory bulb	EjB
Ejaculatory duct	EjD
External genital plates	GenPlate
Fan shaped body	Fb
Fat body	FB
Inferior neuropils	INP
Lateral crescent	LC
Lateral horn	LH
Lateral junction	LJ
Lateral oviduct	OvdL
Malpighian tubule	MT
Mesothoracic ganglion	Msg
Mesothoracic triangle	Mst
Metathoracic ganglion	Mtg
Muscle of Lawrence	MOL
Mushroom body	MB
Neuromuscular junction	NMJ
Olfactory receptor neuron	ORN
Optic lobe	OL
Ovary	Ov
Ovary flap	OvF
Paravoria	Par

Pars intercerberalis	PI
Peduncle	Ped
Perieosophageal neuropils	PENP
Peripheral nervous system	PNS
Prothoracic ganglion	Prg
Protocerebral bridge	Pb
Proventriculus (cardia)	Provent
Salivary gland	SG
Seminal vesicle	SmV
Seminiferous receptacle	SmRcp
Sex comb	SC
Somatic gonadal precursor cells	SGP
Spermatheca	Spt
Spur	Sp
Stomodeal valve	StomV
Suboesophageal ganglion	SOG
Superior neuropils	SNP
Transverse bristles	TVB
Vas deferens	VD
Ventral nerve cord	VNC
Ventromedial neuropils	VMNP
Ventrolateral neuropils	VNLP

Genetic Terms

Abdominal-A	*Abd-A*
Abdominal-B	*Abd-B*
Accessory gland protein	Acp
apterous	*ap*
β-Galactosidase (gene)	*lacZ*
β-Galactosidase (protein)	β-Gal
Broad-complex/Tramtrack/Bric-à-brac	BTB
Canton-Special	CS
Curly of Oster	CyO
don juan	*dj*
doublesex	*dsx*
Doublesex isoforms (female/male)	Dsx^F / Dsx^M
ebony	*e*
embryonic lethal, abnormal vision	*elav*

enhanced Green Fluorescent Protein	eGFP
Flippase site-specific recombinase	FLP
Flippase recognition site	*FRT*
fruitless (gene)	*fru*
Fruitless (proteins)	Fru
Green Fluorescent Protein	GFP
Gustatory receptor gene	*Gr*
Gustatory receptor neuron	GRN
head involution defective	*hid*
hermaphrodite	*her*
Humeral	*Hu*
intersex	*ix*
Ionotropic glutamate receptor (gene)	*Ir*
Ionotropic glutamate receptors (protein)	Ir
Male-specific Fruitless proteins	Fru^{M}
Mosaic analysis with a repressible cell marker	MARCM
Membrane-bound mouse lymphocyte marker CD8	mCD8
mini-white	*mw*
nuclear Green Fluorescent Protein	nGFP
nuclear Red Fluorescent Protein	nRFP
octopamine receptor in the mushroom bodies	OAMB
Olfactory receptor gene	*Or*
Olfactory receptor neuron	ORN
Phalloidin	Phall
pickpocket	*ppk*
Projection neurons	PN
reaper	*rpr*
reversed polarity	*repo*
Serrate	*Ser*
Sex-lethal (gene)	*Sxl*
Sex-lethal (protein)	Sxl
Sex peptide	SP
Sex peptide receptor	SPR
shibire	*shi*
Stable insulated nuclear enhanced GFP	Stinger
Stubble	*Sb*
teashirt	*tsh*
Third multiple of singsong	TMS
transformer (gene)	*tra*

Transformer (protein)	Tra
transformer-2 (gene)	*tra-2*
Transformer-2 (protein)	Tra-2
Tubby	*Tb*
Upstream Activating Sequence	*UAS*
white	*w*
Wild-type	WT
Yeast Transcriptional Activator GAL4	GAL4
yolk protein	*yp*
yellow	*y*
Zinc finger	*Znf*

Measurements

Base pair	bp
Centimetre	cm
Centripetal force = to gravitational acceleration	g
Decibel	dB
Degrees Centigrade	ºC
Hour	hr
Hertz	hz
Kilobases	kb
Melting temperature	Tm
Microgram	µg
Microlitre	µL
Micrometre	µm
Micromolar	µM
Milligram	mg
Millilitre	mL
Millimetre	mm
Millimolar	mM
Millisecond	ms
Minute	min
Molar	M
Nanogram	ng
Nanometre	nm
Optical density	O.D.
Second	sec or s

Behavioural Parameters

Courtship index	CI
Cycles per pulse	CPP
Interpulse interval	IPI
Mean pulses per train	MPPT
Pulse trains per minute	PTPM
Song index	SI
Song bouts per Minute	SBPM
Wing extension index	WEI

Chemicals

2' Deoxyribonucleic acid	DNA
5-bromo-4-chloro-3-indolyl-ß-D-galactopyranoside	X-gal
Bovine serum albumin	BSA
Carbon dioxide	CO_2
Complimentary DNA	cDNA
Ethanol	EtOH
Ethidium Bromide	EtBr
Horseradish peroxidase	HRP
Messenger RNA	mRNA
Phosphate buffered saline	PBS
PBS with Triton-X	PBT
PBS with Triton-X and 5% SNS	PTN
PBS with Triton-X and 0.1% BSA	PAT
Ribonucleic acid	RNA
Ribonuclease A	RNaseA
Normal serum (Sheep/ Goat)	NGS / NSS
Tetramethylrhodamine B isothiocyanate	TRITC

Computing and Statistical Terms

Adobe illustrator file	.ai
Adobe photoshop file	.ps
Analysis of variance	ANOVA
Liquid crystal display	LCD
Look up table	LUT
Quicktime movie file	.mov

Personal computer	PC
Portable document format	pdf
Standard deviation	s.d.
Standard error of the mean	s.e.m.
Tagged image file format	.tif or .tiff

Miscellaneous

7-tricosene	7-T
7,11-heptacosadiene	7,11-HD
7,11-nonacosadiene	7,11-ND
11-*cis*-vaccenyl acetate	cVA
Analysis of variance	ANOVA
Bacterial artificial chromosome	BAC
Cuticular hydrocarbon	CHC
Enteroblast	EB
Enteroendocrine cell	EEC
First, second or third larval molt stage	L1, L2 or L3
Heat shock	hs
Intestinal stem cell	ISC
Neuroblast	NB
Overnight	O/N
Polymerase chain reaction	PCR
P transposable element	P-element
Room temperature	R/T
RNA interference	RNAi
Ultraviolet	UV

1 Introduction

Overall, the primary aim of this study is to establish causal relationships between distinct neurons in the central nervous system and a defined set of reproductive behaviours in the fruit fly, *Drosophila melanogaster*.

Analysing the relationship between genes, neurons and reproductive behaviour requires several steps. The first involves the identification of genes that control the development of neural circuitry that underlies these behaviours. Next, is to characterise how and when these genes specify the development of the neural circuitry, and localise which neurons are required for normal reproductive behaviours to occur. Once established, the final step involves understanding whether the organisation of the behaviours maps onto sub-assemblies of neurons.

I have focused on a circuit that has proven to be pivotal to both male and female reproductive behaviours. The defining element of this circuit is the gene *doublesex* (*dsx*), a transcription factor required for sex determination in *Drosophila* and in a wide variety of species, including our own. However, little is known about the circuit logic of *dsx*-expressing neurons and how components of this circuit coordinate the display of reproductive behaviours.

This study has attempted to address these issues by ascertaining whether components of the *dsx* circuit can be functionally assigned, such that discrete clusters specify distinct modules of reproductive behaviour. Therefore I asked: which neurons are required for a given behavioural module? In other words:

a. Does the activation of these neurons elicit the dispay of this behaviour? (and/or)

b. Does the inactivation of these neurons abrogate the dispay of this behaviour?

With this in mind, I generated a novel transgenic tool that reproducibly grants genetic access to subsets of *dsx*-expressing neurons for such circuit analyses, enabling the above-mentioned questions to be tackled.

Prior to delving into these data, I first present this chapter as a historical perspective and detailed literature review of the genetics of *Drosophila* reproductive behaviours. I also

introduce prevalent genetic tools and amenable approaches that form the foundations of my study. Ultimately, this chapter serves to establish a backdrop of evidence pertinent to the issues at hand and to familiarise the reader with key concepts prior to considering the experimental portions of this study.

1.1 Behaviour

Behaviour can be defined as a response that occurs as a result of an external stimulus, an internal stimulus, or a mixture of the two, in order to facilitate survival and reproduction. This broadly encompasses any action by an organism within its environment. However, most overt actions can be grouped into one of two disparate classes of behaviour that encompass a spectrum between the ends of a continuum (Table 1-1).

Table 1-1 Innate vs. Learned Behaviours.
Comparison of key features/descriptors for innate and learned behaviours. Taken from Mayer, J.R. (2006).

Innate	Learned
Heritable	Non-heritable
Intrinsic	Extrinsic
Stereotypic	Permutable
Inflexible	Adaptable
Consummate	Progressive

In reality most behavioural traits are inherently complex – meaning that they possess components of both classes to varying degrees. This includes innate behaviours that can be modified through experience, and learned behaviours, which depend upon mechanisms of innate behaviour. That innate mechanisms (a common denominator of all complex behaviours) are subject to natural selection highlights the biological underpinnings of behaviour. Thus, it is via the study of innate foundations of behaviours that will allow us to shed light on more complex paradigms of learned behaviours (and/or higher processing)

(Tinbergen, 1951). The different approaches to such investigations can be summed up in Tinbergen's four questions of ethology (Tinbergen, 1963):

Proximate view

1. Causation (mechanism)?
2. Development (genetics/ontogeny)?

Ultimate view

3. Function (adaptive significance)?
4. Evolution (phylogenetic history)?

1.2 Behaviour genetics

As animals spend their lives bombarded by countless stimuli, their nervous system filters the mass of sensory information and selectively responds to those that are determined to be significant for survival. Thus, to understand the biological basis of behaviour, it is important to identify the proximate causal mechanisms and developmental events that allow the nervous system to process the relevant sensory stimuli and generate appropriate behaviour.

In the case of innate mechanisms, a comprehensive definition and method of quantification of the behavioural outputs, in order to establish a baseline for manipulations, marks the first challenge. For the purpose of this study, I will focus on complex innate mechanisms that give rise to complex innate behaviours – namely sexual behaviours. Sexual behaviours are among the most evolutionarily constrained and, due to a strong innate component, are believed to be mostly "hardwired" (Billeter et al., 2006). By definition, these behaviours occur as a stereotypical repertoire of overt, species-specific behaviour(s) that occur without any prior experience. Although modifiable by experience, these behavioural outputs are fundamentally derived from underlying genetic determinants, and thus implicit in the idea of the heritability of innate behavioural responses. Given that the majority of complex behaviours are under the direction of many genes, the identification of candidate genes, which appear to influence a defined/specific behaviour, suggests their involvement in the modulation of that behaviour. Once identified, these genes provide the genetic access required to understand the cellular functions that contribute towards determining the behavioural output(s). Interrogating how, when and in what context these genes might

function in the whole organism begins to form the framework that links genes to behaviour. While the nervous system is crucial for the elicitation of behaviour, additional physiological structures that officiate the processing of sensory stimuli, and regulate the animal's physiology or direction of motor response(s) are necessary to generate these behaviours.

To add complexity, both short- and long-term changes that may occur in the external environment, together with the requirement of an internal homeostatic environment, necessitates that an organism, and therefore its behaviours, must be responsive to change. This constant interdependence between genes and the environment ensures that the genetic substrates that underlie an organism's behaviours are required to maintain a fine balance between specifying a stereotypical response and ensuring that an underlying plasticity exists to allow variations in that response.

It is only after creating a comprehensive picture of the genetic processes that engenders stereotypical responses in an organism, may we begin to ask questions pertinent to the following:

i) Sex-specific behaviours

- *How are sex-specific behaviours built into the nervous system during development and how does this circuitry coordinate with the development and maintenance of a dimorphic organism as a whole?*

ii) Species-specific behaviours

- *How does the changing environment select for modifications that vary the development and/or functioning of behaviour for the purpose of generating behavioural diversity and/or prospective speciation factors?*

1.3 Neurogenetics of behaviour in *D. melanogaster*

As a result of 100 years of research, using *Drosophila melanogaster* as a model organism, much is known about the genetic determinants of behaviours (Vosshall, 2007; Bellen et al., 2010). By means of identifying new genes, proteins and biochemical pathways that underlie an array of complex behaviours (examples include aggression, learning and memory, circadian rhythms and courtship, just to name a few), investigators have been able to

discover homologous genes with analogous functions in mammals (Sokolowski, 2001). The ability to extrapolate, from flies to vertebrates, genetic principles underlying behaviour has contributed to the empowerment of *Drosophila* as a model system for the study of neurogenetics. However, ultimately, its success and sophistication lends itself to milestone discoveries in development and nervous system function through the ongoing creation and modification of the armamentarium of genetic tools available in this model organism. The identification of visible genetic markers, the creation of balancer chromosomes, the ability to carry out mutagenic screens, the use of transposable elements to generate a range of transgenic animals, the ability to target specific genes by homologous recombination, combined with a fully sequenced genome, altogether allow both forward and reverse genetic screens to be performed (reviewed in Sokolowski 2001; Venken and Bellen, 2005; Vosshall 2007; Olsen and Wilson, 2008). Greatly simplifying the identification of individual genes involved in the development and function of neural circuits controlling specific behaviours. In addition, recent development of high-throughput technologies aimed at profiling biological processes (including genomic tiling arrays covering the full *Drosophila* genome, RNA deep sequencing technologies, technologies identifying protein-DNA interactions *in vivo*, in conjunction with powerful tools for computational analysis of genomic sequence and/or bioinformatics data) has made it possible to determine genome-wide genetic function (reviewed by Neville and Goodwin, 2012).

1.4 Prevalent genetic tools in *D. melanogaster*

As previously stated, genetic dissection of behaviours requires a functional understanding of the genes underlying a particular behaviour. Determining how, where and when a gene's product acts during development to specify neural development and/or function, in addition to understanding the effects of manipulations of the function and/or presence of such neurons, begins to unravel the relationship between a gene, the neural circuitry specified by this gene and the behavioural outputs that are displayed as a result of this circuitry. The development of binary and ternary expression systems in *D. melanogaster* has armed geneticists with powerful tools capable of precise spatiotemporal manipulations of gene function, and it is this

reverse-genetics toolkit that has expanded the ability of investigators to elucidate gene function to unprecedented resolution (reviewed by Venken et al., 2011).

1.4.1 Binary expression systems

The implementation of the GAL4/*UAS* binary transcription system to directly target gene expression was the first of its kind in the early 90s (Brand and Perrimon, 1993). Since then, other independent binary expression systems have been developed – *e.g.* the LexA/*LexAop* and Q systems (Figure 1-1; Lai and Lee, 2006; Potter et al., 2010; reviewed in del Valle Rodriguez et al., 2012).

GAL4 is a yeast transcriptional activator protein that directly binds to four related 17 bp sites that define an enhancer-like element called the upstream activating sequence (*UAS*) (Giniger et al., 1985; Ptashne, 1988). As GAL4 has no endogenous targets in *Drosophila*, Fischer et al. (1988) were able to demonstrate that ectopic GAL4 expression could restrictively/specifically activate the transcription of genes engineered under the control of the *UAS* element in *Drosophila*. These findings prompted the development of the *in vivo* GAL4/*UAS* binary system for targeted gene expression in *Drosophila* (Figure 1-1A; Brand and Perrimon, 1993). The elegance in the system lies in the fact that either a defined or random promoter element can be used to drive the expression of GAL4. The random insertion of GAL4 into the genome may result in expression patterns that report the *cis*-regulatory architecture of the insertion location. However, by targeting GAL4 via homologous recombination, GAL4 expression is driven by the endogenous *cis*-regulatory elements of the gene of interest. A hybrid of the two methods entails fusing GAL4 to the known enhancer and/or promoter elements of a gene of interest, and randomly inserting it into the genome – although this makes it susceptible to positional/integration effects (reviewed in Luo et al., 2008; Jones, 2009; del Valle Rodriguez et al., 2012). An additional later development to this system involves the use of the negative regulator GAL80, which inhibits the transcriptional activation of GAL4 by binding to 30 amino acids at the C-terminus of GAL4 (Figure 1-1A; Ma and Ptashne, 1987; Lee and Luo, 1999; McGuire et al., 2003). The abundance of characterized GAL4 lines together with the plethora of *UAS* effector lines the GAL4/*UAS*

system a powerful, highly versatile and most widely used targeted expression system in *Drosophila* genetics today. However, like any system, it has its limitations and can manifest faults. These include 'leaky' transgenes, off target and dose- dependent effects and the inability to recapitulate isoform- or gene-specific restricted patterns of expression spatially and/or temporally, just to name a few.

Generally, transcriptional activators like GAL4 consist of two separable functional domains, the DNA-binding domain (DBD), which binds to specific nucleotide sequences, and the trans-activating domain (AD), which activates local transcription via interactions with basic transcription factors. The LexA/*LexAop* system makes use of this feature by fusing the DBD of the *E.coli* repressor protein LexA with either the viral transcription factor VP16 acidic activation domain (VP16-AD) to generate a GAL80-insensitive transcription factor, or the GAL4 transactivating domain (GAD) to generate a GAL80-suppressible transcriptional factor (Brent and Ptashne, 1985; Lai and Lee, 2006). Both hybrid LexA proteins bind to multiple LexA-binding sites, the LexA operator (*LexAop*), to effectively drive the expression of *LexAop*-controlled transgenes in *Drosophila* (Figure 1-1B; Lai and Lee, 2006). The LexA/*LexAop* system is widely used in combination with the GAL4/*UAS* system as an intersectional strategy for functional or co-labelling studies, and in instances where strong expression of effectors are required due to the unparalleled strength of the VP16 activator (Brent and Ptashne, 1985; Lai and Lee, 2006; Mellert et al., 2010; Pitman et al., 2011).

The third (and most recently developed) binary system known as the 'Q system' is conceptually similar to the repressible GAL4/*UAS* binary system (Figure 1-1C; Brand and Perrimon, 1993; McGuire et al., 2003; Potter et al., 2010; Potter and Luo, 2011). The Q system is based on the regulatory genes from the *Neurospora qa* gene cluster, and consists of three components: the QF transcription factor, a *QUAS* effector, and the QS suppressor (Potter et al., 2010; Potter and Luo, 2011). The *QUAS* element contains five 16 bp QF-binding sites and allows for robust QF-dependent expression of the effector. As such, the Q system contains three similar components (QF, *QUAS* and QS) as the analogous GAL4 system (GAL4, *UAS* and GAL80; Figure 1-1C). The additional use of quinic acid as the

inhibitor of the QS suppressor, allows for a relief of suppression, ultimately making temporal control of the Q system also possible (Potter et al., 2010; Potter and Luo, 2011).

The advantages of developing two systems complementary to the GAL4/*UAS* system are numerous. First, numerous intersectional strategies can be achieved by employing either the LexA/*LexAop* or Q systems in conjunction with the vast array of GAL4 drivers and UAS effector lines to refine gene expression patterns and manipulate sub-populations of cells. Second, all three systems may be used in concert to label and/or manipulate, both agonistically as well as antagonistically, cells of unrelated lineages. Third, to perform both GAL4-independent and coupled lineage tracing, to increase the level of refinement that may be applied to the functional analyses of exclusively labelled cells or clonal groups (Lai and Lee, 2006; Shang et al., 2008; Pfeiffer et al., 2010; Potter and Luo, 2011; del Valle Rodriguez et al., 2012).

1.4.2 Ternary expression systems

As most genes are expressed broadly and dynamically, the expression patterns dictated by the promoters of individual genes are rarely restricted enough to map the functional identities of individual cells/cell clusters within a given neural circuitry. As a result, GAL80's ability to repress GAL4 was introduced as a ternary technique capable of accomplishing such restrictions. By engineering the expression of GAL80 in either a promoter-specific and/or temperature-specific manner, spatial and temporal targeted suppression of intersecting GAL4 expressing cells can be achieved, preventing GAL4 responsive *UAS* gene expression in only a subset of cells of the original neural population that expresses GAL4 (Figure 1-1A; Lee and Luo, 1999; McGuire et al., 2003). Unfortunately, as the Q-system has yet to be widely adopted, a wide variety of QS lines have not yet been generated, however, in principle, similar strategies may be used to generate QS lines that are functionally analogous to the GAL80s available today.

A second use of GAL80 involves coupling it with a separate flippase/*flippase recombination target* (FLP/*FRT*) site-specific recombinase system (McLeod et al., 1986; Golic and Lindquist, 1989; Harrison and Perrimon, 1993; Bischof and Basler, 2008), which forms the

foundations of the mosaic analysis with a repressible cell marker (MARCM) system (Lee and Luo, 1999; Lee and Hou, 2008). Here, a ubiquitously expressed GAL80 transgene is placed in trans to a characterized mutation on chromosomes that have FRT sites engineered into them, while a tissue/gene-specific GAL4, a *UAS-reporter* and a heat inducible FLP recombinase (*hs-FLP*) are engineered onto other chromosomes. Heat shock activation of the *hs-FLP* promotes FRT-mediated recombination between homologous chromosomal arms during mitotic cell division, generating a homozygous mutant cell(s) lacking GAL80 (Lee and Luo, 1999). In the absence of GAL80, the active GAL4 may then drive expression of the *UAS-reporter*, uniquely labelling this mutant clone. Additional effector transgenes under the control of *UAS* may be included to i) create homozygous mutants for a particular gene of interest, ii) modify a gene's activity in, or iii) manipulate the function of these uniquely marked cell(s) in an otherwise wild-type tissue (Lee and Luo, 1999; Liu and Hou, 2008). Since its inception, MARCM has been widely implemented as a high-resolution method for mosaic mutant analysis, lineage analysis, tracing of single/clones of neurons and mosaic analysis of gene function (Liu and Hou, 2008; Luo, 2007). However, the biggest limitation of this method involves the perdurance of the GAL80 protein post-induction of mitotic recombination, which restricts the sensitivity of the system for mosaic lineage analyses to 48 hr post- induction of mitotic recombination (Lee and Luo, 1999).

Intersectional strategies that achieve genetic access to defined populations of cells entails the use of one of two alternative systems - the split-GAL4 and the FLP out systems (Figure 1-1D-E). The split-GAL4 system exploits the fact that the two functional domains of GAL4, the DBD and AD domains, are separable. Similar to the LexA/*LexAop* system, the split-GAL4 system can use either the GAL4 or the more active VP16 ADs (Luan et al., 2006). The elegance of the system is that each domain is under the control of different promoter elements and is fused to a hetero-dimerizing leucine zipper to ensure that the two domains associate when expressed in a cell in which both promoters are active, thereby reconstituting transcriptional activity (Figure 1-1E). One major drawback to this system is that it requires *de novo* generation of both hemi-driver lines (Luan et al., 2006). On the other hand, the FLP out technique uses transgenes that are silenced by a transcriptional stop signal flanked by FRT

sites that can be removed by the expression of FLP to activate the gene of interest (Figure 1-1D; Golic and Lindquist, 1989; Struhl and Basler. 1993; Harrison and Perrimon, 1993; Bischof and Basler, 2008). Although FLP can be induced by heat-shock if a heat-shock promoter is used to drive its expression (as previously described for MARCM), it is only when FLP is placed under the control of a defined promoter, and is combined with pre-existing characterised GAL4 lines, that this method may then be employed to provide iterative reproducible spatial control of intersecting cells. However one limitation of this system to note is that if the promoter element used to drive the FLP is from a gene expressed at a specific developmental stage, or that exhibits a dynamic expression pattern throughout development, additional 'ectopic' cells become labelled/manipulated – contributing to the stochastic nature of the system. Also it should be noted that the excision of the stop codon by FLP that results in active transcription of the *UAS* transgene cannot be undone, causing the perdurance of reporter/effector expression in cells that could potentially have been labelled at any point throughout development at which the promoters of the FLP and GAL4 co-express. Again, as most genes are broadly and dynamically expressed, this system has been shown to produce imprecise access to intersecting cells (Golic and Lindquist, 1989). Finally this system shares the same limitation as that of the split GAL4; that is it requires the generation of *de novo* FLP line(s).

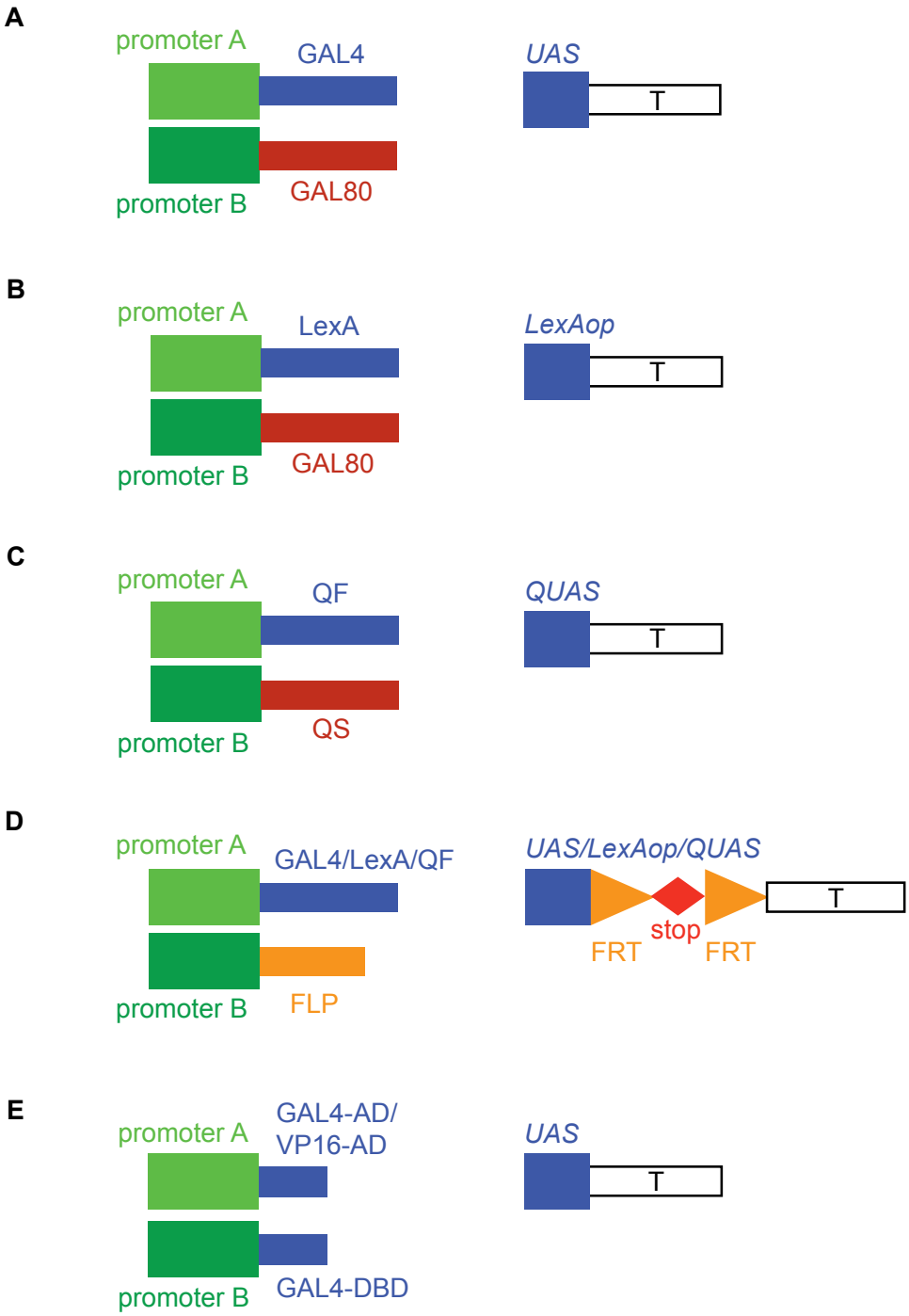


Figure 1-1 Binary and Ternary Methods of Gene Expression.
(A) Yeast transcription factor GAL4 binds to *UAS* and activates target gene 'T' expression in cells where promoter A is active. When including Gal80, target gene is expressed in a subset of cells that are active for promoter A, as Gal80 inhibits GAL4 activity in cells that are active for promoter A but also exhibit activity for promoter B (intersection of the two promoters). (B) Yeast transcription factor LexA binds to *LexAop* and activates target gene 'T' expression in cells where promoter A is active. When including Gal80, target gene is expressed in cells that are active for promoter A but not promoter B, as Gal80 inhibits LexA activity – only when the LexA contains a GAL4-AD. (C) Fungal transcription factor QF binds to *QUAS* and activates target gene 'T' expression in cells where promoter A is active. When including QS, target gene is expressed in cells that are active for promoter A but not promoter B, as QS inhibits QF activity. (D) The combination of any binary expression system in combination with Flp/*FRT* allows the target gene of interest to be expressed in cells that are active for both promoters A and B. (E) Intersectional method that utilizes the reconstitution of two domains of GAL4, which then binds to *UAS* and activates target gene 'T' expression in cells where promoter A and B is active. Adapted from Luo et al., (2008).

1.4.2.1 Realisation of neural morphology and connectivity

The assortment of reporters that have been developed and continuously improved allows experimenters to visualise and more fully characterise neural morphology. The most efficacious of all are the arrays of fluorescent probes, such as green (GFP) and red (RFP) fluorescent proteins and the multitude of associated derivatives that have been placed under the control of *UAS*. Engineering variants of these proteins by creating fusions to cytoplasmic, membrane-, nuclear-, dendritic- or synapse- specific proteins alters their sub-cellular localisations, permitting comprehensive neuroanatomical characterizations of a given neuron or neural circuitry (reviewed in Simpson, 2009; Jones, 2009). Recent developments in 3D digital registration software has made it possible to trace single/clusters of neurons at high-resolution and compile these images onto a common reference brain, in order to perform in-depth digital comparisons of neurons in the same, or different, brain samples (Cachero et al., 2010; Yu et al., 2010; Chiang et al., 2011; von Philipsborn et al., 2011; Lai et al., 2012; Lin et al., 2013). This technique has proved to be a powerful tool for inferring sex-specific differences, potential interconnectivity, and likely pathways of neural processing (Cachero et al., 2010; Yu et al., 2010; Chiang et al., 2011; von Philipsborn et al., 2011; Lai et al., 2012; Lin et al., 2013). Based on digital predictions of the connectivity between component neurons, a largely hypothetical interconnected neural framework of a given circuitry can be generated. However, it is important to confirm the hypothetical connections using additional transgenes that allow downstream/connecting neurons to be identified/visualised. A previously adopted strategy entails expressing photoactivatable cytoplasmic GFP (PA-GFP) using a circuit specific driver to identify potential synaptic partners (Patterson and Lippincott-Schwartz, 2002; Datta et al., 2008). Based on the proximity of post-synaptic termini to the pre-synaptic innervations, photoactivation of an area that contains the axon termini of a known group of neurons triggers the rapid and local conversion of PA-GFP molecules in neighbouring dendritic termini (which intersect the area of photostimulation) to a fluorescent state. Diffusion of the fluorescent PA-GFP from the illuminated dendritic arbors reveals the cell bodies and axonal projections of possible downstream neurons (Patterson and Lippincott-Schwartz, 2002; Datta et al., 2008). Another promising technique termed GFP

reconstitution across synaptic partners (GRASP) involves the expression of separate GFP fragments (which can be engineered to localise at synapses) in different populations of cells using a combination of binary expression systems. The physical proximity of neural membranes, primarily at sites of synapses, allows the reconstitution of a functional and detectable GFP (Feinberg et al., 2008; Gordon and Scott, 2009).

1.4.2.2 Neural ablation or inhibition

Once a comprehensive anatomical map or 'connectome' of a given behavioural circuitry is generated, functional annotations of the circuitry as a whole and/or its component neurons need to be established (reviewed by Pavlou and Goodwin, 2013). This can be achieved using genetically encoded transgenes to ablate or silence neurons (to determine necessity), to artificially trigger the same neurons (to determine sufficiency), and to image neural activity (to establish the natural pattern of activity), which collectively help determine the causal relationships between neurons and their respective behavioural outputs (reviewed in Olsen and Wilson, 2008). A prevalent and successful method to precisely ablate neurons is by targeting the expression of cell death genes *head involution defective* (*hid*) and *reaper* (*rpr*) using the GAL4/*UAS* system (McNabb et al., 1997). Several powerful tools have been established for both irreversible and reversible silencing of neurons. Targeted expression of either the inwardly rectifying potassium ion channel Kir2.1, which reduces neural excitability by hyperpolarisation (Baines et al., 2001), or the light chain of bacterial tetanus toxin (TNT; Sweeney et al., 1995), which cleaves the synaptic vesicle protein synaptobrevin ensuring loss of neurotransmitter exocytosis, in a defined neuron or circuitry, results in irreversible inhibition of neural activity. Alternatively one can express the temperature sensitive version of the *Drosophila* gene encoding a dynamin orthologue, (*shibire*^{ts}), which blocks vesicle endocytosis, and thus synaptic transmission, transiently at restrictive temperatures (Kitamoto, 2001). The consequences of selective ablation or silencing of neurons may be fully determined by assessing modifications in, or the complete lack of, behavioural outputs, demonstrating the necessity of those neurons for a given behaviour.

1.4.2.3 Manipulating neural activity

Conversely, the use of tools that enable selective activation of neurons allows experimenters to demonstrate the sufficiency of that circuitry for a behavioural output. However, unlike the inhibition of neurons, temporal control of neural activation is mandatory – especially given that constant artificial activation of neurons results in the depletion of associated neurotransmitter, ultimately rendering the manipulated neurons permanently inactive (Peabody et al., 2009). With this in mind, three different tools have been developed and successfully implemented in *Drosophila* (reviewed in Olsen and Wilson, 2008; Jones, 2009). Recent optogenetic technologies have engineered optically gated ion channels that evoke an action potential in neurons via a flash of light (Miesenböck and Rothman, 1997; Miesenböck et al., 1998; Zemelman et al., 2002; Lima and Miesenbock, 2005; Nagel et al., 2003; Boyden et al., 2005). The most successful phototriggers include the GAL4 responsive *UAS* transgenes encoding the ATP-gated cation channel $P2X_2$, (Zemelman et al., 2002; Lima and Miesenbock, 2005, Miesenbock and Kevrekidis, 2006; Clyne and Miesenbock, 2008) or the monovalent cation, Channelrhodopsin-2 (ChR2) engineered for *Drosophila* from green algae; both of which have specific photo-stimulatory triggers (Nagel et al., 2003; Boyden et al., 2005; Li et al., 2005; Nagel et al., 2005; Schroll et al., 2006; Hwang et al., 2007; Suh et al., 2007; Zhang et al., 2007; Zimmerman et al., 2009). One limitation of the $P2X_2$ system is that it requires the delivery of caged ATP via microinjection, making it more invasive and less favourable than the ChR2 system, which only requires the delivery of its co-factor retinal via food supplementation. Nonetheless, the larger problem of light penetration, which applies to the umbrella of optogenetics, has forced researchers to continue developing more amenable systems that respond to longer wavelengths of light, capable of deep tissue penetration (Simpson, 2009). One such example is the red light-sensitive opsin (ReaChR) that is capable of penetrating the cuticle and activating neurons of the CNS in freely moving adult flies (Inagaki et al 2014). As elegant as optogenetics is, the more pervasive use of the temperature sensitive non-selective cation channels, TrpA1 and TrpM8, for neural activation, stems from the relatively low costs that these systems offer (Hamada et al., 2008; Pulver et al., 2009; Peabody et al., 2009). By increasing or decreasing the temperature by only a few

degrees, neurons are rendered active, with any behavioural consequences of the activity more easily assayed (Hamada et al., 2008; Pulver et al., 2009; Peabody et al., 2009; Krashes et al., 2009; Alekseyenko et al., 2010; Kohatsu et al., 2011; Pan et al., 2011; von Philipsborn et al., 2011; Pan et al., 2012; Toda et al., 2012).

1.4.2.4 Realising neural activity

To detect which neurons are active during the display of a given behaviour, it is possible to either record precise responses of individual candidate neurons or express genetically encoded calcium indicators (GECI) as a proxy to report neural activity (reviewed in Jones, 2009; Simpson, 2009). Classic electrophysiological recordings can provide precise information about the action potentials of a given neuron, which is an unparalleled advantage in itself. However, the number of neurons that can be recorded at a single time is limited, and, the inherent difficulty of obtaining stable recordings from *Drosophila* brains, given the size of the neurons, deems electrophysiological recording inefficient when compared to more recent light-based visualisations of neural activity. Synaptic vesicles that contain neurotransmitters commit vesicle fusion with the pre-synaptic plasma membrane once the neuron depolarises, and the subsequent opening of voltage-gated Ca^{2+} channels leads to a local influx of Ca^{2+} ions (Muller and Connor, 1991; Jaffe et al., 1992). The concentration of such local Ca^{2+} ions is dependent on the intensity of neural stimulation, thereby making Ca^{2+} dynamics an indicator of neural activity (Yuste and Denk, 1995; Denk et al., 1996; Yuste et al., 1999; Yasuda et al., 2004). Engineering recombinant fluorescent proteins that comprise of a calcium-binding recognition element (that undergoes a Ca^{2+}-dependent conformational change) coupled to an optical reporter (in the form of a fluorescent protein), the properties of which are modulated by the conformational changes of the calcium-binding recognition element, forms the basis of all GECIs (construction, expression and optimisation of GECIs are discussed in detail in Miyawaki and Tsien, 2000; Kootlikiff; 2007; Mank and Griesbeck; 2008, respectively). Several groups have developed a number of fluorescent protein-based GECIs – of which, the most highly developed are GCaMPs (Nakai et al., 2001; Mao et al., 2008). In *Drosophila,* expressing GCaMP using various targeted expression systems has allowed researchers to detect neural activity in candidate neurons during the performance of

a given behaviour, identifying elements of underlying circuitry that are activated during the elicitation of that behaviour (Wang et al., 2003; Suh et al., 2004; Marella et al., 2006; Yu et al., 2006; Fischler et al., 2007; Wang et al., 2008; Cameron et al., 2010; Kohatsu et al., 2011; Thistle et al., 2012; Liu et al., 2012; Min et al., 2013; Flood et al., 2013). Employing GCaMPs to survey different components of neural circuits in action, whilst an animal behaves, is currently the prevailing and most powerful method to map participating neurons involved in directing a given behaviour.

1.5 Courtship behaviours in *D. melanogaster*

Drosophila melanogaster display a rich array of behaviours. One in particular, courtship, is a classic paradigm that has received much attention (Figure 1-2). One of the most significant advantages of studying courtship behaviour, making it particularly amenable to genetic studies, is the sexually dimorphic nature of the behaviour, where two naturally occurring behavioural variants exist: male and female. As a result of this feature, courtship has been the central paradigm of a multitude of studies that have investigated and partially elucidated the genetic basis underlying the development and function of a sex-specific nervous system (reviewed by Billeter *et al*., 2006a; Dickson, 2008; Villella and Hall, 2008; Dauwalder, 2011; Pavlou and Goodwin, 2013). The plethora of investigative tools now available has expanded our capabilities to delineate the underlying neural substrates that direct individual behavioural modalities.

1.5.1 Male courtship behaviours

Courtship can be thought of as a decision-making process, consisting of a series of behaviours designed to find, choose and copulate with the opposite sex. Historically, studies on *Drosophila melanogaster* courtship have largely focused on the male's active behavioural outputs, which are designed to achieve copulation, resulting in successful fertilization of the female's eggs (Billeter et al., 2006a; Dickson, 2008; Villella and Hall, 2008; Dauwalder, 2011; Pavlou and Goodwin, 2013). This is primarily due to the fact that male courtship behaviours are robust, overt and therefore easily quantifiable. These behaviours are innate; naïve males reared in isolation are capable of performing the full repertoire of behaviours when

introduced to a female for the first time (Villella and Hall, 2008). However, courtship conditioning experiments have shown that male flies learn to depress courtship toward a virgin female after an unproductive courting experience with a mated female, demonstrating that these behaviours may also be modified by experience (McRobert et al., 2003; Siegel and Hall, 1979; Siwicki et al., 2005).

Initially, visual, olfactory and acoustic cues stimulate the male to orient on, and follow, a target female (Figure 1-2A-B; Cook, 1979; Tompkins et al., 1983; Markow, 1987). He subsequently 'taps' the female with his foreleg, allowing him to sense non-volatile pheromones from the female's abdomen (Figure 1-2C; Manning, 1959; Venard et al., 1989; Greenspan and Ferveur, 2000; Amrein and Thorne, 2005; Thorne et al., 2005). Next, the male uni-laterally extends and vibrates the wing most adjacent to the female, in order to generate a species-specific courtship song – a male-specific behavioural output that consists of two types of acoustic signals termed "pulse" and "sine" (Figure 1-2D; Ewing and Bennet-Clark, 1968). In *D.melanogaster*, pulse-song (PS) consists of intermittent trains of monocyclic pulses, consisting of one or two cycles of pulses, with an intra-pulse carrier frequency of approximately 240 Hz (Ewing and Bennet-Clark, 1968; Kulkarni and Hall, 1987; Wheeler et al., 1988; Wheeler et al., 1989). The trains of pulses are interrupted by occasional periods of sine-song (SS), which occur as low frequency sinusoidal hums with a carrier frequency of approximately 160 Hz. The time interval between consecutive pulses in *D.melanogaster* (termed the inter-pulse interval; IPI) is 33 ms (Bennet-Clark and Ewing, 1967; Ewing and Bennet-Clark, 1968; Kawanishi and Watanabe, 1980; Cowling and Burnet 1981; Wheeler et al. 1988; Ritchie et al. 1994), which oscillates sinusoidally with a period of approximately 50-60 s (Kyriacou and Hall, 1980; Kyriacou and Hall, 1982; Kyriacou and Hall, 1986; Ritchie et al., 1999). The occurrence of SS, appears to prime the female by increasing her receptivity (Bennet-Clark and Ewing, 1967; von Schilcher, 1976a, b). The duration of the inter-pulse interval (IPI), and the rhythmic oscillation of the IPI, are components to the song output that are characteristic of the species (Bennet-Clark and Ewing, 1967; Ewing and Bennet-Clark, 1968; Kyriacou and Hall, 1980; Kyriacou and Hall, 1982; Kyriacou and Hall, 1986; Ritchie et al., 1999). The ability to produce song is not necessary for mate recognition given that the

complete absence of courtship song in wingless males increases latency to copulate but does not abrogate successful mating (von Schilcher, 1976). Yet, increased mating success in wingless males when playback of the appropriate pre-recorded species-specific song (as opposed to either no song, or song with incorrect species parameters) is employed, suggests that the presence of song, and the species-specific components of song in particular, are important cues for target females to identify con-specific courting males (Kyriacou and Hall, 1982; Ritchie et al., 1999). Another ancient vibrational mode of communication, only recently described for *Drosophila,* is substrate-borne vibrations (Fabre et al., 2013; Mazzoni et al., 2013). Studies have shown that the male abdomen quivers at rate of 6 Hz (Fabre et al., 2013; Mazzoni et al., 2013). Under conditions that transmit substrate-borne vibrations from these abdominal quivers, receptive females appear to reduce their locomotion, evidencing the enhanced receptivity of these females that subsequently facilitate successful copulation (Fabre et al., 2013). Altogether, if the courting male is successful in stimulating a receptive female with the initial steps of his repertoire, she will slow down in order to allow him to lick her genitals and gain additional non-volatile pheromonal cues (Figure 1-2E; Tompkins et al., 1983). The male will then attempt copulation by grasping the female securely using the sex-combs on his forelegs, aligning his genitalia to the female's while curling his abdomen and thrusting his head under the female's wings in attempt to achieve intromission (Figure 1-2F; Spieth, 1974; Cook, 1977; Coyne, 1985). If successful, the male copulates with the female by transferring a complex package of sperm, to fertilise the female, and seminal fluid, which will alter her behavioural state, increasing ovulation rates, locomotor activity and feeding while reducing her receptivity to further courtship attempts (Figure 1-2G; Aigaki et al., 1991; Carvalho et al., 2006; Häsemeyer et al., 2009; Kubli, 2003; Kubli, 2008, 2010; Yang et al., 2009). Finally, male-specific pheromones (present in both the seminal fluid and on the cuticle of the male's abdomen) are deposited onto the female, creating a mated female pheromonal profile that acts to repel subsequent advances by other potential suitors (Ejima et al., 2007).

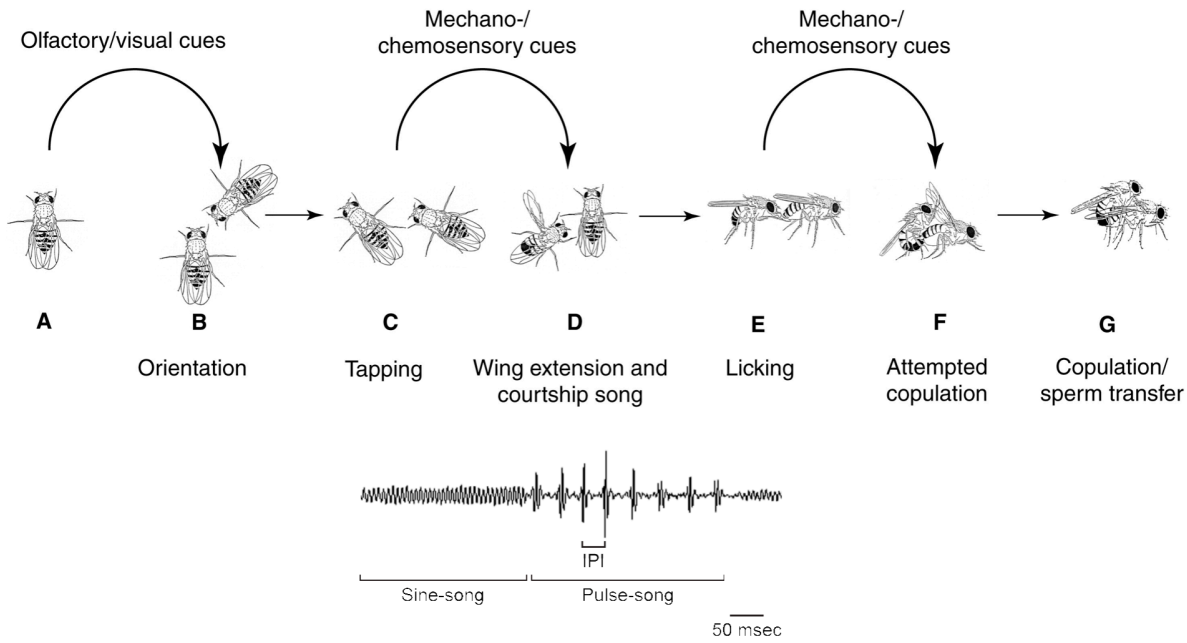


Figure 1-2 Courtship steps performed by male *Drosophila*.
(A) Target female prior to detection by the male fly. (B) The male orients to the female, (C) taps her abdomen with his foreleg, and (D) extends his wing to sing a species-specific courtship song. Male-specific wild-type courtship song illustrated below. Sine- and pulse- components and inter-pulse interval (IPI) indicated. Scale bar = 50 msec. (E) The male then proceeds to lick the target female's genitals with his proboscis, (F) attempt copulation, and if successful, (G) copulation occurs. Figure taken from Billeter et al. (2006a).

1.5.2 Female courtship behaviours

Knowledge about female mating decisions and behaviour is still in its infancy. From the female's perspective, it is essential to summate the varying and intermittent stimuli provided by a courting male, such as auditory and pheromonal cues, to assess both target species and fitness prior to sanctioning copulation (Bastock and Manning, 1955; Manning, 1967; Kyriacou and Hall 1982; Ritchie et al., 1999). If the female is unreceptive to the male, she exhibits subtle rejection behaviours such as wing flicking (in young virgins), kicking (in mature virgins) or ovipositor extrusion (Connolly and Cook, 1973; Ejima et al., 2001; Spieth and Ringo, 1983). If a female is receptive to the male, she will facilitate copulation by slowing down, ceasing rejection behaviours, and opening her vaginal plate for successful intromission (Spieth, 1974; Spieth and Ringo, 1983). The stimuli that trigger such responses, and the effects they have on the behaviour of courting males are still unknown, however, that females are able to actively accept or reject a male's advances demonstrates the fact that successful copulation is largely a female dependent choice. If successful copulation is

allowed to occur, the copulating pair will remain largely stationary (Spieth and Ringo, 1983) and, as stated, the male will transfer a complex package of sperm, to fertilise the female, and seminal fluids, which will engender a change in the female's behavioural and physiological state. While virgin females are highly receptive and rapidly copulate with a suitable partner, mated females actively reject another courting male, reducing their likelihood to remate for approximately 1 week, and maximizing their capacity for producing eggs by increasing their rate of ovulation and oviposition (Aigaki et al., 1991; Liu and Kubli, 2003; Kubli 2008; Ram and Wolfner, 2007; Häsemeyer et al., 2009; Yang et al., 2009). Studies have shown that the frequency to remate is dependent on social context, as a high incidence of remating is observed when flies are housed in groups of six males and six females (Billeter et al., 2012). In addition to these post-mating responses, mated females display changes in their locomotor activity, sleep, feeding, and innate immune response (Carvalho et al., 2006; Ejima and Griffith, 2007; Kubli, 2003; Kubli, 2008; Kubli, 2010). Altogether, a female's decision to copulate is not only based on the mate's features but also on her own reproductive status and readiness to mate. Exceptions to this rule come from a study that has shown that a persistent male can overcome determined rejection behaviours from both virgin and mated females to successfully copulate, demonstrating a complex facet of female behavioural responses that is yet to be understood (Häsemeyer et al., 2009; Yang et al., 2009; Rideout et al., 2010). Deciphering how and whether the change in behaviours from naïve (non-receptive) to mature (potentially receptive) females is guided by stimuli from the male and/or her own internal state will begin to unravel these issues.

1.6 Sex determination in *D.melanogaster*

By definition, sexual dimorphism encompasses differences in external appearance, internal physiology, pheromonal profiles and behaviour between the sexes. In *Drosophila*, genes of the sex-determination hierarchy orchestrate the differentiation and development of sex-specific tissues that establish sex-specific physiology and neural circuitry, and thus, by implication, are involved in all facets of sexual dimorphism. In *Drosophila melanogaster* sex determination is cell-autonomous; the X chromosome to autosome ratio (X:A) specifies the

sex of each cell by activating (in XX females), or repressing (in XY males) the *Sex lethal* (*Sxl*) gene (Christiansen et al., 2002; Camara et al., 2008; Figure 1-3). This produces functional Sxl protein in females only, serving as a cis-acting RNA splicing factor (Cline, 1984). Sxl regulates the splicing of pre-mRNA transcribed by its primary target, *transformer* (*tra*), resulting in expression of functional Tra protein (McKeown et al., 1987; Boggs et al., 1987; Nagoshi et al., 1988; Inoue et al., 1990). In males, neither Sxl, nor Tra proteins are expressed. The presence or absence of Tra, in conjunction with the non-sex-specific Tra-2 protein, determines the presence, or form, of both Dsx and Fru proteins, which in turn determine most aspects of the male and female state. Ultimately, the concerted effects of male-specific proteins, Fru^M and Dsx^M, determines the morphological and neural potential for complete male-specific wild-type behavioural repertoires, while the equivalent processes in females are solely dependent on the function of female specific protein, Dsx^F (Figure 1-3; MacRobert et al., 1985; Villella and Hall, 1996; Lee et al., 2002; Billeter et al., 2006a; Billeter et al., 2006b; Rideout et al., 2007; Kimura et al., 2008; Rideout et al., 2010).

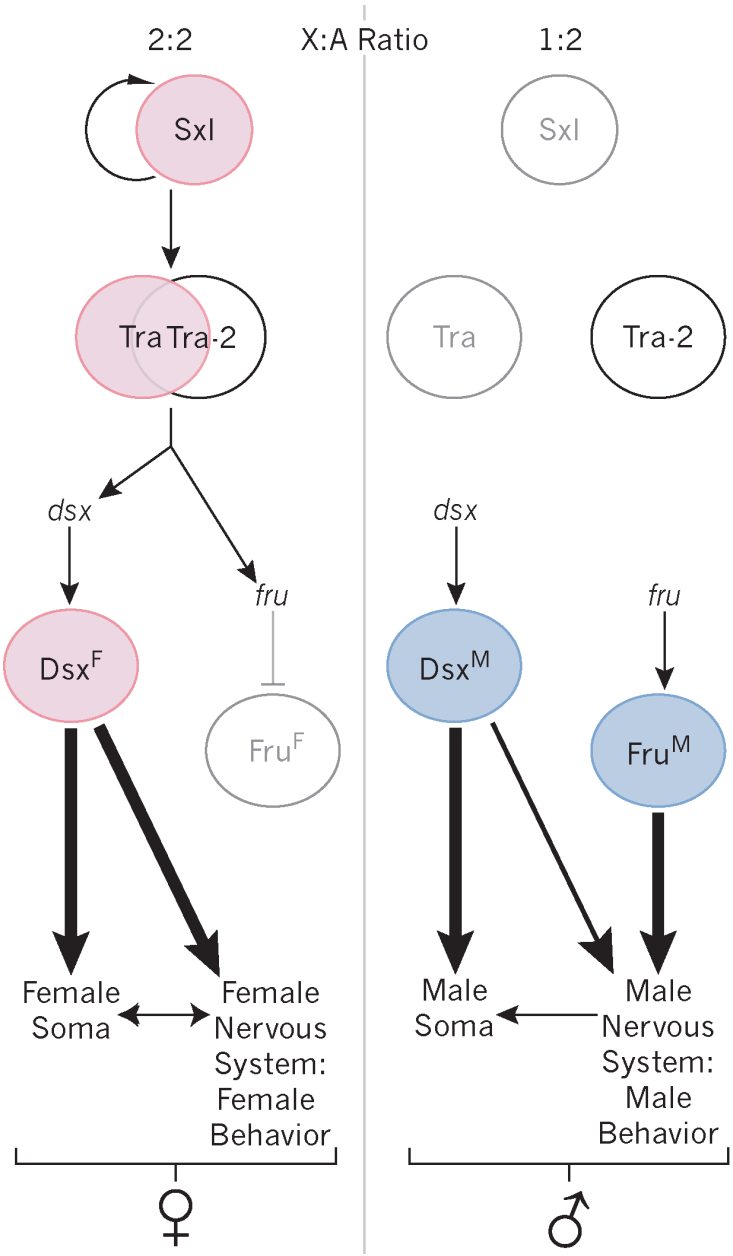


Figure 1-3 Schematic of the sex determination hierarchy highlighting the functional activities of *dsx* and *fru*.
Black lines/bold colours indicate active; grey lines/faded colours indicate inactive or non-functional. Female-specific proteins (pink), male-specific proteins (blue), non-sex-specific proteins (white). *Sex lethal* gene is maintained 'on' in females by positive auto-regulatory splicing of its own pre-mRNA, Sex Lethal (Sxl) protein also controls female-specific splicing of transformer pre-mRNA to generate the Transformer (Tra) protein. Tra in conjunction with Tra-2 regulates the splicing of *doublesex* (*dsx*) and *fruitless* (*fru*) so that a functional female-specific form of Doublesex (Dsx^F) protein is formed and the female-specific fru pre-mRNAs are not translated into a functional Fruitless (Fru^F) protein. Dsx^F determines female somatic structures and external morphology, but has also been shown to regulate female specific behaviours arising from the nervous system. However Dsx^F expression in the soma has also been demonstrated to modulate female-specific behavioural outputs. In the absence of Tra, *dsx* and *fru* are spliced into their functional male Dsx^M and Fru^M proteins. Dsx^M largely determines male somatic structures and external morphology, while Fru^M is required for expression of male behaviours arising from the male nervous system. However Dsx^M has also been shown to be required for the complete organization/complement of some Fru^M expressing neurons and so is also involved in determining the male nervous system and modulating male-specific behavioural outputs. Conversely Fru^M's activity within male-specific structures of the peripheral nervous system may also indicate a function for *fru* within the developing soma of the fly as with the induction of the male-specific muscle of Lawrence. *dsx* appears above *fru* in the linear schematic as it's expression precedes Fru^M's. Figure from Billeter et al. (2006a).

1.7 Genetic correlates of courtship behaviour

Historically, how *fru* and *dsx* regulate courtship came from behavioural analyses in males and females expressing mutations at the respective loci. This provided a handle for identifying neurons involved in sexual behaviour (reviewed in Villella and Hall, 2008; Dauwalder, 2011; Pavlou and Goodwin, 2013). Details of these investigations are discussed below.

1.7.1 Fruitless

The *fru* locus spans approximately 140 kb, from cytogenetic location 91A7-91B3, and encodes a BTB (Broad-complex/Tramtrack/Bric-à-brac) zinc finger (Znf) transcription factor (Figure 1-4A; Ryner *et al*., 1996; Ito *et al*., 1996). Molecular and functional analyses of *fru* revealed it to be a transcriptionally complex pleiotropic gene with at least two major functions: one for the control of male sexual behaviour, and the other for the viability of both sexes (Figure 1-4B; Ito et al., 1996; Ryner et al., 1996; Villella et al., 1997; Goodwin et al., 2000; Anand et al., 2001; Lee and Hall, 2001; Lee et al., 2001; Song et al., 2002; Song and Taylor, 2003; Demir and Dickson, 2005; Dornan et al., 2005; Billeter et al., 2006b). *fru* has only been shown to exist within insect lineages, while its mechanism of sex-specific splicing and isoform choice has been shown to be conserved between Drosophilidae and Mosquito, animals separated by approximately 250 million years of evolution (Gailey et al., 2000; Davis at al., 2000; Gailey et al., 2006).

Alternative splicing at the 5' and 3' ends of *fru* produces a series of transcription factor proteins driven by four promoters, P1-P4, that contain a common BTB N-terminal domain capable of protein:protein interactions and one of four alternative DNA-binding C-terminal Znf ends, A-D (Figure 1-4B; nomenclature as per Ryner et al., 1996; Billeter et al., 2006b). Transcripts from the most distal of the four promoters, P1, are sex-specifically spliced by the female-specific Tra/Tra2 protein complex – such that in females, this introduces a stop codon into the S exon, which inhibits the translation of a functional Fru protein from all P1 transcripts, while in males, the absence of the Tra/Tra-2 protein complex results in the use of a default splice site that produces P1 transcripts capable of translating functional male-

specific Fru proteins collectively referred to as Fru^M (Figure 1-4B-C; Ito et al., 1996; Ryner et al., 1996; Usui-Aoki et al., 2000; Goodwin et al., 2000; Billeter et al., 2006b). As male-specific *fru* transcripts originating from the P1 promoter (as opposed to those produced by the non-sex specific promoters P2, P3 and P4) only contain zinc fingers A, B or C, the Fru^M isoforms comprise Fru^{MA}, Fru^{MB}, and, Fru^{MC} (Figure 1-4C-D; Billeter et al., 2006b). An additional feature of male-specific Fru^M proteins is the inclusion of an additional 101 amino acid N-terminal domain, upstream of the common BTB domain. The features exhibited by *fru* proteins point towards two modes of interactions: i) the presence of alternative Znf C-terminal domains suggests sequence-specific DNA binding capability while ii) the presence of the N-terminal BTB protein:protein interaction domain suggests homo-dimerisation with identical or other isoforms of *fru* proteins and/or hetero-dimerisation with other BTB-containing proteins (Ryner et al., 1996; Ito et al., 1996). The potential for such combinatory interactions implies a multiplicity of potential downstream targets.

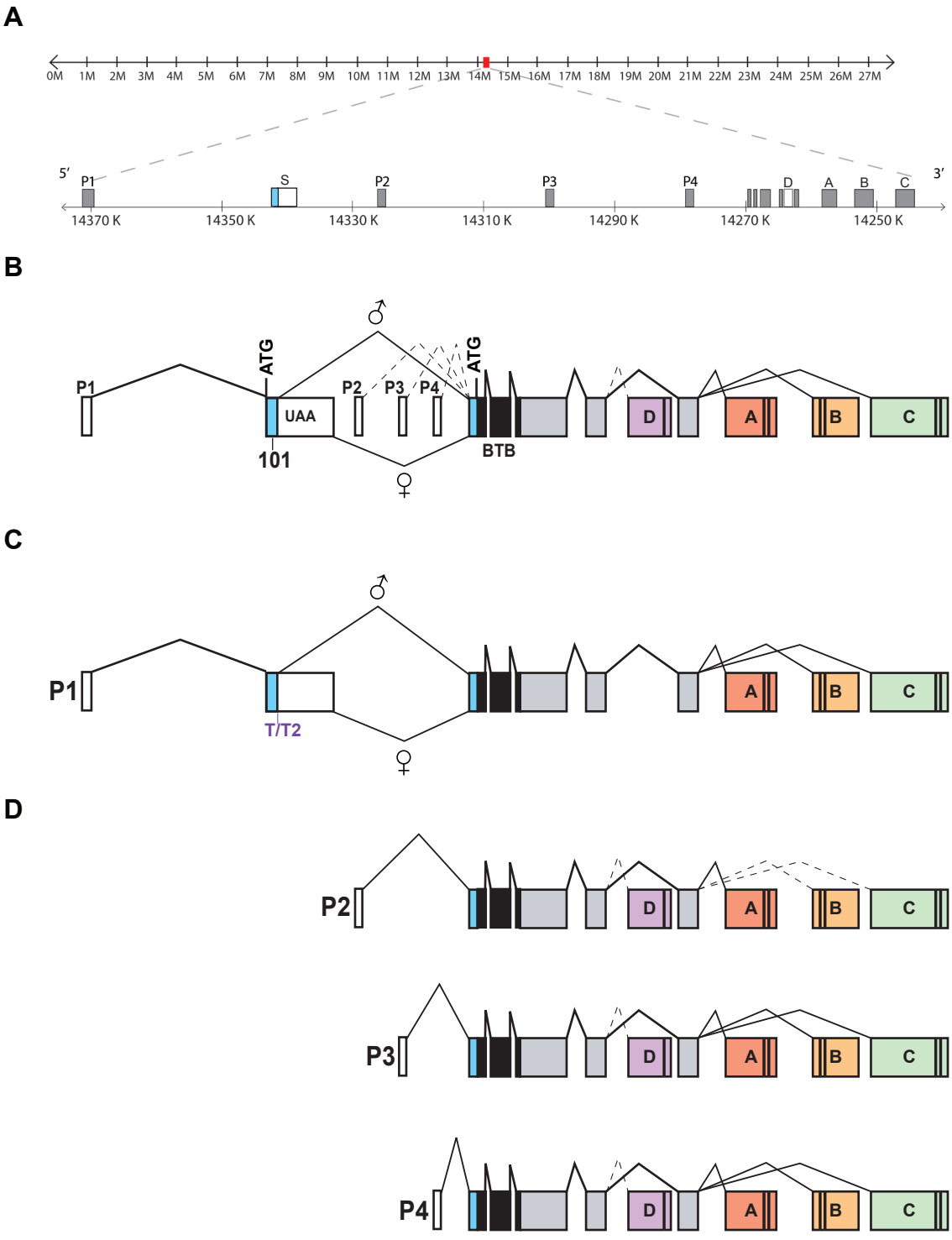


Figure 1-4 Schematic representation of the *fruitless* locus and its predicted transcripts.
(A) Right arm of the third chromosome, *fru* locus indicated by the red box (M=megabases). Expanded region of the *fru* locus below, spanning ~150 kb at cytogenetic location 91A7-91B3. Both sex- and non-sex-specific exons represented (grey boxes). Sex specifically spliced exon represented by blue/white box (S). (B) Schematic of *fru* gene, (C) male and female P1 sex-specific predicted transcripts and (D) P2-P4 non-sex-specific predicted transcripts. Arrows indicate transcriptional start sites, non-coding exons (white boxes). Translational start sites (blue boxes). Common BTB domain (black boxes). Grey and coloured boxes sex- and non-sex-specific coding exons. Transcripts from the P1 promoter undergo sex-specifically splicing at the 5' end in the Sex specifically spliced exon by the female specific splice factor Tra in conjunction with the non-sex-specific splice factor Tra-2 (T/T2). P1 male-specific transcripts include an additional 101 amino acids (101). P1-P4 transcripts incorporate through alternative splicing, one of four C-terminal Znf DNA binding domains (A-D). Figures adapted from E. Rideout (unpublished) and Billeter and Goodwin (2004).

1.7.2 Fruitless and courtship

A mutation in *fru* (*fru*^{1}) was originally isolated in an X-ray mutagenic screen for male sterility (K. Gill, 1965). Behavioural interrogation of this mutant revealed the underlying cause of sterility: abnormal courtship (such that males court males and females indiscriminately) and a failure to attempt copulation (Hall, 1978; Gailey and Hall, 1989). In a similar strategy, using male sterility as a phenotype, additional *fru* mutant alleles were generated in order to investigate the role of *fru* in the manifestation of courtship sub-behaviours. Depending on the mutant allele, *fru* males display a range of pathologies that contribute to their sterility; including i) reduced levels or complete absence of courtship towards females, ii) increased levels of courtship towards males, iii) abnormal or complete lack of courtship song, and iv) failure to attempt copulation; though animals with specific *fru* mutant combinations are able to successfully copulate, these fail to ejaculate (Gailey and Hall, 1989; Gailey et al., 1991; Ito et al., 1996; Ryner et al., 1996; Villella et al., 1997; Goodwin et al., 2000; Lee et al., 2001; Demir and Dickson, 2005; Dornan et al., 2005; Billeter et al., 2006b; Rideout et al., 2007). Morphologically, *fru* mutant males appear normal, the exception being the absence or incomplete formation of a male-specific muscle (the muscle of Lawrence; MOL) (Gailey et al., 1991; Taylor and Knitttel, 1995; Ito et al., 1996; Villella et al., 1997; Anand et al., 2001; Billeter et al., 2006b). Strikingly, mutations in *fru* appear to have little or no discernable effects on female behaviours (Villella et al., 1997). Historically these findings formed the foundations of our understanding of *fru* function: that the products of the *fru* locus are necessary to determine the potential for male courtship behaviour.

The *fru* mutations that specifically disrupted male courtship behaviours impaired transcription of the sex-specific transcripts from the P1 promoter (Goodwin et al., 2000; Lee and Hall, 2001; Anand et al., 2001). As a result, studies since have specifically focused on elucidating the role of Fru^{M} isoforms in the determination of male sexual behaviour. That females do not express Fru^{M} proteins and that female behaviours are unaltered by mutations that disrupt the expression of Fru^{M}, provides an ideal system, in the form of a ‘clean slate’, to test whether Fru^{M} expression in the female is sufficient for the specification of male courtship behaviours.

Two novel alleles of *fru (fru*^{M} and *fru*$^{\Delta tra}$) were generated to force male splicing in both males and females, importantly resulting in ectopic/atypical production of Fru^{M} transcripts/isoforms in females. This was achieved by deleting either the entire female-specific part of the S exon that includes the Tra/Tra-2 binding sites, or by deleting the Tra/Tra-2 binding sites alone (Demir and Dickson, 2005). Females expressing Fru^{M} (which were later termed *'she-males*') perform the early steps of the male courtship ritual, though at subnormal levels, that is: initiation, orientation, following, tapping and wing extension towards wild-type females, although no recognizable song is produced and these females never attempt copulation (Demir and Dickson, 2005; Rideout et al., 2007). To test the effects of no Fru^{M} expression in males, an allele that forces female splicing of *fru* was generated, by introducing a point mutation at the male splice donor site of the S exon. These *fru*^{F} males are able to display typical *fru*-associated courtship behaviours, such as 'chaining', which occurs when these males are grouped together. However, these Fru^{M} mutant males exhibit little to no sexual interest towards females (Demir and Dickson, 2005).

To genetically access and manipulate *fru*-expressing neurons, GAL4 was targeted downstream of the *fru* P1 promoter, creating the novel *fru*^{GAL4} allele (Billeter et al., 2004; Stockinger et al., 2005). These tools express GAL4 in neurons that normally express Fru^{M} in males, albeit imprecisely, and it also gains access to the corresponding neurons in females (Billeter et al., 2004; Stockinger et al., 2005). Silencing the activity of all *fru*^{GAL4} neurons in males results in an overt impairment in the display of male courtship behaviours, when paired with a virgin female (Stockinger et al., 2005). Thus, given that the general sensorimotor functions of these *fru*^{GAL4}-silenced males are still intact, this study showed that *fru*^{GAL4} neurons directly function to determine male courtship and are largely necessary and dedicated to this behaviour. These findings were confirmed when similar experiments were carried out using the enhancer trap line, *NP21,* which contains a P-element insertion in the second intron of the *fru* gene, reiterating GAL4 expression in a subset of Fru^{M} neurons (Kimura et al., 2005).

To determine causal relationships between *fruitless* neurons and behaviour, Clyne and Miesenböck (2008) used an optogenetic strategy to activate all *fru*-expressing neurons in intact and headless flies (Clyne and Miesenböck, 2008). They demonstrated the existence of a central song pattern generator (CPG) in the mesothoracic area of the VNC in both sexes, capable of generating wing extension and courtship song in flies. However, to generate *bona fide* courtship song requires the expression of the male-specific isoforms of both *dsx* (Dsx^M) and *fru* (Fru^M) in the CNS, in addition to direction from male-specific higher-order 'command' neurons (Rideout et al., 2007; Clyne and Miesenböck, 2008). Again, these experiments were confirmed via a thermal activation strategy, whereby all *fru* neurons express *UAS-dTrpA1* (Pan et al., 2011; Kohatsu et al., 2011). At the restrictive temperature, these males display a full courtship repertoire in the absence of a target female (Pan et al., 2011; Kohatsu et al., 2011).

As it may be seen that *fru*, while necessary, is not sufficient to determine the complete male repertoire of behaviours, it must be asked what other genes may be involved in determining these behavioural outputs? That *tra* mutant females, which express the male-specific isoforms of both *fru* and *dsx*, are able to perform all male-specific behaviours (Bernstein et al., 1992; Kyriacou and Hall, 1980), compellingly demonstrated that not only is *tra* is able to regulate all the necessary downstream events that are essential for courtship behaviour, but that *dsx is* the obvious candidate to act alongside of *fru* in the specification of male courtship behaviour.

1.7.3 Doublesex

The *dsx* locus spans approximately 50 kb, from cytogenetic location 84E5-84E6, and encodes a transcription factor that, unlike Fru, is structurally and functionally conserved throughout the animal kingdom (Figure 1-5; Kopp, 2012). The intrinsic DNA binding motif (DM domain of Dsx proteins classifies them as members of the Dmrt (*doublesex* and *mab-3*-related transcription factor) family (Kopp, 2012). Male- and female-specific isoforms of Dsx are comprised of a common N-terminal domain that not only mediates DNA binding via the DM domain, but also mediates protein:protein interactions via a second oligomerization

domain, which suggests similar binding properties; and as a result of sex-specific splicing events, divergent C-terminal domains (Figure 1-5B-C; An et al., 1996; Burtis et al., 1991; Cho and Wensink, 1997; Erdman et al., 1996). These C-terminal domains contain sex-specific regulatory elements as well as a homotypic-binding domain that mediates dimerisation and additional protein:protein interactions (An et al., 1996; Cho and Wensink, 1997; Erdman et al., 1996). It has been speculated that the sex-specific functions of Dsx isoforms are likely to be mediated by the different proteins/cofactors that interact with these sex-specific C-terminal domains (Williams et al., 2008).

Dsx proteins are known to specify most somatic sexual differences outside the nervous system, in addition to a sexually dimorphic circuitry in the CNS (Taylor and Truman, 1992; Lee et al., 2002; Billeter et al., 2006a; Rideout et al., 2007; Sander and Arbeitman, 2008; Rideout et al., 2010; Robinett et al., 2010; Mellert et al., 2010), possibly by way of governing the activity of downstream target genes. However, target genes that are governed by Dsx isoforms may differ based on the mode of regulation (repression of genes or paths leading to inappropriate sexual identity, while ensuring genes or paths leading to the appropriate sexual fate are activated), developmental role (specific or continuous role in regulating target genes for sex-specific development of tissues), and tissue specificity, making the array of processes regulated by *dsx* extremely complex.

1.7.4 Doublesex and courtship

Complete loss of function alleles in *dsx* cause both males and females to differentiate as intersex animals (Hildreth, 1965). As implied by the name ‘doublesex’, these animals develop male-like pigmentation, ambiguous male and/or female internal reproductive organs, and have incomplete sex combs on the foreleg; all of which occur as a result of the loss of both positive and negative regulatory events mediated by normal/endogenous expression of the male- and female-specific isoforms of *dsx* (Hildreth, 1965; Burtis and Baker, 1989; Jursnich and Burtis, 1993; Waterbury *et al*., 1999). Females carrying a dominant *dsx* mutation, dsx^{Dom}, which forces constitutive expression of Dsx^{M}, have been shown to differentiate as morphologically male (Nagoshi and Baker, 1990). Similarly, the expression of Dsx^{F} in males

has been shown to induce the expression of female-specific pheromones, and is sufficient for the development of female internal reproductive organs, abdominal pigmentation and external sexual characteristics (Burtis and Baker, 1989; Waterbury *et al*., 1999). These studies compellingly demonstrate *dsx*'s central role in the determination of most aspects of dimorphic somatic differentiation (discussed in more detail later).

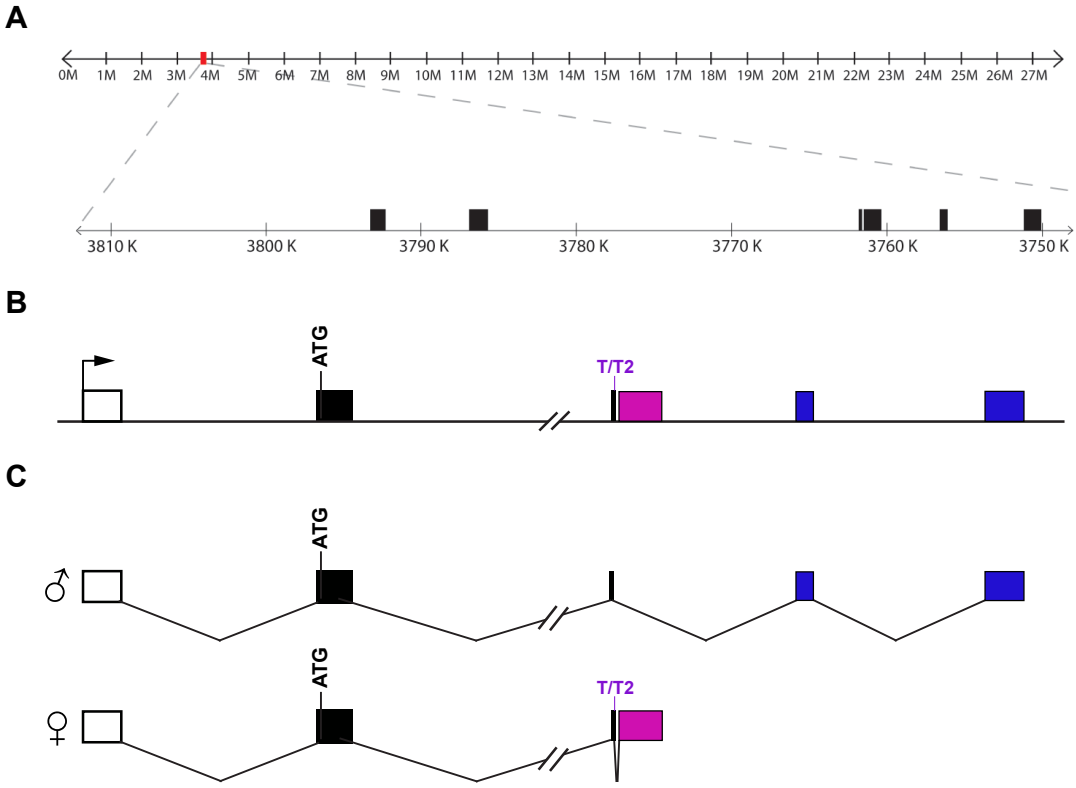


Figure 1-5 Schematic representation of the *doublesex* locus and its predicted transcripts.
(A) Right arm of the third chromosome, *dsx* locus indicated by the red box (M=megabases). Expanded region of the *dsx* locus below, spanning ~43 kb at cytogenetic location 84E5- 84E6. Both sex- and non-sex-specific exons represented (black boxes). (B) Schematic of *dsx* gene and (C) male and female predicted transcripts. Arrows indicate transcriptional start sites, white box non-coding exon. Black and coloured boxes sex- and non-sex-specific coding exons. Transcripts from the *dsx* locus are sex-specifically spliced at the 3' end by the female specific splice factor Tra in conjunction with the non-sex-specific splice factor Tra-2 (T/T2). Figures adapted from E.Rideout (unpublished) and Rideout et al. (2010).

When interrogating the role of *dsx* and courtship behaviour, studies have collectively demonstrated that *dsx* is necessary, but not sufficient, to modulate male sexual behaviour (McRobert and Tompkins, 1985; Villella and Hall, 1996; Rideout et al., 2007; Kimura et al., 2008; Rideout et al., 2010). Expression of the male form of *dsx* (Dsx^M) in chromosomally (XX) female flies results in their physiologically male appearance; yet these masculinised females lack the ability to exhibit male-like behaviours (Taylor et al., 1994). Although males

lacking *dsx* also appear intersexual, these animals are able to perform courtship behaviours though at greatly diminished levels (Villella and Hall, 1996). Further to this, a signature phenotype associated with *dsx* mutant males, is their inability to perform sine song (Villella and Hall, 1996).

Genetic access to *dsx*-expressing neurons was only recently established via the generation of dsx^{GAL4} alleles (Rideout et al., 2010; Robinett et al., 2010), marking the first set of comprehensive investigations of the role of *dsx* in copulatory behaviours (Rideout et al., 2010). Rideout et al. (2010) demonstrated that the disruption of neural function by constitutively expressing *UAS-TNT*, lead to aberrant behaviours and sterility in both sexes (Rideout et al., 2010). More specifically, silencing all *dsx*-expressing neurons in males resulted in severe reduction of courtship behaviours, resulting in increased latency to initiate courtship, beyond which these males engaged only in intermittent following and orientation and never attempted copulation (Rideout et al., 2010). Disrupting synaptic activity of all *dsx*-expressing neurons in virgin females impaired their ability to sample male courtship displays, resulting in their incapability of providing acceptance responses (Rideout et al., 2010). During copulation, this lack of cooperation manifested as continual female movement and rejection behaviours (Rideout et al., 2010). Although sperm and seminal fluids were transferred, these females laid no eggs, re-mated, and were incapable of suppressing further courtship advances, indicating that *dsx* neurons are involved in both pre- and post-copulatory female reproductive behaviours (Rideout et al., 2010).

1.8 Neural correlates of courtship behaviour

Specific genes orchestrate the molecular events necessary for accurate development and wiring of the nervous system, to produce a functional meshwork of parallel neural circuitries that is the CNS. As such, the potential for behaviour intrinsically relies on the operation of a multicellular circuitry that is made up of functionally associated cells, in which impairment of any part of such circuitry is likely to cause decrements in all behaviours that it sub-serves. How *dsx* and *fru* function in specifying sexual behaviour was inferred by their temporal and

spatial patterns of expression in the nervous system; the components of which have been functionally assigned (reviewed in Pavlou and Goodwin, 2013).

1.8.1 Organisation of the adult CNS

Unlike neurons in vertebrates, where both dendrites and axons extend directly from the neural cell body (soma), neurons in insect CNSs are monopolar, sending single neurites (cell body fibres) that extend from the soma deep into the brain, which form arborisations (pre-synaptic axons and post-synaptic dendrites) and synapses en route (reviewed by Strausfeld and Meinertzhagen, 1998). Neural cell bodies are confined to the surface of the CNS in which surface-associated glia ensheath each neural cell body, to form the 'cell body rind' (CBR). Neurons of the CBR are comprised of small locally projecting interneurons, and projection neurons, whose axons project to more distant regions of the CNS, both contributing to the synaptic complexity of the CNS itself; and efferent neurons whose dendrites and cell bodies lie within the CNS but whose axons extend to peripheral targets, including neuro-modulatory and motoneurons that innervate muscles and neurosecretory cells within various organs. The 'neuropil', on the other hand, refers to the inner areas of the CNS, and is occupied by neural fibres, synapses and neuropil-associated glia, and is categorized into two types; the synaptic neuropil – an area which contains neural projecting fibres and synaptic arborisations; and the connecting fibre neuropil, which refers to bundles of neural fibres that are devoid of synapses, including fascicles (i.e. fibre bundles that connect two areas of the ipsi-lateral hemisphere), commissures (i.e. fiber bundles that connect two areas of the contra-lateral hemispheres), and chiasmata (i.e. the area where neural fibres cross-over).

Developmental and evolutionary criteria have historically been used to compartmentalise the *Drosophila* CNS into segmental neuromeres. The synaptic neuropil within each neuromere has also been compartmentalized into mutually exclusive anatomical nerve centres or 'ganglia', determined by physical descriptors of the densities associated with the projecting fibres of the associated cell bodies, and surrounding connecting fibre neuropil. The borders around major brain areas were determined simply by the presence of a sheath of neuropil-

associated glia. More recently, synaptic markers such as anti-*bruchpilot* or -*Synapsin*, as well as pan-neural ectopic expression of synapse targeted reporter genes such as *syaptobrevin*::GFP or *synaptotagmin:*::HA, have been utilised to readily identify physical landmarks of bundles of connecting fibres, allowing for the boundaries to be further refined into comprehensive and mutually exclusive supercategories that are widely used today (Figure 1-6).

In the broadest sense, the CNS is separated into two inter-dependent and inter-connected anatomical entities that are made up of neuroanatomically grouped ganglia: the brain, located in the head capsule, and the ventral nerve cord (VNC), which extends longitudinally in the ventral cavity of the thorax. Connected to the CNS is the peripheral nervous system (PNS), which consists of peripheral nerves, neuromuscular junctions and sensory receptors that allow the fly to receive, transmit and respond to sensory stimuli. The cell bodies of the PNS are typically bipolar and their axonal projections extend to supply the first-order input into the CNS (reviewed by Stocker, 1994; Strausfeld and Meinertzhagen, 1998; Caldwell and Eberl, 2002).

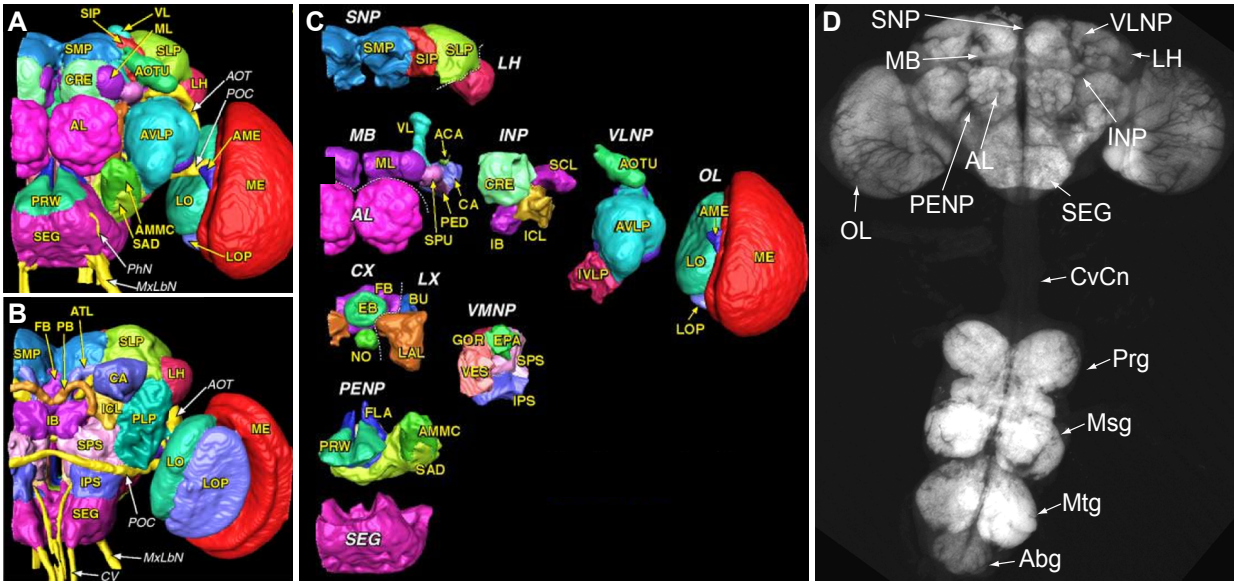


Figure 1-6 Representations of the *Drosophila* nervous system.
(A) Overall anterior, (B) overall posterior and (C) expanded 3D reconstructions of the regions of the *Drosophila* brain neuropil. The 'level 1' neuropil supercategories indicated are optic lobe (OL), mushroom body (MB), central complex (CX), lateral complex (LX), ventrolateral neuropils (VNLP), lateral Horn (LH), superior neuropils (SNP), inferior neuropils (INP), antennal lobe (AL), ventromedial neuropils (VMNP), periesophageal neuropils (PENP) and suboesophageal ganglion (SEG/SOG). (C) 5 D adult CNS stained with anti-nC82 to realize all neuropil. SNP, MB, OL, AL, SEG/SOG, PENP, INP, LH and VNLP indicated in brain. Cervical connexion (CvCn) and prothoracic (Prg), mesothoracic

(Msg), metathoracic (Mtg) and abdominal (Abg) ganglia indicated in VNC. (Ventral view; superior, top). (A-C) Figures taken from Ito et al., 2014, and (D) CNS counterstained with neuropil marker (anti-nc82; shown in white). Image from Dornan A.J. (unpublished).

1.8.1.1 The brain

The *Drosophila* brain consists of two optic lobes (OL) that are large masses of neuropil responsible for the processing of visual information received from the fly's compounds eyes. The OLs are comprised of three main layered regions, the lamina, medulla and lobular complexes (LA; ME; and LO respectively) that are arranged proximal to distal, with respect to the central brain (Figure 1-6; reviewed by Fischbach and Hiesinger, 2008).

The central brain consists of sensory centres specialised for all other sensory modalities, in addition to integrative and associative centres and motor control centres (Figure 1-6A-C; Ito et al., 2008). Developmental and evolutionary data suggest that there are a total of 6 segmental neuromeres within two major ganglia within the central brain; the protocerebrum, deutocerebrum and tritocerebrum exist within the supraoesophageal ganglion (SPG), the majority of which occupy the volume of the brain above the oesophagus, while the mandibular, maxillary and labial neuromeres exist within the suboesophageal ganglion (SOG or SEG), occupying the remaining central brain region below the oesophagus (Figure 1-6A-C; Ito et al., 2008).

The protocerebrum lies dorsal to, and occupies the most area of, the SPG. It is created from a variety of complex neuropils that include, the mushroom bodies (MBs), the central complex (CC), the lateral complex (LC), the lateral horns (LH) and more loosely designated areas as the ventero-lateral and ventero-medial neuropils (VLNP and VMNP) (Figure 1-6). Some of these regions may be subdivided into more isolated regions of interdependent neuropil, while others are seen as discrete anatomical areas. Associated with the protocerebrum are structures such as the superior protocerebral bridge (SPB) and the pars intercerebrialis (PI). The PI runs fully ventero-dorsally through the superior protocerebrum and contributes several neuro-secretory cells, both locally and distally to the CNS (Pathak and Ghosh, 1990). Continued research has elucidated some of the functional contributions these structures perform within the CNS and the organism as a whole; in behaviours such as locomotion,

olfactory learning and courtship visual learning (the MBs) and walking, flying and visual learning (the CC), making this the most studied neuromere in the fly brain (Fahrbach, 2006; Heisenberg, 2003; Ilius et al., 1994; Martin et al., 1998; Martin et al., 1999; Pan et al., 2009; Zars, 2000).

The deutocerebrum lies ventral to the protocerebrum and encompasses major substructures such as the antennal lobe (AL) and the antennal mechanosensory and motor centres (AMMCs) (Figure 1-6). The ALs are composed of >40 glomeruli that receive a number of sensory inputs, primarily from the antennae via the antennal nerves. The olfactory sensory fibres arising from the third antennal segments project to the ALs while the first and second antennal segments fibres, which arise mainly from mechanoreceptors terminate in the lateral deutocerebrum in the AMMCs. The primary functional contributions of the substructures within the deutocerebrum are thought to include the processing of chemosensory, olfactory and mechanosensory stimuli (reviewed by Stocker et al., 1994; Tootoonian et al., 2012; Lai et al., 2012).

The tritocerebrum demonstrates the inefficiency of historical mapping by landmark as opposed to modern functional mapping of neuro-anatomy, remaining obscure as its boundaries have yet to be fully characterised. Theoretically, it lies beneath the deutocerebrum, and is associated with fibre tracts connecting inconspicuous centres that lie behind the AL in the deutocerebrum, via commisures. Functional annotations of this neuromere have yet to be carried out.

The SOG lies ventrally in the brain, separated by a central foramen created by the passage of the oesophageal tract. The SOG incorporates substructures that derive from the three head segments posterior to the oesophagus. As such, the mandibular, maxillary and labial neuromeres receive the peripheral pharyngeal and maxillary-labial nerves from their corresponding head segments, comprised of sensory receptor neurons from the sensillae of the internal mouthparts as well as inputs from other gustatory receptor neurons. The primary functional contributions of the SOG are thought to include the processing of chemosensory stimuli from gustatory receptor neurons of the mouthparts for taste and feeding (Scott et al.,

2001; Wang et al., 2004; Thorne et al., 2004; Bader et al., 2007). In addition, the SOG consists of dendrites of the motor neurons of the head muscles, giving rise to descending and ascending neurons, while neurosecretory fibres projecting from the PI input to this region (Figure 1-6; Rajashekhar and Singh, 1994; Ito et al., 2008). Given that the primary role of the SOG substructures is closely associated with the PNS, the SOG is functionally more similar to the VNC than to the SPG.

1.8.1.2 The ventral nerve cord

As stated the VNC is joined anteriorly by the cervical connection to the SOG of the brain and extends longitudinally into the ventral part of the thorax (Figure 1-6; Miller, 1950). The VNC is subdivided into four main regions, which, running cephalic to caudal, are defined as the pro-, meso- and meta-thoracic (Prg; Msg; and Mtg respectively) and abdominal ganglia (Abg) (Figure 1-6D; Miller, 1950) The Prg, Msg and Mtg give rise to, three bilaterally paired ventral nerves that innervate the muscles of the coxae and extend to the tips of the legs, giving off branches to the muscles and sensory organs therein. Additional dorsally paired nerves within the Msg project to the direct flight muscles, wings and halteres, while shorter accessory paired nerves target muscles proximal to the spiracles. The Abg gives rise to paired nerves that target the first and second abdominal segments, and a thick median abdominal nerve trunk (AbNvTk), which targets structures within the most posterior abdominal segments including the genital segment, while ramifying on the internal reproductive organs of both sexes (Miller, 1950).

1.8.2 CNS foci necessary for courtship behaviour

Pioneering work in the field of *Drosophila* courtship exploited the generation of sex mosaics to identify defined anatomical sites within the CNS in which the primary neural substrate for a given sub-behaviour of courtship is located (termed ‘behavioural foci’; reviewed by Hall, 1978). Cell-autonomous sex determination in *Drosophila* makes this possible by allowing for the creation of flies that are partially male and partially female. Inducing the somatic loss of an X chromosome from a diplo-X zygote (female), results in a sex mosaic in which haplo-X tissues are genetically male, while the rest of the tissue remains female as it retains both

chromosomes (reviewed by Hall, 1978). With the part-male and part-female flies described as gynandromorphs.

That 'female' gynandromorphs with a fully masculinised CNS perform the full male courtship repertoire (Hall, 1977) supported the notion that the generation of gynandromorphs with partial masculinisation of CNS would be sufficient to elicit sub-behaviours of the courtship repertoire, given that the appropriate behavioural foci were masculinised (reviewed by Hall; 1994; Hall, 1977; Greenspan, 1995). Behaviourally screening such gynandromorphs for the emergence of sub-behaviours of courtship, and neuroanatomically determining the masculinised regions of the CNS, allowed for the identification and neuroanatomical positioning of some courtship behavioural foci (Hall, 1977; Von Schilcher and Hall, 1979; Hall 1979). Unfortunately, each animal that was generated via this approach had a unique mosaic cluster of cells that were almost impossible to refine and reproduce. However, Ferveur and Greenspan (1998) overcame these limitations by creating 'transgenic gynandromorphs'. This involved the ectopic expression of female-specific *tra* under the control of UAS (*UAS-tra*^{F}) using a collection of enhancer trap GAL4 lines to reproducibly feminise various regions of the male CNS. The anatomical expression patterns of these regions were precisely determined by driving the expression of *UAS-reporter*s, and subsequently correlating this with the presence, decrement in and/or lack of courtship sub-behaviours displayed by these males (Ferveur and Greenspan, 1998).

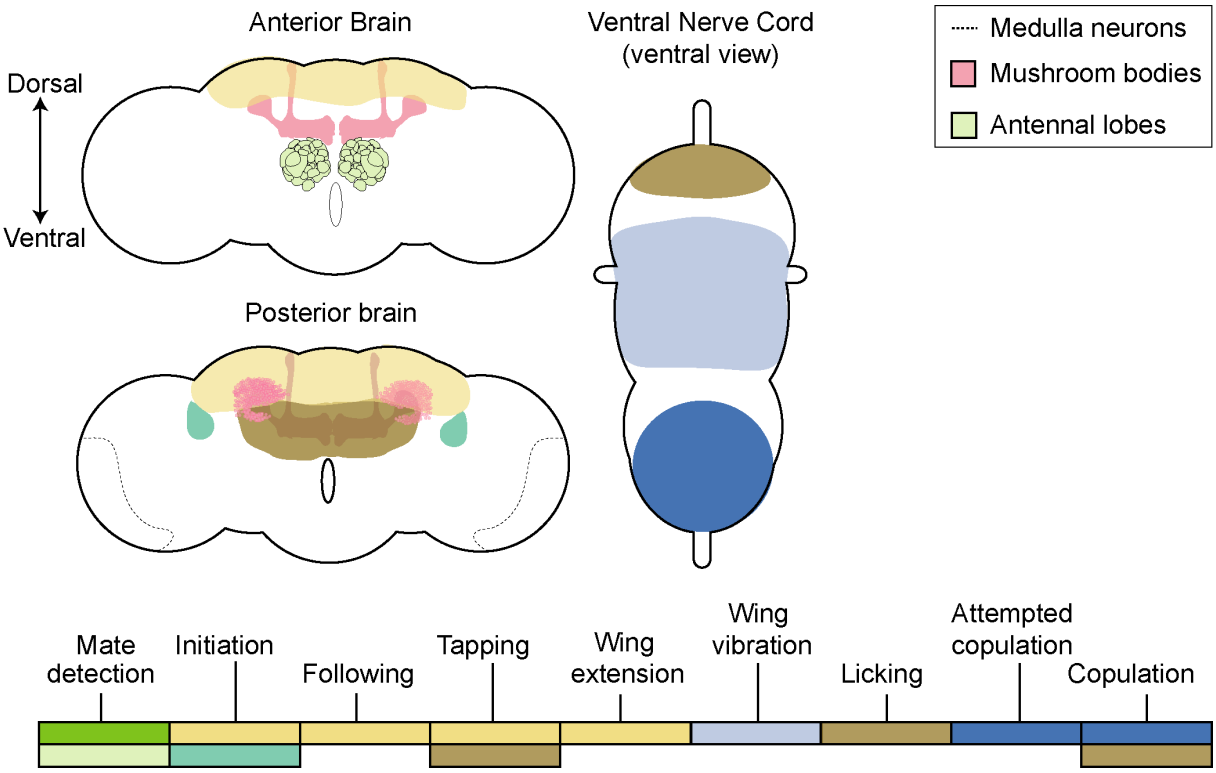
Collectively, these studies demonstrated that the major male courtship foci are:

1. The antennal lobes and a region of the mushroom body – implicated in partner discrimination (Ferveur et al., 1995; O'Dell et al., 1995; Ferveur and Greenspan, 1998).
2. A region of the posterior-dorsal brain - implicated in the initial steps of courtship, which includes orienting and following the female in addition to wing extension (Figure 1-7; Ferveur and Greenspan, 1998; Hall, 1977, 1979).
3. A posterior-medial brain region called the lateral protocerebrum – implicated in licking behaviour (Figure 1-7; Ferveur and Greenspan, 1998; Hall, 1979).

4. The anterior SOG and sites within the dorsal-mid and posterior brain – implicated in attempted copulation and copulation (Figure 1-7; Ferveur and Greenspan, 1998).
5. The prothoracic ganglion – implicated in wing extension and possibly the induction of courtship wing vibrations (Figure 1-7; Ferveur and Sureau, 1996; Ferveur and Greenspan, 1998).
6. The mesothoracic ganglion – implicated in courtship song production (Figure 1-7; von Schilcher and Hall, 1979).
7. The Abg – implicated in attempted copulation without the achievement of actual mating (Figure 1-7; Ferveur and Greenspan, 1998; Hall, 1977, 1979).

Unfortunately, the subtle nature of female behaviour during courtship has made it difficult to identify all female behavioural loci using gynandromorphs. Nevertheless, studies have mapped a region of the dorsal brain that must be female for an animal to be receptive (Szabad and Fajjszi, 1982). In addition, a single successfully identified focus, in the form of bilaterally symmetric cells of the anterior-dorsal brain has also been implicated in female mating receptivity, though this brain region appears to be largely distinct from all male-like courtship foci of the CNS (Tompkins and Hall, 1983). More recently, the VNC has been implicated in the modulation of female post-mating responses, within which the Abg has been identified as the focus specifically involved in ovulation and transfer of eggs into the uterus for fertilization (Monastirioti, 2003; Soller et al., 2006; Rodríguez-Valentín et al., 2006).

Figure 1-7 Cartoon of the neural foci implicated in the modulation of male courtship behavioural outputs.
Areas of the adult male CNS associated with the control of specific courtship steps are colour-coded and refer to the courtship steps indicated below and to the legend on the right. The dorsal posterior brain (yellow) is involved in the initiation of courtship, following, tapping, and wing extension. The posterior midbrain (brown) affects licking and copulation. In the ventral nerve cord, the prothoracic ganglion (light purple) is a site associated with the control of tapping; the mesothoracic ganglion (light blue) regulates wing extension and courtship song; and the abdominal ganglion (dark blue) controls attempted copulation and copulation. Adapted from Billeter et al. (2006a).



1.8.3 Spatiotemporal distribution of Fru^{M} expressing neurons

Spatially, Fru^{M} expression is restricted to subsets of sensory, inter- and motoneurons within the CNS and PNS of an adult male. In the CNS, Fru^{M} neurons are heterogeneously distributed in discrete clusters in, but not limited to, all behavioural loci previously implicated with courtship (Figure 1-8). More specifically, Fru^{M} is expressed in ~1700 neurons, in ~20 spatially designated clusters in the brain, with a further ~5 spatially designated clusters in the VNC (Figure 1-8); in addition to sites in the PNS associated with smell, taste and hearing, all of which have been implicated in the regulation of male courtship behaviours (Lee et al., 2000; Billeter and Goodwin, 2004; Demir and Dickson, 2005; Billeter et al., 2006a; Billeter et al., 2006b). Temporally, Fru^{M} is first expressed at the beginning of metamorphosis in a few neurons of the late third instar larval brain, coinciding with the remodelling of the CNS (Goodwin et al., 2000; Lee et al., 2000; Ryner et al., 1996). The number of Fru^{M} expressing cells increases to a peak in 2-day old pupae, and then remains constant throughout adulthood (Lee et al., 2000).

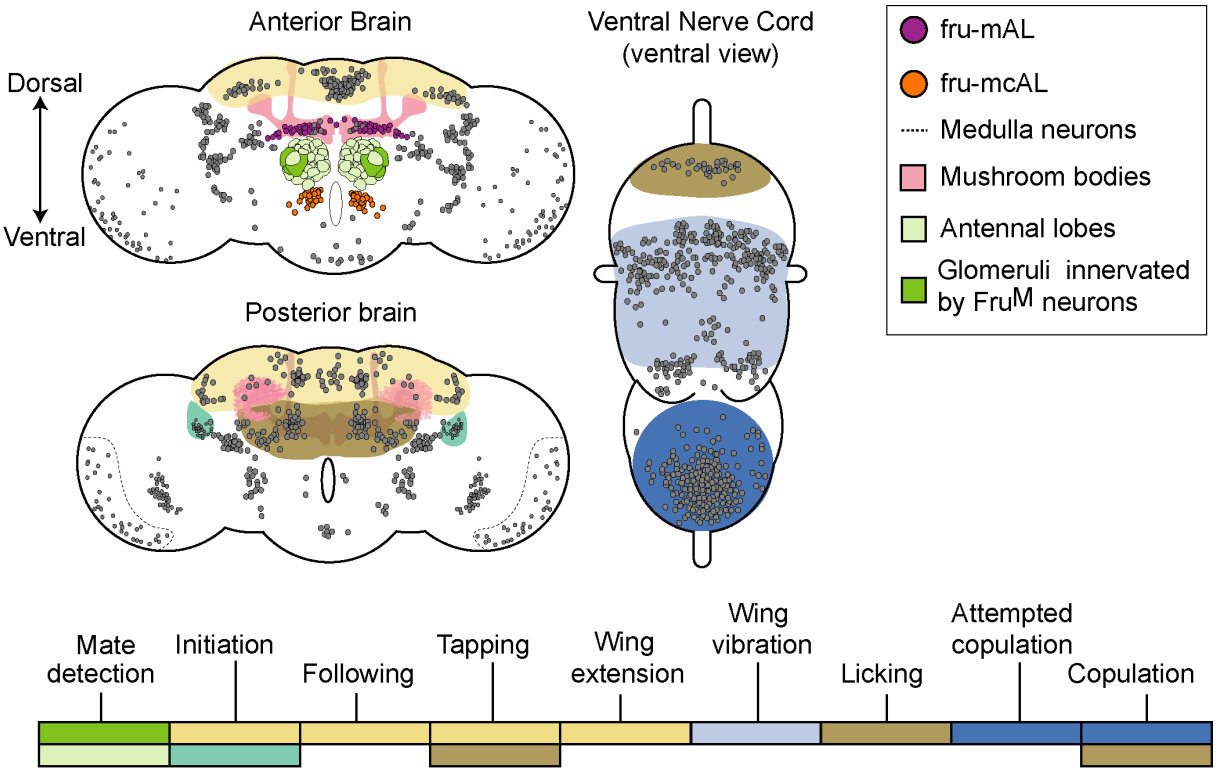


Figure 1-8 Schematic of Fru^{M} expression in the adult male CNS, overlapping with neural foci implicated in the modulation of male courtship behavioural outputs.
Areas of the adult male CNS associated with the control of specific courtship steps are colour-coded and refer to the courtship steps indicated below and to the legend on the right. Fru^{M} neural nuclei of the adult male CNS are represented by grey and coloured dots. The antennal lobes (light green) are involved in partner discrimination and specific glomeruli (darker green) innervated by Fru^{M}-expressing odorant receptor neurons are involved in mate recognition. A cluster of cells in the lateral dorsal brain (teal) regulates courtship initiation. Figure taken from Billeter et al. (2006a).

1.8.4 Spatiotemporal distribution of Dsx$^{M/F}$ expressing neurons

Unlike Fru^{M}, which is expressed solely in the male CNS, Dsx is expressed in the CNSs of both sexes (Figure 1-9; Lee et al., 2002; Rideout et al., 2007; Sanders and Arbeitman, 2008; Rideout et al., 2010; Robinett et al., 2010). Yet, similar to the spatial expression patterns of Fru^{M}, Dsx expression is also restricted to subsets of sensory, inter- and motor neurons within the CNS and PNS respectively of both sexes of adults (Rideout et al., 2010). In the CNS, Dsx neurons are distributed in discrete clusters that are restricted to the behavioural loci previously implicated with courtship (Figure 1-9; Hall, 1977; Von Schilcher and Hall, 1979; Hall 1979; Lee et al., 2002; Rideout et al., 2007; Sanders and Arbeitman, 2008; Rideout et al., 2010; Robinett et al., 2010). More specifically, Dsx^{M} is expressed in ~650 neurons, in 5 spatially designated clusters of neurons in the brain, with a further 3 spatially designated clusters of neurons in the VNC in males (Figure 1-9); while Dsx^{F} is expressed in ~370

neurons, in 4 spatially designated clusters of neurons in the brain with a further single spatially designated neural cluster in the VNC, in females (Figure 1-9); as well as in sites in the PNS associated with taste and proprioception, all of which have been implicated in the regulation of male courtship behaviours (Lee et al., 2002; Rideout et al., 2010; Robinett et al., 2010). Temporally, Dsx is first expressed in the L2 larval CNS in a bilateral cluster of cells at the distal tip of the Abg (Rideout et al., 2010). The appearance of the first clusters of neurons in the central brain occurs at the beginning of metamorphosis in the late third instar larval brain, at which point the pattern of expression becomes noticeably dimorphic (Rideout et al., 2010). The number of Dsx expressing cells increases to a peak in 2-day old pupae. At this critical juncture, the participation of Dsx^F in programmed cell death (PCD) results in a reduction in neural numbers in females by adulthood, while additional male specific clusters appear and persist throughout adulthood, culminating an overt sexually dimorphic expression pattern in adult flies (Sanders and Arbeitman, 2008; Rideout et al., 2010). Thus, by comprehensively exploring the neuroanatomy of *dsx*-expressing cells in both sexes of *D. melanogaster*, various dimorphic features between males and females *dsx* circuitry were identified; including the aforementioned differences in cell numbers in homologous clusters and sex-specific neural development of distinct clusters of neuron, in addition to differences in density, organization and connectivity of axonal projections (Rideout et al., 2010).

Further to this, both the breadth and specificity of *dsx*-expression in an array of somatic tissues that are fundamental to sex determination, endocrine regulation and physiological state changes, were also revealed (discussed in more detail later; Rideout et al., 2010; Robinett et al., 2010); highlighting *dsx*'s fundamental role in the development and differentiation of sex-specific neural circuitry and tissues, along with the establishment and maintenance of a sex-specific physiology.

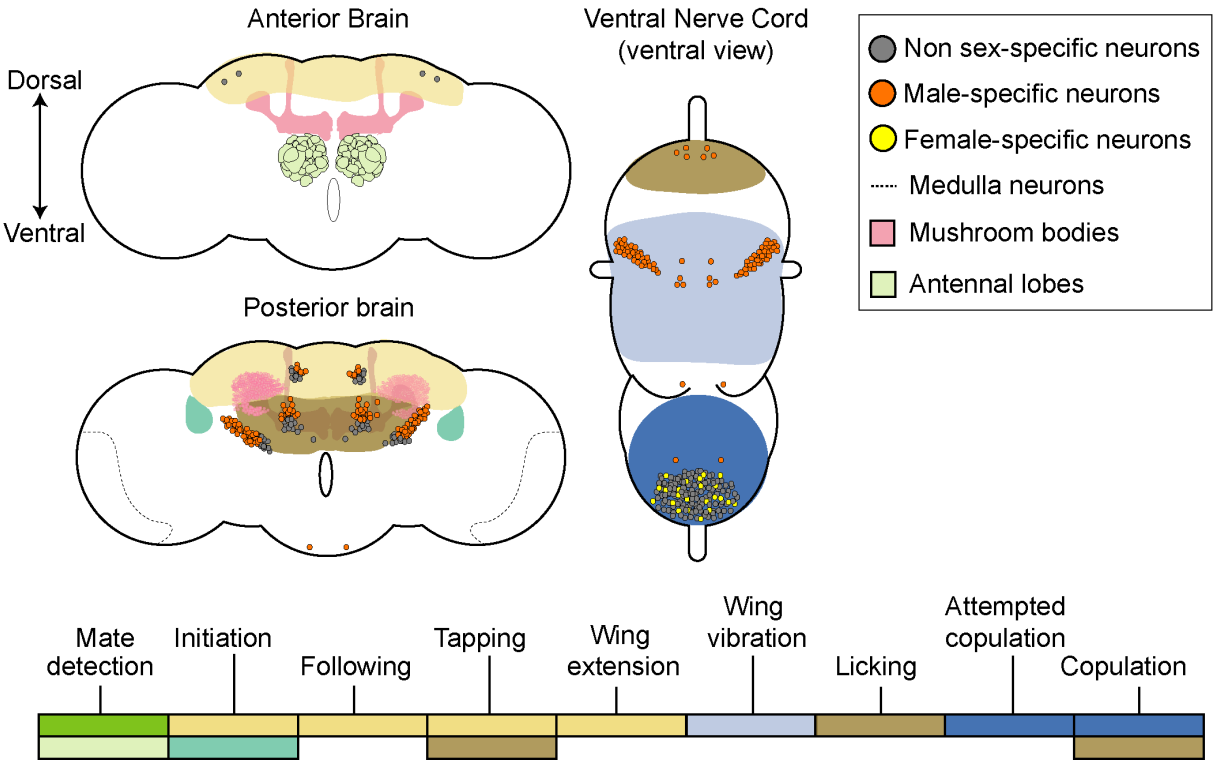


Figure 1-9 Schematic of Dsx expression in the adult male or female CNS, overlapping with neural foci implicated in the modulation of male courtship behavioural outputs.
Areas of the adult male CNS associated with the control of specific courtship steps are colour-coded and refer to the courtship steps indicated below and to the legend on the right. Non sex-specific *dsx*$^{+}$ neural nuclei of the adult CNS are represented by grey dots. Male-specific *dsx*$^{+}$ neural nuclei of the adult male CNS are represented by orange dots, while female-specific *dsx*$^{+}$ neural nuclei of the adult CNS are represented by yellow dots. The bilateral cluster of cells in the medio-lateral dorsal brain regulates courtship initiation.

1.8.5 Co-expression of Dsx^{M}- and Fru^{M}-expressing neurons

fru and *dsx* have been shown individually to be necessary for male-specific courtship behaviours without (complete) sufficiency (Manoli et al., 2005; Rideout et al., 2007; Rideout et al., 2010; Stockinger et al., 2005). That Dsx^{M} and Fru^{M} proteins co-express in several regions important in establishing male sexual behaviour, suggests that they cooperate to dictate development of neural substrates underlying male sexual behaviour (Figure 1-10; Billeter et al., 2006; Rideout et al., 2007; Kimura et al., 2008; Rideout et al., 2010). Although the mode of cooperation between *fru* and *dsx* has yet to be elucidated, that the expression of *dsx* begins earlier than *fru* in both the NS and in sub-sets of somatic tissues, suggests that *dsx* may act independently as an early developmental regulator required to dictate and maintain sexual identity throughout the determination of the final adult 'sexual' state (Hempel and Oliver, 2007; Rideout et al., 2010; Robinett et al., 2010). Yet, that both *dsx*'s and *fru*'s

expression peak at the most critical developmental juncture, during the pupal stages, also suggests cooperation between these two genes in the determination of adult male sexual behaviour (Arthur et al., 1998; Lee et al., 2000; Lee et al., 2002; Rideout et al., 2010). As these are the only two known transcriptional regulators at the bottom of the sex-determination hierarchy, both clearly act in the same sexually dimorphic neural clusters to bring about male-specific neural wiring underlying male-specific behavioural patterns (Kimura et al., 2008a; Rideout et al., 2007b; Rideout et al., 2010; von Philipsborn et al., 2011). This is behaviourally relevant, as the importance of converging fru^{+}/dsx^{+} neurons has been demonstrated by the fact that thermoactivation of either *fru*- or *dsx*-expressing neurons, in both intact and headless solitary males, can elicit elements of courtship behaviour (*e.g.* courtship song, abdominal curling and ejaculation; Pan et al., 2011). Strikingly, activation of *dsx* circuitry in males null for fru^{M} produces courtship outputs as robust as males wild-type for fru^{M}; providing further evidence suggesting that *dsx*-specified circuitry is key to male courtship behaviour (Rideout et al., 2010; Pan et al., 2011). Additional examples that support the importance of fru^{+}/dsx^{+} neurons comes from studies that have parsed *fru* circuitry into component elements responsible for different sub-behaviours of courtship (see section 'Deciding to Court' for more details; Kimura et al., 2005; Kohatsu et al., 2011; von Philipsborn et al., 2011). Distinct clusters that express both *fru* and *dsx* have been implicated in most courtship sub-behaviours; including multimodal sensory integration, initiation of courtship and courtship song production (Kimura et al., 2005; Rideout et al., 2007; Kohatsu et al., 2011; von Philipsborn et al., 2011; Pan et al., 2012).

Although the male CNS consists of ~650 dsx^{+} neurons, which is far fewer than the ~1700 fru^{+} neurons, almost all *dsx* clusters with key subsets of neurons co-localize with *fru* (Figure 1-10). Thus, it appears that *dsx* describes a more restricted circuitry (encompassing a subset of *fru* circuitry) capable of directing male courtship. It is important to re-emphasize that the sex-specific Fru isoform is absent in females; thus any sex-specific circuits in the female are most likely specified by the female Dsx^{F} isoform (Rideout et al., 2010). Therefore analyses of *dsx*-specified circuitry and associated behavioural outputs are not restricted to either males or females but rather encompass both sexual 'states'.

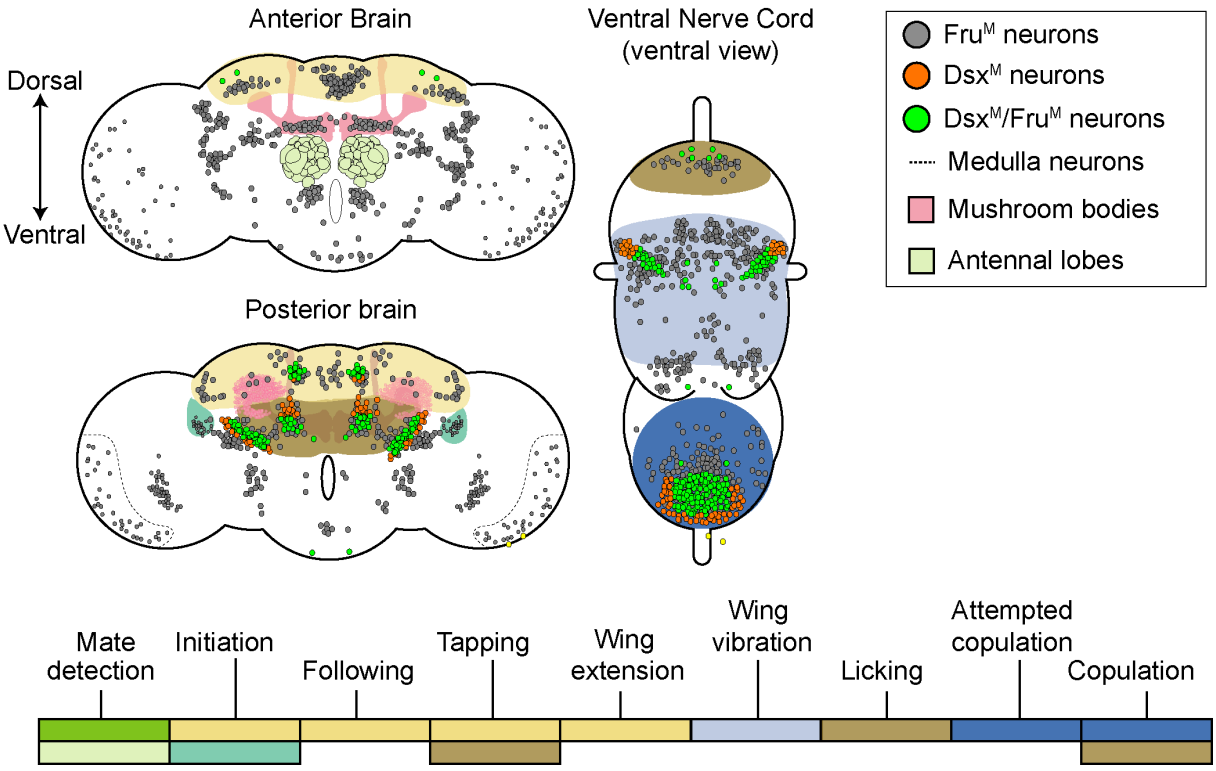


Figure 1-10 Schematic of Fru^M and Dsx^M expression in the adult male CNS, overlapping with neural foci implicated in the modulation of male courtship behavioural outputs.
Areas of the adult male CNS associated with the control of specific courtship steps are colour-coded and refer to the courtship steps indicated below and to the legend on the right. Fru^M neural nuclei of the adult CNS that do *not* co-express Dsx^M are represented by grey dots. Dsx^M neural nuclei of the adult CNS that do *not* co-express Fru^M are represented by orange dots. Male-specific Dsx^M neural nuclei of the adult male CNS that co-express Fru^M are represented by green dots.

1.8.6 Sexual dimorphism in the fly brain

As stated, courtship behaviours are essentially motor outputs that are directed by sexually dimorphic neural circuitries. Therefore it is only by comparing male vs. female circuitry that it is possible to shed light on how differing behavioural outputs may be engendered, via shared circuits that operate differently and/or sex-specific circuits that result from the presence/absence of unique circuit elements.

Previous studies originally described the overall arrangement of the majority of *fru* neural cell bodies, except for a handful of clusters, as sexually isomorphic (Demir and Dickson, 2005; Stockinger et al., 2005; Manoli et al., 2005). One such cluster is the well-characterised GABA-ergic mAL neurons; these have been shown to be dimorphic in both number and projection pattern (Kimura et al., 2005; Koganezawa et al., 2010). In males the mAL cluster consists of ~30 neurons; the projections of which extend both contra- and ipsilaterally in the

SOG, while the equivalent female mAL cluster consists of only ~5 neurons that give rise to a single contralateral projection to the SOG (Kimura et al., 2005). While the male-specific dendritic termini have been shown to overlap with Gr32a axonal termini that project from the foreleg into the SOG, the female-specific dendritic arborisations appear unable to do so (Koganezawa et al., 2010). This feature is behaviourally relevant as inhibition of mAL neurons results in bilateral wing extension during courtship song, in males, suggesting that these neurons serve to inhibit contralateral wing extension via a proposed model of lateral inhibition (Koganezawa et al., 2010).

More recent studies have re-visited this matter, that is sexual dimorphism in *fru* circuitry, exploiting technologies that permit highly accurate neuroanatomical analyses to an unprecedented resolution. By taking advantage of two independent approaches, stochastic MARCM and intersectional strategies employing fru^{FLP} and various GAL4 drivers, *fru* neurons were genetically parsed into distinct subsets, in order to generate a comprehensive digital 3D atlas of all *fru* neurons in males and the corresponding neurons in females (Yu et al., 2001; Cachero et al., 2011). Warping high-resolution tracings of individual neurons onto a common reference brain allowed the identification of neuro-anatomical dimorphisms and, by implication, differences in interconnectivity and likely pathways of neural processing (Cachero et al., 2010; Yu et al., 2010). Direct comparison of male vs. female *fru* neural elements confirmed three distinct modes of sexual dimorphism; i) sex-specific neural clusters; ii) differences in cell numbers within a given cluster; and iii) sex-specific arborisations; all of which may contribute to developing neural architecture capable of eliciting sex-specific behaviour(s) (Billeter and Goodwin, 2004; Manoli et al., 2005; Kimura et al., 2005; Datta et al., 2008; Kimura et al., 2008; Cachero et al., 2010; Mellert et al., 2010; Ruta et al., 2010; Yu et al., 2010; von Philipsborn et al., 2011

Several brain regions, most notably the PI, lateral protocerebral complex (made up of arch, ring and junction), Prg, Mtg and Abg, consist of ~10 clusters of *fru* neurons that are either are male-specific clusters or dimorphic in cell number, in addition to 19 clusters of *fru* neurons that differ in their arborisations between in males than in females (Yu et al., 2010; Cachero et

al., 2010). Volumetric differences between male and female standardised brains were documented, with male and female expanded regions (MERs and FERs) present in areas that are heavily enriched in sexually dimorphic *fru* neural projection density and connectivity (Cachero et al., 2010). Exhaustive neuroanatomical analyses lead to the hypothesis that non-sex-specific neurons that have dimorphic arborisations exist within early sensory processing or terminal motor pattern generation, while sex-specific neurons are postulated to function in sensory integration and motor control (Yu et al., 2010; Cachero et al., 2010). Examples of this include the male-specific P1, and sexually dimorphic aSP1 and aSP2 clusters that are more numerous in cell numbers in males (Kimura et al., 2008; Yu et al., 2010; Cachero et al., 2010). That these clusters are intrinsic to the lateral cerebral complex, a brain region implicated in multimodal sensory integration supports the model implicating sex-specific neurons in sensory integration. That the non sex-specific aSP4 and aSP6 neurons that are also intrinsic to this region, but exhibit both male- and female-specific arborisations supports the model that implicates non-sex-specific neurons that exhibit dimorphic arborisations in early in sensory processing (Yu et al., 2010). Focusing on *fru* circuitry involved in olfaction, the sensory modality with the highest number of dimorphic processes, Cachero et al. (2010) analysed the projection patterns and patterns of connectivity between 2nd order projection neurons and 3rd order lateral horn (LH) neurons. A large proportion of LH neurons, which have input regions in the LH and output regions in other parts of the brain, were found to have dimorphic projections. Further to this, the most dimorphic *fru* clusters in the central brain, pMP-e and aSP-a clusters, were found to innervate the LH in males and not in females; a feature suggestive of sex-specific multimodal sensory integration (Cachero et al., 2010). Overlapping *fru* projection neurons (PNs) and LH neurons revealed sex-specific connectivity between distinct clusters of neurons. For example, aSP-f and aSP-h LH neurons have the potential to form connections with aDT-e and aDT-a PNs only in males, while aSP-g LH neurons can only form synapses with aDT-e, aDT-a and aDT-f PNs in females (Cachero et al., 2010). These data provide evidence for dimorphic anatomical connectivity that may explain sex-specific responses to the same pheromone between males and females. That LH neurons overlap with the descending pIP-1

neuron, which has dendrites widely distributed in MERs, and axons that project to the three thoracic ganglia, suggests its role in relaying sensory information to motor centres in the VNC (Cachero et al., 2010).

Gaining genetic access to *dsx*-expressing cells was only recently accomplished (Rideout et al. 2010; Robinett et al., 2010). As such, exhaustive mapping of *dsx* circuitry has yet to be undertaken. By simply observing the patterns of expression of *dsx* neural nuclei and associated projections, several modes of dimorphism are overtly apparent. First, there exist three distinct clusters, SN, TN1 and TN2, the latter two of which are implicated in wing extension and courtship song, which are present in males only (Lee et al., 2002; Rideout et al., 2007; Rideout et al. 2010; Robinett et al., 2010; von Philipsborn et al., 2011). Second, there are a handful of clusters that consist of differences in cell numbers between males and females; the only cluster of *dsx* neurons that is larger in number in females than in males is in the Abg, while all other clusters in the dorsal brain (pC1, pC2 and pC3) are more numerous in males than in females (Rideout et al. 2010). Lastly, the sole distinct cluster that is non-sex specific is aDN (Rideout et al. 2010). The pattern of expression of projections associated with the male and female neural clusters is similar, except for the overtly attenuated density of projections exhibited in females when compared to males. The most conspicuous feature would be the complete absence of the contralateral projections within the VNC, this being most notable with respect to projections from the foreleg that project to, and through, the Prg that do not form a trans-commissural line in females as compared to males (Possidente and Murphey, 1989; Rideout et al., 2010).

Ultimately, the realisation of these dimorphic features within the *fru* and *dsx* circuitries clearly demonstrates differences in almost all aspects of neural architecture that exist in areas of the CNS associated with the sex-specific behavioural foci. It is only logical that these exhaustive neuroanatomical characterisations serve as a neuroanatomical framework for successive functional studies.

1.9 Assigning function to elements of the courtship circuitry

Given that courtship requires communication between the sexes and therefore that sensory information acting on various sensory modalities must be efficaciously exchanged, it is likely that this sensory information converges within specific brain areas capable of integrating and assigning 'weighting' effects associated with any competing agonistic and antagonistic stimuli. Sex-specific differences at the level of sensory processing are therefore responsible for ultimately relaying the correct information so that the most appropriate behavioural outputs are elicited. Some of the major sensory, integration and output elements within the *fru* and/or *dsx* circuitries have been functionally assigned; these are discussed below.

1.9.1 Relaying sensory information

fru^{GAL4} is expressed in approximately 15% of the olfactory receptor neurons (ORNs) on the third antennal segment that innervate the olfactory trichoid sensilla (Manoli et al., 2005; Stockinger et al., 2005). Blocking synaptic transmission in these ORNs profoundly reduces male courtship, demonstrating their importance in detecting sex-pheromones (Stockinger et al., 2005). The afferent projections of these *fru*^{GAL4} ORNs have been mapped to three sexually dimorphic antennal lobe glomeruli; DA1, VA1lm and VL2a, which appear to overlap with dendrites of second order *fru*^{GAL4} PNs (Figure 1-11; Kondoh et al., 2003; Stockinger et al., 2005). A complete map of higher olfactory centres showed that pheromone-responsive PNs project to distinct compartments of the LH of the protocerebrum, a region thought to be the 'sensory integration/processing centre' (Figure 1-11; Jefferis et al., 2007; Cachero et al., 2010; Yu et al., 2010).

To date our knowledge of the neural circuitry underlying the detection, processing and possible outputs of olfactory pheromones has come exclusively from studies on the male pheromone 11-*cis*-vaccenyl acetate (cVA) (Figure 1-11; Butterworth, 1969; Datta et al., 2008; Ruta et al., 2010. cVA, sensed by Or67d ORNs in both males and females, elicits aggression amongst males (Ha and Smith, 2006; Kurtovic et al., 2007; Wang and Anderson, 2010), inhibits male courtship towards males and females (Ejima et al., 2007; Kurtovic et al., 2007), and promotes receptivity in females. Mapping the cVA-responsive circuit showed that it was

comprised of only four physiologically connected neurons, with the fourth neuron projecting into the ventral nerve cord (VNC) and terminating in the Abg (Figure 1-11; Ruta et al., 2010) While some components within this circuit are male-specific others exhibit male-specific arborisations and/or synaptic connections (Datta et al., 2008; Ruta et al., 2010). Given that dimorphic anatomical connections are particularly enriched in third order olfactory interneurons of the LH (Cachero et al., 2010), these neurons may be the first elements in the olfactory pathway that respond sex-specifically to the same stimulus. In particular, dimorphic connections between DA1 PNs and higher-order olfactory neurons might explain the sex-specific behavioural responses elicited by cVA (Cachero et al., 2010; Ruta et al., 2010), though additional electrophysiology experiments would be essential to determine this.

While the association between pheromones, olfaction and courtship may seem obvious; an intriguing relationship has been identified between food-olfaction and male courtship (Grosjean et al., 2011). Members of a novel family of chemosensory receptors, the ionotropic glutamate receptors (Irs), localize to distinct sensory cilia of the antennae and are expressed in olfactory neurons lacking olfactory receptors (ORs) (Benton et al., 2009). In particular, ORNs that express Ir84a have been shown to co-express fru^{M} and innervate VL2a, one of the three fru^{+} sexually dimorphic glomeruli (Figure 1-11; Grosjean et al., 2011). Although $Ir84a^{+}$ neurons are not tuned to respond to sex-specific odours, two volatile compounds normally found in *Drosophilid* food sources (phenylacetaldehyde and phenylacetic acid) were found to elicit responses in both males and females. Ir84a mutant males court females at diminished levels, while restoring Ir84a function re-establishes normal courtship levels, implicating Ir48a in the regulation of male courtship. Neuroanatomical analyses of second order VL2a PNs revealed distinctive intercalation with pheromonal PNs of fru^{+} DA1 and VA1lm glomeruli, rather than with general food odor pathways (Figure 1-11; Grosjean et al., 2011). PNs from all three sexually dimorphic glomeruli target a specialized pheromone-processing region of the LH, suggesting a point of integration of food and pheromonal pathways within the *fru* courtship circuitry. The reception of such food indicators demonstrates how non sex-specific olfactory stimuli are able to drive a sex-specific behavioural response (Grosjean et al., 2011). This makes logical sense, as sites of food

deposition have been implicated in female egg-deposition choice and the presence of food may in some way serve as a positional cue for the formation of possible *Drosophila* leks (Joseph et al., 2009; Spieth, 1974).

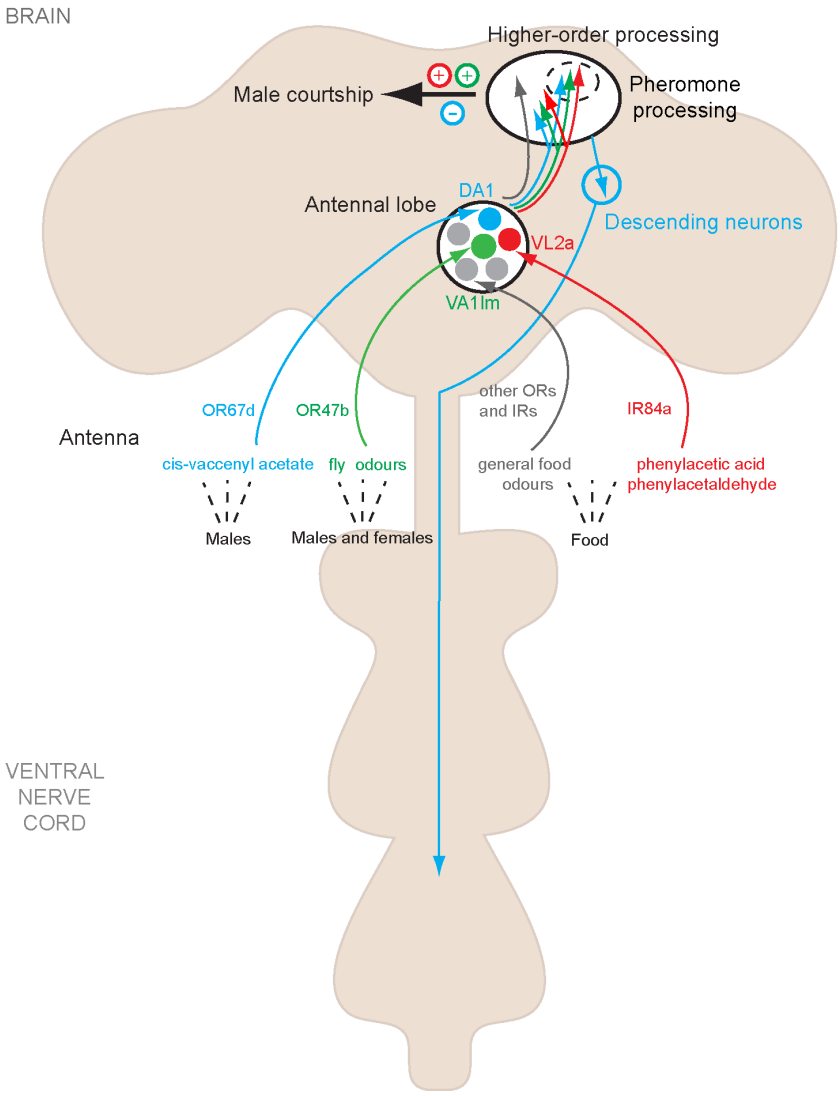


Figure 1-11 Proposed model for the perception and integration of olfactory sensory signals that regulate *Drosophila* male courtship.
Olfactory receptor neurons (ORNs) in the antenna detect odors and send axons to glomeruli of the antennal lobe of the brain. DA1 and VA1 lm glomeruli receive pheromonal information from *Or67d*-expressing neurons (which respond to the male pheromone 11-cis-vaccenyl acetate, cVA) (Datta et al., 2008; Kurtovic et al., 2007) and *Or47b*-expressing neurons (which respond to unidentified female- and male-derived odors) (van der Goes, van Naters and Carlson, 2007; Vosshall et al., 2000, respectively). While Or67d ORNs express *fru,* Or47b ORNs do not. Olfactory information is propagated through projection neurons to higher brain centres, such as the mushroom body and lateral horn. OR67d/DA1 neurons target *fru*-expressing second order neurons in a specific region of the lateral horn associated with pheromone processing. Ultimately these second order neurons form downstream *fru*-expressing connections (via third and fourth order neurons) that terminate in the abdominal ganglia (Ruta et al., 2010; Datta et al., 2008). VL2a glomerulus receives information from *Ir84a*-expressing neurons, which respond to odors derived from host food/oviposition substrates (Grosjean et al., 2011). VL2a projection neurons are segregated from projection neurons responding to general food odour pathways but they are anatomically interconnected with the VA1 lm/DA1 pheromone pathways and target a specific area in the lateral horn involved in pheromone processing (Grosjean et al., 2011). Note that only half of the male CNS is shown in the schematic. (Figure taken from from Pavlou and Goodwin, 2013).

During the 'tapping' and 'licking' stages of courtship males are believed to assess a mate's sex and species via non-volatile pheromones, with the reception of essential information occurring largely via gustatory receptor neurons (GRN) of the foreleg (Figure 1-12; Spieth, 1974). Studies suggest that detection of female-enriched long-chain cuticular hydrocarbons (CHCs) stimulates male-female courtship while the detection of male-enriched CHCs promotes male-male repulsion, preventing inappropriate male-male courtship (Ferveur and Cobb, 2010). To date, only three gustatory receptors (Gr) have been implicated in the reception of pheromones - Gr39a is thought to detect female-enriched CHCs (Watanabe et al., 2011), while Gr32a and Gr33a may serve to detect male-enriched CHCs (Lacaille et al., 2007; Miyamoto and Amrein, 2008; Moon et al., 2009). GRNs expressing each of these Grs do not express *fru*. However, axons of *Gr32a*-expressing GRNs terminate in the SOG and are likely to form connections with second-order *fru*-expressing neurons of the ventrolateral protocerebrum that relay this signal to higher-order centres in the lateral protocerebrum (Figure 1-12; Koganezawa et a., 2010). This implies that sensory neurons that do not express *fru* may be capable of relaying information to fru^{+} downstream 'processing' circuitry.

Members of the degenerin/epithelial sodium channel subunit family *pickpocket-23* (*ppk23*) and *pickpocket-29* (*ppk29*) are expressed in Fru^{M}-positive GRNs of the foreleg tarsi (Lu et al., 2012; Thistle et al., 2012; Toda et al., 2012). There appears to be twice the number of $ppk23^{+}$ neurons in the male foreleg, when compared to the female (Lu et al., 2012; Thistle et al., 2012; Toda et al., 2012), with contralateral projections within the VNC that terminate in the SOG, a sex-specific feature previously attributed to Fru^{M}-expressing gustatory neurons (Possidente and Murphey, 1989; Mellert et al., 2010). Males with silenced $ppk23^{+}$ neurons display reduced levels of courtship towards females and increased levels towards males, while males with silenced $ppk29^{+}$ neurons display defects in courtship towards females only (Lu et al., 2012; Thistle et al., 2012; Toda et al., 2012). Coupling thermogenetics with electrophysiology demonstrated that $ppk23^{+}$ neurons, which are restricted to two cells per bristle, respond to specific female pheromones (Thistle et al., 2012; Toda et al., 2012). G-CaMP imaging of $ppk23^{+}$ neurons in response to pheromonal stimulation showed that the two neurons innervating each bristle perform opposing roles forming two directly competing

populations; one specifically responding to male-enriched pheromones, the second responding to female-enriched pheromones, suggesting a direct role in mediating attractive and aversive cues (Thistle et al., 2012). A third subunit, *pickpocket-25*, is expressed in sexually dimorphic *fru*$^{+}$ tarsal gustatory neurons that also give rise to characteristic sexually dimorphic projections within the VNC (Figure 1-12). Though these neurons appear to be necessary for normal courtship initiation, specific ligands and further neural connections remain unknown (Lin et al., 2005; Starostina et al., 2012).

Parsing the neural basis of female sexual behaviours has only recently come into play with studies primarily focusing on sensory elements that modulate post-mating responses (Figure 1-13; Häsemeyer et al., 2009; Yang et al., 2009). Post-mating responses are triggered primarily by the allohormone pheromone sex peptide (SP), a small peptide synthesized in the male accessory glands that is transferred to the female during insemination (Kubli, 2003). A SP-responsive G protein-coupled receptor for SP-mediated post-mating responses has been identified; females lacking this sex peptide receptor (SPR) remain receptive, exhibiting virgin-like behaviours, post-mating (Yapici et al., 2008). Transfer of male SP during copulation mediates these post-mating responses by SPR activation in sensory neurons that co-express *fru* and a DEG/ENaC ion channel *pickpocket* (*ppk*) in the female reproductive system (Figure 1-13; Häsemeyer et al., 2009; Yang et al., 2009). These sensory neurons are thought to relay sensory information related to mating state via their projections, which terminate in the Abg, and, possibly, the SOG (Figure 1-13).

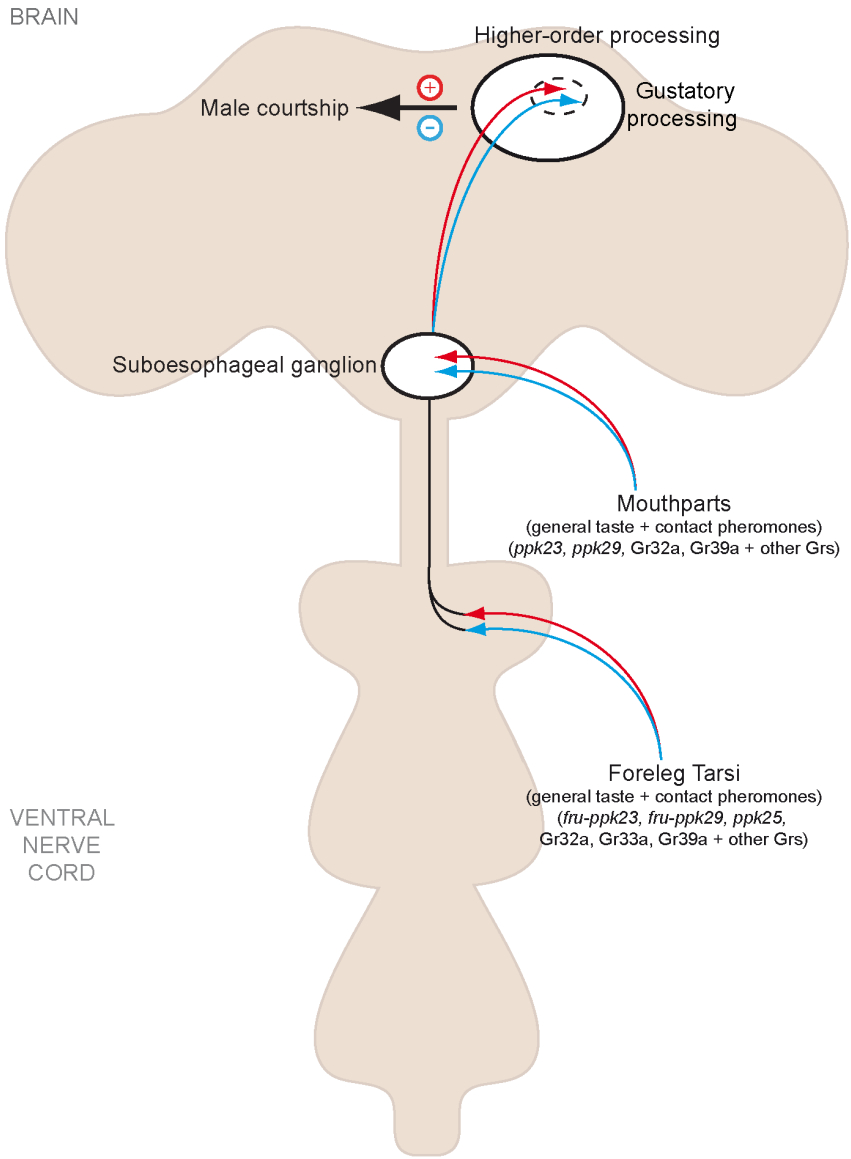


Figure 1-12 Proposed model for the perception and integration of gustatory sensory signals that regulate courtship.
In males, non-volatile pheromones are primarily detected by gustatory receptor neurons (GRNs) of the foreleg tarsi. Gustatory receptors (Gr) Gr32a, Gr33a and Gr39a have been implicated in courtship (Miyamoto and Amrein, 2008; Moon et al., 2009; Watanabe et al., 2011). Gr33a and Gr32a are thought to detect female-specific pheromones (acting as aphrodisiacs) and Gr39a has is thought to detect male-specific pheromones (acting as aversive stimuli) (Miyamoto and Amrein, 2008; Moon et al., 2009; Watanabe et al., 2011). GRNs expressing these Grs do not express *fruitless.* However, projections of *Gr32a*-expressing terminate in the SOG are likely to form connections with *fru*-expressing neurons of the ventrolateral protocerebrum that relay this signal to the higher-order lateral protocerebrum (Koganezawa et al., 2010). Projections of *Gr33a*- and *Gr39a*-expressing GRNs remain unknown. GRNs expressing proprioceptive receptors *pickpocket-23* (ppk23), *ppk29* or *ppk25* co-express *fruitless* and have also been implicated in courtship (Lin et al., 2005; Starostina et al., 2012. Yu et al., 2012; Thistle et al., 2012; Toda et al; 2012). All three send sexually dimorphic projections to the first thoracic ganglia, of which *ppk23*- and *ppk29*-expressing GRNs ascend to terminate in the SOG (Starostina et al., 2012. Yu et al., 2012; Thistle et al., 2012; Toda et al; 2012). Although downstream connections have not been described, studies have shown that gustatory information is relayed from the SOG to a distinct region of the lateral protocerebrum (Kimura et al., 2005; Yu et al., 2012). One population of *ppk23*-expressing GRNs respond to male-specific pheromones (to promote male-male repulsion) (Thistle et al., 2012) while a second population responds to female-specific pheromones (to promote male-female courtship) (Thistle et al., 2012; Toda et al., 2012). Most aforementioned receptors are also expressed in the mouthparts; however, their specific role in these tissues has not been determined. Note that only half of the neural clusters are shown in the schematic. (Figure taken from Pavlou and Goodwin, 2013).

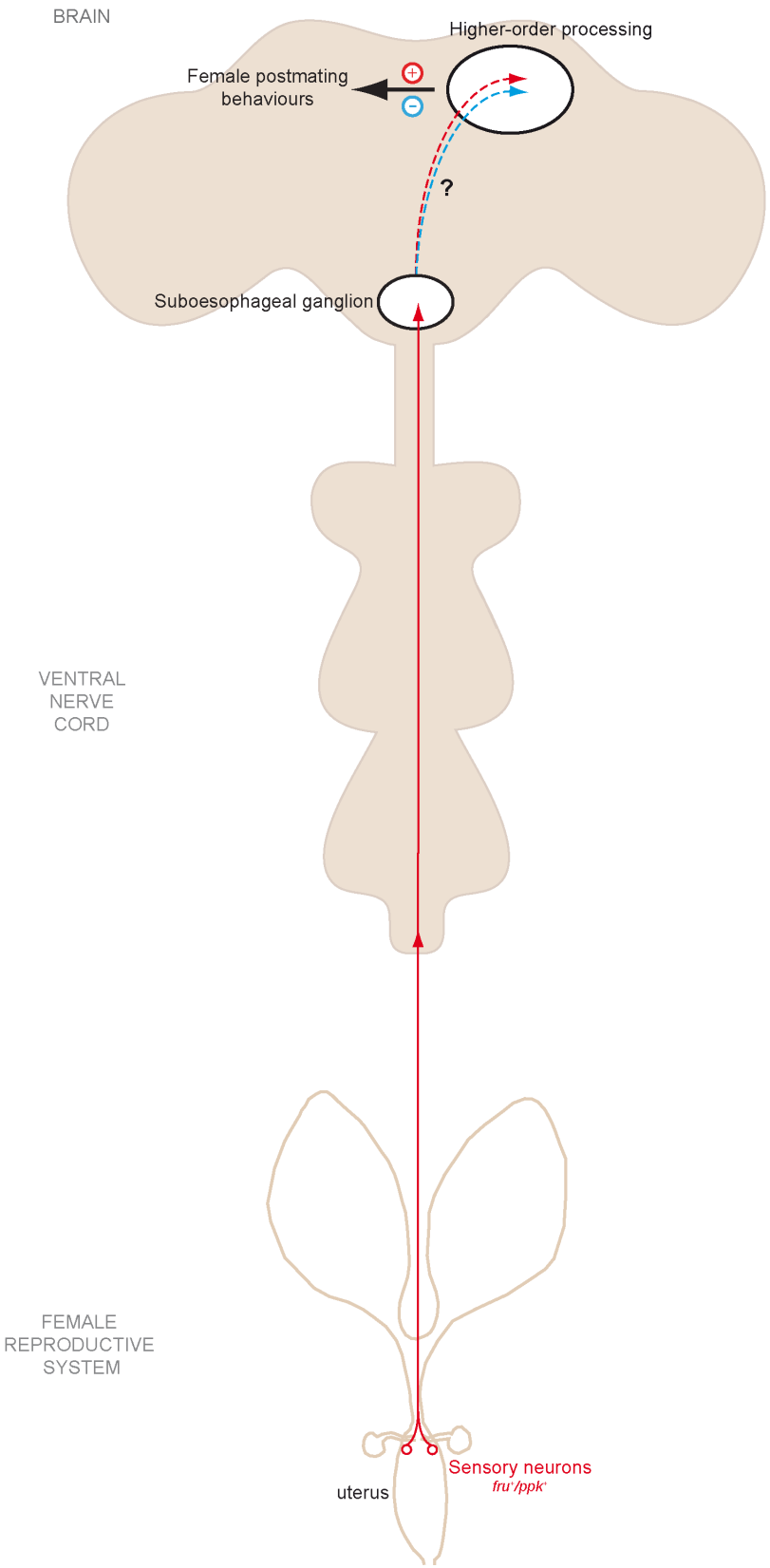


Figure 1-13 Proposed model for the perception and integration of sex peptide (SP) sensory signals that regulate female post-mating responses.
SP-responsive sensory neurons expressing *fru* and *ppk* are localized to the uterus and project into the abdominal ganglia (Abg) and possibly into the suboesophageal ganglion (Hasemayer et al., 2009; Yang et al., 2009). Higher-order central pathways may process these signals (dotted lines) to regulate female behaviour, however, studies have yet to identify these processing/command elements. Note that only half of the female CNS is shown in the schematic. (Figure taken from Pavlou and Goodwin, 2013).

1.9.2 Deciding to court

As stated previously, to generate *bona fide* courtship song requires the expression of Dsx^M and Fru^M in the CNS, in addition to direction from male-specific higher-order 'command' neurons (Rideout et al., 2007; Clyne and Miesenbock, 2008). Continuing with the logic that higher-order command neurons exist that initiate courtship behaviours, Kimura et al. (2008) identified a *fru*- and *dsx*-expressing neural cluster in the dorsal posterior brain, P1, as pivotal for initiation of male courtship. Restrictively thermoactivating the P1 cluster is sufficient to initiate courtship and trigger pulse song, even in the absence of a target female (Kohatsu et al., 2011l von Philipsborn et al., 2011), while silencing P1 neurons in the male brain impairs song and other courtship elements (Figure 1-14; Kimura et al., 2008; Kohatsu et al., 2001; von Philipsborn et al., 2011). Since P1 neurons are male-specific and are located in the lateral protocerebrum (which receives multimodal sensory input), they are ideal candidates to be the 'decision-making' neural element(s) capable of integrating environmental stimuli to make the decision to court. A remarkable experiment demonstrated not only that contact between the male tarsus and a female's abdomen provokes real-time activation of P1 neurons, but also that the presence of cVA can attenuate this response (Kohatsu et al., 2011), demonstrating a role for P1 neurons in integrating gustatory and olfactory information. In line with this, Pan et al. (2012) showed that restricted activation of P1 neurons resulted in heightened levels of following and orientating when exposed to a moving object (Pan et al., 2012). Although visual processing appears independent of the P1 neural pathway, these data support the view that, by integrating multimodal sensory signals, P1 interneurons mediate the decision to initiate courtship, effectively acting as a switch for courtship initiation (Figure 1-14; Kohatsu et al., 2011; von Philipsborn et al., 2011; Pan et al., 2012).

Thermoactivation of fru^+ descending interneurons, P2b and pIP10, is has also been shown to be sufficient to initiate courtship and trigger pulse song, again even in the absence of a target female (Kohatsu et al., 2011; von Philipsborn et al., 2011). However, it has been hypothesized that these serve a downstream 'command' role, relaying information from

integration/higher-processing centres to motor centres in the VNC (Kohatsu et al., 2011; von Philipsborn et al., 2011). Within the VNC, three distinct *fru*$^{+}$ interneuron classes are thought to be components of the CPG, as thermoactivation of these neurons did not lead to faithful recapitulation of pulse song; that is 1) activation of the *fru*$^{+}$/*dsx*$^{+}$ prothoracic, dPR1, neuron elicits courtship song with a significantly longer inter-pulse interval (IPI); 2) the level of activation of the *fru*$^{+}$/*dsx*$^{+}$ mesothoracic neural cluster, vPR6, appears to be indirectly correlated to IPI; and 3) activation of the *fru*$^{+}$ mesothoracic neural cluster, vMS11, induces wing extension without the production of song (Figure 1-14; von Philipsborn et al., 2011). By overlapping axonal and dendritic arborizations, von Philipsborn et al. (2011) described a hypothetical interconnected circuit for courtship song, linking all 5 aforementioned *fru*$^{+}$ neural classes (P1, pIP10, dPR1, vPR6 and vMS11). Yu et al. (2011) were able to neuroanatomically map a single mesothoracic cluster of *fru*-expressing motoneurons, vMS2, which innervates the direct flight muscles, which could be critical for song production (Figure 1-14). However, connections between vMS2 and neurons of the CPG have yet to be confirmed.

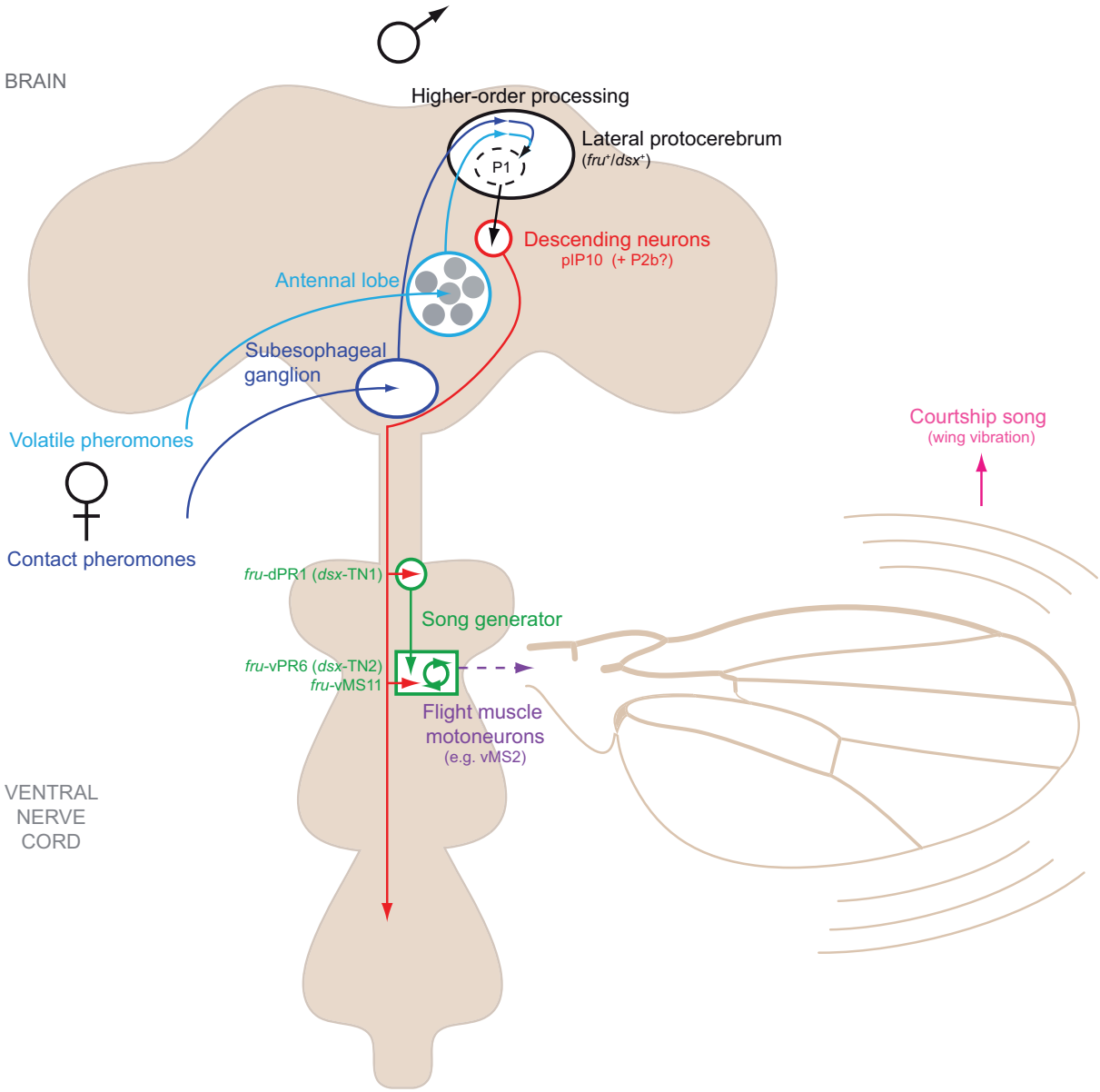


Figure 1-14 Proposed circuitry underlying the initiation of courtship and pulse song in the male CNS.
During courtship, a male unilaterally extends and vibrates a wing to generate a species-specific courtship song. Five distinct *fru*-expressing clusters of neurons that consist of command/decision-making neurons (P1), descending interneurons (pIP10), and components of the central pattern generator (dPR1, vPR6 and vMS11) are thought to form an interconnected circuit (von Philipsborn et al., 2011). Thermoactivation of these neurons triggers unilateral wing extension and/or vibration in isolated males deprived of the sensory inputs that would normally induce males to sing (von Philipsborn et al., 2011). Thermoactivation of P1 and the descending neuron P2b independently initiate male courtship in the presence of a female. Thus P1 and P2b are thought to play a key role in triggering male courtship (Kohatsu et al., 2011). Although the descending cluster, P2b, is connected to P1 neurons its downstream connections within the VNC have yet to be identified. A cluster of flight muscle motoneurons, vMS2, may form connections (dotted line) with the CPG (Yu et al., 2010). Note that only half of the neural clusters is shown in the schematic. (Figure taken from Pavlou and Goodwin, 2013).

1.10 Other somatic correlates of behaviour

An entirely different facet of the sex determination genes is their role in specifying other sexually dimorphic somatic tissues that collectively create an animal that looks and smells like the appropriate sex. Many of these tissues have been shown to rely on the action of *dsx* to combine sexual identity with an initially non-sexually specified and patterned tissue, to create a sexually dimorphic tissue that may either develop or function differently between the sexes (reviewed in Christiansen et al., 2002; Camara et al., 2008). That simultaneous expression of Dsx^M and Dsx^F results in an intersexual phenotype, similar to that of a *dsx* null mutant, suggests that the two isoforms are able to hinder each other's activity (Nagoshi and Baker, 1990). Since the only feature that is different between the two isoforms is the C-terminal domain, this is likely the mode by which their transcriptional regulation differs. By binding to different proteins (cofactors), each isoform (and their respective complex of cofactors) may impart different effects on the same gene and/or result in the targeting of different downstream genes (Camara et al., 2008). One such cofactor is the non-sex-specific gene *intersex* (*ix*), which is an obligate partner of Dsx in females, but not males, and therefore acts to direct differences in transcriptional regulation between the sexes (Waterbury et al., 1999; Garrette-Engele et al., 2002). This is supported by the fact that *ix* mutant females appear intersexual, albeit less overt than *dsx* mutant females, while *ix* mutant males appear largely normal, with the exception of sex comb and genital bristle morphology (Baker and Ridge, 1980; Chase and Baker, 1995; Acharyya and Chatterjee, 2002).

Therefore, although the dimorphic CNS is key to directing courtship behaviours, the importance of gender appropriate physiology is evident by its necessity for the generation of natural sex-specific behaviours (Waterbury et al., 1999; Dauwalder et al., 2002; Fujii and Amrein, 2002; Fujii et al., 2008; Lazareva et al., 2007). This may seem a truism when considering the numerous tissues, outwith the NS that express *dsx*. In the adult fly, these include cells associated with the fat body, oenocytes, external cuticle, alimentary tract, proboscis and mouthparts, and most obviously, the internal and external genitalia (Rideout et al., 2010; Robinett et al., 2010). As most of these tissues differ in function and/or morphology

between the larval and adult stages, spatiotemporal characterisations of *dsx* expression in these tissues, throughout development, is indicative of when *dsx* may act to determine sexual identity. As an example, the fat body and the oenocytes may be used to describe *dsx*-dependent regulation in specific tissues that have associated roles in courtship.

Larval fat body cells differentiate from embryonic mesodermal cells and are involved in the regulation of energy storage and metabolism, as well as being involved in the fly's immune response (Petersen et al., 1999; Aguila et al., 2007; Liu et al., 2009). Despite their similar name the adult fat body cells are derived from larval histoblasts and serve a broader range of metabolic functions including energy and nutrient sensing, steroid hormone signalling, innate immune response, growth and ageing (Camara et al., 2008; Hoshizaki, 2005). Ubiquitous expression of *dsx* throughout the development of both the larval and adult tissues is indicative of continuous transcriptional regulation that serves to maintain its sexual identity (Rideout et al., 2010). The behavioural relevance of such regulation is demonstrated by the fact that specific feminisation of the fat body of sexually mature adults, and not that of larvae, strongly reduces the competence of males to perform courtship; conceivably by disturbing the synthesis of male-specific secreted circulating proteins that influence the function of the CNS (Lazareva et al., 2007). Indeed, one such protein is Takeout, which is secreted into the hemolymph and has been shown to influence courtship levels/behaviour (Lazareva et al., 2007). Screens that have examined downstream targets of *dsx* have identified a number of genes that are expressed in the fat body, some of which have subsequently been shown to be differentially regulated by *dsx* (Arbeitman et al., 2004). The most characterised of these target genes are the yolk protein genes (*yp).* The continuous transcriptional activation and repression of *yp* genes by Dsx^F and Dsx^M respectively, throughout the adult, demonstrates the requirement for continual maintenance of this facet of the female's sex-specific physiology for the assurance of neural and non-neural synchrony (Bownes, 1994).

Adult oenocytes are specialized, peri-cuticular, polyploid cells of ectodermic origin that are located in the abdomen, and are involved in detoxification, lipid metabolism, and cuticular hydrocarbon (CHCs) production (Jallon et al., 1988; Ferveur et al., 1997; Savarit et al., 1999;

Ferveur, 2005; Siwicki et al., 2005; Chertemps et al., 2006; Grillet et al., 2006; Chertemps et al., 2007; Lacaille et al., 2007; Legendre et al., 2008; Billeter et al., 2009). Some of the CHCs produced in the oenocytes function as species- or sex-specific pheromones, capable of modulating behavioural outputs of the progenitor and interacting fly (Ferveur et al., 1997; Savarit et al., 1999; Ferveur, 2005; Siwicki et al., 2005; Grillet et al., 2006; Lacaille et al., 2007; Billeter et al., 2009). Interestingly, the production of sex-specific pheromones is under the direct control of *dsx* (Waterbury et al., 1999). In females, this occurs via the direct activation of the oenocyte- and female-specific pheromone biosynthesis gene *desaturase* (*desat*^{F}) by Dsx^{F}, which results in the production of female pheromones that stimulate male courtship behaviour (Shirangi et al., 2009). Expression of *dsx* in both male and female oenocytes, throughout development and adulthood, reflects the requirement for *dsx* to modulate pheromonal production, presumably through the regulation of additional genes involved in pheromone biosynthesis (Jallon et al., 1988; Ferveur et al., 1997; Savarit et al., 1999; Ferveur, 2005; Siwicki et al., 2005; Chertemps et al., 2006; Grillet et al., 2006; Chertemps et al., 2007; Lacaille et al., 2007; Legendre et al., 2008; Billeter et al., 2009; Shirangi et al., 2009)

Altogether, it is evident that these studies demonstrate the role of somatic tissues as ‘inputs’ into the courtship circuitry that are able to influence behavioural outcomes. Again, this is not limited to the fat body and oenocytes, as the male-specific sex combs of the foreleg, sexually dimorphic abdominal pigmentation and internal and external reproductive systems have also been shown to modulate courtship behavioural outputs (reviewed by Camara et al., 2008).

Fundamentally, the development and maintenance of the complete morphological and behavioural sexual state is dependent on a highly complex network of genetic factors that serve to orchestrate and regulate the entwined workings of somatic and nervous tissues.

1.11 Aims and objectives

I have attempted in this chapter to bring together the decades of work that have served as building blocks underlying, what is now referred to as, the 'courtship connectome'. By focusing on generating a comprehensive map of courtship circuitry, it has been proposed that the integration of neuroanatomical and behavioural data for each class of neurons will allow us to understand circuit organisation as a whole. By generating and testing hypotheses about how information may flow through the system from sensory input, through the brain, to motor outputs, the workings of the miniscule fly brain may soon come to light.

Much of the work that has contributed to understanding of courtship circuitry has come from comprehensive neuroanatomical and functional interrogations of *fru* circuitry, while the contiguous *dsx* circuitry has yet to be pursued. The fact that *dsx* is expressed in numerous somatic tissues, in addition to the NS in both sexes, confounds the ability to ensure that any behavioural consequences of genetic manipulations are a true indication of the underlying neural operations, and not of somatic modifications/ malformations.

In order to overcome this limitation, the primary purpose of the investigations which form the basis of this thesis was to generate a novel intersectional tool capable of solely and restrictively targeting *dsx*-expressing neurons. With the objective of paralleling *fru* functional mapping efforts, I spatially targeted distinct clusters of *dsx* neurons, in order to map and manipulate specific *dsx* neural circuitry underlying different aspects of male and female sexual behaviours; establishing causative relationships between distinct clusters of *dsx*-expressing neurons and behaviour.

More specifically, these investigations included:

1) Targeting QF and GAL4-DBD (separately) into the *dsx* locus by homologous recombination, of which I was able to generate a novel *dsx* allele ($dsx^{GAL4\text{-}DBD}$ split-GAL4) that can be exploited in combination with the previously published pan-neural hemidriver, $elav^{VP16\text{-}AD}$ (Luan et al., 2006).
2) Neuroanatomical and behavioural characterision (via silencing experiments) of the new allele, demonstrating its ability to restrict genetic access solely to *dsx*-expressing neurons.

3) Successful utilisation of this allele to parse *dsx* neural circuitry into functional component parts. This entailed performing a behavioural screen in which a thermal activation strategy was employed for the elicitation of sub-behaviours of courtship, which were scored for following activation of differential intersecting neurons using a collection of enhancer trap hemi-driver lines (Luan et al., 2006; M. Landgraf, unpublished).
4) Neuroanatomical and behavioural characterision (via silencing experiments) of candidate lines that revealed restricted expression in distinct clusters of *dsx*-expressing neurons. This neuroanatomical mapping was then correlated with behavioural results.
5) Finally (and ideally), to derive from these investigations the logic for how these neurons function to generate sex-specific behavioural outputs and contribute to the current body of knowledge on courtship circuitry architechture and organisation.

2 Materials and Methods

2.1 Drosophila

2.1.1 Drosophila melanogaster stocks

A description of all the *Drosophila* stocks used in this work can be found in Table 2-1. A full description of all mutations and balancer chromosomes used can be found in FlyBase (http://www.flybase.org).

Table 2-1 Drosophila stocks used in this study.
"w*" or "y*" indicates that the precise allele for w or y is unknown.

Strain/Genotype	Description	Reference
Isogenised Strains		
Canton-Special (Canton-S; CS)	Isogenic wild-type strain.	Flybase.
white^{honey} (*w*^{h})	*w* mutant allele isogenised to CS.	Flybase.
w^{1118}	*w* mutant used for microinjections	Flybase.
Balancer Chromosome Strains		
w^{h};*ap*^{Xa}/*CyO*;+	Strain isogenised to CS. Second chromosome balancer Curly of Oster(*CyO*) and dominant marker (*ap*^{Xa}).	Flybase.
TM3,Sb,Ser/TM6B,Tb,Hu,e	Strain isogenised to CS. Third Multiple series of chromosome balancers (*TM*). *TM*3 with dominant markers (*Sb* and *Ser)* and *TM*6B with dominant markers (*Tb, Hu,* and *e)*.	Flybase.
Homologous Recombination Stocks		
y,w*,ey*-FLP	*P*-element insertion of Flippase recombinase (FLP) under the control of the *eyeless* gene promoter (*ey)* on the X chromosome, used during the first stage of gene targeting by homologous recombination.	B.Dickson (unpub.).
y,w*;ey*-FLP	*P P*-element insertion of Flippase recombinase (FLP) under the control of the *eyeless* gene promoter (*ey)* on the 2nd chromosome, used during the first stage of gene targeting by homologous recombination.	B.Dickson (unpub.).

y,w*,ey*-FLP;*Pin/CyO*	*P*-element insertion of Flippase recombinase (FLP) under the control of the *eyeless* gene promoter (*ey)* on the X chromosome, in a second chromosome balancer background; used during the first stage of gene targeting by homologous recombination.	B.Dickson (unpub.).
y,w*,ey*-FLP;+;*Ly/TM3,Sb*	*P*-element insertion of Flippase recombinase (FLP) under the control of the *eyeless* gene promoter (*ey)* on the X chromosome, in a third chromosome balancer background; used during the first stage of gene targeting by homologous recombination.	B.Dickson (unpub.).
y,w*,Sco,hs*-I-*Sce*I,*hs*-FLP/*Y,hs-hid*	*P*-element insertions of heat shock (*hs*) I-*Sce*I restriction enzyme (I-*Sce*I) and heat shock Flippase recombinase (*hs*-FLP) on the X chromosome and heat shock *head involuted defective gene (hs*-hid) on the Y chromosomes; used during first stage of gene targeting by homologous recombination to excise the donor *P*-element from genome and create a double-strand break in the extra-chromosomal DNA prior to integration at the desired locus.	B.Dickson (unpub.).

GAL4, Split-GAL4, LexA, and FLP drivers

+;+;*dsx*^{GAL4}/*TM3*,*Sb*,*Ser, e*	GAL4 element inserted into *doublesex* (*dsx*) locus via ends-in HR.	Rideout et al., 2010.
+;+;*dsx*^{GAL4}/*TM6b*,*Tb*,*Hu*,*e*	GAL4 element inserted into *dsx* locus via ends-in HR.	Rideout et al., 2010.
+;+;*dsx*^{GAL4},*P{w*$^{+mc}$*= UAS-mCD8::GFP.L}*LL6/*TM3*,*Sb*,*Ser*	GAL4 element inserted into *dsx* locus, recombined with the GAL4 responsive UAS transgene expressing a fusion protein between mouse lymphocyte marker CD8 and Green Fluorescent Protein (mCD8::GFP).	Rideout et al., 2010.
+;+;*dsx*$^{GAL4\text{-}DBD}$/*TM3*,*Sb*,*Ser*	GAL4 DNA binding domain (DBD) element inserted into *doublesex* (*dsx*) locus via ends-in HR.	Pavlou and Goodwin (unpubl.).
+;+;*dsx*$^{GAL4\text{-}DBD}$/*TM6b*,*Tb*,*Hu*,*e*	GAL4 DNA binding domain (DBD) element inserted into *dsx* locus via ends-in HR.	Pavlou and Goodwin (unpubl.).
+;*P{w[+mc]=UAS-pStingerII}/ Cyo*;*dsx*$^{GAL4\text{-}DBD}$/*TM3*,*Sb*,*Ser*	GAL4-DBD element inserted into *dsx* locus, in conjuction with the GAL4 responsive UAS transgene expressing a stable insulated nuclear enhanced GFP (nGFP).	Pavlou and Goodwin (unpubl.).

+;*P{w[+mc]= UAS-mCD8::GFP.L}LL6*/*Cyo*;*dsx*$^{GAL4-DBD}$/*TM3*,*Sb*,*Ser*	GAL4-DBD element inserted into *dsx* locus, in conjuction with the GAL4 responsive UAS transgene expressing a fusion protein between mouse lymphocyte marker CD8 and GFP (mCD8::GFP).	Pavlou and Goodwin (unpubl.).
*w**;*P{w[+mC]=UAS-2xEGFP}AH2*/*Cyo*;*dsx*$^{GAL4-DBD}$/*TM3*,*Sb*,*Ser*	GAL4-DBD element inserted into *dsx* locus, in conjuction with the GAL4 responsive UAS transgene expressing a dicistronic insulated cytoplasmic enhanced GF (2xEGFP).	Pavlou and Goodwin (unpubl.).
w^{+};*P{w[+mC]=UAS-TeTxLC.tnt} G2*/*Cyo*;*dsx*$^{GAL4-DBD}$/*TM3*,*Sb*,*Ser*	GAL4-DBD element inserted into *dsx* locus, in conjuction with GAL4 responsive UAS transgene expressing tetanus neurotoxin light chain (*tnt*).	Pavlou and Goodwin (unpubl.).
*w**;+;*P{w[+mC]=elav-VP16.AD}G3A1*	VP16 transcription activation domain-leucine zipper fusion protein under the control of the *embryonic lethal abnormal vision* gene (*elav*) promoter, on the 3rd chromosome.	Luan et al., 2006.
*w**;*P{w[+mC]=elav-VP16.AD}G3A1*	VP16 transcription activation domain-leucine zipper fusion protein under the control of the *embryonic lethal abnormal vision* gene (*elav*) promoter, on the 2nd chromosome.	Pavlou and Goodwin (unpubl.); Luan et al., 2006.
*w**;*P{w[+mC]=UAS-2xEGFP}AH2*;*P{w[+mC]=elav-VP16.AD}G3A1*	VP16 transcription activation domain-leucine zipper fusion protein under the control of the *embryonic lethal abnormal vision* gene (*elav*) promoter, in conjunction with the GAL4 responsive UAS transgene expressing a insulated cytoplasmic enhanced GF (EGFP).	Luan et al., 2006.
w^{+};*P{w[+mC]=UAS-TeTxLC.tnt}G2*/*Cyo*;*P{w[+mC]=elav-VP16.AD}G3A1*/*TM3,Sb,Ser*	VP16 transcription activation domain-leucine zipper fusion protein under the control of the *embryonic lethal abnormal vision* gene (*elav*) promoter, in conjuction with GAL4 responsive UAS transgene expressing tetanus neurotoxin light chain.	Pavlou and Goodwin (unpubl.).
P{w[+mC]=ET.VP16.AD}N9	VP16 transcription activation domain-leucine zipper fusion protein under the control of a minimal promoter for use in enhancer trap screens on either the X, 2nd or 3rd chromosome.	Luan et al., 2006; Landgraf (unpubl.).
P{y^{+}*, dVP16ADvGlut*^{OK371}*}*	VP16 transcription activation domain-leucine zipper fusion protein under the control of *vGlut* gene enhancer. Line generated by transposon swap exchanging GAL4 coding sequence to VP16-AD.	Gao et al., 2008.

fru^{GAL4}/TM3,Sb,Ser	GAL4 knock-in at the *fru* locus by homologous recombination. Drives expression in all *fruitless*-expressing (*fru*) neurons. Homozygous courtship behaviour defective, partially fertile.	Stockinger et al., 2005.
*y*w*;UAS-pStingerII,lexAop-FRT-tdTomato::Nls;fru$^{PI.LexA}$*	*fru^{PI}* driven nuclear Tomato via LexA/LexAop binary system in conjunction with the UAS transgene expressing a stable insulated nuclear enhanced GFP (nGFP).	Mellert et al., 2010.
fru^{FLP}/TM3,Sb,Ser	FLP recombinase knock-in at the *fru* locus by homologous recombination. Drives expression in *fru* neurons.	Yu et al., 2010.
P{w[+mC]=ET.FLP}	FLP recombinase under the control of a minimal promoter for enhancer trap screens on either the X, 2nd or 3rd chromosome.	Rezaval et al., 2012.
w;P{w[+mC]=ppk-GAL4}*	GAL4 element under the control of the *pickpocket* (*ppk*) promoter.	Grueber et al. 2003; Yang et al., 2009.
w;P{w[+mC]=Cha-GAL4.7.4}19B*	GAL4 element under the control of a 7.4 kb 5' flanking regulatory sequence from the *choline acetyltransferase* (*Cha*) gene locus.	Salvaterra and Kitamoto, 2001.
w;P{w[+mC]=Tdc2-GAL4.C}2*	GAL4 element under the control of the 5' flanking regulatory sequence of the *tyrosine decarboxylase 2* enzyme (*Tdc2*) gene locus.	Cole et al., 2005.
w;;P{w[+mC]=Trh-GAL4}*	GAL4 element under the control of the long upstream regulatory sequence of the *tryptophan hydroxylase* (*Trh*) enzyme gene locus.	Alekseyenko et al., 2010.
w;;P{w[+mC]=Th-GAL4}*	GAL4 element inserted between the regulatory sequences from the *tyrosine hydroxylase* (*Th*) enzyme gene 5' flanking and downstream coding sequences.	Friggi-Grelin et al., 2003.
w^{1118};P{w[+mW.hs]=GawB}VGlut [OK371]	GAL4 enhancer trap element that is inserted in the proximity of promoter of the Drosophila *vesicular glutamate transporter* (*DVGLUT*) gene locus.	Mahr and Aberle, 2006.
*y*w*;P{w+;GAD1-GAL4}II*	GAL4 element under the control of a 3.1 kb 5' upstream regulatory sequence of the *glutamic acid decarboxylase* (*GAD1*) enzyme gene locus.	Ng et al., 2002.
gat1-GAL4	GAL4 element under the control of the *vesicular GABA transporter* (*gat1*) gene promoter.	J. Simpson, (Janelia Farm VA, USA).

UAS Reporter/Effector Strains		
w^{1118}; P{w[+mC]=UAS-StingerII}	GAL4 responsive UAS transgene expressing a stable insulated nuclear enhanced GFP (nGFP).	Barolo et al., 2000.
*y^{1},w^{*};P{ w[+mC]=UAS-mCD8::GFP.L}*LL5	GAL4 responsive UAS transgene expressing a fusion protein between mouse lymphocyte marker CD8 and the Green Fluorescent Protein (mcD8::GFP). Labels cell membranes, highly concentrated in neuronal processes.	Lee and Luo, 1999.
w;P{w[+mC]=UAS-2xEGFP}AH2*	GAL4 responsive UAS transgene expressing an a dicistronic insulated cytoplasmic enhanced Green Fluorescent Protein (EGFP).	Halfon et al., 2002.
w^{1118};P{w[+mC]=UAS-RedStinger}4/CyO	GAL4 responsive UAS transgene expressing a nuclear dsRed Flourescent Protein (RFP).	Flybase.
UAS-*synaptotagmin*–HA	GAL4 responsive UAS transgene expressing a pre-synaptic marker recombined with Human influenza hemagglutinin (HA) tag.	Kimura et al., 2005.
w;P{w[+mC]=UAS-TeTxLC.tnt}G2* (*aka UAS-TNT_G*)	GAL4 responsive UAS transgene expressing tetanus neurotoxin light chain.	Sweeney et al., 1995.
w;P{w[+mC]=UAS>stop>nLacZ}*	GAL4 responsive UAS transgene expressing the transcriptional stop cassette flanked by the FLP recombinase target sites *(>stop>),* upstream of the nuclear- localised *beta-galactosidase* (*nLacZ*) reporter gene.	Yu et al., 2010.
w;P{w[+mC]=UAS>stop>mCD8::GFP}*	GAL4 responsive UAS transgene expressing the transcriptional stop cassette flanked by the FLP recombinase target sites *(>stop>),* upstream of the membrane bound mcD8::GFP fusion protein.	Yu et al., 2010.
w;P{w[+mC]=UAS>stop>nSyb::GFP}*	GAL4 responsive UAS transgene expressing the transcriptional stop cassette flanked by the FLP recombinase target sites *(>stop>),* upstream of the fusion protein between synapse specific protein, synaptobrevin, and the Green Fluorescent Protein (*nSyb*::GFP).	Yu et al., 2010.

w;P{w[+mC]=UAS>stop>TNT}*	GAL4 responsive UAS transgene expressing the transcriptional stop cassette flanked by the FLP recombinase target sites (>*stop*>), upstream of the tetanus neurotoxin light chain.	Yu et al., 2010.
w;P{w[+mC]=UAS>stop>dTrpA1}*	GAL4 responsive UAS transgene expressing the transcriptional stop cassette flanked by the FLP recombinase target sites (>stop>), upstream of the Transient receptor potential A1 ion channel protein (*TrpA1*).	von Philipsborn et al., 2011.
w;P{w[+mC]=UAS>stop>dTrpA1^{mcherry}}*	GAL4 responsive UAS transgene expressing the transcriptional stop cassette flanked by the FLP recombinase target sites (>stop>), upstream of the membrane bound RFP (mCherry) tagged Transient receptor potential A1 ion channel protein (*TrpA1*).	von Philipsborn et al., 2011.
P{w[+mC]=UAS-SPR-IR}1	GAL4 responsive UAS-driven inverted repeat of a short fragment of the sex peptide receptor (SPR).	Dietzl et al.,2007.
P{w[+mC]=UAS-mSP};;P{w[+mC]=UAS-mSP}	GAL4 responsive UAS transgene expressing the membrane-bound, non-diffusible form of Sex peptide (*mSP*; achieved by N-terminal fusion of SP to human c-glutamyl trans-peptidase type II membrane protein).	Nakayama et al., 1997.
Sex Determination Mutants		
Dp(1;Y)B^{S}Y;+;Df(3R)dsx15/TM6B,Tb,Hu,e	Deletion covering the doublesex (dsx) locus, from cytogenetic location 84D11-84E8. haplo-X vs. diplo-X progeny identified by Bar-marked Y chromosome.	Baker et al., 1991; Taylor et al., 1994; Ring and Martinez Arias 1993.
In(3R)dsx^{23},dsx^{23},Ubx^{bx-1},sr^{1},e^{s}/TM3,Sb^{1}	Revertant, (no. R3), of the dominant mutation of *dsx* (*dsx*^{D}) which has lesions 3' to the acceptor site in the female exon, via insertion of repetitive elements, that does not disrupt the intron or the acceptor site. *dsx*^{23} is synonymous to *dsx*$^{D+R3}$. Homozygous intersexual in appearance.	Duncan and Kaufman, 1975; Baker et al., 1991.
Gal80 and Miscellaneous Strains		
w^{-};tsh-Gal80/Cyo	GAL80 repressor of GAL4 driven by the *teashirt* (*tsh*) promoter.	Clyne, and Miesenböck, 2008
w^{-};;elav-Gal80	GAL80 repressor of GAL4 driven by the *embryonic lethal abnormal vision* gene (*elav*) promoter.	Rideout et al., 2010.

w⁻;nsyb-Gal80/Cyo	GAL80 repressor of GAL4 driven by the *synaptobrevin* (*syb*) promoter that carries a nuclear localisation sequence (*n*).	J. Simpson, (Janelia Farm VA, USA).
w⁻;ppk-Gal80	GAL80 repressor of GAL4 driven by the *pickpocket* (*ppk*) promoter.	Yang et al., 2009.
w⁻;Cha-Gal80	GAL80 repressor of GAL4 driven by the *acetyl-choline transferase* (*Cha*) promoter.	Kitamoto, 2002.
ppk::eGFP	*pickpocket* (*ppk*) promoter fusion expressing enhanced GFP.	Grueber et al. 2003; Yang et al., 2009.
Df(1)Exel6234 *(a.k.a Df(1)SPR)*	Deficiency removing 88 kb from the X-chromosomal region including Sex peptide receptor and four other annotated genes.	Yapici et al., 2008.

Fly strains were raised as per Billeter and Goodwin (2004), unless stated otherwise. All transgenes are in a w^+ background for behavioural studies.

2.1.2 Wild-type strain

Unless otherwise stated the wild-type strain used in this study was Canton-Special (Canton-S; CS).

2.1.3 Sex determination mutant genotypes

Null mutations in the *doublesex* (*dsx*) gene were obtained using heterozygous combinations of either $dsx^1/Df(3R)dsx^{15}$ or $In(3R)dsx^{23}/Df(3R)dsx^{15}$ (as per Villella and Hall, 1996).

2.1.4 Fly husbandry

Drosophila stocks were raised on 'Oxford' *Drosophila* medium. Stocks were maintained at room temperature in the laboratory (~22ºC). Unless otherwise stated for genetic crosses and experiments, the flies were mated and their progeny raised in either an incubator or a designated fly room at 25°C at 45% humidity in 12:12 hr light-dark cycles. TNT crosses were performed at 21°C, while RNAi crosses were performed at 29°C.

Oxford Medium: 70 g malt, 20 g maize meal, 7.69 g agar, 4 g dried yeast, 2.3 g soy flour, 20 ml molasses, 5 ml of 94 % propionic acid and 6 % orthophosphoric acid, 30 ml of Nipagin M

(4-hydroxybenzoic acid methylester, 10% (w/v) in absolute ethanol), per litre of distilled water.

2.1.5 Drosophila microinjection

2.1.5.1 DNA preparation

Plasmids for microinjection were purified from *E. coli* DH5α using the Plasmid Maxi Kit (QIAGEN), following the standard manufacturer protocol. Approximately 30-50 µg of plasmid was sent for microinjection.

2.1.5.2 Microinjection

Drosophila embryos of genotype w^{1118} were microinjected with a DNA solution that contains the *P*-element transformation vector containing the transgene of interest, together with the helper plasmid pUCHSπΔ2-3 to provide a source of transposase, using standard microinjection procedures performed by Genetic Services Inc. (Cambridge, MA).

2.1.5.3 Selecting *P*-element transformants

Larvae were returned by post approximately 48 hr after injection. They were allowed to develop into adults in a food vial at 25°C. Single adults were collected after eclosion and mated with w^{1118} flies of the opposite sex. The progeny of these crosses were screened for the presence of orange eyes, indicating *P*-element integration. The *P*-elements used in this study all bear the *mini-white (mw)* gene, which confers varying degrees of eye colour to flies when in a w^{1118} genetic background.

2.1.5.4 Determining chromosomal insertion

P-element lines were crossed to different balancer chromosomes with dominant genetic markers to determine the chromosome of insertion. Since all the *P*-elements used in this work contain the *mini-white* gene as a marker, all genetic crosses were carried out using flies with balancer chromosomes in a w^- background. The *P*-elements were followed using the eye colour conferred by the presence of the *mw* transgene.

To determine whether an insertion occurred on the second chromosome, flies heterozygous for the presence of the *P*-element were crossed to $w^h;ap^{Xa}/CyO$. The $w^h;+/CyO$ progeny with

orange eyes were then backcrossed to *w^h;ap^Xa/CyO*. Insertion on the second chromosome was determined by the absence of *w^h;ap^Xa/CyO* progeny with orange eyes (Figure 2-1).

Similarly, insertions on the third chromosome were determined by crossing the *P*-element line to *w^1118;+;TM3,Sb,Ser/TM6B,Tb,Hu,e* and by following the same logic as for the second chromosome.

For insertion on the first chromosome (X), males carrying the *P*-element insertion were crossed to *w^118* females. Integration on the first chromosome was determined by the absence of male progeny with orange eyes (inherited *mini-white* marker). After excluding insertions on the first, second and third chromosome, the insertion was determined to have occurred on the fourth chromosome (Figure 2-1. No insertions are usually found on the Y chromosome.

Once the chromosome bearing the *P*-element was determined, the insert was balanced with the appropriate chromosomal balancer. Homozygous viable lines were kept both as homozygous stocks and as heterozygotes with an appropriate balancer chromosome. Lethal insertion lines were only kept as heterozygotes with the appropriate balancer chromosome.

2.1.5.5 Outcrossing of transgenic strains into an isogenised wild-type background

All generated transgenic strains were outcrossed to isogenise their genetic background with that of a *Canton-S* wild type strain. White-eyed virgin females of the *Canton-S* (*w^h*) strain were collected and crossed to red-eyed males of the line of interest. The *mini-white* marker was used to follow the transgene throughout the outcrossing procedure. At the F1 stage, one orange-eyed virgin female was crossed to three *Canton-S* (*w^h*) males. At the F2 stage, one orange-eyed virgin female was crossed again to Canton-S (*w^h*) males. This process was repeated for at least five generations. After outcrossing, a single virgin female was collected and crossed to three sibling males, and the homozygous progeny from this cross were used to generate the final outcrossed stock.

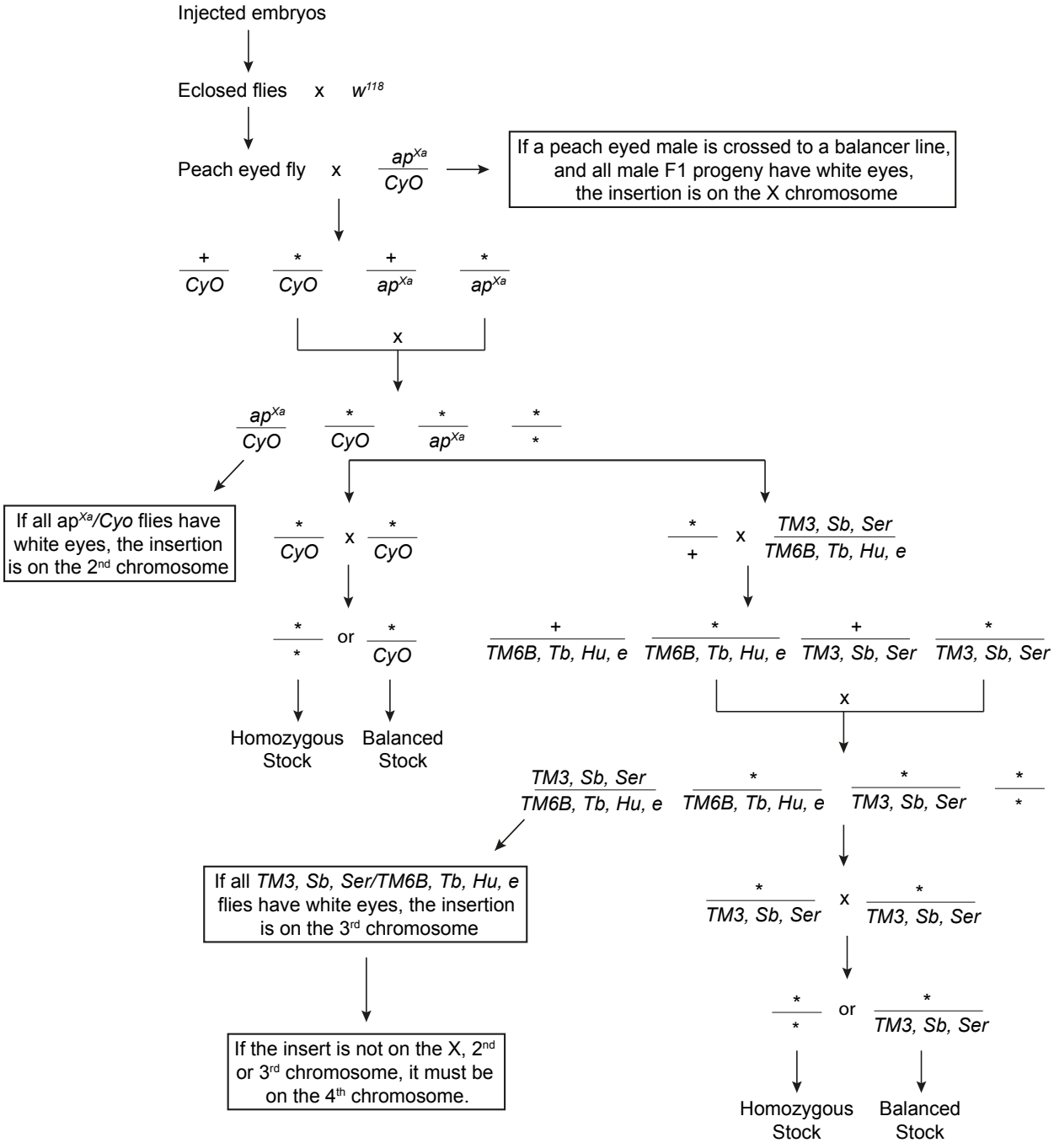


Figure 2-1 Crossing scheme for balancing an integrant.
The series of crosses identifies the chromosomal location of an insert within the genome. Once the location is established, homozygous and/or heterozygous stocks are established and maintained.

2.1.6 Dissection techniques

2.1.6.1 Whole-mount dissection of adult CNS and/or other somatic tissues

Unless otherwise stated for adult dissections flies were aged for 5 days prior to dissecting, except in the case of pharate adults. After light CO_2-anaesthesia, flies were immersed in ethanol for 5 sec. They were then transferred into 300µl phosphate-buffered saline (PBS;

137 mM NaCl, 2.7 mM KCl, 10 mM Na_2HPO_4, 2 mM KH_2PO_4) on a blacked-out concave dissecting slide. Their wings and legs were removed using No. 5 Biology Grade dissection forceps (Dumont). The brain was exposed by first removing the proboscis, and then by tearing the head capsule in half by pulling at the lower corner of each eye. The brain was left attached to the rest of the body by the cervical connection. The abdomen was then severed using dissection scissors. The forceps were used to cut the thoracic cuticle transversely at the midline from posterior/caudal to anterior/cephalic severing the cuticle surrounding the cervical connection. The dorsal cuticle with attached muscles and then oesophagus would be lifted away to reveal the dorsal surface of the ventral nerve cord (VNC). The VNC, with Brain attached, would then be gently lifted from the thorax. Finally the whole isolated CNS would be transferred using a siliconised Pasteur pipette to a dish for fixation and incubations.

In the case of dissections requiring the abdominal nerve trunk (AbNvTk) to remain attached to the internal genitalia the dissection is as above, except the abdomen would be left attached and the abdominal and thoracic cuticle would be severed at the midline from the anal plates up to the cervical connection. The dorsal cuticular structure then would be lifted away and the internal genitalia lifted out ensuring the AbNvTk remained attached to both the genitalia and VNC. The final stages of the dissection would then proceed as normal.

Somatic tissues such as the internal genitalia, guts, proboscis, appendages etc. are removed as required and treated as per the protocol described above. For cuticular preps the cuticles were excised using dissecting forceps and, if required, muscle and fat body scraped away to present the cuticle alone.

2.1.6.2 Whole-mount pupal CNS

Wandering 3rd instar (L3) larvae make their way out of the food and up the side of the vial. These would be collected and sexed by the size of their gonads (Ashburner, 1989). Sexed L3 larvae would be transferred onto 3M Whatman paper in a 50 mm Petri dish humidified with an underlying tissue moistened with water. These larvae would then evert their spiracles and stop moving, developing into white pre-pupae (Bainbridge and Bownes, 1981). The pupae would then be aged at 25°C for a fixed time period. Pupae at the desired stage would

be transferred to 300 µl PBS on a blacked-out concave dissecting slide for dissection. The operculum would first be removed using forceps. The rest of the pupal case would then get gently peeled off to reveal the pupa. A slit would be made with forceps along the dorsal part of the abdomen, extending to just below the top of the brain. A Gilson P20 micropipette fitted with a yellow tip would then be used to jet 20 µl of PBS in and out of this opening, which clears the inside of the thorax and allows visualization of the pupal CNS. The CNS would be dislodged from surrounding connective tissues with continued gentle jetting of PBS until the whole CNS could be lifted from the capsule using the forceps. The whole isolated CNS would then be transferred using a siliconised Pasteur pipette to a dish for fixation and incubations.

2.1.6.3 Whole-mount larval CNS and/or other somatic tissues

L3 larvae were gently selected with forceps and transferred to PBS. Larvae were sexed according to the size of their gonads (Ashburner, 1989). No. 5 dissecting forceps were used to tear a small opening in the caudal end of the larvae. The mouthparts were then firmly taken hold of by one set of forceps and, using the other forceps, the cuticle was slid along effectively inverting the larvae while leaving the internal tissues intact and *in situ*. The desired tissues (CNS, imaginal disc, gonads, fat body etc.) could then be removed for processing.

2.1.6.4 Embryo collection

Approximately 100 *Drosophila* adult females and 50 *Drosophila* adult males were pooled in an inverted plastic beaker and allowed to lay eggs on a plastic Petri dish containing grape juice agar medium with a dab of yeast paste (dried yeast dissolved in distilled water, which is subsequently heat inactivated) covering the open bottom of the beaker. *Drosophila* adult females were allowed to lay eggs on the grape juice agar plates for approximately 12 – 16 hr at 25°C. The plate was removed the following morning for collection; embryos were detached from the egg laying plate using a paintbrush and a stream of distilled water, and collected in a fine-mesh sieve.

Grape Juice Agar: 20 g agar, 26 g sucrose, 52 g glucose, 7 g dried yeast, and 9% (v/v) preservative free grape juice per litre of distilled water.

For this media, distilled water was heated to boiling to dissolve the agar. The remaining reagents were then added and allowed to dissolve. The media was allowed to cool to 60°C before being supplemented with Nipagin M (4-hydroxybenzoic acid methylester, 10% (w/v) in absolute ethanol) to inhibit fungal growth.

2.2 Visualisation techniques

2.2.1 Immunofluorescence

2.2.1.1 Incubations for larval, pupal and adult tissues.

All samples dissected and treated as per Lee et al. (2000) and Billeter and Goodwin (2004). Samples were dissected in PBS and fixed in 4% (w/v) paraformaldehyde (in PBS) for 20 min at room temperature (RT). Samples were then washed three times in PBS for 15 min each, three times in PBT (1x PBS, 0.4 % Triton X-100) for 10 min each, and incubated for 1 hr in PTN (PBT, 5% normal goat serum; Scottish Diagnostics and Molecular Probes). The specimens were incubated for 24 – 48 hr at 4ºC in PTN containing the primary antibody at the appropriate concentration (see table 2.2). They were washed four times in PBT for 1 hr each and incubated in PTN containing the appropriate species-specific fluor-conjugated secondary antibody (see table 2.3) for 24 hr at 4ºC. They were washed four times in PBT for 1 hr and three times in PBS for 30 min. Stained specimens were mounted in VectaShield (Vector Lab) on Poly-L-Lysine treated microscope slides (BDH).

2.2.1.2 Embryonic incubations

Embryos were collected as described previously, and dechorionated by placing the sieve into a 50% solution of bleach in distilled water for exactly 3 min, after which the embryos were washed thoroughly with distilled water to remove all traces of bleach. The embryos were then transferred to 5 ml heptane in a glass container using a paintbrush, in which 5 ml of 4% paraformaldehyde (in PBS) was added. This solution containing the embryos was shaken vigorously, and then left for 10 – 30 mins at room temperature for embryo fixation. After fixation, the aqueous bottom layer was completely removed, and a 5 ml solution of 95% methanol/5% EGTA (ethylene glycol tetra-acetic acid, pH 8.0) was added to the glass container, and swirled gently. De-vitellinized embryos sank to the bottom of the container.

Embryos were then transferred to a clean 1.5 ml Eppendorf tube containing 1.0 ml of PBS using a Pipette with a cut tip. After the embryos had fallen to the bottom of the tube, most of the PBS was removed and several drops of PAT (PBS, 1% Triton-X, 0.1% bovine serum albumin) were added. The embryos were then washed an additional three times with PAT, followed by two washes in PBS. They were incubated for 1 hr in PTN (PBT, 5% normal goat serum; Scottish Diagnostics and Molecular Probes), followed by a 24 – 48 hr incubation at 4ºC, in PTN containing the primary antibody at the appropriate concentration (see table 2.2). They were washed four times in PBT for 1 hr each and incubated in PTN containing the appropriate species-specific fluor-conjugated secondary antibody (see table 2.3) for 24 hr at 4ºC. They were washed four times in PBT for 1 hr and three times in PBS for 30 min. Stained specimens were mounted in VectaShield (Vector Lab) on Poly-L-Lysine treated microscope slides for viewing.

2.2.1.3 Phalloidin muscle preparations

Muscle preparations were fixed for 30 min in 4% (w/v) paraformaldehyde (in PBS). Preparations were then washed three times for 10 min per wash in PBS, followed by a single wash in PBT (PBS, 0.5% (v/v) Triton-X). The preparations were then incubated with 100 nM TRITC- (tetramethylrhodamine B isothiocyanate) conjugated phalloidin (F-Actin specific fungal toxin; Sigma) for 20 min. The preparations were given three 10 min washes with PBT, followed by three 10 min washes in PBS before being mounted in VectaShield (Vector Lab) on a slide.

2.2.1.4 Primary and secondary antibodies utilised in immunofluorescent characterisations

Table 2-2 Primary antibodies used in this study.

Antibody	Description	Dilution	Source/Reference
Anti-Dsx	Rat, polyclonal against common DM DNA-binding domain of Dsx.	1:50	Hempel and Oliver, 2007
Anti-SPR	Rabbit, polyconal against an amino-terminal region of SPR.	1:500 - CNS, 1:2000 - reproductive system	Yapici et al., 2008

Anti-Horseradish Peroxidase (Anti-HRP)	Cy3 conjugated affinity-purified goat polyclonal against HRP.	1:300	Jackson ImmunoResearch Laboratories
Anti-HRP::Cy3	Cy3-AffiniPure conjugated Goat Anti-HRP.	1:400	Jackson ImmunoResearch Laboratories
Anti-ßgal	Rabbit, polyclonal against *E.coli* ß-galactosidase	1:1500	Invitrogen Molecular Probes
Anti-Green Fluorescent Protein (Anti-GFP)	Chicken, polyclonal against GFP.	1:1500	Abcam
Anti-GFP	Rabbit, polyclonal against GFP.	1:1000	Invitrogen Molecular Probes
Anti-mCD8	Rat, monoclonal against mouse lymphocyte marker CD8a-subunit.	1:20	Invitrogen Molecular Probes
Anti-nc82	Mouse, monoclonal against Bruchpilot (neuropil marker).	1:10	DSHB (Univ of Iowa)
Anti-Elav	Mouse, monoclonal against Elav (neuronal marker).	1:10	DSHB (Univ of Iowa)
Anti-Prospero	Mouse, monoclonal against prospero (enteroendocrine cell marker).	1:10	DSHB (Univ of Iowa)
Anti-HA	Rat, monoclonal against human influenza Hemagglutinin.	1:1000	Invitrogen Molecular Probes
Phalloidin-TRITC	TRITC- (tetramethylrhodamine B isothiocyanate) conjugated Phalloidin (F-Actin specific fungal toxin).	100 nm	Sigma

Table 2-3 Secondary antibodies used in this study.

Antibody	Description	Dilution	Source/Reference
Anti-rat IgG-Alexa Fluor 488	Goat, polyclonal against rat IgG, conjugated to Alexa Fluor 488.	1:600	Invitrogen Molecular Probes
Anti-rabbit IgG-Alexa Fluor 488	Goat, polyclonal against rabbit IgG, conjugated to Alexa Fluor 488.	1:600	Invitrogen Molecular Probes
Anti-mouse IgG-Alexa Fluor 488	Goat, polyclonal against mouse IgG, conjugated to Alexa Fluor 488.	1:600	Invitrogen Molecular Probes
Anti-chicken IgG-Alexa Fluor 488	Goat, polyclonal against chicken IgG, conjugated to Alexa Fluor 488.	1:600	Invitrogen Molecular Probes
Anti-rat IgG-Alexa Fluor 546	Goat, polyclonal against rat IgG, conjugated to Alexa Fluor 546.	1:600	Invitrogen Molecular Probes

Anti-rabbit IgG-Alexa Fluor 546	Goat, polyclonal against rabbit IgG, conjugated to Alexa Fluor 546.	1:600	Invitrogen Molecular Probes
Anti-mouse IgG-Alexa Fluor 546	Goat, polyclonal against mouse IgG, conjugated to Alexa Fluor 546.	1:600	Invitrogen Molecular Probes
Anti-rat IgG-Alexa Fluor 633	Goat, polyclonal against rat IgG, conjugated to Alexa Fluor 633.	1:600	Invitrogen Molecular Probes
Anti-mouse IgG-Alexa Fluor 633	Goat, polyclonal against mouse IgG, conjugated to Alexa Fluor 633.	1:600	Invitrogen Molecular Probes
Anti-mouse IgG-Cy5	Goat, polyclonal against mouse IgG, conjugated to Cy5.	1:600	Invitrogen Molecular Probes

*IgG stands for Immunoglobin Gamma.

2.2.2 Confocal microscopy

Stained whole mount preparations were examined using a Leica TCA SP5, an Olympus Flowview FV1000, or a Zeiss LSM 710 Meta confocal micro-system equipped with x10, x20, x40 (oil immersion), and x63 (oil/water immersion) objectives. The Diode laser excites in the visibe spectrum at 405 nm. The Ar laser can excite fluorophores with the following wavelengths in the visible spectrum: 458, 477, 488 and 514 nms. The He/Ne lasers can excite fluorophores with the following wavelengths in the visible spectrum: 543 and 633 nm. Alexa fluor-405-conjugated secondary antibodies excited with the 405 nm line and emit at ~420 nms. Alexa fluor-488-conjugated secondary antibodies excited with the 488 nm line emit at ~520 nms. TRITC-conjugated phalloidin and the Alexa Fluor 546-conjugated secondary antibodies excited with 543 nm line emit at ~575 nm.

For multi-track (multiple fluorophore labels) imaging, each wavelength was sequentially scanned for each optical section through the sample to excite each fluorophore individually and avoid bleed-through. Stacks of optical sections were generated at 1 μm intervals, unless stated otherwise.

2.2.3 Image processing

After acquisition of confocal images, files were opened with Imaris (Bitplane Scientific, AG, Zürich) software and transformed into “maximum Z-stack projections” which superimpose serial optical sections into a single image. Unless stated otherwise images presented in this study represent maximal Z-stack projections.

Imaris was also used to add pseudocolour to images generated by confocal microscopy, using the 'Look Up Table' (LUT) function. For single track/single fluorochrome preparations no pseudocolour was applied as greyscale provides a higher degree resolution for the image. A green LUT was applied to images obtained from samples stained with Alexa fluor 488-conjugated secondary antibodies; and a magenta LUT was applied to samples stained with either Alexa fluor 546- or TRITC-conjugated secondary antibodies. LUTs replaced the greyscale value produced by the confocal microscope with colours. If a third fluorochrome label was present, a blue LUT was applied to images obtained from samples stained with Alexa fluor 633- or TRITC-conjugated secondary antibodies. Three-dimensional (3D) reconstruction of confocal stacks were performed using Imaris software via the 'Maximum Projection' function, which is a flattened composite of the brightest pixels found through the vertical (or *Z*) axis of a given number of optical sections. Pseudocoloured 3D reconstructions or individual optical sections for co-localisation experiments were merged by first separating individual fluorochrome images by adjusting the 'output levels' of the green or red and blue channels to zero using Adobe Photoshop 7.0. The separated individual fluorochrome images were saved as .tiff (Tagged Image File Format) files, opened in Adobe Photoshop 7.0. and then merged as layers. These .tiff images files were processed, with brightness and contrast adjusted if necessary, using Adobe Photoshop 7.0. (Adobe Systems Inc., San Jose, CA). Figures were then assembled using Adobe Illustrator 10 (Adobe Systems Inc., San Jose, CA).

2.2.4 Cell counts

For cell counts, stacks of optical sections obtained by confocal microscopy were opened using Imaris (Bitplane Scientific, AG, Zürich) software and transformed into "maximum-Z-stack projections" which superimpose serial optical sections into a single image. Unless stated otherwise, the display properties of images that were processed for cell counts were modified, such that the single fluorophore labelling the cells of interest was used as the 'source channel' for automatic detection of spots, while all other fluorophores were unchecked and thus absent from the image. Using the 'Spots' detection tool in Imaris, the

maximum-Z-stack projection of the optical stack was automatically examined for spherically labelled nuclei with a minimum of 3 μm in diameter. This often marked the most obvious nuclei. However, as a precautionary step to ensure that all obvious cells were labelled, the threshold was manually shifted to the point at which it automatically detects the maximum number of spherical nuclei, without any observable ectopic detection. Then, using 'orthoslicer' tool, each optical slice was examined, and any un-marked nuclei that fell short of automatic-detection were manually labelled using the 'Edit' function within the 'Spots' detection tool. Once the cell counts were finalised using this semi-automatic technique, the 'Statistics' tab within the 'Spots' detection tool provided a count of the number of nuclei that were marked, providing comprehensive descriptions of each individual nucleus.

2.3 Bacterial protocols

2.3.1 Strains and plasmids

The *Escherichia coli* strains used in this study included the chemically competent and electrocompetent DH5α and NEB 10-beta respectively (Hanahan, 1983); genotypes listed below.

Table 2-4 *E.coli.* strains used in this study.

Strain	Genotype	Source/ Reference
DH5α	F-, φ80d*lac*ZΔM15 Δ(*lac*ZYA-*arg*F)U169 *deo*R *rec*A1 *end*A1 *hsd*R17(rk-, mk+) *pho*A *sup*E44 λ- *thi*-1 *gyr*A96 *rel*A1	Hanahan et al., 1983
NEB 10-beta	*araD139 Δ(ara,leu)7697 fhuA lacX74 galK16 galE15 mcrA φ80d(lacZΔM15) ecA1 relA1 endA1 nupG rpsL rph spoT1Δ(mrr-hsdRMS-mcrBC)*	New England Biolabs

Plasmids used in this study, other than those whose construction is described elsewhere in this thesis, are listed below.

Table 2-5 Plasmids used in this study.

Plasmid	Size (bp)	Description	Antibiotic Resistance	Source/ Reference
Strataclone®p SC-B-amp/kan	4300	Sub-cloning vector for cloning PCR products using topoisomerase	Ampicillin/ Kanamycin	Agilent Technologies

PCR® 2.1-TOPO®	3900	Sub-cloning vector for cloning PCR products using topoisomerase.	Ampicillin	Invitrogen
pED22-*dsx*	~23000	Vector generated for *dsx* gene targeting by homologous recombination. Contains three regions of *dsx* homology, GAL4 coding sequence, multiple cloning sites, *P*- element transposition sequences, a mini- white marker gene and the I-*Sce*I and I- *Cre*I recognition sites. The I-*Cre*I site contain cryptic modifications to two essential nucleotides deeming it inoperative.	Ampicillin	pED22 construct originally from B.J. Dickson; Rideout et al., 2010; J. Walker, pers. comm.
pattB-QF-sv40	~10500	Vector generated for gene targeting by homologous recombination. Contains QF coding sequence, multiple cloning sites, *P*-element transposition sequences, a mini- white marker gene, the I-*Sce*I and I- *Cre*I recognition sites and the sv40 termination sequence.	Ampicillin	Potter et al., 2010; Addgene
pattB-QF-hsp70	~10500	Vector generated for gene targeting by homologous recombination. Contains QF coding sequence, multiple cloning sites, *P*-element transposition sequences, a mini- white marker gene, the I-*Sce*I and I- *Cre*I recognition sites and the hsp70 termination sequence.	Ampicillin	Potter et al., 2010; Addgene

2.3.2 Culture Media

SOC: 2% tryptone (Sigma-Aldrich), 0.5% yeast extract (Difco™, BD Biosciences), 10 mM NaCl, 2.5 mM KCl, 10 mM $MgCl_2$, 10 mM $MgSO_4$, 20 mM glucose, pH 7.0

L-Broth: 10 g Bacto-tryptone (Difco™, BD Biosciences), 5 g yeast extract (Difco™, BD Biosciences), and 10 g NaCl per litre of water; pH was adjusted to 7.0 with NaOH.

L-Agar: As above with the addition of Bacto-agar (Difco) to 1.5% (w/v).

All culture media were sterilised by autoclaving at 120°C for 15 min.

2.3.3 Antibiotics and Indicators

When necessary, antibiotics were added to culture media for plasmid selection. Antibiotics were added to broth at room temperature and to molten agar at 50°C. Final concentrations of antibiotic used were as follows: 100 µg/ml for ampicillin, 25 µg/ml for kanamycin and 20 µg/ml for chloramphenicol. All antibiotics were purchased from Sigma.

X-Gal and Isopropyl-ß-D-thiogalactopyranoside (IPTG) were added to L-Agar to detect recombinant clones by α-complementation (blue/white selection). 40 µl of X-Gal (20 mg/ml in DMF) and 4 µl of IPTG (200 mg/ml in sterile distilled water) were spread on the surface of a solidified L-Agar Petri dish (98 mm diameter) (Sambrook and Russell, 2001).

2.3.4 *E. coli* Transformation Techniques

2.3.4.1 Chemical transformation

50-150 ng of DNA in a maximum volume of 1 µl was added to 50 µl of chemically competent DH5α cell suspension and incubated on ice for 15 min. The cells were heat shocked at 42°C for 90 sec, cooled on ice for 2 min and supplemented with 900 µl of SOC. The suspension was then incubated at 37°C with vigorous shaking (250 revolutions per min; rpm) for 1 hr. 100 µl of the cell suspension was then plated onto L-Agar Petri dishes with the appropriate antibiotics and indicator, and incubated overnight at 37°C to select for transformants.

2.3.4.2 Electroporation

1 µl of DNA solution was added to 50 µl of NEB 10-beta electrocompetent cells. Individual aliquots of cells and DNA were transferred into pre-chilled electroporation cuvettes (0.2 cm gap electrode, BioRad). The cells were then electroshocked at 2.5 kV in a MicroPulserTM (BioRad). 950 µl of SOC medium that was pre-warmed to 37°C in a water bath was added into each cuvette immediately following electroshock. The cell suspension was quickly transferred to a fresh microcentrifuge tube and incubated for 1 hour at 37°C with vigorous shaking (250 rpm). 100 µl of the cell suspension was then plated onto L-agar containing Petri dishes with the appropriate antibiotic and indicators, and incubated overnight at 37°C to select for transformants.

2.3.5 Isolation of plasmid DNA from *E. coli*

2.3.5.1 Small-Scale isolation of plasmid DNA

DNA was purified from 5-10 ml of overnight culture grown in L-Broth at 37°C with shaking in the presence of the appropriate concentration and type of antibiotic. Plasmid DNA for sequencing and cloning was isolated using the QIAprep spin miniprep kit (QIAGEN) according to the manufacturer's instructions.

2.3.5.2 Large-Scale Isolation of ultra-pure plasmid DNA

Large-scale preparations of plasmid DNA were performed using the Maxiprep kit (QIAGEN) according to the manufacturer's instructions.

2.4 General molecular biology protocols

2.4.1 Polymerase chain reaction (PCR)

Taq polymerase (New England Biolabs) was used for diagnostic PCR, and Phusion high fidelity DNA polymerase (New England Biolabs) was used for applications requiring high fidelity amplification. The PCR mix was set according to manufacturer's instruction. For PCR using *Taq* polymerase (New England Biolabs) the conditions were the following: initial denaturation- 5 min at 95ºC; denaturation- 50 sec at 94ºC, annealing- 40 sec at a temperature °C appropriate to the primer pair employed as determined by TmºC – 5ºC, extension- 1 min at 72ºC, where denaturation through extension was repeated for 30-35 cycles, followed by a final extension at 72ºC for 5 min. For high fidelity PCR with Phusion DNA Polymerase (New England Biolabs) the conditions were the following: initial denaturation step- 30 sec at 98°C; denaturation- 15 sec at 98°C, annealing- 30 sec at 50-60°C, extension- 15 sec per kb at 72°C, where denaturation through extension was repeated for 29 cycles, followed by a final extension at 72°C for 10 min.

2.4.1.1 Primer design

Primers used in this study were designed with the help of MacVector 7.2.2 (Oxford Molecular) software purchased from Invitrogen. The T_m of primers was calculated using

MacVector software. The primers were ordered from Sigma-Aldrich (Dorset, UK). A description of the primers used for PCR can be found below:

Table 2-6 Primers used in this study.

Primer Name	Sequence	Comment	Tm (°C)
GAL4DBD-SeqR1	TTCTTTGGAGCACTTGAGC	Gal4DBD-seq(R)	55.1
GAL4DBD-SeqR1	AAGCCAATCTATCTGTGAC	Gal4DBD-seq(R)	48.2
GAL4DBD-SeqF1	CGGTTACATAAACTTAGACGCTCG	Gal4DBD-seq(F)	60.0
GAL4DBD-SeqF1	CAAGTGTCTGAAGAACAACTGG	Gal4DBD-seq(F)	55.9
GAL4DBD-SeqF1	AGTGATGATGAGGCTACTGC	Gal4DBD-seq(F)	53.8
GAL4DBD-SeqF1	CAGCCATACCACATTTGTAGAG	Gal4DBD-seq(F)	55.8
HJP-38s	CCTGGAGAACGAGGTGAGC	Gal4DBD-seq(F)	59.7
HJP-39s	CTCTTCCGATGATGATGTCG	Gal4DBD-seq(R)	57.9
HJP-40s	TGAAAAACCCCTGGCAGAC	FRT-seq(F)	59.8
HJP-41s	CCAAAACCAATCACCACCC	FRT-seq(R)	59.8
HJP-49s	CATCACGGACCAAAAGATTG	QF-seq(R)	57.8
HJP-50s	CTAGCCATGCCGATCTGTTC	Insert 3-seq(F)	59.6
HJP-51s	CGACATAAAAACAGCCATGC	Insert 3-seq(R)	58.1

2.4.1.2 Cloning PCR Products

PCR products were cloned into vector pCR®2.1-TOPO® using the TOPO-TA cloning kit (Invitrogen) following manufacturer's instructions.

2.4.2 Restriction digest of DNA

DNA was digested in the appropriate buffer for the enzyme(s) according to manufacturer recommendations (New England Biolabs). 2 units of enzyme were used per µg of DNA to ensure complete restriction of DNA. Digests were carried out at 37°C for 1-2 hours for plasmid DNA, and 4 hours for genomic DNA.

2.4.3 DNA gel electrophoresis

DNA fragments were resolved on agarose (Boehringer Mannheim) gels. The DNA solution was mixed with loading buffer and loaded into agarose gels containing 1 X TAE (40 mM Tris/AcOH (pH 8.2), 20 mM NaOAc, 1 mM EDTA). A range of agarose concentrations (0.6%-2.0% (w/v)) was used depending on the size of the fragments to be resolved (Sambrook and Russell, 2001). The gels were run from 1 hour to overnight at voltages ranging from 25 mV to 120 mV. DNA size markers were the 100 bp or the 1 kb ladders (New England Biolabs).

2.4.4 Visualization and photography of gels

The UVIdoc HD2 (UVITEC, Cambridge) gel documentation hardware was used to visualise DNA by UV induced fluorescence on either a short wave (254 nm) or long wave (365 nm) transilluminator after staining the agarose gels in an ethidium bromide (EtBr) solution (0.5 µg/ml) in a shaker tray for 40 min and then de-staining in a bath of dH_2O twice for 15 min. A 1.4 megapixel scientific Sony chip CCD camera was used to capture and save the image to the internal memory of the gel documentation, while a Sony UP-D897MD digital thermal printer was used to print captured/saved images. For very large DNA fragments, the DNA was visualized on a light box after staining the agarose gels for 1 hour with crystal violet (0.0025% (w/v) in distilled water; Yang *et al*., 2001), and de-staining for 20 min in distilled water.

2.4.5 Gel extraction of DNA fragments

Size-selected DNA fragments were excised from agarose gels using a clean razor blade, on the long wave (365 nm) UV transilluminator. Purification of the DNA fragment from agarose, salt and enzymes was carried out with the QIAquick gel extraction kit (QIAGEN), or the QIAEXII Gel Extraction Kit (for fragments >10 kb)(QIAGEN) following manufacturer's instructions.

2.4.6 Subcloning DNA Fragments into plasmid vectors

The insert to be sub-cloned and the target plasmid vector were digested with the appropriate restriction enzymes as described in 2.4.1. When the plasmid vectors were cut with a single

enzyme, the over-hanging 5' or 3' nucleotides triphosphate were dephosphorylated to prevent vector re-ligation. 1 µl of Antarctic Phosphatase (New England Biolabs) was added directly to the completed plasmid digest reaction and incubated at 37°C for 1 hour. The alkaline phosphatase was then heat-inactivated for 15 min at 68°C. Both insert and vector were size fractionated and gel purified as described in 2.4.2 and 2.4.4.

2.4.7 Ligation

Purified inserts and vectors were mixed at a ratio of 3:1 (insert:vector) for cohesive end ligation and 1:1 for blunt end ligation. The DNA mix was combined with 1 µl (1 Weiss Unit) of T4 DNA ligase and 2 µl of 5x T4 DNA ligase buffer (New England Biolabs) in a total volume of 10 µl. The ligation mixture was incubated overnight at room temperature and transformed as described in 2.3.4.2 and 2.3.4.5. Transformants were selected on L-Agar plates in the presence of the appropriate antibiotics and indicators.

2.4.8 Purification of genomic DNA

Fly genomic DNA was prepared by a modification to the procedure described in Hamilton and Zinn (1994). 0.04 g of flies (approx. 30 flies) were frozen on dry ice and homogenized with a micro-pestle in 200 µl of grinding buffer (5% sucrose, 80 mM NaCl, 100 mM Tris, pH 8.5, 0.5% SDS, 50 mM EDTA). The homogenate was then incubated at 70ºC for 30 min, supplemented with 35 µl of 8 M KOAc, transferred to ice for 30 min and centrifuged at 12000 g for 10 min at 4°C. The supernatant was then transferred into a clean tube. Excess protein was extracted from the solution using a phenol:chloroform:isoamyl alcohol (25:24:1) (Sigma) extraction (as described in Sambrook and Russell, 2001). The DNA was then precipitated by adding 150 µl of isopropanol to the supernatant and allowed to stand at room temperature for 5 min. The genomic DNA was pelleted by centrifugation at 12000 g for 15 min at 4°C. The pellet was rinsed with 500 µl of 70% EtOH and allowed to dry at room temperature. The pellet of genomic DNA was re-suspended in 50 µl of TE (10 mM Tris-HCl, 1 mM EDTA, pH 8.0) with 0.1 mg/ml of RNase A (Sigma).

2.4.9 Quantification of nucleic acids

The amount of DNA or RNA in a sample was estimated by taking Optical Density (O.D.) measurement at a wavelength of 260 nm using a NanoDrop 1000 spectrophotometer (Thermo Scientific). An $O.D._{260}$ =1 corresponded to ~50 µg/ml of double stranded DNA. An $O.D._{260}$ =1 corresponded to ~40 µg/ml of double stranded RNA.

2.4.10 DNA sequencing

Automated sequencing was carried out by Source Bioscience using Sanger sequencing SpeedREAD™ technology. The requirements for the concentration of plasmid DNA was 100 ng/µl. Primers used for sequencing can be found in Table 2-6.

2.5 Behavioural analyses

2.5.1 Equipment

2.5.1.1 Chambers

Prior to behavioural recordings, flies were introduced into the appropriate chamber by aspiration through a small opening in the side of the chamber. For thermoactivation experiments, round chambers 1 cm in diameter and 0.4 cm in height with a nylon mesh base were used, while male and female courtship behavioural experiments were carried out in larger round chambers (2 cm diameter x 4 mm height). The chambers have a Perspex top to allow the camera to record the movements and activities of the flies.

2.5.1.2 Cameras

A Sanyo VCC-3972P CCD video camera was used for all behavioural recordings. The camera was mounted on an adjustable mount and positioned over the courtship chambers. The image on the LCD screen was sharpened using the focus and zoom rings. Upon formatting DVD+RW discs, the connected DVD player/writer was used to initiate and stop recordings. During the recording, each DVD was given a name, and the date, genotype and comments on recording.

2.5.2 Behavioural assays

For behavioural assays, including silencing experiments, flies were raised at 21°C in a 12:12 hr light:dark cycle. Individual virgin adults were collected and aged for 5 - 7 days post-eclosion at 25°C and assays carried out at 25°C.

For thermoactivation experiments, *UAS-dTrpA1*-expressing flies were reared at 21°C in a 12:12 hr light:dark cycle. Individual virgin adults were collected and aged for 10 - 14 days post-eclosion at 21°C and assays carried out at the permissive temperature of 25°C, or the restrictive temperature of 32°C (achieved by placing the chambers on a temperature controlled heating plate).

2.5.2.1 Male courtship behaviour

Courtship behaviour was as described in Villella et al. (1997) and was measured in the chambers as described above. Essentially an individual male aged 3 - 5 days old (of varying genotype) and a single wild-type CS virgin 'target' female of the same age were introduced into the chamber and observed for a 10 min period.

- *Courtship index (CI*): measured as the proportion of time in 10 min that the 'courter' spent exhibiting courtship behaviours towards the 'target' female (as per Villella *et al*., 1997). Courtship behaviours are defined here as: following, orientation, tapping, wing extension, and abdominal curling/attempted copulation.
- *Courtship initiation:* is the time elapsed between introduction of flies and first exhibition of courtship behaviour by the male towards the target female (as per Villella et al., 1997).
- *% Mating:* number of male flies, as a percentage, that were observed successfully copulating within in a 2 hr period (Rideout et al., 2010).
- *Fertility*: males tested for fertility were collected at eclosion (kept in groups ≤10) and aged for 5 days. Then they were placed individually in food vials containing three wild-type virgin females of the same age. All vials were scored for presence of larval progeny over a 7 day period (Gailey and Hall, 1989). Vials containing a dead male and no progeny were discounted. Females in vials in which no progeny were apparent after 7

day were then re-mated with wild-type males to then assure the receptivity/fertility of these target females.

2.5.2.2 Female courtship behaviour

- *Fertility*: females tested for fertility were collected at eclosion (kept in individual vials) and aged for 5 days. They were then introduced individually into food vials containing three wild-type virgin males of the same age. All vials were scored for presence of larval progeny over a 7 day period (Rideout et al., 2010). Vials containing a dead female and no progeny were discounted. Males in vials in which no progeny were apparent after 7 days were then re-mated with wild-type males to assure their fertility.
- *Receptivity*: equivalent to % mating and refers to the number of female flies, as a percentage, that were observed to successfully copulate within a 1 hr period (Yapici et al., 2008; Häsemeyer et al., 2009; Rideout et al., 2010).
- *Egg laying*: the number of eggs present per day in vials in which individual females (of varying genotypes) were introduced to three wild-type males (Rideout et al., 2010). After two days the females and males were transferred to a fresh vial and the old vial was then examined for the presence of eggs. Any set of vials in which the target female died during the assay was discounted.
- *Line crossings:* a measure of the number of times a copulating pair crossed a demarcated line in the courtship chamber per min during the time spent copulating (as per Waterbury et al., 1999).
- *Copulation duration*: measure of the observed time (in sec) elapsed between the beginning of mating and its termination (as per Billeter et al., 2006a).
- *% re-mating*: measure of the number of females (of varying genotypes), as a percentage, that were successfully re-mated by the same wild-type male over the same 1 or 2 hr period in which females mated for the first time (Rideout et al., 2010).
- *% re-mating after 48 hrs*: measure of the number of females (of varying genotypes) that successfully re-mated with a wild-type male, 48 hrs post initial mating, over a 1 or 2 hr period.

- The following locomotion and rejection behavioural parameters were measured during a 3 min observation period (or until mating occurred) starting from courtship initiation (first bout lasting over 3 seconds):
- *Movement during courtship*: percentage of time females spent moving while being actively courted by the male.
- *Movement in the absence of active courtship*: percentage of time females spent moving when male was not actively courting.
- *Ovipositor extrusion*: number of ovipositor extrusion(s) performed by the female per minute during the observation period of courtship.
- *Female 'attractiveness' index*: percentage of time during which a male displays any of the courtship steps, including following, tapping, wing extension, licking, and attempted copulation, from the time of courtship initiation to either the time to copulation or within a 10 min observation period (depending on which occurred first). This parameter was used as a determinant of females' 'attractiveness' (Villella and Hall, 2008).
- *Male courtship index with decapitated females*: percentage of time during which a male displays any of the courtship steps, including following, tapping, wing extension, licking, and attempted copulation, within a 10 min observation period from the time of courtship initiation. Here, male courtship towards decapitated female targets was measured in individual chambers of 12-well polystyrene plates (each chamber dimension is 10 mm diameter × 5 mm height). 'Headless' females were placed in the centre of the chamber ~30 min before transferring an individual naïve *Canton-S* male.

2.6 Statistics

All the data obtained in this thesis were tested for normal distribution prior to statistical analyses. As such, overall analyses of variance (ANOVAs) of behavioural means were subjected to pairwise comparisons using the non-parametric Kruskal-Wallis One Way Analysis of Variance on ranks and Dunn's post hoc statistical test between relevant groups. Fisher's exact probability test was used for fertility assay data, within which 2-tail *p*-values were compared to those of wild type controls. Egg laying data were subjected to Dunnett's

test; all comparisons were made against the wild type control group. As data from cell counts followed a normal distribution, comparisons between males and female means were carried out using the Student's t-test.

Statistical tests were performed and graphed with JMP v6.0 software (SAS Institute), Prism v5.0b software (SPSS Inc.) and SigmaPlot v.11 software (Systat Software Inc.) respectively.

3 Generation of Intersectional Tools

3.1 Introduction

Both *fru* and *dsx* are necessary, but not sufficient, for the specification of male courtship behaviours (Villella and Hall, 2008). Yet, of the two sex determination genes, the role of *fru* in *Drosophila* copulatory behaviours has received more attention over the last few decades; until the conspicuous effects on male and female courtship and fertility, associated with impairing *dsx* neural function, demonstrated the neural aetiology underlying *dsx* related behavioural phenotypes (Rideout et al., 2007; Rideout et al., 2010). In support for the role of *dsx* circuitry in copulatory behaviours, *dsx* has been shown to be expressed in a sexually dimorphic manner in the larval, pupal and adult CNS, with Dsx^M co-expressing and coordinating with Fru^M, in a restricted subset of neurons in behaviourally relevant regions of the male CNS, to confer the potential for male-specific reproductive behaviours (Billeter et al., 2006b; Kimura et al., 2008; Rideout et al., 2007; Rideout et al., 2010; Sanders and Arbeitman, 2008; von Philipsborn et al., 2011). These observations are validated by investigations that showed that artificial activation of either all fru^M- or all dsx^M-expressing neurons results in the elicitation of almost all steps of courtship, from courtship song to ejaculation. However more strikingly when *dsx* circuitry was activated in males null for fru^M this generated courtship outputs equitable to males that are wild type for fru^M; providing compelling evidence for a more restricted *fru*-independent *dsx*-circuitry underlying male courtship behaviours (Clyne and Miesenboek, 2008; Pan et al., 2011).

Given that the correct sexual identity of non-neural adult tissues, such as the fat body and oenocytes, is also critical for normal sex-specific behaviours, this strongly suggests a supporting role of somatic tissues in the advancement of copulatory behaviours (Waterbury et al., 1999; Lazareva et al., 2007; Shirangi et al., 2009). This is further supported by the fact that *dsx* is expressed in an array of somatic tissues fundamental to sex determination, endocrine regulation and physiological state changes (Rideout et al., 2010; Robinett et al., 2010).

To date however, studies have been limited by the lack of amenable reagents and their inability to delineate and spatially target various *dsx*-expressing cell types. For this reason, in

this study, I aimed to refine our understanding of how *dsx* neurons instruct sex-specific neural programs, by way of separating the relative contribution of *dsx* circuitry from that of dsx-expressing non-neuronal tissues in the generation and maintenance of reproductive behaviours.

3.2 Intersectional strategies

As previously stated, restricting genetic access from all *dsx*-expressing cells to specific, spatially targeted, *dsx*-expressing neurons only, requires the implementation of intersectional strategies. Given recent applications of the GAL4-inhibitor, GAL80, the Flippase recombinase, FLP and the development of the novel LexA/*LexAop* and QF/*QUAS* binary expression systems, there are at least four different genetic tools that could be used in conjunction with the ever increasing number of GAL4 expression lines, enhancer trap lines and swappable driver lines (reviewed by Simpson, 2009; Rodriguez et al., 2012); theoretically allowing *dsx* to be manipulated in any cell type at any developmental stage (Figure 3-1). An alternative to these strategies is the ternary split-GAL4 system, which entails placing each functional domain of GAL4 under control of a different promoter, and fusing them to a heterodimerizing leucine zipper, so that the two domains are able to associate when expressed in the same cell, reconstituting transcriptional activity (Luan et al., 2006). This restricted activation can be used in combination with the vast array of available GAL4 responsive *UAS-reporters* and *UAS-effectors*, and/or in conjunction with independent binary systems, such as the LexA/*LexAop* and/or QF/*QUAS* systems (Figure 3-1B).

Each of these aforementioned approaches has its limitations, some of which are less challenging than others. GAL80 for example, must be expressed at a sufficiently high level in order to neutralise the transcription-promoting activity of GAL4 (Johnston and Hopper, 1982; Salmeron et al., 1989; Yun et al., 1991; Travern et al., 2006). However, the dosage of GAL80 is a promoter-independent stochastic feature that may not be predicted or considered for, when generating the novel allele (Pfeiffer et al., 2010). Further, the use of FLP for intersectional methods has been shown to result in imprecise expression patterns in the adult (Bohm et al., 2010). This is conceivably a result of the irreversible excision of the >*stop*>

cassette in cells that intersect at some point in development, resulting in perdurance of *UAS*-effector or -*reporter* expression from earlier developmental stages (Bohm et al., 2010). Although the LexA/*LexAop* system is conceptually similar to the Q system, studies have shown that LexA is a weaker transcriptional activator than GAL4, and that the *colE1*-derived binding site used in most *LexAop*-reporters or effectors 'leaks' expression in the absence of the LexA protein (Lai and Lee, 2006).

In comparison, the limitations of both the split-GAL4 and Q systems are restricted to reduced expression levels when compared to GAL4, and a limited number of available reagents (Luan et al., 2006; Potter et al., 2010). These observed weak expression levels have already been overcome in the split-GAL4 system, by the use of the more potent viral VP16-AD (Luan et al., 2006). The fact that both these systems have limited available reagents is impermanent, as groups that adopt these novel strategies will contribute to the growth of the reagent collection. When put into perspective, these limitations are less onerous than those of other systems.

Again, as no one strategy is a panacea when it comes to spatially targeting the nervous system, I chose to employ both (complementary) stratagems: that is the ternary split-Gal4 system approach, and the binary Q system approach. Both approaches are genetically heritable, allowing for the replication of genetic access to intersecting neurons for subsequent behavioural and neuroanatomical studies (Luan et al., 2006; Potter et al., 2010). The generation of such novel tools requires a large investment in time, with no guaranteed success that resultant transgenic reagents will successfully recapitulate the endogenous gene expression; thus it was deemed that the generation of two, rather than one, complementary novel alleles would increase the chance of a successful outcome.

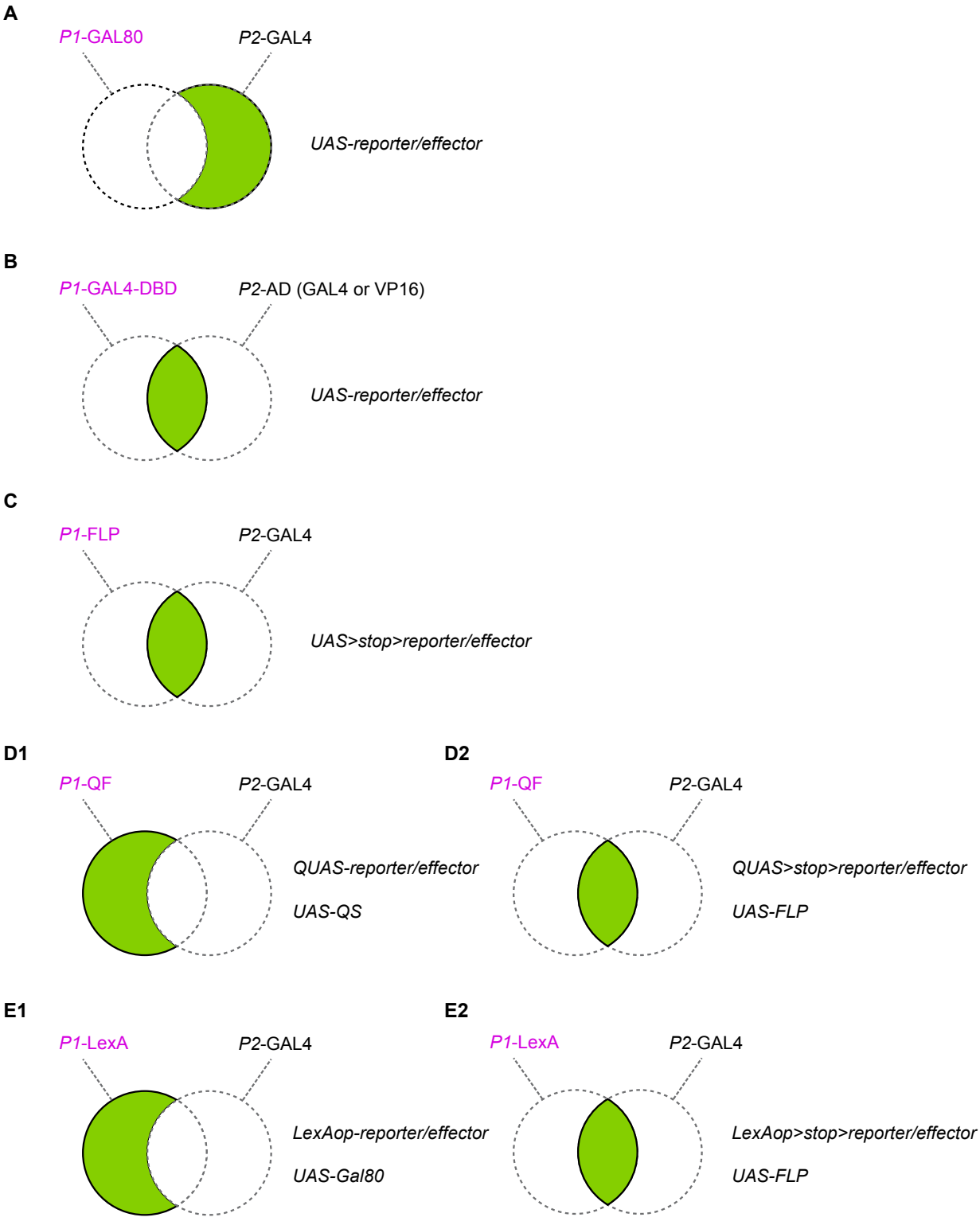


Figure 3-1 Optional intersectional tools and combinations.
(A) GAL80 with GAL4. (B) Split-GAL4. (C) FLP with GAL4. (D1) Subtractive and (D2) intersectional approaches to utilising QF with GAL4. (E1) Subtractive and (E2) intersectional approaches to utilising LexA with GAL4. Possible reagents that could be generated in this study are shown in magenta. The combination of responsive reporters and effectors, shown to the right of each schematic, determine the resultant subtractive (A, D1, E1) or intersectional (B, C, D2, E2) reporter/effector expression (shown in green).

Accordingly, I generated a novel *dsx* allele that expresses the GAL4 DNA-binding domain (*dsx*$^{GAL4\text{-}DBD}$), which in combination with the previously published pan-neuronal hemi-driver *elav*$^{VP16\text{-}AD}$ (Luan et al., 2006) restricts access to the intersection (∩) of the two promoters (i.e. *dsx* expression exclusively in the nervous system). This *dsx*$^{GAL4\text{-}DBD}$ hemi-driver was also used to screen a collection of extant split-GAL4 enhancer-trap lines (*ET*$^{VP16\text{-}AD}$) to restrict expression to subsets of *dsx*-expressing neurons and identify various functional components within *dsx* circuitry (Luan et al., 2006). Further, I attempted to generate a novel *dsx*^{QF} allele, to be used in combination with numerous QF responsive *QUAS* reporters and effectors, in conjunction with various pan-neuronal GAL4 expression lines (Potter et al., 2010; Potter and Luo, 2012). This approach offers a more versatile means of parsing component elements of the *dsx*-circuitry, given that a vast number of publically available promoter-fusion, enhancer trap, and cell- or tissue-specific GAL4 driver lines, may be exploited here (Potter and Luo, 2012).

3.3 Gene targeting by homologous recombination

Prior to recent developments, *P*-element- or mutagenic (i.e. ethane methyl sulphonate or isotope induced) mediated screens were implemented to isolate mutations in a gene of interest (Engels, 1996). The stochastic nature of these traditional approaches, however, meant that the majority of mutations generated were imprecisely directed, rarely resulting in null alleles, and were reliant on screening a number of mutagenic events using genetic markers or PCR to detect modifications within the gene of interest. Arguably the most powerful method to decipher gene function entails gaining access to its endogenous locus to precisely disrupt, alter or mimic the expression of the endogenous gene, but traditional methods lack the necessary precision to generate such modifications, resulting in largely imperfect tools. However, since the development of gene targeting by homologous recombination, *Drosophila* geneticists have been armed with an approach capable of directly targeting insertions, deletions or modifications to a specific locus within the *Drosophila* genome (Rong and Golic, 2000). Despite being labour intensive, this technology is enticing as it allows direct manipulation of large genes with multiple promoters and/or protein

isoforms, in addition to genes with complex *cis*-acting regulation, making it ideal for disrupting or altering specific aspects of a gene's function (reviewed by Bi and Rong, 2003). Modified from yeast, gene targeting by homologous recombination utilizes endogenous DNA repair and recombination machinery to either substitute or integrate an engineered extra-chromosomal DNA molecule (termed "the donor") into the chromosomal target gene locus (Rong and Golic, 2000). This donor element is engineered to contain four essential components:

2) Regions of homology to that of the target gene essential for the process of homologous recombination. Donor to target homology may range from 2.9 kb to 8.9 kb, though typically around 4 kb has proven to be sufficient (Bi and Rong, 2003; Hasty et al., 1991a; Rong and Golic, 2000, 2001; Rong et al., 2002).
3) P-element transposition sequences and *flippase recognition target* (*FRT*) sites in direct orientation flanking the entire donor molecule for excision of the donor molecule upon expression of FLP site-specific recombinase.
4) A marker gene (such as *mini-white*$^{+}$*;* *mw*$^{+}$ or *yellow*$^{+}$; *y*$^{+}$) for the identification of targeting events.
5) A recognition site for the site-specific rare-cutting endonuclease I-*Sce*I for the linearization of the donor element.

Once constructed, the donor element is first randomly inserted into the genome by standard *P*-element mediated transformation (Rubin and Spradling, 1983). Upon integration into the genome, the expression of FLP and I-SceI enzymes result in the excision and linearization of the donor element. The now linear and mobile DNA utilises the engineered regions of homology to participate in homologous recombination with the endogenous target. Depending on the desired end product, the arrangement of both the I-SceI cut site and the marker gene can be preselected during the construction of the donor element in order to configure it for one of two alternative strategies of gene targeting by homologous recombination: ends-in or ends-out (Rong and Golic, 2000; Rong et al., 2002; Gong and Golic, 2003).

3.3.1 Ends-out homologous recombination

Gene targeting by homologous recombination via the ends-out strategy is most often used if the desired end product is simply a null mutation in the gene of interest (Rong and Golic, 2000; Rong *et al*., 2002). This may be achieved in one of two ways, by either disrupting or replacing or deleting the endogenous locus, dependent on the genomic region chosen as the donor/target homology (Rong and Golic, 2000; Rong *et al*., 2002). Engineering regions of homology that consist of sequences within the targeted locus results in a disruption of the endogenous locus by the insertion of the donor construct. Whereas, engineering regions of homology that consist of sequences flanking the desired locus results in the replacement/deletion of the endogenous locus by the donor construct (Figure 3-2; reviewed by Bi and Rong, 2003).

By placing the marker gene between the regions of donor/target homology, and ensuring that the placement of the I-*Sce*I cut site is not in close proximity to the regions of homology or the marker gene, the donor construct is sufficiently tailored for the single step gene targeting provided by the ends-out process (Figure 3-2A; Rong and Golic, 2000, 2001; Rong et al., 2002). Once the donor construct has been inserted into the genome at random by *P*-element transformation, the transgenic fly then undergoes a series of genetic crosses to generate a null mutant in the gene of interest (Rong and Golic, 2000; Rong and Golic, 2001; Rong *et al*., 2002). First, the strain of flies carrying the donor *P*-element is crossed to a strain of flies carrying heat shock inducible FLP and I-*Sce*I. The F1 progeny of this cross are heat-shocked early in development, resulting in the excision of the donor element from the genome by the activation of FLP, and the generation of a double-stranded break via the action of I-*Sce*I (Figure 3-2A,B). The excision of the donor element from the genome renders it mobile, while the generation of a double strand break in the donor element induces it to be highly recombinogenic (Rong and Golic, 2000). As a result of these features, the linearized mobile donor element may be integrated at the desired locus by homologous recombination, where integration events are scored for via the presence of expression of the marker gene (i.e the appearance of eye colouration in a w^- genetic background due to the incorporation of a

transgenic donor element carrying the *mw*$^{+}$ genetic marker) followed by use of molecular techniques to confirm successful integration at the chosen locus (Figure 3-2C; Rong and Golic, 2000; Rong *et al*., 2002). Ultimately, the integration event should replace/disrupt the target gene, creating the desired genetically marked mutant. In some cases however, the presence of a marker at the gene locus may prove to be a disadvantage, as it may interfere with mutant analyses (Bi and Rong, 2003). In such cases, a second step must be incorporated, subsequent to the ends-out strategy, to remove the interfering marker (as described by Stockinger *et al*., 2005).

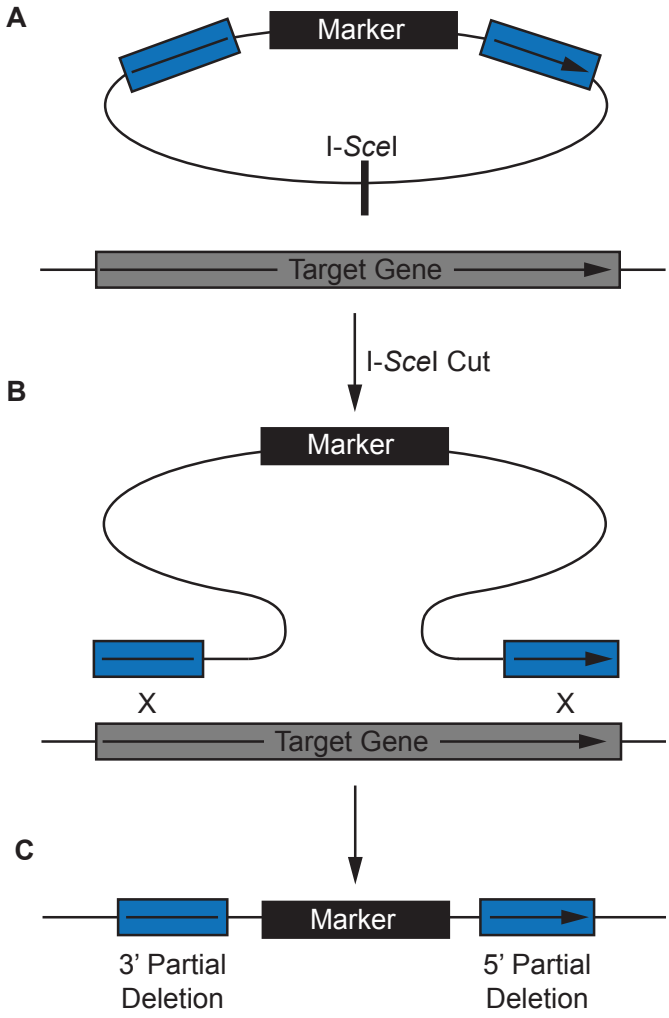


Figure 3-2 Schematic representation of gene targeting by ends-out homologous recombination.
(A) Targeting vector contains two regions of donor: target homology separated by a marker; the I-*Sce*I recognition site is located at a separate region within the vector that is far from the regions of homology and marker. (B) The donor vector is cut at the I-*Sce*I recognition site, creating a double-strand break. The donor vector is then integrated into the desired locus by homologous recombination. (C) Given that the regions of donor: target homology are located at either end of the targeted locus, integration of the vector at the target locus results in the deletion of all the sequence flanking the regions of donor: target homology. Adapted from Rong and Golic (2000).

3.3.2 Ends-in homologous recombination

The ends-in gene targeting strategy involves a slightly more complex two-step process that is better suited for the creation of subtle modifications to the endogenous locus (Figure 3-3; Rong and Golic, 2000; Rong et al., 2002). Examples of the types of modifications ends-in gene targeting is capable of include the creation of deletions or insertions within a target gene, or the disruption of a single isoform of a gene (Rong *et al*., 2002).

By first introducing the donor element in tandem to the endogenous allele to create a duplication at the locus, the endogenous portion of this 'hybrid' locus is subsequently removed to leave a single mutated allele within the chromosome (Figure 3-3A-C; Rong et al., 2002; Bi and Rong, 2003; Maggert et al., 2008). To achieve this, the donor construct is tailored to include a genetic marker and three regions of donor/target homology separated by recognition sites for the I-*Sce*I and I-*Cre*I site-specific endonucleases (Figure 3-3A). Following random insertion of the donor construct into the genome by *P*-element transformation, the fly strain carrying the donor *P*- element is crossed to a strain of flies carrying heat shock inducible FLP and I-*Sce*I (Figure 3-3A). Similar to ends-out gene targeting, the F1 progeny of this cross are heat-shocked early in development, resulting in the excision of the donor element from the genome by the activation of FLP, and the generation of a double-stranded break via the action of I-*Sce*I (Figure 3-3B). The linearized mobile donor element may then integrate at the desired locus by homologous recombination, where integration events are again scored for via the presence of expression of the marker gene. However, this integration event leads to a duplication, rather than a disruption/replacement of the gene locus as a result of the difference associated with the ends-out donor construct design (Figure 3-3C).

Thus, the initial steps of ends-in gene targeting are identical to those of ends-out gene targeting. The main differences between the approaches arises from differences in the design of the donor construct, which enable the introduction a second step in ends-in gene targeting, which aims to eliminate the duplication and the marker gene from the gene locus (Figure 3-3C-E). First, the recombinant flies that carry the duplication are crossed to a strain

of flies carrying a heat-shock inducible I-*Cre*I (Figure 3-3C). The F1 progeny of this cross are heat-shocked to induce a double-strand break in the locus, which is subsequently repaired by homologous recombination, via a third region of donor to target homology, ultimately resolving the duplication at the locus, and eliminating the marker gene (Figure 3-3D,E). This final event is scored for by the loss of the previously observed phenotypic expression of the chosen marker (i.e. the loss of eye colouration due to the elimination of the transgenic *mw*$^{+}$ genetic marker ((Figure 3-3E; Rong et al., 2002).

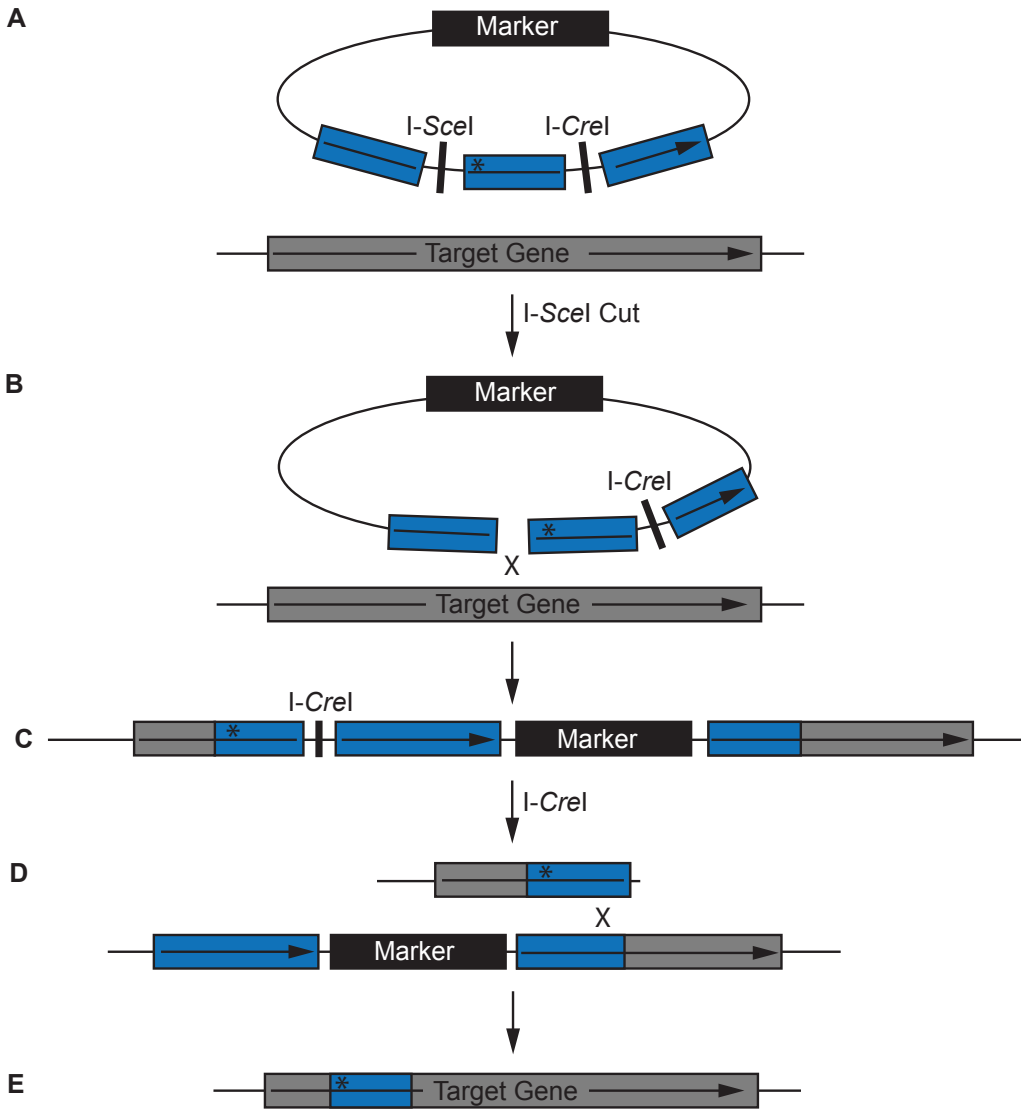


Figure 3-3 Schematic representation of gene targeting by ends-in homologous recombination. (A) Donor vector contains a genetic marker and three regions of donor: target homology, separated by the recognition sites for I-*Sce*I and I-*Cre*I restriction endonucleases. * indicates the desired alteration to be made at the targeted locus. (B) A double-strand break is made at the I-*Sce*I site in the donor vector, and is integrated into the target locus by homologous recombination. (C) A duplication is created at the targeted locus. (D) A double-strand break is made at the I-*Cre*I site at the targeted locus, and the break is repaired by homologous recombination, also eliminating the marker and the duplicated portion of the gene. (E) Resolved end product containing the desired alteration (*). Adapted from Rong and Golic (2000).

The development of these homologous recombination-based gene targeting techniques has meant that investigators can now directly target the endogenous loci of, and consequently manipulate genes that have been shown to be involved in specific behaviour(s). Moreover, by coupling homologous recombination-based gene targeting technology with the remarkably versatile expression systems that have been adapted for *Drosophila*, researchers are now able to fully characterise the expression patterns and delineate the functions of these genes.

3.3.3 Chosen strategy

In this study, the ends-in strategy of homologous recombination was chosen to insert GAL4-DBD and QF (separately) into the *dsx* locus. The main reason being that this strategy provides the option of removing the marker gene, via a second step of genetic crosses, enabling the generation of a true *dsx* null mutant, which has yet to be created. An even more important reason to have the option of removing the marker gene is that the *mini-white* (*mw)* gene, which serves as a marker within the *P*-element donor construct used in this study, has been previously shown to trigger high levels of inter-male courtship (Zhang and Odenwald, 1995). Given that the novel alleles created in this study will be used to study courtship behaviour, any possible interference of the marker gene must be eliminated. However, it is important to mention that the original dsx^{GAL4} allele consists of a tandem duplication in which the mw^{+} marker gene remained (Rideout et al., 2010). Yet, despite the presence of mw^{+}, no inter-male courtship was observed (Rideout et al., 2010). Further, the proven record of success of this strategy in numerous publications, in addition to the readily available *P*-element targeting vectors, further supports the choice of the ends-in strategy of gene targeting (Rong and Golic, 2000; Rong and Golic, 2001; Rong et al., 2002; Stockinger et al., 2005; Rideout et al., 2010; Yu et al., 2010). Of the two published dsx^{GAL4} alleles available today, the first was made via the ends-in strategy, while the second was made via an ends-out strategy (Rideout et al., 2010; Robinett et al., 2010 respectively). The first remained as a tandem duplication at the *dsx* locus, yet it did not result in a hypomorph, as it is clear that the presence of the GAL4 insert did not is affect any facet of morphology or behaviour (Rideout et al., 2010). However, it became clear that the second allele did result in a hypomorphic

mutant as the presence of GAL4 clearly affected viability and fertility at the very least (Robinett et al., 2010). In light of these studies, the GAL4-DBD and QF targeting vectors were separately inserted into the *dsx* locus in an almost identical manner to that described by Rideout et al. (2010).

3.4 Generation of gene targeted GAL4 and QF 'donor' constructs

3.4.1 QF donor construct

3.4.1.1 Parent vector

The parent vector, pED22 (B. Dickson, unpublished) was used to generate the original *dsx*^{GAL4} donor vector pED22-*dsx*GAL4 (Rideout et al., 2010). This parent vector included an I-*Cre*I site-specific endonuclease recognition site that is recognised and cleaved by the heat-shock inducible I-*Cre*I site-specific endonuclease to create a double-strand break (B.Dickson, unpublished). This reaction is pivotal for subsequent DNA repair events via homologous recombination that ultimately serve to resolve the duplication at the locus and eliminate the marker gene (Rong et al., 2002). Unfortunately, this I-*Cre*I recognition site was later shown to consist of polymorphisms in the conserved and non-conserved regions of each half-site, when compared to wild-type I-*Cre*I recognition site, resulting in a degenerate 22 bp palindrome sequence that prevented resolution events from occurring (J.Walker, unpublished data). As a consequence of this, the *dsx*^{GAL4} allele could not be resolved and remained as a duplication at the locus (Rideout et al., 2010).

To amend this, annealed complementary primers were used to introduce an additional *I-CreI* site into the *Bam*HI site of the targeting vector, pED22 (Dickson, B., unpublished), creating the novel parent vector pED22+*I-CreI* (Figure 3-4C; M.Neville, unpublished) used in this study. pED22+I*Cre*I contains the same elements of the original pED22 vector, except for the addition of a faithful wild-type I*Cre*I recognition site that should enable the resolution of the marker gene and subsequent generation of a true null mutant. To re-iterate, the different elements within the vector now include: i) the *mw*$^{+}$ gene as a selectable marker ii) *P*-element transposition repeat sequences at the extreme 5' and 3' ends for random insertion of the vector into the genome prior to initiating the steps of gene targeting, iii) FRT sites at the 5'

and 3' ends, internally flanking the transposition sequences, in order to mediate the excision of the construct from the genome in the first step of the gene targeting protocol, iv) the coding sequence of GAL4 and the SV40 termination sequence that lies between the second and third fragment; v) an I-*Sce*I site-specific endonuclease recognition site in order to induce a double-strand break during the first stage of the targeting process; and finally vi) a newly introduced wild-type I-*Cre*I site-specific endonuclease recognition site that serves to create a double-strand break during the second step of the targeting process (Figure 3-4C).

3.4.1.2 Cloning strategy

The exact same regions of homology that were used to generate the original pED22-*dsx*GAL4 targeting vector were used here (Figure 3-4C). The first two fragments with homology to the *dsx* genomic region were PCR amplified using the following primers (5′ to 3′): Fragment I **GGA TCC** CAC TAA ACG AGA ATC AAA AAC containing a *Bam*HI site (bold) and **TCT AGA** GAG AAA GAC CCT GCT GGC TAT CAG containing an *Xba*I site (bold), and Fragment II **CCT AGG** CTT AAA GTG GCT CTT CGG AGG containing an *Avr*II site (bold) and **GGA TCC** GAT TCC AGC TTC TGA TAT CCT A containing a *Bam*HI site (bold) (Figure 3-4A-C).

The first of the two fragments was cloned between the I*Cre*I and I*Sce*I sites of the pED22+I*Cre*I vector via complementary ends generated by digestion with *Bgl*II and *Spe*I (Figure 3-4B,C). Subsequent to this, the second fragment was cloned between the I*Sce*I recognition site and GAL4 coding sequence of the pED22+I*Cre*I vector via complementary ends generated by digestion with *Nhe*I and *Bam*HI (Figure 3-4B,C). Next, the GAL4 coding sequence and SV40 termination sequence were excised via flanking *Bam*HI and *Not*I recognition sites, and replaced with the QF coding sequence and hsp70 termination site that were obtained as a single fragment from digesting the pattB-QF-hsp70 targeting vector (Addgene, Cambridge, M.A., Plasmid No. 24368; deposited by L. Luo) with *Bam*HI and *Not*I (Figure 3-4C,D). The last cloning step involved the introduction of the third fragment. Rather than PCR amplification, this fragment was excised from the original pED22-*dsx*GAL4 vector via flanking *Not*I recognition sites, and cloned downstream of the hsp70 termination

sequence (Figure 3-4B,C) generating the final pED22-*dsx*QF donor construct (Figure 3-4D). Each fragment that was PCR amplified was done using high-fidelity Phusion polymerase to ensure no alterations in the predicted sequence (New England Biolabs). The PCR products were then purified and cloned into the TOPO-TA Cloning vector (Invitrogen) for sequencing. Sequencing confirmed no missense or nonsense mutations were induced during PCR amplification. The junctions of the QF + hsp70 insert and those of the third fragment were sequenced directly from the final construct, to ensure precise ligations (data not shown). Further confirmation of the final pED22-*dsx*QF came from restriction enzyme digestion analyses (data not shown).

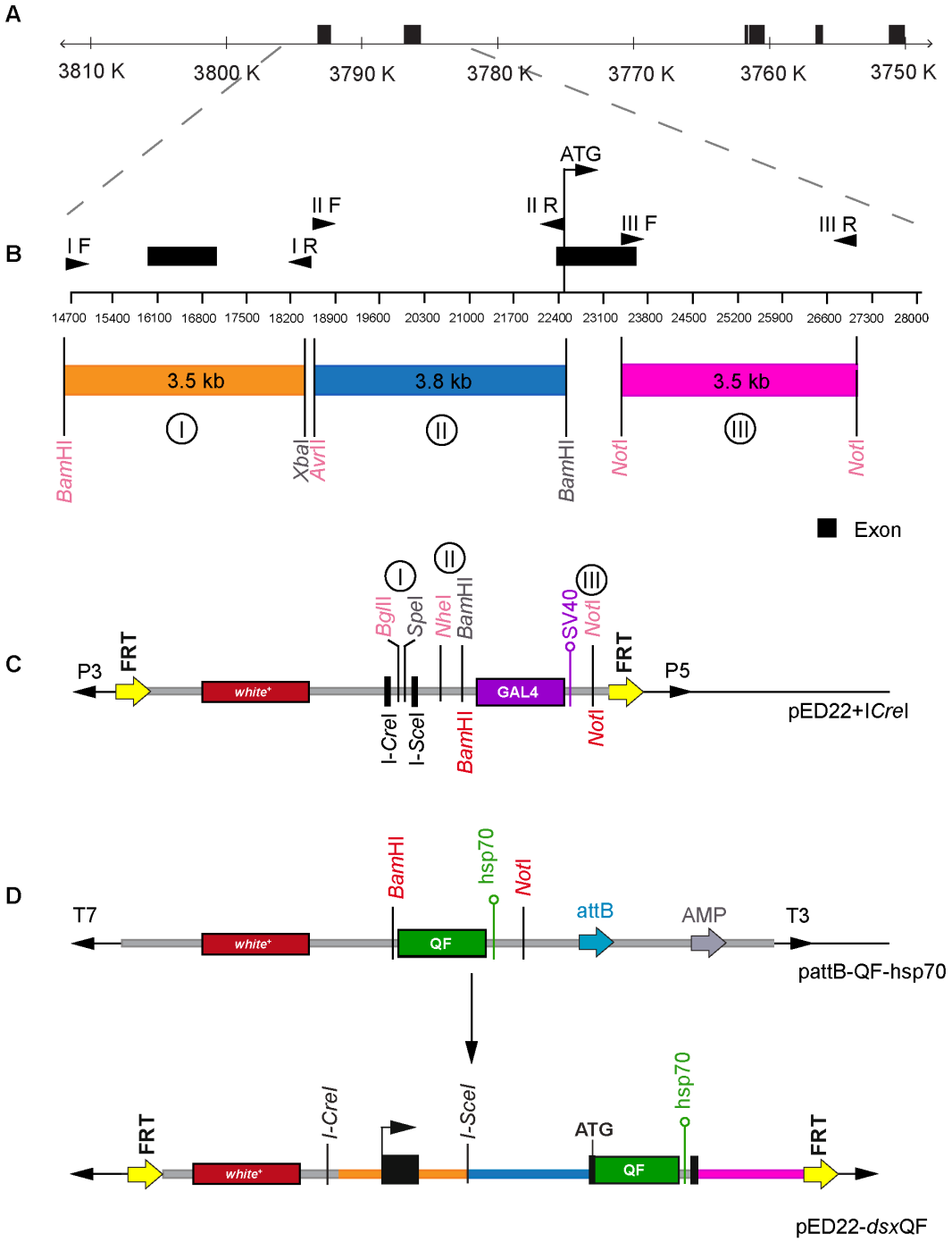


Figure 3-4 Cloning strategy of QF donor construct of ends-in homologous recombination.
(A) Entire dsx locus from which regions of homology were isolated. Black boxes indicate exons. (B) Closer view of the region surrounding the first two exons, shown as different coloured boxes, from which the fragments of homology were amplified. Forward (F) and reverse (R) primers for each of the three fragments of homology are shown, while each pair of restriction sites incorporated into the forward and reverse primers are shown in pink and grey. The size of each fragment to be inserted into targeting vector pED22+I*Cre*I is shown. (C) The pED22+I*Cre*I targeting vector is identical to the original pED22 targeting vector (B.Dickson) with the exception of a newly replaced I*Cre*I site (M. Neville). In order to ligate the *dsx* fragments into pED22+I*Cre*I, restriction sites with compatible ends were used for fragment I (orange box) and II (blue box), shown in the corresponding pink and grey; while fragment III (pink box) is inserted using an endogenous *Not*I site shown in pink. (D) pattB-QF-hsp70 vector was used to excise QF and hsp70 sequences via digestion with *Bam*HI and *NotI* (shown in red). Replacement of GAL4 and SV40 terminator with QF and hsp70 terminator was made possible via a corresponding *Bam*HI and *Not*I sites in pED22+I*Cre*I (shown in red). (E) Final targeting construct is called pED22-dsxQF. This was achieved following sequential cloning of the following fragments: fragment I, fragment II, QF + hsp70, and finally fragment III.

3.4.2 GAL4-DBD donor construct

3.4.2.1 Parent vector

The original *dsx*^{GAL4} donor vector pED22-*dsx*GAL4, created by Rideout et al. (2010), was used as the backbone/template for the generation of the *dsx*$^{GAL4\text{-}DBD}$ donor construct (Figure 3-5A). This original *dsx*^{GAL4} donor vector consists of i) the *mw* selectable marker ii) *P*-element transposition sequences at the extreme 5' and 3' ends for random insertion of the vector into the genome prior to initiating the steps of gene targeting, iii) FRT sites at the 5' and 3' ends, internally flanking the transposition sequences, in order to mediate the excision of the construct from the genome in the first step of the gene targeting protocol and iv) three regions of *dsx* homology that are a minimum of 3.5 kb in size sequentially cloned into three different multiple cloning sites (Figure 3-5A). Rideout et al., (2010) chose to replace the first coding exon of *dsx* with GAL4, while preserving the splice donor site at the 3' end of this exon in order to maintain the sex-specific splicing that occurs downstream of this exon. To accomplish this, two regions of homology were chosen immediately upstream of the translational start site, while the third region included the splicing enhancers at the 3' end of this first coding exon (Rideout et al., 2010). Additional features include v) the coding sequence of GAL4 and the SV40 termination sequence inserted between the second and third fragment; vi) an I-*Sce*I site-specific endonuclease recognition site lying between the first and second regions of homology in order to induce a double-strand break during the first stage of the targeting process; and finally vii) an I-*Cre*I site-specific endonuclease recognition site lying between the third region of homology and the *mw*$^{+}$ marker gene, to create a double-strand break during the second step of the targeting process in order to resolve the gene duplication (Figure 3-5A). As previously stated, this I-*Cre*I recognition site consisted of polymorphisms in the conserved and non-conserved regions of each half-site, resulting in a degenerate 22 bp palindrome sequence that prevented resolution events from occurring (J.Walker, unpublished data). As a consequence of this, the *dsx*^{GAL4} allele could not be resolved and remained as a duplication at the locus (Rideout et al., 2010).

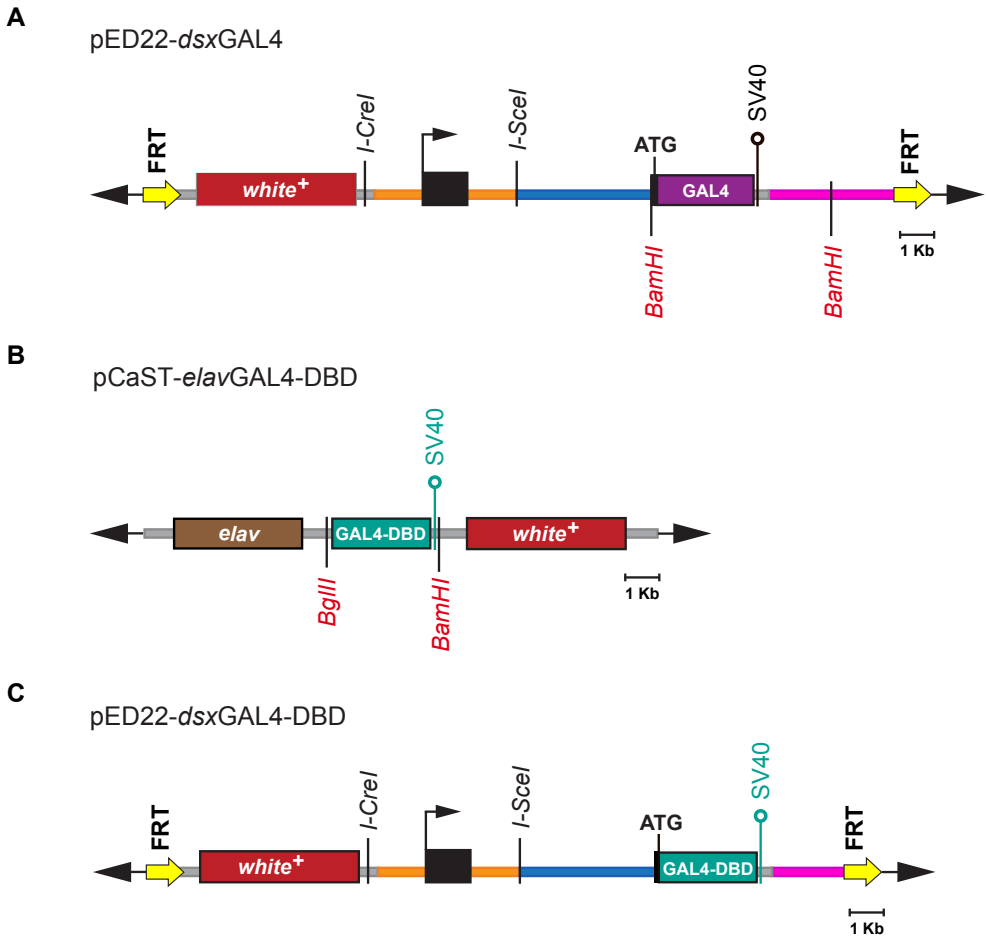


Figure 3-5 Single-step cloning strategy of GAL4-DBD donor construct for ends-in homologous recombination.
(A) Original pED22-*dsx* donor targeting vector used for the generation of the *dsx*^{GAL4} allele. The three regions of *dsx* homology are included (fragment I as orange box, fragment II as blue box, and fragment III as pink box) in addition to the GAL4 coding sequence (purple box) and SV40 termination sequence. First step involved excision of GAL4, SV40 and ~1.7 kb of fragment three, via flanking *BamH*I recognition sites (B) The pCaST-*elav*GAL4-DBD vector used to excise GAL4-DBD coding sequence and SV40 termination sequence (shown in green) via flanking *Bgl*II and *Bam*HI recognition sites (B. White). (C) Final pED22-*dsx*GAL4-DBD targeting vector; achieved by annealing compatible ends of GAL4-DBD + SV40 fragment into *Bam*HI digested pED22-*dsx.*

3.4.2.2 Cloning strategy

A single cloning step was carried out to achieve the replacement of the GAL4 coding sequence with the GAL4-DBD coding sequence (Figure 3-5). Recognition sites for the restriction enzyme *Bam*HI were used to excise a single fragment of ~5.2 kb in size that included the GAL4 coding sequence, the SV40 termination sequence and ~1.7 kb of the third region of *dsx* homology (Figure 3-5A). It is important to note that, as the remaining vector sequence consists of the degenerate I-*Cre*I site that persists in the final GAL4-DBD construct, a resolution step could not be carried out; ultimately resulting in a duplication at the locus, much like the original *dsx*^{GAL4} allele.

Typically, the double-strand break produced by I-*Cre*I at its respective recognition site is repaired by recombination between the homologous regions that flank the double-strand break, which based on the donor construct for ends-in homologous recombination, is the third region of donor to target homology (Rong et al., 2002). Hence, the fact that a resolution step could not be carried out due to the degenerate I-*Cre*I recognition site, meant that the third region of donor to target homology is expendable, given that it primarily serves to enable DNA repair during the resolution step. As such, the excision of ~1.7kb of homology from the third region of donor to target homology, should not impede homologous recombination from occurring when incorporated into the fly's genome, and should not bear a consequence on the final outcome. A second pCasT-*elav*GAL4-DBD vector (generously provided by B.White) was used to excise a 1.3 kb fragment, consisting of the GAL4-DBD coding sequence and SV40 termination sequence via recognition sites for the restriction enzymes *Bgl*II and *Bam*HI (Figure 3-5B). The resulting compatible ends were used to anneal it to the *Bam*HI digested pED22-*dsx*GAL4 construct, resulting in the generation of the final pED22-*dsx*GAL4-DBD (Figure 3-5C). The GAL4-DBD + SV40 insertion was sequenced directly from the final construct, to ensure correct sequence and orientation (data not shown). Further confirmation of the final pED22-*dsx*GAL4-DBD came from restriction enzyme digestion analyses.

3.4.3 *P*-element transformation of donor constructs

Prior to initiating the process of targeting either the insertion of GAL4-DBD or QF into the *dsx* locus, the donor constructs, pED22-*dsx*GAL4-DBD and pED22-*dsx*QF, must first be inserted randomly into the genome by *P*-element transformation (Engles, 1989). Each construct was microinjected into embryos of a w^{1118} strain with an immobile helper plasmid capable of producing the *P* transposase (Genetic services Inc.; Cambridge, MA). The transposase acts on the inverted repeat transposition sequences within each donor construct, facilitating its integration into random chromosomal sites of the embryo's germ line. Transformants were then selected on the basis of eye colour conferred by the mw^{+} marker gene contained within each construct. The chromosome insertion of each independent transformant line was then

determined. When targeting a locus on the 3rd chromosome, as in this case, it is ideal to use a transformant with a *P*-elements donor insertion event on either the 2nd or X chromosome. This makes it easier to differentiate between events where the *P*-element has re-inserted into the original insertional locus, and events where the donor has inserted into the desired endogenous locus. In line with this, two second chromosome transformant lines (no. 35.1 and 35.2) were recovered from pED22-*dsx*GAL4-DBD injected embryos. However, multiple rounds of pED22-*dsx*QF injected embryos resulted in the recovery of only a single third chromosome transformant line (no. 67.2). As such, one of the ensuing *dsx*GAL4-DBD second chromosome transformant lines (no. 35.2) and the single *dsx*QF third chromosome transformant line were chosen to proceed with ends-in gene targeting by homologous recombination.

3.5 Generation of *dsx*^{QF} and *dsx*$^{GAL4\text{-}DBD}$ via genetic crosses

3.5.1 Integration

3.5.1.1 Crossing scheme for *dsx*^{QF}

Approximately 750 transformant virgin females (no. 67.2) were crossed to ~300 males of the genotype *y,w,hs-I-SceI,hs-FLP//Y,hs-hid* (Figure 3-6A). First instar larvae were heat shocked for 2 hr at 38°C on the 3rd day following the cross and again on the following day for 1hr. Taking in consideration the fact that the crosses in this study were set up in large bottles, rather than smaller vials, I modified the original 1 hr treatment that was implemented on the on the 3rd day that was discovered to be optimal by Rong et al. 2002, to a 2 hr heat-shock treatment. The following fly stocks were used to identify and balance all third chromosomal *mw*$^{+}$ recombinants: *y,w; ey*-FLP5*, y,w,ey*-FLP2*; Pin/CyO, y,w,ey*-FLP2*;;Ly/TM3,Sb* (Figure 3-6B-F; provided by B. Dickson). A schematic of genetics events underlying the integration of pED22-*dsx*QF into the endogenous *dsx* locus can be found in Figure 3-7. Approximately 20,000 flies were screened, and a single independent targeted recombination event that mapped to the third chromosome, was recovered. Animals from this line exhibited an overt wings-up phenotype. Multiple attempts to generate a stable stock of this integrant proved it to be impossible, as it appeared too weak to maintain a healthy stock. While the males

appeared to have reduced fertility, the main concern was that the majority of pupae were unable to eclose properly, resulting in their mortality mid-eclosion (data not shown). The few that did survive eclosion, exhibited similar or often, a more severe wing phenotype, that entailed severe defects in post-eclosion wing expansion (data not shown).

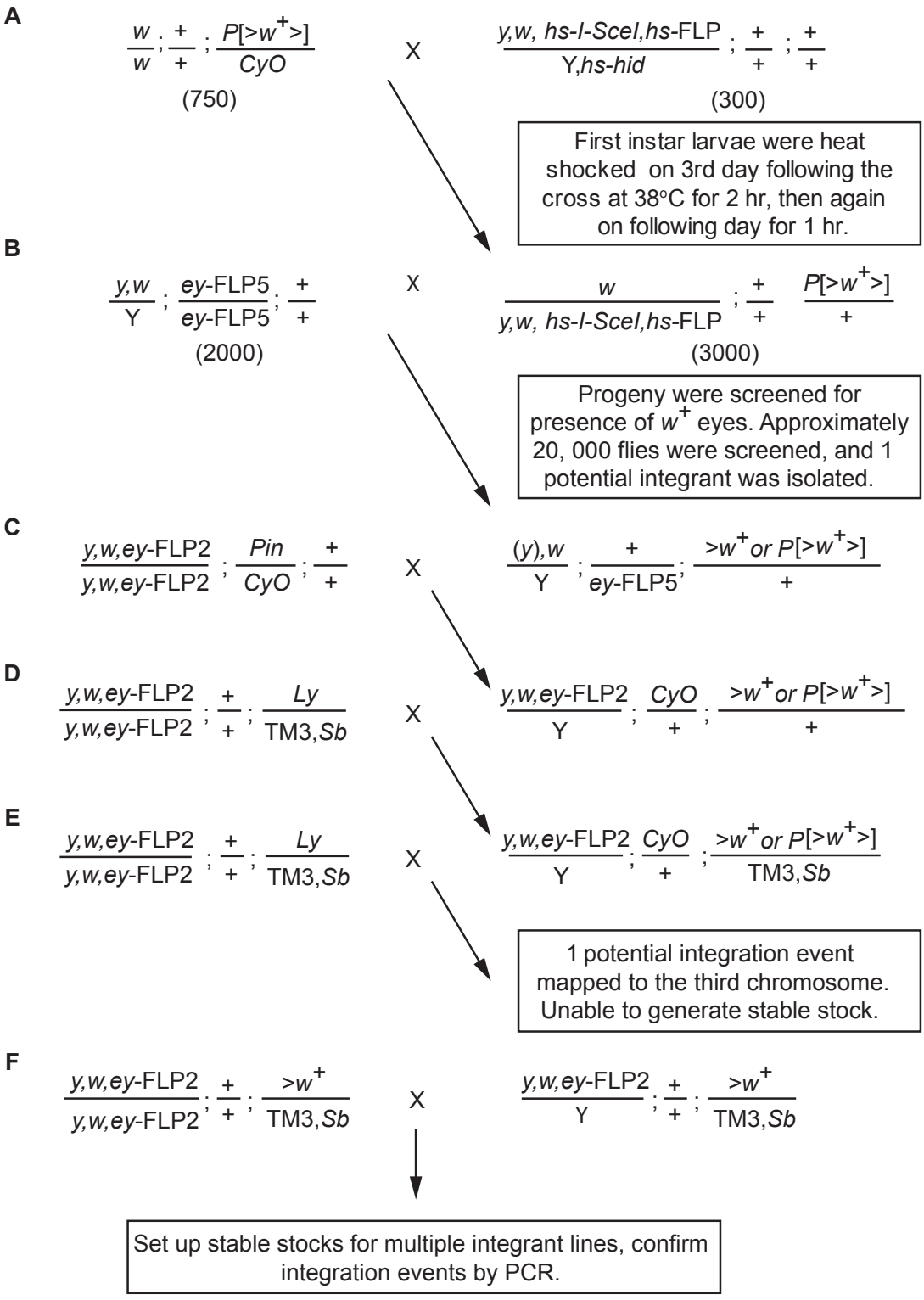


Figure 3-6 Genetic crosses to integrate QF donor construct into the *dsx* locus.
(A) First instar larvae from the first cross are heat-shocked to kill male progeny, excise *P*-element donor and make a double-stranded break; this is then integrated into the target by homologous recombination. (B) Progeny from this cross are screened for the presence of w^+ eyes from the *mw* marker gene indicating a successful integration event. (C-F) Crosses to second and third chromosome balancers to map the chromosome of insertion for all independent w^+ integrant lines. (F) Individual w^+ integrant lines that map to the third chromosome are established as stable balanced stocks. Subsequent confirmation of the insert is done by PCR. The number of flies crossed is indicated between parentheses.

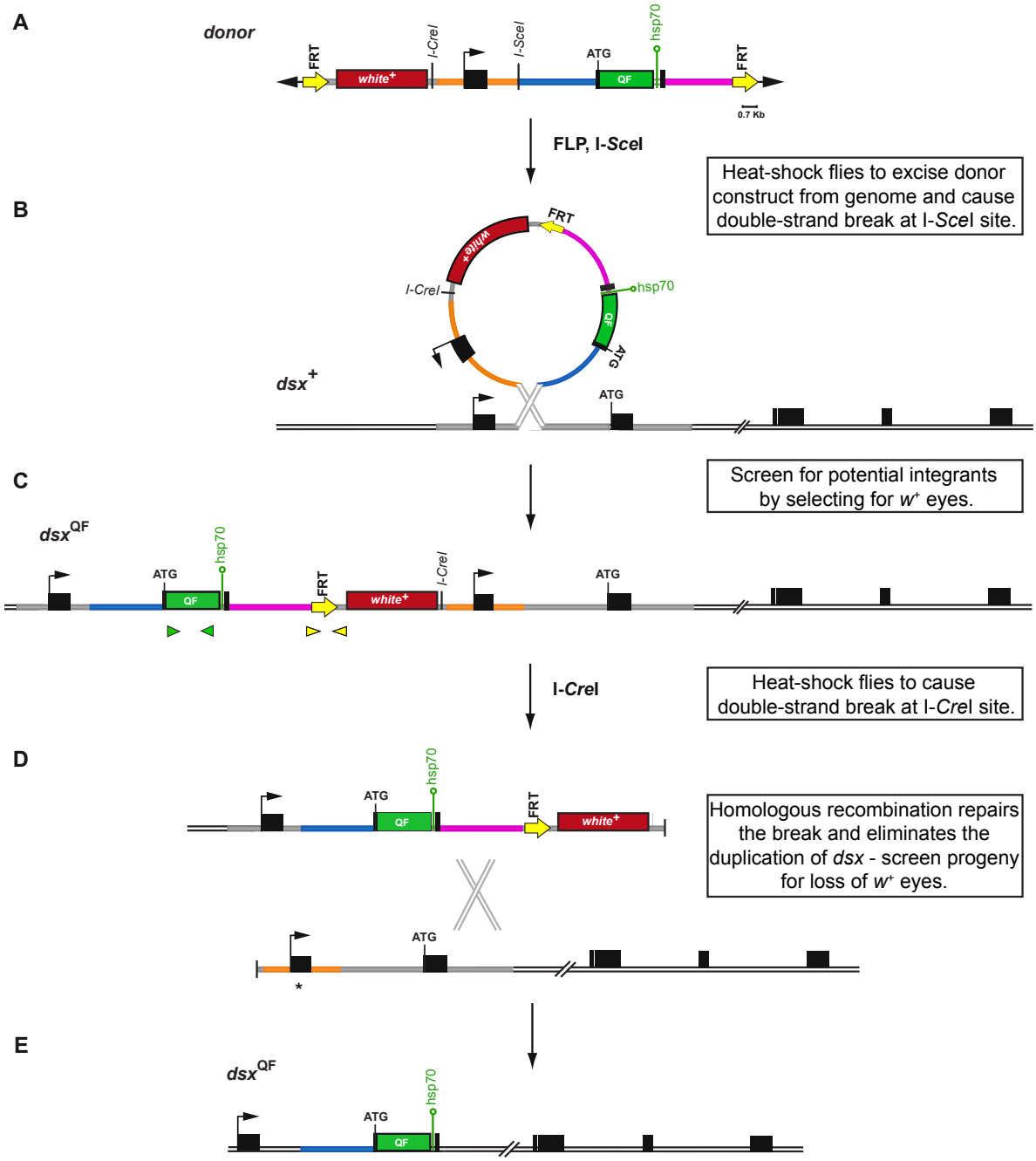


Figure 3-7 Insertion of QF into *dsx* locus by homologous recombination.
(A) 'Donor' construct pED22-*dsx*QF containing three regions of homology (in orange, blue and purple boxes), the QF open reading frame and hsp70 termination sequence (in green), the *mw*$^{+}$ marker gene (labelled *white*$^{+}$ in red box), two FLP-recombinase recognition sequences (FRT; yellow arrows), the I-*Cre*I recognition site, the I-*Sce*I recognition site, and the QF open reading frame. Solid black boxes indicate the position of exons and black arrows represent transcriptional start sites. (B) The donor sequence is excised, creating a double strand break, and linearised via *hs*-FLP and *hs*-I*Sce*I respectively. Linearised donor construct is incorporated by homologous recombination into the endogenous *dsx* locus, creating a tandem duplication (C). (D) A second double-strand break is induced via *hs*-I*Cre*I, allowing a second repair step to take place via homologous recombination. This generates the final resolved allele that no longer has the *mw*$^{+}$ marker gene (E).

3.5.1.2 Relative frequency of episomal integration for *dsx*^{QF}

Of the 20, 000 flies screened, a single independent line that exhibited an almost wild-type solid red eye colouration was recovered. Independent integrants that have precise integration events into the endogenous *dsx* locus develop gradients of orange pigmentation across their eye (as seen with *dsx*^{GAL4} and *dsx*$^{GAL4\text{-}DBD}$ - see below). Rather than exhibiting the mosaic/gradient pigmentation common to other *dsx* integrants, a deeper wild type tone that was observed here, which may be indicative of a higher level of gene expression, leakiness or even cytotoxic events that can have transcriptional impact (Rezaval et al 2007). The fact that this animal displayed an overt wing deformity, and weak fertility levels is suggestive of either imprecise integration into the third chromosome or effects of cytotoxicity and immunogenicity of the pED22-*dsx*QF vector in the endogenous *dsx* locus. Still, based on the recovery of this integrant, the estimated frequency of integration into the *dsx* locus is approximately 1 in 20, 000 gametes, which is almost double the frequency that was reported during the generation of *dsx*^{GAL4} (Rideout, 2007).

3.5.1.3 Crossing scheme for *dsx*$^{GAL4\text{-}DBD}$

Approximately 1500 transformant virgin females (no. 35.2) were crossed to ~500 males of the genotype *y,w/Y,hs-hid; Sco,hs-I-SceI,hs-FLP/CyO* (Figure 3-8). First instar larvae were heat shocked for 2 hr at 38°C on the 3rd day following the cross and again on the following day for 1hr. Again, taking in consideration the fact that the crosses in this study were set up in large bottles, rather than smaller vials, I modified the original 1 hr treatment that was implemented on the on the 3rd day that was discovered to be optimal by Rong et al. 2002, to a 2 hr heat-shock treatment. The following fly stocks were used to identify and balance all third chromosomal *white*$^{+}$ recombinants: *y,w; ey*-FLP5*, y,w,ey*-FLP2*; Pin/CyO, y,w,ey*-FLP2*;;Ly/TM3,Sb* (Figure 3-8B-F; provided by B. Dickson). A schematic of genetics events underlying the integration of pED22-*dsx*GAL4-DBD into the endogenous *dsx* locus can be found in Figure 3-9. Approximately 75,000 flies were screened, with 15 independent targeted recombination events recovered; 11 of which mapped to the third chromosome. Stable stocks for all 11 integrant lines were successfully generated.

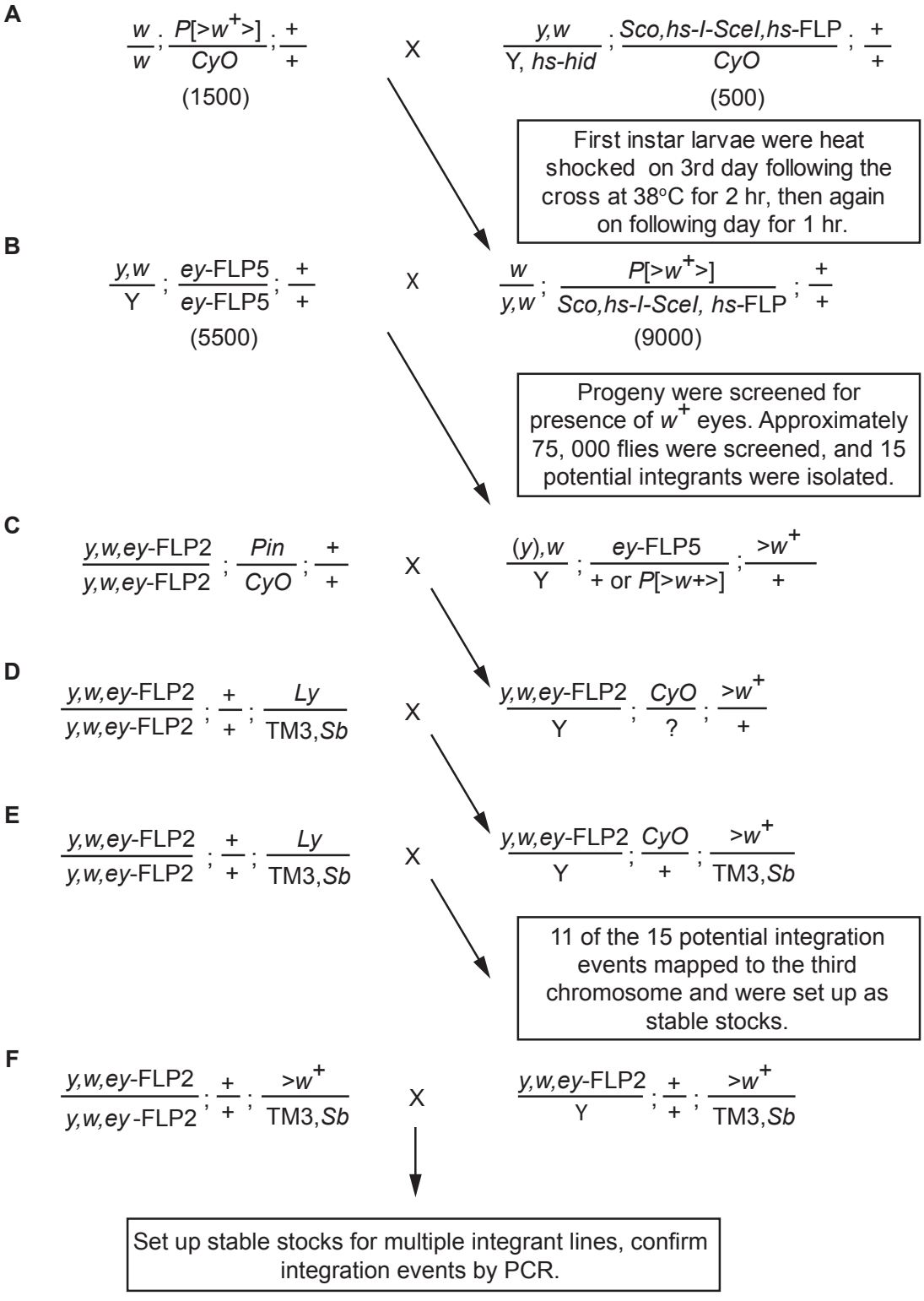


Figure 3-8 Genetic crosses to integrate GAL4-DBD donor construct into the *dsx* locus.
(A) First instar larvae from the first cross are heat-shocked to kill male progeny, excise *P*-element donor and make a double-stranded break; this is then integrated into the target by homologous recombination. (B) Progeny from this cross are screened for the presence of w^+ eyes from the *mw* marker gene indicating a successful integration event. (C-F) Crosses to second and third chromosome balancers to map the chromosome of insertion for all independent w^+ integrant lines. (F) Individual w^+ integrant lines that map to the third chromosome are established as stable balanced stocks. Subsequent confirmation of the insert is done by PCR. The number of flies crossed is indicated between parentheses.

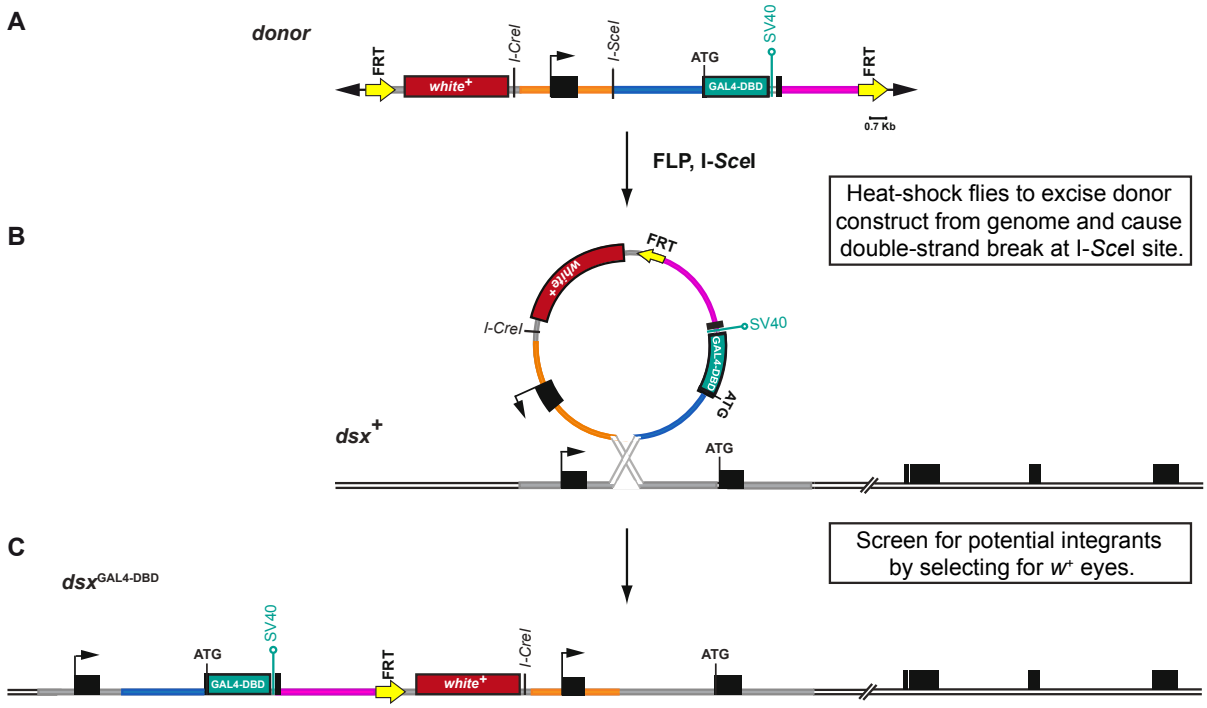


Figure 3-9 Insertion of GAL4-DBD into *dsx* locus by homologous recombination.
(A) 'Donor' construct pED22-*dsx*GAL4-DBD containing three regions of homology (in orange, blue and purple boxes), the *mw*$^{+}$ marker gene (labelled *white*$^{+}$ in red box), two FLP-recombinase recognition sequences (FRT; yellow arrows), the I-*Cre*I recognition site, the I-*Sce*I recognition site, and the GAL4-DBD open reading frame and SV40 termination sequence (in green). Solid black boxes indicate the position of exons and black arrows represent transcriptional start sites. (B) The donor sequence is excised, creating a double strand break, and linearised via *hs*-FLP and *hs*-I*Sce*I respectively. Linearised donor construct is incorporated by homologous recombination into the endogenous *dsx* locus, creating a tandem duplication (C). (D) A second double-strand break is induced via *hs*-I*Cre*I, allowing a second repair step to take place via homologous recombination. This generates the final resolved allele that no longer has the *mw*$^{+}$ marker gene (E).

3.5.1.4 Relative frequency of episomal integration for *dsx*$^{GAL4-DBD}$

Of the 75, 000 flies screened, 15 independent lines with varying degrees of orange colouration were recovered; some flies exhibited solid orange eye colouration while others possessed a gradient of orange pigmentation across the eye. This variability in independent integrant eye colour was also reported during the generation of the original dsx^{GAL4} integrant (Rideout, 2007). However, once mapping of the integrant was carried out, flies that exhibited a gradient orange pigmentation across the eye were all found to map to the third chromosome. Again, this feature had previously been reported with the original dsx^{GAL4} integrants that were recovered (Rideout, 2007). Given that the solid eye colour, displayed in 4 independent lines, was identical to the original *P*-element transformant line (no. 35.2), and given that these events mapped to the second chromosome in all 4 lines, suggests re-integration events in which the excised and linearised pED22-*dsx*GAL4-DBD donor construct

was re-inserted into its original site. Thus, based on the recovery of integrants that mapped to the third chromosome, the estimated frequency of integration into the *dsx* locus is approximately 1 in 6800 gametes. This is almost half the frequency that was reported during the generation of *dsx*^{GAL4} (Rideout, 2007).

3.5.1.5 Verification of *dsx*$^{GAL4\text{-}DBD}$ integration by PCR

Primers flanking the FRT sites (yellow arrows), and primers against the GAL4-DBD coding sequence (green arrows) were designed to confirm precise integration of the pED22-*dsx*GAL4-DBD donor construct into the endogenous *dsx* locus (Figure 3-10). The primers that flank the FRT sites do not orientate correctly in the pED22-*dsx*GAL4-DBD donor construct to be able to generate/amplify a product, whereas the GAL4 primers (blue arrowheads) will generate/amplify a product of approximately 500 bp (Figure 3-10A,B). However, when the FRT sites come together to form the circularized extrachromosomal plasmid in the first step of the gene targeting by homologous recombination, creating a duplication at the *dsx* locus upon integration (Figure 3-10B), the primers flanking the FRT sites are then orientated correctly to amplify a product of approximately 650 bp. While the GAL4-DBD primers will continue to amplify a 500 bp product, provided that GAL4-DBD has been inserted intact into the *dsx* locus (Figure 3-10A,B).

Genomic DNA was isolated from all eleven 3rd chromosomal integrant lines and the amplifications using the FRT and GAL4-DBD primer pairs were performed to verify that the two events described above had occurred (Figure 3-10C). The PCR results are shown in Figure 3-10C2 confirming that the FRT sites came together during the excision of the pED22-*dsx*GAL4-DBD donor construct from the second chromosome in each of the independent integrant lines. In addition to this, each line is demonstrated to contain intact GAL4-DBD coding sequence (Figure 3-10C1). Genomic DNA from *w*^{118}, the line into which pED22-*dsx*GAL4-DBD donor construct was microinjected, was used as a negative control for GAL4-DBD and the FRT paired primer amplification. A no DNA control was also included as a negative control (Figure 3-10C).

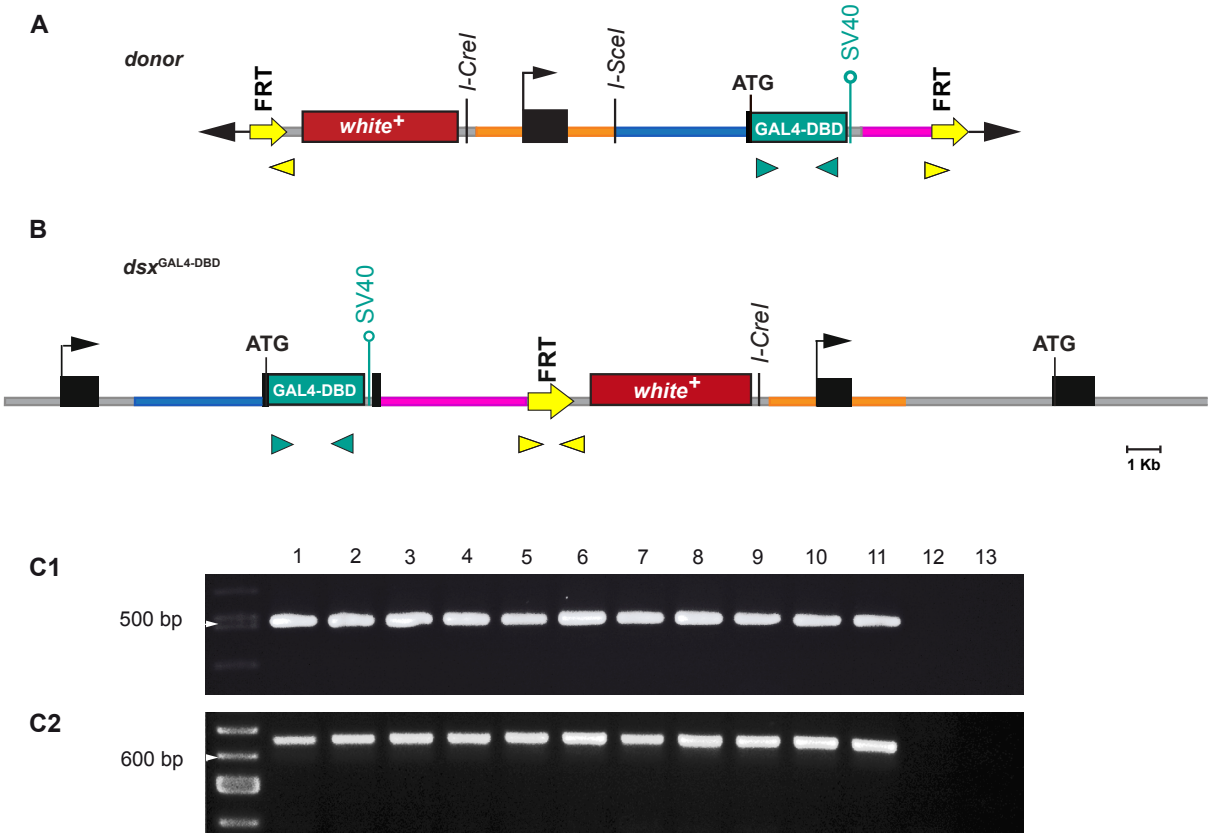


Figure 3-10 Confirmation of donor *P*-element excision and GAL4 presence in the genome by PCR.
(A) pED22-*dsx*GAL4-DBD donor targeting vector is integrated randomly into the genome by P-element transformation. FRT primers (yellow arrowheads) are not orientated correctly to give a product, whereas the GAL4 primers (blue arrowheads) will give a product of approximately 500 bp. (B) pED22-*dsx*GAL4-DBD integrated into the *dsx* locus, creating a tandem duplication. Because the FRT sites have come together to form the circularized extrachromosomal plasmid during the initial step of gene targeting, a product of approximately 650 bp should be generated with the FRT primers. (C1-2) The PCR products were run on a 2% agarose gel and visualized with ethidium bromide on a shortwave UV transilluminator to visualise successful amplification products with the GAL4 primers (C1) and the FRT primers (C2). All eleven lines potentially carrying the *P*-element donor integrated at the *dsx* locus were screened, in addition to a w^{1118} negative control strain. Lanes 1-13 loading as follows: (1-11) lines potentially carrying the integration at the *dsx* locus, (12) w^{1118} negative control strain, (13) no DNA control. 100 bp DNA ladder (New England Biolabs) is shown on far left hand side of the gel. Primers are indicated by arrowheads, and direction is also shown.

3.5.1.6 Phenotype of independent integrant fly lines

Nine out of the eleven recovered integrant lines were homozygous viable; displaying wild-type abdominal pigmentation, external genitalia and sex combs (in males) (Figure 3-11). Of these nine lines, males and females were found to be fertile (n=20 for each group) both when homozygous and heterozygous for the duplication. Strikingly, one of the lines excluded from these criteria (Line J) displays wild-type abdominal pigmentation, external genitalia and sex combs (in males) only as heterozygotes, even when ‘cantonised’ for six generations (Figure

3-12). Although homozygous animals from this line were found to be viable, they all appear intersexual, as their external abdominal pigmentation is male-like, though they lack sex combs, and possess external genitalia with aberrant morphology, which are somewhat hybrid in appearance. These homozygous intersexual animals from Line J were also found to be infertile (n=20). The final strain (named Line A) were completely homozygous inviable. When all lines were examined in *trans* with the *dsx* deficiency (*Df*(*3R*)*dsx*^{15}), neither males nor females exhibited any overt abnormalities in their morphology or external sexual characteristics, with the exception of Line J (data not shown) All animals from Line J that were examined in *trans* of (*Df*(*3R*)*dsx*^{15}) displayed intersexual external morphology, much like the features animals homozygous for the duplication.

These results confirmed that the pED22-*dsx*GAL4-DBD donor has been successfully excised from its original site of insertion on the second chromosome, and for 9/11 integrants, was now located on the third chromosome. From the evidences shown here, it seems likely that the pED22-*dsx*GAL4-DBD donor has been successfully targeted into the *dsx* locus, resulting in the generation of 9 bona fide independent tandem duplications.

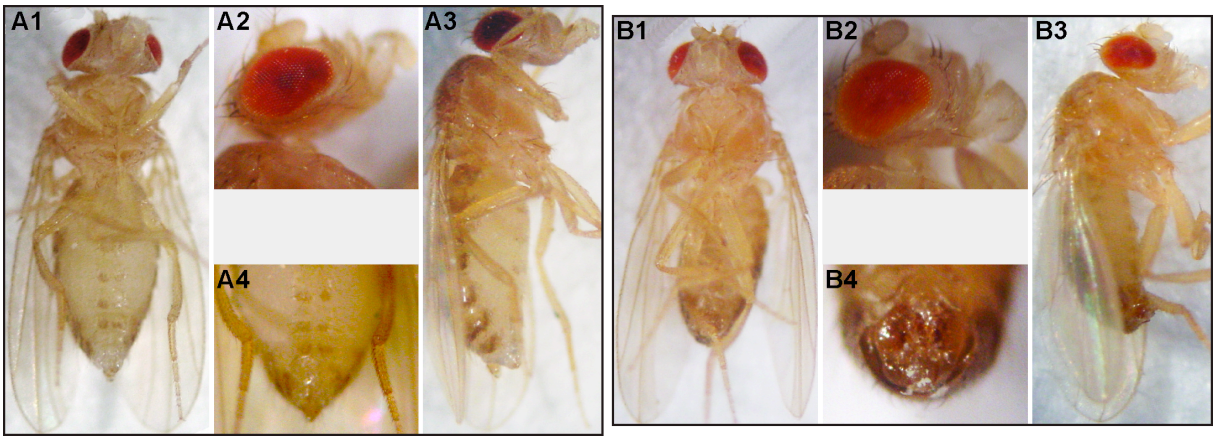


Figure 3-11 Wild-type external phenotype of flies containing a duplication at the *dsx* locus.
(A) Female external morphology; (A1). Ventral view of female external morphology; (A2). Higher magnification of compound eyes, sagittal view; (A3). Lateral view of external morphology; (A4) Higher magnification of female external genitalia, ventral view. (B) Male external morphology; (B1). Ventral view of male external morphology; (B2). Higher magnification of compound eyes, sagittal view; (B3). Lateral view of male external morphology; (B4) Higher magnification of external genitalia, ventral view. Flies shown here are homozygous for the integration at the *dsx* locus. Gradient eye colour exhibited by all integrant lines that mapped to the third chromosome, likely representing *bona fide* integration at the *dsx* locus.

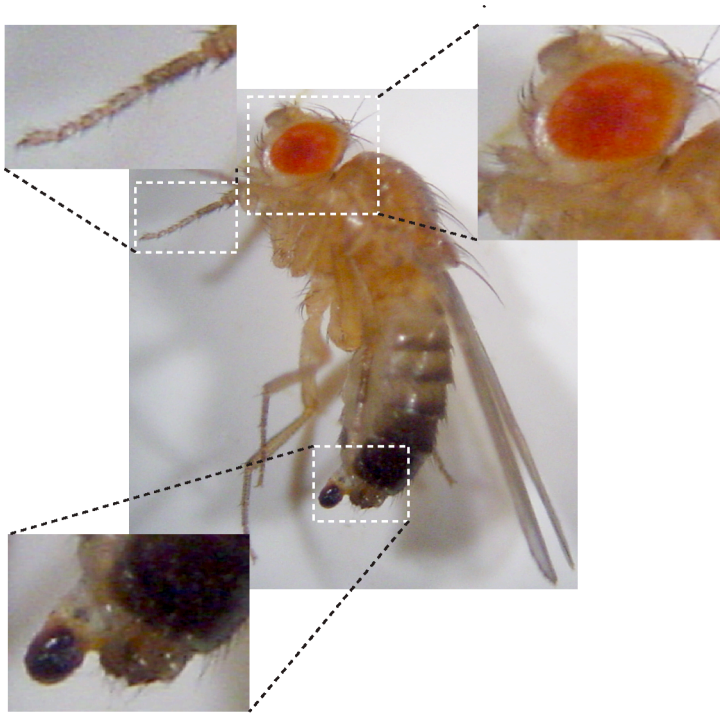


Figure 3-12 Intersexual external phenotype of flies homozygous for the duplication at the *dsx* locus from 'cantonised' line J.
Lateral view of intersexual animal. Overt intersexual external morphology can be verified based on the absence of sex combs, male-like abdominal pigmentation, and hybrid external genitalia (shown at higher magnification on the left) Gradient eye colour is exhibited here (shown at higher magnification on the right), much like the eye colour of all other integrant lines that mapped to the third chromosome, likely representing *bona fide* integration at the *dsx* locus.

3.5.2 Resolution

Eleven independent lines that consist of a duplication of the *dsx* locus as a result of the integration of the donor pED22-*dsx*GAL4-DBD targeting vector were identified, although only 9 of the 11 are considered to be completely successful. Given that the construct contains the degenerate I*Cre*I recognition site from the original pED22-*dsx*GAL4 targeting vector, the resolution of the duplication in order to eliminate the marker gene, and generate a null mutant is not an option here.

The re-design of the pED22-*dsx*QF targeting vector with a faithful I*Cre*I recognition site would have meant that a resolution step was possible, given that the integration of the donor element into the endogenous *dsx* locus was successful. However, the first step of gene targeting failed using this vector. Although a single integrant was recovered, it was impossible to maintain a healthy stock for future experimentation. Further, it appears that the rate of integration for this vector specifically was significantly lower than those reported using

pED22-*dsx*GAL4 or pED22-*dsx*GAL4-DBD (Rideout, 2007), signifying possible adverse effects resulting from the integration of the pED22-*dsx*QF targeting vector into the endogenous *dsx* locus.

3.6 Discussion

In this chapter, I have described the process of gene targeting by ends-in homologous recombination, with the aim of separately inserting GAL4-DBD and QF into the *dsx* locus. Here I demonstrated the successful generation of the novel allele called $dsx^{GAL4\text{-}DBD}$. Ideally, this novel allele should drive expression of GAL4-DBD in all *dsx*-expressing cells, and when combined with the pan neuronal hemi-driver, $elav^{VP16\text{-}AD}$, should restrict expression of reconstituted GAL4 in *dsx*-expressing neurons only. This vital tool will permit the investigation of the structure and function of *dsx*-expressing neurons within, and outwith, the CNS.

3.6.1 Approach

In this study, I employed the ends-in strategy of gene targeting by homologous recombination to insert GAL4-DBD and QF into the endogenous *dsx* locus. This strategy has been used in a number of studies to make subtle alterations in a gene of interest, and was successfully used to insert GAL4 into both the *fru* and *dsx* locus (Rong and Golic, 2000; Rong and Golic, 2001; Rong et al., 2002; Stockinger et al., 2005; Rideout et al., 2010, Robinett et al., 2010, Pan et al., 2011).

Given the proven success of the GAL4 targeting vector used to generate dsx^{GAL4} via ends-in homologous recombination, I cloned identical regions of homology, and replaced GAL4 and the SV40 termination site with QF and the hsp70 termination site, to construct the final QF targeting vector. By further incorporating a wild-type *ICre*I site, the final construct would permit the second resolution step generating a dsx^{QF} null mutant, unlike the original GAL4 targeting vector.

Having built a targeting vector that was capable of generating a null mutant, transforming the original GAL4 targeting vector into the GAL4-DBD targeting vector via a single cloning step,

served as a contingency plan in the event that the QF targeting vector did not succeed. The simple replacement of GAL4 with GAL4-DBD meant that the only difference between the new targeting vector and the original would be just that. Given the relatively high rate of integration of the original GAL4 targeting vector into the *dsx* locus, the generation of a $dsx^{GAL4\text{-}DBD}$ integrant is almost expected.

3.6.2 Modifications

The main difference between the original GAL4 targeting vector, and the QF targeting vector, that may affect the outcome is the change in the transcriptional terminator from SV40 to hsp70. This feature was carried out based on the recommendation of C. Potter, as a way of attenuating the expression of QF (C. Potter pers. comm.). Reports of toxicity were brought to light upon unsuccessful generation of tubP-QF transgenic animals (Potter et al., 2010). The authors report considerable difficulty in obtaining transgenes from microinjection or transposition, and that QF is more toxic and harmful to flies, than GAL4, when expressed ubiquitously and/or at high levels, during particular developmental stages or within particular tissues (Potter et al., 2010). This is thought to occur as a consequence of repressing/obstructing the transcriptional machinery.

In light of this, it appears that the failure of the QF targeting vector could be attributed to the manifestation of any one of the pathologies associated with the Q system. From the difficulty in obtaining transformants post-microinjection, to the intractability of achieving successful re-mobilisation to the third chromosome, to the compromised health of the only recovered integrant implies QF toxicity as the underlying problem; especially when considering the fact that *dsx* is expressed at high levels in a plethora of tissues, throughout development. Recent studies have shown that both QF and GAL4 vectors with the SV40 transcriptional terminator result in increased expression levels, when compared to those with hsp70 (Potter et al., 2010; Pfeiffer et al., 2010). As hsp70 termination sequence contains degradation sequences that cause rapid turnover in non-heat-shock conditions, replacing it with SV40 is thought to result in greater mRNA stability that results in higher protein expression levels (Petersen and Lindquist, 1989; Potter et al., 2010; Pfeiffer et al., 2010). Yet in most cases where reiteration

of endogenous gene expression is desired, increased protein expression is not necessary, nor desirable.

In the case of targeting the *dsx* locus, it appears that even utilising a stratagem designed to attenuate overall expression, the toxic effects of QF are inescapable. A recent attempt to reduce QF expression, and perhaps toxicity, involved the use of a *Drosophila* codon optimised QF cDNA (Potter et al., 2011). This modification has had a demonstrated degree of success in the generation of promoter-QF constructs that had been previously difficult to generate (such as pan-neuronal QF lines) (Potter et al., 2011). Still, alternative efforts are underway to modify the QF gene itself to reduce its toxicity when broadly expressed (C. Potter pers. comm.) As such it may be prudent to wait for these investigations to be completed prior to re-attempting targeting the QF into the *dsx* locus; especially in the practical sense, given the costs, with respect to time and effort, of employing HR stratagems, even more so if the end-results could potentially again prove to be negative.

With regards to the GAL4-DBD targeting vector, the minor difference with regards the original dsx^{GAL4} construct, besides replacing GAL4 with GAL4-DBD, was the excision of almost half of the third fragment of *dsx* homology. Given that the third region of homology primarily serves to enable homologous recombination during the resolution step, the fact that the final resolution step of the tandem duplication was not possible due to the presence of the faulty I*Cre*I site, suggests that this modification should not affect the overall efficacy of the targeting vector, Indeed, this appeared to be the case, as eleven integrants were recovered at the end of the first step of ends-in HR. Of the eleven established lines, Line A was found to be non-viable as a homozygote. This could potentially be a result of multiple integration events of the donor element in more than one site of the third chromosome, resulting in the disruption of unknown genes. Alternatively, these effects could merely be a reflection of cytotoxic and/or immunogenic effects of the donor element in the endogenous *dsx* locus. The second distinctive integrant Line J displayed intersexual external morphology when homozygosed. When placed in *trans* with the *dsx* deficiency (*Df*(*3R*)dsx^{15}*),* the intersexual phenotype persisted, suggesting that Line J consists of an imprecise integration into, and probable

disruption of, the endogenous *dsx* locus. Outcrossing these lines not only serves to isogenise their genetic background, but also aids in eliminating multiple integration events that may have occurred; yet still, the phenotypes of both line A and J persist. Uncovering the intricacies of the insertion in these two lines will require sequencing of the *dsx* locus.

The original *dsx*^{GAL4} allele, which comprises a duplication at the *dsx* locus, expresses *GAL4* transcripts that reiterate the endogenous *dsx* expression, in conjunction with endogenous gene transcripts (Rideout et al., 2010). This was shown to be distinctly different from a second *dsx*^{GAL4} allele, which presents as a hypomorph (Robinett et al, 2010). The presence of the GAL4 insert as a duplication did not affect viability, fertility, external morphology or general behaviours (locomotion/flight/smell/taste), nor did it appear to impinge upon transcription of endogenous Dsx (Rideout et al. 2010). It is expected the novel *dsx*$^{GAL4\text{-}DBD}$ allele generated in this study will behave in a similar manner to the original *dsx*^{GAL4} allele (Rideout et al., 2010).

3.6.3 Ends-in vs. Ends-out

Ends-out homologous recombination is a chosen strategy to direct the generation of null knockout or knockin mutations of the targeted gene of interest (Rong et al., 2003). The latter knockin method of creating a null mutation has been the most applied approach in the ~30 successful reports since the inception of the ends-out strategy (Supplemental Table 1 of Huang et al., 2008). This approach however, is not desirable when targeting genes with alternative splice forms, like *dsx*, as studies have shown that disrupting splicing may lead to the production of novel splice variants with unpredictable phenotypes (Manoli et al., 2005, Villella and Hall, pers. comm.). When comparing recent attempts in generating a *dsx*^{GAL4} null mutants, both ends-out and ends-in approaches have been attempted (Rideout et al., 2010; Robinett et al., 2010). The ends out approach resulted in the generation of a hypomorphic mutant, while the ends-in strategy resulted in a wild-type behaving transgenic mutant; albeit a duplication at the locus (Robinett et al., 2010; Rideout et al., 2010 respectively). The fact that an ends-in approach was more successful than ends-out in targeting the endogenous *dsx* locus, together with the fact that a number of studies that have demonstrated the

successful application of the ends-in protocol, prompted its use in this study (Egli et a., 2003; Liu and Kubli, 2003; Lankenau et al. 2003; Sogame et al., 2003; Dolezal et al., 2004; Stockinger, 2005; Kurtovic et al., 2007; Roy et al., 2007; Xu et al., 2009; Chen et al., 2010; Rideout et al., 2010, Yagi et al., 2010; Nagel et al., 2012).

3.6.4 Frequency of integration

The efficacy of targeting a donor element is locus-dependent, and can range from as high as 1 targeting event in ~1500 gametes to as low as 1 in 34,000 gametes (Rong et al., 2002). However, this frequency of integration can be improved with increased donor: target homology (Rong et al., 2002). The two targeting vectors constructed in this study, were targeting the same gene (*dsx)*, using similar donor: target homology. Yet, vast differences in the frequency of integration were found; the GAL4-DBD donor element displayed a high frequency of integration with 1 in ~6800 gametes, while the QF donor element integration occurred in 1 in ~20,000 gametes; both of which differ from the original GAL4 donor element that displayed a frequency of integration of 1 in ~12,1000 gametes (Rideout, 2007). Although these reports all fall within the range of frequencies for other loci (Rong et al., 2002), the limited number of successful reports have failed to elaborate on the efficacies of their respective targeting elements, making it difficult to assess the relative efficacy of the donor elements generated in this study. Nevertheless, the dramatic variations observed here suggest that additional factors may influence the efficacy of integration.

It is important to note that the efficiency of the ends-in method is thought to vary independently of features of the donor construct, with positional or sequence differences between target loci contributing to such inexplicable variation (Wesolowska and Rong, 2010). One such factor may be based on pre-existing chromosomal site of the donor DNA (Rong et al., 2002). That the donor element is already packaged as chromatin, which may be bound by different proteins, would influence their targeting efficacy; explaining the variation seen when using the same donor element transformed into different chromosomal sites (Rong et al., 2002). As such, there are no clear set of principles that determine, *a priori,* the efficacy of any given gene targeting construct.

3.7 Conclusion

In this chapter, I present my attempts to generate two independent tools (*dsx*$^{GAL4\text{-}DBD}$ and *dsx*^{QF}) via the insertion of the coding sequence of the yeast transcription activator GAL4, and the fungal transcription activator QF, into the first, non-sex-specific, coding exon of *dsx.* These tools should theoretically be able to direct expression of GAL4-DBD or QF in all *dsx*-expressing cells. I describe the construction of the two targeting vectors and their random insertion into the genome via *P*-element transformation. Following this I describe the process by which they were excised from the genome and integrated into the endogenous *dsx* locus. I report the successful integration of both vectors. Unfortunately, subsequent to these events, the only recovered *dsx*^{QF} integrant was not able to maintain a healthy stock, and was therefore lost. However eleven *dsx*$^{GAL4\text{-}DBD}$ integrants were recovered and verified by PCR; of these eleven independent events, one was shown to be homozygous lethal and a second as homozygous intersexual.

In the following chapter I will describe the selection of one of the remaining nine *dsx*$^{GAL4\text{-}DBD}$ integrants which was then combined with a pan neuronal hemi-driver, in order to validate via comprehensive extensive genetic analyses that the associated expression patterns of GAL4-DBD were restricted to *dsx*-neurons. I will also describe the detailed neuroanatomical characterisations carried out of *dsx*-expressing neurons in the PNS; a task that had, up to this point, proved genetically intractable given then limitations of the available genetic tools. And lastly, I will describe how this novel tool was employed to parse *dsx* circuitry into functional units underlying the sub-behaviours of male courtship behaviours.

4 Characterisation of the novel *dsx*$^{GAL4\text{-}DBD}$ allele

4.1 Introduction

To distinguish the effects of *dsx*-expressing neural circuitry in the specification of male and female courtship behaviours, from those mediated by *dsx*-expressing somatic tissues, I have generated a novel intersectional *dsx*$^{GAL4\text{-}DBD}$ allele that should, theoretically, gain genetic access to *dsx*-expressing neurons exclusively, when combined with the pan neural hemi-driver *elav*$^{VP16\text{-}AD}$ (Luan et al., 2006). In this chapter, I demonstrate the validity of the *dsx*$^{GAL4\text{-}DBD}$ allele as a reporter of endogenous *dsx* neural expression, revealing novel patterns of *dsx*-expressing in the peripheral nervous system (PNS), and confirm the role of *dsx* circuitry in specifying reproductive behaviours in both sexes.

I utilised the *dsx*$^{GAL4\text{-}DBD}$ allele in conjunction with the pan-neural hemidriver, *elav*$^{VP16\text{-}AD}$, to direct expression of a variety of GAL4 responsive reporters specifically in *dsx*-expressing neurons. I first performed a spatiotemporal survey of the expression of *dsx*$^{GAL4\text{-}DBD}$/*elav*$^{VP16\text{-}AD}$ within the central nervous system (CNS) of both males and females to, qualitatively and quantitatively, document the topology of expression specified by this novel allele. To assess the degree of spatial restriction offered by the intersection of these two promoters, I used the original *dsx*^{GAL4} allele, which has been previously comprehensively characterised (Rideout et al., 2010), to check the fidelity and accuracy of the novel *dsx*$^{GAL4\text{-}DBD}$ in conjunction with *elav*$^{VP16\text{-}AD}$, within a range of tissues.

While *dsx* has been shown to regulate the development of specific sense organs of the peripheral nervous system (PNS), namely those of the foreleg and genitalia, the lack of amenable reagents has previously prohibited systematic characterisation of *dsx*-expression within the PNS (Hildreth, 1965; Lee and Baker, 1998; Rideout et al., 2010; Robinett et al., 2010; Mellert et al., 2010; Mellert et al., 2012). As such, I carried out a comprehensive spatial survey of *dsx*-expression in the adult male and female PNS, revealing novel patterns of expression that are both restricted and functionally telling.

Finally, to functionally link the neuroanatomy of this novel allele to behaviour, I expressed the tetanus neurotoxin light chain (TNT) in *dsx*$^{GAL4\text{-}DBD}$ cells, which acts to disrupt synaptic activity

in neurons by acting specifically on neural synaptobrevin and assayed the resultant behavioural deficits (Sweeney et al., 1995).

4.2 Testing the fidelity of the novel *dsx*$^{GAL4\text{-}DBD}$ allele

Early studies documented the presence of *dsx* transcripts in the CNS of both males and females and, by exploiting a polyclonal anti-Dsx antibody, were able to demonstrate sexually dimorphic expression of Dsx in the CNS from late larval stages to the fully formed adult (Lee et al., 2002). Validations of this data have come from more recent studies that demonstrated a role for Dsx in establishing sexual dimorphism in the CNS, notably in males this involves a cooperation between Dsx^{M} with Fru^{M}, in an isoform dependent manner (Billeter et al., 2006b; Rideout et al., 2007; Sanders and Arbeitman, 2008; Kimura et al., 2008; Rideout et al., 2010). To gain genetic access to *dsx*-expressing cells, targeted insertion of GAL4 into the endogenous *dsx* locus was carried out, generating novel *dsx*^{GAL4} alleles (Rideout et al., 2010; Robinett et al., 2010). The comprehensive molecular, somatotopic, functional and behavioural characterisations of Rideout et al.'s *dsx*^{GAL4} transgenic line validated its ability to recapitulate endogenous *dsx* expression and thoroughly demonstrates that the exogenous insert does not impinge on endogenous *dsx* function (Rideout et al., 2010). Conversely, the presence of the GAL4 insert in the alternative dsx^{GAL4} allele (generated by Robinett et al., 2010) was shown to affect fertility, hinting at the possibility that it may be hypomorphic mutant (Robinett et al., 2010). Unfortunately however, the lack of behavioural data using this allele makes it difficult to assess the extent of loss of gene function. Furthermore, given the analogous construct design and ends-in targeting stratagem that the novel *dsx*$^{GAL4\text{-}DBD}$ allele shares with the original *dsx*^{GAL4} line, it would be most logical to neuroanatomically compare the expression pattern of *dsx*$^{GAL4\text{-}DBD}$ in combination with *elav*$^{VP16\text{-}AD}$ with that of the original Rideout et al. (2010) *dsx*^{GAL4}. As such, I carried out a series of comparisons, within and outwith the CNS, using various genetic reporters, to systematically assess the similarities and differences in expression patterns between the two transgenic expression systems.

4.2.1 Pairing *dsx*$^{GAL4\text{-}DBD}$ with *elav*$^{VP16\text{-}AD}$ faithfully recapitulates *dsx*^{GAL4} expression in the adult CNS

Dsx is expressed in both the male and female adult CNS in identifiable small clusters of neurons (Lee et al., 2002; Billeter et al., 2006b; Rideout et al., 2007; Sanders and Arbeitman, 2008; Rideout et al., 2010; Robinett et al., 2010). In males, 5 clusters of neurons reside in the posterior brain (pC1, pC2, pC3, aDN and SN; Figure 4-1A), 2 clusters in the pro- and mesothoracic ganglia (Prg and Msg respectively) (TN1 and TN2; Figure 4-1C) of the ventral nerve cord (VNC), and a single large cluster of neurons in the abdominal ganglion (Abg; Figure 4-1C). In females, there are only 4 corresponding clusters of neurons within the posterior brain (pC1, pC2, pC3 and Figure 4-1B), no cells in the pro- and mesothoracic ganglia, and an analogous cluster of neurons in the Abg (Figure 4-1D). Interestingly the pC2 cluster has recently been shown to consist of two distinct clusters of cells, pC2m and pC2l, in males and not in females (Robinett et al., 2010; Dornan, 2011), that appear to contribute to separate axonal fascicles to the overall *dsx* circuitry (Dornan, 2011). As such, the correct assignment of pC2 neurons to one of the two subclasses requires the simultaneous realisation of their axons. In the absence of such data, I refer to these clusters collectively pC2. It is evident that sexual dimorphism is not limited to neural clusters being present or absent but may also be defined by a divergence in neuronal populations/numbers and the associated differences in connections that then arise (Lee et al., 2002; Sanders and Arbeitman, 2008; Rideout et al., 2010; Robinett et al., 2010).

Previous studies have demonstrated that the transcription levels derived by coupling GAL4-DBD with GAL4-AD are significantly diminished when compared with intact GAL4 (Ma and Ptashne, 1987). Even in instances in which the leucine zipper of GAL4-AD is optimised for efficient reconstitution, it remains overtly weaker than the viral VP16-AD, which promotes higher transcriptional activity, permitting even weak effector transgenes to be used at single-copy dosages (Luan et al., 2006). The initial pairing of *dsx*$^{GAL4\text{-}DBD}$ allele with the less transcriptionally active *elav*$^{GAL4\text{-}AD}$ hemi-driver resulted in weak and unfaithful expression in the adult CNS (data not shown). Thus, to test the specificity and efficacy of the novel *dsx*$^{GAL4\text{-}}$

^{DBD} allele, I used *dsx*$^{GAL4\text{-}DBD}$ in conjunction with the more potent *elav*$^{VP16\text{-}AD}$ hemi-driver to drive the expression of a GAL4-responsive transgenic reporter expressing nuclear GFP (nGFP); this was directly compared to the expression of nGFP using *dsx*^{GAL4}. This experiment demonstrated that the new pairing of *dsx*$^{GAL4\text{-}DBD}$ with *elav*$^{VP16\text{-}AD}$ directs GAL4 expression in all described *dsx*-expressing neural clusters in the adult CNS of both sexes (Figure 4-1E-H). Not only does it faithfully recapitulate endogenous *dsx*-expression, it does so at an even stronger level than that of intact GAL4. Based on the Dsx expression patterns documented by Lee et al. (2002), both the original and novel *dsx* drivers do not entirely reiterate endogenous *dsx*-expression (Rideout et al., 2010). However, given their identical iterations of *dsx*-expression, our novel *dsx*$^{GAL4\text{-}DBD}$ allele, much like the original *dsx*^{GAL4} driver, compellingly demonstrates its sensitivity and specificity as a reporter of *dsx* neurons (Figure 4-1).

4.2.2 Pairing *dsx*$^{GAL4\text{-}DBD}$ with *elav*$^{VP16\text{-}AD}$ faithfully recapitulates *dsx*^{GAL4} neural architecture in the adult CNS

To further test the specificity and efficacy of the *dsx*$^{GAL4\text{-}DBD}$ allele, I crossed this line to *elav*$^{VP16\text{-}AD}$, in the presence of the cytoplasmic enhanced GFP (*UAS-EGFP*) reporter. By using a cytoplasmic reporter, neural, projection and synaptic patterns are simultaneously realised, clearly demonstrating their respective contribution to the sexually dimorphic neural architecture of *dsx*-expressing neurons. Comparison of our novel split GAL4 allele to the original *dsx*^{GAL4} allele revealed identical projection and synaptic patterning associated with these neurons in the CNS (Figure 4-2; Rideout et al., 2010). In both cases, despite the conspicuous dimorphism in neuron numbers in the brain, the topology of the projections between males and females are shown to be superficially similar, the main difference being the marked increased density of projections in males when compared to females (Figure 4-2). Our *dsx*$^{GAL4\text{-}DBD}$ allele revealed extensively connected bilateral dorsal clusters in the central brain that give rise to the lateral protocerebral complex, made up of the arch, lateral junction (LJ), lateral crescent (LC) and ring in both sexes, albeit at a largely attenuated level in female brains (Figure 4-2E,F; Rideout et al., 2010; Yu et al., 2011). Connections from the

dorsal clusters also extend to the suboesophageal ganglion (SOG), the point of termination for projections originating from gustatory neurons of the labellum and foreleg tarsi; both of which are implicated in the processing of non-volatile pheromones (Figure 4-2E,F; reviewed by Pavlou and Goodwin, 2013). Striking dimorphisms are also shown to occur in the VNC, as seen with the original *dsx*^{GAL4} allele (Figure 4-2C,D,G,H; Rideout et al., 2012). In accord with the original *dsx*^{GAL4} allele, our new allele also showed male specific *dsx*-TN1 clusters communicating directly with each other and with local TN2 cells, giving rise to the male-specific mesothoracic triangle (MsT; Yu et al., 2011), while also communicating with regions of the brain responsible for higher order processing of sensory cues via projections through the cervical connective (Figure 4-2C,G; Rideout et al., 2010). That the mesothoracic ganglion (Msg) is a neural focus for male-specific unilateral wing extension implicated in the production of courtship song is one of the many examples in which the dimorphisms in neural numbers and architecture overtly link *dsx*-expressing neurons in behaviourally relevant brain regions to different sub-behaviours of courtship (reviewed in Pavlou and Goodwin, 2013). However, the dimorphisms that lend themselves to the presence (in males) or absence (in females) of cells in the Msg of the VNC does not entirely explain the most conspicuous dimorphic feature in the VNC; the presence (in males) and absence (in females) of a trans-commissural bridge from the contralateral projections that run from the foreleg into the prothoracic region (Figure 4-2C,D,G,H). Studies have demonstrated a role for Dsx^{M} in the determination of this male-specific midline crossing of the gustatory receptor neurons (GRNs) of the foreleg (Rideout et al., 2010; Robinett et al., 2010; Mellert et al., 2010; Mellert et al., 2012). Additional dimorphic features in the neural architecture of *dsx*$^{GAL4\text{-}DBD}$-expressing cells occurs in the Abg, as there appear to be more dense projections in females than in males, comparable to the expression patterns seen with the original *dsx*^{GAL4} line (Figure 4-2C,D,G,H; Rideout et al., 2010).

In summary, *dsx*$^{GAL4\text{-}DBD}$ paired with *elav*$^{VP16\text{-}AD}$ reveals indistinguishable topographical positioning of neurons and associated projections in the adult CNS, when compared to the original *dsx*^{GAL4} allele (Figure 4-1; Figure 4-2). By constructing a schematic of the cell numbers and associated projections of *dsx* circuitry, both analogous and distinct

characteristics are easily and overtly depicted; with considerable dimorphism between males and females occurring in neural number and axonal projections in behaviourally relevant regions of the brain (Figure 4-3).

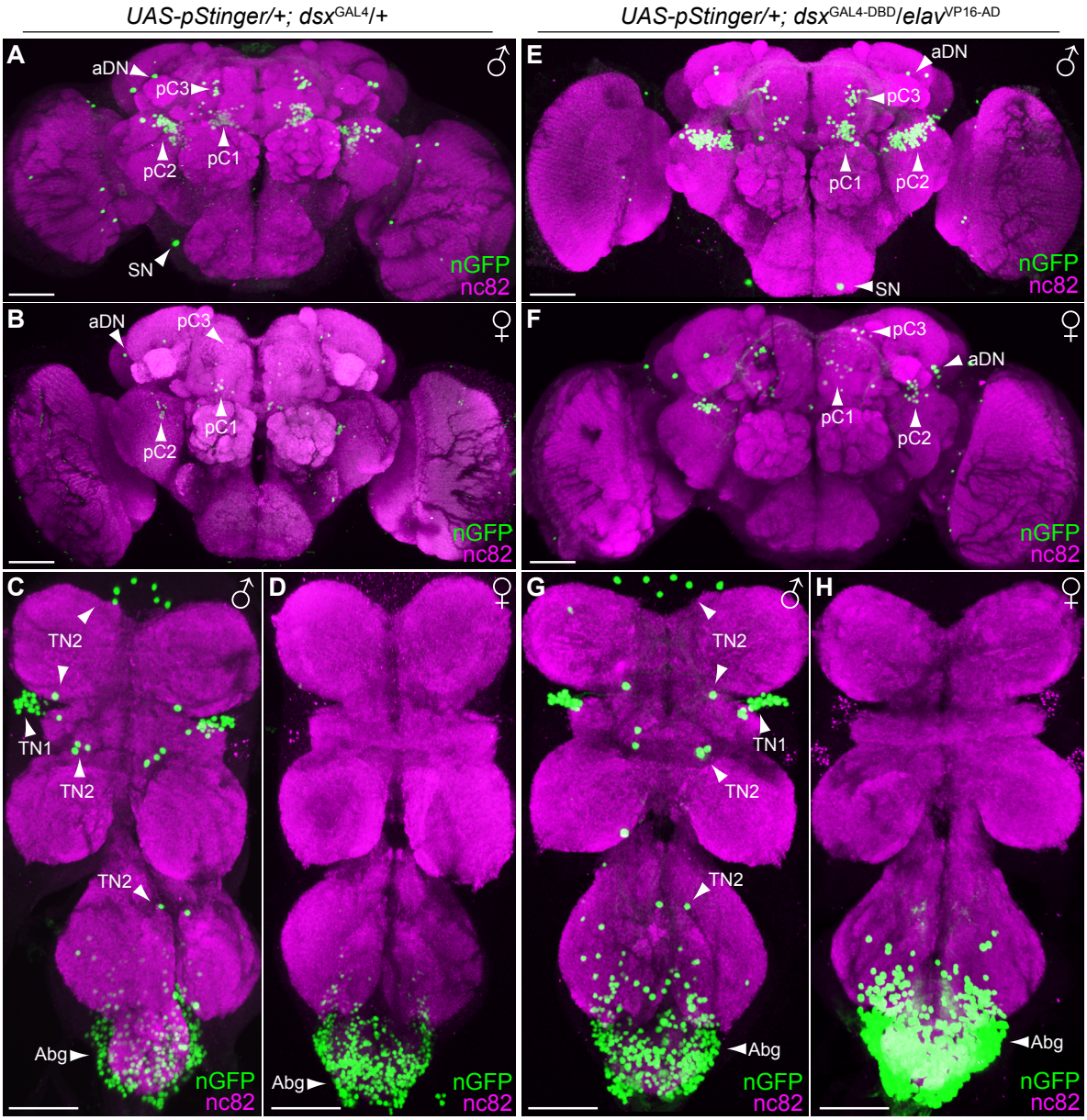


Figure 4-1 Comparison of *dsx*^{GAL4} vs. *dsx*$^{GAL4\text{-}DBD}$ paired with *elav*$^{VP16\text{-}AD}$ expressing nGFP in male and female 5 day old adult CNSs.
(A-D) *dsx*^{GAL4} expressing *UAS-pStinger* in male and female adult CNSs. (A) Adult male brain, expression in the *dsx*-aDN, -pC1,-pC2, -pC3, -SN, clusters. (B) Adult female brain, expression in the *dsx*-aDN, -pC1, -pC2, -pC3, clusters. (C) Adult male VNC, expression in the *dsx*-TN1,-TN2, and -Abg clusters. (C) Adult female VNC, expression in the *dsx*-Abg cluster. Expression is absent in the *dsx*-SN, -TN1, and -TN2 cells. (E-H) *dsx*$^{GAL4\text{-}DBD}$ paired with *elav*$^{VP16\text{-}AD}$, expressing *UAS-pStinger* in male and female adult CNSs. (A) Adult male brain, expression in the *dsx*-aDN, -pC1, -pC2, -pC3, -SN, clusters. (B) Adult female brain, expression in the *dsx*-aDN, -pC1, -pC2, -pC3, clusters. (C) Adult male VNC, expression in the *dsx*-TN1, -TN2, and -Abg clusters. (C) Adult female VNC, expression in the *dsx*-Abg cluster. Expression is absent in the *dsx*-SN, -TN1, and -TN2 cells. Cluster designation as per Lee et al., 2002 and Rideout et al., 2010. nGFP realised with anti-GFP antibody (green) and neuropil counterstained with nc82 (magenta). All views are ventral, with anterior up. Scale bar = 50 µm.

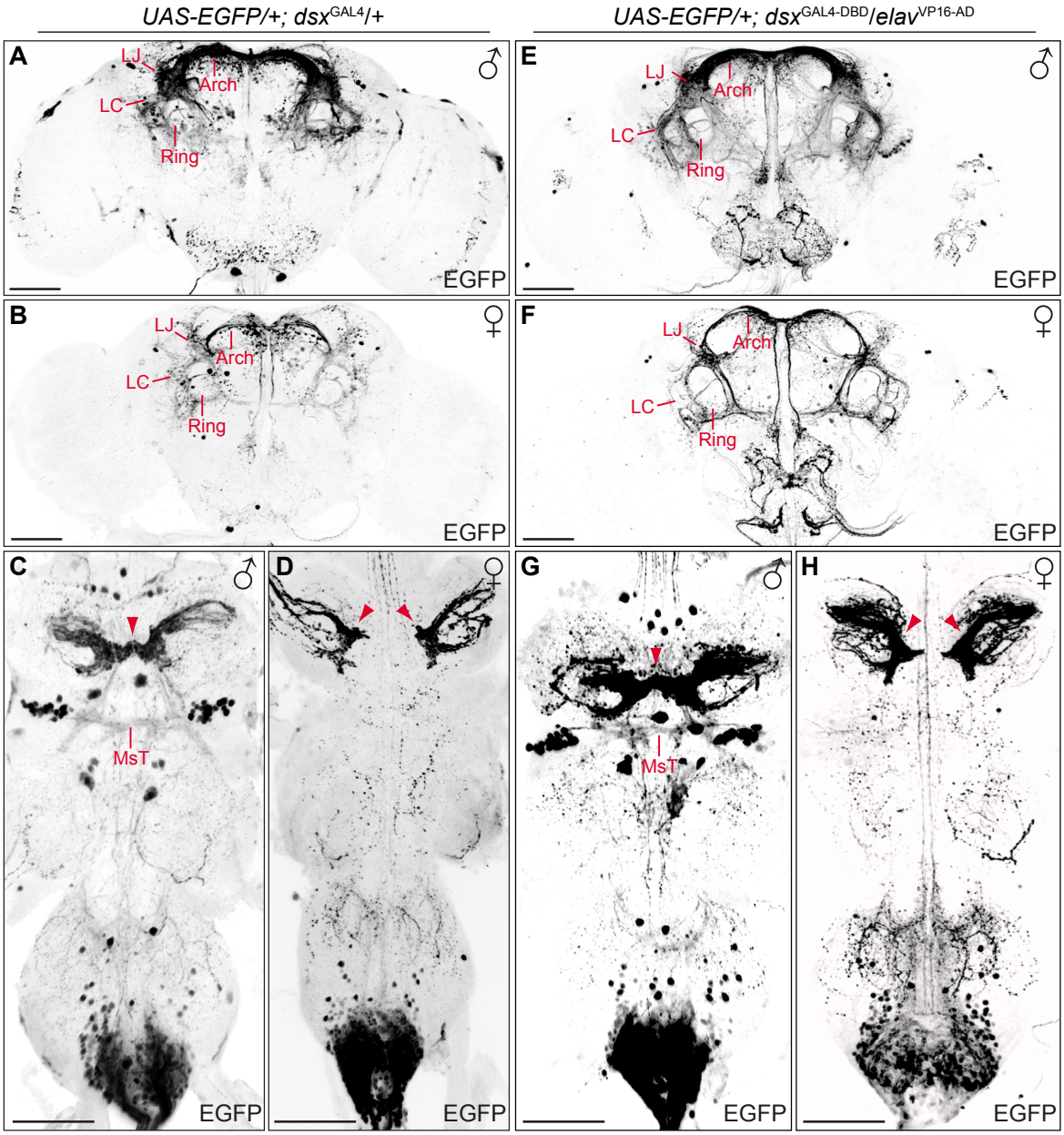


Figure 4-2 Comparison of *dsx*^{GAL4} vs. *dsx*$^{GAL4\text{-}DBD}$ paired with *elav*$^{VP16\text{-}AD}$ expressing cytoplasmic EGFP in male and female 5 day old adult CNSs.
(A-D) *dsx*^{GAL4} expressing *UAS-EGFP* in male and female adult CNSs highlighting expression in *dsx* neurons, associated projection and synapses. (A) Adult male brain, expression shows lateral protocerebral complex (B) Adult female brain, expression shows attenuated lateral protocerebral complex (C) Adult male VNC, expression shows male-specific dorsal mesothoracic triangle (MsT) and notable projections from the foreleg forming a male-specific contralateral commissural bridge (red arrowhead). (D) Adult female VNC, expression shows projections from the foreleg that fail to form a contralateral commissural bridge (red arrowheads). (E-H) *dsx*$^{GAL4\text{-}DBD}$ paired with *elav*$^{VP16\text{-}AD}$, expressing *UAS-EGFP* in male and female adult CNSs highlighting expression in *dsx* neurons, associated projection and synapses. (E) Adult male brain, expression shows lateral protocerebral complex (F) Adult female brain, expression shows attenuated lateral protocerebral complex (G) Adult male VNC, expression shows male-specific MsT and notable projections from the foreleg forming a male-specific contralateral commissural bridge (red arrowhead). (H) Adult female VNC, expression shows projections from the forelegs that overtly fail to form a contralateral commissural bridge (red arrowheads). Lateral protocerebral complex (Arch, LJ, Lateral Junction; LC, Lateral Complex; Ring) and mesothoracic triangle (MsT) indicated as per Yu et al., 2011. EGFP realised with anti-GFP antibody showing skeleton structure in black. All views are ventral, with anterior up. Scale bar = 50 µm.

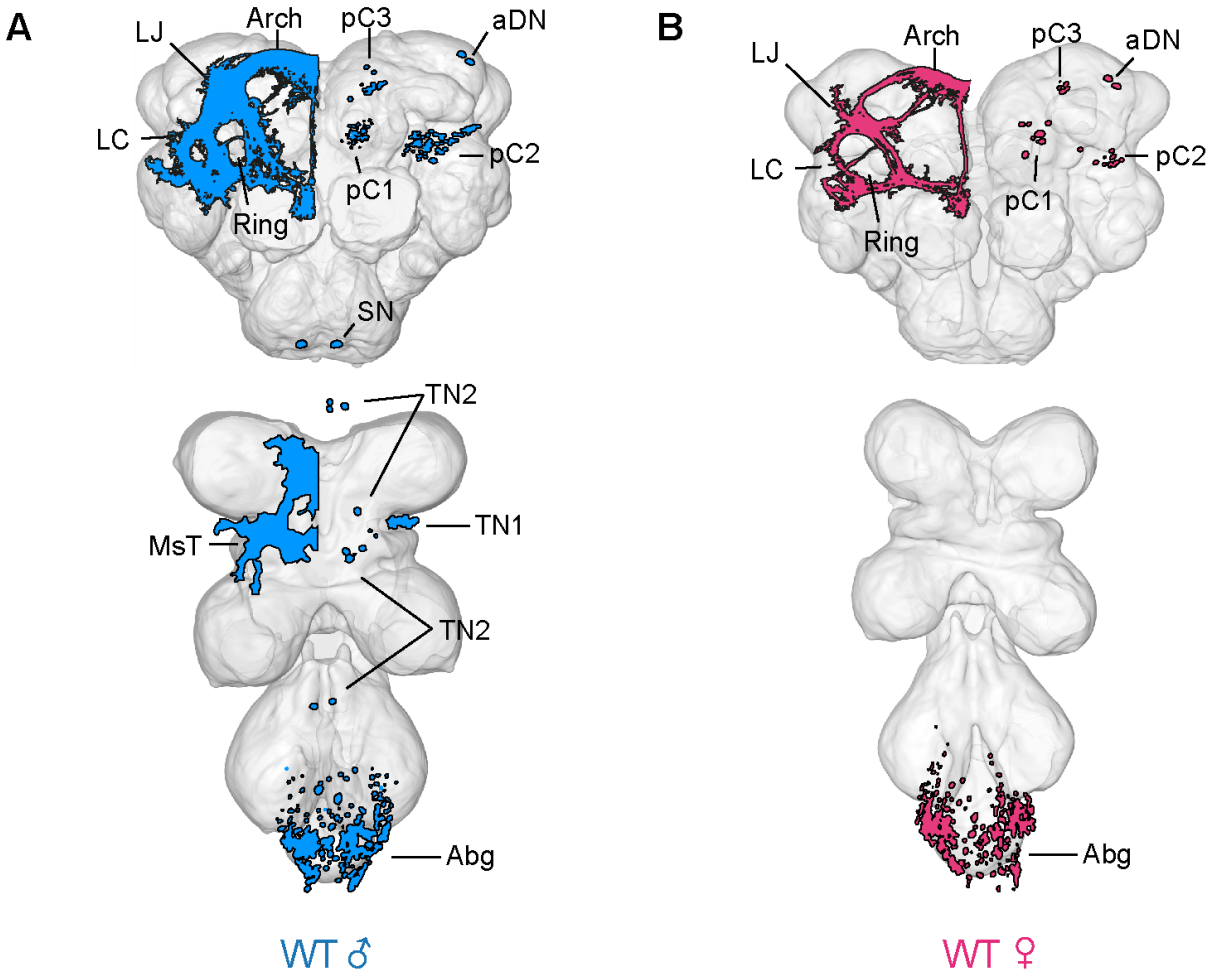


Figure 4-3 Schematic representation of *dsx*$^{GAL4\text{-}DBD}$ paired with *elav*$^{VP16\text{-}AD}$ showing topographical positioning of neurons and associated projections in the 5 day old adult CNS.
(A) Adult male CNS. (B) Adult female CNS. Neural clusters in the CNS indicated as per Lee et al., 2002 and Rideout et al., 2010. Lateral protocerebral complex (Arch; LJ, lateral junction; LC, lateral crescent; Ring) and male-specific mesothoracic triangle (MsT) indicated as per Yu et al., 2011.

4.2.3 *dsx*$^{GAL4\text{-}DBD}$/*elav*$^{VP16\text{-}AD}$ vs. *dsx*^{GAL4} expression in other somatic tissues

Based on the fact that *dsx* mutants exhibit an intersexual phenotype, genetic studies have gone on to demonstrate a central role for *dsx* in the establishment of secondary sexual characteristics in both males and females (reviewed by Christiansen et al., 2002 and Camara et al., 2008). Having focused primarily on the role of Dsx in several overtly dimorphic somatic tissues including the reproductive system, foreleg, fat body and abdomen, *dsx* has been shown to regulate non-sex-specific transcription factors and cell signalling molecules in a dynamic manner (that may depend on developmental time- or tissue-specificity); giving rise to a fully co-ordinated, mature, sexually dimorphic adult (reviewed by Christiansen et al., 2002 and Camara et al., 2008). However, the rich diversity of *dsx* function was only brought

to light through systematic spatiotemporal characterisation of *dsx* expression using *dsx*^{GAL4} transgenenic lines (Rideout et al., 2010; Robinett et al., 2010). These surveys confirmed what was inferred by previous genetic studies; that *dsx* is expressed in a restricted manner throughout the soma (Rideout et al., 2010; Robinett et al., 2010). However, when considering the presence or absence of *dsx* expression across all somatic tissues, it becomes apparent that although primarily expressed in a restricted manner, practically every somatic tissue of the developing and mature adult fly expresses *dsx* (Rideout et al., 2010; Robinett et al., 2010). It is for this reason that we generated a novel allele: to dissociate expression of the nervous system from that of somatic tissues and functionally interrogate *dsx* neurons exclusively.

Thus, in order to elucidate the extent by which our novel tool restricts *dsx*-expression, I drove the expression of EGFP using the original and the novel *dsx* drivers, comparing the expression patterns of the two drivers within various somatic tissues.

4.2.3.1 An overall view of expression in the mature adult

As a first step to interrogating the extent of restriction obtainable by the split GAL4 system, a broad, yet telling, survey of EGFP expression in whole fly preparations was carried out; systematically comparing observable expression patterns to analogous *UAS-EGFP*; *dsx*^{GAL4} flies. Using whole mount fly preparations and realising the fluorescent signals via epi-fluorescent excitation, EGFP expression from the nervous system, internal organs and peri-cuticular cells can be viewed in unison (Figure 4-4).

EGFP expression driven by the *dsx*^{GAL4} driver demonstrated the striking levels of expression in the fat body and sub-cuticular cells of the head thorax and abdomen, and in neural and non-neural cells associated with sensory organs including the legs, halteres and mouthparts, in both males and females (Figure 4-4A-E). Contrary to the expression patterns observed with the *dsx*^{GAL4} driver, *UAS-EGFP*; *dsx*$^{GAL4\text{-}DBD}$/ *elav*$^{VP16\text{-}AD}$ whole mount adult male and females are devoid of EGFP expression, with the exception of the foreleg, mouthparts and thorax of the adult male and female fly (Figure 4-4F-I). It is presumed however, that the observed thoracic signal originates from the robust EGFP expression in the VNC of the CNS.

Comparing expression patterns in the head capsule revealed broad patterns of *dsx*^{GAL4} expression in the mouthparts and pericuticular cells, with little or no expression seen in the antennae (Figure 4-4E), while *dsx*$^{GAL4\text{-}DBD}$/ *elav*$^{VP16\text{-}AD}$ driven expression revealed practically no expression in the head capsule, except for a highly restricted pattern in the labella of the mouthparts (Figure 4-4J).

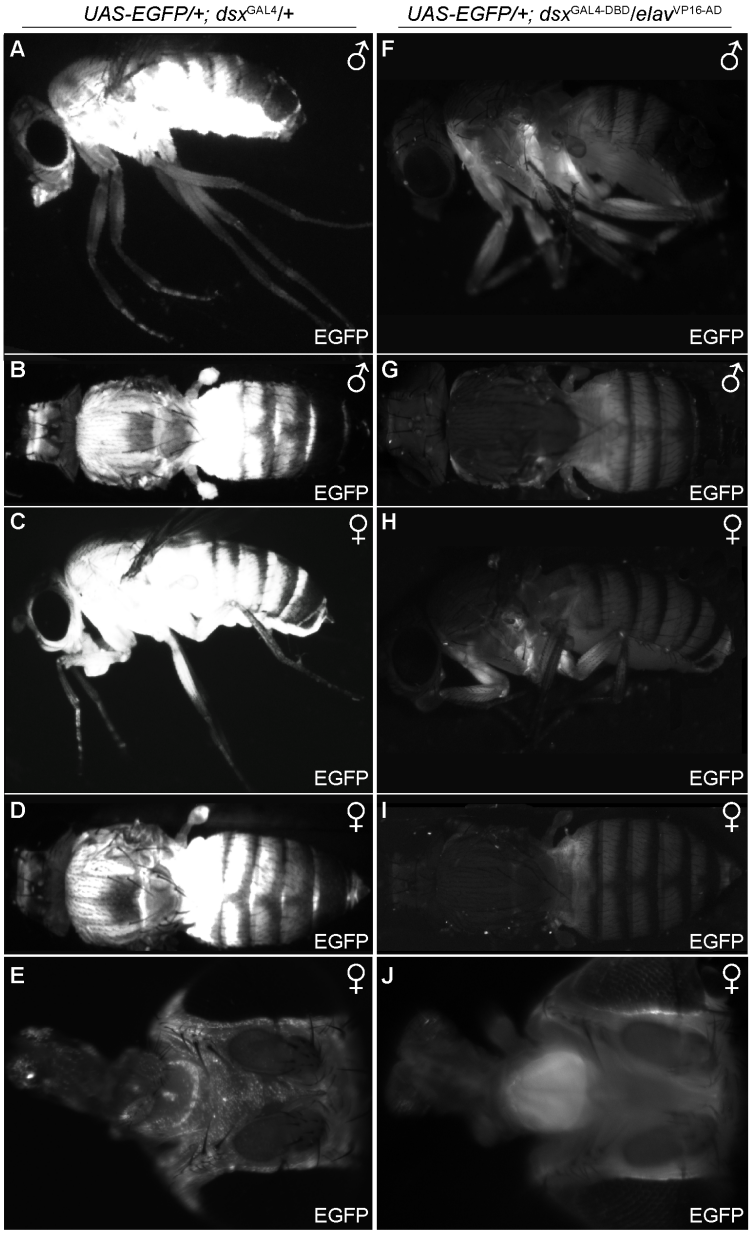


Figure 4-4 Comparison of *dsx*^{GAL4} vs. *dsx*$^{GAL4\text{-}DBD}$ paired with *elav*$^{VP16\text{-}AD}$ expressing cytoplasmic EGFP in whole mount 5 day old male and female adult flies.
(A-E) *dsx*^{GAL4} driven expression of EGFP in whole mount 5 day old male and female adult flies. Lateral (A) and dorsal (B) view of adult male. Lateral (C) and dorsal (D) view of adult female. (E) Dorsal view of adult female head. (F-J) *dsx*$^{GAL4\text{-}DBD}$ paired with *elav*$^{VP16\text{-}AD}$ driven expression of EGFP in whole mount 5 day old male and female adult flies. Lateral (F) and dorsal (G) view of adult male. Lateral (H) and dorsal (I) view of adult female. (J) Dorsal view of adult female head.

4.2.3.2 Fat body, Oenocytes and the Alimentary tract

Continuing with the comparative approach of paralleling the expression patterns of the split GAL4 driver to that of the *dsx*^{GAL4} driver, I focused on two pivotal somatic tissues that ubiquitously express *dsx*^{GAL4} from early larval stages to the mature adult: the oenocytes and fat body (Figure 4-5A-D; Rideout et al., 2010). Additional tissues of choice include those of the alimentary tract, as they appear not to differ between the sexes, and are made up of varying cell types exhibiting patterns of *dsx*^{GAL4} expression that are restricted to components parts, including the malphigian tubules and midgut (Figure 4-5E; Rideout et al., 2010; Robinett et al., 2010).

Driving EGFP expression using the *dsx*$^{GAL4\text{-}DBD}$/ *elav*$^{VP16\text{-}AD}$ hemi-drivers compellingly shows no observable expression in larval and adult FB and oenocytes (Figure 4-5F-I). However, when surveying the alimentary tract of adult males and females, restricted expression of the reporter was found to occur in the midgut, albeit in far fewer cells than those labelled with *dsx*^{GAL4} (Figure 4-5J) The continued prevalence of reporter expression in a subset of cells of the midgut is seemingly indicative of the neural nature of these cells, and through their morphology and localisation, would lead me to speculate that these cells may be *dsx*- and *elav*-expressing enteroendocrine (EE) cells. As all EE cell nuclei express the transcription factor Prospero (Ohlstein and Spradling, 2006), I further investigated this hypothesis by co-staining the gut with anti-Pros; the results of which will be discussed in section 4.3.2.3.

4.2.3.3 Reproductive system

High levels of *dsx*^{GAL4} expression are observed in a restricted manner in various tissues of the male and female internal reproductive systems (Figure 4-6A,B; Rideout et al., 2010; Robinett et al., 2010). In males this includes expression in cells associated with the epithelium of the testes, vas deferens (VD), and ejaculatory duct (EjD), as well as in secondary cells in the apex of the accessory glands (AcGl), in the muscles of the apodeme, in secretory cells of the ejaculatory bulb (EjB), and in the aedeagus (Aed) (Figure 4-6A; Rideout et al., 2010). Similarly in females, high levels of *dsx*^{GAL4} expression are observed in the lateral and common oviducts (OvL and OvC respectively), the seminal receptacles

(SmRcp), the spermathecae (Sp), uterus and paravoria (Figure 4-6B; Rideout et al., 2010), and external genital plates of both males and females (Rideout et al., 2010). Surveying split Gal4 driven EGFP revealed little or no expression in all aforementioned sites of the internal reproductive system of males, with the exception of the ejaculatory bulb and associated muscles of the apodeme (Figure 4-6C). The striking lack of reporter expression in almost all tissues of the female internal reproductive system, with the exception of the Sp and uterus is comparable to the restricted levels of expressions seen in the male internal reproductive system (Figure 4-6D). Such persistence of expression is analogous to that of the midgut, all of which are extant with the split GAL4 driver; indicating that the cells are of a neural origin.

In summary, comparing the expression patterns between *dsx*^{GAL4} and the novel split-GAL4 driver, demonstrated that the pairing of *dsx*$^{GAL4\text{-}DBD}$ with *elav*$^{VP16\text{-}AD}$ systemically targets a significantly smaller population of *dsx*-expressing cells compared with the expression exhibited with the original *dsx*^{GAL4} driver, this subset presumably restricted to neurons or cells of neural origin (Figure 4-5; Figure 4-6). The level of magnification applied in these comparative immunohistochemical experiments did not permit detailed characterisations of *dsx*$^{GAL4\text{-}DBD}$/ *elav*$^{VP16\text{-}AD}$ expression patterns at the connective or synaptic level. However, it is important to note, that although rudimentary in nature, these initial experiments have been instrumental in corroborating the restrictive capabilities of the novel Split GAL4 driver.

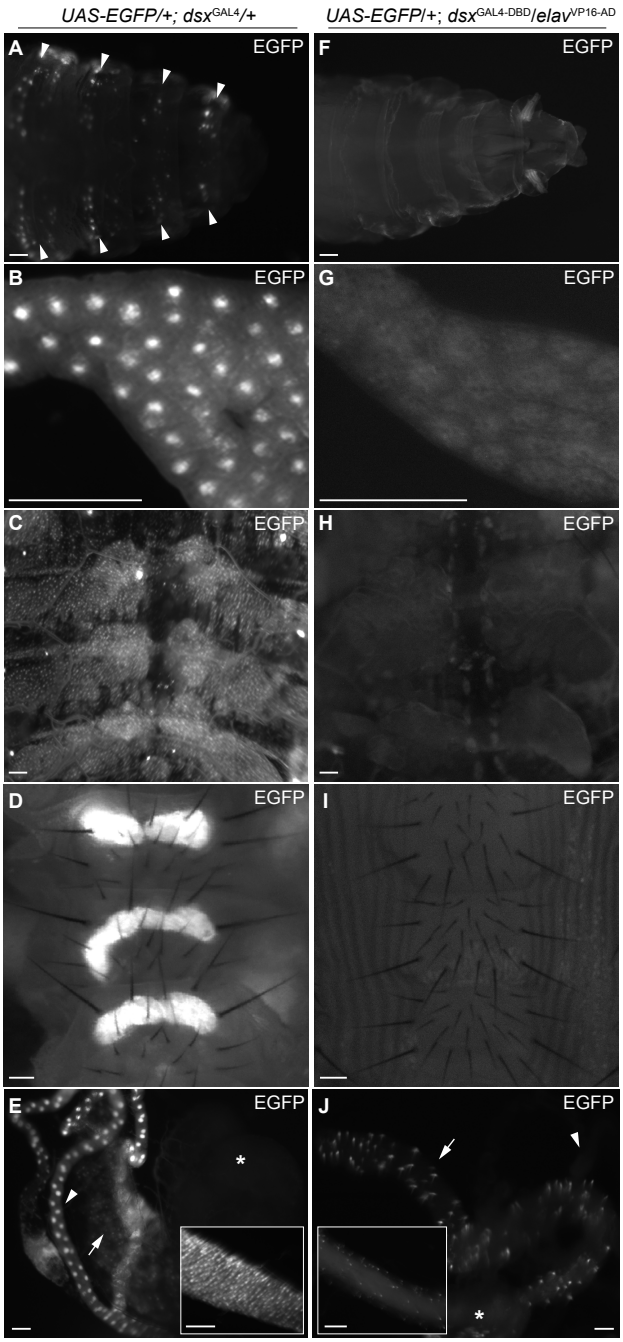


Figure 4-5 Comparison of *dsx*^{GAL4} vs. *dsx*$^{GAL4\text{-}DBD}$ paired with *elav*$^{VP16\text{-}AD}$ expressing cytoplasmic EGFP in sub-cuticular tissues and the alimentary tract of 5 day old of adult flies.
(A-E) *dsx*^{GAL4} driven expression of EGFP in 5 day old adult somatic tissues. (A) Anterior (cephalic) dorsal view of sub-cuticular cells present in each hemi-segment of late 3rd instar larva (arrowheads). (B) Late 3rd instar larval fat body (C) Ventral view of filleted dorsal abdominal wall revealing expression in adult fat body. (D) Ventral view of filleted ventral abdominal wall revealing expression in adult oenocytes. (E) Reporter expression in the adult alimentary tract including the malphigian tubule (arrowhead) and midgut (arrow), with no expression detected in the hindgut (asterix). Inset shows higher magnification of adult midgut and associated reporter expression. (F-J) *dsx*$^{GAL4\text{-}DBD}$ paired with *elav*$^{VP16\text{-}AD}$ driven expression of EGFP in 5 day old adult somatic tissues. (F) Anterior (cephalic) dorsal view of late 3rd instar larva showing a lack of reporter expression in sub-cuticular cells of each hemi-segment. (B) Late 3rd instar larval fat body lacking reporter expression. (C) Ventral view of filleted dorsal abdominal wall revealing no expression EGFP in adult fat body. (D) Ventral view of filleted ventral abdominal wall revealing no expression in adult oenocytes. (E) Reporter expression in the adult alimentary tract, showing no expression in the malphigian tubule (arrowhead) and hindgut (asterix), and expression of EGFP in a subset of cells of the adult midgut (arrow). Inset shows higher magnification of adult midgut and associated reporter expression. Cytoplasmic EGFP, white. Scale bar = 50 µm.

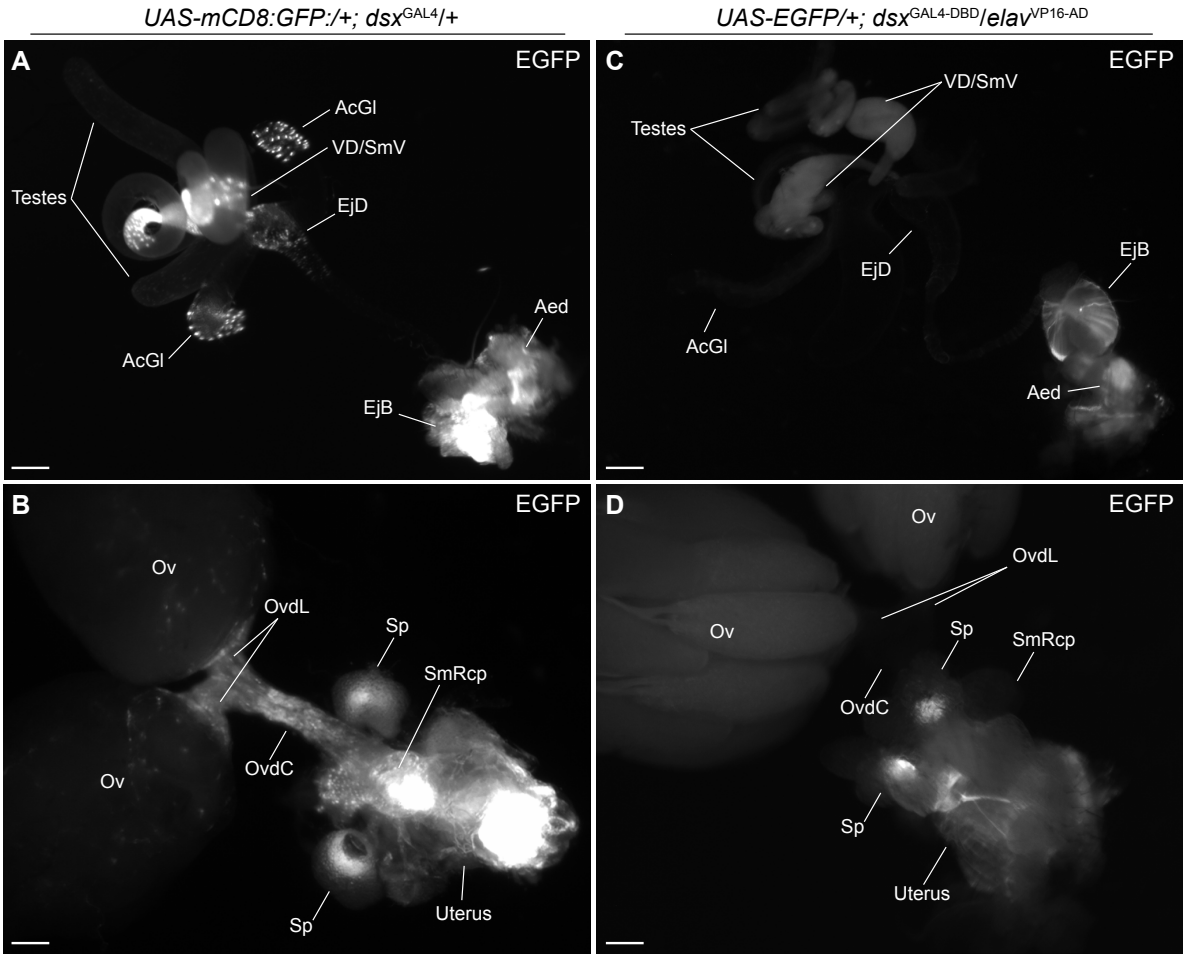


Figure 4-6 Comparison of *dsx*^{GAL4} vs. *dsx*$^{GAL4\text{-}DBD}$ paired with *elav*$^{VP16\text{-}AD}$ expressing cytoplasmic EGFP in the genitalia of 5 day old male and female adult flies.
(A-B) *dsx*^{GAL4} driven expression of *UAS-EGFP* in internal genitalia of adult male and female flies. (A) *UAS-EGFP*; *dsx*^{Gal4} male internal genitalia; expression in testes, vas deferens (VD), seminal vesicles (SmV), ejaculatory duct (EjD), secondary cells of the accessory glands (AcGl), and ejaculatory bulb (EjB) are indicated. All other expression is repressed. (B) *UAS-EGFP*; *dsx*^{Gal4} female internal genitalia; expression in ovaries (Ov), lateral and common oviducts (OvL and OvC respectively), seminal receptacle (SmRcp), spermathecae (Spt) and uterus are indicated. All other expression is repressed. (C-D) *dsx*$^{GAL4\text{-}DBD}$/*elav*$^{VP16\text{-}AD}$ driven expression of *UAS-EGFP* in internal genitalia of adult male and female flies. (C) *UAS-EGFP*; *dsx*$^{GAL4\text{-}DBD}$/*elav*$^{VP16\text{-}AD}$ male internal genitalia; expression in ejaculatory bulb is observed. All other expression is repressed. (D) *UAS-EGFP*; *dsx*$^{GAL4\text{-}DBD}$/*elav*$^{VP16\text{-}AD}$ female internal genitalia; expression in spermathecae (Spt) and uterus are observed. All other expression is repressed. Cytoplasmic EGFP, white. Scale bar = 50 µm.

4.3 Characterisation of *dsx*$^{GAL4\text{-}DBD}$/*elav*$^{VP16\text{-}AD}$ neural circuitry both within, and outwith, the CNS

I have shown that coupling the *dsx*$^{GAL4\text{-}DBD}$ hemi-driver to *elav*$^{VP16\text{-}AD}$ not only labels neurons of the CNS (Figure 4-1; Figure 4-2), but also of the PNS, evidenced by reporter expression in the gut and reproductive systems of these animals (Figure 4-4; Figure 4-5; Figure 4-6). It is important however, as a novel allele of *dsx,* and as a tool that, for the first time, is capable of reporting *dsx* expression in the PNS, to carry out a comprehensive set of characterisations

that fully validate and elucidate the particulars of the patterns of expression revealed in these initial surveys. Data from these experiments are discussed below.

4.3.1 Spatiotemporal expression of *dsx*$^{GAL4\text{-}DBD}$/*elav*$^{VP16\text{-}AD}$ in the central nervous system of males and females

Using *dsx*$^{GAL4\text{-}DBD}$ in combination with *elav*$^{VP16\text{-}AD}$, to express nGFP, I was able to systematically describe the full pattern of *dsx*$^{GAL4\text{-}DBD}$/*elav*$^{VP16\text{-}AD}$ expression in both males and females within the developing CNS (Figure 4-7; Figure 4-8; Figure 4-9). This not only served as a way of further validating the novel tool, but to again demonstrate the dynamic nature of development, beginning with a handful of cells in the larva to the final expanded dimorphic expression in the adult that sub-serves their specific behavioural outputs (Lee et al., 2002; Rideout et al., 2010; Robinett et al., 2010).

Studies have shown that *dsx*^{GAL4} specified expression is apparent in the developing gonad, and absent in the nervous system, throughout mid to late embryonic stages (Rideout et al., 2010; Robinett et al., 2010). While *dsx*$^{GAL4\text{-}DBD}$/*elav*$^{VP16\text{-}AD}$ specified expression of nGFP demonstrated the complete absence of expression in the gonads, throughout in stages 11-12 and 14-15 in the embryo, as expected these animals also lacked expression in the CNS and PNS (Rideout et al., 2010; Robinett et al., 2010); demonstrated by the lack of co-expression with the nervous tissue specific anti-HRP (Figure 4-7A-D; Jan and Jan 1982; Snow et al., 1987). Again as previously described, similar to the embryonic stages, no expression was observed in the CNS of L1 larva of either sex (Figure 4-7E; Rideout et al., 2010). In keeping with previous findings, expression becomes apparent in L2 larvae, which is restricted to a bilateral cluster of cells in the distal tip of the Abg in both males and females (Figure 4-7F; Rideout et al., 2010). Further in development, in the L3 larval stage, the pattern of expression is shown to expand to include increased number of cells in the Abg (Figure 4-7G,H; Rideout et al., 2010). At this developmental stage, this cluster appears to be the only cluster present in the VNC (Figure 4-7G,H; Arthur et al, 1998; Lee et al., 2000; Lee et al., 2002; Rideout et al., 2010). However, expression is not limited to the VNC, as expression was also observed in discrete clusters of cells in the brain; topographically consistent with the *dsx*-pC1 and *dsx*-

pC2 and *dsx*-pC3 clusters previously described (Lee et al., 2002; Rideout et al., 2010); contributing to the first instance of a noticeably dimorphic pattern of expression that exists between CNSs of the sexes (Figure 4-7G,H). No expression in cells consistent with the non sex-specific *dsx*-aDN and male-specific *dsx*-SN neurons described in pupae and adults was observed in the larval brain (Figure 4-7G,H). So far, these features are congruent with the previous descriptions of *dsx*-expression throughout these developmental stages (Lee et al., 2002; Rideout et al., 2010). The dimorphic pattern of expression exhibited in L3 larvae has been shown to continue into pupariation, with only a few clusters expanding incrementally, and with the emergence of the anteriorly positioned cells of the non-sex-specific *dsx*-aDN, in both males and females (Rideout et al., 2010). However, the most critical juncture in development is 48 hrs into pupariation, at which point the CNS undergoes rapid remodelling; metamorphosising from one that determines the behaviour of the foraging larva, to one that determines the behaviour of the mature adult (Arthur et al., 1998). At this critical stage, the male-specific *dsx*-SN, –TN2 and –TN1 neuronal clusters have been shown to appear, with continuous expansion of both male and female *dsx*-Abg neuronal clusters (Lee et al., 2002; Rideout et al., 2010). By carrying out cell counts throughout development, Rideout et al. (2010) also demonstrated that the number of neurons in the female *dsx*-Abg cluster overtakes that of the male. Altogether, these profound changes in expression in both male and female CNSs are indicative of a period that is pivotal in the sculpting of the mature sexually dimorphic neural architecture (Rideout et al., 2010).

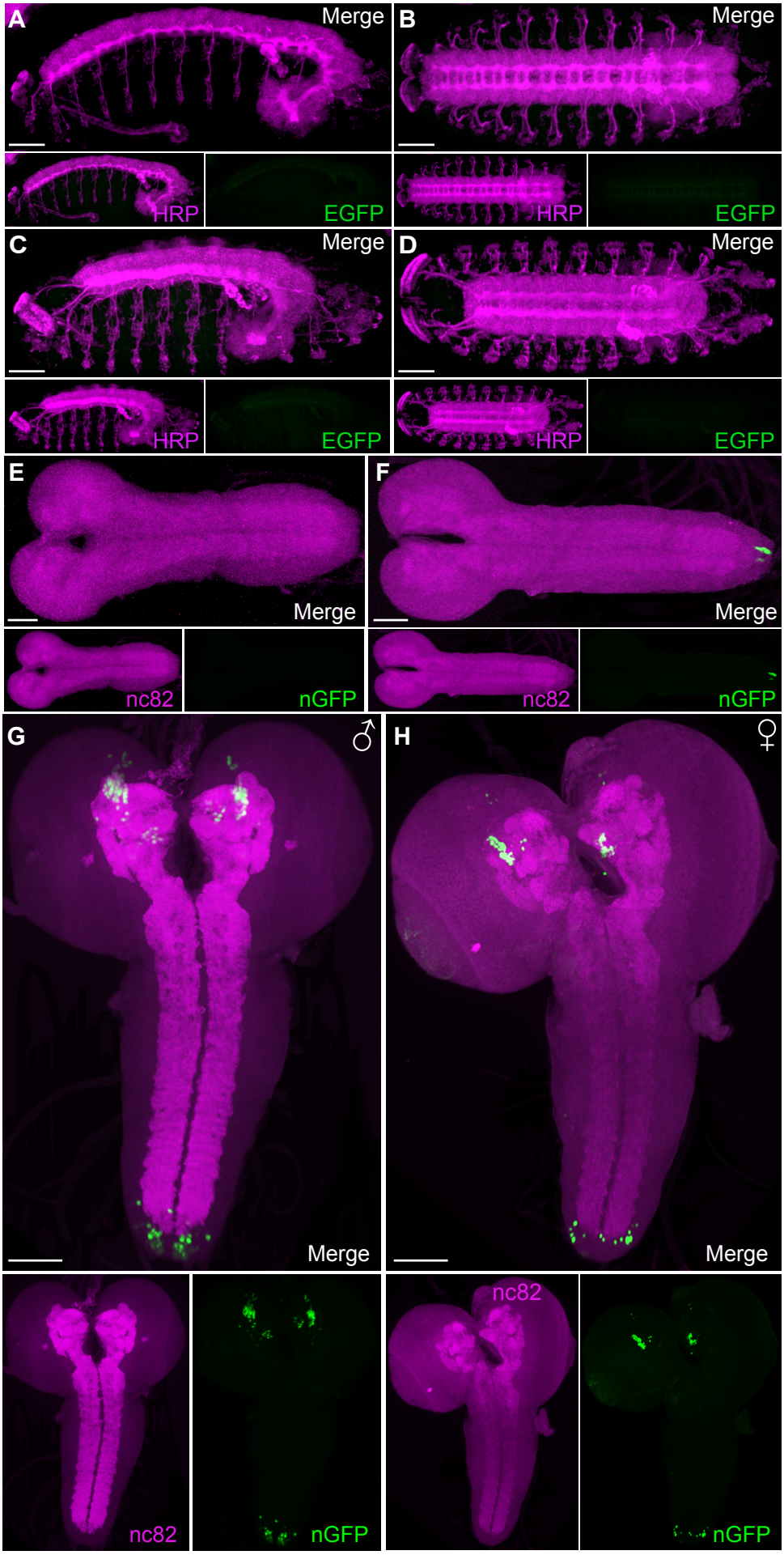

A
Merge
HRP
EGFP
B
Merge
HRP
EGFP
C
Merge
HRP
EGFP
D
Merge
HRP
EGFP
E
Merge
nc82
nGFP
F
Merge
nc82
nGFP
G
♂
Merge
nc82
nGFP
H
♀
Merge
nc82
nGFP

Figure 4-7 *dsx*$^{GAL4\text{-}DBD}$/*elav*$^{VP16\text{-}AD}$ driven nuclear GFP expression in embryonic and larval CNSs of males and females.
(A-B) Stage 11 – 12 (A) Cephalic, left; ventral, bottom (B) Cephalic, left; ventral, top and (C-D) Stage 14 – 15 (C) Cephalic, left; ventral, bottom (D) Cephalic, left; ventral, top embryos counterstained with the neural tissue specific marker anti-HRP (magenta) (Jan and Jan, 1982; Snow et al., 1987) demonstrating no co-expression with *dsx*$^{GAL4\text{-}DBD}$/*elav*$^{VP16\text{-}AD}$ driven nGFP (green). (E) L1 larva, no expression apparent (F) L2 larva, expression in a bilateral cluster of cells at distal tip of the Abg (G) L3 male larva, expression apparent in the *dsx*-pC1, -pC2, -pC3 and -Abg clusters. No dsx-TN1 and -TN2 neurons expression is observed. (H) L3 female larva, expression in the *dsx*-pC1, -pC2, -pC3 and -Abg clusters, though reduced in numbers with respect to the male. Cluster designation as per Lee et al., 2002 and Rideout et al., 2010. nGFP realised with anti-GFP antibody (green) and neuropil counterstained with anti-nC82 (magenta). Unless noted, all views ventral, anterior up. Scale bar = 50 µm.

Compellingly, the expression patterns observed at this critical juncture using the novel split GAL4, are predominantly in accordance with previous descriptions of expression; consistent with the fact that this time point in pupal development is critical in the establishment of the neural substrates that govern sex-specific reproductive behaviours (Figure 4-8A-D; Arthur et al., 1998; Belote and Baker, 1987). *dsx*-SN neurons and -TN2 cells are thought to arise in the CNSs of both sexes, but then disappear specifically in adult females, while the *dsx*-TN1 neuronal clusters appear solely in males, but never females (Lee et al., 2002; Rideout et al., 2010). Conversely, when using the novel split GAL4 driver, the presence of *dsx*-SN was not observed in the brains of either sex, and neither was the presence of *dsx*-TN2 neurons in female VNCs at this developmental stage (Figure 4-8A-D). This may be a consequence of the split GAL4 system itself: given that it requires two hemi-domains to come together to reconstitute a functional GAL4 protein, even the slightest lag in expression or reconstitution would result in, what would be considered, a lack of expression. Programmed cell death (PCD) has been shown to be a key method of determining the final adult *dsx* expression (Kimura et al., 2005; Kimura et al., 2008; Sanders and Arbeitman, 2008; Rideout et al., 2010). Indeed, the loss of *dsx*-SN and *dsx*-TN2 from pupal to adult stages in the female CNS has specifically been shown to occurs as a result of female-specific PCD (Rideout et al., 2010). Hence, given the ± 2-3 hour window of dissections, PCD may have already occurred, resulting in expression patterns reminiscent of a later pupal time point.

Nevertheless, the most undeniable data demonstrating that the pairing of *dsx*$^{GAL4\text{-}DBD}$ with *elav*$^{VP16\text{-}AD}$ does in fact reiterate *dsx*^{GAL4}-expression comes from the adult neuroanatomical expression patterns in the CNS of males and females, together with their respective cell

counts (Table 4-1; Figure 4-9E-H; Figure 4-10). Contiguous to previous findings, I observed *dsx*$^{GAL4\text{-}DBD}$/*elav*$^{VP16\text{-}AD}$ expression in ~650 neurons divided into 8 groups in males, and ~350 neurons divided into 5 groups in females; resulting in, as shown in section 4.2.2, overt and substantial dimorphisms in the topology of the associated axonal projections and synaptic pattern of expression (Table 4-1; Figure 4-9E-H; Figure 4-10; Lee et al., 2002; Rideout et al., 2010; Robinett et al., 2010). Realisation of this pattern of expression, together with carrying out cell counts, clearly demonstrates a profound difference in neuronal cell numbers between males and females. That *dsx*-pC1, -pC2 and -pC3 clusters have higher numbers of neurons in males, and that *dsx*-SN, -TN1 and, -TN2 clusters are male-specific, and finally that the cell numbers of the Abg cluster of neurons is higher in females that in males, altogether compellingly validate the sensitivity and specificity of *dsx*$^{GAL4\text{-}DBD}$/*elav*$^{VP16\text{-}AD}$ as reporter of *dsx* neurons (Figure 4-10).

Table 4-1 Comparison between *dsx*$^{GAL4\text{-}DBD}$/*elav*$^{VP16\text{-}AD}$ cell counts obtained in this study and the previously described cell counts for *dsx*^{GAL4}.
dsx^{GAL4} counts taken from Rideout et al., 2010. Single labeling with GFP applied to CNSs from *UAS-pStinger; dsx*$^{GAL4\text{-}DBD}$/*elav*$^{VP16\text{-}AD}$ flies. [a]Neuronal cluster away from CNS midline. Count represents one cluster per hemisegment of the CNS. [b]Neuronal cluster spans the CNS midline. Count given is for the complete VNC. Counts represent mean ± standard deviation. n's listed in parentheses.

Neural Clusters	*dsx*^{GAL4}		*dsx*$^{GAL4\text{-}DBD}$/*elav*$^{VP16\text{-}AD}$	
	Male	Female	Male	Female
-aDN[a]	2 ± 0 (10)	2 ± 0 (10)	2 ± 0 (12)	2 ± 0 (12)
-SN[a]	1 ± 0 (10)	0 ± 0 (10)	1 ± 0 (12)	0 ± 0 (12)
-pC1[a]	57 ± 5.0 (10)	9 ± 2.0 (10)	52 ± 4.8 (12)	8 ± 1.6 (12)
-pC2[a]	77 ± 3.1 (10)	11 ± 1.9 (10)	78 ± 4.8 (12)	14 ± 1.5 (12)
-pC3[a]	14 ± 1.0 (10)	6 ± 1.4 (10)	14 ± 0.9 (12)	8 ± 1 (12)
-TN1[a]	22 ± 1.7 (10)	0 ± 0 (10)	23 ± 1.5 (12)	0 ± 0 (12)
-TN2[a]	7 ± 3.0 (10)	0 ± 0 (10)	8 ± 0.3 (12)	0 ± 0 (12)
-Abg[b]	277 ± 22.1 (10)	312 ± 15.9 (10)	275 ± 21.7 (10)	315 ± 18.9 (10)

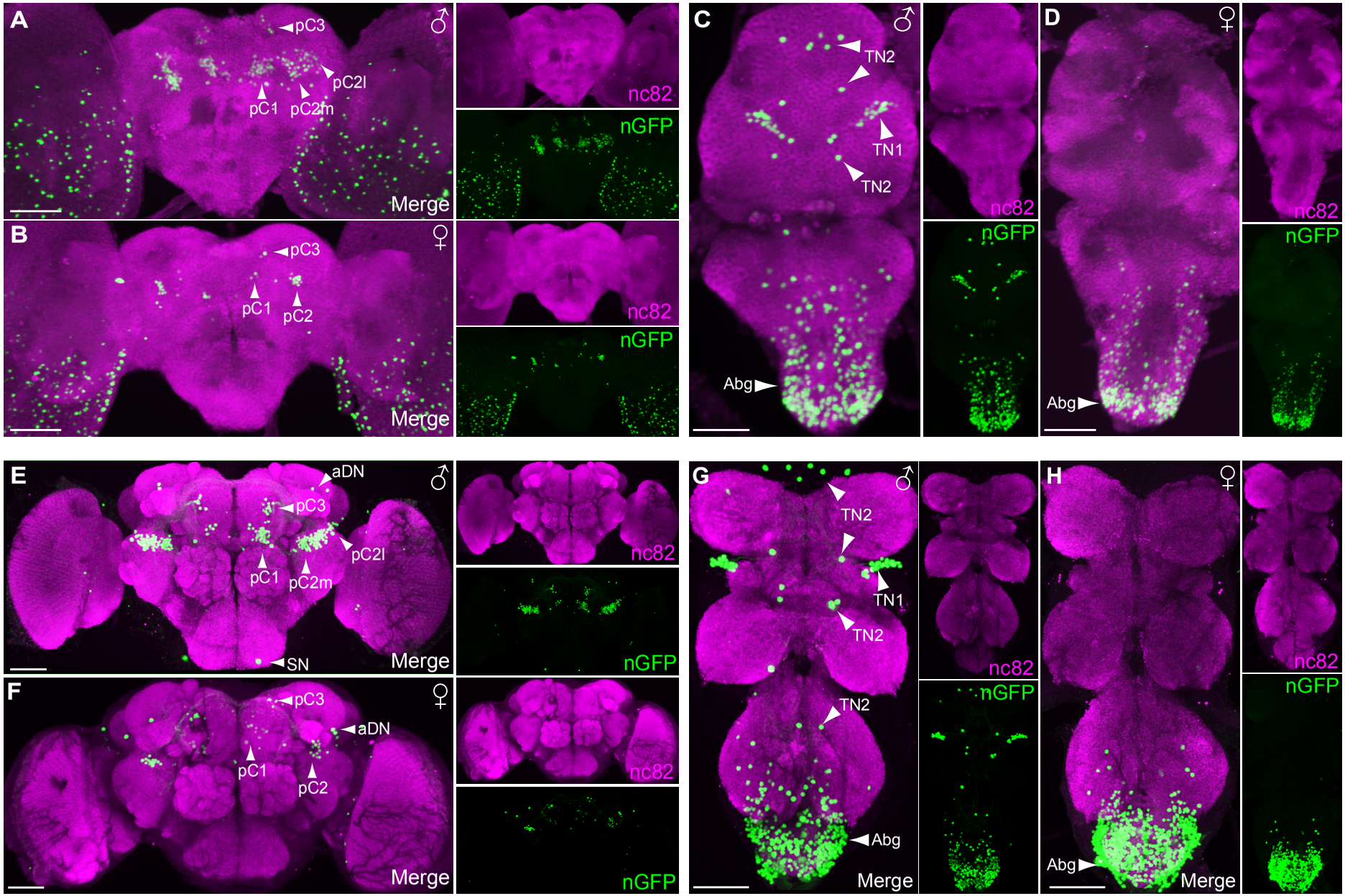

A
pC3
pC2l
pC1
pC2m
Merge
nc82
nGFP
B
pC3
pC1
pC2
Merge
nc82
nGFP
C
TN2
TN1
TN2
Abg
nc82
nGFP
D
Abg
nc82
nGFP
E
aDN
pC3
pC2l
pC1
pC2m
SN
Merge
nc82
nGFP
F
pC3
aDN
pC1
pC2
Merge
nc82
nGFP
G
TN2
TN1
TN2
TN2
Abg
Merge
nc82
nGFP
H
Abg
Merge
nc82
nGFP

Figure 4-8 *dsx*$^{GAL4\text{-}DBD}$/*elav*$^{VP16\text{-}AD}$ driven nuclear GFP expression in embryonic and larval CNSs of males and females.
(A) 48 hr male pupal brain; expression in the *dsx*-pC1, -pC2, and -pC3 clusters. (B) 48 hr female pupal brain, expression in the *dsx*-pC1, - pC2, and -pC3 clusters. (C) 48 hr male pupal VNC; expression in the *dsx*-TN1, -TN2 and -Abg clusters. (D) 48 hr female pupal VNC, expression in the *dsx*-Abg cluster. (E) 5-day-old adult male brain, expression in the *dsx*-aDN, -pC1, -pC2, -pC3, and –SN clusters. (F) 5-day-old adult female brain, expression in the *dsx*-aDN, -pC1, -pC2, and -pC3 clusters. (G) 5-day-old adult male VNC, expression in the *dsx*-TN1, -TN2, and -Abg clusters. (H) 5-day-old adult female VNC, expression in the *dsx*-Abg cluster. All clusters remain reduced in numbers with respect to the male except the *dsx*-Abg. Counts for designated clusters in adult stage given in Figure 4-9. Cluster designation as per Lee et al., 2002 and Rideout et al., 2010. nGFP realised with anti-GFP antibody (green) and neuropil counterstained with anti-nC82 (magenta). All views ventral, anterior up. Scale bar = 50 µm.

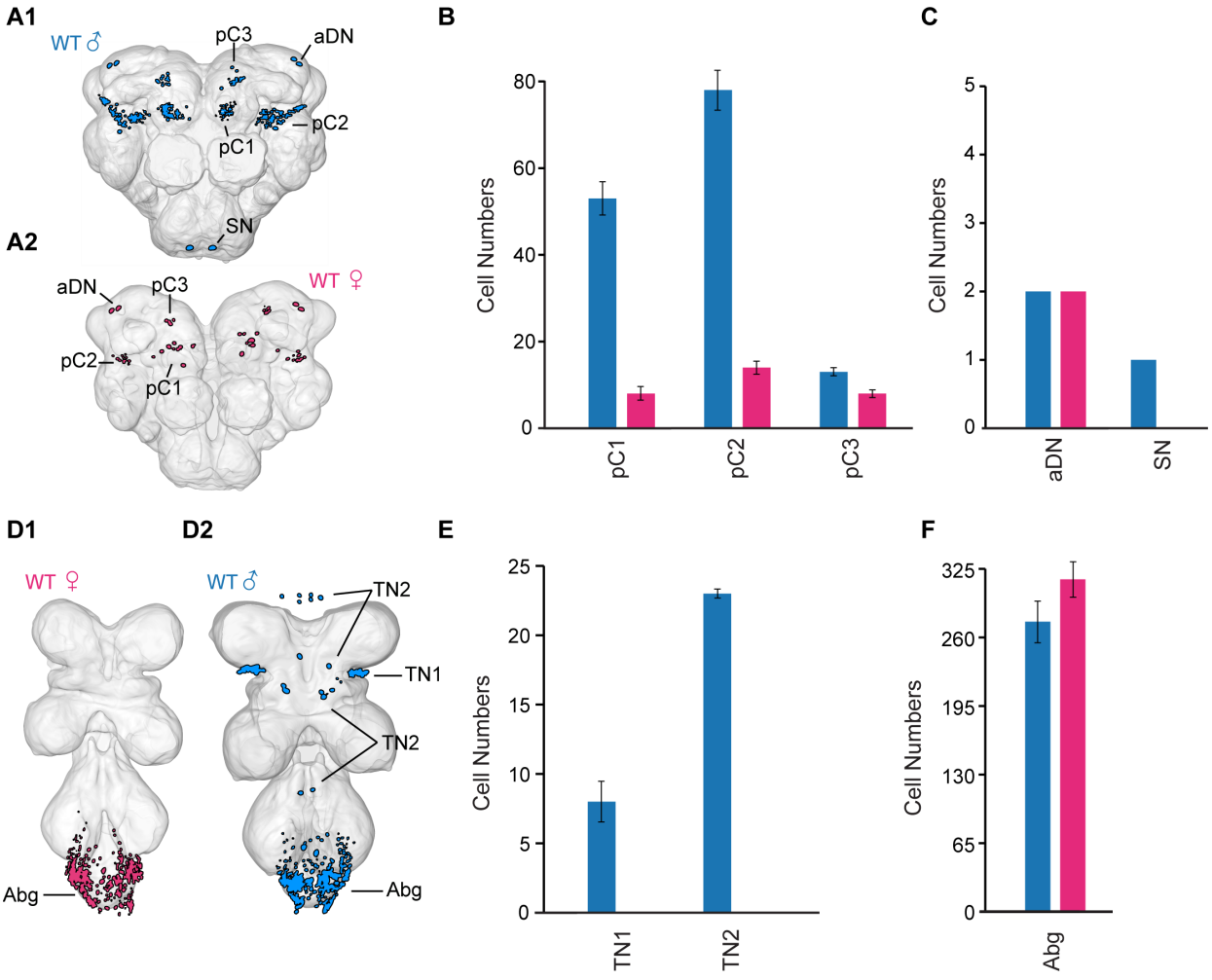


Figure 4-9 Graphical representation of the distribution of *dsx*$^{GAL4\text{-}DBD}$/*elav*$^{VP16\text{-}AD}$ driven nuclear GFP expression in the adult male and female CNS.
(A1) Schematic representation of *dsx*$^{GAL4\text{-}DBD}$/*elav*$^{VP16\text{-}AD}$ neuronal expression in the adult male brain. (A2) Schematic representation of *dsx*$^{GAL4\text{-}DBD}$/*elav*$^{VP16\text{-}AD}$ neuronal expression in the adult female brain. (B) Graphical representation of cell counts for neuronal clusters *dsx*-pC1, -pC2, and –pC3 in the adult male and female brain. (D) Graphical representation of cell counts for neuronal clusters *dsx*-aDN and –SN in the adult male and female brain. (D1) Schematic representation of *dsx*$^{GAL4\text{-}DBD}$/*elav*$^{VP16\text{-}AD}$ neuronal expression in the adult male VNC. (D2) Schematic representation of *dsx*$^{GAL4\text{-}DBD}$/*elav*$^{VP16\text{-}AD}$ neuronal expression in the adult female VNC. (B) Graphical representation of cell counts for neuronal clusters *dsx*-TN1 and –TN2 in the adult male and female VNC. (D) Graphical representation of cell counts for neuronal cluster *dsx*-Abg in the adult male and female VNC. Neuronal clusters indicated as per Lee et al., 2002 and Rideout et al., 2012. Counts represent mean ± standard deviation.

4.3.2 Spatial expression patterning of *dsx*$^{GAL4\text{-}DBD}$/*elav*$^{VP16\text{-}AD}$ in the peripheral nervous system of adult males and females

dsx neural circuitry is thought to include sensory neurons, interneurons, and motoneurons, much like that of *fru* circuitry, specifying circuit elements capable of receiving, processing and transferring information to elicit sexual behaviour (reviewed in Pavlou and Goodwin, 2012). With the expression of *dsx* within the CNS, encompassing both interneurons and motoneurons as a whole, little attention has been focused on comprehensively characterising and/or interrogating the 'receiving' components of this circuitry, with the exception of GRNs of the forelegs (Kimura et al., 2008; Rideout et al., 2010; Robinett et al., 2010; Mellert et al., 2010; Mellert et al., 2012).

As already exemplified in this study, observations of expression within spatially restricted regions of various somatic tissues including the mouthparts, alimentary tract, and internal reproductive systems (described in above section 4.2.3), is indicative of the complex network of sensory neurons that must almost certainly be the neuroanatomical sites at which somatic tissues relay information to, or communicate with, the CNS. As such, I dedicate the following section in this chapter to comprehensive descriptions of *dsx*$^{GAL4\text{-}DBD}$/*elav*$^{VP16\text{-}AD}$ expression in the above-mentioned tissues of both males and females, revealing components of *dsx* peripheral neural circuitry that have yet to be identified.

4.3.2.1 *dsx*$^{GAL4\text{-}DBD}$/*elav*$^{VP16\text{-}AD}$ is expressed in gustatory neurons of the labellum

I observed *dsx*$^{GAL4\text{-}DBD}$/*elav*$^{VP16\text{-}AD}$ expression within restricted regions of the proboscis, namely the labellum, which appears not to differ in topology or cell numbers between males and females (Figure 4-10A,C). Expression is apparent in ~6 bipolar cells per labial palp; the cell bodies of which lie beneath the surface of the cuticle, giving rise to a single dendrite that extends to the tip of the sensilla and an axon that innervates the subesophageal ganglion (SOG) region of the brain (Figure 4-10). Although the morphology of the observed innervations on the SOG does not appear to differ between the sexes, females appear to exhibit denser projections and synapses throughout. Based on their neural morphology, these cells are essentially *dsx*$^{GAL4\text{-}DBD}$/*elav*$^{VP16\text{-}AD}$-expressing gustatory receptor neurons

(GRNs). The level of auto fluorescence exhibited by the cuticle compromised the observation of all axonal projections of the GRNs. However, by cropping the Z-stack by a minimal set of initial cuticular sections, I was able to reveal axons of the GRNs projecting through the labial nerve, and terminating in the SOG (Figure 4-10A1,C1). Axonal arborisations and associated synapses can be seen in the SOG of both males and females, superficially revealing dimorphic patterns of expression, while confirming the destination of the labial GRNs (Figure 4-10B). There appears no expression elsewhere in the mouthparts, including cells associated with the cuticle, the labrum, maxillary palps and the cibarium (Figure 4-10A,C).

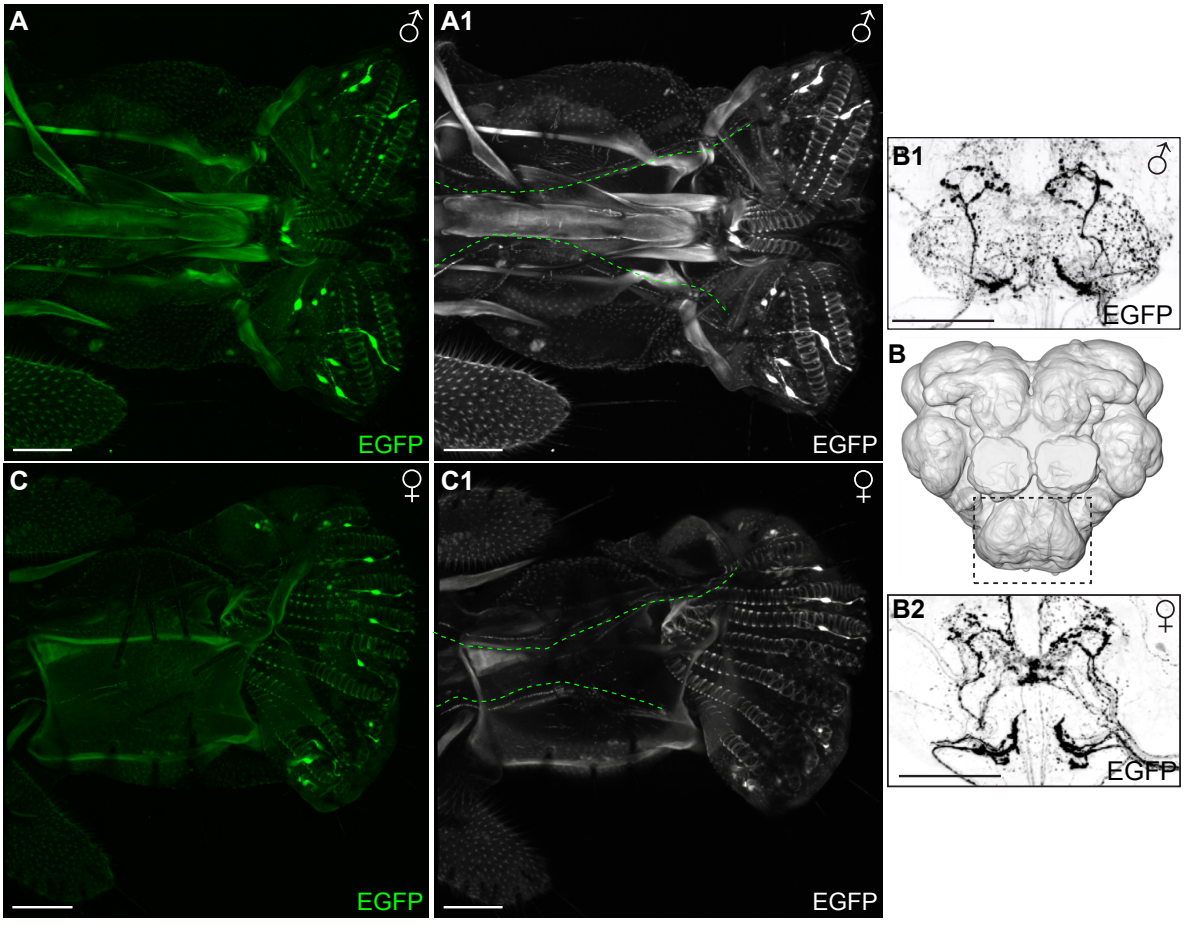


Figure 4-10 *dsx*$^{GAL4\text{-}DBD}$/*elav*$^{VP16\text{-}AD}$ driven cytoplasmic GFP expression in the proboscis, mouth parts, and associated innervations of the subesophageal ganglion (SOG) of 5 day old male and female adults.
(A) Male proboscis and mouthparts demonstrating restricted expression in gustatory receptor neurons (GRNs). (A1) Sectional Z-stack of male proboscis and mouthparts demonstrating GRN projections via the labial nerve (also shown in green dotted line). (B) Schematic of brain depicting region of SOG (black dotted box). (B1) 5 day old adult male SOG, analogous to region shown in (B), demonstrates GRN innervations. (B1) 5 day old adult female SOG, analogous to region shown in (B), demonstrates GRN innervations. (C) Female proboscis and mouthparts demonstrating restricted expression in GRNs; lateral view (C1) Sectional Z-stack of female proboscis and mouthparts demonstrating GRN projections via the labial nerve (also shown in green dotted line); lateral view. EGFP realised with anti-GFP antibody (green in A and C; white in A1 and C1; black in B1 and B2). Scale bar = 50 μm.

4.3.2.2 *dsx*$^{GAL4\text{-}DBD}$/*elav*$^{VP16\text{-}AD}$ is expressed in gustatory neurons of the forelegs

In the foreleg, *dsx*$^{GAL4\text{-}DBD}$/*elav*$^{VP16\text{-}AD}$ expression was found to be restricted to clusters of GRNs, in T1-5 tarsi of both male and female forelegs (Figure 4-11A, female is not shown). In keeping with previous findings, the observed patterns of expression in neurons of the foreleg appeared to be sexually dimorphic, with males overtly exhibiting more neurons, when compared to females (Figure 4-11A-D; Nayak and Singh, 1983; Possidente and Murphey, 1989; Rideout et al., 2010; Mellert et al., 2010; Mellert et al., 2012). No expression was observed in hind legs of both males and females (data not shown). The five tarsal segments of the foreleg consist of approximately 180 sensory bristles (or sensillae); most of which are mechanosensory in origin and are innervated by a single neuron (Orenic et al., 1993). However, the remaining sensillae are chemosensory/gustatory, in origin and are innervated by 4 GRNs and a single mechanosensory neuron (Nayak and Singh, 1983; Shanbhag et al., 2001). Males have a greater number of gustatory sensillae, and therefore more GRNs, in the four most proximal tarsal segments of their forelegs, when compared to females; most of which project across the midline of the VNC (in males but not in females) (Possidente and Murphey, 1989). That *dsx*$^{GAL4\text{-}DBD}$/*elav*$^{VP16\text{-}AD}$-expression occurs in clusters of neurons in the tarsi, the dendrites of which converge to a single sensilla, morphologically classifies them as GRNs (Figure 4-11A,B). The sexually dimorphic topology of the arborisations of these neurons, in the prothoracic ganglia (Prg) of the VNC, further supports this categorization (Figure 4-11C,D). However, whether *dsx*$^{GAL4\text{-}DBD}$/*elav*$^{VP16\text{-}AD}$ is also expressed in the mechanosensory neuron innervating each of these sensillae remains to be elucidated.

Given that *dsx* has known isoform-specific roles in both aspects of these dimorphisms, that is (in specifying the development of the GRNs of the foreleg and regulating VNC midline crossing by GRN axons), the observed dimorphic expression of *dsx*$^{GAL4\text{-}DBD}$/*elav*$^{VP16\text{-}AD}$ GRNs and their associated dimorphic projection patterns, is not entirely surprising (Figure 4-11C,D; Hildreth 1965; Mellert et al., 2010; Mellert et al., 2012). The most intriguing aspects of this work will come from future studies that exploit the *dsx*$^{GAL4\text{-}DBD}$/*elav*$^{VP16\text{-}AD}$ driver to electrophysiologically and functionally interrogate the role of these sexually dimorphic GRNs in eliciting sex-specific responses/behaviours. Nevertheless, the sexually dimorphic

expression of *dsx*-expressing GRNs in the male and female foreleg presented here, has for the first time, been observed in a restricted manner that separates it from all other *dsx*--expressing cells of the foreleg (Figure 4-11).

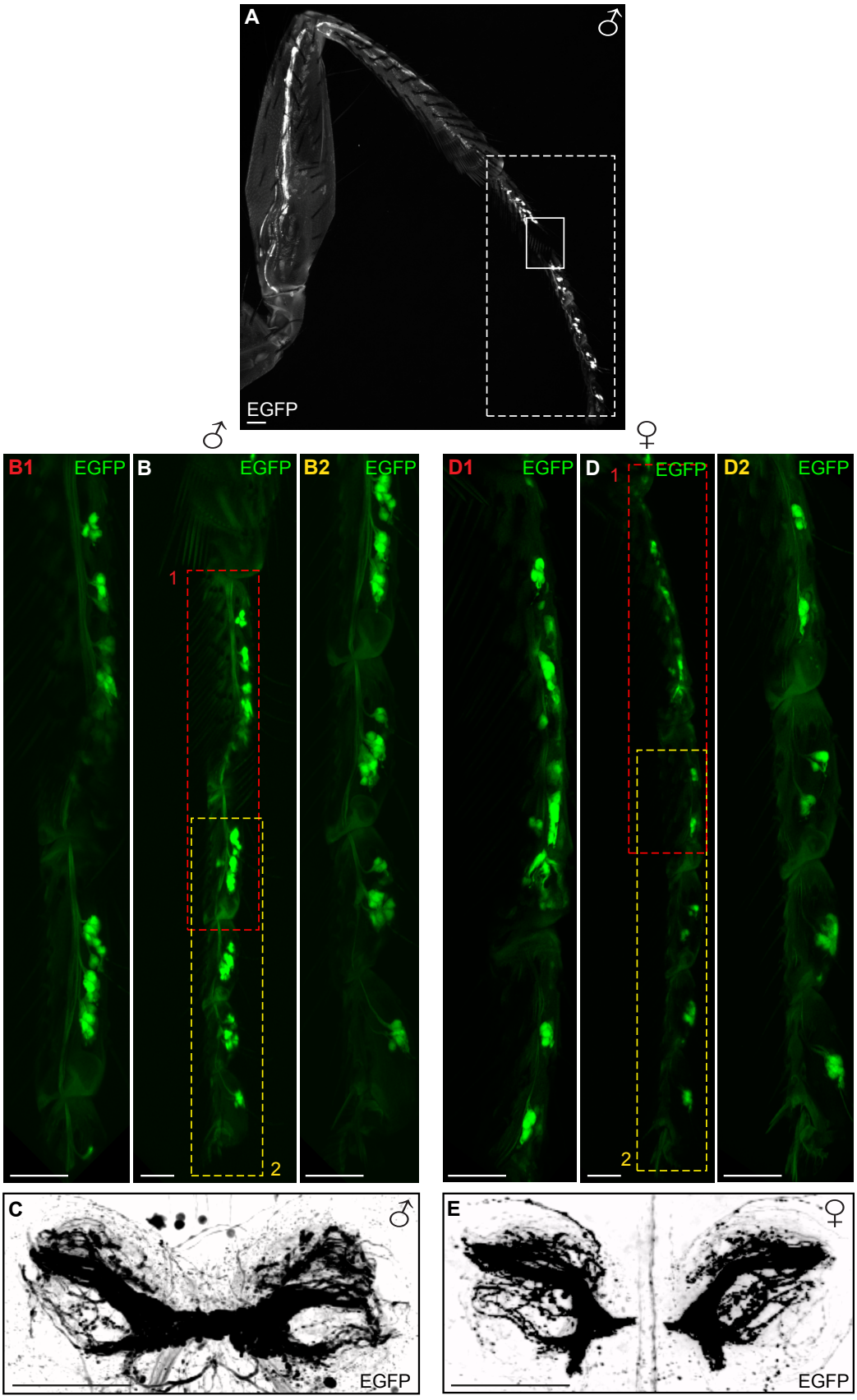


Figure 4-11 Sex-specific expression of cytoplasmic GFP using the *dsx*$^{GAL4\text{-}DBD}$/*elav*$^{VP16\text{-}AD}$ driver, in the forelegs of adult males and females.
(A) Expression in the adult male foreleg. Cell bodies expressing EGFP are restricted to the T1-T5 tarsi (white dotted box), while associated axons project through the foreleg and terminate in the prothoracic ganglia of the VNC. Sex combs shown in solid white box. (B) Expression in the T1 tarsi of the male foreleg. (B1) Expression in the T1-2 tarsi the male foreleg at higher magnification (region of magnification shown in red dotted box of (B)). (B2) Expression in the T2-5 tarsi the male foreleg at higher magnification (region of magnification shown in yellow dotted box of (B)). (C) 5 day old adult male prothoracic ganglia, demonstrating gustatory receptor neuron innervations and male-specific midline crossing.(D) Expression in the T1 tarsi of the female foreleg. (D1) Expression in the T1-2 tarsi the female foreleg at higher magnification (region of magnification shown in red dotted box of (D)). (D2) Expression in the T2-5 tarsi the female foreleg at higher magnification (region of magnification shown in yellow dotted box of (D)). (E) 5 day old adult female prothoracic ganglia, demonstrating gustatory receptor neuron innervations and the lack of a midline crossing. Cytoplasmic EGFP realised with anti-GFP antibody (white in A. green in B and D; black in C and E). Scale bar = 50 μm.

4.3.2.3 *dsx*$^{GAL4\text{-}DBD}$/*elav*$^{VP16\text{-}AD}$ is expressed in the alimentary tract

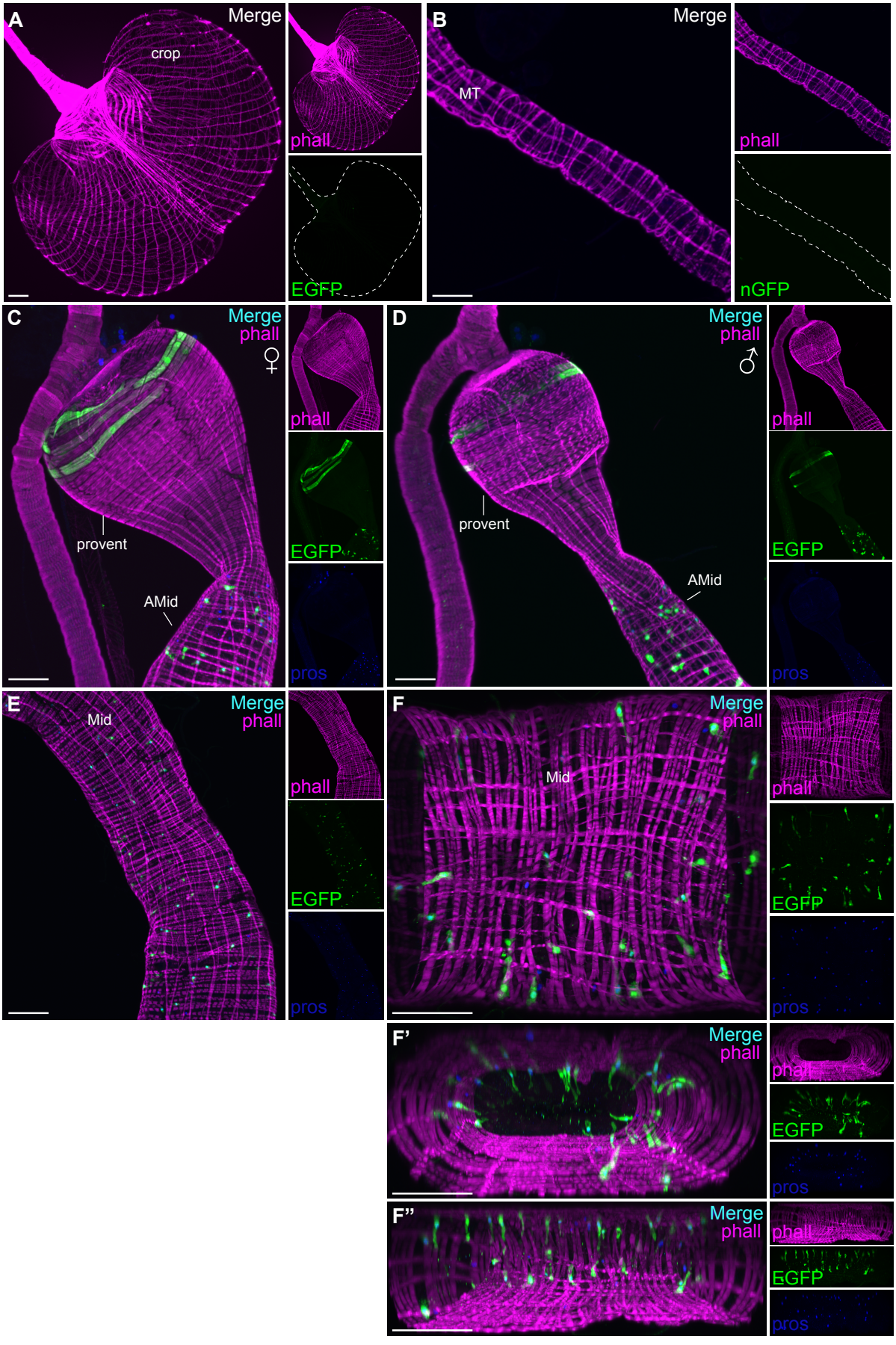
I observed *dsx*$^{GAL4\text{-}DBD}$/*elav*$^{VP16\text{-}AD}$ expression within the digestive tract of both males and females, with little dimorphism in the patterns documented (Figure 4-12). All associated tissues, including the crop and Malphigian tubules, revealed no *dsx*$^{GAL4\text{-}DBD}$/*elav*$^{VP16\text{-}AD}$ expression (Figure 4-12A,B).

Analyses of the topographical distribution of expression revealed a restricted population of cells within the muscle layer of the proventriculus that give rise to band-like pattern of expression similar to that of the scattered muscle fibres of the outermost layer of the proventriculus (Figure 4-12C,D). These bands of cells appear to be more numerous in males than in females (Figure 4-12C,D). As studies have demonstrated an abundance of neural innervations in this region (Cognini et al., 2011), these cells most probably act like, or form, sphincters that may be regulated by the nervous system itself. Additional *dsx*$^{GAL4\text{-}DBD}$/*elav*$^{VP16\text{-}AD}$ expression was observed in a restricted pattern of cells of the midgut that do not appear to differ between the sexes (Figure 4-12E,F). The epithelial monolayer of the midgut is composed of at least 4 cell types; enterocytes (EC) involved in nutrient absorption, interspersed hormone-producing enteroendocrine (EE) cells, dispersed intestinal stem cells (ISC) that continuously replenish the intestinal cells via their daughter enteroblasts (EB) that ultimately become ECs and less frequently EEs (Ohlstein and Spradling, 2006; Micchelli and Perrimon, 2006). Based on the dispersal of the expression patterns observed in the preparations, these cells could be one of two types of cells: EEs or EBs. Given that all EE cell nuclei express the transcription factor Prospero (Ohlstein and Spradling, 2006), I

performed co-expression analyses using and an anti-Prospero antibody, while visualising the muscle fibres with F-actin phalloidin staining (Figure 4-12E,F). Undeniably, all EGFP-expressing *dsx*$^{GAL4\text{-}DBD}$/*elav*$^{VP16\text{-}AD}$ cells were found to co-express Prospero; however, not all Prospero expressing nuclei co-expressed EGFP (Figure 4-12E,F). Having used an EGFP reporter, I was also able to visualise the cytoplasm of these cells, allowing for the realisation of their morphology. Indeed, the morphology of these cells is in keeping with that of EEs, as they associate with the overlying longitudinal muscle and extend internally through the endothelial epithelium (Figure 4-12F; Ohlstein and Spradling, 2006). The expression of *dsx*$^{GAL4\text{-}DBD}$/*elav*$^{VP16\text{-}AD}$ in a subset of EE cells implies a requirement for sexual identity in the functioning of these cells. This would make logical/functional sense as these chemosensory cells continuously sense nutrients and/or chemicals, and are capable of producing regulatory peptides that act on nearby cells or neural innervations in a paracrine manner to ultimately mediate the contraction of intestinal muscles, and/or on distant targets such as the brain in an endocrine manner (Nässel, 1999; Bendena et al., 1999; Park and Kwon, 2013).

Again, that the aforementioned cells express *dsx*$^{GAL4\text{-}DBD}$/*elav*$^{VP16\text{-}AD}$ is indicative of the neural nature of these cells. However, given that little is known about the components and/or mechanisms of the stomatogastric nervous system of the fly, the functions of, and the role of *dsx*-expression in, these cells remain to be elucidated. Again, importantly, the novel *dsx*$^{GAL4\text{-}DBD}$ transgenic demonstrably provides an avenue to gain insight into the function and activity of the largely uncharacterised enteric NS.

Figure 4-12 Expression of cytoplasmic GFP using the *dsx*$^{GAL4\text{-}DBD}$/*elav*$^{VP16\text{-}AD}$ driver, in the alimentary tract of 5 day old adult males and females.
(A) Detail of 5 day old crop. (B) Detail of 5 day old Malphigian tubule. (C) Detail of procentriculus (provent) and anterior midgut (Amid) from a 5 day old adult female alimentary canal. Expression is observed in cells within the muscle layer that give rise to band-like expression patterns, and in enteroendocrine cells (EEs) labelled with anti-prospero (Pros) in the Amid. (D) Detail of procentriculus (provent) and Amid from a 5 day old adult male alimentary canal. Expression is observed in cells within the muscle layer that give rise to band-like expression patterns, and in EEs (labelled with anti-prospero) in the Amid. (E) Detail of the midgut (mid) of a 5 day old adult alimentary canal. Expression is observed in EEs, co-labelled with anti-prospero. (F) Higher resolution image showing detail of the midgut (mid) of a 5 day old adult alimentary canal. Expression is observed in EEs, co-labelled with anti-prospero. (F') Coronal plane view of (F) showing morphology of cells, extending from the muscle layer interiorly within the intestinal epithelial wall. (F'') Transverse plane view of (F) revealing morphology of cells, extending from the muscle layer interiorly within the intestinal epithelial wall. Cytoplasmic EGFP realised with anti-GFP antibody (green). Anti-Phalloidin (Phall) is shown in magenta. EEs marker Anti-Prospero is shown in blue. Scale bar = 50 μm.


A
Merge
crop
phall
EGFP
B
Merge
MT
phall
nGFP
C
Merge
phall
♀
provent
AMid
phall
EGFP
pros
D
Merge
phall
♂
provent
AMid
phall
EGFP
pros
E
Merge
phall
Mid
phall
EGFP
pros
F
Merge
phall
Mid
phall
EGFP
pros
F'
Merge
phall
phall
EGFP
pros
F''
Merge
phall
phall
EGFP
pros

4.3.2.4 *dsx*$^{GAL4\text{-}DBD}$/*elav*$^{VP16\text{-}AD}$ is expressed in the genitalia of male and females

As previously demonstrated (in section 4.2.3.3), *dsx*$^{GAL4\text{-}DBD}$/*elav*$^{VP16\text{-}AD}$ expression occurs in a restricted manner in select tissues of both the male and female internal genitalia. In males, in depth characterisation of *dsx*$^{GAL4\text{-}DBD}$/*elav*$^{VP16\text{-}AD}$-expression revealed four primary sites of expression including the testes, the ejaculatory duct (EjD), and the apodeme (Apo) of the ejaculatory bulb (EjB) and aedeagus (Aed) (Figure 4-13; Figure 4-14). More specifically, *dsx*$^{GAL4\text{-}DBD}$/*elav*$^{VP16\text{-}AD}$-expressing cells are associated with i) the epithelium of the internal lumen of both the testes and EjD, ii) the crown of striated muscle fibres that are connected to the Apo of the EjB, and iii) the most proximal tip of muscle fibres of the adeagus (Figure 4-13; Figure 4-14). In addition to these cells, sagittal sections of the EjB revealed *dsx*$^{GAL4\text{-}DBD}$/*elav*$^{VP16\text{-}AD}$-expression in ~5-6 cells that lie underneath the crown of striated muscles, external to the Apo (Figure 4-13C; Figure 4-14D). Realising the morphology of these cells by expressing EGFP allowed the classification of these cells as neurons that extend from the internal EjB plate towards the crown of muscles that attach the Apo of the EjB to the EjB (Figure 4-13C; Figure 4-14D).

In the female, I observed a highly restricted pattern of expression that is limited to five regions of the internal genitalia, that is; one cell per lateral oviduct; two anterior bilateral clusters of ~3 and ~5 cells, and one posterior bilateral cluster of cells of ~5 cells on the uterus; cells associated with the endothelial lumen of the lateral and common oviducts (OvL and OvC respectively) and seminal receptacle (SmRcp); and finally, cells associated with the muscles of the uterus and spermathecae (Spt) and the Spt itself (Figure 4-15; Figure 4-16). By expressing EGFP, the projections of the neurons in the lateral oviduct, and of all three clusters on the uterus were realised (Figure 4-15B,C; Figure 4-16C,D); the characteristics of which are topologically reminiscent of neurons that have been previously implicated in the regulation of female post-mating behavioural responses (Grueber et al., 2003; Grueber et al., 2007; Häsemeyer et al., 2009; Yang et al., 2009). I have, through co-expression and behavioural assays, demonstrated that these neurons do in fact comprise a subset of *dsx*$^{+}$/*fru*$^{+}$/*ppk*$^{+}$ neurons involved in post-mating behavioural responses (Rideout et al., 2012). These investigations however, will be discussed in greater detail in Chapter 6.

The realisation of *dsx*$^{GAL4\text{-}DBD}$/*elav*$^{VP16\text{-}AD}$-expression in the genitalia of both males and females demonstrated the intriguing presence of restricted clusters of sensory neurons and neurons associated with the epithelial or muscle layers of component parts (Figure 4-13; Figure 4-15). Given the relatively different cell types labelled here, I co-expressed anti-ELAV, as a form of validation, ensuring that all aforementioned cells are in fact neural in nature (Figure 4-14; Figure 4-16).

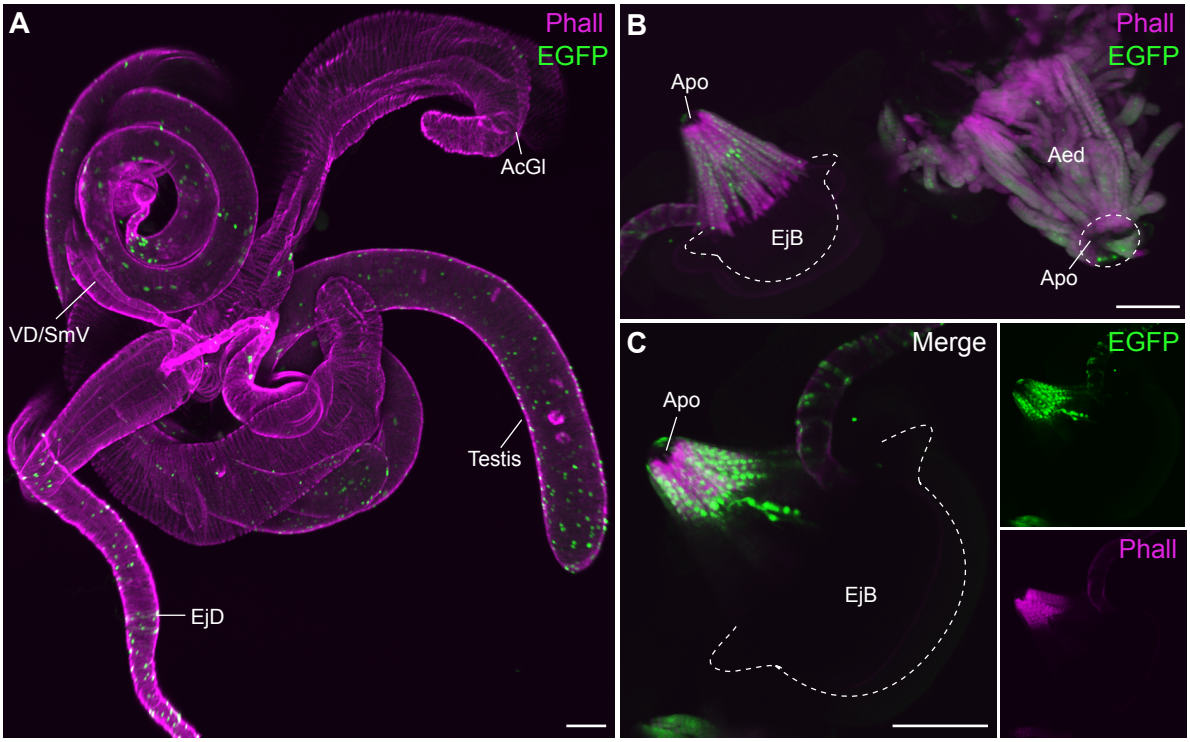


Figure 4-13 *dsx*$^{GAL4\text{-}DBD}$/*elav*$^{VP16\text{-}AD}$ driven expression of cytoplasmic EGFP in the internal genitalia of 5 day old adult male flies counterstained with the F-actin specific antibody Phalloidin.
(A) Detail of internal genitalia; testes, seminal vesicles (SmV), vas deferens (VD), accessory glands (AcGl) and ejaculatory duct (EjD) indicated. (B) Detail of internal genitalia; ejaculatory bulb (EjB), apodeme (Apo) and aedeagus (Aed) indicated. Dotted line shows outline of EjB. (C) Higher magnification, and subset of the maximal confocal stack, showing detail of EjB. Dotted line shows outline of EjB. Detail revealing expression in numerous cells within musculature associated with the Apo and the secretory cells of the ejaculatory bulb (dotted line), and in sensory neurons internal to the EjB. Cytoplasmic EGFP realised with anti-GFP antibody (green). Anti-Phalloidin (Phall) is shown in magenta. Scale bar = 50 μm.

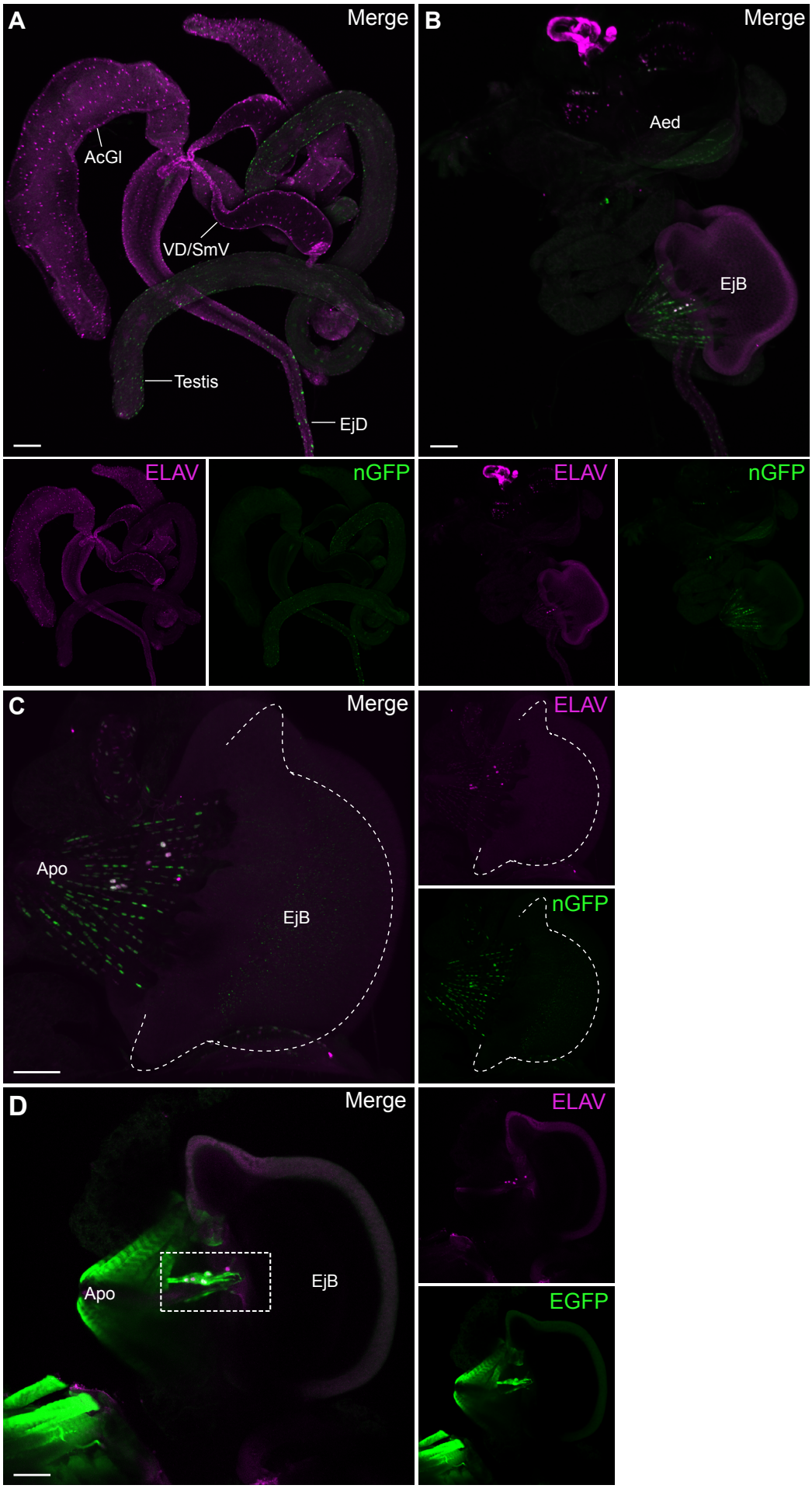

A
Merge
AcGl
VD/SmV
Testis
EjD
B
Merge
Aed
EjB
ELAV
nGFP
ELAV
nGFP
C
Merge
Apo
EjB
ELAV
nGFP
D
Merge
Apo
EjB
ELAV
EGFP

Figure 4-14 *dsx*$^{GAL4\text{-}DBD}$/*elav*$^{VP16\text{-}AD}$ driven expression of nuclear or cytoplasmic GFP in the internal genitalia of 5 day old adult male flies counterstained with the neuron specific antibody ELAV.

(A) Detail of nuclear GFP (nGFP) expression in internal genitalia; testes, seminal vesicles (SmV), vas deferens (VD), accessory glands (AcGl) and ejaculatory duct (EjD) indicated. (B) Detail of nGFP expression in internal genitalia; ejaculatory bulb (EjB), apodeme (Apo) and aedeagus (Aed) indicated. (C) Higher magnification, and subset of the maximal confocal stack, showing detail of nGFP expression in EjB. Dotted line shows outline of EjB secretory cells. (D) Higher magnification, and subset of the maximal confocal stack, showing detail of cytoplasmic GFP (EGFP) expression in EjB. Detail revealing expression in sensory neurons, that co express ELAV, internal to the EjB. Nuclear and cytoplasmic GFP (nGFP and EGFP respectively) realised with anti-GFP antibody (green). Anti-ELAV (ELAV) is shown in magenta. Scale bar = 50 µm.

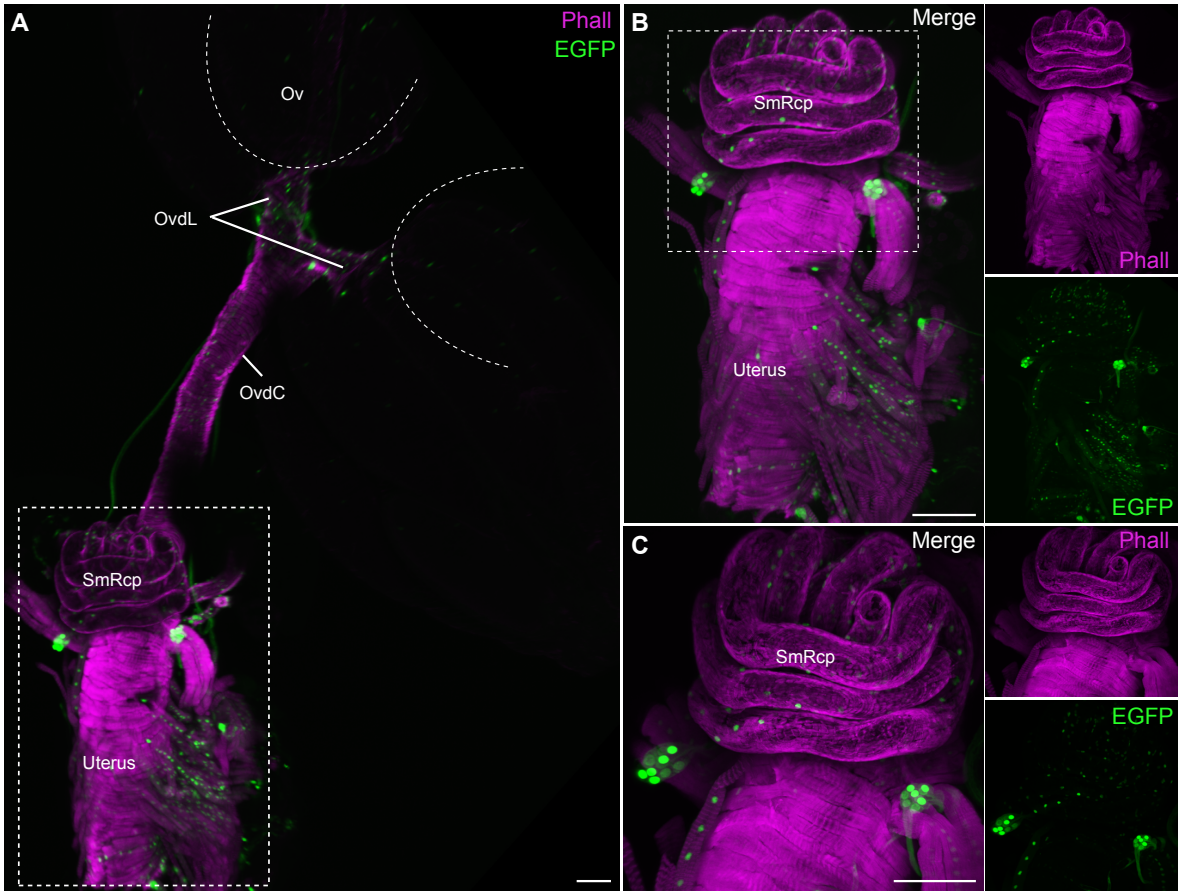


Figure 4-15 *dsx*$^{GAL4\text{-}DBD}$/*elav*$^{VP16\text{-}AD}$ driven expression of cytoplasmic EGFP in the internal genitalia of 5 day old adult female flies counterstained with the F-actin specific antibody Phalloidin.

(A) Detail of female internal genitalia; lateral and common oviducts (OvdL and OvdC), seminal receptacle (SmRcp), and uterus indicated. (B) Higher magnification showing detail of female internal genitalia; seminal receptacle (SmRcp), and uterus indicated. Demonstrating expression in bilateral anterior clusters of sensory neurons and associated projections on the uterus, in cells associated with endothelium of SmRcp, and in cells associates with the musculature surrounding the uterus. (C) Higher magnification showing detail of female internal genitalia; SmRcp indicated. Demonstrating expression in bilateral anterior clusters of sensory neurons and associated projections on the uterus, and in cells associated with endothelium of SmRcp. Cytoplasmic EGFP realised with anti-GFP antibody (green). Anti-Phalloidin (Phall) is shown in magenta. Scale bar = 50 µm.

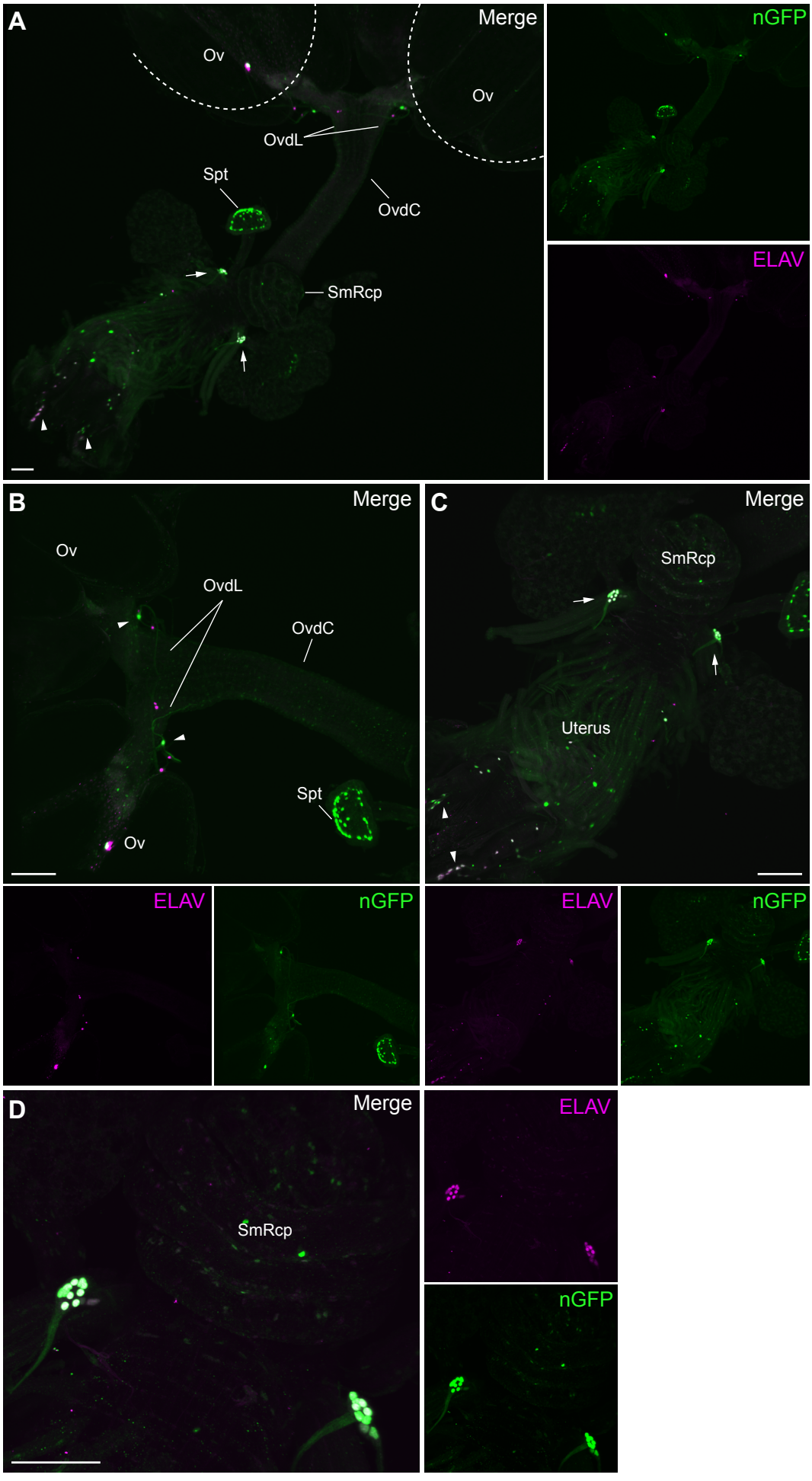

A
Merge
Ov
Ov
OvdL
Spt
OvdC
SmRcp
nGFP
ELAV
B
Merge
Ov
OvdL
OvdC
Spt
Ov
ELAV
nGFP
C
Merge
SmRcp
Uterus
ELAV
nGFP
D
Merge
SmRcp
ELAV
nGFP

Figure 4-16 *dsx*$^{GAL4\text{-}DBD}$/*elav*$^{VP16\text{-}AD}$ driven expression of cytoplasmic EGFP in the internal genitalia of 5 day old adult female flies counterstained with the neuron specific antibody ELAV. (A) Detail of female internal genitalia; ovaries (Ov), lateral and common oviducts (OvdL and OvdC), seminal receptacle (SmRcp), spermathecae (Spt) and uterus indicated. Demonstrating expression in bilateral anterior (arrows) and posterior (arrowheads) clusters of sensory neurons and associated projections on the uterus, in cells associated with endothelium of SmRcp, and in cells associates with the musculature surrounding the uterus. (B) Higher magnification showing detail of female internal genitalia; Ov, OvdL, OvdC and Spt indicated. Demonstrating expression in single bilateral sensory neuron (arrowheads) and associated projection on the OvdL, in cells associated with endothelium of OvdL, OvdC and Spt. (B) Higher magnification showing detail of female internal genitalia; SmRcp), and uterus indicated. Demonstrating expression in bilateral anterior (arrows) and posterior (arrowheads) clusters of sensory neurons and associated projections on the uterus, in cells associated with endothelium of SmRcp, and in cells associates with the musculature surrounding the uterus. (C) Higher magnification showing detail of female internal genitalia; SmRcp indicated. Demonstrating expression in bilateral anterior (arrows) and posterior (arrowheads) clusters of sensory neurons and associated projections on the uterus, and in cells associated with endothelium of SmRcp. Cytoplasmic GFP (EGFP) realised with anti-GFP antibody (green). Anti-ELAV (ELAV) is shown in magenta. Scale bar = 50 μm.

4.3.2.5 *dsx*$^{GAL4\text{-}DBD}$/*elav*$^{VP16\text{-}AD}$ is expressed in sensory neurons of the terminalia of 5 day old adult males and females

Studies exploiting *dsx*^{GAL4} drivers have demonstrated high levels of reporter expression in almost all cells of the male and female genital disc, with the exception of cells along the lateral edges (Rideout et al., 2010; Robinett et al., 2010). Extrapolating from these data, *dsx* is essentially expressed in all major regions of this disc that give rise to sexually dimorphic structures of the adult genitalia and analia (Sanchez and Guerrero, 2001). Indeed, this has been shown to be the case given the broad expression patterns of *dsx*^{GAL4} in the male and female adult internal and external reproductive systems (Rideout et al., 2010; Robinett et al., 2010). However, that both the peripheral sensory neurons and their associated bristle organs also arise from precursors in the genital disc epithelium (Taylor, 1989; Taylor, 1989b) prompted me to interrogate the presence of peripheral neurons in male and female adult terminalia.

Driving the expression of *UAS-EGFP* using the *dsx*$^{GAL4\text{-}DBD}$/*elav*$^{VP16\text{-}AD}$ revealed/exhibited overt expression in several bilateral clusters of sensory neurons of the male and female adult terminalia (Figure 4-17). Interestingly, in males, these neurons are associated with bristles of the clasper teeth, lateral plates and anal plates (Figure 4-17C). A lateral view of the projection patterns associated with these sensory neurons demonstrates their convergence into a single bilateral nerve bundle (Figure 4-17A,B). In females, the observed sensory neurons are associated with bristles of the anal and vaginal plates (Figure 4-17D,G). The

projections of the sensory neurons associated with bristles of the anal plates converge into a single bilateral nerve bundle, which appear to converge with the axons of the sensory neurons of the vaginal plates (Figure 4-17D,E). The fragility of the female terminalia meant that an all-encompassing lateral view of the female terminalia was practically challenging, however this data is necessary to certify the convergence of axons of all *dsx*$^{GAL4\text{-}DBD}$/*elav*$^{VP16\text{-}AD}$-expressing sensory neurons of the female terminalia.

Studies have shown that the number and morphology of the bristles associated with the terminalia differ between the sexes (Taylor, 1989); this may seem obvious, however this appears to be the case even when considering bristles of analogous structures such as the anal plates (Taylor, 1989). Characterisations of the sensory neurons innervating bristles of the terminalia demonstrated that these are mechanosensory in origin, in males, while in females, it has been postulated that small sensillae of the vaginal plates may be chemosensory in origin (Taylor, 1989b). In both cases however, sensory neurons of the terminalia appear to arborize on the Abg of the VNC in a sex specific manner (Taylor, 1989b). Based on these characterisations, it is safe to presume that the neurons observed here are predominantly mechanosensory in origin, except for the chemosensory neurons of the vaginal plate, which also appear to express *dsx*$^{GAL4\text{-}DBD}$/*elav*$^{VP16\text{-}AD}$ (Figure 4-17C,F,G). The sexually dimorphic density and topology of synaptic expression previously described in the Abg of *dsx*$^{GAL4\text{-}DBD}$/*elav*$^{VP16\text{-}AD}$ males and females may, in part, be a consequence of the arborisations of the sensory neuron of the terminalia (Figure 4-2E-H). Functional investigations that exploit restrictive ablation of these bristles and/or associated sensory neurons, together with fully characterising their morphology and arborisations, would shed light on the role of these neurons in courtship/copulation.

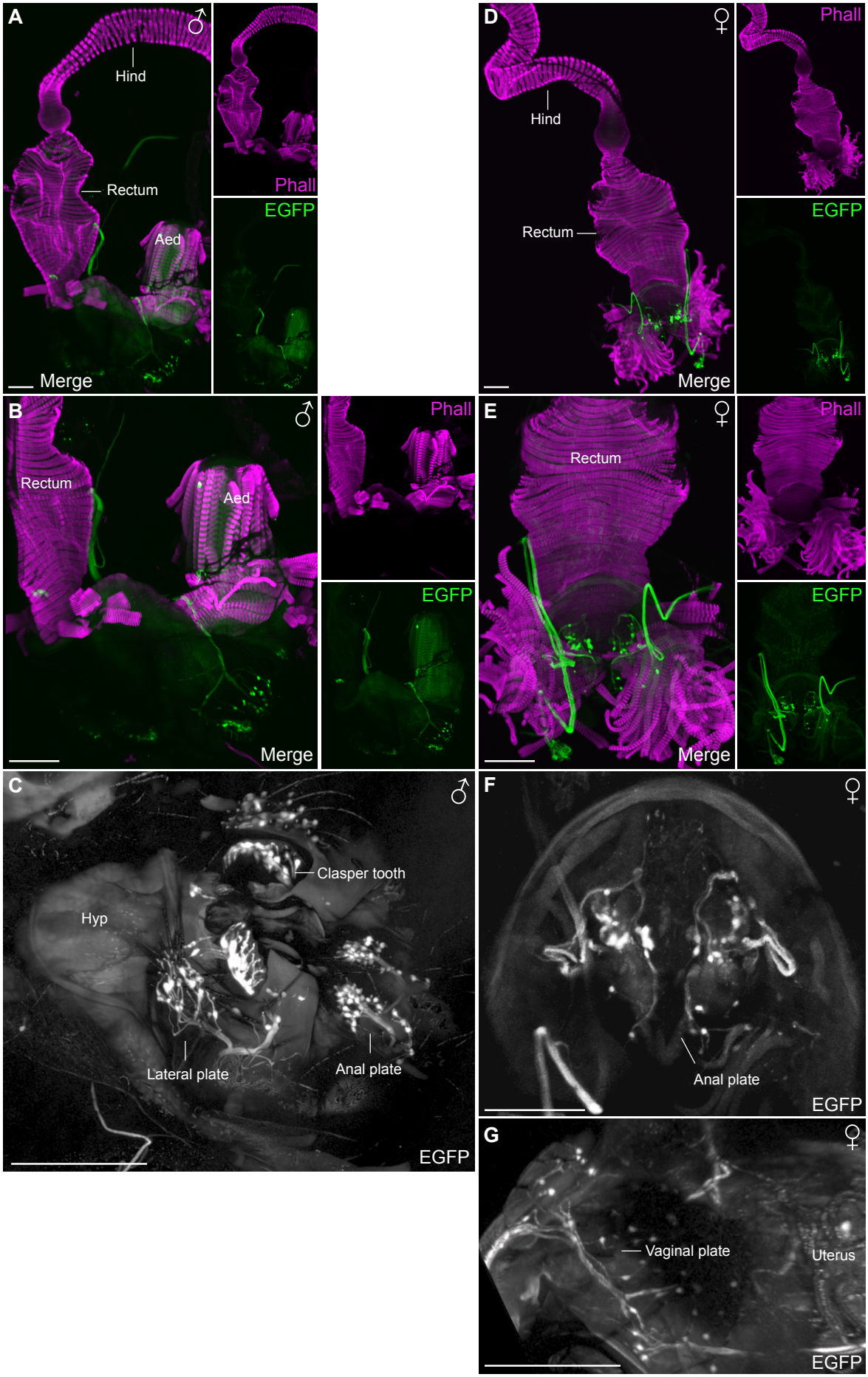

A
Hind
Rectum
Aed
Merge
Phall
EGFP
B
Rectum
Aed
Merge
Phall
EGFP
C
Clasper tooth
Hyp
Lateral plate
Anal plate
EGFP
D
Hind
Rectum
Merge
Phall
EGFP
E
Rectum
Merge
Phall
EGFP
F
Anal plate
EGFP
G
Vaginal plate
Uterus
EGFP

Figure 4-17 *dsx*$^{GAL4\text{-}DBD}$/*elav*$^{VP16\text{-}AD}$ driven expression of cytoplasmic EGFP in terminalia of 5 day old adult female flies counterstained with the F-actin specific antibody Phalloidin.
(A) Detail of male genitalia and analia; hindgut (Hind), rectum, and aedeagus (Aed) indicated. Lateral view. (B) Higher magnification showing detail of male genitalia and analia; rectum, and Aed indicated. Demonstrating expression in bilateral clusters of sensory neurons and associated projections in the terminalia. Lateral view. (C) Higher magnification showing skeleton of sensory neurons and respective projections associated with bristles of the clasper teeth, lateral plates and anal plates. Hypandrium (Hyp) also indicated. (D) Detail of female terminalia; rectum indicated. Demonstrating expression in bilateral clusters of sensory neurons and associated projections in the terminalia. (E) Higher magnification showing detail of female terminalia; rectum indicated. Demonstrating expression in bilateral anterior clusters of sensory neurons and associated projections. (F) Higher magnification showing skeleton of sensory neurons and respective projections associated with bristles of the anal plates. (G) High magnification image showing skeleton of sensory neurons and respective projections associated with bristles of the vaginal plates. Uterus also indicated. Cytoplasmic EGFP realised with anti-GFP antibody (green in A,B, D and E; black in C, F and G). Anti-Phalloidin (Phall) is shown in magenta. Scale bar = 50 μm.

4.3.3 Innervations of *dsx*$^{GAL4\text{-}DBD}$/*elav*$^{VP16\text{-}AD}$-expressing neurons in adult males and females

Characterising the topology of *dsx*$^{GAL4\text{-}DBD}$/*elav*$^{VP16\text{-}AD}$-expressing neurons in the PNS demonstrated a widespread presence of *dsx*-expression within neurons of various sense organs. Realising the projection patterns of these neurons demonstrated their respective arborisations into different regions of the CNS, which is indicative of direct communication between somatic tissues and the CNS. The interneurons present in such target regions of the CNS (including the Prg, Msg and Abg) have been shown to be involved in the transmission of information to higher order centres of the brain that are responsible for the processing of converging sensory information (reviewed by Pavlou and Goodwin, 2013). However, the specific neural loci of the CNS and their associated outputs responsible for reciprocating communication and regulating physiology (and, by implication, behaviour) remain to be fully determined.

Scrutinizing *dsx* neural architecture for expression in cephalic and/or thoracic nerve trunks helps specify which neural foci consist of *dsx*-expressing neurons that project to, and target, somatic tissues. In this way, a subset of *dsx*-expressing neurons of the Abg and their associated output projections via the abdominal nerve trunk (AbNrTr) were found to be the only ‘outputs’ of the circuitry (Rideout et al., 2010; Robinett et al., 2010). This is not to say that other *dsx*-expressing neurons do not synapse with non-*dsx*-expressing output neurons; however, as the primary goal here is to comprehensively describe functionally distinct

components of *dsx* circuitry, I focused on uncovering target organs innervated by *dsx*-expressing neurons of the Abg.

4.3.3.1 *dsx*$^{GAL4\text{-}DBD}$/*elav*$^{VP16\text{-}AD}$-expressing neurons innervate adult male and female reproductive systems

Some of the neurites of *dsx*$^{GAL4\text{-}DBD}$/*elav*$^{VP16\text{-}AD}$-expressing neurons project through the AbNrTr and bilaterally innervate the internal reproductive systems of adult males and females (Figure 4-18; Rideout et al., 2010; Robinett et al., 2010). The extremely low levels of EGFP reporter expression in these innervations required amplification of the signal in two ways: staining the whole mount preparations with anti-GFP (the fragility of these samples meant that at least one of the innervating bilateral nerve trunks was damaged during the staining process), and increasing the gain during confocal imaging. Although these modifications allowed for accurate realisation of the patterns of innervations, the majority of fluorescent signals from previously identified sensory neurons, and even auto-fluorescence signals from muscles developed into overtly saturated patterns of expression.

Nonetheless, in males, I observed ramifications on the testes, ejaculatory duct, accessory glands, vas deferens and seminiferous tubules of the internal genitalia (Figure 4-18A). These patterns of expression are in keeping with the topology of innervations of *dsx*^{GAL4}-expressing neurons in the male reproductive system (Rideout et al., 2010). Interestingly, expression of *dsx* has been shown to be necessary for the determination of a full complement of *fru*-expressing, male-specific, serotonergic neurons of the abdominal ganglia (SAbg) that innervate the ejaculatory duct, accessory glands, vas deferens and seminiferous tubules (Billeter et al., 2006b). The co-localisation of *dsx*^{GAL4}-expression with ~3 neurons, each of both the dorsal and ventral SAbg clusters, suggests that the innervations described here, baring those ramifying on the testes, are essentially from *dsx* and *fru* positive SAbg neurons (Billeter et al., 2006b; Dornan, 2011). On the other hand however, neurons that do ramify on the testes appear functionally distinct, as they have been shown not to co-localise with serotonin (Dornan, 2011). Unfortunately, the congruence of *dsx*$^{GAL4\text{-}DBD}$/*elav*$^{VP16\text{-}AD}$-expressing

neural innervations with serotonin was not investigated here, however, descriptions of these neurons will be determined as part of future work.

Further to these findings, *dsx*$^{GAL4\text{-}DBD}$/*elav*$^{VP16\text{-}AD}$-expressing neurons were also found to innervate the protractor muscles of the aedeagus (Figure 4-18B). The external portion of the aedeagus consists of a medial sclerotised pointed lobe through which the ejaculatory duct discharges, while a long apodeme extends into the body from the base of the aedeagus (Miller, 1950). The protractor muscles connect the aedeagal apodeme to the hypandrium, and are capable of causing conformational changes and protraction of the phallic organs during copulation (Kamimura, 2010). It is possible that the innervations from *dsx*$^{GAL4\text{-}DBD}$/*elav*$^{VP16\text{-}AD}$-expressing motoneurons are capable of controlling the contraction of these muscles, and thus, by implication, control protraction of the phallic organs for accurate genital coupling during copulation. Additional muscle groups associated with the aedeagus did not appear to exhibit innervations from *dsx*$^{GAL4\text{-}DBD}$/*elav*$^{VP16\text{-}AD}$-expressing motoneurons (Figure 4-18B); however, given the saturated non-specific fluorescence signals in the muscles that occurred as a consequence of amplifying the reporter signal, the complete pattern of innervations within other muscles of the aedeagus remain inconclusive. Further analyses using more potent and/or multiple copies of reporters may improve the strength of reporter expression and detection in these whole mount preps, allowing for a more detailed characterisation of the innervations on the aedeagus.

In females, I observed a pattern of expression of a fine network of neurites encapsulating the ovaries and lateral oviducts, analogous to that seen ramifying on the male internal genitalia (Figure 4-18C,D). These observations are again complementary with that of to the reported patterns of innervations using the *dsx*^{GAL4} driver (Rideout et al., 2010). However, I also observed innervations ramifying on the muscles of the seminal receptacle, spermathecae and parovarian ducts, and uterus (Figure 4-18C,D). It is conceivable that the motoneurons innervating these structures modulate/control their contractions, ultimately regulating insemination and oviposition. In support of this hypothesis, silencing the activity of all *dsx*^{GAL4}-expressing neurons in females renders them sterile (Rideout et al., 2010). Given that the observed infertility was not a consequence of failure to transfer sperm or seminal fluid,

and that these females did not display live births, this suggests that the infertility is due to an inability to ovulate eggs into the uterus and/or a lack of sperm release from the seminal receptacle and spermathecae (Rideout et al., 2010); both of which prevent sperm from penetrating through the egg's micropyle to fertilize the embryo (Miller, 1950).

It is important to note that the observations described here identify novel components of *dsx* circuitry: motoneuron innervations that ramify on muscles of the male and female internal reproductive systems (Figure 4-18). Given the broad patterns of *dsx*-expression throughout the entire adult reproductive system of males and females (Rideout et al., 2010), these observations would not have been made possible without restricting patterns of expression to *dsx*-expressing neurons with the novel $dsx^{GAL4\text{-}DBD}/elav^{VP16\text{-}AD}$ driver.

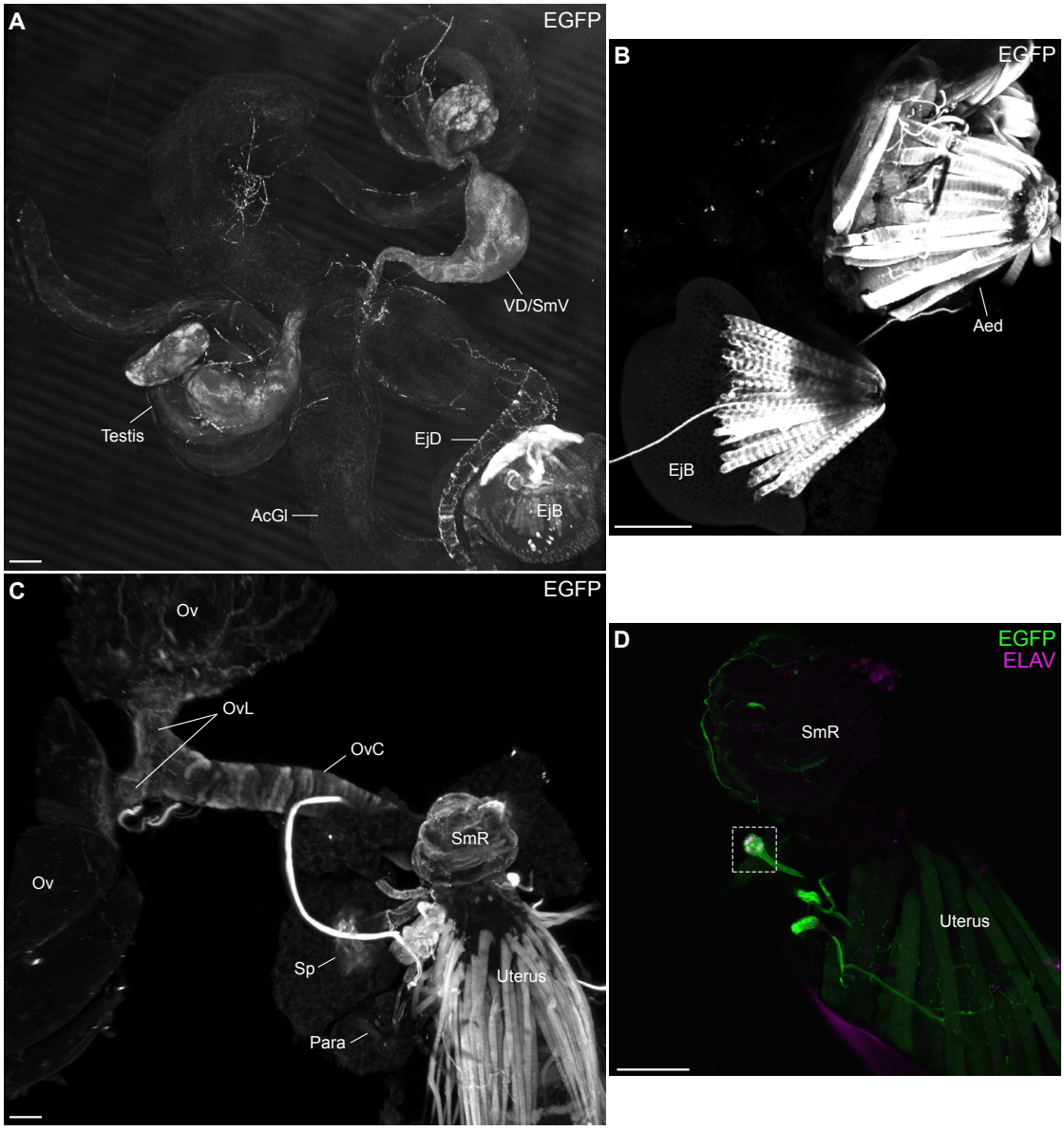


Figure 4-18 5 day old adult *dsx*$^{GAL4\text{-}DBD}$/*elav*$^{VP16\text{-}AD}$-expressing neurons innervate male and female internal reproductive systems.
(A) Detail of innervations to the male internal genitalia; testes, seminal vesicles (SmV), vas deferens (VD), accessory glands (AcGl) and ejaculatory duct (EjD) indicated. (B) Detail of innervations to the aedeagus (Aed) with no observable innervations to the ejaculatory bulb (EjB) indicated. (C) Detail of innervations to female internal genitalia; ovaries (Ov), lateral and common oviducts (OvdL and OvdC), seminal receptacle (SmRcp), spermathecae (Sp), paravoria (Para) and uterus indicated. (D) Higher magnification, and subset of the maximal confocal stack, showing detail of innervations that target the muscles of the uterus. Sensory neurons of the uterus, co-expressing ELAV (magenta) shown in white dotted box. Cytoplasmic EGFP realised with anti-GFP antibody (white in A-C, green in D). Anti-ELAV (ELAV) is shown in magenta in D. Scale bar = 50 μm.

4.3.3.2 *dsx*$^{GAL4\text{-}DBD}$/*elav*$^{VP16\text{-}AD}$-expressing motoneurons innervate longitudinal muscles of the dorsal abdomen in adult males and females

Neurons of the Abg gives rise to a pair of nerves that innervate the first and second abdominal segments, in addition to the thick median AbNrTr that gives off nerves to more posterior abdominal segments, of which the most terminal branches innervate the internal reproductive organs (Miller, 1950). The weak levels of *dsx*$^{GAL4\text{-}DBD}$/*elav*$^{VP16\text{-}AD}$-driven EGFP expression in neural projections emerging from neurons of the abdominal ganglia made the search for smaller nerves that branch off the trunk of the AbNrTr before reaching the internal reproductive systems challenging and inconclusive. However, as the longitudinal muscles of the abdominal segments are the only other structures, besides those of the internal reproductive system, that may be innervated by the AbNrTr, I went on to interrogate the presence of ramifications on the abdominal muscles.

The ventral and dorsal plates found in each segment of the adult abdomen are called sternites and tergites respectively. In dorsal abdominal segments, muscle fibres attach midway into each tergite and to the anterior edge of the next segment. Amongst these dorsal abdominal muscles is the male-specific muscle of Lawrence (MOL), a structure that spans the border between abdominal segments 5 and 6 (Lawrence and Johnston, 1984). The presence of *dsx*$^{GAL4\text{-}DBD}$/*elav*$^{VP16\text{-}AD}$-expressing abdominal nerve innervations, to dorsal abdominal muscles, was investigated via flat preparations of the dorsal abdominal segments of both males and females expressing EGFP under the control of *dsx*$^{GAL4\text{-}DBD}$/*elav*$^{VP16\text{-}AD}$ (Figure 4-19). By staining the samples with anti-GFP, and realising the muscle fibres with phalloidin antibody, I was able to observe expression in innervations of the complete set of longitudinal muscles of abdominal segment 6 (A6) in both males and females (Figure 4-

19A,C). The size and number of longitudinal muscles differ between the sexes (Figure 4-19), which may be a consequence of the sexually dimorphic number of abdominal segments (6 in males and 8 in females, excluding the anal segment). Much like A8 in females, A6 in males is directly connected to the anal segment; suggesting that this segment must house additional muscles that are analogous to the supraspiracular, sternal, supra- and sub-anal muscles (to name a few) that attach to parts of the internal reproductive system and analia including the uterus and anal plates, that have been documented in females (Miller, 1950). Interestingly in males, the preparations revealed lateral muscles that also appear to be innervated by *dsx*$^{GAL4\text{-}DBD}$/*elav*$^{VP16\text{-}AD}$-expressing motoneurons (Figure 4-19B); however, the target organs to which these muscles attach remain unknown.

Interestingly, in both males and females, all the observed motor nerve terminals are large boutons of the Ib-type (Figure 4-19A1,B1,C1); a feature associated with adult glutamatergic motoneurons (Atwood et al., 2003; Rivlin et al., 2004). A lack of precise neuroanatomical descriptions and/or functional interrogations of these A6 dorsal muscles compound the difficulties associated with my ability to make interpretations of these findings. It can be postulated however, that these muscles may, in part, control abdominal unbending in males for successful copulation, and possibly abdominal contractions in females that facilitate oviposition.

Much attention has been given to the male-specific MOL that is innervated by a *fru*-expressing, MOL-inducing, glutamatergic motoneuron (also known as the ‘Mind’ neuron; Lawrence and Johnston, 1986; Gailey et al., 1991; Billeter et al., 2006b; Usui-Aoki et al., 2000; Nojima et al., 2010), that gives rise to large Ib-type synaptic boutons, and a second uncharacterised octopminergic neuron that gives rise to smaller type-II boutons (Nojima et al., 2010). Given that allelic variations at the *dsx* locus do not influence the development or morphology of the MOL (Taylor, 1992), suggests that *dsx* is not expressed in the Mind neuron. However, it is possible that *dsx* may still be expressed in the second octopaminergic neuron that does not serve to provide and inductive developmental signal, but is thought to have a neuromodulatory role (Nojima et al., 2010). Using the flat abdominal preps, I was

unable to observe any *dsx*$^{GAL4\text{-}DBD}$/*elav*$^{VP16\text{-}AD}$-expressing innervations to the MOL (data not shown). The complete absence of *dsx* positive innervations to the MOL, by implication, demonstrates that both the Mind and octopaminergic neurons do not express *dsx.*

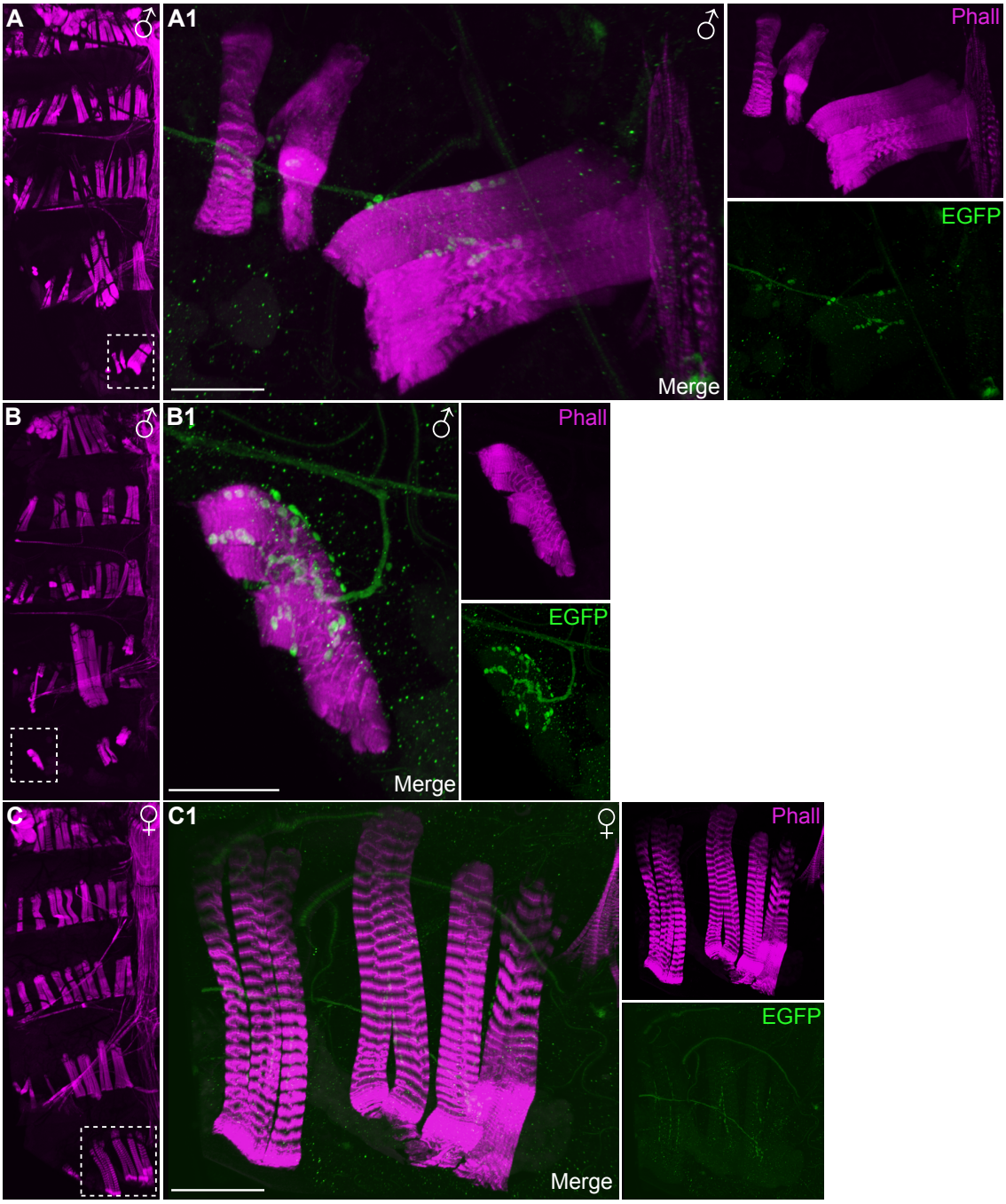


Figure 4-19 *dsx*$^{GAL4\text{-}DBD}$/*elav*$^{VP16\text{-}AD}$-expressing motoneurons innervate longitudinal muscles of the dorsal abdomen in 5 day old adult males and females.
(A) Flat dorsal abdominal preparation of 5 day old adult males demonstrating longitudinal muscles associated with abdominal segments A2-A6 that are counterstained with phalloidin. Longitudinal muscles of abdominal segment A6 shown in white dotted box. (A1) Higher magnification of longitudinal muscles of abdominal segment A6 with realised morphology of *dsx*$^{GAL4\text{-}DBD}$/*elav*$^{VP16\text{-}AD}$-expressing motoneuron innervations and synaptic termini. (B) Flat dorsal abdominal preparation of 5 day old adult males demonstrating lateral longitudinal muscles associated with abdominal segments A2-A6 that are counterstained with phalloidin. Lateral longitudinal muscles of abdominal segment A6 shown in white dotted box. (B1) Higher magnification of lateral longitudinal muscles of abdominal

segment A6 with realised morphology of *dsx*$^{GAL4\text{-}DBD}$/*elav*$^{VP16\text{-}AD}$-expressing motoneuron innervations and synaptic termini. (C) Flat dorsal abdominal preparation of 5 day old adult females demonstrating longitudinal muscles associated with abdominal segments A2-A6 that are counterstained with phalloidin. Longitudinal muscles of abdominal segment A6 shown in white dotted box. (B1) Higher magnification of longitudinal muscles of abdominal segment A6 with realised morphology of *dsx*$^{GAL4\text{-}DBD}$/*elav*$^{VP16\text{-}AD}$-expressing motoneuron innervations and synaptic termini. Cytoplasmic EGFP realised with anti-GFP antibody (green). Anti-Phalloidin (Phall) is shown in magenta. Scale bar = 50 µm.

4.3.4 *dsx*$^{GAL4\text{-}DBD}$/*elav*$^{VP16\text{-}AD}$-expressing neurons and their role in reproductive behaviours

dsx mutants are known to display aberrant courtship behaviours (McRobert and Tompkins, 1985; Villella and Hall, 1996; Waterbury et al., 1999; Rideout et al., 2007; Rideout et al., 2010); however, evidence substantiating a role of *dsx*-expressing neurons in directing sex-specific courtship behaviours only recently came to light (Rideout et al., 2010). Expressing the tetanus neurotoxin light chain (TNT) in *dsx*^{GAL4} cells disrupted synaptic activity in *dsx*-expressing neurons by acting specifically on neural synaptobrevin (n-Syb; Sweeney et al., 1995). As a result of silencing all *dsx*-expressing neurons, Rideout et al. (2010) demonstrated complete behavioural and physiological sterility, the details of which are discussed in more detail below (Rideout et al., 2010). To verify the neural aetiology of the observed behavioural defects, Rideout et al. (2010) co-expressed the pan neuronal GAL4 inhibitor *elav-GAL80,* demonstrating significant recovery of courtship behaviours and fertility (Rideout et al., 2010). Using the same approach, I carried out silencing experiments to behaviourally compare the novel *dsx*$^{GAL4\text{-}DBD}$ allele to the original *dsx*^{GAL4} allele (Figure 4-20; Figure 4-21). To allow for an independent, impartial comparison, I not only assayed the behaviour of animals expressing UAS-TNT using the novel *dsx*$^{GAL4\text{-}DBD}$/*elav*$^{VP16\text{-}AD}$, I also repeated the original experiment using the *dsx*^{GAL4} driver; the results of which are discussed below.

4.3.4.1 *dsx*$^{GAL4\text{-}DBD}$/*elav*$^{VP16\text{-}AD}$ neurons are necessary for male sexual behaviour

After one week in the presence of two virgin females, males of both genotypes, *dsx*^{GAL4} and *dsx*$^{GAL4\text{-}DBD}$/*elav*$^{VP16\text{-}AD}$, were completely infertile ($P<0.0001$; Figure 4-20A). A more detailed investigation of these males was then carried out, demonstrating that this infertility phenotype was a consequence of defects in courtship and mating behaviours. When paired with a virgin

female, the time to initiate courtship by UAS-TNT;*dsx*^{GAL4} and UAS-TNT;*dsx*$^{GAL4\text{-}DBD}$/*elav*$^{VP16\text{-}AD}$ males was significantly higher than controls (P<0.001 and P<0.0001 respectively; Figure 4-20B), and once initiated, consisted entirely of brief intermittent bouts of orientation and following, with a complete lack of wing extension and with no subsequent attempts to copulate. Hence, the computed amount of courtship performed by males of both genotypes was significantly reduced (P<0.0001; Figure 4-20C). During an extended 2-hour observation period, approximately 95% of all cohorts of control flies successfully copulated; however, none of the experimental genotypes successfully copulated (P<0.0001; Figure 4-20D). Courtship duration was measured for, as an added parameter to assess control groups; all of which showed no significant difference (Figure 4-20E).

In accord with the observations of Rideout et al. (2010), our experiments directly demonstrate that the specific disruption of the entire *dsx* neural circuitry effectively inhibits male courtship behaviours; and in doing so, these data reveal the necessity of *dsx* neural circuitry for all fundamental aspects of male copulatory behaviours.

4.3.4.2 *dsx*$^{GAL4\text{-}DBD}$ neurons are critical for female sexual behaviour

A similar approach to that of the male was used to investigate the role of *dsx*$^{GAL4\text{-}DBD}$ cells in female sexual behaviour. After one week in the presence of two males, females expressing UAS-TNT were completely infertile in both experimental cohorts (*dsx*^{GAL4} and *dsx*$^{GAL4\text{-}DBD}$/*elav*$^{VP16\text{-}AD}$) (P<0.0001; Figure 4-21A). When scored for courtship behaviour, females of both cohorts actively rebuffed wild-type males during copulation through sustained wing flicks, kicking and a failure to remain stationary during copulation, as previously described (Rideout et al., 2010). Although males often managed to grasp hold of a female, they never manage to spread the female's wings during copulation. All together, this resulted in a marked increase in locomotion of copulating pairs compared with controls (P<0.001; Figure 4-21B). Although the majority of females of all cohorts copulated within the first 10 minutes of a 2-hour observation period (data not shown), in the case of the experimental cohorts, this appears more a testament to the persistence of the courting wild-type male. As such, a significant decrease in the duration of copulation of these experimental females was

observed, when compared with controls ($P<0.001$; Figure 4-21D), presumably as a consequence of the vigorous rejection and persistence of locomotion displayed by these females. Interestingly, and in accord with previous findings, approximately 35% of *UAS-TNT*; dsx^{GAL4} females and approximately 45% of *UAS-TNT*; $dsx^{GAL4\text{-}DBD}$/$elav^{VP16\text{-}AD}$ females were observed to re-mate with the same male during the 2 hr observation period, although they continued to exhibit vigorous rejection behaviours throughout ($P<0.001$, $P<0.0001$ respectively; Figure 4-21D) (Rideout et al., 2010). Control females never re-mated during the observation period (Rideout et al., 2010).

That our observations, using both *dsx* alleles, reiterate those of Rideout et al. (2010) validates that the specific disruption of the entire *dsx* neural circuitry effectively impinges on distinct female-specific behaviours (Figure 4-21). Not only do these data demonstrate the necessity of this neural substrate for the specification of female behavioural outputs, but also demonstrate a pivotal role for *dsx*-dependent female behaviours in the successful completion of the wild-type courtship repertoire.

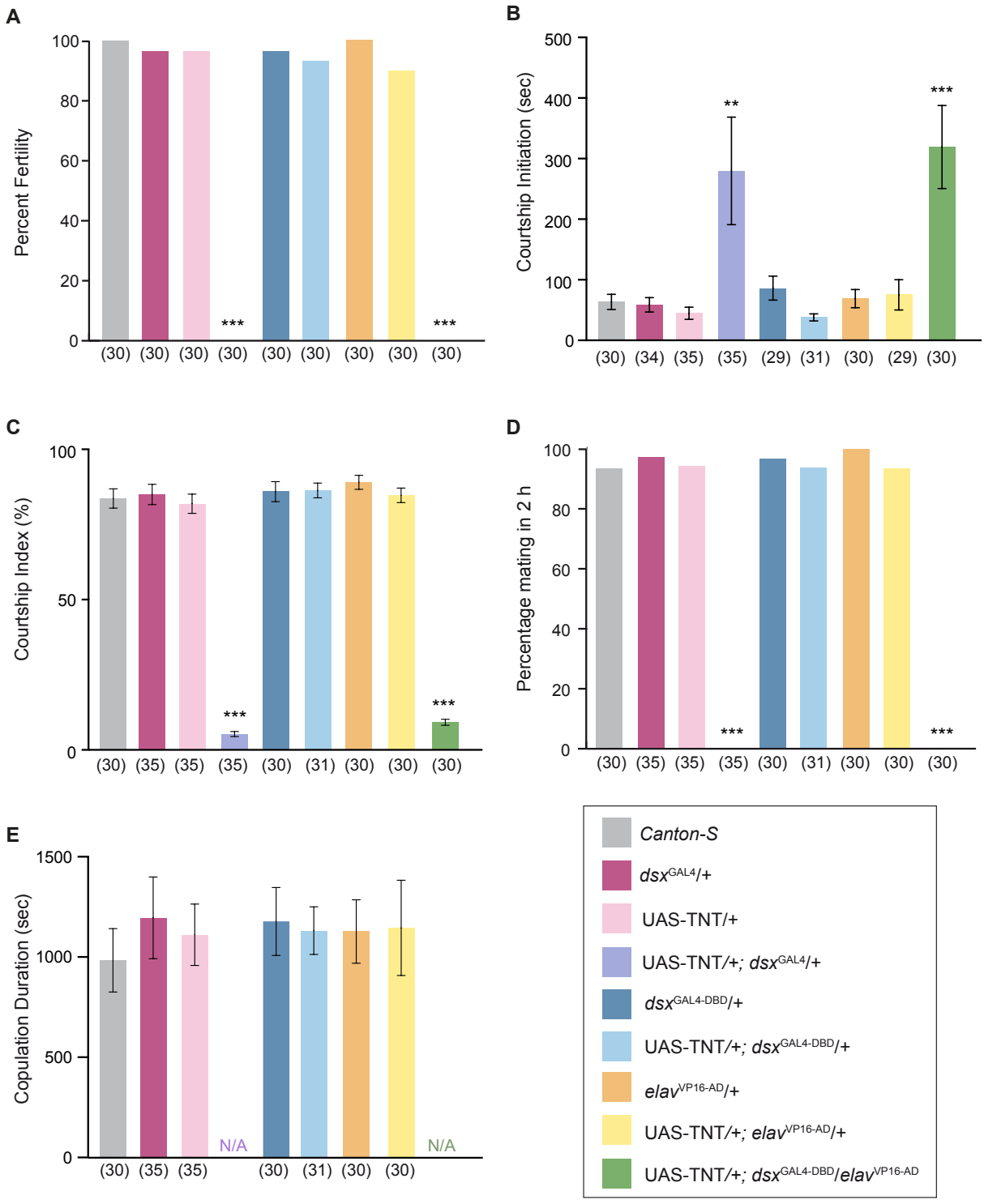


Figure 4-20 *dsx*$^{GAL4\text{-}DBD}$/*elav*$^{VP16\text{-}AD}$-expressing neurons control male sexual behaviour.
(A) Male fertility (***P<0.0001, Fisher exact test). (B) Courtship initiation (mean ± s.e.m.. **P<0.001, ***P<0.0001, Kruskal-Wallis and Dunn's test). (C) Courtship index (mean ± s.e.m., ***P<0.0001, Kruskal-Wallis and Dunn's test). (D) Percentage of male matings in 2 h (***P<0.0001, Fisher exact test). (E) Copulation duration (mean ± s.e.m. Kruskal-Wallis and Dunn's test).

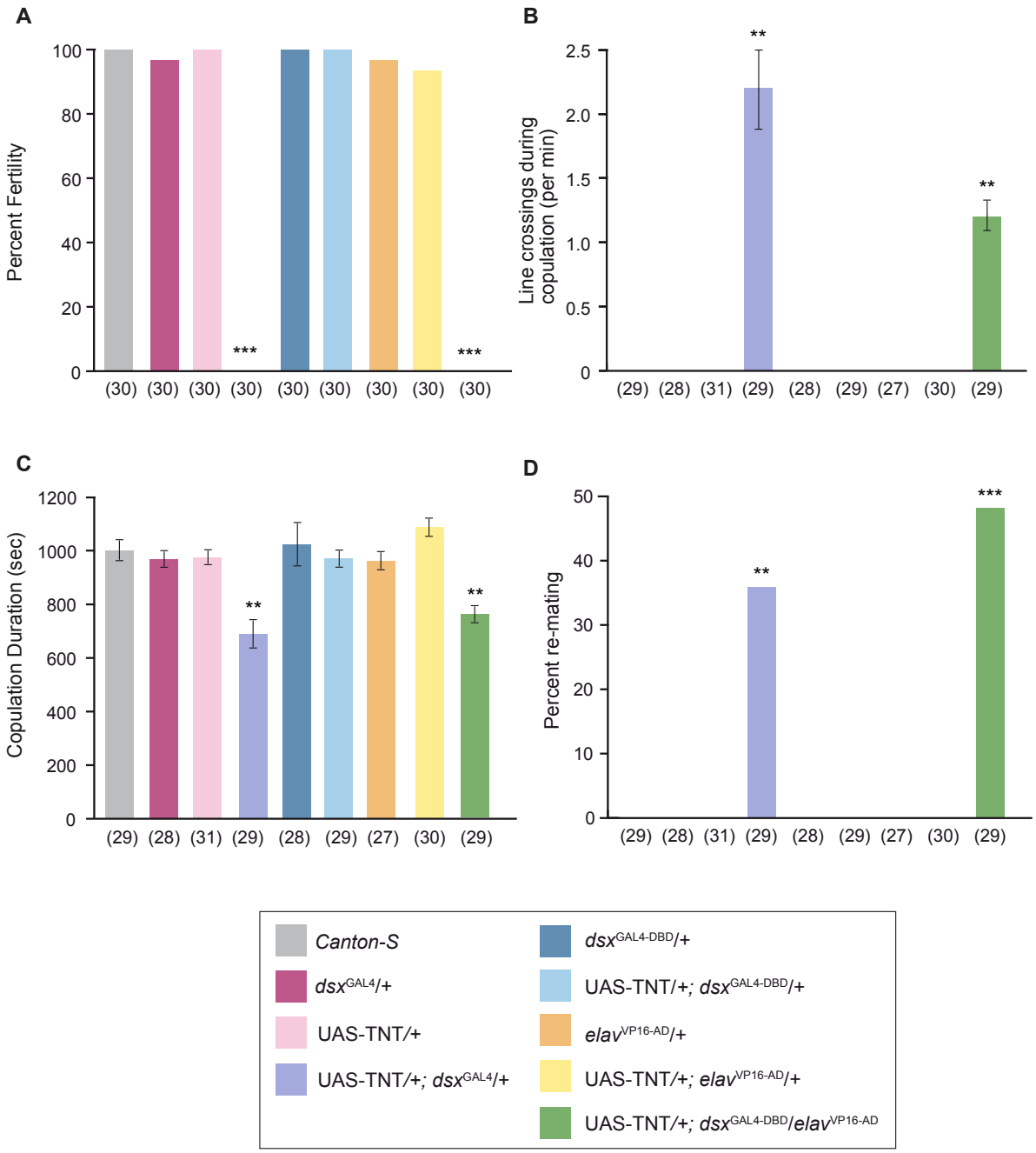


Figure 4-21 *dsx*$^{GAL4\text{-}DBD}$/*elav*$^{VP16\text{-}AD}$-expressing neurons are critical for female sexual behaviour. (A) Female fertility (***P<0.0001, Fisher exact test). (B) Line crossings during copulation (mean ± s.e.m., **P<0.001, Kruskal-Wallis and Dunn's test). (C) Copulation duration (mean ± s.e.m., **P<0.001, Kruskal-Wallis and Dunn's test). (D) Percentage of females that re-mate with the same male in 2 h (**P<0.001, ***P<0.0001, Fisher exact test).

4.4 Discussion

I have, through these investigations, demonstrated that an operative GAL4-DBD element has been successfully integrated into the endogenous *dsx* locus via homologous recombination. Importantly, this transgenic line remains viable, and flies homozygous for the *dsx*$^{GAL4\text{-}DBD}$ allele appear to be wild-type in gross morphology and fertility, suggests no impingement on normal gene expression. I have, by pairing this novel allele with the previously published pan neuronal hemidriver *elav*$^{VP16\text{-}AD}$ (Luan et al., 2006), demonstrated the complete reiteration of *dsx*^{GAL4}-expression within the CNS. Further to this, I have revealed novel patterns of *dsx*-expression in the PNS, and, finally, demonstrated that manipulating *dsx* function specifically in *dsx*$^{GAL4\text{-}DBD}$/ *elav*$^{VP16\text{-}AD}$-expressing neurons reprises the functional roles of endogenous *dsx* in specifying male and female sexual behaviours, ultimately validating of this tool for this and future studies.

It should be noted that since the inception of the Split-GAL4 system, (Luan et al., 2006), this study represents one of the, if not the, first attempts at targeting the insertion of the GAL4-DBD hemidomain into an endogenous gene locus via homologous recombination, that has proved to be successful. It is by validating this tool in this chapter, that I demonstrate the experimental elegance and sophistication that this system presents. As this novel tool lends itself to a plethora of approaches, its utilisation will not only enable the neuroanatomical and functional dissection of the dsx circuitry specifying male and female reproductive behaviours, but it will also provide insight into how the sexually dimorphic nervous system and the soma orchestrate to generate the 'complete' male or female adult.

4.4.1 Expression dictated by *dsx*$^{GAL4\text{-}DBD}$/*elav*$^{VP16\text{-}AD}$ in the CNS

The initial sections of this chapter dealt with the overall spatial expression patterns generated by the *dsx*$^{GAL4\text{-}DBD}$/*elav*$^{VP16\text{-}AD}$ driver via a general comparative approach. To assess the extent to which the *dsx*$^{GAL4\text{-}DBD}$/*elav*$^{VP16\text{-}AD}$ driver reflects *dsx*^{GAL4} neural expression, I compared the expression patterns of nuclear and cytoplasmic reporters both within and outwith the NS, between the two drivers. It is important to mention that the comparative analyses performed in this chapter involved the solitary use of the original *dsx*^{GAL4} allele generated by Rideout et

al. (2010), and did not include comparisons with the second *dsx*^{GAL4} allele generated by Robinett et al. (2010). Given the analogous construct design, strategy of gene targeting and the comprehensive neuroanatomical and behavioural characterisations provided by Rideout et al. (2010), it made logical sense to compare the novel allele to this 'parent' *dsx*^{GAL4} allele.

In doing so, I focused on the most overt features of dimorphic expression in the CNS, including: i) increased number of neurons in pC1, pC2 and pC3 clusters of the dorsal brain in males, when compared to females, ii) presence of male-specific SN cluster of the SOG and TN1 and TN2 clusters of the Msg, iii) higher density of projection patterns associated with the lateral protocerebral complex of the brain in males, when compared to females iv) male-specific projections that give rise to the MsT and v) male-specific midline crossings of GRNs of the foreleg in the Msg. That the novel allele exhibited all these key features, demonstrates that it's patterns of expression are congruous with previous characterisations of *dsx*-expression in the CNS (Lee et al., 2002; Billeter et al., 2006b; Kimura et al., 2008; Rideout et al., 2007; Rideout et al., 2010; Robinett et al., 2010), and are practically identical to the patterns of expression exhibited by the original *dsx*^{GAL4} allele (Rideout et al., 2010). Formal validation of the novel allele, as a reporter of *dsx*-expression, came from a spatiotemporal survey or expression in the CNS together with cell counts of the final male and female adult circuitry. In realising the expression patterns of *dsx* circuitry, three distinct modes of sexual dimorphism were confirmed: (i) sex-specific neuronal clusters; (ii) differences in cell numbers within a given cluster; and (iii) sex-specific arborisations (Lee et al., 2002; Billeter et al., 2006b; Kimura et al., 2008; Rideout et al., 2007;Rideout et al., 2010; Robinett et al., 2010). These features ultimately demonstrate the multiplicity of possible differences in connectivity within *dsx* circuitry itself, and between *dsx* circuitry and non-*dsx*-expressing circuitry; all of which concertedly contribute to determining a neural architecture capable of eliciting sex-specific behaviours. Altogether, these data categorically validate this novel allele as a genetic tool capable of faithful reiteration of *dsx* expression in the CNS and of precise spatial restriction of expression to the NS.

In mapping *fru* circuit elements, Yu et al. (2011) hypothesised that the majority of non-sex-specific neurons that possess differences in connectivity serve to receive sensory information or generate motor outputs; superficially assigning these neurons as the start and end points to a given circuitry (Yu et al., 2011). Further to this, Yu et al. (2011) hypothesised that the majority of sexually dimorphic cells and/or cell clusters function to process sensory information to subsequently command the appropriate downstream response(s) (Yu et al., 2011). Given the overlap between *dsx* and *fru* circuitry in males, it would be interesting to determine if the same principles of functional organisation will apply to different *dsx* circuit elements. Indeed from the perspective of higher-order processing, studies have already implicated dimorphic *dsx*- and *fru*- intersecting clusters in sensory integration and in commanding motor response (Rideout et al., 2007; Kimura et al., 2008; Clyne and Miesenbock, 2008; Kohatsu et al., 2011; von Philipsborn, 2011; Pan et al. 2011; Pan et al., 2012). Considering the differences in the number of neurons that comprise *fru* and *dsx* circuitries (~2000 *fru* neurons *vs.* ~650 *dsx* neurons), it is clear that *dsx* offers a more restricted paradigm of male courtship (Lee et al., 2000; Lee et al., 2002; Billeter and Goodwin, 2004; Demir and Dickson, 2005; Billeter et al., 2006a; Rideout et al., 2010; Robinett et al., 2010). Hence, utilising the novel $dsx^{GAL4\text{-}DBD}$ allele to parse *dsx* circuitry into functionally distinct components may prove to be an essential step towards dissecting the circuitry required for the performance of male sexual behaviours.

It is also important to re-emphasise is that any circuitries that are actively specified in the female are likely to depend on the female isoform Dsx^{F}, as a sex-specific Fru isoform is absent in females. Thus, expanding these interrogations to the female will not only enable the functional delineation of *dsx* circuit elements underlying female behaviours, but will also serve to better understand the differences in the operation of this circuitry, between males and females.

4.4.2 Expression dictated by $dsx^{GAL4\text{-}DBD}$/$elav^{VP16\text{-}AD}$ in the PNS

The comparative survey of expression between $dsx^{GAL4\text{-}DBD}$/$elav^{VP16\text{-}AD}$ and dsx^{GAL4} included several somatic tissues. The most compelling demonstration of the efficacy of the split

dsx$^{GAL4\text{-}DBD}$/*elav*$^{VP16\text{-}AD}$ system to restrict expression to the NS (in comparison to the original *dsx*^{GAL4}) was illustrated by the complete absence of expression in larval and adult fat body and oenocytes, together with a severe reduction in expression observed in the reproductive system and tissues of the alimentary tract. The lack of amenable reagents has, up till now, meant that there has been no encompassing understanding of where *dsx* may be expressed within the fly's PNS. However, based on, and subsequent to, these preliminary findings, the investigations performed within the latter parts of this chapter aimed at providing a far more comprehensive survey of the spatial patterns of expression for all *dsx* neurons of the PNS. In doing so, this has vastly increased our understanding of *dsx* expression in sensorium of the PNS in both males and females.

The expression of *dsx* in the PNS, namely in sexually dimorphic gustatory neurons of the foreleg, has previously been demonstrated (Rideout et al., 2007; Kimura et al., 2008; Mellert et al., 2010; Rideout et al., 2010; Robinett et al., 2010). However as exemplified in this study, the expression of *dsx*$^{GAL4\text{-}DBD}$/*elav*$^{VP16\text{-}AD}$-expression in the PNS further encompasses numerous sensory neurons associated with various sense organs within the labial palps and internal and external reproductive systems of adult males and females. Much like the patterns of *dsx*-expression in the CNS, *dsx*$^{GAL4\text{-}DBD}$/*elav*$^{VP16\text{-}AD}$-expression has allowed me to restrictively assign expression within the PNS to a subset of neurons within specific sensory structures.

During the 'tapping' and 'licking' stages of courtship males are believed to assess a potential mate's sex and species (and perhaps fitness) via non-volatile contact-mediated pheromones, the reception of essential gustatory information occurring largely via GRNs of the foreleg and labial palps (reviewed by Pavlou and Goodwin, 2013). The sexually dimorphic pattern of *dsx*$^{GAL4\text{-}DBD}$/*elav*$^{VP16\text{-}AD}$-expression in neurons of the foreleg, together with the dimorphic projections associated with these neurons, are reminiscent of previously identified GRNs; a small subset of which have been shown to express *fru* in males (reviewed by Pavlou and Goodwin, 2013). Classification of both foreleg and labial GRNs by surveying them for expression of different gustatory receptors and ion channel genes has been attempted,

however the pheromones that the majority of these receptors recognise and their relationship to *dsx*-expressing GRNs has yet to be investigated.

Further experiments in which $dsx^{GAL4\text{-}DBD}/elav^{VP16\text{-}AD}$-expression is shown to correspond to *bona fide* Dsx expression via antibody and/or *in-situ* hybridisation, will be necessary to confirm *dsx* activity. Using *dsx* mutants, the role of Dsx in the development of these neurons may then be interrogated. Finally examining the function of these neurons, via additional intersectional strategies, should identify which Grs and/or ion channels are expressed in these neurons; while electrophysiological recordings from these neurons, upon exposure to female- and/or male-enriched hydrocarbons, could functionally assign these neurons based on the pheromones they detect. Given that the vast extant Gr-GAL4 collection cannot, unfortunately, be used in combination with the current split GAL4 system, future experiments will require the generation of novel *dsx* drivers that are capable of being used combination with extant GAL4 lines to gain genetic access to, and functionally characterise, these neurons.

Axons of *Gr32a*-expressing GRNs have been shown to terminate in the SOG, and are thought to form connections with second-order *fru*-expressing neurons that subsequently relay this signal to the higher-order centres of the brain, implying that sensory neurons that do not express *fru* are capable of relaying information to *fru*-expressing downstream 'processing' circuitry (Koganezawa et al., 2010; reviewed by Pavlou and Goodwin). That non-*dsx*-expressing GRNs may connect to *dsx*-downstream circuitry is certainly a possibility, and must be kept in mind. Although formal examples of *dsx* circuitry connecting to non-*dsx* circuitry have yet to be revealed, the fact that *dsx* has been shown to act both in concert and in complement to *fru* in males (Kimura et al., 2005; Rideout et al., 2007; Kimura et al., 2008; Sanders and Arbeitman, 2008; Rideout et al., 2010), and appears to act by itself in an analogous manner in females, to provide a neural substrate necessary to the generation of pivotal dimorphic courtship behaviours would lend itself strongly to the supposition that *dsx* circuitry also connects to non-*dsx* circuitry to support these dimorphic behavioural outputs. A foretaste of this comes from the artificial activation of *dsx*-expressing male-specific neurons

of the Msg, which elicits unilateral wing extension and courtship song production; the fact that all the neurons activated here are interneurons demonstrates their relationship with non-*dsx*-expressing motoneurons that are capable of directing the flight muscles to extend a wing and generate courtship song (Pan et al., 2011). In this example, *dsx* neurons take on the role of a dimorphic remote control, which acts upon independent circuit elements that need not be sexually dimorphic (such as the direct flight muscles), however a multiplicity of such connections may occur with practically each circuit element within the *dsx* circuitry.

The intestinal tract plays a central role in absorption and digestion of nutrients, maintaining energy homeostasis by exchanging neural and endocrine signals with other organs (reviewed by Lemaitre and Miguel-Aliaga, 2013). The differing homeostatic requirements of males and females may be met by means of dimorphic neural feedback from and/or control of the intestinal tract. One aspect, modulation of intestinal transit, is thought to be carried out by *OK371-GAL4*-expressing motoneurons that ramify on three segments of the intestine that contain valves or sphincters, including the muscles of the proventriculus (Cognini et al., 2011). In the case of the observed *dsx*$^{GAL4\text{-}DBD}$/*elav*$^{VP16\text{-}AD}$-expressing cells within specific muscle layers of the proventriculus, these cells may serve to contract upon direction from the CNS. The most intriguing observation of expression within the intestinal tract is the expression of *dsx*$^{GAL4\text{-}DBD}$/*elav*$^{VP16\text{-}AD}$ in a subset of EECs of the midgut. EECs are not only abundant, but given that different EECs produce different hormonal peptides, EECs of the midgut are also functionally diverse (reviewed by Lemaitre and Miguel-Alliaga, 2013). Interestingly, EECs undergo a conserved developmental program, similar to that of neurons (Harteinstein et al., 2010; Takashima et al., 2011), and since the midgut exhibits the least number of innervations when compared to other portions of the intestinal tract (Cognini et al., 2011), it has been postulated the EECs may function like neurons in conveying information on nutritional state to other organs, and/or directly regulating intestinal physiology (Lemaitre and Miguel-Alliaga, 2013). That *dsx*$^{GAL4\text{-}DBD}$/*elav*$^{VP16\text{-}AD}$ in expressed in only a subset of these EECs, implicates them in a sex-specific role that may serve to maintain appropriate sex-specific physiology, that is not only pertinent to diet, but also to reproductive state. It is also possible that the limited expression within the putative EECs may be reflective of an

immunofluorescence ‘snapshot’, as different populations of cells may actively express *dsx* while others remain quiescent; the specification of which may depend upon the developmental/physiological state. Mated females appear to decrease the intestinal transit speed, resulting in highly concentrated faecal outputs, as a result of receiving a dose of sex peptide (SP) during copulation (Cognini et al., 2011). The dramatic physiological switch that is SP has also been shown to impose changes in caloric intake, physiology (for egg production), post-mating behaviours, and immune responses (Liu and Kubli, 2003; Peng et al., 2005; Carvalho et al., 2006; Hasemeyer et al., 2009; Yang et al., 2009). Comparative experiments which involve assaying such behaviours as measuring food intake, faecal output and faecal pH, using both virgins and mated males and females, after the directed/restricted ablation of $dsx^{GAL4\text{-}DBD}/elav^{VP16\text{-}AD}$-expressing EECs may help functionally assign a role for these cells.

The presence of $dsx^{GAL4\text{-}DBD}/elav^{VP16\text{-}AD}$-expression in restricted peripheral neurons of the internal and external reproductive system and terminalia is quite telling of their function. During copulation, the ejaculatory bulb gradually squeezes the entire volume of sperm contained within the sperm chamber through the short posterior ejaculatory duct and the aedeagus into the female genital tract, forming a typical viscous plug (Bairati, 1968; Lung and Wolfner, 2001). The observed expression of $dsx^{GAL4\text{-}DBD}/elav^{VP16\text{-}AD}$ associated with the crown of muscles operating the compression mechanism is likely to be responsible for the modulation of contractions and ultimately ejaculation. Further expression was observed in ~5 neurons within the sperm chamber itself, the morphology of which resembles that of mechanoreceptors. Although little is known about the function of these neurons, Bairati (1968) referred to them collectively as a “peculiar receptive apparatus controlling bulb compression”. It is possible to envision that the active pumping of sperm and seminal fluid into the sperm chamber of the ejaculatory bulb, by the anterior ejaculatory duct, would prime the compression mechanism through the activation of these mechanoreceptors. Alternatively, these neurons may act to regulate the contractions of the crown muscles, by sensing the capacity of the sperm chamber; inhibiting muscular contraction until the chamber is full. Although previous studies have shown that thermoactivation of the *dsx* circuitry is

sufficient for ejaculation (Pan et al., 2011), definitive proof of the involvement of these neurons in mediating contraction of the ejaculatory bulb is warranted.

During copulation, a wild-type female will receive a complex package of sperm, to fertilise the eggs, and a mixture of various accessory gland proteins (AcGl), including SP, to induce a suite of stereotypical post-mating responses (Kubli, 2003; Liu and Kubli, 2003). These postmating responses include increased ovulation rates, altered locomotor activity, feeding and intestinal regulation, induced upregulation in her innate immune responses, and a reduction in the female's receptivity to further competitive courtship attempts (Aigaki et al., 1991; Liu and Kubli, 2003; Carvalho et al., 2006; Ejima and Griffith, 2007; Ram and Wolfner, 2007; Kubli, 2003, 2008, 2010; Häsemeyer et al., 2009; Yang et al., 2009; Cognini et al., 2011). Some of these effects, namely the increased ovulation rates, decreased receptivity and altered intestinal regulation, have been demonstrated to arise as a consequence of successful uptake of SP in the female, via activation of its respective G protein-coupled receptor (Sex Peptide Receptor; SPR; Liu and Kubli, 2003; Chapman et al., 2003; Yapici, et al., 2008; Cognini et al., 2011). SP is thought to regulate post-mating responses by modulating a restricted number of SPR-expressing, fru^{GAL4} positive (fru^{+}) neurons that co-express the proprioceptive marker *pickpocket* (ppk^{+}) in the female reproductive tract (Grueber et al., 2003; Grueber et al., 2007; Häsemeyer et al., 2009; Yang et al., 2009). The full pattern of expression of ppk^{+} neurons innervating the female genitalia are described as having two neurons ramifying on each lateral oviduct with approximately a further thirty neurons organized in three bilateral clusters on each side of the uterus (Yang et al., 2009). The toplogical positioning of these ppk^{+} neurons, together with the fact that no other sensory cells are observed in the female internal reproductive tract, compellingly implies that the observed neurons expressing $dsx^{GAL4\text{-}DBD}/elav^{VP16\text{-}AD}$ within the internal reproductive tract may in fact be a subset of ppk^{+} neurons. The possibility of overlap is further strengthened by the aberrant post-mating behaviour(s) exhibited by mated females that express UAS-TNT in all *dsx* neurons (using both dsx^{GAL4} and $dsx^{GAL4\text{-}DBD}/elav^{VP16\text{-}AD}$ drivers; Rideout et al., 2010). To validate this connection I, in conjunction with Dr. Carolina Rezaval, performed a series of neuroanatomical and behavioural assays that corroborate the role of *dsx* neurons in the

female post-mating switch (Rezaval et al., 2012). These data will be discussed in detail in Chapter 6.

Further to these data, I demonstrated that *dsx*$^{GAL4\text{-}DBD}$/*elav*$^{VP16\text{-}AD}$ is expressed in sensory neurons associated with the bristles of the external reproductive system and analia in adult males and females. Studies have documented the presence of gustatory neurons of the oviduct that are involved in sensing sugar and modulating oviposition; the mode by which they function and the downstream neural targets of these neurons have yet to be identified (Dethier, 1976). In the wild, as adult flies thrive on rotting fruit, gustatory neurons associated with the vaginal plate may enable the female to 'taste' the environment, conveying nutritional information to the CNS. In this manner, gravid females are able to preferentially deposit their eggs on a rich environment that enhances the survival of their offspring (Scott, 2001). This may be of real importance for wild-type behaviours as non-specific olfactory stimuli driving a sex-specific behavioural response has been demonstrated in the reception of food indicators (Grosjean et al., 2011). This then makes logical sense, as sites of food deposition have been implicated in female egg-deposition choice and the presence of food may in some way to serve as a positional cue for the formation of possible *Drosophila* leks (Joseph et al., 2009; Spieth, 1974).

Interestingly in males, *fru*-expression has also been documented in the mechanosensory neurons described here (Billeter et al., 2006; Manoli et al., 2005;). Studies that have ablated the bristles of the genital claspers and lateral plates have demonstrated their role in mediating the genitalia during attempted copulations, while also mediating species-specificity (Dufour, 1984; Acebes et al., 2003) That both *dsx* and *fru* are expressed in these neurons suggests that the functioning of these neurons may be key to copulatory success.

4.4.3 *dsx*$^{GAL4\text{-}DBD}$/*elav*$^{VP16\text{-}AD}$ motor control

Motoneurons exhibit stereotypical projections into the periphery, exhibiting synaptic connections with various muscles (reviewed by Thor and Thomas, 2002). The identification of *dsx*$^{GAL4\text{-}DBD}$/*elav*$^{VP16\text{-}AD}$-expressing motoneuron synapses on muscles of the internal reproductive system and longitudinal muscles of the A6 segment in adult males and females,

implies sex-specific control over the contractions of these muscles. In this manner, these neurons may be perceived to be essential for the actualisation of copulation. Obviously, the functioning of these motoneurons relies on a direct and/or indirect command structure made up of higher-order interneurons in the brain, to ultimately regulate their activity. However, the multiplicity of pathologies that males and females exhibit, upon silencing *dsx*-circuitry, makes it difficult to pinpoint the dedicated roles of these neurons. Do males fail to attempt copulation because of decreased receptivity or aberrant motor control? And, do females fail to lay eggs due to their inability to contract muscles of the uterus, or is this a consequence of a failure to fertilise the eggs? Separating the command structure from motoneurons will allow a better understanding of the control that *dsx*$^{GAL4\text{-}DBD}$/*elav*$^{VP16\text{-}AD}$ circuitry specifies over these structures.

Glutamate is the primary excitatory neurotransmitter in *Drosophila*, and is widely expressed throughout the CNS and in all Type I synaptic terminals (Jan and Jan, 1976; Johansen et al., 1989). Fortunately, a VP16-AD hemi-driver for the *Drosophila* vesicular glutamate transporter (*vGlut*^{OK371}*-VP16AD*,) has been published (Gao et al., 2008). This tool was generated via a transposon swap using the original *vGlut*^{OK371}*-GAL4 enhancer trap line, and when combined with the pan neuronal elav*$^{GAL4\text{-}DBD}$*, recapitulates expression in glutamatergic moto- and sensory neurons; in an identical manner to the original line (Mahr and Aberle, 2006; Gao et al., 2008). Pairing this hemidriver with dsx*$^{GAL4\text{-}DBD}$ permits genetic access to *dsx*-expressing glutamatergic neurons; allowing for both neuroanatomical and behavioural investigations to be carried out. Data from these investigations will be discussed in Chapter 5.

4.4.4 *dsx*$^{GAL4\text{-}DBD}$/*elav*$^{VP16\text{-}AD}$-expressing neurons are necessary for male and female reproductive behaviours

In the brain of the adult male, *dsx*$^{GAL4\text{-}DBD}$/*elav*$^{VP16\text{-}AD}$-expressing neurons are localised to areas that gynadromorph studies identified previously as foci involved in initiation, following, tapping, wing extension and copulatory behaviours (Hotta and Benzer, 1976; Hall, 1977; Hall, 1979; von Schilcher and Hall, 1979). Within the adult male VNC, the *dsx*$^{GAL4\text{-}DBD}$/*elav*$^{VP16\text{-}AD}$ neurons appear to be expressed in those areas identified by gynandromorph

studies as containing foci associated with tapping, wing extension, courtship song and with copulatory behaviours (Hall, 1977, 1979; Hotta and Benzer, 1976; von Schilcher and Hall, 1979). Given the overlap between *dsx* and *fru*, in key neurons of the clusters described here, lessons of circuit organisation and information processing may be taken from studies that have neuroanatomically mapped and functionally assigned component parts of the *fru* circuitry (Rideout et al., 2010 and expanded in Dornan, 2011). These extrapolations suggest that *dsx*$^{GAL4\text{-}DBD}$/*elav*$^{VP16\text{-}AD}$ clusters of the brain are involved in higher-order processing of multi-modal sensory stimuli inputs; specifically from the auditory, visual and olfactory circuitries, given their convergence to regions of the lateral protocerebral complex (Cachero et al., 2010; Kimura et al., 2008; Kohatsu et al., 2011; Yu et al., 2010). *dsx*$^{GAL4\text{-}DBD}$/*elav*$^{VP16\text{-}AD}$ neurons of the Prg and Msg may be associated with the transmission and processing of stimulatory inputs for the *dsx*$^{GAL4\text{-}DBD}$/*elav*$^{VP16\text{-}AD}$ gustatory neurons of the foreleg, and therefore potentially modulate signals involved in the generation of unilateral wing extension and song production (Cachero et al., 2010; Kimura et al., 2008; Kohatsu et al., 2011; Rideout et al., 2007; Rideout et al., 2010; Yu et al., 2010). And finally, neurons of the Abg and their associated projections, both descending to the genitalia and abdominal muscles and ascending to the protocerebrum, together with potential connections with mechanosensory neurons of the terminalia, may be associated with regulation and generation of copulatory behaviours (Billeter et al., 2006b; Cachero et al., 2010; Kimura et al., 2008; Kohatsu et al., 2011; Rideout et al., 2010; Yu et al., 2010). All these *dsx*$^{GAL4\text{-}DBD}$/*elav*$^{VP16\text{-}AD}$ neural substrates, within and outwith the CNS, potentially describe circuitry essential for the initiation and continuation, in a coordinated manner, of the sub-behaviours of courtship (e.g., tapping, wing extension, courtship song, etc.), culminating in successful copulation. As stated inhibition of *dsx*$^{GAL4\text{-}DBD}$/*elav*$^{VP16\text{-}AD}$ neural function in males leads to disruption of the early steps of courtship (orientation, following) and the complete absence of the later steps (wing extension, courtship song, attempted copulation and copulation), resulting in complete behavioural sterility. This strongly implies that this *dsx*$^{GAL4\text{-}DBD}$/*elav*$^{VP16\text{-}AD}$-specified circuitry encompasses the neural components that contribute to and/or direct all steps of the male

courtship repertoire. Consequently, these results demonstrate that *dsx*$^{GAL4\text{-}DBD}$/*elav*$^{VP16\text{-}AD}$ neurons are necessary for all fundamental aspects of male courtship behaviours.

In the brain of an adult female, *dsx*$^{GAL4\text{-}DBD}$/*elav*$^{VP16\text{-}AD}$-expressing neurons are localised to areas that gynadromorph studies identified as foci involved in receptivity (Szabad and Fajszi, 1982; Tompkins and Hall, 1983), while in the VNC, *dsx*$^{GAL4\text{-}DBD}$/*elav*$^{VP16\text{-}AD}$ neurons appear to be restricted to the Abg; a neuroanatomical focus previously implicated in the modulation of female post-mating responses, ovulation and oviposition (Monastirioti, 2003; Soller et al., 2006; Rodríguez-Valentín et al., 2006). Although females do not express Fru, studies have exploited the *fru*^{GAL4} driver to allow direct genetic manipulation of the neurons in the female CNS that are analogous to the Fru^{M}-expressing neurons of the male CNS (Cachero et al., 2010; Yu et al., 2010). In this manner, comparing male and female *fru*^{GAL4} circuitries allows comprehensive assessment of the extent to which these neural networks are sexually dimorphic, and how they might be organized into differentially functional circuits (Cachero et al., 2010; Yu et al., 2010). Again, it would seem likely that *dsx*$^{GAL4\text{-}DBD}$/*elav*$^{VP16\text{-}AD}$ neurons in the brain contribute to female mating decisions in an analogous manner to the involvement of analogous neurons in male mating decisions; via higher-order processing of multi-modal sensory stimuli inputs (Broughton et al., 2004; Kimura et al., 2008; Cachero et al., 2010; Yu et al., 2010). In the case of the female however, these may specifically come from the auditory (to assess courtship song), and olfactory and gustatory circuitries (to assess sex and species via volatile and non-volatile pheromones). However, given that females exhibit two distinct behavioural states: pre- and post-mating, *dsx*$^{GAL4\text{-}DBD}$/*elav*$^{VP16\text{-}AD}$ neurons in the brain must also be able to command the behavioural switch upon receipt of SP-dependent sensory information regarding the reproductive state of the female (Liu and Kubli, 2003; Carvalho et al., 2006; Grueber et al., 2007; Häsemeyer et al., 2009; Yang et al., 2009; Rideout et al., 2010; Rezaval et al., 2012). Again in an analogous manner to that of the male, female *dsx*$^{GAL4\text{-}DBD}$/*elav*$^{VP16\text{-}AD}$-expressing Abg neurons and their associated projections, both descending to the genitalia and abdominal muscles and ascending to the protocerebrum, together with the potential connections with mechanosensory/chemosensory neurons of the terminalia, and SP-sensing proprioceptive neurons of uterus, may therefore be associated

with regulation of copulatory behaviours, oviposition, and in mediating the post-mating behavioural switch (Liu and Kubli, 2003; Carvalho et al., 2006; Grueber et al., 2007; Häsemeyer et al., 2009; Yang et al., 2009; Rideout et al., 2010; Rezaval et al., 2012). That the inhibition of *dsx*$^{GAL4\text{-}DBD}$/*elav*$^{VP16\text{-}AD}$ neural function in females leads to leads to a complete lack of receptivity, sterility and no post-mating switch, demonstrates that the *dsx*$^{GAL4\text{-}DBD}$/*elav*$^{VP16\text{-}AD}$ circuitry encodes for, and is necessary to, all fundamental aspects of female courtship behaviours.

4.5 Conclusions

In this chapter, I have presented compelling results validating the novel *dsx*$^{GAL4\text{-}DBD}$ allele as a reporter of *dsx* expression. I demonstrated that the novel pairing of *dsx*$^{GAL4\text{-}DBD}$ with the pan neuronal *elav*$^{VP16\text{-}AD}$ is capable of spatially restricting expression and genetic access to *dsx*-expressing neurons only. I subsequently verified that the patterns of expression realised by *dsx*$^{GAL4\text{-}DBD}$/*elav*$^{VP16\text{-}AD}$, in the CNS, completely reiterate previous descriptions of *dsx* expression. I then undertook to comprehensively survey of *dsx*$^{GAL4\text{-}DBD}$/*elav*$^{VP16\text{-}AD}$ expression in the PNS, revealing patterns of expression in various sense organs of the periphery that have been previously documented. Finally, I disrupted synaptic activity of *dsx*$^{GAL4\text{-}DBD}$/*elav*^{VP16} circuitry, causally linking and further cementing the critical importance of *dsx* neurons in the specification of male and female copulatory behaviours.

Following from these spatial and behavioural surveys, my investigations will centre on attempting to neuroanatomically and functionally parse male *dsx* circuitry into its component parts. Spatially targeting small clusters of neurons may help to determine whether certain subsets of neurons are necessary and/or sufficient for a given sub-behaviour of the male behavioural repertoire. The long-term goal of these studies is thus to try and provide insight into the functional organisation of *dsx* circuitry as a whole and thereby gain insight into the underlying logic behind how neural substrates are sculpted and maintained, and how they then act to direct specific behavioural outputs.

5 Enhancer-Trap Screen

5.1 Introduction

Recent studies that have attempted to functionally parse *fru* circuitry have successfully employed the two key approaches of clonal analyses and intersectional strategies to directly target specific subsets of *fru*-expressing neurons, allowing for the interrogation of their distinct roles in specifying male courtship behaviours (reviewed by Pavlou and Goodwin, 2013).

The finding that artificial activation of *fru*-expressing neurons via the thermosensitive d*TrpA1* channel (Hamada et al., 2008; Pulver et al., 2009) induces the entire repertoire of courtship in solitary males (Kohatsu et al., 2011) formed the foundations of a valiant study in which mosaic analysis with a repressible marker (MARCM; Lee and Luo, 1999) was used to generate single clones of neurons in the male CNS that express *dTrpA1* (Kohatsu et al., 2011). In this manner, defined clusters of neurons were artificially activated, and the behavioural consequences, if any, were assayed; allowing for direct correlations to be made between labelled *TrpA1-expressing* neurons and the sub-behaviours of courtship that were elicited (Kohatsu et al., 2010). The unmatched resolution of the clonal MARCM approach (down to individual neurons) justifies its prevalent use. However that every recombination event generated within each animal is unique, limits the reproducibility of animals with identical marked clones, making it practically impossible to substitute reporters and effectors for detailed neuroanatomical and functional analyses of any given animal (Lee and Luo, 1999). A further limitation comes from the fact that this technique is restricted to clonally derived neurons, which is dependant on the developmental timing of mitosis in the neurons of interest (Lee and Luo, 1999).

There are a variety of alternate ways to spatially target neurons using intersectional methods (as reviewed in Simpson, 2009), however it should be recognised that as yet no one strategy is a panacea when it comes to dissecting neural circuits. Again, using a thermogenetic approach, a recent study employed a behavioural screen to identify *fru*-specified song circuitry, by combining a novel intersectional fru^{FLP} allele, that drives FLP-mediated recombination specifically in *fru*-expressing neurons, with numerous GAL4 lines, enhancer

trap lines, and molecularly defined enhancer-GAL4 transgenes, in the presence of the *UAS>stop>TrpA1* effector (von Philipsborn et al., 2011). This combination allows for the expression of *TrpA1* in all intersecting neurons (*fru* ∩ GAL4/ET) in which FLP has excised the transcriptional stop cassette (>*stop*>). Candidate lines that displayed a wing extension phenotype upon heating were then neuroanatomically characterised, of which, lines exhibiting sparse patterns of expression were then used for more detailed neuroanatomical and behavioural analyses (von Philipsborn et al., 2011). The ability to replicate the intersectional expression patterns with a single genetic cross, and exchange reporters for effectors (or *vice-versa*) for subsequent neuroanatomical and functional analyses of any given candidate line are powerful traits that enable rigorous and comprehensive analyses to be carried out. Such features of intersectional strategies means that they should be considered as a favourable initial approach when attempting to parse neural circuitry. Though as the resolution obtained by these strategies is inferior to that of MARCM, subsequent single cell analyses are typically warranted.

The split-GAL4 system utility is not limited to the targeting of transgene expression to known neural groups by exploiting hemidrivers with known promoters (Luan et al., 2006). It has also been used to as an intersectional strategy for behavioural screens, exploiting split-GAL4 VP16AD enhancer trap lines ($ET^{VP16\text{-}AD}$), to functionally dissect a known neural circuitry into independent component parts that specify distinct behaviour(s) (Luan et al., 2006; Peabody et al., 2009; Luan et al., 2012). Given the limited number of available hemidrivers with defined promoters that are currently available, the latter intersectional 'enhancer trap' approach is particularly pertinent to the cause at hand: that is dissecting *dsx* circuitry into functionally distinct component elements. The fact that thermoactivation of *dsx* circuitry elicits all components of courtship behaviour in males, qualitatively similar to those elicited upon the activation of *fru* circuitry in males (Pan et al., 2011; Pan et al., 2012), while analogous thermoactivation of *dsx* circuitry in females does not elicit any overt behaviours (Pan et al., 2011), would appear to restrict the efficacy of a thermogenetic screen to males only. However this is not to say that the identification of candidate $ET^{VP16\text{-}AD}$ lines that display restricted patterns of expression in males would not display corresponding restricted patterns

of expression in females. On the contrary, it is likely that the products of this screen may be used to parse *dsx* circuitry underlying female behaviours. Unfortunately however, given the realm and time constraints of this thesis, I primarily focused on parsing *dsx* circuity underlying male reproductive behaviours, with the hope of extending this work to encompass both sexes in the near future.

As such, I performed a thermogenetic intersectional strategy similar to that executed by von Philipsborn et al. (2011) for *fru*-specified song circuitry. I combined the novel *dsx*$^{GAL4\text{-}DBD}$ hemidriver with extant split-GAL4 VP16AD (*ET*$^{VP16\text{-}AD}$) enhancer trap lines (Luan et al., 2006; M. Landgraf, unpublished), in the presence of the *UAS-dTrpA1* effector, to isolate and identify functional components of the overall *dsx* circuitry that specify sub-behaviours of the male courtship repertoire.

5.2 Activation of all *dsx*$^{GAL4\text{-}DBD}$/*elav*$^{VP16\text{-}AD}$ neurons is sufficient to elicit male courtship

To first test the efficacy of the split-GAL4 system, I assayed the behavioural consequences of artificially activating all *dsx*-expressing neurons in males by driving the expression of *UAS-dTrpA1* with *dsx*$^{GAL4\text{-}DBD}$/*elav*$^{VP16\text{-}AD}$. Activation of *dsx* circuitry was accomplished by shifting the temperature of the flies from a permissive 23 °C to a restrictive 30 °C. In accord with Pan *et al.* (2011), solitary males (in the absence of any target female) displayed unilateral wing extension and vibration, followed by abdominal bending and finally attempted copulation (n=30). Although *UAS-dTrpA1*/+; *dsx*$^{GAL4\text{-}DBD}$/*elav*$^{VP16\text{-}AD}$ males sequentially display wing extension and abdominal curling behaviours, once both behaviours have been elicited, they are continuously and simultaneously exhibited for the entire duration of the 3 min observation period. The distinction between abdominal bending and attempted copulation is that the latter is a momentary thrusting action during which a male fully curls its abdomen, surpassing a 90º angle of bending.

It is important to note that I merely observed the occurrence of these behaviours, rather than quantified distinct parameters (*e.g*. time to elicitation of both behaviours); primarily due to the technical limitations of the available heating apparatus. That even the slightest shifts in

temperature affect the kinetics of these behaviours (Pan et al., 2011), means that quantification of behavioural parameters post-thermal activation requires the use of temperature controlled incubators and/or a thermoelectric heat-pump (*e.g.* Peltier), capable of maintaining the temperature within fractions of a degree (Pulver et al., 2009; Berni et al., 2010; Galio et al., 2011; Pan et al., 2011; Tayler et al., 2012; Pan et al., 2012; Wang et al., 2012; Melom et al., 2013). Unfortunately, such precise thermal control was practically unattainable.

Grouping *UAS-dTrpA1*/+; *dsx*$^{GAL4\text{-}DBD}$/*elav*$^{VP16\text{-}AD}$ males together during themoactivation strikingly resulted in the display of male-male courtship and 'chaining' behaviours (n=30). Solitary males of this genotype did not display any courtship behaviours at the permissive temperature (n=30), nor did solitary and grouped control males of *UAS-dTrpA1*/+; *dsx*$^{GAL4\text{-}DBD}$/+ and *UAS-dTrpA1*/+; *elav*$^{VP16\text{-}AD}$ /+ genotypes at the restrictive and permissive temperatures (n=30 per genotype). In line with previous findings, thermoactivation of *dsx*-circuitry in solitary *UAS-dTrpA1*/+; *dsx*$^{GAL4\text{-}DBD}$/*elav*$^{VP16\text{-}AD}$ females failed to elicit any overt behaviours (n=20; Pan et al., 2011).

Previous studies did not group 'thermoactive' males together, explaining why these observations have not been previously reported. However, studies have demonstrated that *UAS-dTrpA1*/+; *dsx*^{GAL4}/+ males are able to discriminate between the sexes and species at both permissive and restrictive temperatures; although the targets used in these assays were headless and immobile (Pan et al., 2011). To test the dependency of these males on visual cues, recent experiments assayed courtship behaviours using males with thermoactivatable *dsx* neurons that were separated from intact females targets by a thin transparent plastic barrier (Pan et al., 2012). At the permissive temperature, these males rarely courted the female targets, consistent with the behavioural phenotype of controls males, however, at restrictive temperatures, males with activated *dsx* circuitry showed consistently high levels of courtship towards these targets (Pan et al., 2012). This phenotype was lost when the target females were immobilised, suggesting that there remains a strong dependence on motion cues for the elicitation of courtship behaviour even when *dsx* circuitry has been activated

(Pan et al., 2012). Whether these males are able to differentiate the motion cues of a male *vs.* those of a female would be an interesting paradigm to test; however, based on the male-male courtship behaviour observed in this study, I would anticipate that these males are merely unable to do so.

Studies have implicated *dsx*- expressing neurons of protocerebrum (that co-express *fru)* in higher-order processing of olfactory and gustatory information (reviewed by Pavlou and Goodwin, 2013), while the processing of motion cues is thought to be independent of *dsx*-circuitry (Pan et al., 2012). If activation of the entire *dsx* circuitry includes the activation all *dsx*-expressing sensory neurons, and assuming that not all sensory information received will generate excitatory responses/activation signals (an example of this being the functionally opposing *ppk*25-expressing gustatory neurons in the male foreleg, within which one sensorium mediates attractive pheromonal cues and the other mediates aversive pheromonal cues; Thistle et al., 2012), then it is not unreasonable to also assume that such global activation results in the transmission of conflicting information. This concept is not entirely new, as Clyne and Miesenböck (2008) implemented the use of male headless 'flyPods' in the optogenetic activation of *fru* circuitry to specifically circumscribe predicted conflicting information from the brain. The receipt of conflicting information upon *dsx* circuit activation may result in impeding variant *dsx*-dependent sensory modalities, that might normally positively drive initiation and subsequent maintenance of courtship, from overcoming the sensory threshold necessary to initiate courtship; resulting in the sole reliance on sensory information that is processed independently of *dsx*-circuitry, motion being the obvious cue (Pan et al., 2012). It is possible that these males now only require a moving target to tip the level of 'positive' sensory stimulation over the threshold, eliciting a 'command' mode response from the higher-order processing centres in which the behavioural outputs of courtship behaviour are elicited as a simple motor response, irrespective what the mobile target may be.

Still, that solitary *UAS-dTrpA1*/+; $dsx^{GAL4\text{-}DBD}/elav^{VP16\text{-}AD}$ males sequentially display unilateral wing extension and vibration, abdominal bending and attempted copulation upon

thermoactivation, inarguably demonstrated the successful utility of the novel *dsx*$^{GAL4\text{-}DBD}$ hemidriver in eliciting all sub-behaviours of the courtship repertoire via a thermogenetic approach. That thermoactivation of *dsx*$^{GAL4\text{-}DBD}$/*elav*$^{VP16\text{-}AD}$-expressing neurons is sufficient to elicit all male courtship behaviours underpins the strategy by which the enhancer trap collection was screened.

5.3 Strategy to utilise the *ET*$^{VP16\text{-}AD}$ enhancer trap collection

I devised a three-phase stratagem to exploit and maximise the use of the split-GAL4 VP16AD (*ET*$^{VP16\text{-}AD}$) enhancer trap collection (Luan et al., 2006; M.Landgraf, unpublished) to identify and functionally interrogate candidate lines that exhibit restricted patterns of transgene expression (Figure 5-1). A methodical filtering system was implemented whereby at each experimental phase, the relevant lines were scrutinised for their fulfilment of a defined set of criteria; each of which is discussed in more details in the following sections. This process facilitated the selection of the most significant candidate lines.

The first phase involved a 'grand' thermogenetic screen, exploiting *UAS-dTrpA1,* to behaviourally identify lines that display a defined behavioural response upon thermoactivation (section 5.5). All candidate lines that fell out of this screen were subsequently neuroanatomically characterised in phase 2 of the stratagem (section 5.6). Based on their patterns of expression, candidate lines that exhibited sparse and restricted clusters of neurons in the CNS were then used for silencing experiments via *UAS-TNT* transgene expression in the final third phase (section 5.7). The methodology, results and enforced criteria from each of these stages are discussed in the following sections.

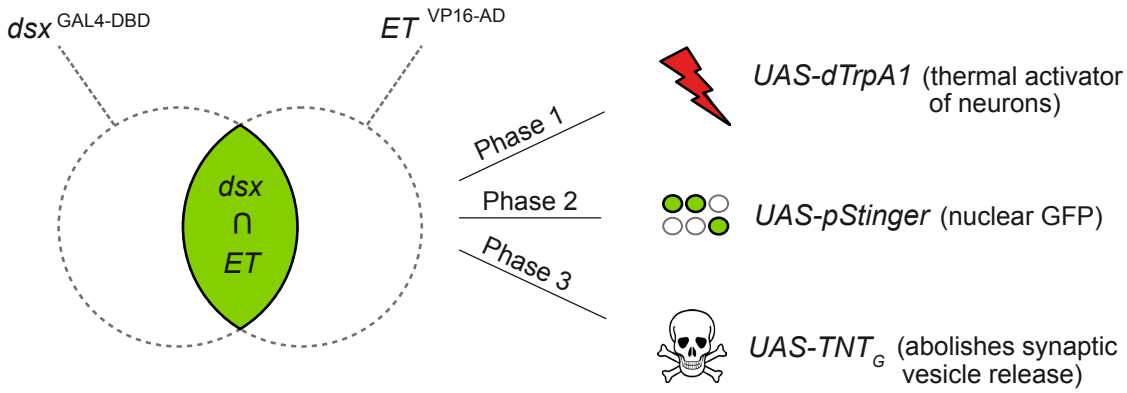


Figure 5-1 Schematic of the implemented experimental strategy to isolate and interrogate functionally distinct subsets of *dsx* neurons.
Phase 1 includes a thermogenetic screen of a collection of ETVP16-AD lines for the elicitation of sub-behaviours of male courtship. Phase 2 involves neuroanatomical characterisation of all candidate lines via expression of nuclear GFP. Phase 3 involves utilising candidate lines with sparse and restricted patterns of expression in silencing experiments, addressing the necessity of the intersecting neurons in the elicitation of their respective sub-behaviours.

5.4 *ET*$^{VP16\text{-}AD}$ collection

As previously stated, to target patterns of expression that are both heritable, and relatively fixed, I exploited the extant *ET*$^{VP16\text{-}AD}$ lines (Luan et al., 2006; M.Landgraf, unpublished) in a thermogenetic behavioural screen. Approximately 350 *ET*$^{VP16\text{-}AD}$ lines were generated by *P*-element mobilization using the transposase-bearing line, *w*; +; K_i, Δ2-3 by Luan et al. (2006), while an additional 60 *ET*$^{VP16\text{-}AD}$ lines were generated in the same way (kind gift of Matthias Landgraf). Of these two collections, only lines from the Landgraf collection were pre-screened for nervous system expression (Landgraf, M., pers. comm.). Both collections were made with the original VP16AD construct, which has been shown to drive very high levels of transgene expression, and is capable of realising patterns of expression in cells in which the levels of activity of the VP16-AD are relatively low (Luan et al., 2006). Although the expression patterns of the *ET*$^{VP16\text{-}AD}$ lines have not been systematically characterised, reports of broad patterns of expression have been documented (Luan et al., 2006; White, B.H., pers. comm.). This is potentially due to the fact that integration of *P*-elements has been shown to biased towards highly recombinogenic 'hotspots' in the genome (Bellen et al., 1992; Kania et al., 1995; Salzberg et al., 1997). As the VP16-AD construct's minimal promoter depends on local enhancer elements near the site of the transgene's integration into the genome for transcriptional activation, thereby directing expression in arbitrary/unknown patterns, it is possible that the broad patterns of expression associated with many of the VP16-AD constructs are to do with the non-random genes/loci these constructs are inserted into. Unfortunately, reports of low promoter fidelity and resultant ectopic patterns of transgene expression have revealed problematic features of these 'first generation' *ET*$^{VP16\text{-}AD}$ lines (Luan et al., 2006). Further reports of lethality of pan-neural VP16-AD and GAL4-DBD co-expression have indicated a link between high levels of transgene co-expression and cytotoxicity (Luan et al., 2006). Finally that numerous *ET*$^{VP16\text{-}AD}$ lines were found to be weak

and unhealthy is suggestive of deleterious/disruptive effects associated with insertion of the construct itself. These described limitations have since been overcome, by codon optimising the VP16-AD sequence for expression in *Drosophila (*dVP16-AD) and ablating a potential cryptic enhancer site within the construct (Luan, H. and White, B.H., unpublished). However, only a handful of these 'second generation' enhancer trap lines have, to date, been generated (White, B.H., unpublished). A recent study however, performed a targeted replacement of an extant GAL4 element already inserted downstream of the vesicular glutamate transporter (*vGlut*) locus for the 'drosophilised' dVP16-AD element, ultimately generating the novel *vGlut*^{OK37}1-VP16-AD hemidriver (Gao et al., 2008). The original enhancer trap OK371-GAL4 is expressed almost exclusively in glutamatergic motoneurons, confirmed via vGLUT antibody staining, with the exception of a limited number of non-glutamatergic neurons in the brain and sensory neurons of the foreleg and labellum (Mahr and Aberle, 2006). Since its characterisation, the OK371-GAL4 genetic tool has provided a means to selectively target and functionally interrogate glutamatergic motoneurons. Having generated the split-GAL4 counterpart, I employed the novel *vGlut*^{OK37}1-VP16-AD hemidriver (Gao et al., 2008) in combination with *dsx*$^{GAL4\text{-}DBD}$, to spatially restrict, neuroanatomically characterise and functionally interrogate the role of *dsx* motoneurons in male courtship behaviour. Therefore, I employed all the available ~410 'first generation' *ET*$^{VP16\text{-}AD}$ lines, as well as the *vGlut*^{OK371}-VP16-AD hemidriver (Luan et al., 2006; Landgraf, M., unpublished, Gao et al., 2008), all of which had been generously shared with me, for the behavioural screen described within this chapter.

5.5 Phase 1 - Enhancer trap thermogenetic screen

5.5.1 Method

The vigorous wing extension and abdominal bending responses of thermally activated *UAS-dTrpA1*/+; *dsx*$^{GAL4\text{-}DBD}$*/elav*$^{VP16\text{-}AD}$ males provided an efficient and robust assay for a thermogenetic screen to isolate candidate *ET*$^{VP16\text{-}AD}$ lines that restrict genetic access to subsets of *dsx* neurons ultimately involved in either song production or copulatory behaviours. I initially chose to include an assay for 'chaining' behaviour for two reasons: 1) it

is possible that scoring for this behaviour may lead to the identification of circuit elements involved in courtship initiation and/or mate-choice, and 2) by grouping males into a single chamber, I was able to assay both group chaining behaviour and individual behavioural outputs for wing extension and/or abdominal curling; increasing the number of animals tested, per genotype and thereby increasing the throughput of the methodology. However, it quickly became obvious that scoring for 'chaining' was far more complex than previously presumed. In many cases, males in which a behavioural response was elicited quickly became immobile, a consequence of a continual display of vigorous abdominal curling and attempted copulation phenotypes; prohibiting my ability to reliably assess the manifestation of 'chaining' behaviour. For this reason, I omitted this parameter from the study, but continued to group males as a way of increasing the number of animals tested.

To this end, I devised a strategy in which recombinant *dsx*$^{GAL4\text{-}DBD}$, *UAS-dTrpA1*/+ virgin females were crossed to males from individual *ET*$^{VP16\text{-}AD}$ lines, using lines with inserts on the X chromosome as internal negative controls. The fact that the chromosomal locations of the majority of the inserts mapped to the 2nd and 3rd chromosomes, with only 20 lines exhibiting the insert on the X chromosome (see Appendix; Luan et al., 2006; Landgraf, unpublished), permitted the use of this crossing scheme, rather than the reciprocal use of virgin females from each individual *ET*$^{VP16\text{-}AD}$ line. This was favourable for two reasons: to circumvent the laborious collection of virgin female flies from the numerous weak and unhealthy lines, and given the time constraints, this approach enabled me to easily synchronise the set up of 100 crosses at any one time. Upon set up, all crosses were reared at 21°C. The F1 *UAS-dTrpA1*-expressing male progeny were collected shortly after eclosion and aged in groups of 10–20, for 10–15 days at 21°C, prior to behavioural screening.

For the first round of the screen, five males were aspirated in isolation, while an additional 4-5 males were aspirated in a group, into Perspex chambers (1 cm diameter × 4 mm height) placed on a heating plate heated between 30–31°C (Figure 5-2). All males were screened for emergence of wing extension and abdominal curling behaviours. Flies that exhibited any combination of these behaviours were recorded for 3 minutes.

Still, based on the premise that the neurons that specify wing extension are distinct from those that specify abdominal curling (reviewed in Pavlou and Goodwin, 2013), elicitation of wing extension or abdominal curling exclusively is suggestive of spatial restriction of transgene expression to sub-sets of distinct neural circuitry involved in directing either of these two distinct behavioural outputs. As previously stated, *UAS-dTrpA1*/+; *dsx*$^{GAL4\text{-}DBD}$*/elav*$^{VP16\text{-}AD}$ males sequentially display wing extension and abdominal curling behaviours, once both behaviours have been elicited, they are continuously exhibited. Hence, it is also possible that even slight variations in the behavioural response, such as an animal that exhibits one dominant behaviour such as overt wing extension or abdominal curling, while also presenting the alternate behaviour in a partial/weak manner, may also be suggestive of spatial restriction of transgene expression in which a sub-set of the neural circuitry may impinge on more than one behavioural process. Based on the above-mentioned rationale, I focused on identifying candidate lines that elicited one of three defined behavioural responses:

i) wing extension exclusively,

ii) abdominal curling exclusively, and

iii) a 'partial' behaviours category, which strictly incorporated candidates that display either overt wing extension with partial abdominal curling or overt abdominal curling with occasional bouts of wing extension.

ET$^{VP16\text{-}AD}$ candidate lines that fell into any of the three defined behavioural categories were scored as positive, and were then taken through a second round of screening, identical to the first, to repeat and verify the described observation.

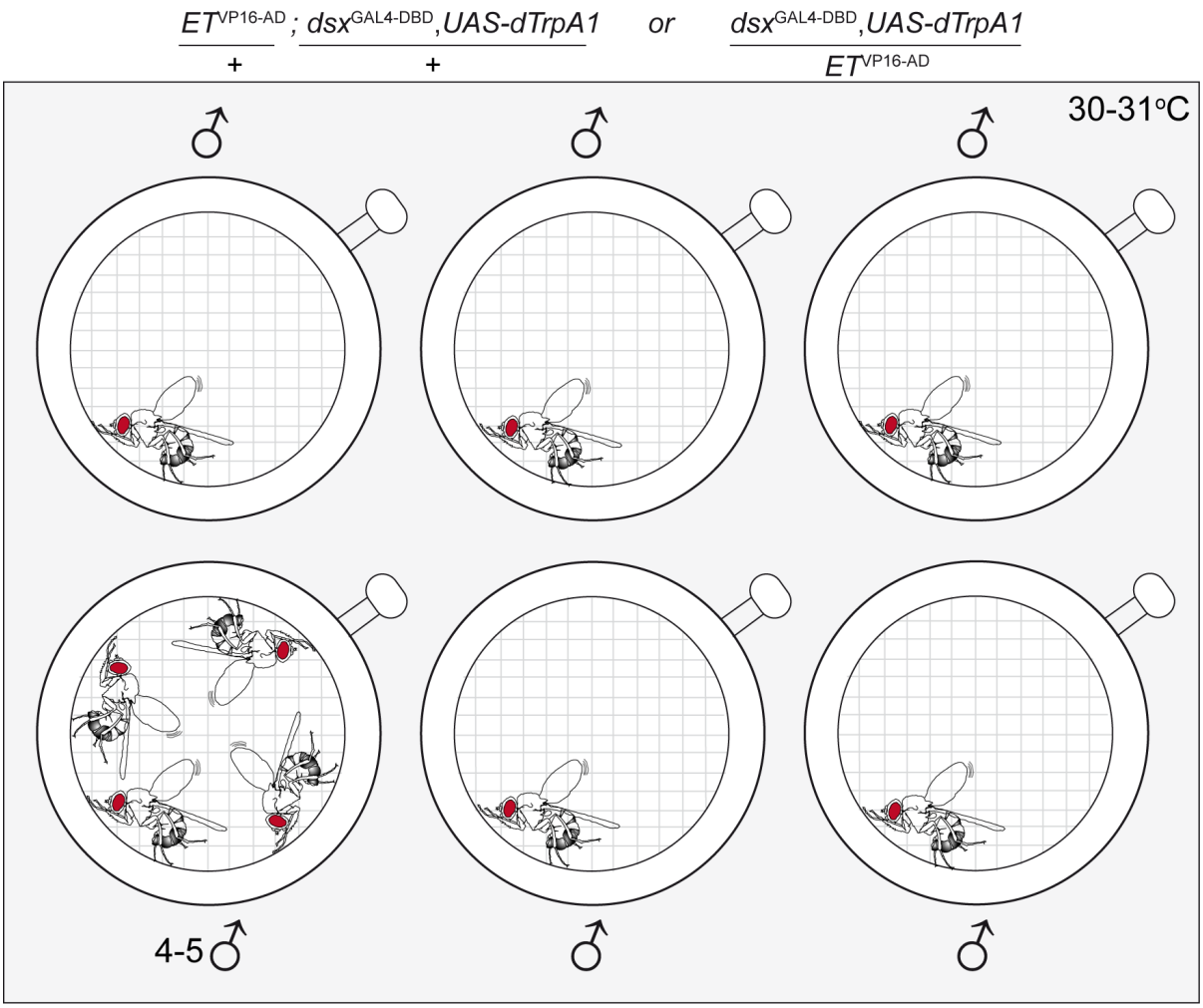


Figure 5-2 Thermal activation strategy to screen ~410 *ET*VP16-AD lines.
Schematic of the behavioural set up. Up to 6 chambers (1-cm diameter × 4-mm height) are placed on a heating plate, heated between 30–31°C. Five of these chambers contain a single isolated male, while one chamber contains 4-5 grouped males. All animals have been aged in groups of 10-20 for 10-15 days at 21°C. All males are scored for wing extension and/or abdominal curling.

5.5.2 Results

Males from approximately 33% (~135 of the total 410 lines) of the screened $ET^{VP16\text{-}AD}$ collection displayed the full courtship repertoire upon thermoactivation, similar to the behaviours elicited in *UAS-dTrpA1*/+; $dsx^{GAL4\text{-}DBD}$/$elav^{VP16\text{-}AD}$ males. This is unsurprising as, based on the reports of a high incidence of $ET^{VP16\text{-}AD}$ lines with broad patterns of expression (B.H. White, pers. comm.), the intersected expression patterns of these lines may be predicted to encompass all *dsx* circuitry. For further information, a comprehensive list of candidate lines and associated behavioural scores can be found in the Appendix.

5.5.2.1 Wing extension candidates

Only seven lines displaying a robust wing extension behavioural response were retrieved from the screen: 5 of which showed bilateral wing extension that was akin to wing scissoring, while the remaining 2 displayed unilateral wing extension (Table 5-1). Although bilateral wing extension is not a characteristic of courtship, studies have shown that gustatory inputs from the foreleg that are processed in higher order centres of the brain ensure laterality of wing extension; contributing to the controlled inhibition of the contralateral wing so that it remains in resting position during unilateral wing extension (Koganezawa et al., 2010). Bilateral wing extension within these animals may potentially be due to a restricted pattern of expression that excludes higher-order sensory integration and/or command centres of the brain that would normally direct the inhibition of the motor output to the contralateral wing. This scenario would involve activation of the localised thoracic central song pattern generator (CPG) (Rideout et al., 2007; Clyne and Miesenböck, 2008) and/or motor centres for wing extension (von Philipsborn et al., 2011) while circumventing higher order processing centres within the brain. In support of this hypothesis, the display a wing scissoring phenotype, similar to that observed in this study, was shown to occur as a consequence of activating a subset of *fru* neurons that comprise the thoracic central song pattern generator (CPG) (von Philipsborn et al., 2011).

5.5.2.2 Abdominal curling candidates

Scoring abdominal curling phenotypes proved more difficult than anticipated. It quickly became obvious that an abdominal curling phenotype is not an all-or-nothing behavioural response. Rather, it appeared as more of a continuum within which some animals exhibited an extreme >90^{o} angle abdominal curl, similar to *UAS-dTrpA1*/+; $dsx^{GAL4\text{-}DBD}$/$elav^{VP16\text{-}AD}$ males, and other animals exhibited less conspicuous abdominal curls (referred to as partial abdominal curling) during which the genital segments were found to be in close proximity to the chamber walls, almost as if the terminalia were being dragged against the surface of the chamber. Confining the assignment of candidate lines to one of two abdominal curling behavioural response groups (extreme or partial), I retrieved 11 candidate lines that fell into

the ‘extreme’ group, while a substantially larger number of lines, 38 to be exact, were assigned to the ‘partial’ group (tabulated in Appendix). Taking into consideration the amount of time it would take to neuroanatomically characterise all these lines, I chose to limit my analyses to candidate lines that displayed ‘extreme’ abdominal curling responses (Table 5-1). I reasoned that, depending on the level of spatial restriction I obtain with these lines, I could incorporate the remaining 38 candidate lines at a later stage; however, I did include two candidate lines (No. 61 and 199) that displayed abdominal curling responses that fell short of the ‘extreme’ group, but did not warrant their placement in the ‘partial’ group as a way of exploring the prospects of the remaining 38 lines (Table 5-1).

As previously stated, analyses of thermoactive *UAS-dTrpA1*/+; dsx^{GAL4} males, revealed that these males display all sub-behaviours of courtship (Pan et al., 2011). This was confirmed in this study, via analyses of thermoactive *UAS-dTrpA1*/+; $dsx^{GAL4\text{-}DBD}$/$elav^{VP16\text{-}AD}$ males. Upon severing the brain however, headless *UAS-dTrpA1*/+; dsx^{GAL4} males are reported to lose one facet of the repertoire; attempted copulation (Pan et al., 2011). This suggests this behavioural modality may be under direct descending control from higher-order neurons in the brain. For this reason, I scored all candidate lines that displayed an abdominal curling behavioural response for attempts to copulate (Table 5-1). The rationale being that the presence/absence of expression in higher-order neurons in the brain of these intersectional animals may specifically correlate with the presence/absence of attempted copulation, shedding light on the circuitry underlying this sub-behaviour of the courtship repertoire.

Combining *UAS-dTrpA1*/+; $dsx^{GAL4\text{-}DBD}$ with the $vGlut^{OK371}$-VP16-AD hemidriver did not result in an obvious behavioural response upon thermoactivation, rather these males exhibited partial abdominal curling. Based on the comprehensive neuroanatomical characterisations of $dsx^{GAL4\text{-}DBD}$/ $elav^{VP16\text{-}AD}$-expressing neurons presented in the previous chapter, the presence of motoneurons in the Abg of the VNC that target the longitudinal muscles of the ventral abdominal wall and the internal genitalia (shown in Chapter 4), advocates their role in the late stages of the courtship repertoire (including attempting copulation, and copulation itself). That these neurons are the only $dsx^{GAL4\text{-}DBD}$/ $elav^{VP16\text{-}AD}$-expressing motoneurons of the *dsx*-

circuitry would imply a role for them in the abdominal curling phenotype. That *vGlut*^{OK371}-VP16-AD;*dsx*$^{GAL4\text{-}DBD}$–expressing neurons should theoretically comprise of all *dsx* motorneurons, one would expect to observe and abdominal curling phenotype. Their falure to do so warranted further neuroanatomical and behavioural investigations of this line. It is possible that although glutamatergic neurons are excitatory in origin, fine-tune modulation of motor response may be necessary to elicit abdominal curling. Presumably, abdominal curling requires the simultaneous contraction of a specific set of muscles, and the relaxation of an opposing set of muscles, enabling the ventral abdomen to distend, and the dorsal abdomen to contract. If so, excitation of all the motoneurons targeting these muscle groups would result in conflicting contractions that could manifest as a 'partial' abdominal curl response. To investigate this further, I observed the abdomens of thermoactive *vGlut*^{OK371}-VP16-AD; *dsx*$^{GAL4\text{-}DBD}$ males at higher magnification, using a stereo-dissecting microscope. In this way, I observed a back and forth 'bobbing' phenotype of the abdomen. Furthermore, given that *vGlut*^{OK371}-VP16-AD;*dsx*$^{GAL4\text{-}DBD}$–expressing neurons should theoretically comprise of *dsx*-expressing motoneurons that innervate muscles of the aedaegus, I attempted to observe movements of the external genitalia that may reflect modulation/extrusion of the aedeagus; however, no apparent movement of the external genitalia was observed (Table 5-1). Although the observed bobbing phenotype is far from overt, gaining genetic access to *dsx*-expressing motoneurons exclusively, by way of exploiting the *vGlut*^{OK371}-VP16-AD, not only enables functional interrogation of these neurons, but also provides a piece of the courtship connectome puzzle. As previously stated, the *dsx* neural circuitry consists of sensory neurons, interneurons and motoneurons, suggesting that there are functionally separable components capable of receiving, processing and transferring information to direct and maintain sexual behaviour. Combining the novel *dsx*$^{GAL4\text{-}DBD}$ hemidriver with *vGlut*^{OK371}-VP16-AD would artificially focus on a single component of the circuitry – in this case identifying and studying motoneurons, to ultimately begin to refine the mechanics of this circuitry as a whole. For these reasons, I included this line for further analyses.

5.5.2.3 Candidates displaying 'partial' behaviours

Lastly, for the final group of candidate lines, a total of 9 candidate lines were found to exhibit partial behaviours (Table 5-1). To reiterate, the criteria for selecting these lines entailed a faithful display of either wing extension or abdominal bending, during which the alternative behaviour is simultaneously displayed in an unfaithful manner. Four of these lines displayed overt unilateral wing extension responses with deficits in the abdominal curling response, evidenced by a partial abdominal curl response (in 3 lines) and a display of attempts to copulate without continuous abdominal bending (1 line; Table 5-1). The remaining 5 lines displayed extreme abdominal curling responses with bouts of unilateral wing extension, the occurrence of which is significantly lower than the wing extension phenotype elicited in *UAS-dTrpA1*/+; $dsx^{GAL4\text{-}DBD}$/$elav^{VP16\text{-}AD}$ males (Table 5-1). Further to these candidates, I retrieved an additional ~17 lines that displayed unfaithful renditions of both wing extension and abdominal curling responses simultaneously (See Appendix for more detail). Again, I chose to omit these lines from further analyses until neuroanatomical characterisations of the initial 8 lines were carried out. I reasoned that the use of the most robust lines as indicators of successful spatial restriction would enable an informed decision to be made on whether to include additional lines at a later stage.

Table 5-1 Phase 1 list of candidate lines retrieved from thermogenetic screen.
Candidate names (as per Luan et al., 2006; M.Landgraf, unpublished), primary behavioural description and additional behaviours and/or descriptors are listed below. Candidate lines were classed into one of three groups based on their behavioural responses (wing extension, abdominal curling, and partial behaviours); candidate lines showing similar behavioural responses are grouped together.

Candidate I.D.	Primary Behavioural Description	Additional behaviours and/or descriptors
Wing Extension Candidates		
BF01	Bilateral wing extension	Paralytic
CH11	Bilateral wing extension	Paralytic
ML153	Bilateral wing extension	Paralytic
VK29	Bilateral wing extension	-
92RWIII	Bilateral wing extension	-
147	Unilateral wing extension	-
79	Unilateral wing extension	Weak wing posture

Abdominal Curling Candidates		
AZ16	Extreme abdominal curling	No overt attempt to copulate
BF59	Extreme abdominal curling	No overt attempt to copulate
MB01	Extreme abdominal curling	No overt attempt to copulate
N9A100A	Extreme abdominal curling	No overt attempt to copulate
VK02	Extreme abdominal curling	No overt attempt to copulate
141	Extreme abdominal curling	No overt attempt to copulate
165	Extreme abdominal curling	No overt attempt to copulate
61	Abdominal curling	No overt attempt to copulate
119	Abdominal curling	No overt attempt to copulate
ML156	Extreme abdominal curling	Attempts to copulate
N9A25	Extreme abdominal curling	Attempts to copulate
N9A47A	Extreme abdominal curling	Attempts to copulate
N9A61	Extreme abdominal curling	Attempts to copulate
vGlut^{OK371}	Partial abdominal curling	No overt attempt to copulate
Candidates that display partial behaviours		
105	Unilateral wing extension	Attempts to copulate
179	Unilateral wing extension	Partial abdominal curl
177RA	Unilateral wing extension	Partial abdominal curl
2	Unilateral wing extension	Partial abdominal curl
N4A10	Extreme abdominal curling	Attempts to copulate & bouts of unilateral wing extension
88R	Extreme abdominal curling	Attempts to copulate & bouts of unilateral wing extension
N9A96B	Extreme abdominal curling	Bouts of unilateral wing extension
111	Extreme abdominal curling	Bouts of unilateral wing extension
112	Extreme abdominal curling	Bouts of unilateral wing extension

In summary, 7 wing extension candidates, 14 abdominal curling candidates and 9 partial behaviours candidates were identified, creating a total of 30 candidate lines advanced to Phase 2 of the stratagem – neuroanatomical characterisations of reporter expression (Figure 5-3).

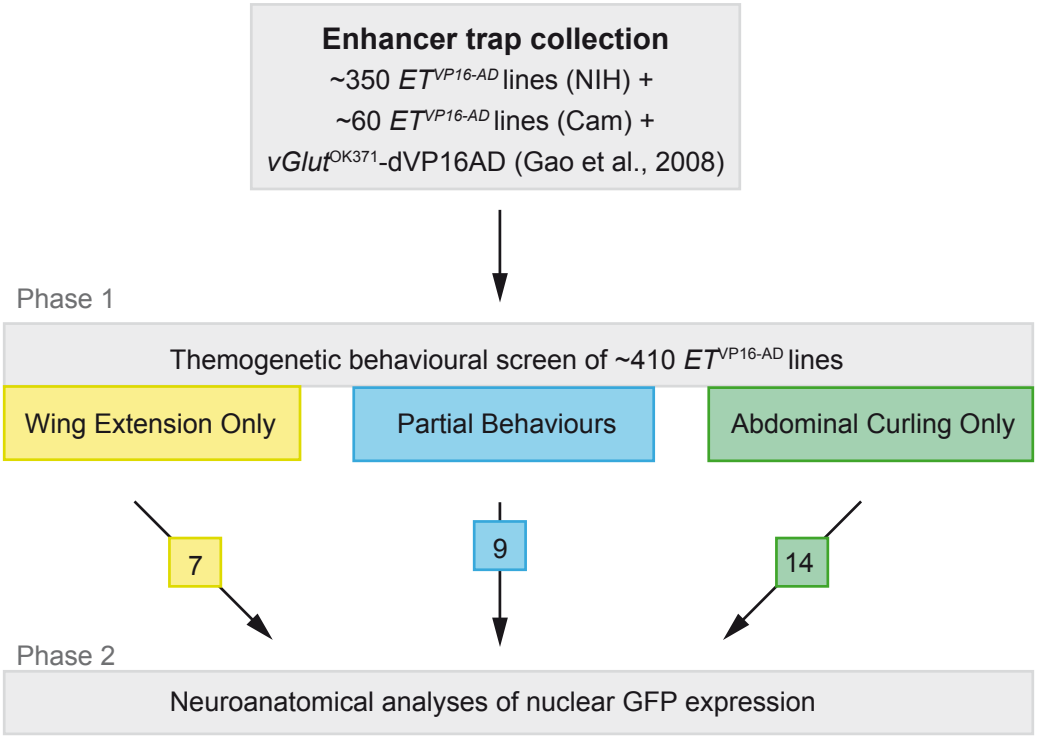


Figure 5-3 Flowchart depicting the strategy and results of the thermogenetic behavioural screen.
Behavioural response categories and associated number of candidate lines retrieved from the screen are shown. A total of 30 candidate lines proceed to Phase 2 neuroanatomical analyses of nuclear GFP expression.

5.6 Phase 2 - Neuroanatomical characterisation of *ET*$^{VP16-AD}$ candidate lines

5.6.1 Method

Lines that were recovered from the second screen underwent neuroanatomical characterisation by crossing each candidate line to *UAS-pStinger*/+; *dsx*$^{GAL4-DBD}$/+. The CNSs of male and female progeny expressing nuclear GFP (nGFP) were stained for GFP and the neuropil marker, nc82, realising the expression patterns and topology of intersecting nGFP-expressing neurons.

The rationale for the inclusion of the female CNS in these neuroanatomical characterisations is two-fold. First, comparing male patterns of reporter expression to analogous females served as a form of validating patterns of expression observed in the male. More importantly however, by way of surveying the patterns of expression of the analogous female CNSs, identification of any lines that showed restricted patterns of expression could be exploited in

the study of female sexual behaviours at a later stage. As previously stated, that *UAS-dTrpA1*/+; *dsx*$^{GAL4\text{-}DBD}$/*elav*$^{VP16\text{-}AD}$ females do not display overt reproductive behaviours upon thermoactivation meant that carrying out a thermogenetic screen for female behaviours would entail time consuming assays, deeming it impractical for a screen of this size. Behavioural analyses of both virgin females and mated females during courtship to assess pre- and post-mating behaviours, the assessment of male courtship behaviours towards these females as a method of measuring female attractiveness, and fertility and even egg-laying experiments would all need to be factored into a global screen that would aim to comprehensively parse different components of female reproductive behaviours. However I felt it warranted, in order to maximise the potential benefits of the screen preformed in this study, that candidate lines that elicited specific behavioural responses in males were also surveyed for spatial restriction in the female CNS; to possibly prime prospective studies on parsing *dsx* circuitry underling female copulatory behaviours.

5.6.2 Results

5.6.2.1 Omitting candidate lines with ectopic patterns of reporter expression

Previous studies have demonstrated that the intersection of split-GAL4 hemidrivers resulted in an expansion of expression to numerous cells not observed in either parental line (Luan et al., 2006; Pfeiffer et al., 2010). This is thought to occur as a result of the strong activation domain that subsequently drives broader patterns of expression than with an intact GAL4 (Pfeiffer et al., 2010). Attempts to address this phenomenon via the generation of additional split-GAL4 reagents, using activation domains of various strengths, have been unsuccessful (Pfeiffer et al., 2010). Here, four out of the 30 candidate lines revealed such ‘ectopic’ patterns expression, and as such, were omitted from subsequent experiments (Table 5-2; example shown in Figure 5-4A-E; regions of ectopic expression marked by asterisks). Interestingly the expansion of expression to cells that are not observed in either parental line was not the only ectopic pattern of expression observed. Four additional lines revealed widespread patterns reporter expression that lacked expression in *dsx*-expressing neural clusters (Table 5-2; example shown in Figure 5-4E-H). Given that studies have pointed towards the presence of

a cryptic enhancer element within the VP16-AD construct (Luan et al., 2006; Luan, H. and White, B.H., unpublished) this 'globally ectopic' phenotype may manifest in lines within which the VP16-AD *P*-element is positioned nearby an exceptionally strong enhancer element. In such instances, the accumulation of transcriptional machinery may result in its binding to the cryptic enhancer element, resulting in globally ectopic patterns of expression; the topology of which would not be expected to differ between such lines. Indeed all 4 lines exhibited a reiterated pattern of expression (data not shown). Unfortunately, any lines that fall into this category are practically flawed, and must also be omitted from further experimental use. A list of candidate lines and the type of associated ectopic pattern of expression realised by their use is shown in Table 5-2.

Figure 5-4 Examples of ectopic patterns of nGFP expression in male and female 5 day old adult CNSs.
(A-D) *dsx*$^{GAL4\text{-}DBD}$ paired with 177RA$^{VP16\text{-}AD}$ expressing *UAS-pStinger* in male and female adult CNSs. (A) Adult male brain, expression in the *dsx*-aDN, -pC1, -pC2, -pC3, -SN, clusters. Ectopic expression marked by asterisks. (B) Adult male VNC, expression in the *dsx*-TN1, -TN2, and -Abg clusters. (C) Adult female brain, expression in the *dsx*-aDN, -pC1, -pC2, -pC3, clusters. Ectopic expression marked by asterisks. (D) Adult female VNC, expression in the *dsx*-Abg cluster. (E-H) *dsx*$^{GAL4\text{-}DBD}$ paired with MB01$^{VP16\text{-}AD}$ expressing *UAS-pStinger* in male and female adult CNSs. (E) Adult male brain. Overt globally ectopic expression of nGFP is observed, with no expression detected in *dsx* clusters. (E) Adult male brain. (F) Adult male VNC. (E) Adult female brain. (E) Adult female VNC. Cluster designation as per Lee et al., 2002 and Rideout et al., 2010. nGFP realised with anti-GFP antibody (green) and neuropil counterstained with nc82 (magenta). All views are ventral, with anterior up. Scale bar = 50 µm.

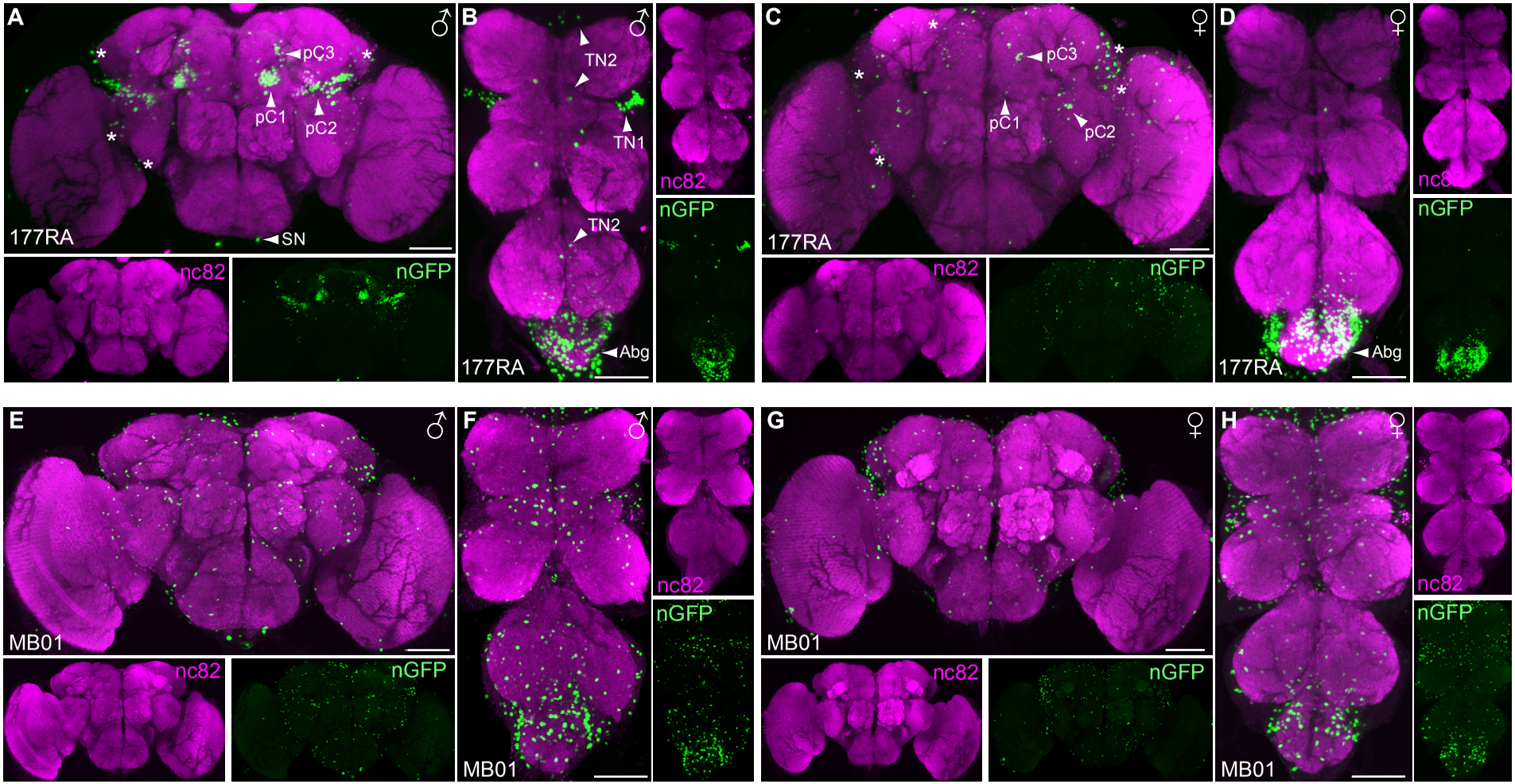

A
♂
pC3
pC1
pC2
SN
177RA
nc82
nGFP
B
♂
TN2
TN1
TN2
Abg
177RA
nc82
nGFP
C
♀
pC3
pC1
pC2
177RA
nc82
nGFP
D
♀
Abg
177RA
nc82
nGFP
E
♂
MB01
nc82
nGFP
F
♂
MB01
nc82
nGFP
G
♀
MB01
nc82
nGFP
H
♀
MB01
nc82
nGFP

Table 5-2 Phase 2 Candidate lines in which intersected male CNSs exhibit ectopic patterns of reporter expression.
Candidate names (as per Luan et al., 2006; M.Landgraf, unpublished), description of male and female neuroanatomical reporter expression listed. Ectopic patterns of expression were found to occur in two different modes; 'globally ectopic' refers to widespread expression of the reporter that does not include expression in neurons of the *dsx* circuitry, while 'ectopic' refers to expression patterns in which neurons of the *dsx* circuitry, in addition to non *dsx*-expressing neurons are realised. Intersected male and female CNSs from the same candidate lines revealed identical modes of ectopic expression.

Candidate I.D.	Male Neuroanatomical Expression Analyses	Female Neuroanatomical Expression Analyses
Wing Extension Candidates		
BF01	Globally ectopic	Globally ectopic
CH11	Globally ectopic	Globally ectopic
ML153	Globally ectopic	Globally ectopic
92RWIII	Ectopic	Ectopic
Abdominal Curling Candidates		
MB01	Globally ectopic	Globally ectopic
VK02	Ectopic	Ectopic
Candidates that display partial behaviours		
177RA	Ectopic	Ectopic
88R	Ectopic	Ectopic

5.6.2.2 Omitting candidate lines with extensive patterns of reporter expression

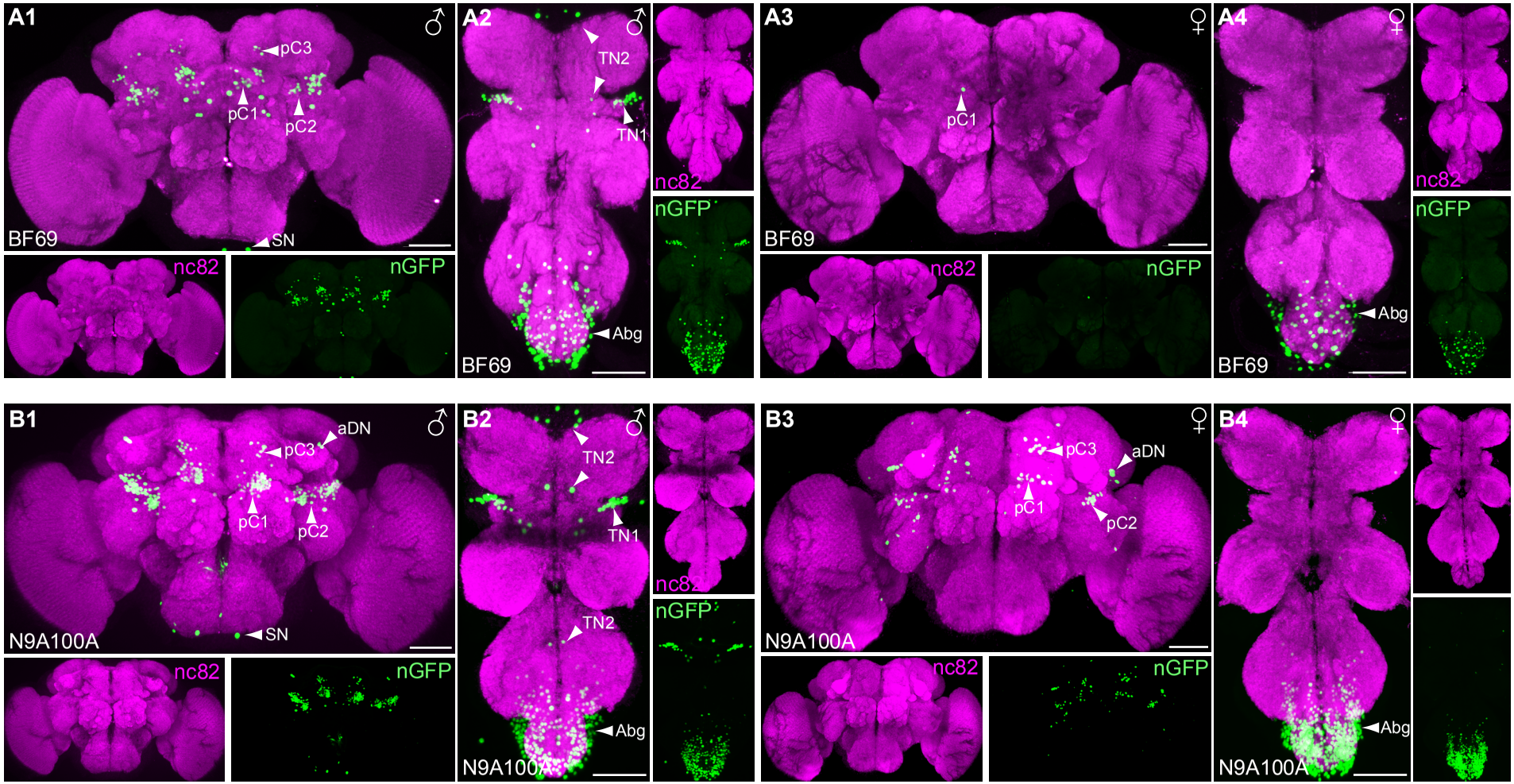
Candidate lines that realise extensive patterns of intersected expression are superfluous to the project at hand, as this study necessitates restriction of spatial expression for the purpose of functionally mapping subsets of the *dsx* circuitry. By way of scoring for variations in the display of two mutually exclusive behaviours, wing extension and abdominal curling, via a thermogenetic screen, I anticipated a requirement for a level of restriction not met by the majority of the candidate lines. Strikingly, 16 out of the remaining 22 lines retrieved from the screen realised extensive patterns of expression that were, superficially, indistinguishable from the expression patterns realised by $dsx^{GAL4\text{-}DBD}/elav^{VP16\text{-}AD}$ (Table 5-3; Figure 5-5). This included all candidate lines that displayed partial behaviours, in addition to 9/12 abdominal curling candidate lines (Table 5-3; Figure 5-5). This is not to say that these lines are identical to wild-type expression patterns. It is likely that a 'critical' set of neurons necessary for the

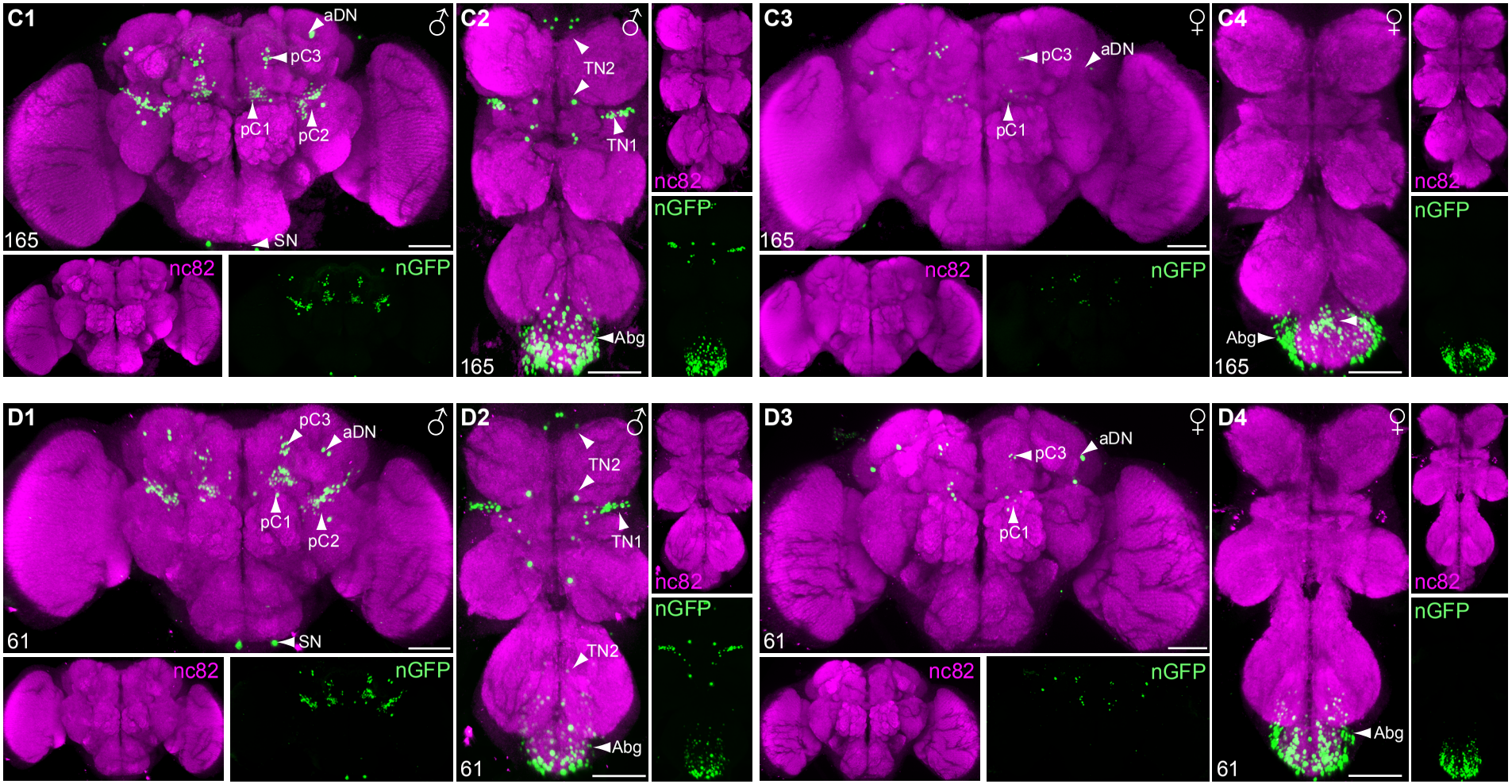
appropriate behavioural outputs are absent in these intersected lines, resulting in the deficit of a given behaviour. By way of registering these images onto a reference brain, it may be possible to identify individual neurons absent from these lines, revealing their requirement in the generation of faithful unilateral wing extension or abdominal curling. Yet even then, these lines are functionally of less interest, as they do not grant genetic access to interrogate or neuroanatomically map these 'critical' neurons. For these reasons, these lines were omitted from further investigations.

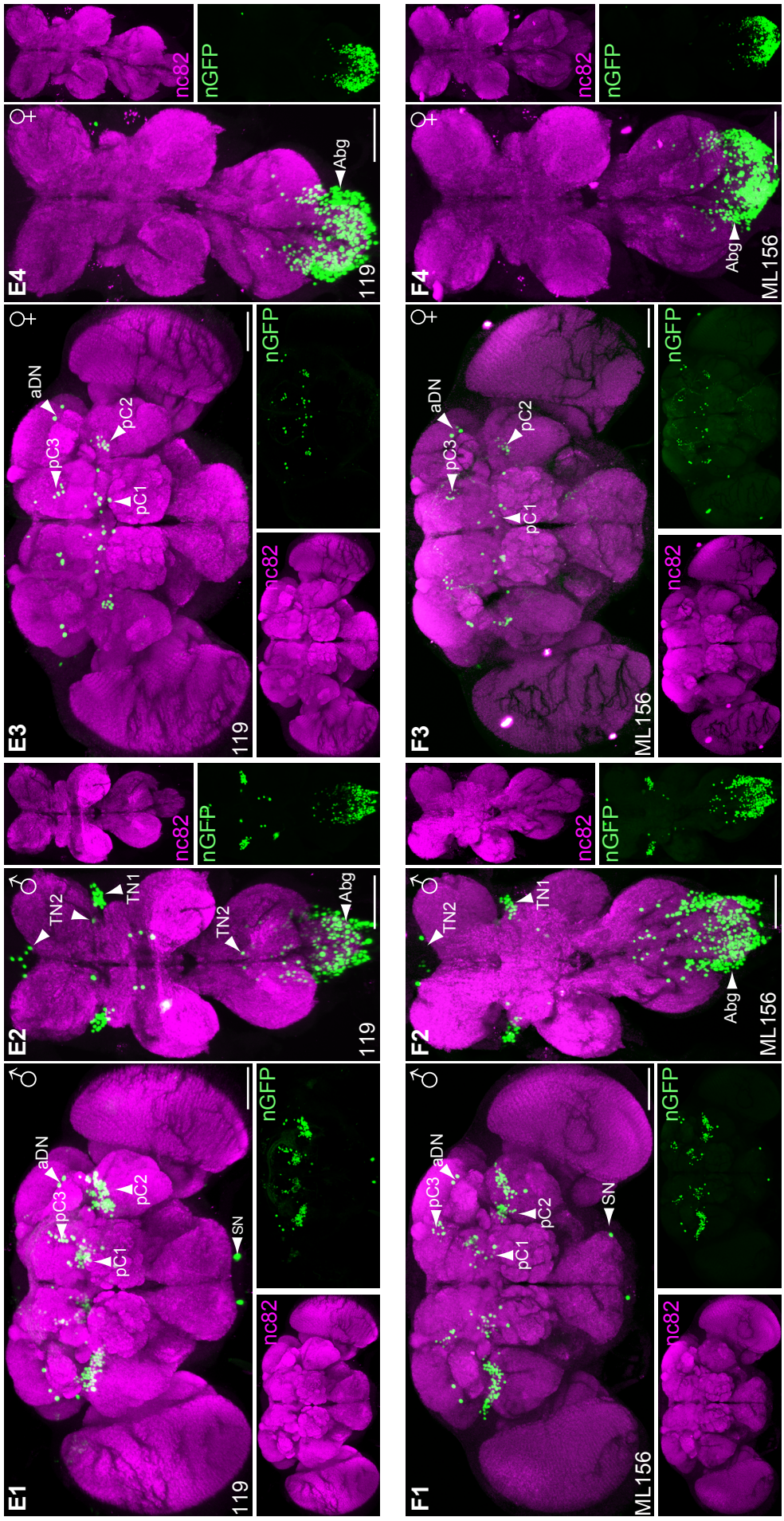
As previously stated, I aimed to exploit all the candidate lines retrieved from the screen not only to isolate lines with restricted patterns of expression in the male CNS, but also as an indirect way to isolate lines that may reveal restricted patterns of expression in the female CNS for future work on parsing neural circuitry underlying female behaviour. Although the male CNSs of these candidate lines show broad patterns of intersected expression, female CNSs did not always reveal analogous patterns of expression (Table 1 3; Figure 1 5). Seven of the 16 lines showed restricted patterns of expression in females and not in males (Table 5-3; Figure 5-5). For example, coupling BF69 with *dsx*$^{GAL4\text{-}DBD}$ restricts expression to a subset of neurons in the Abg only (Figure 5-5A3-4). While coupling 165 or 61 with *dsx*$^{GAL4\text{-}DBD}$ realises the full *dsx* circuitry, barring the *dsx*-pC2 cluster (Figure 5-5C3-4, Figure 5-5D3-4). It is for this reason that I have included the full set of lines; displaying both male and female patterns of expression as a reference point for selecting possible candidate lines for future studies on female behaviour.

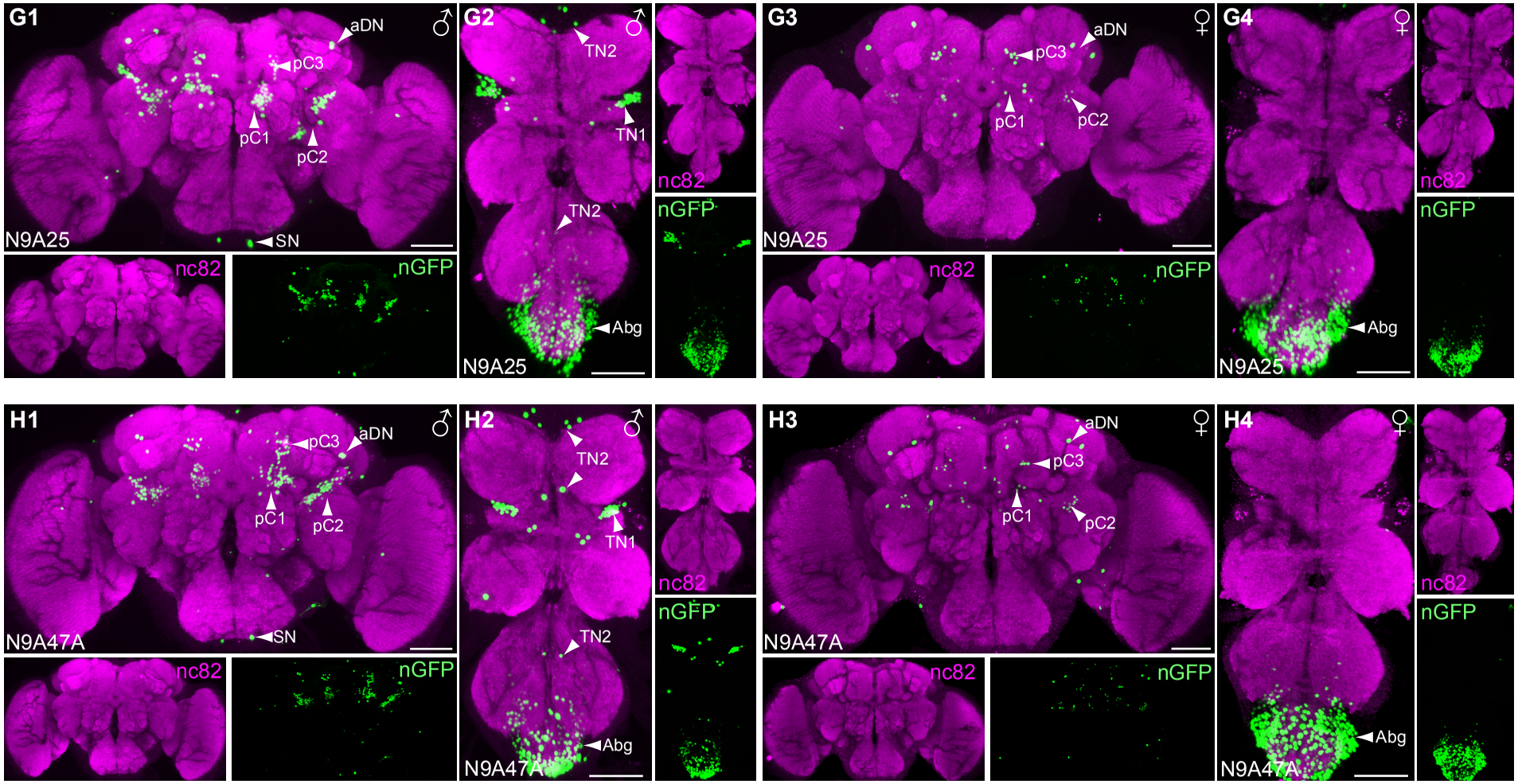
Table 5-3 Phase 2 Candidate lines in which intersected male CNSs exhibit extensive patterns of reporter expression.
Candidate names (as per Luan et al., 2006; M.Landgraf, unpublished), description of male and female neuroanatomical reporter expression listed. Although males from these candidate lines all exhibit broad patterns of reporter expression, analogous female CNSs did not always reveal similarly broad patterns of expression. Specifically, seven candidate lines revealed restricted patterns of expression in females only.

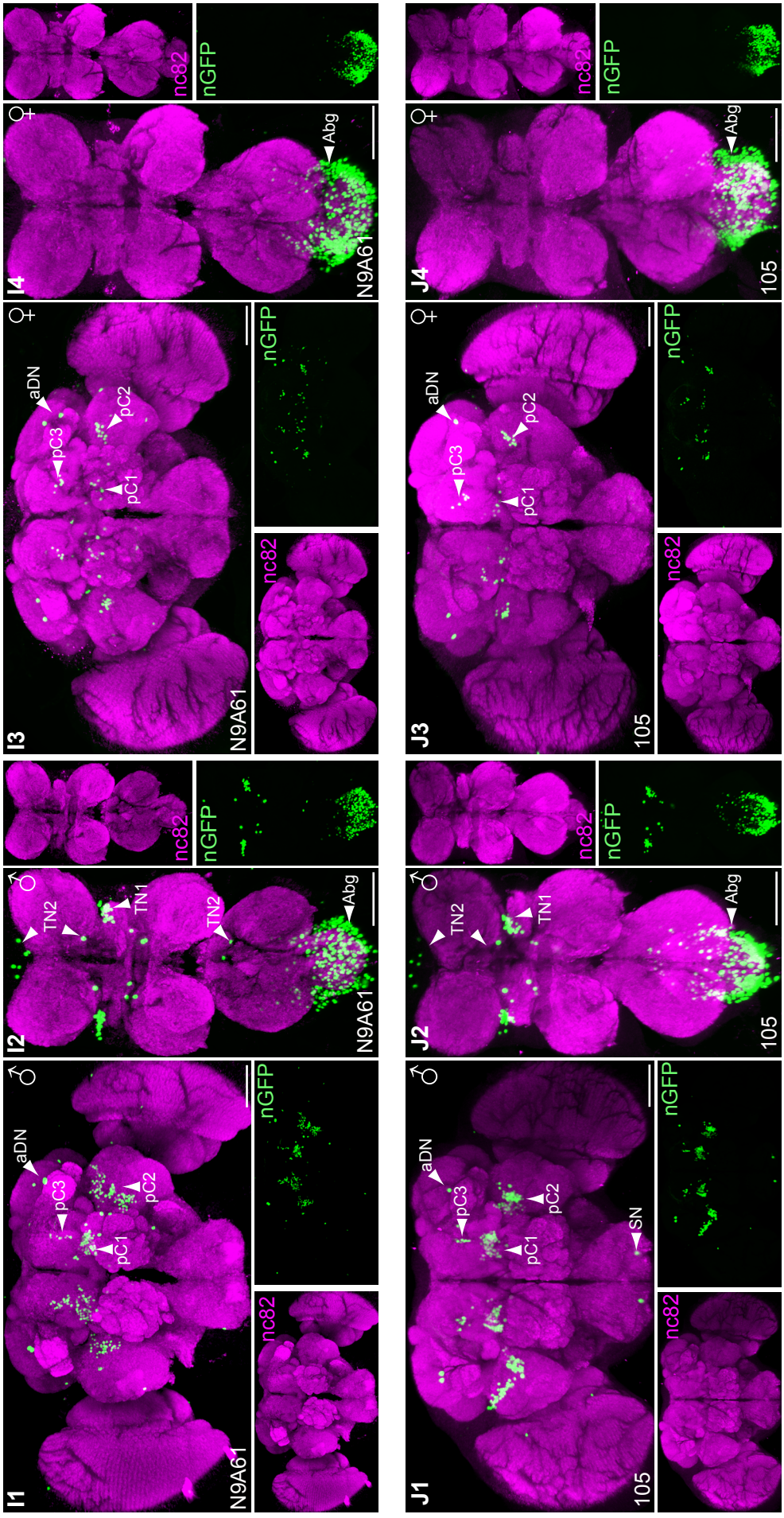
Candidate I.D.	Male Neuroanatomical Expression Analyses	Female Neuroanatomical Expression Analyses
Abdominal Curling Candidates		
BF69	Extensive	Restricted
N9A100A	Extensive	Extensive
165	Extensive	Restricted
61	Extensive	Restricted
119	Extensive	Extensive
ML156	Extensive	Extensive
N9A25	Extensive	Restricted
N9A47A	Extensive	Extensive
N9A61	Extensive	Extensive
Candidates that display partial behaviours		
105	Extensive	Extensive
179	Extensive	Restricted
2	Extensive	Restricted
N4A10	Extensive	Extensive
N9A96B	Extensive	Extensive
111	Extensive	Restricted
112	Extensive	Extensive

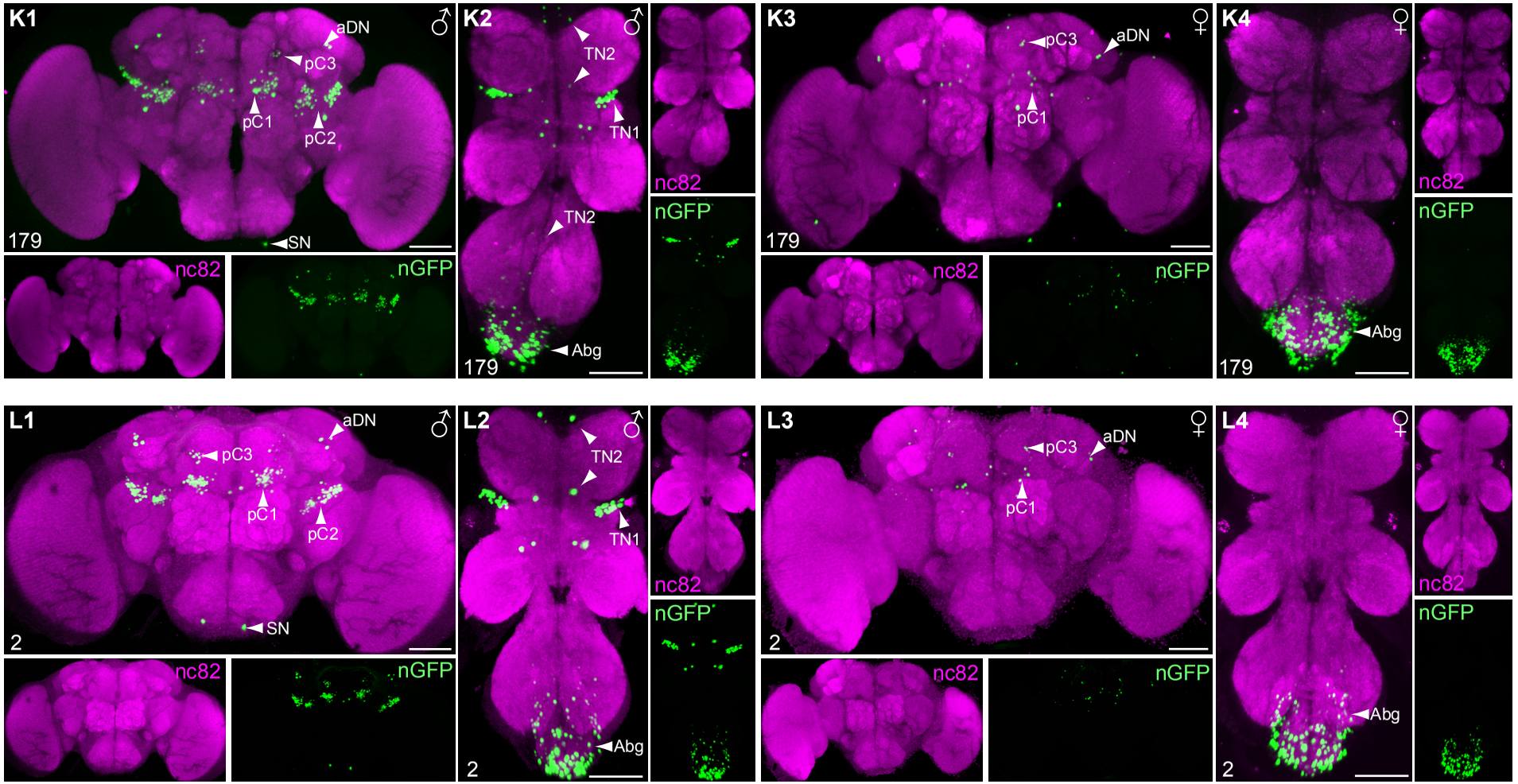

A1
♂
pC3
pC1
pC2
BF69
SN
nc82
nGFP
A2
♂
TN2
TN1
nc82
nGFP
BF69
Abg
A3
♀
pC1
BF69
nc82
nGFP
A4
♀
nc82
nGFP
Abg
BF69
B1
♂
aDN
pC3
pC1
pC2
N9A100A
SN
nc82
nGFP
B2
♂
TN2
TN1
nc82
nGFP
TN2
Abg
N9A100A
B3
♀
pC3
aDN
pC1
pC2
N9A100A
nc82
nGFP
B4
♀
nc82
nGFP
Abg
N9A100A

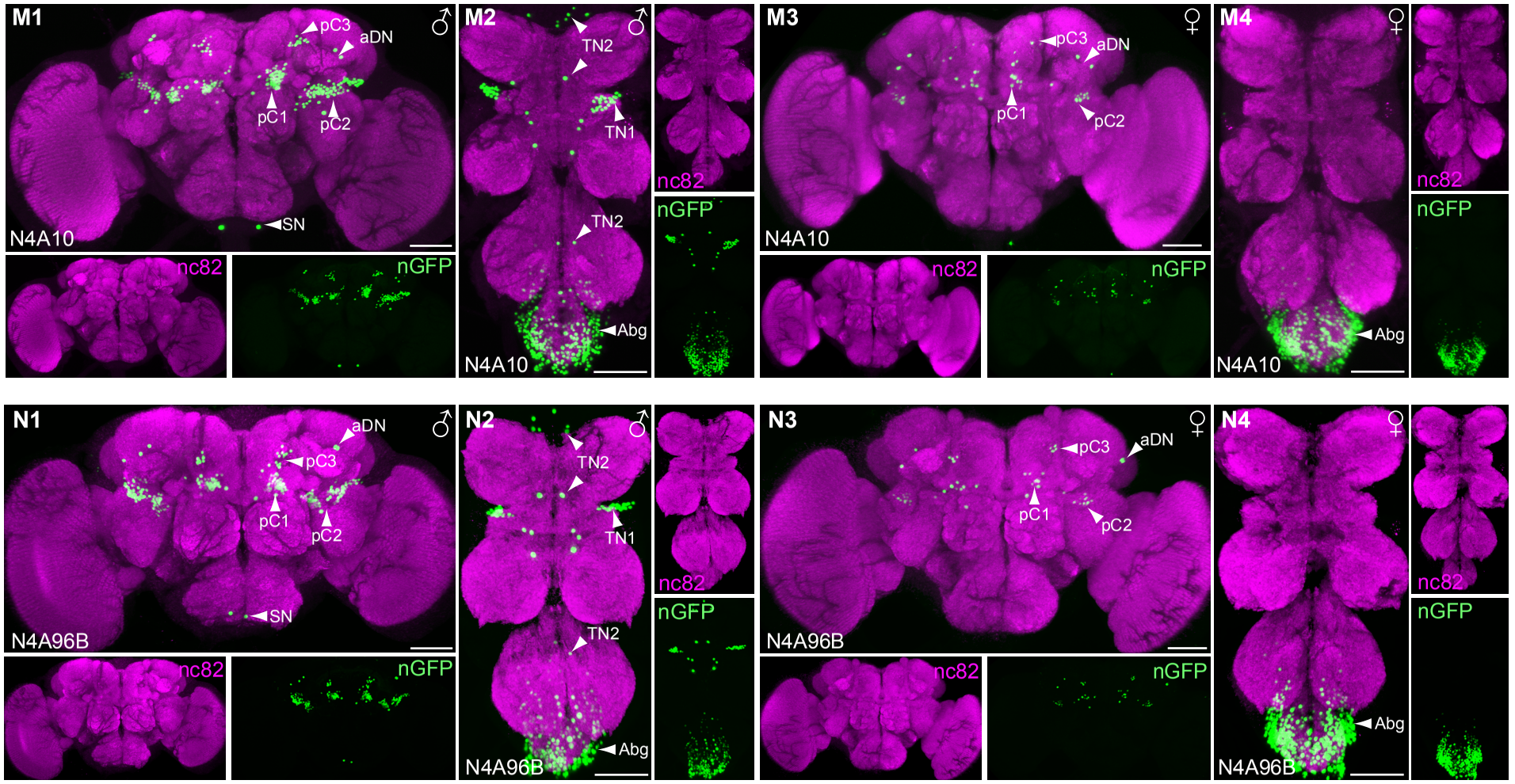

C1
aDN
pC3
pC1
pC2
SN
165
nc82
nGFP
C2
TN2
TN1
Abg
165
nc82
nGFP
C3
pC3
aDN
pC1
165
nc82
nGFP
C4
Abg
165
nc82
nGFP
D1
pC3
aDN
pC1
pC2
SN
61
nc82
nGFP
D2
TN2
TN1
TN2
Abg
61
nc82
nGFP
D3
pC3
aDN
pC1
61
nc82
nGFP
D4
Abg
61
nc82
nGFP


E1
119
aDN
pC3
pC2
pC1
SN
nGFP
nc82
E2
TN2
TN1
TN2
Abg
119
nc82
nGFP
E3
119
aDN
pC3
pC2
pC1
nGFP
nc82
E4
Abg
119
nc82
nGFP
F1
ML156
aDN
pC3
pC1
pC2
SN
nGFP
nc82
F2
TN2
TN1
Abg
ML156
nc82
nGFP
F3
ML156
aDN
pC3
pC2
pC1
nGFP
nc82
F4
Abg
ML156
nc82
nGFP


G1
aDN
pC3
pC1
pC2
SN
N9A25
nc82
nGFP
G2
TN2
TN1
TN2
Abg
N9A25
nc82
nGFP
G3
aDN
pC3
pC1
pC2
N9A25
nc82
nGFP
G4
Abg
N9A25
nc82
nGFP
H1
pC3
aDN
pC1
pC2
SN
N9A47A
nc82
nGFP
H2
TN2
TN1
TN2
Abg
N9A47A
nc82
nGFP
H3
aDN
pC3
pC1
pC2
N9A47A
nc82
nGFP
H4
Abg
N9A47A
nc82
nGFP


I1
aDN
pC3
pC1
pC2
N9A61
nc82
nGFP
I2
TN2
TN1
TN2
Abg
N9A61
nc82
nGFP
I3
aDN
pC3
pC1
pC2
N9A61
nc82
nGFP
I4
Abg
N9A61
nc82
nGFP
J1
aDN
pC3
pC1
pC2
SN
105
nc82
nGFP
J2
TN2
TN1
Abg
105
nc82
nGFP
J3
aDN
pC3
pC1
pC2
105
nc82
nGFP
J4
Abg
105
nc82
nGFP


K1
aDN
pC3
pC1
pC2
SN
179
nc82
nGFP
K2
TN2
TN1
TN2
Abg
179
nc82
nGFP
K3
pC3
aDN
pC1
179
nc82
nGFP
K4
Abg
179
nc82
nGFP
L1
aDN
pC3
pC1
pC2
SN
2
nc82
nGFP
L2
TN2
TN1
Abg
2
nc82
nGFP
L3
pC3
aDN
pC1
2
nc82
nGFP
L4
Abg
2
nc82
nGFP


M1
♂
pC3
aDN
pC1
pC2
SN
N4A10
nc82
nGFP
M2
♂
TN2
TN1
TN2
Abg
N4A10
nc82
nGFP
M3
♀
pC3
aDN
pC1
pC2
N4A10
nc82
nGFP
M4
♀
Abg
N4A10
nc82
nGFP
N1
♂
aDN
pC3
pC1
pC2
SN
N4A96B
nc82
nGFP
N2
♂
TN2
TN1
TN2
Abg
N4A96B
nc82
nGFP
N3
♀
pC3
aDN
pC1
pC2
N4A96B
nc82
nGFP
N4
♀
Abg
N4A96B
nc82
nGFP

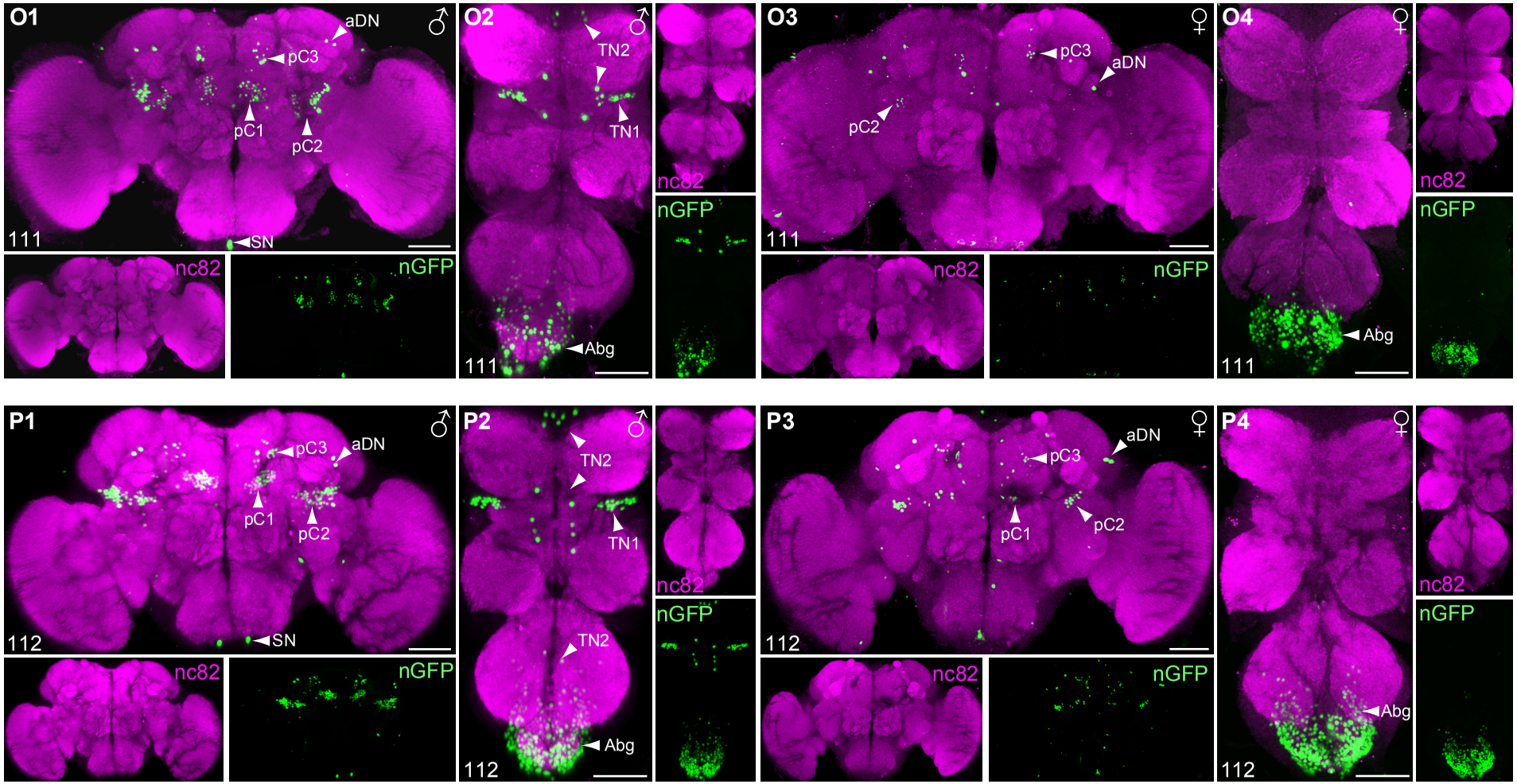

O1
aDN
pC3
pC1
pC2
111
SN
nc82
nGFP
O2
TN2
TN1
nc82
nGFP
111
Abg
O3
pC3
aDN
pC2
111
nc82
nGFP
O4
nc82
nGFP
111
Abg
P1
pC3
aDN
pC1
pC2
112
SN
nc82
nGFP
P2
TN2
TN1
nc82
nGFP
TN2
112
Abg
P3
aDN
pC3
pC1
pC2
112
nc82
nGFP
P4
nc82
nGFP
112
Abg

Figure 5-5 Candidate lines with broad patterns of nGFP expression in male and female 5 day old adult CNSs.
(A-I) Wing extension candidate lines with broad patterns of nGFP expression in male and female 5 day old adult CNSs. (A1-4) *dsx*$^{GAL4\text{-}DBD}$ paired with BF69$^{VP16\text{-}AD}$ expressing *UAS-pStinger* in male and female adult CNSs. (B1-4) *dsx*$^{GAL4\text{-}DBD}$ paired with N9A100A$^{VP16\text{-}AD}$ expressing *UAS-pStinger* in male and female adult CNSs. (C1-4) *dsx*$^{GAL4\text{-}DBD}$ paired with 165$^{VP16\text{-}AD}$ expressing *UAS-pStinger* in male and female adult CNSs. (D1-4) *dsx*$^{GAL4\text{-}DBD}$ paired with 61$^{VP16\text{-}AD}$ expressing *UAS-pStinger* in male and female adult CNSs. (E1-4) *dsx*$^{GAL4\text{-}DBD}$ paired with 119$^{VP16\text{-}AD}$ expressing *UAS-pStinger* in male and female adult CNSs. (F1-4) *dsx*$^{GAL4\text{-}DBD}$ paired with ML156$^{VP16\text{-}AD}$ expressing *UAS-pStinger* in male and female adult CNSs. (G1-4) *dsx*$^{GAL4\text{-}DBD}$ paired with N9A25$^{VP16\text{-}AD}$ expressing *UAS-pStinger* in male and female adult CNSs. (H1-4) *dsx*$^{GAL4\text{-}DBD}$ paired with N9A47A$^{VP16\text{-}AD}$ expressing *UAS-pStinger* in male and female adult CNSs. (I1-4) *dsx*$^{GAL4\text{-}DBD}$ paired with N9A61$^{VP16\text{-}AD}$ expressing *UAS-pStinger* in male and female adult CNSs. (J-P) Abdominal curling candidate lines with broad patterns of nGFP expression in male and female 5 day old adult CNSs. (J1-4) *dsx*$^{GAL4\text{-}DBD}$ paired with 105$^{VP16\text{-}AD}$ expressing *UAS-pStinger* in male and female adult CNSs. (K1-4) *dsx*$^{GAL4\text{-}DBD}$ paired with 179$^{VP16\text{-}AD}$ expressing *UAS-pStinger* in male and female adult CNSs. (L1-4) *dsx*$^{GAL4\text{-}DBD}$ paired with 2$^{VP16\text{-}AD}$ expressing *UAS-pStinger* in male and female adult CNSs. (M1-4) *dsx*$^{GAL4\text{-}DBD}$ paired with N4A10$^{VP16\text{-}AD}$ expressing *UAS-pStinger* in male and female adult CNSs. (N1-4) *dsx*$^{GAL4\text{-}DBD}$ paired with N9A96B$^{VP16\text{-}AD}$ expressing *UAS-pStinger* in male and female adult CNSs. (O1-4) *dsx*$^{GAL4\text{-}DBD}$ paired with 111$^{VP16\text{-}AD}$ expressing *UAS-pStinger* in male and female adult CNSs. (P1-4) *dsx*$^{GAL4\text{-}DBD}$ paired with 112$^{VP16\text{-}AD}$ expressing *UAS-pStinger* in male and female adult CNSs. (1) Adult male brain, expression in the *dsx*-aDN, -pC1, -pC2, -pC3, -SN, clusters. (2) Adult male VNC, expression in the *dsx*-TN1, -TN2, and -Abg clusters. (3) Adult female brain, expression in the *dsx*-aDN, -pC1, -pC2, -pC3, clusters. (4) Adult female VNC, expression in the *dsx*-Abg cluster. (E-H) *dsx*$^{GAL4\text{-}DBD}$ paired with MB01$^{VP16\text{-}AD}$ expressing *UAS-pStinger* in male and female adult CNSs. Cluster designation as per Lee et al., 2002 and Rideout et al., 2010. nGFP realised with anti-GFP antibody (green) and neuropil counterstained with nc82 (magenta). All views are ventral, with anterior up. Scale bar = 50 µm.

5.6.2.3 Candidate lines with restricted patterns of reporter expression

Barring candidate lines that revealed ectopic or broad patterns of expression, six remaining candidate lines revealed restricted patterns of expression in both male and female CNSs: three wing extension candidates, and three abdominal curling candidates (Table 5-4; Figure 5-6 to Figure 5-11). To quantify the level and topology of restriction, I carried out cell counts of nGFP expression in the CNSs of 5-7 day old adult males (Table 5-5; Figure 5-12).

Table 5-4 Phase 2 Candidate lines in which intersected male CNSs exhibit restricted patterns of reporter expression.
Candidate names (as per Luan et al., 2006; M.Landgraf, unpublished), description of male and female neuroanatomical reporter expression listed. Intersected male and female CNSs from the same candidate lines revealed similarly restricted patterns of reporter expression.

Candidate I.D.	Male Neuroanatomical Expression Analyses	Female Neuroanatomical Expression Analyses
Wing Extension Candidates		
VK29	Restricted	Restricted
79	Restricted	Restricted
147	Restricted	Restricted
Abdominal Curling Candidates		
AZ16	Restricted	Restricted

141	Restricted	Restricted
vGlut^{OK371}	Restricted	Restricted

VK29 (Figure 5-6; Table 5-5): Male brain expression restricted to subsets of *dsx*-pC1, -pC2 -pC3 clusters. Male VNC expression restricted to *dsx*-TN1 and a small subset of -TN2 and -Abg clusters. No expression observed in the female brain. Superficially, expression in a subset of the *dsx*-Abg cluster in the female VNC is observed.

79 (Figure 5-7; Table 5-5): Male brain expression restricted to *dsx*-aDN and -SN clusters, and subsets of *dsx*-pC1, -pC2 -pC3 clusters. Male VNC expression restricted to *dsx*-TN1 and a subset of the -TN2 and -Abg clusters. Female brain expression restricted to *dsx*-aDN cluster and subsets of *dsx*-pC1 and -pC2 clusters. Overt expression in the *dsx*-Abg cluster of the female VNC.

147 (Figure 5-8; Table 5-5): Male brain expression restricted to subsets of *dsx*-pC1, -pC2 -pC3 clusters. Male VNC expression restricted to *dsx*-TN1 and a small subset of -TN2 and -Abg clusters. Female brain expression restricted to subsets of *dsx*-pC1 and -pC2 clusters. Expression in a subset of the *dsx*-Abg cluster in the female VNC is observed.

141 (Figure 5-9; Table 5-5): Male brain expression restricted to subsets of *dsx*-pC1 and -pC2 clusters. Male VNC expression restricted to *dsx*-TN1 and a small subset of -TN2 and -Abg clusters. Female brain expression restricted to *dsx*-aDN cluster and subsets of *dsx*-pC1, -pC2 and -pC3 clusters. Expression in the *dsx*-Abg cluster in the female VNC is observed

AZ16 (Figure 5-10; Table 5-5): Male brain expression restricted to subsets of *dsx*-pC1, -pC2 and -pC3 clusters. Male VNC expression restricted to a small subset of *dsx*-TN1 and -Abg clusters. Superficially, female brain expression restricted to *dsx*-aDN cluster and a small subset of the *dsx*-pC1 cluster. Expression in a subset of the *dsx*-Abg cluster in the female VNC is observed.

***vGlut*^{OK371} (**Figure 5-11; Table 5-5): Male brain expression is restricted to *dsx*-aDN cluster. Male VNC expression is restricted to a subset of the *dsx*-Abg cluster. Female brain

expression restricted to *dsx*-aDN cluster. Female VNC expression is restricted to a subset of the *dsx*-Abg cluster.

Comparing expression patterns between the wing extension candidates revealed the similarities between them (Figure 5-6 to Figure 5-8; Figure 5-12; Table 5-5). The most reassuring being the presence a full complement of *dsx*-TN1 cluster, that comprises the local song CPG in the VNC (Rideout et al., 2007; Clyne and Miesenböck, 2008; von Philipsborn et al., 2011), in all three lines; although each of the lines showed varying numbers of neurons in *dsx*-pC1, -pC2, pC3 clusters of in the brain, and the *dsx*-TN2 and -Abg clusters of the VNC (Figure 5-6 to Figure 5-8; Figure 5-12; Table 5-5). Similarly, comparing expression patterns between the abdominal candidates revealed a commonality between them; all three lines lacked *dsx*-TN2 expression in the VNC, and all three lines presented a subset of *dsx*-Abg neurons of the VNC (Figure 5-9 to Figure 5-12; Table 5-5). That only a subset of *dsx*-TN1 neurons is realised with both 141 and AZ16, while a complete lack of expression in these neurons in observed in $vGlut^{OK371}$, is practically the opposite of what is seen with the wing extension candidates (Figure 5-6 to Figure 5-8; Figure 5-12; Table 5-5), implicating, as previously reported, the necessity of *dsx*-TN1 and -TN2 neurons of the VNC in wing extension and ultimately in song production (von Philipsborn et al., 2011).

Rather than discussing the significance of the neuroanatomical realisations here, with respect to the behavioural data obtained from the thermogenetic screen, I have held off discursive text in section 5.8 of this chapter. In this way, behavioural data from both the thermogenetic screen and from silencing experiments of the next section can differentially contribute towards deciphering the significance of each unique neuroanatomical pattern of intersected expression realised by each of the candidate lines. In essence, it is only by considering the conditions of sufficiency and necessity of these defined patterns of expression, that I am able to correlate function to specific clusters of *dsx*-expressing neurons.

In summary of the neuroanatomical analyses performed here, a total of 8 lines have been omitted due to observed ectopic patterns of expression, and an additional 16 lines because

they exhibited extensive patterns of expression that precluded fine-functional mapping (Figure 5-13). However a final 6 candidate lines revealed spatially restricted patterns of expression, upon which detailed neuroanatomical and topological analyses were carried out (Figure 5-13).

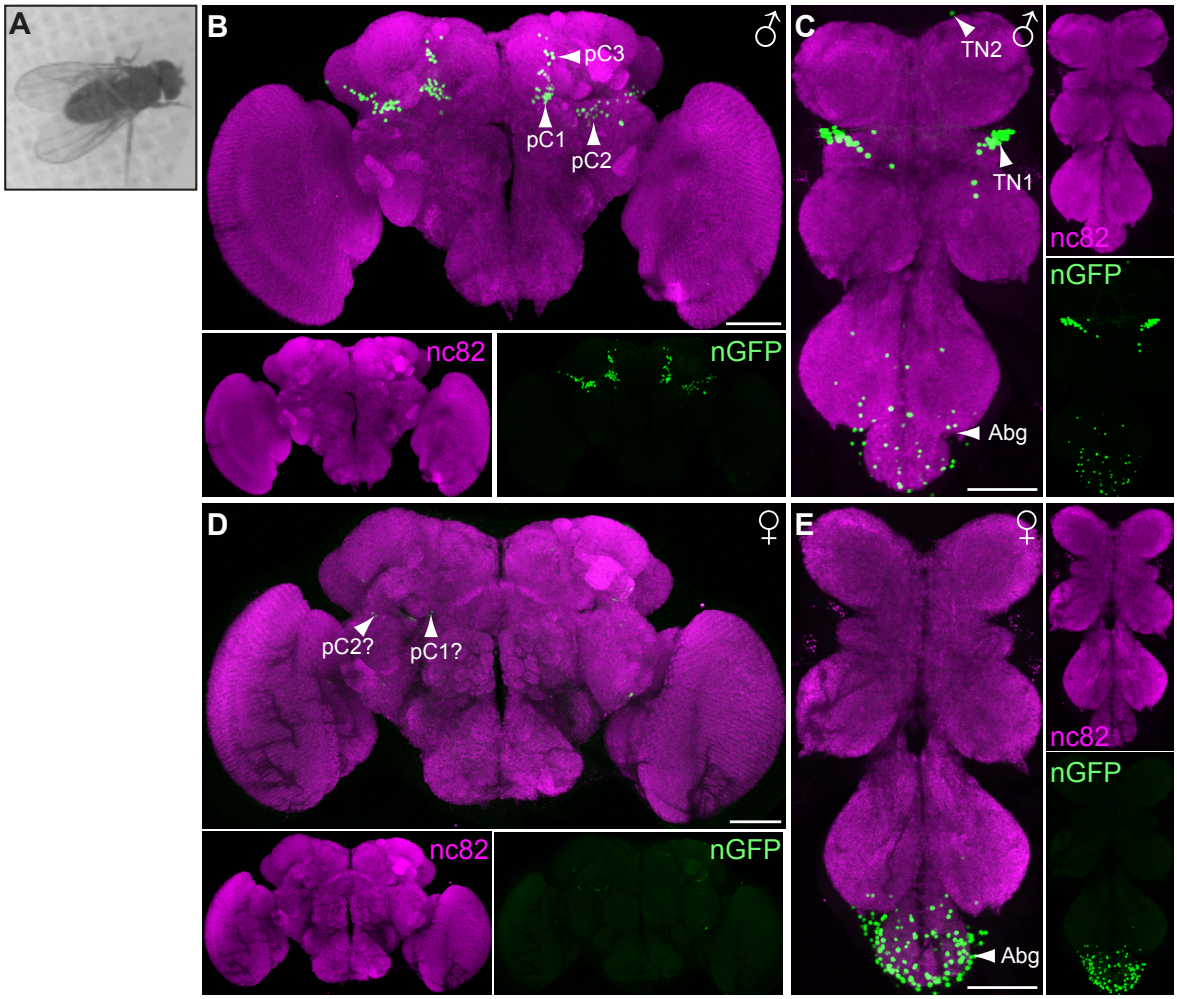


Figure 5-6 *dsx*$^{GAL4\text{-}DBD}$ paired with VK29$^{VP16\text{-}AD}$ expressing *UAS-pStinger* in male and female adult CNSs.
(A) Snapshot of wing scissoring elicited in thermogenetic screen. (B) Adult male brain, expression in the *dsx*-pC1, -pC2, -pC3 clusters. (C) Adult male VNC, expression in the *dsx*-TN1 and -Abg clusters. (D) Adult female brain, expression in the *dsx*-pC1 and -pC2, clusters. (E) Adult female VNC, expression in the *dsx*-Abg cluster. Cluster designation as per Lee et al., 2002 and Rideout et al., 2010. nGFP realised with anti-GFP antibody (green) and neuropil counterstained with nc82 (magenta). All views are ventral, with anterior up. Scale bar = 50 µm.

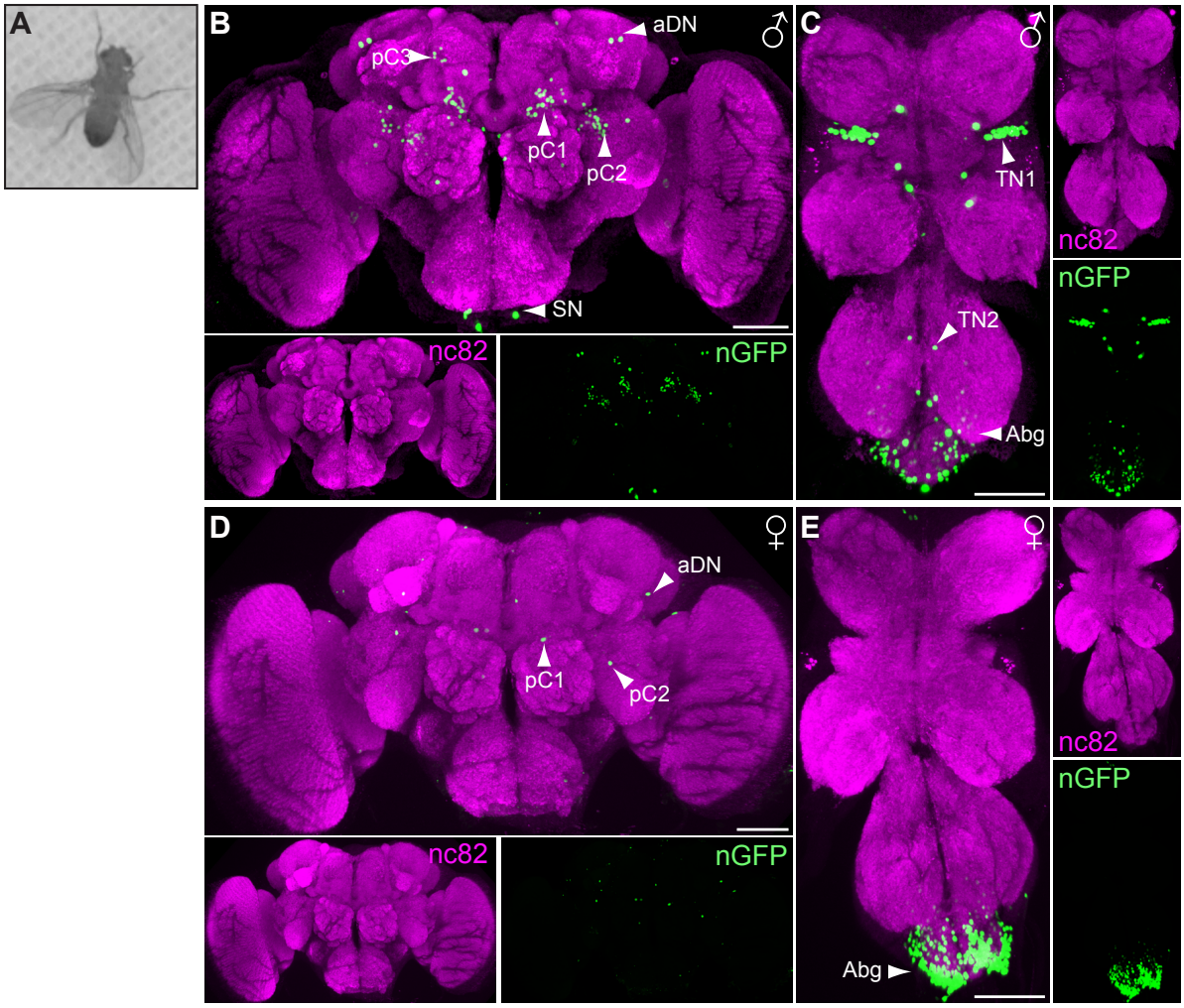


Figure 5-7 *dsx*$^{GAL4\text{-}DBD}$ paired with 79$^{VP16\text{-}AD}$ expressing *UAS-pStinger* in male and female adult CNSs.

(A) Snapshot of unilateral wing extension elicited in thermogenetic screen. (B) Adult male brain, expression in the *dsx*-aDN, -pC1, -pC2, -pC3, -SN, clusters. (C) Adult male VNC, expression in the *dsx*-TN1, -TN2, and -Abg clusters. (D) Adult female brain, expression in the *dsx*-aDN, -pC1 and -pC2 clusters. (E) Adult female VNC, expression in the *dsx*-Abg cluster. Cluster designation as per Lee et al., 2002 and Rideout et al., 2010. nGFP realised with anti-GFP antibody (green) and neuropil counterstained with nc82 (magenta). All views are ventral, with anterior up. Scale bar = 50 µm.

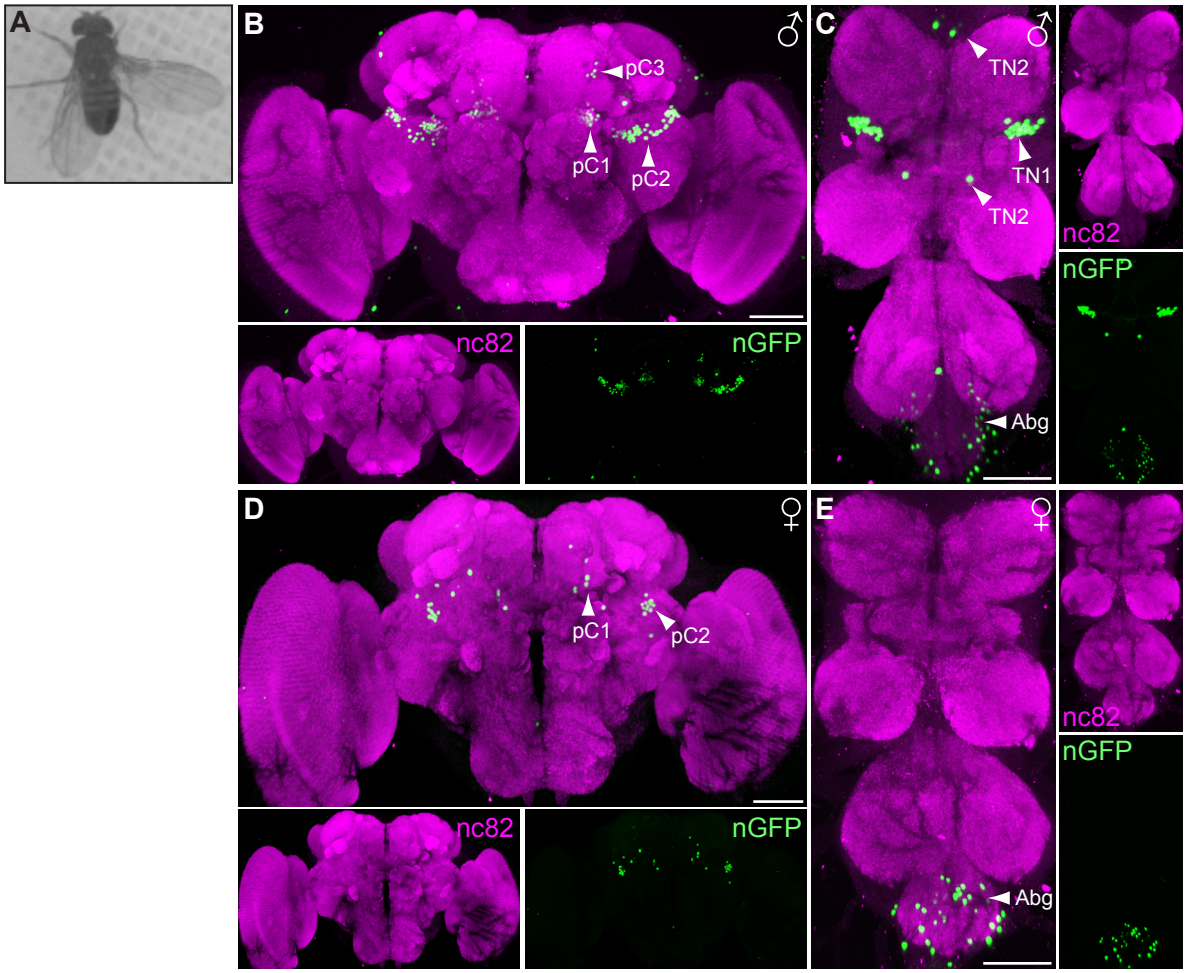


Figure 5-8 *dsx*$^{GAL4\text{-}DBD}$ paired with 147$^{VP16\text{-}AD}$ expressing *UAS-pStinger* in male and female adult CNSs.

(A) Snapshot of unilateral wing extension elicited in thermogenetic screen. (B) Adult male brain, expression in the *dsx*-pC1, -pC2, -pC3 clusters. (C) Adult male VNC, expression in the *dsx*-TN1, -TN2 and -Abg clusters. (D) Adult female brain, expression in the *dsx*-pC1 and -pC2, clusters. (E) Adult female VNC, expression in the *dsx*-Abg cluster. Cluster designation as per Lee et al., 2002 and Rideout et al., 2010. nGFP realised with anti-GFP antibody (green) and neuropil counterstained with nc82 (magenta). All views are ventral, with anterior up. Scale bar = 50 µm.

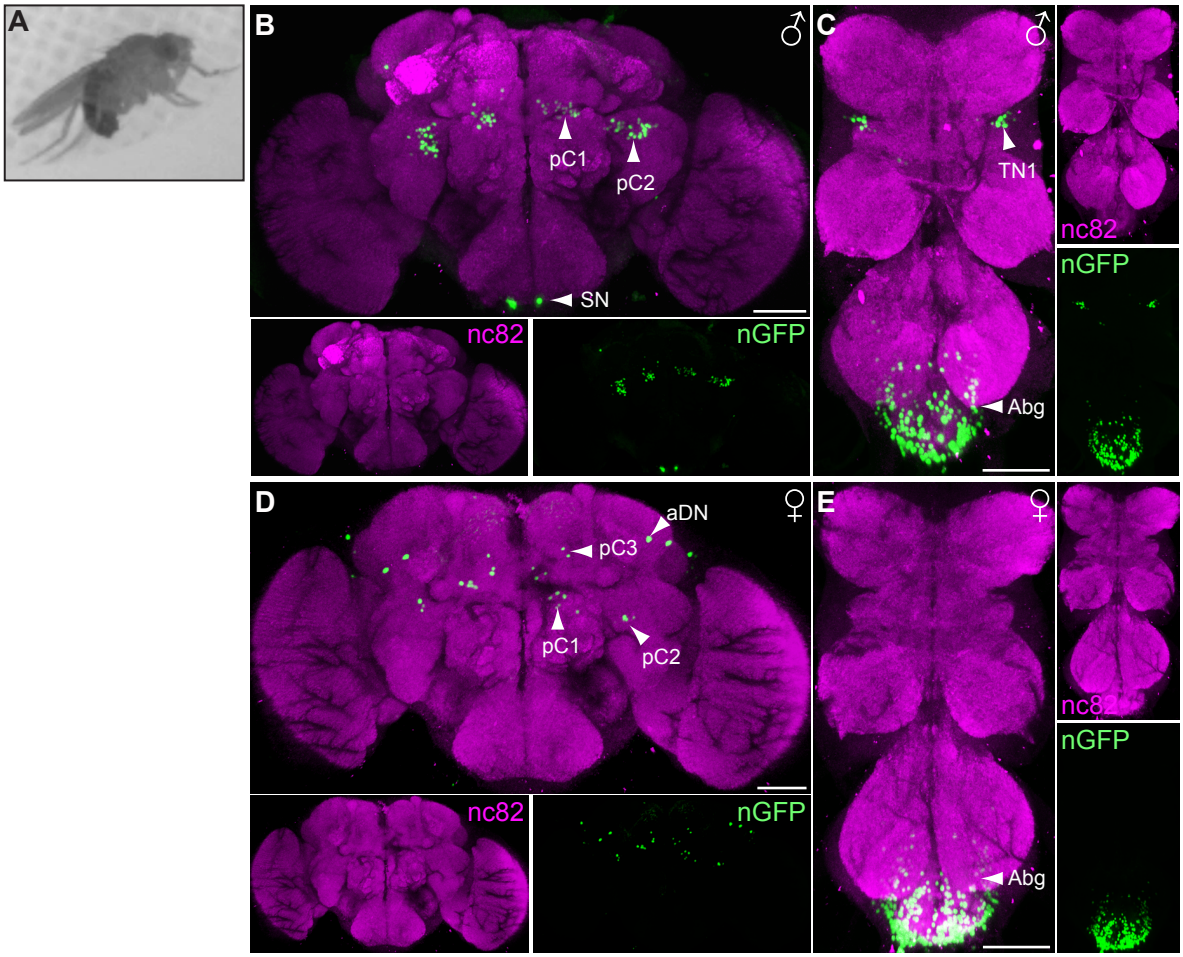


Figure 5-9 *dsx*$^{GAL4\text{-}DBD}$ paired with 141$^{VP16\text{-}AD}$ expressing *UAS-pStinger* in male and female adult CNSs.
(A) Snapshot of abdominal curling elicited in thermogenetic screen. (B) Adult male brain, expression in the *dsx*-pC1, -pC2 and -SN clusters. (C) Adult male VNC, expression in the *dsx*-TN1 and -Abg clusters. (D) Adult female brain, expression in the *dsx*-pC1, -pC2, -pC3 and -aDN clusters. (E) Adult female VNC, expression in the *dsx*-Abg cluster. Cluster designation as per Lee et al., 2002 and Rideout et al., 2010. nGFP realised with anti-GFP antibody (green) and neuropil counterstained with nc82 (magenta). All views are ventral, with anterior up. Scale bar = 50 µm.



Figure 5-10 *dsx*$^{GAL4\text{-}DBD}$ paired with AZ16$^{VP16\text{-}AD}$ expressing *UAS-pStinger* in male and female adult CNSs.
(A) Snapshot of abdominal curling elicited in thermogenetic screen. (B) Adult male brain, expression in the *dsx*-pC1, -pC2 and –pC3 clusters. (C) Adult male VNC, expression in the *dsx*-TN1 and -Abg clusters. (D) Adult female brain, expression in the *dsx*-pC1 and -aDN clusters. (E) Adult female VNC, expression in the *dsx*-Abg cluster. Cluster designation as per Lee et al., 2002 and Rideout et al., 2010. nGFP realised with anti-GFP antibody (green) and neuropil counterstained with nc82 (magenta). All views are ventral, with anterior up. Scale bar = 50 µm.

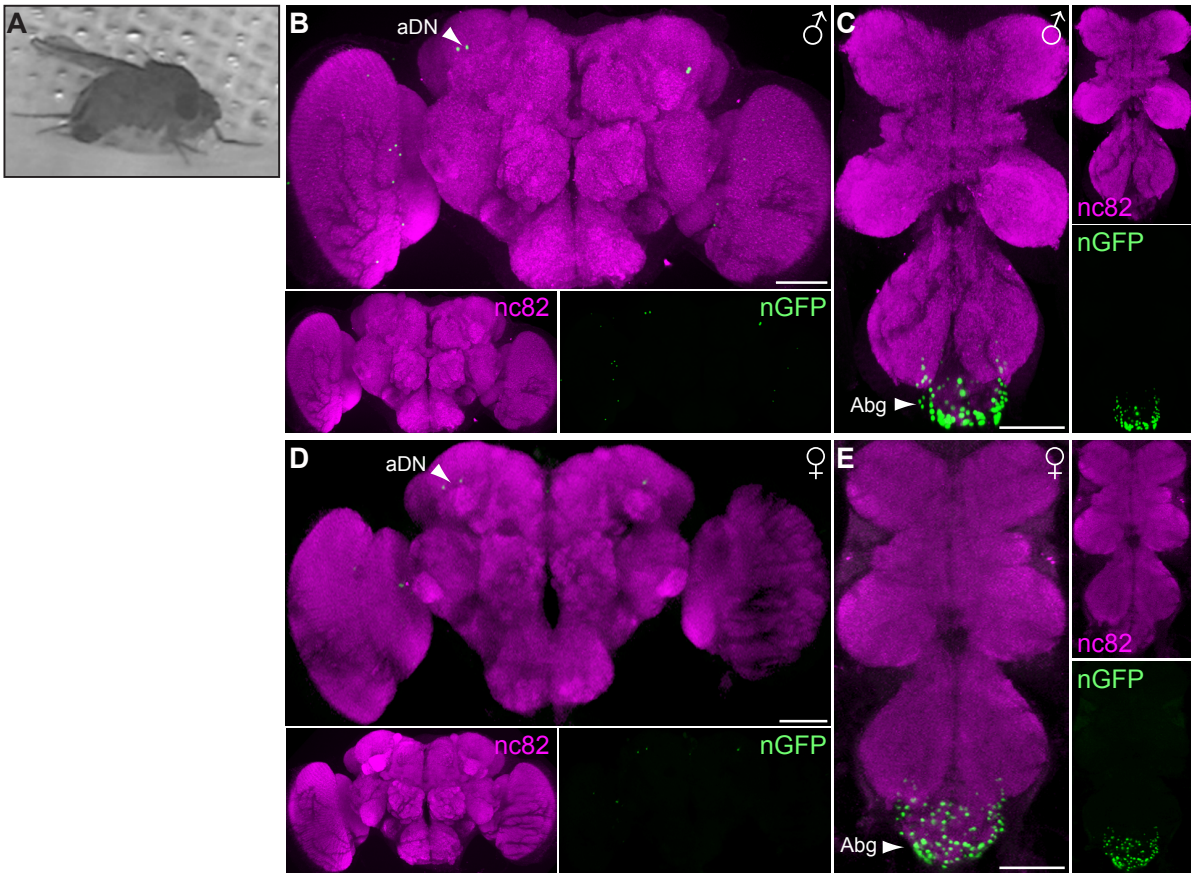


Figure 5-11 *dsx*$^{GAL4\text{-}DBD}$ paired with *vGlut*^{OK371}-VP16-AD expressing *UAS-pStinger* in male and female adult CNSs.
(A) Snapshot of abdominal curling elicited in thermogenetic screen. (B) Adult male brain, expression in the *dsx*-aDN cluster. (C) Adult male VNC, expression in the *dsx*-Abg cluster. (D) Adult female brain, expression in the *dsx*-aDN cluster. (E) Adult female VNC, expression in the *dsx*-Abg cluster. Cluster designation as per Lee et al., 2002 and Rideout et al., 2010. nGFP realised with anti-GFP antibody (green) and neuropil counterstained with nc82 (magenta). All views are ventral, with anterior up. Scale bar = 50 µm.

Table 5-5 Cell counts of candidate lines in adult 5-7 day old male CNS. *UAS-pStinger*/+; *dsx*$^{GAL4\text{-}DBD}$/+ crossed to seven different VP16-AD hemidrivers. *elav* (positive control), wing extension candidates *VK29, 79, 147,* and abdominal curling candidates; *141, AZ16 and vGlut*^{OK371}. Single-labelling with GFP applied to CNS. [a]Neural cluster away from CNS midline. Count represents one cluster per hemisegment of the CNS. [b]Neural cluster spans the CNS midline. Count is given for the complete VNC. Counts represent mean ± standard deviation. n's listed in parentheses.

Neural Clusters	*elav*	*VK29*	*79*	*147*	*141*	*AZ16*	*vGlut*^{OK371}
Brain							
-aDN[a]	2 ± 0 (12)	0 ± 0 (12)	2 ± 0 (12)	0 ± 0 (12)	0 ± 0 (12)	0 ± 0 (12)	2 ± 0 (12)
-SN[a]	1 ± 0 (12)	0 ± 0 (12)	1 ± 0 (12)	0 ± 0 (12)	1 ± 0 (12)	0 ± 0 (12)	0 ± 0 (12)
-pC1[a]	52 ± 4.8 (12)	17 ± 3.0 (12)	23 ± 1.5 (12)	33 ± 2.1 (12)	16 ± 3.2 (12)	9 ± 1.7 (12)	0 ± 0 (12)
-pC2[a]	78 ± 4.8 (12)	24 ± 1.8 (12)	24 ± 2.7 (12)	29 ± 5.6 (12)	23 ± 2.3 (12)	13 ± 1.9 (12)	0 ± 0 (12)
-pC3[a]	14 ± 0.9 (12)	6 ± 0.9 (12)	5 ± 0.7 (12)	4 ± 1.0 (12)	2 ± 0.9 (12)	0 ± 0 (12)	0 ± 0 (12)
VNC							
-TN1[a]	23 ± 1.5 (12)	20 ± 1.1 (12)	22 ± 0.8 (12)	23 ± 2.0 (12)	11 ± 1.4 (12)	3 ± 1.0 (12)	0 ± 0 (12)
-TN2[a]	8 ± 0.3 (12)	3 ± 0.5 (12)	5 ± 1.5 (12)	3 ± 0 (12)	0 ± 0 (12)	0 ± 0 (12)	0 ± 0 (12)
-Abg[b]	275 ± 21.7 (10)	42 ± 2.4 (10)	141 ± 7.8 (10)	43 ± 2.6 (10)	181 ± 12.5 (10)	99 ± 8.1 (10)	80 ± 2.3 (10)

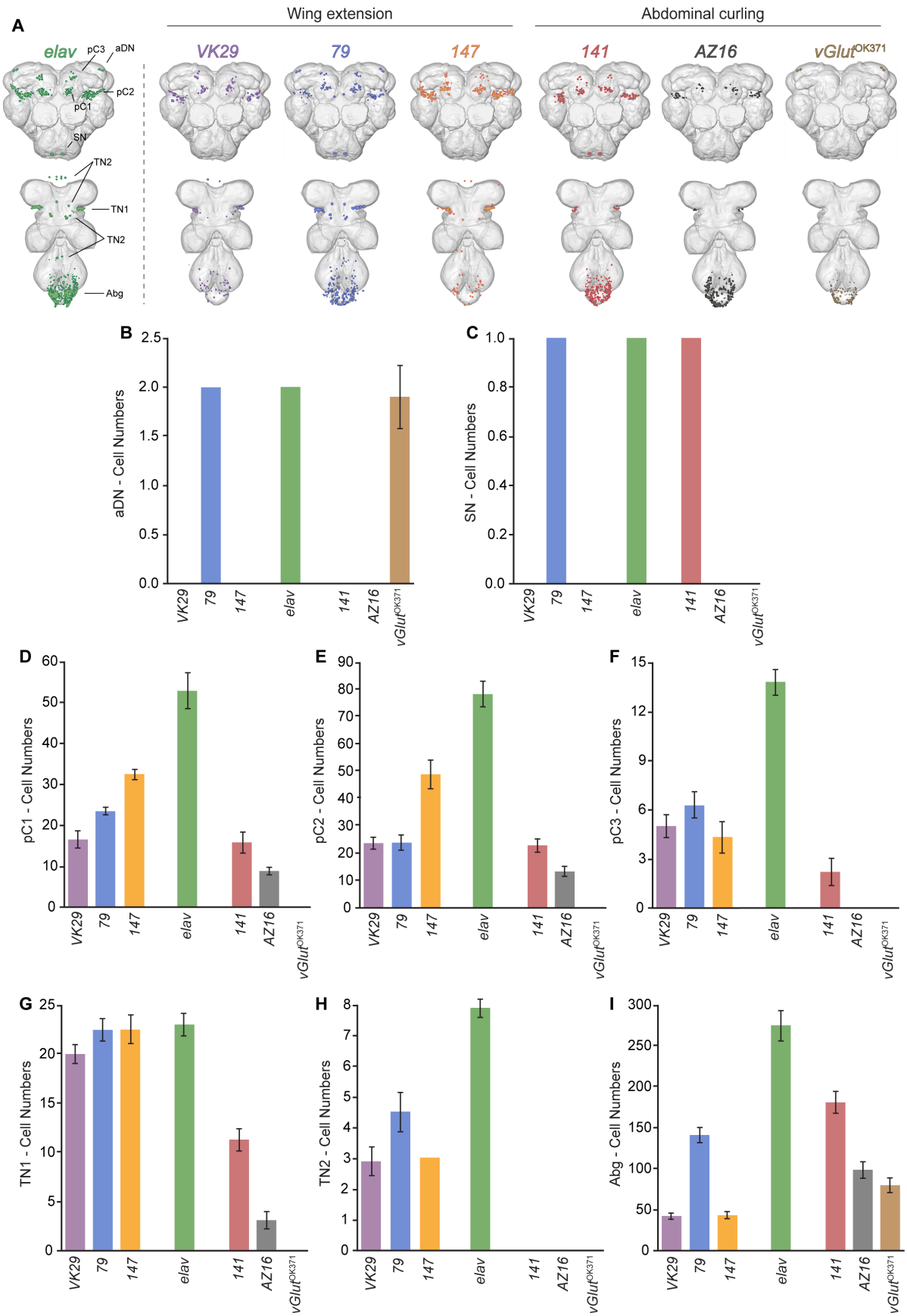


Figure 5-12 Graphical representation of the distribution of intersected nGFP expression realised by each candidate line in the adult male CNS.

(A) Schematic representation of the intersected neural expression realised by each candidate line in the adult male CNS. Graphical representation of cell counts for neural clusters *dsx*-aDN (B), *dsx*-SN

(C), *dsx*-pC1 (D), *dsx* -pC2 (D), and *dsx*-pC3 (E), in the adult male brain. Graphical representation of cell counts for neural clusters *dsx*-TN1 (G), *dsx*-TN2 (H) and *dsx*-Abg in the adult male VNC. Neural clusters indicated as per Lee et al., 2002 and Rideout et al., 2012. Counts represent mean ± standard deviation.

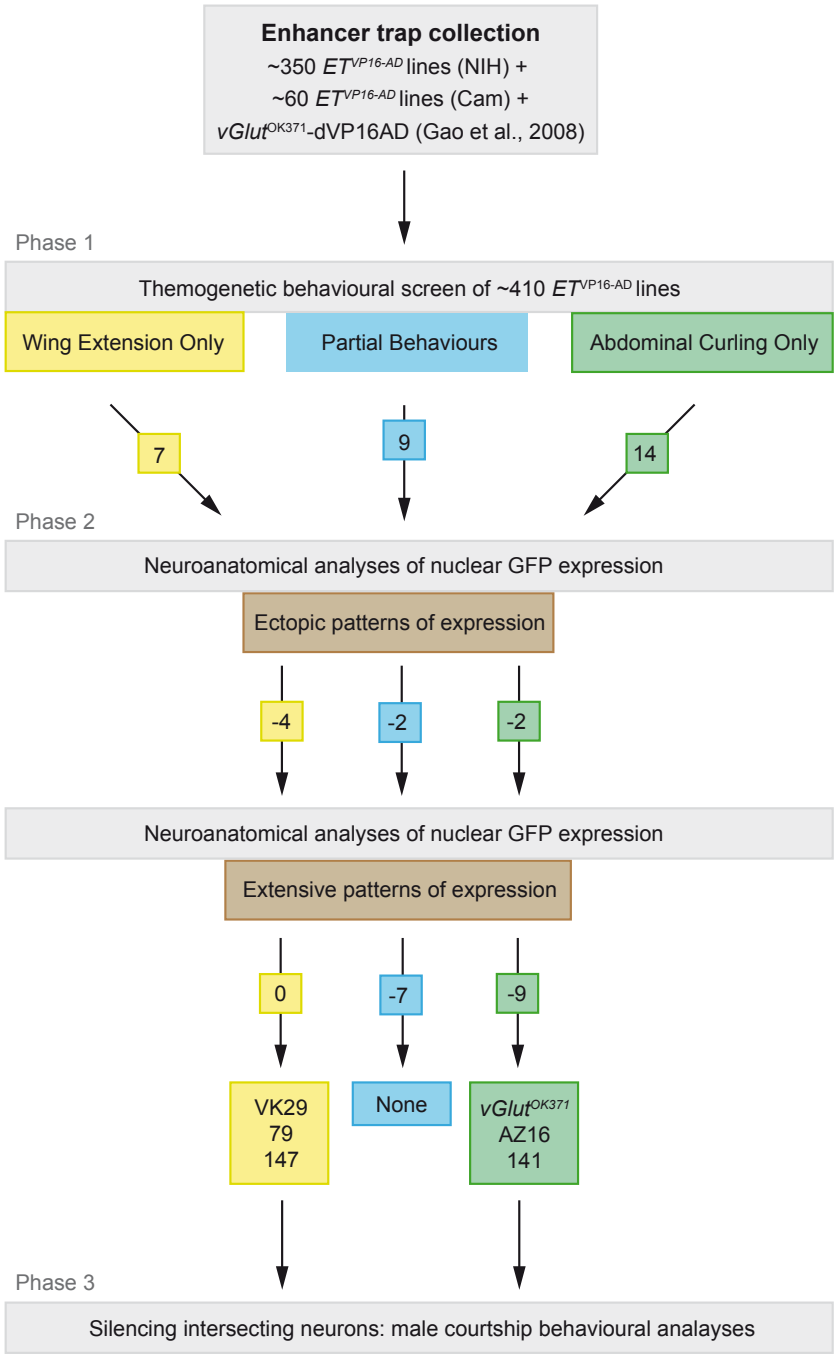


Figure 5-13 Flowchart summarising the strategy, filtering criteria and results of neuroanatomical analyses of candidate lines.
Lines displaying any form of ectopic patterns of expression were omitted from further investigations; Number of candidate lines removed from the screen based on these criteria is shown. Lines displaying extensive/broad patterns of expression were omitted from further investigations; Number of candidate lines removed from the screen based on these criteria is shown. A total of 6 candidate lines continue to silencing experiments via TNT expression in Phase 3.

5.7 Phase 3 – Silencing intersected neurons using *ET*$^{VP16\text{-}AD}$ candidate lines

Next, to test the necessity of the clusters realised in each candidate line, I employed all 6 lines in the final phase of experiments; neural silencing. Expression of tetanus toxin (*UAS-TNT*) results in the inhibition of neurotransmitter exocytosis and the elimination of synaptic transmission, allowing for the consequence of such neural inhibition to be assayed (Sweeney et al., 1995).

5.7.1 Method

To this end, I crossed each candidate line to *UAS-TNT*/+; *dsx*$^{GAL4\text{-}DBD}$/+. Naïve male progeny, in which the intersected neural circuitry accessed by each candidate line was silenced, and a single wild-type CS virgin 'target' female, were introduced into a courtship chamber. Males were subsequently analysed for male courtship behaviours and fertility (Figure 5-14). Behavioural parameters included time to initiate courtship, the percentage of time each male spent courting upon initiation within a 10 minute observation period (courtship index; CI), copulation duration, and the percentage of males that copulated within a 2 hr observation period (Figure 5-14).

5.7.2 Results

VK29: The time taken for *UAS-TNT*/VK29$^{VP16\text{-}AD}$; *dsx*$^{GAL4\text{-}DBD}$/+ males to initiate courtship was not significantly different from control males (Figure 5-14B). However, once courtship was initiated, the amount of courtship performed was significantly reduced (CI of ~73%) when compared to control males (CI of ~96%); though significantly different, comparatively, this phenotype was not nearly as severe as that observed with *UAS-TNT*/+; *dsx*$^{GAL4\text{-}DBD}$/*elav*$^{VP16\text{-}AD}$ males (CI of ~10%) (Figure 5-14C). While no overt abnormalities in the display of the courtship repertoire were observed (i.e. faithful displays of unilateral wing extension, abdominal curling, and attempts to copulate were all observed), the time to copulation was significantly longer than that of controls (1175 ± 239 vs. 298 ± 46.5 sec respectively; $P > 0.001$; data not graphically shown). During an extended 2 hr observation period, ~98% of control flies successfully copulated, while only ~73% *UAS-TNT*/VK29$^{VP16\text{-}AD}$; *dsx*$^{GAL4\text{-}DBD}$/+

males copulated (Figure 5-14E); within which, the duration of copulation was significantly longer than control males (2823 ± 296 vs. 1012 ± 23.7 sec respectively; Figure 5-14D). These males frequently cannot withdraw from the female, and thus remain attached for prolonged periods of time during which both the male and female display agitated behaviours in attempt to dissociate themselves from one another; this is reminiscent of behaviours observed in stuck (*sk*) mutants (Hall et al. 1980). After one week in the presence of several virgin females, these males were completely fertile (n=30) (Figure 5-14F).

79: The time taken for *UAS-TNT*/+; $dsx^{GAL4\text{-}DBD}/79^{VP16\text{-}AD}$ males to initiate courtship was significantly increased, when compared to controls (440 ± 140.7 vs. 63 ± 9.4 sec respectively) (Figure 5-14B) and, once courtship was initiated, the amount of courtship performed was severely reduced (CI of ~38%) (Figure 5-14C), consisting entirely of intermittent following, orientation and wing extension with no overt attempts to copulate. During an extended 2 hr observation period, ~98% of control flies successfully copulated, yet no *UAS-TNT*/+; $dsx^{GAL4\text{-}DBD}/79^{VP16\text{-}AD}$ males copulated (Figure 5-14E). After one week in the presence of several virgin females, these males were completely infertile (n=30), likely as a result of their behavioural sterility (Figure 5-14F).

147: The time taken for *UAS-TNT*/$147^{VP16\text{-}AD}$; $dsx^{GAL4\text{-}DBD}$/+ males to initiate courtship was significantly increased, when compared to controls (509 ± 120.5 vs. 107.1 ± 28.2 sec respectively) (Figure 5-14B) and, once courtship was initiated, the amount of courtship performed was severely reduced (CI of ~15%) (Figure 5-14C), consisting entirely of intermittent following and orientation with no overt attempts to extend their wings and attempt copulation. The behavioural pathologies observed here are reminiscent of the severe behavioural deficits observed in *UAS-TNT*/+; $dsx^{GAL4\text{-}DBD}/elav^{VP16\text{-}AD}$ males (Figure 5-14). During an extended 2 hr observation period, ~98% of control flies successfully copulated, yet no *UAS-TNT*/$147^{VP16\text{-}AD}$; $dsx^{GAL4\text{-}DBD}$/+ males copulated (Figure 5-14E). After one week in the presence of several virgin females, these males were completely infertile (n=30); again, likely as a result of their inability to achieve copulation (Figure 5-14F).

141: The time taken for *UAS-TNT*/+; *dsx*$^{GAL4\text{-}DBD}$/141$^{VP16\text{-}AD}$ males to initiate courtship was significantly increased, when compared to controls (487.8 ± 187.4 vs. 79.6 ± 11.2 sec respectively) (Figure 5-14B) and, once courtship was initiated, the amount of courtship performed was severely reduced (CI of ~47%) (Figure 5-14C), consisting entirely of following, orientation and wing extension with no overt attempts to copulate. Intriguingly, these males display bouts of courtship behaviours that terminate at the point of abdominal curling. It is apparent that these males attempt to curl their abdomens, yet no matter how forced these attempts are; these males rarely manage to sufficiently curl their abdomens > 90^{o} in order to properly align the external genitalia and attempt copulation. As a consequence, during an extended 2 hr observation period, no *UAS-TNT*/+; *dsx*$^{GAL4\text{-}DBD}$/141$^{VP16\text{-}AD}$ males copulated (Figure 5-14D). After one week in the presence of several virgin females, these males were completely infertile (n=30) (Figure 5-14F); again, likely as a result of their inability to achieve copulation.

AZ16: The time taken for *UAS-TNT*/AZ16$^{VP16\text{-}AD}$; *dsx*$^{GAL4\text{-}DBD}$/+ males to initiate courtship was not significantly different from control males (Figure 5-14B). However, once courtship was initiated, the amount of courtship performed was significantly reduced (CI of ~75%) when compared to control males (CI of ~96%), though comparatively, this phenotype was not nearly as severe as that observed with *UAS-TNT*/+; *dsx*$^{GAL4\text{-}DBD}$/*elav*$^{VP16\text{-}AD}$ males (CI of ~10%) (Figure 5-14C). Their courtship display consisted entirely of following, orientation and wing extension with no overt attempts to copulate. Similar to *UAS-TNT*/+; *dsx*$^{GAL4\text{-}DBD}$/141$^{VP16\text{-}AD}$ males, *UAS-TNT*/AZ16$^{VP16\text{-}AD}$; *dsx*$^{GAL4\text{-}DBD}$/+ males display bouts of highly aggressive courtship behaviours that terminate at the point of abdominal curling. It is apparent that these males attempt to curl their abdomens, yet no matter how forced these attempts are; these males rarely manage to sufficiently curl their abdomens > 90^{o} in order to properly align the external genitalia and attempt copulation. As a consequence, during an extended 2 hr observation period, no *UAS-TNT*/AZ16$^{VP16\text{-}AD}$; *dsx*$^{GAL4\text{-}DBD}$/+ males copulated (Figure 5-14E). After one week in the presence of several virgin females, these males were completely fertile (n=30) (Figure 5-14F), again, likely as a result of their inability to achieve copulation.

OK371: The time taken for *UAS-TNT*/*vGlut*^{OK371}-VP16-AD; *dsx*$^{GAL4\text{-}DBD}$/+ males to initiate courtship was not significantly different from control males (Figure 5-14B). However, once courtship was initiated, the amount of courtship performed was significantly reduced (CI of ~75%) when compared to control males (CI of ~96%), though comparatively, this phenotype was not nearly as severe as that observed with *UAS-TNT*/+; *dsx*$^{GAL4\text{-}DBD}$/*elav*$^{VP16\text{-}AD}$ males (CI of ~10%) (Figure 5-14C). While no overt abnormalities in the display of the courtship repertoire were observed (i.e. faithful displays of unilateral wing extension, abdominal curling, and attempts to copulate were all observed), these males were clearly unable to attach themselves to the female. Even during the extreme persistence of these males during an extended 2 hr observation period, none of these males were able to mount the female appropriately to successfully assume copulation. After one week in the presence of several virgin females, these males were completely infertile (n=30) (Figure 5-14B), again, likely as a result of their inability to achieve copulation.

5.7.2.1 Behavioural similarities and differences between candidate lines

Quantification of the behavioural parameters discussed above revealed correlations between various pathologies and the candidate lines that displayed them. It is important to first mention that although 5/6 candidate lines were unsuccessful in copulating within a 2 hr observation period and were found to be infertile, these two pathologies are merely a consequence of the behavioural deficits that have manifested by silencing the intersected neurons dictated by each candidate line. Thus, focusing on the two key telling parameters, latency to initiate courtship and CI, candidate lines can be behaviourally categorised into groups that display similar pathologies. In this manner, the candidate lines cluster into two groups: **Group A** incorporating 79$^{VP16\text{-}AD}$, 147$^{VP16\text{-}AD}$ and 141$^{VP16\text{-}AD}$ and **Group B** incorporating VK29$^{VP16\text{-}AD}$, AZ16$^{VP16\text{-}AD}$ or *vGlut*^{OK371}-VP16-AD.

Group A lines all demonstrate significant and analogous increases in their latency to initiate copulation, and severe (<50%) but varying deficits in CI (Figure 5-14B,C). All three lines display the early steps of courtship including orientating and following; yet only *UAS-TNT*/+; *dsx*$^{GAL4\text{-}DBD}$/79$^{VP16\text{-}AD}$ and *UAS-TNT*/+; *dsx*$^{GAL4\text{-}DBD}$/141$^{VP16\text{-}AD}$ males display faithful unilateral

wing extension. And lastly, while all three lines fail to attempt copulation, *UAS-TNT*/+; *dsx*$^{GAL4\text{-}DBD}$/141$^{VP16\text{-}AD}$ is the only line in which the males attempt to curl their abdomen. These observations suggest that the *dsx* neurons targeted by all three candidate lines directly contribute to early stages of male courtship behaviours.

Group B lines on the other hand, show wild-type latencies to initiate copulation, and display practically identical deficits in CI, that are moderate (>50%) compared to those displayed in Group A (Figure 5-14B,C). All three lines display the early steps of courtship including orientating and following the target female, and unilateral wing extension. However, the lines all diverge at the late steps of courtship, each candidate displaying a unique behavioural deficit within the temporal sequence of behaviours that are designed to achieve copulation. *UAS-TNT*/AZ16$^{VP16\text{-}AD}$; *dsx*$^{GAL4\text{-}DBD}$/+ males are unable to fully curl their abdomen, resulting in a stall in the courtship repertoire at 'abdominal curling' as these males never overtly attempt to copulate. *UAS-TNT*/*vGlut*^{OK371}-VP16-AD; *dsx*$^{GAL4\text{-}DBD}$/+ males are able to faithfully curl their abdomens and attempt copulation. Their downfall comes at the point of genital coupling, as these males are never able to attach to the female. Lastly, *UAS-TNT*/VK29$^{VP16\text{-}AD}$; *dsx*$^{GAL4\text{-}DBD}$/+ males are able to curl their abdomens, attempt copulation and copulate; leaving them with their only pathology – significantly longer copulation duration due to their inability to withdraw from the target female post-copulation. These three candidates demonstrate a breakdown of the courtship repertoire within temporally distinct stages of attempting copulation and copulation itself, suggesting that the *dsx* neurons targeted by all three candidate lines directly contribute to the final stages of the male courtship repertoire.

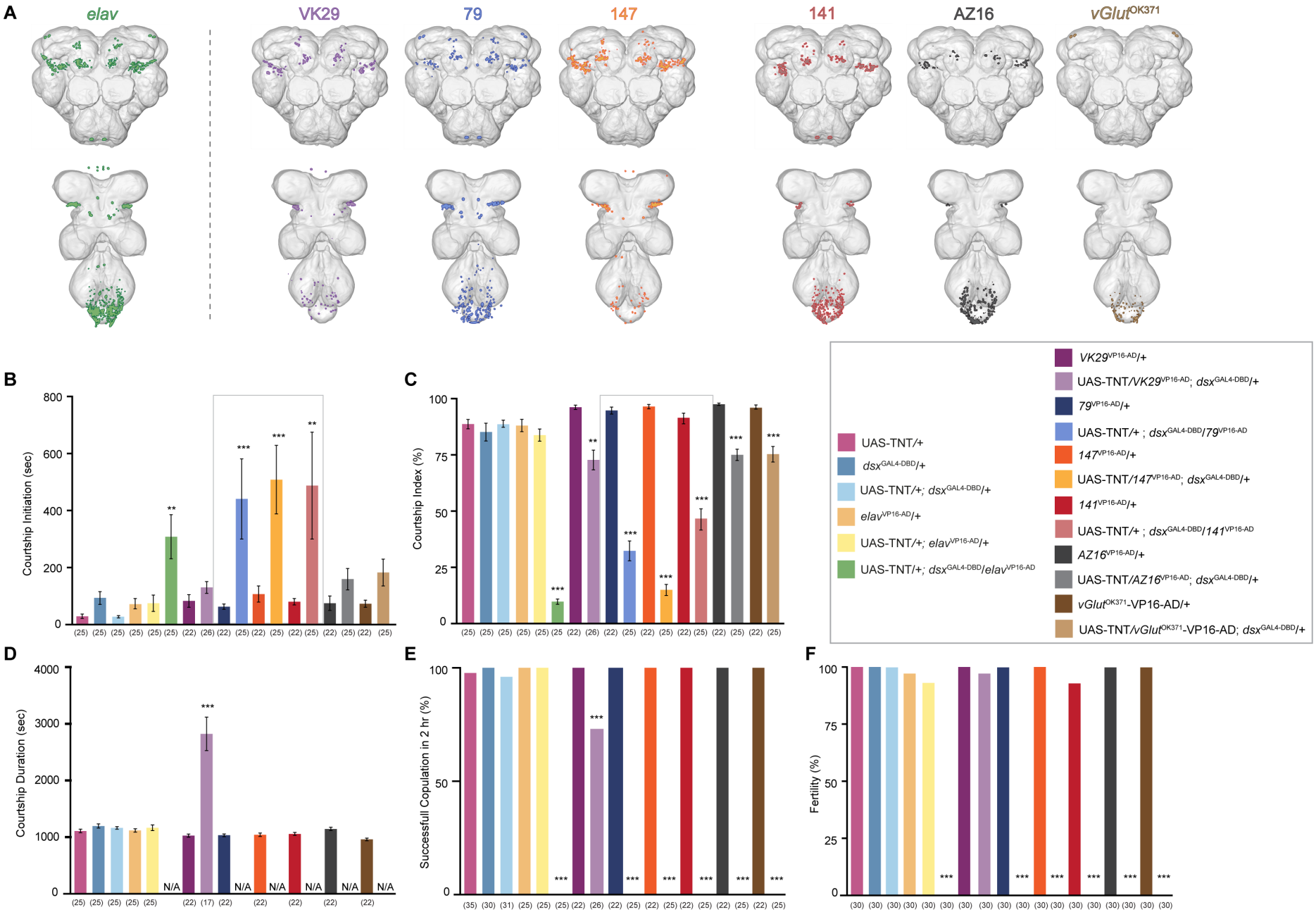

A
elav
VK29
79
147
141
AZ16
vGlutOK371
B
Courtship Initiation (sec)
C
Courtship Index (%)
UAS-TNT/+
dsxGAL4-DBD/+
UAS-TNT/+; dsxGAL4-DBD/+
elavVP16-AD/+
UAS-TNT/+; elavVP16-AD/+
UAS-TNT/+; dsxGAL4-DBD/elavVP16-AD
VK29VP16-AD/+
UAS-TNT/VK29VP16-AD; dsxGAL4-DBD/+
79VP16-AD/+
UAS-TNT/+ ; dsxGAL4-DBD/79VP16-AD
147VP16-AD/+
UAS-TNT/147VP16-AD; dsxGAL4-DBD/+
141VP16-AD/+
UAS-TNT/+ ; dsxGAL4-DBD/141VP16-AD
AZ16VP16-AD/+
UAS-TNT/AZ16VP16-AD; dsxGAL4-DBD/+
vGlutOK371-VP16-AD/+
UAS-TNT/vGlutOK371-VP16-AD; dsxGAL4-DBD/+
D
Courtship Duration (sec)
E
Successfull Copulation in 2 hr (%)
F
Fertility (%)

Figure 5-14 Intersected neurons control aspects of male sexual behaviour.
(A) Schematic representation of the intersected neural expression realised by the pairing of *dsx*$^{GAL4\text{-}DBD}$ with each candidate line, in the adult male CNS. (B) Courtship initiation (mean ± s.e.m.. **P<0.001, ***P<0.0001, Kruskal-Wallis and Dunn's test). (C) Courtship index (mean ± s.e.m., **P<0.001, ***P<0.0001, Kruskal-Wallis and Dunn's test). (D) Copulation duration (mean ± s.e.m. ***P<0.0001, Kruskal-Wallis and Dunn's test). (E) Percentage of male mating's in 2 h (***P<0.0001, Fisher exact test). (F) Male fertility (***P<0.0001, Fisher exact test).

5.8 Correlating neuroanatomy with behaviour

In the brain, *dsx* neurons are localised to areas identified by gynandromorph studies as foci involved in initiation, following, tapping, wing extension and copulatory behaviours (Hall, 1977, 1979; Hotta and Benzer, 1976; von Schilcher and Hall, 1979), while in the VNC, *dsx* neurons localise to foci associated with tapping, wing extension, courtship song and with copulatory behaviours (Hall, 1977, 1979; Hotta and Benzer, 1976; von Schilcher and Hall, 1979). The overlapping relationship between *dsx* and *fru* in the male enables the utilization of clonal analyses of *fru* neurons (Cachero et al., 2010; Kimura et al., 2005; Yu et al., 2010) to make predictions about the function of distinct clusters of *dsx*-expressing neurons. In this way, *dsx* neural clusters of the brain are implicated with higher-order processing of multi-modal sensory stimuli inputs (Cachero et al., 2010; Kimura et al., 2008; Kohatsu et al., 2011; Yu et al., 2010); while neurons of the Prg and Msg are implicated with the transmission and processing of stimulatory inputs of gustatory neurons of the foreleg, and subsequent modulation of higher-order signals involved in the generation of unilateral wing extension and song production (Cachero et al., 2010; Kimura et al., 2008; Kohatsu et al., 2011; Rideout et al., 2007; Rideout et al., 2010; Yu et al., 2010), and finally neurons of the Abg with regulation and generation of copulatory behaviours (Billeter et al., 2006b; Cachero et al., 2010; Kimura et al., 2008; Kohatsu et al., 2011; Rideout et al., 2010; Yu et al., 2010). When considered all together, these neural substrates appear to describe an all-encompassing circuitry that not only specifies the initiation of courtship, but also the assurance of the continuation of the individual sub-behaviours of courtship modalities in a coordinated manner, culminating in successful copulation.

The generation of a hypothetical map of *fru* circuitry, based on *fru* clonal analyses, has not only enabled predictions to be made about the function of specific neurons, but also about

the organisation of the circuit as a whole (Cachero et al., 2010; Yu et al., 2010). Therefore, in the same manner, extending principles of *fru* circuit organisation to that of *dsx* allows informed predictions to be made about the consequences of impairing neural activity in distinct clusters of *dsx*-expressing neurons. Males, in which neural activity is impaired specifically in *dsx*-expressing neurons of the brain, would be expected to present with aberrant behavioural phenotypes related to latency to initiate courtship and the proper coordination and expression of any subsequent courtship steps. That is presenting with significant decrements in the later courtship steps, such as tapping, wing extension and song generation, and copulatory behaviours generally represented by the courtship index. Males, in which neural activity is impaired specifically in *dsx*-expressing neurons of the Prg and Msg, would be expected to present with significant decrements in the early courtship steps, including tapping, wing extension and song generation. Finally, males in which neural activity is impaired specifically in *dsx*-expressing neurons of the Abg, would be expected to present with significant decrements in the final courtship steps, including attempting copulation and successful copulation.

Although the current models of *fru* circuit function and organisation that incorporate *fru* clonal analyses are largely hypothetical, they serve as a framework for more sophisticated functional studies (Kohatsu et al., 20011; von Philipsborn et al., 2011). Data from these studies have been used to draw comparisons to the findings presented in this study; both of which are discussed below.

5.8.1 Functionally assigned *fru* neurons involved in courtship initiation, wing extension and courtship song

Three clusters of *fru* neurons in the central brain, that co-express *dsx,* have been shown to be involved in the initiation of courtship and modulation of courtship song. These include:

1) *fru*-P1 which is equivalent to a subset of the *dsx*-pC1 cluster (Cachero et al., 2010; Rideout et al., 2010; Dornan, 2011; Kohatsu et al., 2011; von Philipsborn et al., 2011).

2) *fru*-P2b which is equivalent to a subset of *dsx*-pC2-medial (-pC2m) cluster (Rideout et al.,2010; Cachero et al., 2010; Dornan, 2011; Kohatsu et al., 2011) and
3) *fru*-pIP10 which operates in a contiguous manner to *fru*-P2b and thus may represent a sub-set of the *dsx*-pC2m cluster (Cachero et al., 2010; Dornan, 2011; von Philipsborn et al., 2011).

Thermoactivation of any of these *fru/dsx* co-expressing clusters has been shown to elicit the initiation of courtship and unilateral wing extension (Kohatsu et al., 2011; von Philipsborn et al., 2011), within which both *fru*-P1 and *fru*-pIP10 are capable of producing pulse song (von Philipsborn et al., 2011). In the case of *fru*-P1 neurons however, depolarization of at least 50% of the neural cluster is necessary to obtain pulse song (von Philipsborn et al., 2011). This either represents an integral subtype of neurons, or a possible threshold system that is in place to ensure appropriate elicitation of courtship song (von Philipsborn et al., 2011). Contrasting experiments in which either of these neural clusters are silenced results in significant deficits in courtship index (Kohatsu et al., 2011; von Philipsborn et al., 2011), and unfaithful pulse song (von Philipsborn et al., 2011). Though these neurons exhibit analogous functions, the topology of these neurons and their associated projections disclose their differences (Kohatsu et al., 2011; von Philipsborn et al., 2011).

The male-specific *fru*-P1 interneuron cluster is located in the lateral protocerebrum (Kimura et al., 2008; Yu et al., 2010), which receives multimodal sensory input (Kimura et al., 2008; Yu et al., 2010; Kohatsu et al., 2011); making it an ideal ‘decision-making’ candidate capable of integrating environmental stimuli to make the decision to court. That *fru*-P1 interneurons comprise third-order neurons associated with the olfactory circuit (Cachero et al., 2010), components of which are important for sensory stimulation leading to courtship initiation (Ferveur, 2005b; Datta et al., 2008; Billeter et al., 2009; Ruta et al., 2010), coupled with the fact that they are rendered active in response to stimuli arising from foreleg tarsal contact with a female abdomen or the male-specific pheromone cis-vaccenyl acetate (cVA) (Kohatsu et al., 2011), suggests that appropriate olfactory and gustatory stimuli may act to trigger these neurons to command the initiation of courtship in the presence of a target female.

Axonal arborisations of the *fru*-P1 cluster superimpose on the dendritic arbors of the *fru*-P2b cluster that projects its axons to the SOG and VNC (terminating in the pro-, meso- and meta-thoracic ganglia); making the *fru*-P2b cluster an ideal candidate for relaying 'trigger' signals that drive the motor pattern generators of the VNC for specific behavioural outputs (Kohatsu et al., 2011; Yu et al., 2010). Though this second cluster is not thought to interact with motor neurons directly (Yu et al., 2010), is it predicted to make synaptic connections with localised inter-eurons (a possibility being with the male-specific *dsx*-TN2 neurons present in midline position in all three thoracic ganglia) (Rideout et al., 2010).

Similar to the *fru*-P2b clonal group, *fru*-pIP10 neurons are localised to the postero-medial portion of the protocerebrum and are thought to be functionally comparable to the *fru*-P2b neurons (Cachero et al., 2010b; von Philipsborn et al., 2011). Again, axonal arborisations of the *fru*-P1 cluster superimpose on the dendritic arbors of *fru*-pIP10 neurons, only this time, the *fru*-pIP10 neurons project to processing centres within the central song-pattern generator (CPG) in the Msg of the VNC (von Philipsborn et al., 2011). These neurons are therefore also ideal candidates for relaying 'trigger' signals that drive the motor pattern generators of the VNC for specific behavioural outputs (von Philipsborn et al., 2011).

Based on the above-mentioned findings, it is conceivable that stimuli received and processed by the *fru*-P1 command cluster are directed in a coordinated manner to various downstream circuit elements, including both *fru*-P2b and *fru*-pIP10 neurons, to achieve cumulative and/or sequential behavioural outputs. This method of multiplexing information to different downstream command neurons would result in a multiplicity of ways in which same information is interpreted and/or acted upon; and only when all the interpretations of the information are considered in unison, does this generate the appropriate response.

The Msg of the VNC has been demonstrated to contain the CPG, within which, the cooperation of Fru^M and Dsx^M is necessary to obtain the full complement of cells for the production of wild-type male-specific courtship song (Rideout et al., 2007; Clyne and Miesenböck, 2008). That *fru*-dPR1 and -vPR6 neurons of the CPG appear to be direct targets of -IP10 projections, is suggestive of a second occurrence of multiplexing, as

functional analyses of both clusters indicate that they are separately involved in the modulation of song inter-pulse interval (IPI) (von Philipsborn et al., 2011). Though both neural groups co-express *dsx*, identifying -dPR1 as a subpopulation of the prothoracic *dsx*-TN2 neurons and -vPR6 as a subset of the *dsx*-TN1 neural cluster (von Philipsborn et al., 2011), additional circuit elements that appear to overlap with the *fru*-dPR1 and - vPR6 neurons, but do not co-express *dsx* appear to be involved in the promotion and motor response of unilateral wing extension (von Philipsborn et al., 2011).

Based on these studies, subsets of only 4 ‘classes’ of neurons that co-express *dsx* have been functionally assigned (-pC1, -pC2, -TN1 and -TN2) and although aspects of these elements may form a predicted circuitry, from command structures to pre-motor output, any one group of neurons is thought to be capable of eliciting wing extension and courtship song (von Philipsborn et al., 2011).

5.8.2 Correlating *dsx* circuit elements with courtship initiation and wing extension

Considering the neuroanatomy of candidate lines that displayed wing extension upon thermoactivation (VK29$^{VP16\text{-}AD}$, 79$^{VP16\text{-}AD}$, and 147$^{VP16\text{-}AD}$), the intersected patterns of expression included a subset of *dsx*-pC1 and -pC2 of the central brain in addition to a subset of *dsx*-TN2, and a full complement of *dsx*-TN1 neurons of the CPG in the VNC (Rideout et al., 2007; Clyne and Miesenböck, 2008; von Philipsborn et al., 2011) in all three lines (Figure 5-6; to Figure 5-8; Figure 5-14; Table 5-5). However, that two of abdominal curling candidates showed similar numbers of neurons in the *dsx*-pC1 and -pC2 clusters of the central brain (Figure 5-12; Table 5-5), but did not elicit wing-extension, suggests that, by way of elimination, the activation of those neurons alone are not sufficient to elicit a wing extension response. The conspicuous absence of all *dsx*-TN2 and the majority of -TN1 neurons in abdominal curling candidates that do not exhibit wing extension upon thermoactivation (Figure 5-12; Table 5-5), is directly contrasting to the presence of a subset of *dsx*-TN2 and a full complement of -TN1neurons observed in all wing extension candidates.

Thus, based on these data, I conclude that *dsx*-TN1 and -TN2 neurons alone account for the elicitation of wing extension in the thermal activation experiments.

When analysing the results of silencing experiments, $79^{VP16\text{-}AD}$, and $147^{VP16\text{-}AD}$ and $141^{VP16\text{-}AD}$ behaved similarly, in that they displayed significant increases in the latency to initiate courtship and significant deficits in courtship index (Figure 5-14). By comparing their intersected patterns of expression, it becomes clear that the commonality between them is the presence of subsets of neurons assigned to three clusters of the central brain (*dsx*-pC1, -pC2 and pC3) (Figure 5-7; to Figure 5-9; Figure 5-14; Table 5-5). The fact that $141^{VP16\text{-}AD}$ deviates in its expression pattern (Figure 5-9), from $79^{VP16\text{-}AD}$, and $147^{VP16\text{-}AD}$, by lacking all *dsx*-TN2 neurons and exhibiting only a small subset of –TN1 neurons (Figure 5-12; Table 5-5), points towards the clusters in the brain as being necessary for these behaviours. Interestingly, the intersected pattern of expression of $VK29^{VP16\text{-}AD}$ (Figure 5-6) is highly comparable to that of $79^{VP16\text{-}AD}$, and $147^{VP16\text{-}AD}$ (Figure 5-12; Table 5-5); yet silencing these neurons did not result in any significant increase in the time to initiate courtship, nor did they display such severe deficits in courtship index. However given that only a subset of neurons within all *dsx* clusters co-express *fru* (comprehensive cell counts found in Dornan, 2011) it is likely that neurons of the brain intersected by $VK29^{VP16\text{-}AD}$ vary in the composition of *fru* co-expressing neurons. By further characterising these candidate lines for Fru^{M} expression, a second dimension to the identity of these neurons would be added, allowing for a better correlation to be made between subsets of dsx^{+} and/or dsx^{+}/fru^{+} neurons and male courtship. Nevertheless, these data demonstrate the necessity of subsets of *dsx*-pC1, -pC2 and -pC3 neurons in the initiation and maintenance of courtship (Figure 5-12; Figure 5-14; Table 5-5).

5.8.3 Previously identified neurons involved in copulation

The behaviours presented by two previously isolated mutants that show deficits in the late steps of courtship are pertinent to the observations in this study. Males expressing a variant of *stuck* (*sk*) presents an inability to disengage from the female, though they appear to be trying to do so after 20 min of copulation, resulting in a duration of copulation that exceeds 400 min (Hall et al. 1980). Similar to *sk* mutants, *lingerer* (lig^{P}) hypomorphic mutant males fail

to withdraw their genitalia at the end of copulation (Kuniyoshi et al., 2002). As a result, the male and female tug in opposite directions for lengthened periods of time until disengagement is achieved (Kuniyoshi et al., 2002). Interestingly, males null for *lig* continue to repeatedly attempt copulation, but fail to achieve genital coupling, resulting in their complete inability to achieve copulation (Kuniyoshi et al., 2002). As the above mentioned mutant males exhibit no morphological abnormalities of the external genitalia (Hall, 1980), the behavioural defects presented in these animals are thought to be neural in aetiology, with the primary speculation being that these phenotypes are a consequence of defective neural mediation of copulatory organs during attempts to copulate (Hall, 1981; Kuniyoshi et al., 2002).

That gynandromorph studies have implicated neurons of the central brain to be involved in attempting and achieving copulation (Ferveur and Greenspan, 1998), together with the fact that thermoactivation of *dsx* circuitry in headless males results in the loss of attempted copulation (Pan et al. 2011), is indicative of a feedback loop that may serve to transmit ongoing visual, olfactory and gustatory information about the target female from sensory integration centres of the brain to motor centres in the Abg. In this manner, such interactive communication between the brain and Abg would serve to provide sufficient stimulation to surpass the necessary threshold to attempt copulation. Once achieved, it is only logical that distinct populations of motoneurons that differentially mediate control of the appropriate abdominal muscles and muscles of the genitalia, communicate with one another in a timely manner to coordinate curling of the abdomen prior to protraction of the penis and associated appendages to ensure successful coupling and copulation.

Such fine motor control has been demonstrated in the circuitry underlying a novel parameter of male courtship, copulation persistence (Crickmore and Vosshall, 2013). Copulation persistence refers to the probability of a stressful stimulus interrupting copulation, and is based on the finding that a decline in persistence occurs over time as the probability of successful mating increases (Crickmore and Vosshall, 2013). Approximately eight sexually dimorphic, *dsx*-expressing, GABAergic interneurons in the male Abg have been

demonstrated to be involved in promoting the decline of this response over time (Crickmore and Vosshall, 2013). Silencing these neurons increases the male's persistence, resulting in significantly longer copulations than required for successful mating, while artificial activation of these neurons decreases persistence and significantly shortens the duration of copulations (Crickmore and Vosshall, 2013). Interestingly, a second functionally opposing cluster of dopaminergic neurons of the Abg appears to promote copulation persistence and extend copulation duration; suggesting that, copulation duration is a product of gradually declining persistence that is regulated by opposing neural populations (Crickmore and Vosshall, 2013).

5.8.4 Correlating *dsx* circuit elements with attempting copulation and copulation

When considering the patterns of expression intersected by the three abdominal curling candidates ($141^{VP16\text{-}AD}$, $AZ16^{VP16\text{-}AD}$, and $vGlut^{OK371}$-VP16-AD) (Figure 5-9 to Figure 5-11 respectively); a direct correlation between the presence of neurons in the Abg and the elicitation of abdominal curling upon thermoactivation is apparent (Figure 5-12; Table 5-5). However, that two of the candidate lines display more extreme abdominal curling phenotypes ($141^{VP16\text{-}AD}$ and $AZ16^{VP16\text{-}AD}$), whereby their abdomens curl >90^{o} upon thermoactivation, may lend itself to one of two neuroanatomical differences; the presence of more numerous neurons of the Abg, and/or the presence of a subset of neurons of the *dsx*-pC1 and -pC2 clusters of the central brain (Figure 5-12; Table 5-5). That several wing extension candidates display numerous neurons in the central brain, yet do not curl their abdomens upon thermoactivation, suggests that a critical cluster of neurons in the Abg necessary for an abdominal curling phenotype is absent in these males (Figure 5-6 to Figure 5-8; Figure 5-12; Table 5-5). Hence, implicating the necessity of distinct subsets of neurons of the Abg in eliciting abdominal curling upon thermoactivation.

Silencing the highly restricted $vGlut^{OK371}$-VP16-AD intersected neurons in males, resulted in a phenotype similar to that presented by mutants null for *lgr* (Figure 5-11; Figure 5-12; Figure 5-14; Table 5-5). That these males were capable of attempting copulation, but failed at

genital coupling suggests that glutamatergic *dsx*-expressing neurons of the Abg may serve to mediate motor control of copulatory organs in order to achieve successful genital coupling and copulation. The opposite was found when, VK29$^{VP16\text{-}AD}$ intersected neurons were silenced (Figure 5-14). This resulted in successful copulation, but unsuccessful genital uncoupling, analogous to the behaviours presented by *sk* mutants (Figure 5-14). These data suggest the presence of a second distinct set of neurons that may functionally oppose or actively inhibit motor control of the above-mentioned glutamatergic *dsx*-expressing neurons. Topologically, based on neuroanatomical comparisons of VK29$^{VP16\text{-}AD}$ with all other candidate lines, these neurons would most likely reside in the Abg of the VNC, as a number of candidate lines that similarly intersect numerous neurons in analogous clusters of the brain do not exhibit this phenotype upon inhibition (Figure 5-6; Figure 5-12; Figure 5-14; Table 5-5). Further neuroanatomical and functional characterisation of the population of neurons intersected by both *vGlut*^{OK371}-VP16-AD and VK29$^{VP16\text{-}AD}$ may help elucidate the mechanism by which these neurons may coordinate with each other and with gender-appropriate physiology to engender successful copulation. These would include realising associated axons, dendrites and patterns of expression outwith the CNS, identifying target organs innervated by these neurons, and finally, performing additional behavioural experiments that involve incorporating temporal control of neural inhibition so that these neurons are rendered inactive *in-copulo.*

The only pairing that displayed atypical attempts to copulate due to incomplete abdominal curling upon neural silencing is that of AZ16$^{VP16\text{-}AD}$. Although an overt correlation between the neuroanatomy and behaviour is not evident, it would be logical to speculate that this behaviour results from faulty modulation of abdominal muscle control; either via the inhibition of higher order neurons necessary for maintaining interactive regulation of motoneurons of the Abg, or by direct inhibition of a subset of motoneurons in the Abg necessary for accurate contraction/relaxation of abdominal muscles to achieve faithful attempts of abdominal curling (Figure 5-10; Figure 5-12; Figure 5-14; Table 5-5). Due to the presence of neurons in both the central brain and in the Abg, additional experiments that further restrict genetic access to

subsets of these neurons would be necessary to identify the circuit elements responsible for this phenotype.

5.9 Discussion

The somatotopic mapping of *dsx*$^{GAL4\text{-}DBD}$/*elav*$^{VP16\text{-}AD}$ neurons coupled with the loss of all male-specific courtship behaviours by specific impairment of *dsx*$^{GAL4\text{-}DBD}$/*elav*$^{VP16\text{-}AD}$ neural function, demonstrated in the previous chapter, provides compelling evidence that these neurons comprise the neural circuitry necessary for the specification of all sub-behaviours of the male courtship repertoire.

In this chapter, I successfully demonstrated the utilisation of the novel *dsx*$^{GAL4\text{-}DBD}$ allele in parsing *dsx* neural circuitry into functional component parts. Via a thermal activation strategy, I first screened a collection of extant *ET*$^{VP16\text{-}AD}$ lines (Luan et al., 2006; M.Landgraf, unpublished), isolating lines that scored positive for the elicitation of defined sub-behaviours of courtship, determining the sufficiency of the intersected neurons in eliciting distinct sub-behaviours of male courtship. Neuroanatomical analyses were subsequently performed in pursuance of candidate lines that realised spatially restricted patterns of expression. Ultimately, these isolated lines were then employed in neural silencing experiments, determining the necessity of the intersected neurons in specifying distinct sub-behaviours of courtship.

In carrying out this three-phased stratagem, I have demonstrated the collective functional role of *dsx*-pC1, -pC2 and -pC3 of the brain in courtship initiation and maintenance, and of *dsx*-TN1 and -TN2 neurons of the Prg and Msg in unilateral wing extension. In demonstrate the potential involvement of *vGlut*-expressing *dsx* neurons of the Abg in genital coupling, together with a functionally opposing second subset of neurons in the Abg that appears to be involved in genital disengagement, post-copulation.

5.9.1 The approach

In this study, the use of the temperature sensitive non-selective cation channel, TrpA1 for neural activation, stems from the simplicity, efficiency, immediate reversibility and proximity

to the physiological norm that this system offers (Hamada et al., 2008; Pulver et al., 2009; Simpson, 2009). By increasing the temperature by only a few degrees, neurons are rendered active, allowing behavioural consequences associated with this activity to be assayed (Hamada et al., 2008; Pulver et al., 2009; Alekseyenko et al., 2010; Kohatsu et al., 2011; Pan et al., 2011; von Philipsborn et al., 2011; Pan et al., 2012; Toda et al., 2012). In this manner, a single neuron (or cluster of neurons) whose stimulation results in the evocation of an endogenous behavioural output may be identified.

However, it is becoming increasingly obvious that our faith in the power of thermogenetics to identify key elements and suggest a scheme for their action must be tempered by the realisation that functional modularity in the brain is relative. Some regions are somewhat specialised with respect to others, but all are highly interconnected and interdependent; within which extensive excitatory feedback loops between neural elements are present. As a consequence of these features, activation of any given neuron is capable of initiating activity in other elements of both the specific circuit examined as well as associated connected circuitry; making it almost impossible to definitively assign a primary initiating function to any one given element (Kupfermann and Weiss, 1978). Thus, rather than assigning primary function to any given cluster of neurons that appear to elicit a given behavioural response in such experiments, it is more realistic to appoint their participation in generating that behaviour.

The majority of lines recovered from the screen performed here revealed extensive numbers of neurons, limiting interpretations to correlations between the presence/absence of neurons and their respective behavioural output. One definite correlation reported in this study was the presence of *dsx*-TN1 and -TN2 neurons that comprise the CPG for courtship song (Rideout et al., 2007; Clyne and Miesenböck, 2008; von Philipsborn et al., 2011) in lines that elicited wing extension upon thermoactivation. In addition, the presence of neurons in the Abg correlated with the elicitation of the late copulatory behaviours of the courtship repertoire, and by process of elimination, it became apparent that *dsx*-aDN and -SN neurons of the central brain did not correlate with any of the designated behavioural phenotypes

assayed, rendering their activity inconsequential to the specification of the behaviours in question. An obvious limitation of the system became apparent when considering correlations between higher-order neurons of the central brain and behaviour. The presence of subsets of neurons in all three clusters of the central brain in 5/6 lines made it practically impossible to draw any conclusive correlations between them and a given behaviour. This is primarily due to the fact that the subsets of labelled neurons may differ in composition between the lines. For this reason, more comprehensive characterisations of these neurons, coupled with more substantial spatial restriction would be necessary to enable unambiguous correlative relationships to be established. Though the thermogenetic approach did serve its function in aiding in the identification of lines whose intersected patterns of expression represents circuit elements sufficient to evoke a given behavioural response, additional supporting experiments are necessary to demonstrate cause and effect between these neurons and behaviour. Thus by rendering neurons inactive, the bona fide function of the intersected neurons comes to light.

In the most fundamental sense, a sequential repertoire of innate behaviours is modulated by innate releasing mechanisms that rely on the response of higher order command/decision making neurons to a defined set of stimuli (Ewert, 1985). A command element is composed of a population of neurons programmed to appropriately select and process stimuli in exacting combinations, by assigning “weighting“ effects associated with any competing agonistic and antagonistic stimuli that they receive (Ewert, 1987). As numerous command elements exist in such circuitries, activation of a downstream motor pattern generator may require simultaneous and appropriate inputs from all of them. Only then do the motor pattern generators mediate the generation of physical actions via direct modulation of motoneurons (Ewert, 1987). Such linearity of circuit organisation imposes a temporal sequence of activity that is executed in a small fraction of time; starting with sensory neurons → command neurons → pattern generators → motorneurons, resulting in the generation of physical actions.

Basing the organisation of the *dsx* circuitry on this simplistic model, clusters within the brain would be classified as command elements, neurons in the Msg as a motor pattern generator, and the Abg as both a motor pattern generator and motoneurons. Silencing neurons at any stage of the circuit would result in the abrogation of all processes specified by that stage and of those downstream of it. It is therefore telling that disruption of neurons in the central brain, namely *dsx*-pC1, -pC2 and -pC3 in males, resulted in a behaviourally sterile animal that exhibited significantly extended time to initiate any courtship behaviours and severe deficits in all latter stages of courtship indicated by the significantly reduced courtship index. To add complexity, the differences in the numbers of neurons expressed in each subset, between candidate lines, was reflected in the behavioural discrepancies between them. These differences may be indicative of a gated system that requires a minimum number of neurons to be silenced prior to behavioural shutdown. The only line that faithfully enabled neural inactivation downstream of the command neurons of the brain was that of *vGlut*^{OK37}1-VP16-AD. Restrictively silencing a subset of motoneurons in the Abg, resulted in a breakdown in the final step of the courtship repertoire; copulation. Interestingly, these males also exhibited a significant deficit in the amount of courtship these males displayed. It is possible that blocking the latter steps of courtship may affect/inhibit sensory information that is fed back to command centres. The resulting imbalance/lack of information may subsequently affect the gating mechanism of these command neurons, presenting as a deficit in the amount of courtship displayed.

5.9.2 Prospective avenues and experiments

In order to make sense of the behavioural pathologies presented by the candidate lines isolated in this study, a series of additional experiments are necessary. These would include comprehensive neuroanatomical characterisations (including neurotransmitter classification), *fru* co-expression analyses, the quantification of additional behavioural parameters (*e.g.* thermal activation of headless males, courtship song analyses and assays for ejaculation), and finally, mosaic analyses. The most important feature of the lines isolated in this study is the specificity of behavioural pathologies that arise in each of the six candidate lines. Such

behavioural specificity may serve to focus subsequent mosaic studies on clusters that have been predicted to be functionally important, ultimately advancing and facilitating the identification of neurons that participate in the specification of that behaviour. Given the amount of time it takes to carry out such extensive investigations, focusing prospective investigations on a single facet of the study is conceivably a more advantageous proceeding.

One such path would involve focusing on the novel isolation of distinct, functionally opposing clusters of neurons in the Abg that modulate successful copulation; the most findings originating from functional interrogations of the the highly restricted cluster of neurons realised with the novel pairing of *dsx*$^{GAL4\text{-}DBD}$ with the *vGlut*^{OK37}1-VP16-AD hemidriver (Gao et al., 2008). Whether the neurons intersected by the *vGlut*^{OK37}1-VP16-AD pairing are glutamatergic in origin requires confirmation using either a glutamate or vGlut antibody. However, that the majority of glutamatergic neurons are motoneurons (Jan and Jan, 1976; Johansen et al., 1989; Mahr and Aberle, 2006), suggests that this novel pairing may potentially have uncovered, for the first time, a subset of motoneurons of the *dsx* circuitry. Strikingly, rendering these neurons inactive in males presented with a highly distinct behavioural deficit: the inability to achieve genital attachment. This finding in itself is the first of its kind, as neurons that participate in the execution of copulation have, until now, failed to be identified. Even when considering motoneurons of *fru* circuitry, which includes i) motoneurons innervating direct flight muscles, which could be critical for song production (Rideout et al., 2007; Yu et al., 2011); ii) a cluster of serotonergic neurons within the Abg that innervate the internal genitalia (Lee and Hall, 2001; Billeter and Goodwin, 2004) and controls the synchronized transfer of sperm and seminal fluids during copulation (Acebes et al., 2004); and finally iii) a separate cluster of Abg motoneurons that innervate abdominal muscles (Billeter and Goodwin, 2004), of which a single glutamatergic motoneuron in the ventral Abg induces the formation of the male-specific Muscle of Lawrence MOL (Billeter et al., 2006; Nojima et al., 2010); none of these neurons have been functionally implicated with the execution of the late stages of the courtship repertoire.

Unfortunately, given the time constraints of this study, the above-mentioned experiments have yet to be carried out. However, as a glimpse of what is to come (in the near future), I broadly present additional neuroanatomical characterisations of *vGlut*^{OK37}1-VP16-AD; *dsx*$^{GAL4\text{-}DBD}$ males expressing the cytoplasmic EGFP reporter; realising neurons of the Abg as motoneurons that innervate the internal reproductive system and abdominal muscles in males (Figure 5-15). Analogous characterisations have been carried out in females; revealing dimorphism in the number of neurons expressed in the Abg (females exhibiting more neurons than males), and their respective innervations on muscles of the uterus and abdomen (data not shown). Interestingly, expression was also realised in a subset of gustatory neurons in both male and female forelegs that give rise to sexually dimorphic innervations to the Msg (male expression pattern shown only; Figure 5-15B). In presenting this data, albeit superficially, I am trying to assert the importance of this novel pairing, particularly as an approach to understanding the mechanism by which *dsx* neural circuitry sex-specifically instructs motor control. Continued analyses of the neural circuitry directing these tissues, in both males and females, will be essential to fully describe how the late steps of courtship are initiated and executed.

Ultimately, this requires investigating these processes at the level of single neurons. Using an elegant heat-shock inducible flipase/*flipase recombination target* (FLP/*FRT*) site specific recombinase approach (Lee and Luo, 1999; von Philipsborn et al., 2011), functional interrogations and intricate neuroanatomical maps of individual *dsx*-motoneurons can be achieved, enabling the isolation of *dsx*-motoneurons that are involved in the modulation of the internal reproductive system, from those that modulate the abdominal muscles. Artificially activating these neurons, and monitoring muscle activity using live calcium imaging (Nakai et al., 2001) would serve to demonstrate their excitatory control over their respective muscles. Finally, using photo-activatable fluorescent proteins (Patterson and Lippincott-Schwartz, 2002), upstream neurons that modulate the activity of these glutamatergic motoneurons can be identified. The proposed experiments will allow me to model the higher-order processing/command signals from the brain that are required to activate these motorneurons, while shedding light on how these motorneurons function to control motor

output and, potentially, muscle development. Ultimately, correlating the connectivity, function and activity of these neurons will provide the logic for how this sexually dimorphic circuitry might be coordinated to generate a sex-specific motor response.

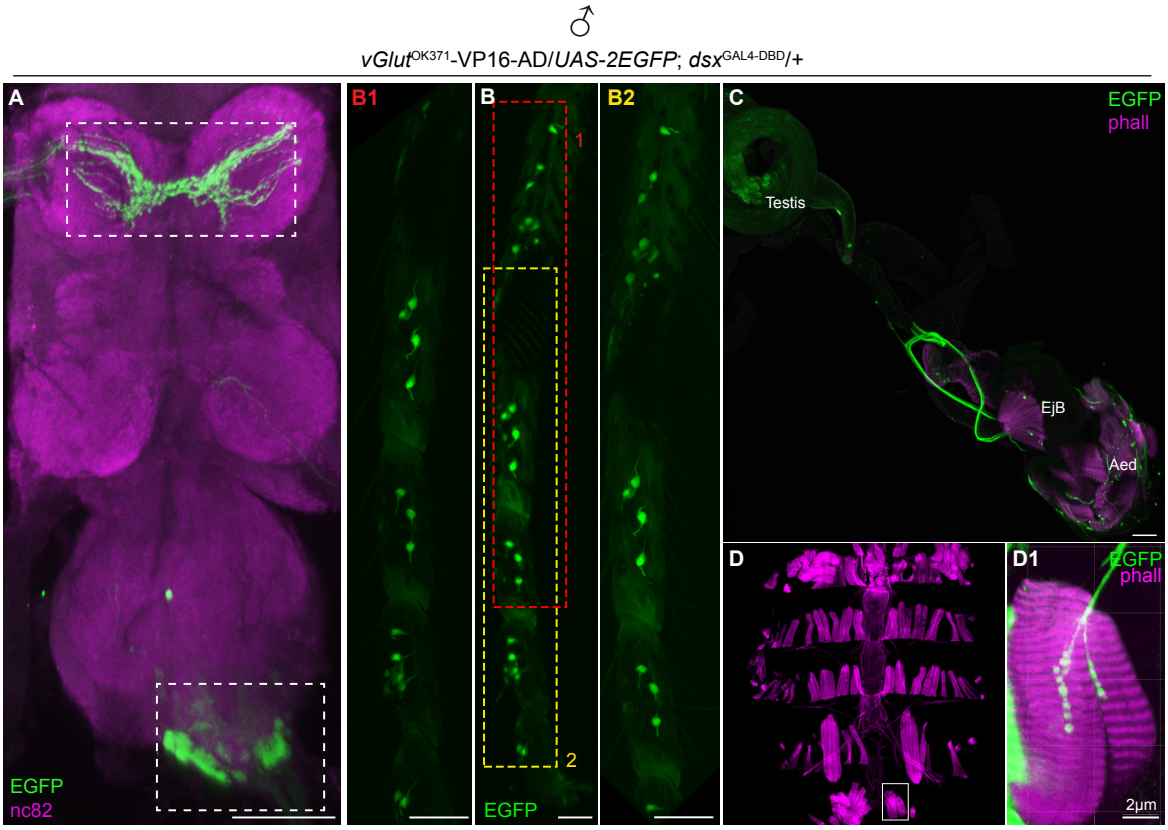


Figure 5-15 *dsx*$^{GAL4\text{-}DBD}$ paired with *vGlut*^{ok371}-VP16-AD, expressing *UAS-EGFP* in 5 day old male. (A) Male VNC revealing expression projections from the foreleg forming a male-specific contralateral commissural bridge, and neurons of the Abg and their associated projections both descending to the genitalia and abdominal muscles (white dotted boxes). Ventral view, anterior up. (B) Expression in the T1 tarsi of the male foreleg. (B1) Expression in the T1-2 tarsi the male foreleg at higher magnification (region of magnification shown in red dotted box of (B)). (B2) Expression in the T2-5 tarsi the male foreleg at higher magnification (region of magnification shown in yellow dotted box of (B)). (C) Abg motoneuron innervations on the internal genitalia of 5 day old adult male flies counterstained with the F-actin specific antibody Phalloidin. Detail of internal genitalia; testes, ejaculatory bulb (EjB), and aedeagus (Aed) indicated. (D) Flat dorsal abdominal preparation of 5 day old adult males demonstrating longitudinal muscles associated with abdominal segments A2-A6 that are counterstained with phalloidin. Longitudinal muscles of abdominal segment A6 shown in white box. (D1) Higher magnification of longitudinal muscles of abdominal segment A6 with realised morphology of *dsx*-expressing glutamatergic motoneuron innervations and synaptic termini. Cytoplasmic EGFP realised with anti-GFP antibody (green). Neuropil in (A) counterstained with anti-nC82 (magenta). Anti-Phalloidin (Phall) is shown in magenta. Scale bar = 50 µm unless otherwise indicated.

5.10 Conclusion

By way of exploiting the novel *dsx*$^{GAL4\text{-}DBD}$ allele, I performed a large thermogenetic screen of extant split-GAL4 VP16AD enhancer trap lines to functionally delineate the roles of specific *dsx*-expressing neural clusters in specifying distinct sub-behaviours of the male courtship repertoire. I retrieved 6 lines in total that exhibited relatively restricted patterns of *dsx*-

expression in the CNS and that, upon thermoactivation, elicited specific behavioural phenotypes; 3 lines that exclusively elicited a wing extension phenotype, and 3 lines that exclusively elicited an abdominal phenotype. Specific inhibition of function in neurons intersected by each candidate line resulted in unique behavioural pathologies pertinent to specific steps of the courtship repertoire. Correlating behavioural data with the neuroanatomical profiles of each candidate line revealed four distinct functional associations:

i) the activity of a critical subset of *dsx*-pC1, -pC2 and -pC3 neurons of the brain is necessary for the initiation and maintenance of courtship behaviours;

ii) the activity of *dsx*-TN1 and -TN2 neurons of the Ptg and Msg correlate with the elicitation of wing extension;

iii) the activity of a critical subset of *dsx*-Abg neurons of the VNC is necessary for the achievement of the late steps of courtship that includes abdominal curling and attempting copulation

iv) the specific activity of glutamatergic *dsx*-Abg motoneurons of the VNC appears necessary for successful genital coupling, while a second set of *dsx*-Abg neurons may be involved in genital uncoupling.

Based on the level of spatial restriction attained by these efforts, it is clear that additional experiments are necessary to winnow down to the minimal subset of neurons that specify the distinct sub-behaviours of the male repertoire. Fortunately, the candidate lines retrieved here may be applied in diverse ways to achieve this.

It is my intent with these investigations, in complement with associated studies, to gain insight into the processes of how the nervous system is wired to engender an associated stereotypical pattern of action/reaction. By describing how this might be achieved we are opening a window into the underlying genetic processes governing physiological functioning in the organism as a whole. By extending these experiments to the female, we can then apply our model to encompass how the generic model may be sculpted so that differing behavioural outputs may then be engendered.

6 Parsing *dsx* neural circuitry underlying female post-mating behavioural responses

6.1 Introduction

The most basic prerequisite for employing thermogenetics is the ability to evoke the display of wild-type motor outputs by activating the underlying neural circuitry. The fact that thermoactivation of *dsx* circuitry in females does not elicit any immediate/overt behaviours (Pan et al., 2011), meant that the dissection of *dsx* circuitry underlying female copulatory behaviours required an alternative strategy.

Typically, prior to copulation, females assess potential mates for species type and fitness before sanctioning mating (Villella and Hall, 2008). An unreceptive female exhibits rejection behaviours such as kicking and ovipositor extrusion (Connolly and Cook, 1973; Spieth and Ringo, 1983; Ejima et al., 2001; Kubli, 2003). A receptive female facilitates copulation by slowing down, ceasing rejection behaviours and opening her vaginal plates (Villella and Hall, 2008). While virgin females are highly receptive and rapidly copulate with a suitable partner, mated females undergo a substantial change in their physiology and behaviour, becoming temporarily sexually unreceptive to further copulatory attempts, while increasing oviposition (Kubli, 2003).

Interestingly, disrupting synaptic activity of *dsx*-expressing neurons in females impairs all the above-mentioned pre- and post-copulatory female reproductive behaviours (Rideout et al., 2010). Pre-mating, virgin females are incapable of sampling the male's courtship displays and therefore incapable of providing acceptance responses. During copulation, this lack of cooperation is evident by continual female movement and rejection behaviours. Although sperm and seminal fluids are transferred, these females lay no eggs, re-mate, and remain incapable of suppressing further courtship (Rideout et al., 2010). These data suggest an important role for *dsx* in building the neural framework necessary for mediating all aspects of female behaviour, including 'summation' prior to copulation, acceptance during copulation, and post-copulatory changes. Identifying specific *dsx* neurons that control different components of this behavioural repertoire is an essential step towards dissecting the circuitry required for the performance of these behaviours.

Much of the work on female behaviours have specifically focused on elucidating the mechanism and neural circuitry underlying female post-mating behavioural responses; revealing that they are triggered primarily by sex peptide (SP), a small peptide synthesized in the male accessory glands and transferred to the female during insemination (Kubli, 2003). Females mated to SP-deficient males readily mate again (Liu and Kubli, 2003; Chapman et al, 2003), while virgin females injected with SP are rendered unreceptive (Chen et al., 1988). Recently a SP-responsive G-protein-coupled receptor for SP-mediated post-mating responses has been identified (Yapici et al., 2008). Females lacking this sex-peptide receptor (SPR) remain receptive, exhibiting virgin-like behaviours, post-mating. It was shown that post-mating responses could be mediated by SPR activation in a set of 6–8 sensory neurons located on the reproductive tract (Häsemeyer et al., 2009; Yang et al., 2009). These neurons express both the sex-specific transcripts of the *fruitless* gene (fru^{+}), a marker for neurons likely to have sex-specific functions, and *pickpocket* (ppk^{+}), which is believed to encode a marker for proprioceptive neurons (Adams et al., 1998; Grueber et al., 2003; Häsemeyer et al., 2009; Yang et al., 2009). As these fru^{+}/ppk^{+} sensory neurons project to the Abg and may target the subesophageal ganglion (SOG), these regions in the CNS are proposed to be involved in processing of SP-sensory information (Häsemeyer et al., 2009; Yang et al., 2009).

The suppression of post-mating responses via disruption of *dsx* neural function, together with the observed $dsx^{GAL4\text{-}DBD}/elav^{VP16\text{-}AD}$-expression in sensory neurons of the female internal genitalia observed in this study (reported in Chapter 4), suggested an overlap between *dsx* and the SP-responsive fru^{+}/ppk^{+}-expressing neurons in the reproductive system. To establish whether *dsx* neurons are in indeed involved in modulating SP-dependent post-mating responses. I, in conjunction with Dr. Carolina Rezával performed a series of behavioural and neuroanatomical assays using the original dsx^{GAL4} line (Rideout et al., 2010). Principally, the rationale for reverting to the original dsx^{GAL4} line for these experiments was simply because the $dsx^{GAL4\text{-}DBD}$ allele had not been behaviourally validated at that point in time.

In focusing our efforts on the post-mating behavioural switch, we not only aimed to identify and functionally isolate component elements of the *dsx* circuitry that specify these behaviours, but also aimed to determine, for the first time, the relationship between *fru* and *dsx*-expressing neurons in females. As the results for individual experiments are really only meaningful when considered in concert and, as many assays were conducted as a joint effort, the experiments presented within this chapter must, as a necessity, reflect the work performed not only by myself, but by my colleague, and will in large part be presented as per our paper, Rezával et al., 2012.

6.2 Results

6.2.1 Targeted expression of membrane-bound SP in *doublesex*-expressing neurons triggers post-mating behaviours

Expression of a membrane-bound form of SP (mSP) in the CNS has been shown to be sufficient to induce post-mating responses in virgin females and has been used to identify SP-responsive cells and tissues (Nakayama et al., 1997; Yang et al., 2009). Employing a similar strategy, we targeted expression of *UAS-mSP* to *dsx* cells under the control of dsx^{GAL4} in virgin females, allowing us to assess the role of such cells in sensing SP. These virgin females exhibited levels of receptivity comparable to mated control females (<20% copulated within 1 hr), involving levels significantly lower than those of control virgin females (>80% copulated within 1 hr) (Figure 6-1A). As a corollary, dsx^{GAL4}/*UAS-mSP* virgin females displayed significant levels of rejection behaviours towards courting males as demonstrated by the increased frequency of ovipositor extrusions (Figure 6-1B and Connolly and Cook, 1973). We also observed an increase in oviposition in dsx^{GAL4}/*UAS-mSP* virgin females, similar to levels observed with mated controls (Figure 6-1E).

Studies have shown the importance of female locomotor activity for stimulating male courtship (Siegel and Hall, 1979; Tomkins et al., 1982; Ejima and Griffith, 2008). Consistent with this, we observed increased locomotor activity in virgin females while being courted compared with mated wild-type females (Figure 6-1C). Tellingly, dsx^{GAL4}/*UAS-mSP* virgin females displayed a marked decrease in locomotion while being courted (Figure 6-1C). It has

been suggested that a female's movement could produce subtle sounds alerting males to the female's presence and initiating courtship behaviours (Ejima and Griffith, 2008). During courtship observation periods, both *dsx*^{GAL4}/*UAS-mSP* virgin females and mated control females exhibited reduced levels of activity while the male was not courting; remaining static for significantly greater periods of time than control virgin females (Figure 6-1D). These results show that locomotion during courtship is another behaviour that undergoes a dynamic change in response to the copulatory 'state' of an individual female.

The male courtship index (CI) is a measure of the attractiveness of a female: naive males court virgin females persistently but display lower levels of courtship when paired with unreceptive mated females (Villella and Hall, 2008). Intriguingly, wild-type naive males courted *dsx*^{GAL4}*/UAS-mSP* virgin females significantly less than control virgin females (<40% vs. >80%, Figure 6-1F). To verify the observed decrement in male CI's was a consequence of female behaviour, rather than a response to potential changes in the experimental female's pheromonal profile, we repeated these experiments with decapitated (i.e. non-behaving) *dsx*^{GAL4}/*UAS-mSP* virgin females, and observed that the males' CI's were indistinguishable to those displayed in the presence of wild-type virgins (Figure 6-2A). This suggests that the male's courtship behavioural outputs are undergoing dynamic modification in response to the target female's behavioural state.

We confirmed the neural aetiology of the observed defects in post-mating responses in *dsx*^{GAL4}/*UAS-mSP* virgin females by employing *elav-Gal80* (Rideout et al., 2010) specifically to inhibit neural expression of mSP; *elav-Gal80; dsx*^{GAL4}/*UAS-mSP* virgin females were not significantly different from controls (Figure 6-1A-F).

During our analyses of *dsx*^{GAL4} driven nGFP expression in conjunction with *elav-Gal80* we noted repression in non-neural cells in the reproductive system (Figure 6-3B). To ensure that this repression did not impinge upon the neural aetiology of the observed *dsx*^{GAL4}/*UAS-mSP* phenotypes, we reiterated these experiments using an alternative pan-neural repressor, *syb-Gal80* (Rubinstein et al., 2010; (Figure 6-3C). *dsx*^{GAL4} driven mSP expression in conjunction with *syb-Gal80* yielded behavioural results consistent with those observed using *elav-Gal80*;

that is, receptivity levels were restored in *dsx*^{GAL4}/*UAS-mSP* co-expressing *syb-Gal80* to ~90% (n=34), and egg-laying was reduced to control levels (7.5 ± 2.4, n=45).

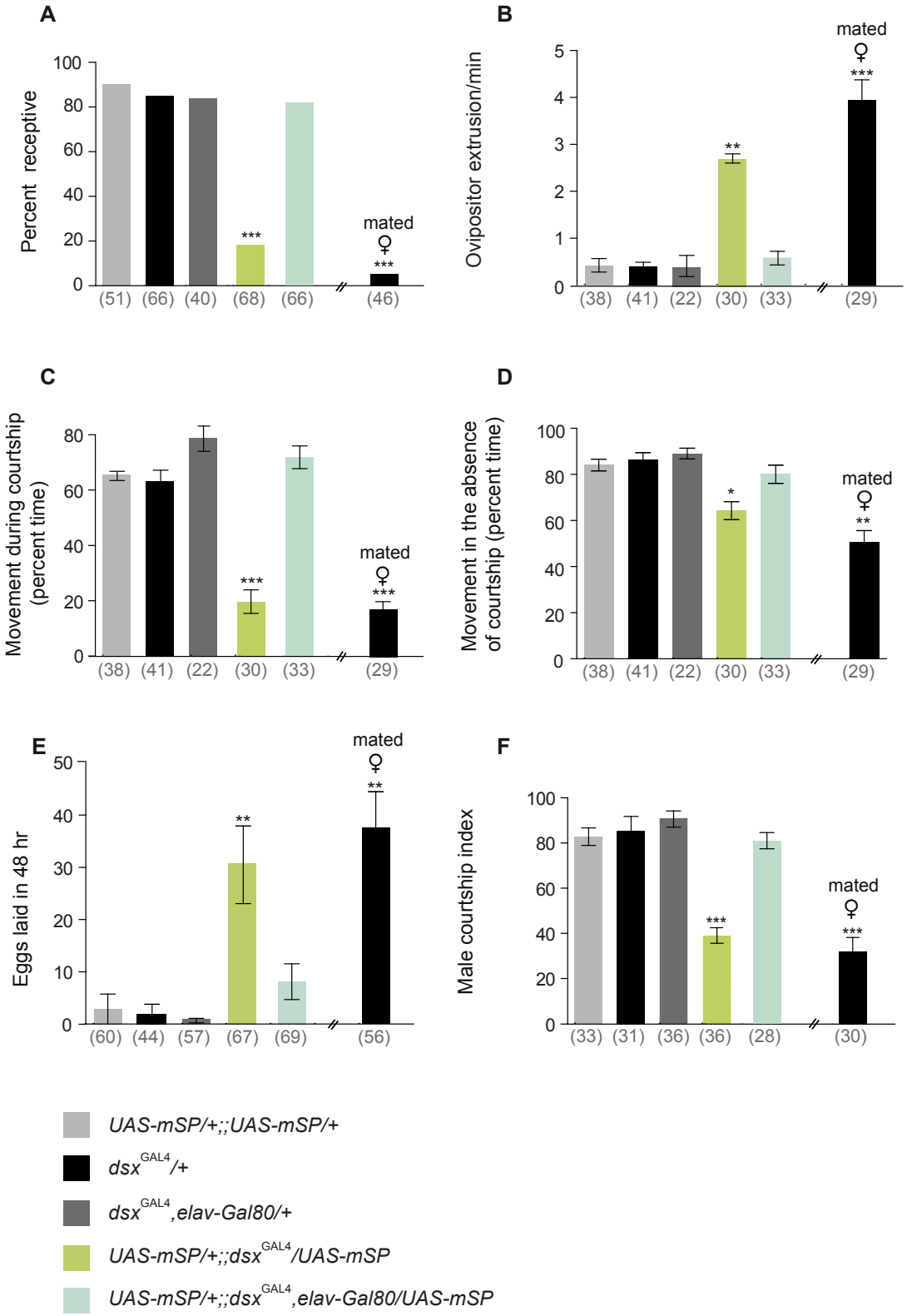


Figure 6-1 Behavioural effects of mSP expression in *dsx* neurons in virgin females.
(A) Percentage receptivity (***P<0.0001, Fisher exact test) (B) Ovipositor extrusion during courtship (**P<0.001, ***P<0.0001, Kruskal-Wallis ANOVA test). (C) Percentage of time spent moving while being actively courted (***P<0.0001, Kruskal-Wallis ANOVA test). (D) Percentage of time spent moving in the absence of active courtship (*P<0.05, **P<0.001, Kruskal-Wallis ANOVA test). (E) Egg-

laying (**P<0.001, Kruskal-Wallis ANOVA test). (F) Male courtship index of naïve males (***P<0.0001, Kruskal-Wallis ANOVA test). Error bars indicate SEM. Genotypes indicate virgin females, unless stated otherwise. Target males were wild-type. n values shown in parentheses. (Figure taken from Rezával et al., 2012).

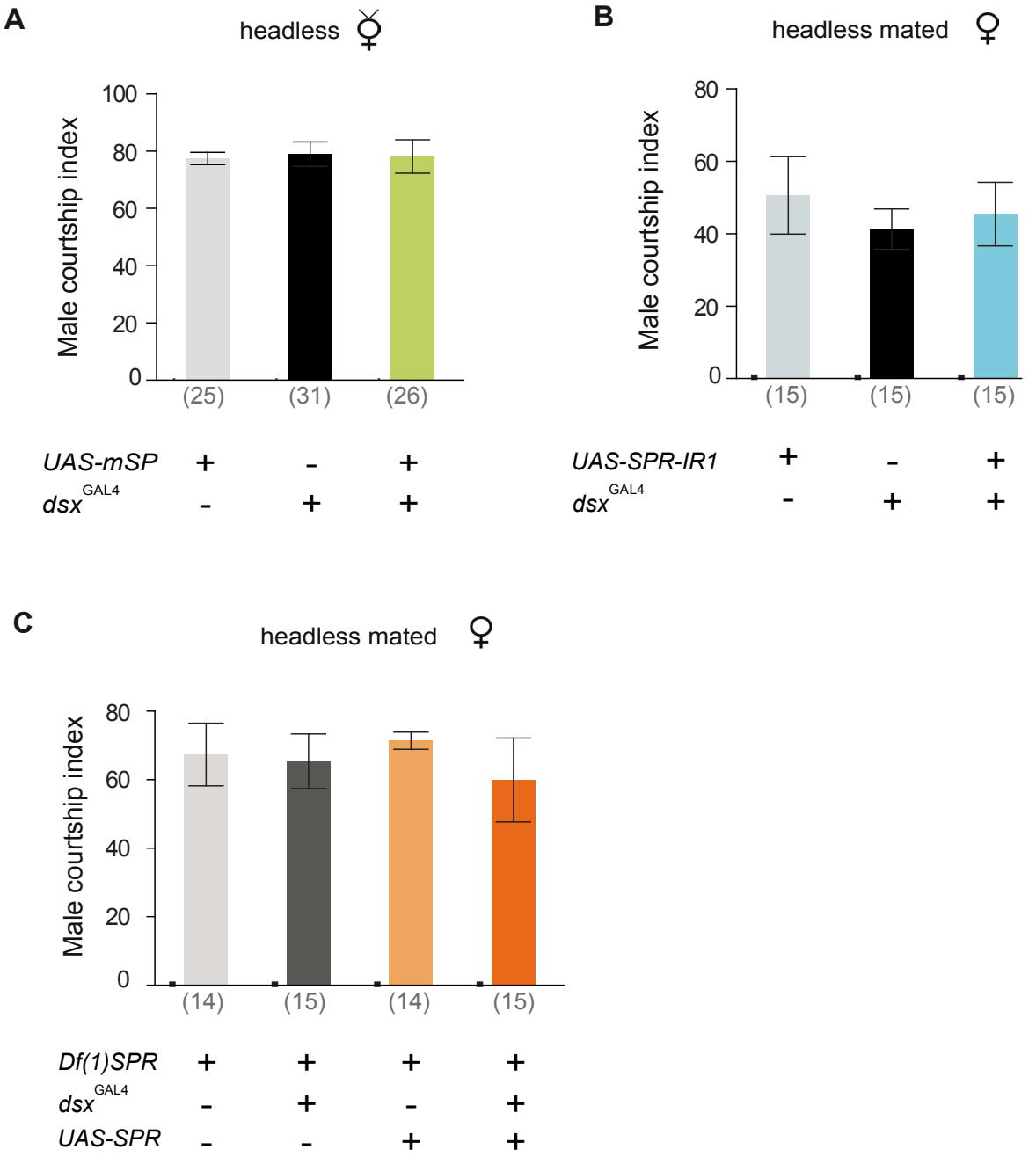


Figure 6-2 Male courtship index in the absence of female behavioural cues.
Male courtship index of naïve wild-type males paired with (A) decapitated virgin females and (B-C) decapitated mated females (Kruskal-Wallis ANOVA test). No significant differences found between the genotypes of each experimental cohort. Error bars indicate SEM. Genotypes indicate virgin females, n values shown in parentheses. (Figure taken from Rezával et al., 2012).

These results demonstrate that expression of mSP in *dsx*-neurons is sufficient to induce female post-mating behaviours in virgin females, and these changes can engender complex behavioural responses in individual females as well as in potential mates.

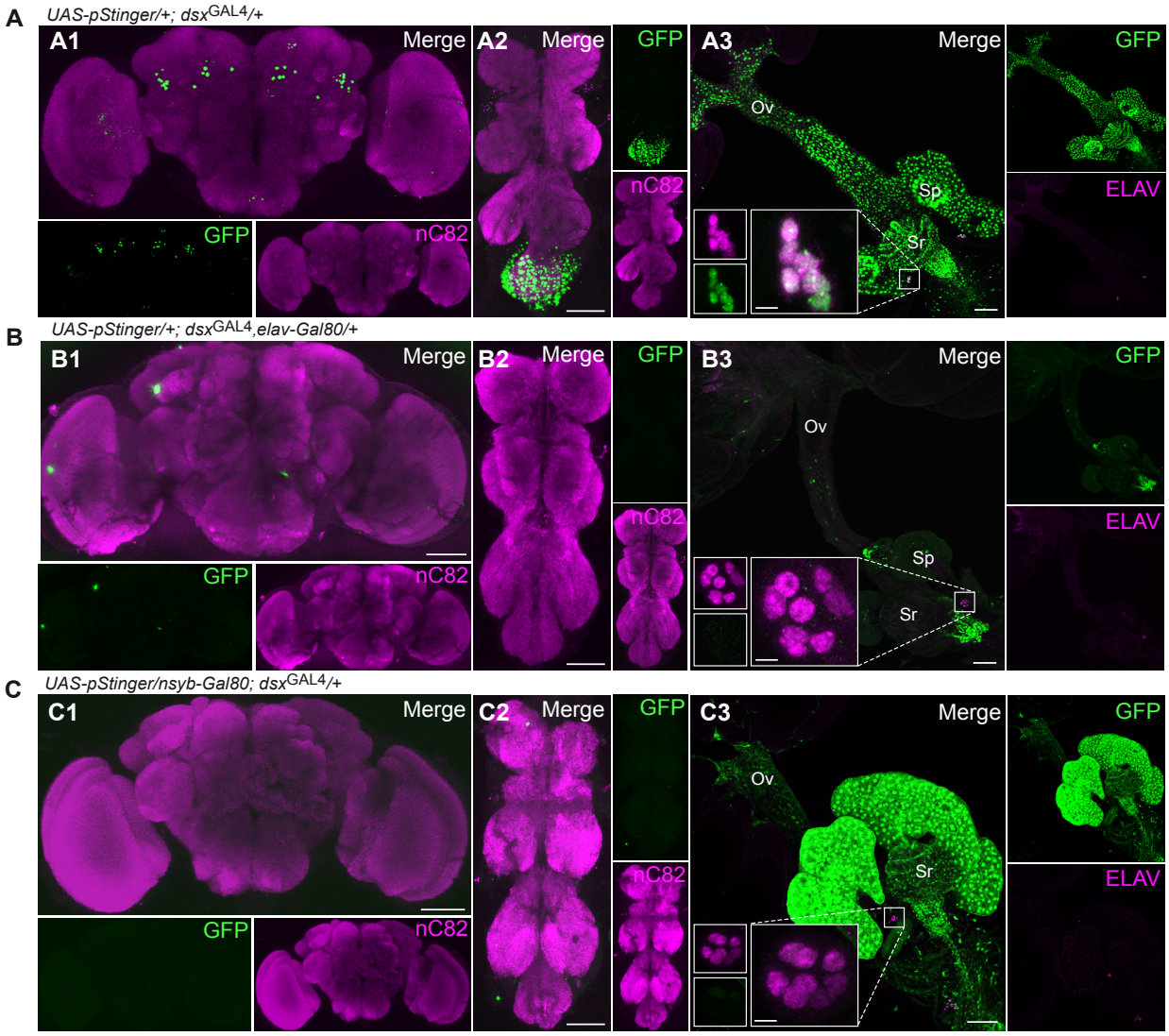


Figure 6-3 Differential effects of neural GAL4 inhibitors, *elav-Gal80* and *syb-Gal80*, on *dsx* expression.
(A) Expression of nGFP (green) in *UAS-pStinger/+; dsx*^{GAL4}/+ 5 day-old female (A1) brain, (A2) VNC and (A3) reproductive system. Inset in (A3) shows co-localisation between anti-ELAV (magenta) and *dsx* (green). (B1-3) Expression of nGFP (green) in *UAS-pStinger/+; dsx*^{GAL4}/+ 5 day-old female, also expressing the neural GAL4 repressor *elav-Gal80.* No expression of GFP is detected in any *dsx*^{GAL4}-neural clusters in the (B1) brain and (B2) VNC. (B3) Ectopic repression of nGFP in non-neural *dsx*^{GAL4}-expressing cells is observed within the lateral and common oviduct (Ov), spermathecae (Sp), seminal receptacle (Sr) and uterus. Inset in (B3) shows absence of nGFP in neurons (ELAV-positive cells, magenta). (C1-3) Expression of nGFP (green) in *UAS-pStinger/+; dsx*^{GAL4}/+ 5 day-old female, also expressing the neural Gal4 repressor *nsyb-Gal80.* No expression of nGFP is detected in any *dsx*^{GAL4}-neural clusters within the (C1) brain and (C2) VNC. (C3) No apparent ectopic repression of non-neural *dsx*^{GAL4}-expressing cells is detected within the internal reproductive system. Inset in (C3) shows absence of nGFP in neurons (ELAV-positive cells, magenta). nGFP expression is shown in green and neuropil was counterstained with anti-nC82 (magenta). Reproductive systems were counterstained with anti-ELAV (magenta). Ventral views; anterior, top. Scale bars = 50 µm. Scale bars in insets = 10 µm. (Figure taken from Rezával et al., 2012).

6.2.2 Knocking down SPR function specifically in *dsx*-expressing neurons abolishes post-mating behavioural responses

The sex-peptide receptor (SPR) is broadly expressed in the CNS and reproductive tract (Yapici et al., 2009; Figure 6-4) and is required for SP-mediated post-mating behavioural responses, as females lacking SPR remain receptive, exhibiting virgin-like behaviours, even after mating or SP injection (Yapici et al., 2009). To show that *dsx*^{GAL4}-expressing cells respond to SP, we employed RNA interference to knockdown SPR expression (Häsemeyer et al., 2009) and evaluated the effects on post-mating responses. While virgin *dsx*^{GAL4}/*UAS-SPR-IR1* females were typically receptive (data not shown), post-mating they displayed no decrement in receptivity nor any increase in ovipositor extrusions compared with mated controls (~80% versus <4% remated, respectively; Figure 6-5A and B). *dsx*^{GAL4}/*UAS-SPR-IR1* mated females displayed locomotor activity comparable to virgin females (Figure 6-5C and D) and significantly decreased levels of oviposition (Figure 6-5E). Males spent significantly more time courting *dsx*^{GAL4}/*UAS-SPR-IR1* mated females compared to controls *(*CI >60% versus <40%, respectively; Figure 6-5F). These effects were not observed when males were paired with decapitated *dsx*^{GAL4}/*UAS-SPR-IR1* females (Figure 6-2B).

We then attempted to rescue the behavioural deficits observed in SPR-null mated females by restrictively expressing SPR in *dsx*-expressing cells in a SPR-deficient genetic background (*Df(1)SPR*). Post-mating responses were restored in *Df(1)SPR*;*UAS-SPR;dsx*^{GAL4} mated females. Rescued females exhibited significantly reduced levels of receptivity, increased ovipositor extrusion, egg-laying, and decreased locomotion; they also elicited lowered levels of male courtship (Figure 6-6A-F). Decapitated *Df(1)SPR*;*UAS-SPR;dsx*^{GAL4} mated females were found to be as attractive as decapitated mated control females to naïve males (Figure 6-2C). We used *elav-Gal80* to confirm the neural aetiology of phenotypic effects arising from impairment of SPR function in *dsx*^{GAL4}-expressing neurons. Expression of *elav-Gal80* in conjunction with *dsx*^{GAL4}/*UAS-SPR-IR1* in mated females rescued all observed behavioural deficits, including percentage of females remating and levels of egg-laying (Figure 6-5A-F).

These findings demonstrate the necessity and sufficiency of SPR function in *dsx* neurons to respond to, and convey, the stimulatory cues engendered by SP, resulting in the induction of post-mating behavioural responses.

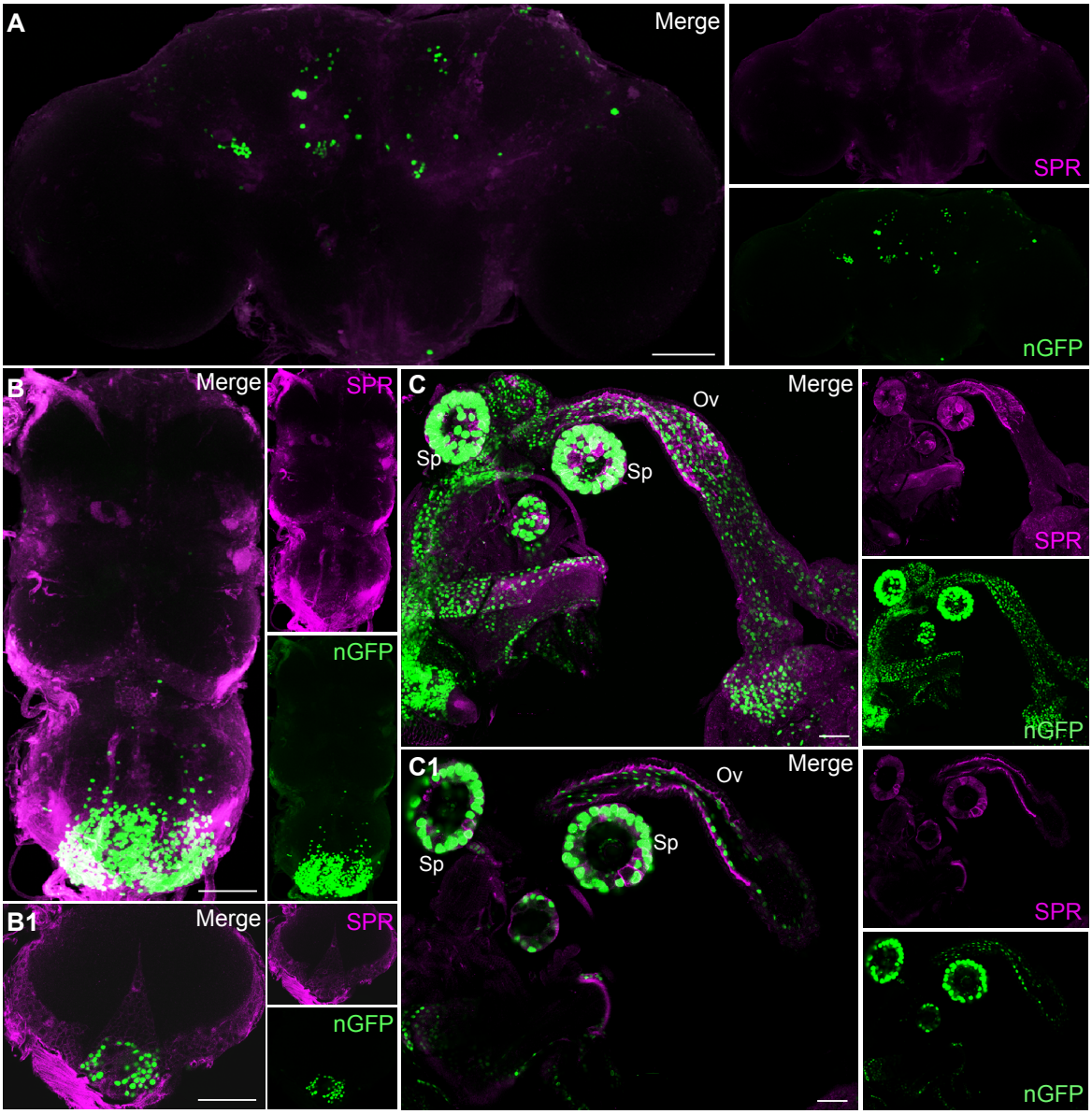


Figure 6-4 *dsx*^{GAL4} and SPR expression in the CNS and internal genitalia of 5-day-old adult females.
(A-B) *UAS-pStinger/+; dsx*^{GAL4}/+ female CNS co-stained with anti-SPR. (A) No apparent co-localization detected in the brain; however, (B) a small subset of *dsx*^{GAL4}-expressing neurons of the Abg in the VNC appears to express SPR on their membrane. (B1) Subset of confocal sections of the VNC (B) appear to show expression of SPR on the membrane of *dsx* neural cell bodies in the dorsal Abg. (A-B) ventral views; anterior, up. (C) Reproductive tract of *UAS-pStinger/+*; *dsx*^{GAL4}/+ females stained with anti-SPR. Co-localization between *dsx*^{GAL4} and SPR occur within the lower common oviduct (Ov) and spermathecae (Sp). (C1) Subset of confocal sections detailing co-expression of SPR and *dsx* within the structures indicated. Anti-SPR (magenta) and nGFP (green). Scale bars = 50 µm. (Figure taken from Rezával et al., 2012).

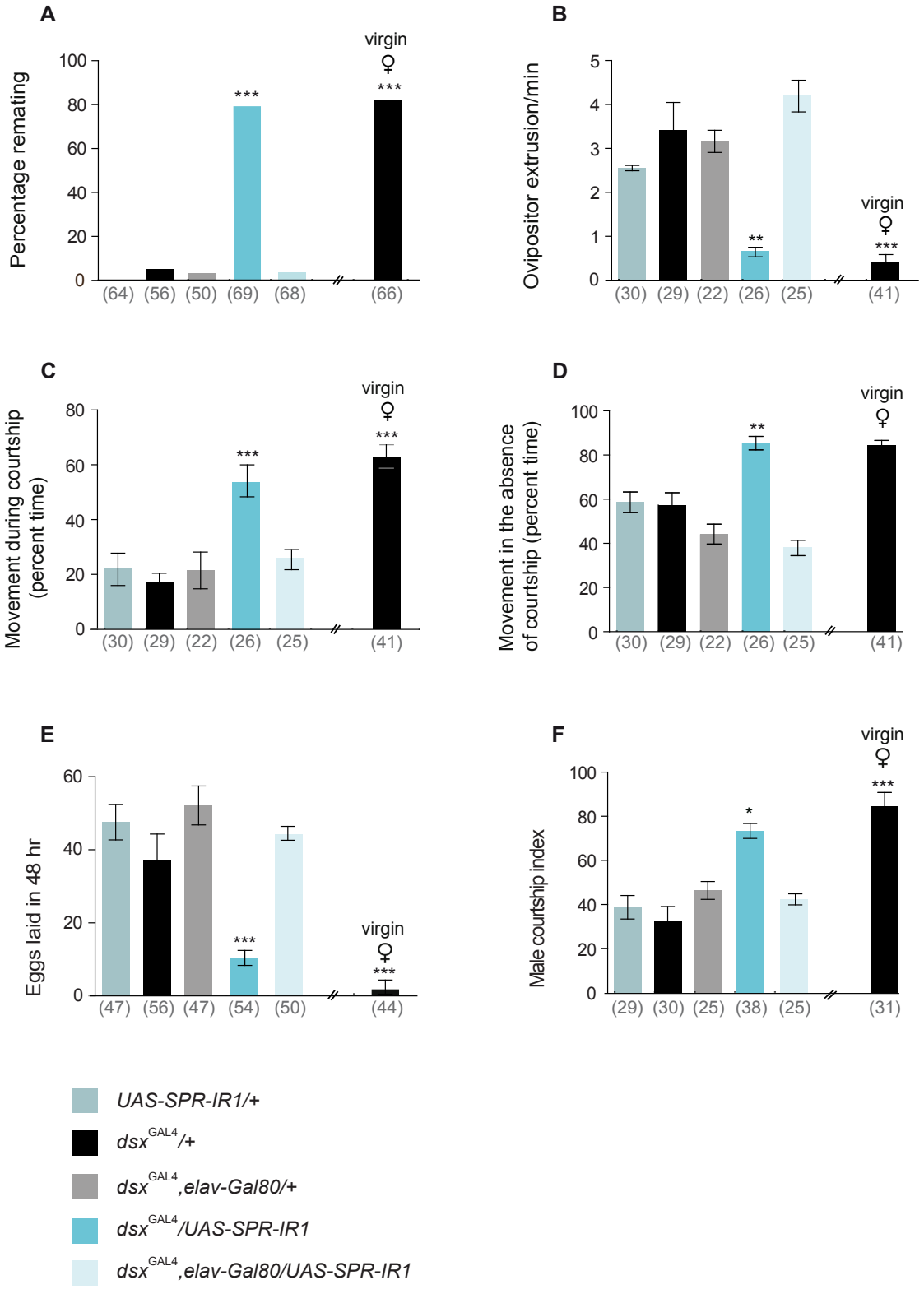


Figure 6-5 Knocking down SPR expression in *dsx* neurons reduces post-mating behaviours in mated females.
(A) Percentage remating (***P<0.0001, Fisher exact test) (B) Ovipositor extrusion during courtship (**P<0.001, ***P<0.0001, Kruskal-Wallis ANOVA test). (C) Percentage of time spent moving while being actively courted (***P<0.0001, Kruskal-Wallis ANOVA test). (D) Percentage of time spent moving in the absence of active courtship (**P<0.001, Kruskal-Wallis ANOVA test). (E) Egg-laying (***P<0.0001, Kruskal-Wallis ANOVA test). (F) Male courtship index of naïve males (*P<0.05, ***P<0.0001, Kruskal-Wallis ANOVA test). Error bars indicate SEM. Genotypes indicate mated females, unless stated otherwise. Target males were wild-type. n values shown in parentheses. (Figure taken from Rezával et al., 2012).

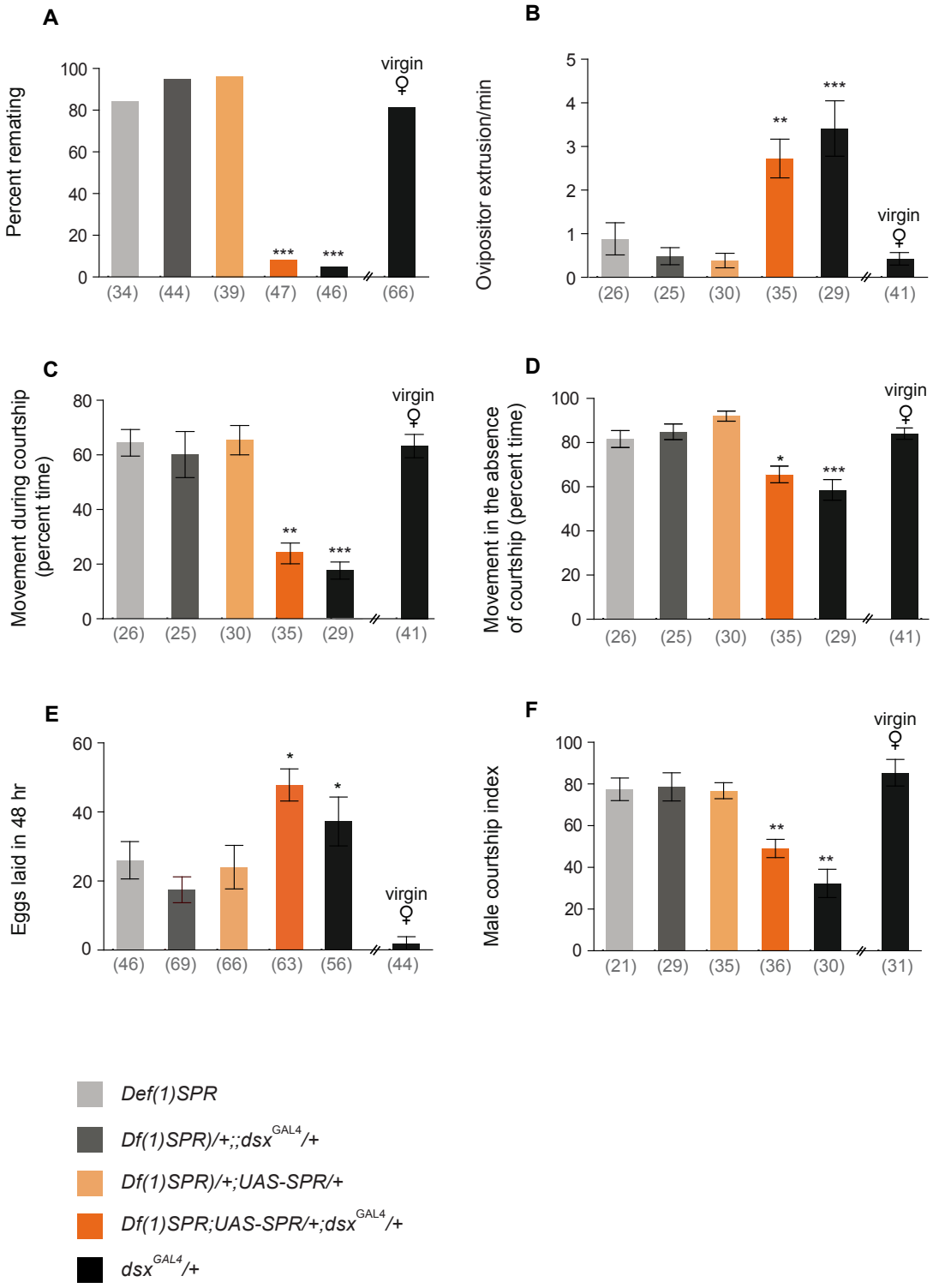


Figure 6-6 Expression of SPR in *dsx* cells alone is sufficient to rescue post-mating responses in *SPR*-deficient line *Df(1)SPR*.
(A) Percentage remating (***P<0.0001, Fisher exact test) (B) Ovipositor extrusion during courtship (**P<0.001, ***P<0.0001, Kruskal-Wallis ANOVA test). (C) Percentage of time spent moving while being actively courted (**P<0.001, ***P<0.0001, Kruskal-Wallis ANOVA test). (D) Percentage of time spent moving in the absence of active courtship (*P<0.05, ***P<0.0001, Kruskal-Wallis ANOVA test). (E) Egg-laying (*P<0.05, Kruskal-Wallis ANOVA test). (F) Male courtship index of naïve males (**P<0.001, Kruskal-Wallis ANOVA test). Error bars indicate SEM. Genotypes indicate mated females, unless otherwise stated. Target males were wild-type. n values shown in parentheses. (Figure taken from Rezával et al., 2012).

6.2.3 *dsx* neurons are part of the *fru*$^{+}$/*ppk*$^{+}$ circuitry involved in sensing SP

Although SPR is detected broadly on the female reproductive tract and superficial regions of the ventral nerve cord (VNC) and brain (Yang et al., 2009), only a restricted subset of *fru*$^{+}$/*ppk*$^{+}$ sensory neurons expressing SPR in the reproductive system appear necessary and sufficient for inducing SP-mediated post-mating responses (Häsemeyer et al., 2009; Yang et al., 2009).

Our behavioural observations suggest *dsx* neurons respond directly to SP to elicit the post-mating switch. To ascertain if the *fru*$^{+}$/*ppk*$^{+}$ neurons involved in modulation of post-mating responses to SP signaling were also *dsx* positive, we expressed *UAS-redStinger* using *dsx*^{GAL4} alongside *ppk-eGFP*. The full population of *ppk* neurons associated with the female genitalia consists of two neurons on each lateral oviduct plus approximately thirty neurons organized in three bilateral clusters, on the uterus (see Figure 6-7C; Yang et al., 2009). Co-localization was observed with *dsx* in most *ppk* sensory neurons; this included a pair of neurons on the lateral oviducts and the two most anterior bilateral clusters on the uterus (Figure 6-7A and 4C, Nos. 1 and 2). In agreement with previous characterizations, the most anterior clusters (No. 1, Figure 6-7C) on the uterus are bilateral clusters comprised of 3 neurons, while the more posterior clusters (No. 2, Figure 6-7C) are bilateral clusters comprised of 7 neurons (Häsemeyer et al., 2009; Yang et al., 2009). Further support that *dsx*$^{+}$/*ppk*$^{+}$ neurons are required for activating the post-copulatory switch was evidenced by the reduction in post-mating responses observed when *dsx*^{GAL4} drove expression of mSP in virgin females in the presence of *ppk-Gal80* (Yang et al., 2009; Figure 6-7D,E).

A specific subset of *ppk* neurons, one per lateral oviduct and a bilateral cluster of 3 neurons in the uterus has been shown to co-express with marker expression driven by *fru*^{GAL4} (Häsemeyer et al., 2009; Yang et al., 2009). We exploited the LexA/lexAop binary system (Lai and Lee, 2006) to confirm co-expression between *dsx* and *fru* using *UAS-pStingerII* (nGFP) and *lexAop-dsTomato* responsive elements in conjunction with the *dsx*^{GAL4} and *fru*^{P1LexA} drivers (Mellert et al., 2010). Co-expression was restricted to 3 *fru*$^{+}$ neurons on each

side of the uterus (Figure 6-7B and C, No. 2), with no co-expression observed on the lateral oviducts (data not shown). We have refined the originally described *fru*$^{+}$/*ppk*$^{+}$ SP-sensory circuit to two pivotal bilateral clusters of 3 *dsx*$^{+}$/*fru*$^{+}$/*ppk*$^{+}$ neurons.

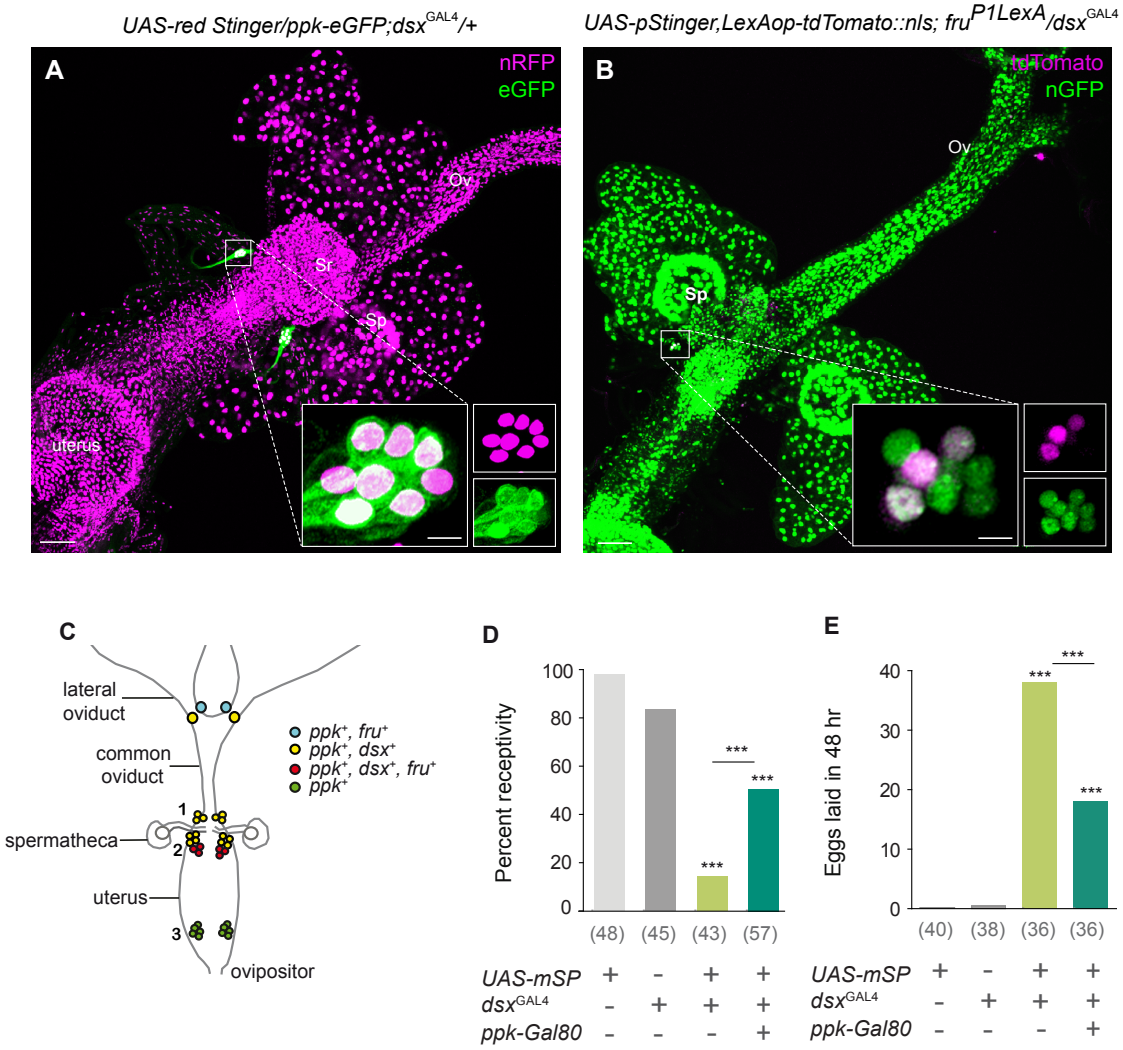


Figure 6-7 *dsx* neurons are part of the circuitry involved in sensing SP.
(A) Co-localisation of *ppk*- and *dsx*-expressing neurons in the female genital tract. *ppk-eGFP* was used to visualise *ppk* neurons (green), while *dsx*-expressing cells were visualised with *dsx*^{GAL4} and *UAS-redStinger* (nRFP; magenta). Inset in (A) shows overlap between *ppk*- and *dsx*-expressing neurons at higher optical magnification. (B) Co-localisation of *fru*- and *dsx*-expressing neurons in the female genital tract. *fru* neurons visualised with *LexAop-tdTomato::nls* under the control of *fru*^{P1LexA} (tdTomato; magenta), *dsx* neurons visualised with *dsx*^{GAL4} and *UAS-pStinger* (nGFP; green). Inset in (B) shows overlap between *fru*- and *dsx*-expressing neurons at higher magnification. (A-B) Scale bars= 50 µm and 10 µm in insets. Seminal receptacle (Sr), Spermathecae (Sp), Common oviduct (Ov) indicated. (C) Schematic representation of the *Drosophila* female reproductive system showing different clusters of sensory neurons expressing *ppk*, *fru* and/or *dsx*. Each lateral oviduct possesses two *ppk*-expressing neurons (Yang et al., 2009), one of which is *fru*$^{+}$ (blue dots), while the other is *dsx*$^{+}$ (yellow dots). Within the uterus, the most anterior cluster (no. 1) comprises 3 bilateral *dsx*$^{+}$/*ppk*$^{+}$ neurons (yellow dots), the more posterior cluster (no. 2) comprises 7 bilateral *dsx*$^{+}$/*ppk*$^{+}$ neurons, 3 of which also express *fru* (yellow and red dots respectively), while the most posterior cluster in the uterus (no. 3) appears to solely express *ppk* (green dots). (D-E) *ppk-Gal80* expression reduces post-mating behavioural responses in *dsx*^{GAL4}/*UAS-mSP* virgin females. (D) Percentage receptivity (***P<0.0001, Fisher exact test) (E) Egg-laying (***P<0.0001, Kruskal-Wallis ANOVA test). Error bars indicate SEM. Genotypes indicate virgin females. Target males were wild-type. n values shown in parentheses. (Figure taken from Rezával et al., 2012).

6.2.4 *dsx* sensory neurons in the female reproductive system appear cholinergic

To investigate the neurochemical properties of the neurons implicated in triggering SP-mediated post-copulatory changes, we behaviourally screened neurotransmitter GAL4 lines driving mSP (data not shown). Of the lines tested, only *Cha-GAL4* (Salvaterra and Kitamoto, 2001) resulted in a reduction in receptivity in virgin females; fewer than 7% of which achieved copulation in 1 hr (Figure 6-8C). Expression of *Cha-GAL4* driving nGFP in the reproductive system co-stained with the pan-neural marker anti-ELAV identified neurons that appear anatomically and topographically congruent with the identified *dsx* neurons: that is two of the three neurons of the anterior bilateral cluster on the uterus (No. 1 in Figure 6-8C), all seven neurons of the posterior bilateral cluster on the uterus (No. 2 in Figure 6-8C), and one neuron per lateral oviduct (Figure 6-8A and Figure 6-8A).

Consistent with these findings, *Cha-Gal80* abolished nGFP expression in all *dsx* neurons within the reproductive system (Figure 6-8B). Moreover, dsx^{GAL4}/*UAS-mSP* virgin females expressing *Cha-Gal80* demonstrated high levels of receptivity (~80%) and reduced levels of egg-laying (Figure 6-8C and D, respectively). These results suggest that SP-responsive *dsx* neurons may be cholinergic.

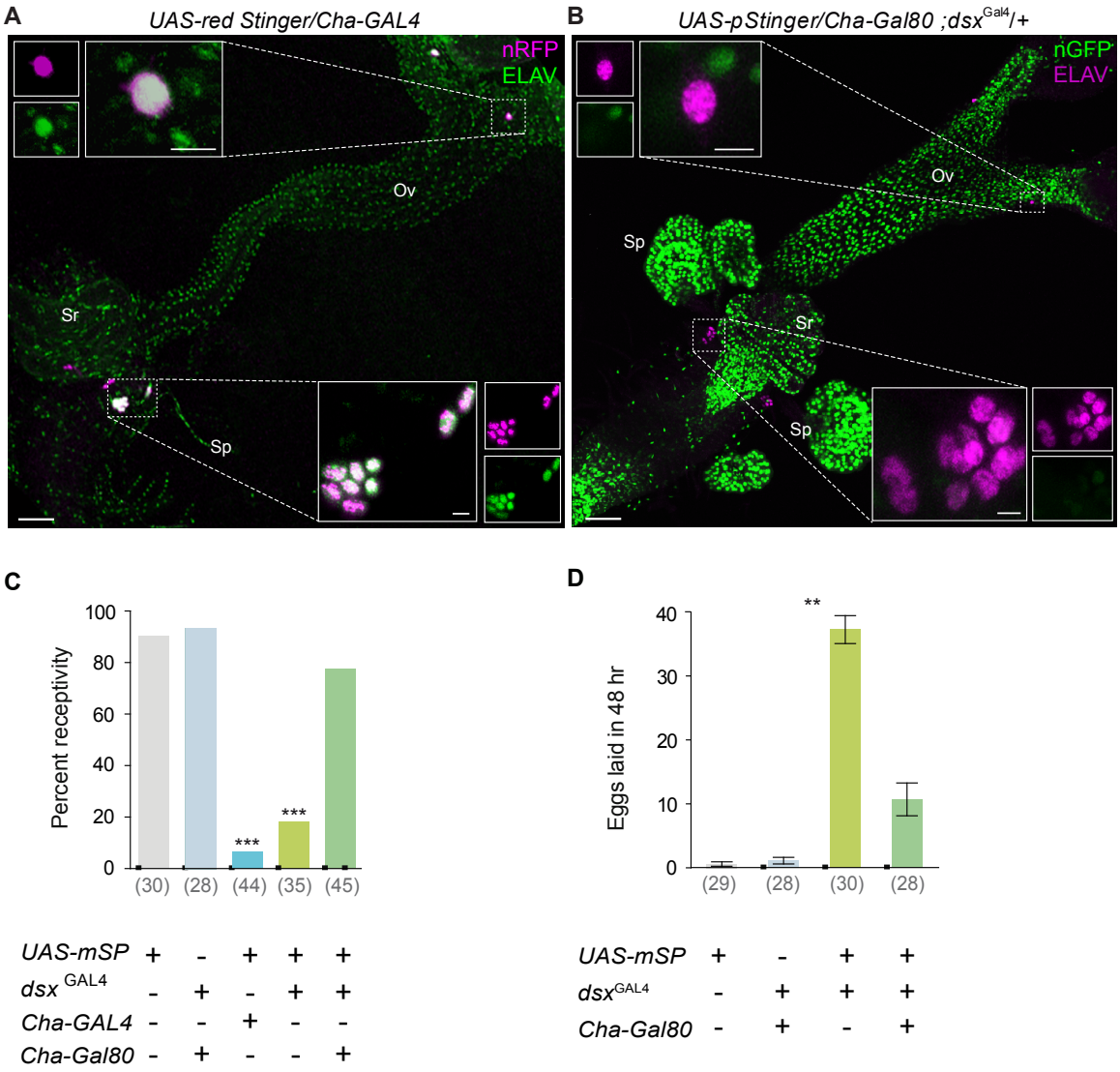


Figure 6-8 *dsx* sensory neurons in the female reproductive system appear cholinergic.
(A) Sensory neurons in the adult female reproductive system are positive for *Cha-GAL4*. Pan-neural antibody, anti-ELAV (green), is shown to co-localize with *Cha-GAL4*/*UAS-redStinger* cells (nRFP; magenta). Insets in (A) show clear overlap between *Cha-GAL4* expressing cells and ELAV in the lateral oviduct and uterus, at higher magnification. (B) *Cha-Gal80* represses nGFP expression in *dsx* neurons of the genital tract. *UAS-pStinger*; dsx^{GAL4} (nGFP, green) female reproductive system also expressing *Cha-Gal80* co-stained with anti-ELAV (magenta). Insets in (B) clearly demonstrate repression of nGFP in *dsx*-expressing neurons in the lateral oviduct and uterus, at higher magnification. Scale bars = 50 µm in (A) and (B), and 10 µm in insets. Seminal receptacle (Sr), spermathecae (Sp), common oviduct (Ov) indicated. (C-D) *Cha-Gal80* expression reduces post-mating behaviours in *UAS-mSP/+*;;dsx^{GAL4}/*UAS-mSP* virgin females. (C) Percentage receptivity (***P<0.0001, Fisher exact test). (D) Egg-laying (***P<0.0001, Kruskal-Wallis ANOVA test). Error bars indicate SEM. Genotypes indicate virgin females. Target males were wild-type. n values shown in parentheses. (Figure taken from Rezával et al., 2012).

6.2.5 Intersecting *dsx* neurons critical for mediating post-mating behavioural responses

Although progress has been made identifying Sex-Peptide responsive sensory neurons (Häsemeyer et al., 2009; Yang et al., 2009), little is known about the downstream neural circuitry underlying post-mating responses. Silencing all dsx^{GAL4} neurons impairs post-mating behaviours, such that mated females failed to lay eggs, remained attractive to courting males, and remated with a second male (Rideout et al., 2010). *dsx* is expressed in ~50 neurons in the female brain and ~300 neurons in the Abg (Rideout et al., 2010). We found a sub-population of *dsx*-Abg neurons sending two bilateral fascicles along the abdominal nerve trunks that ramify on the uterus and vaginal plates (Figure 6-10), suggesting that *dsx* neurons might play a role downstream of the SP-sensory neurons in mediating post-mating responses.

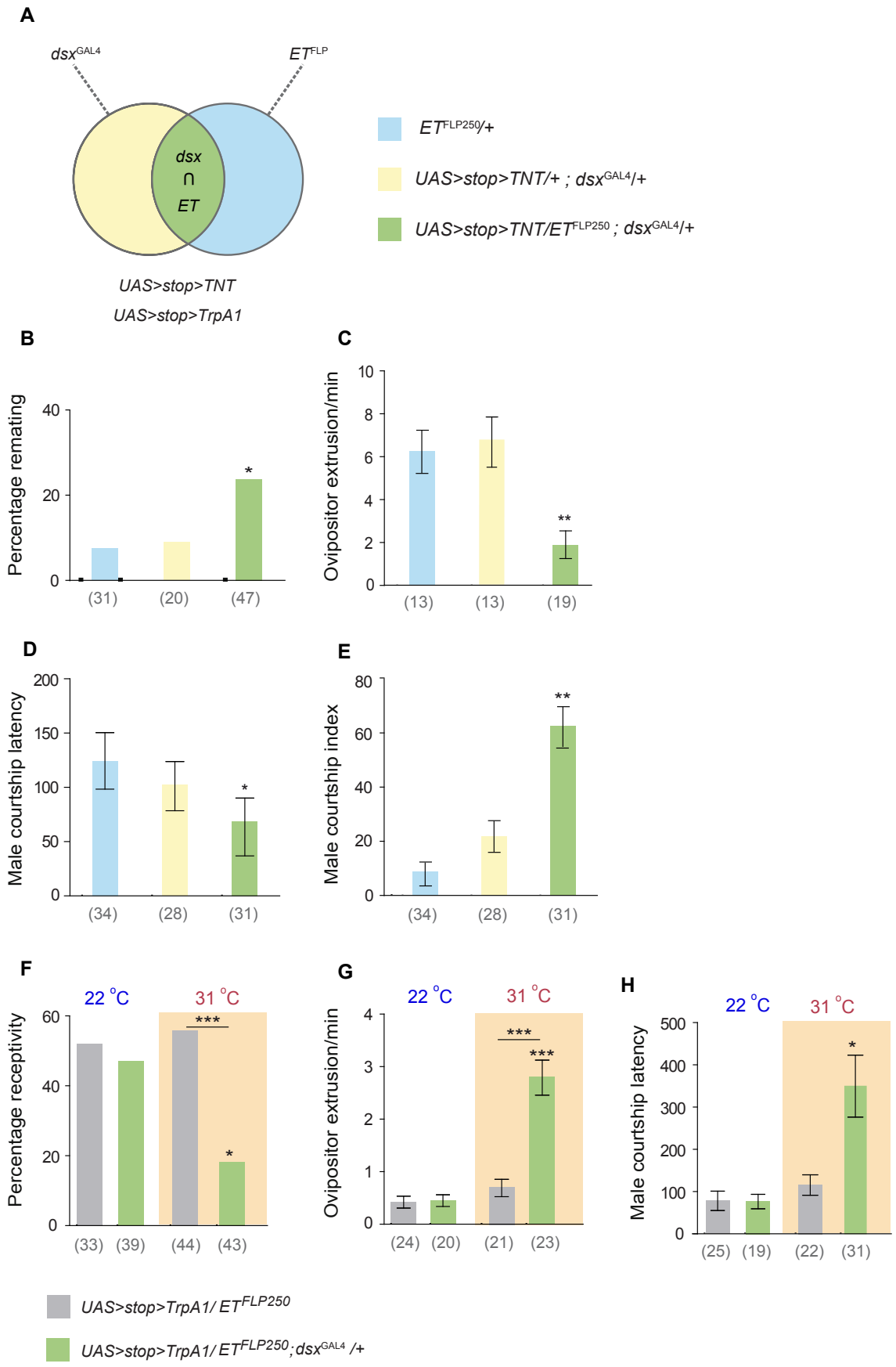
We implemented a FLP/FRT intersectional strategy (Bohm et al., 2012) to subdivide the *dsx* circuitry into functionally defined subsets of neurons underlying post-mating behaviours. This involves crossing an enhancer-trap FLP (ET^{FLP}) line with dsx^{GAL4} and a given reporter (*e.g., UAS>stop>mCD8::GFP)* or effector (*e.g., UAS>stop>TNT)* to express membrane-bound GFP or the synaptic vesicle blocker *TNT* in neurons in which FLP has excised the transcriptional stop cassette (>*stop*>) (Figure 6-9A). Screening a collection of ET^{FLP} lines specific to the nervous system by expressing *UAS>stop>TNT* in combination with dsx^{GAL4}, we identified one line (ET^{FLP250}) that showed robust impairment of post-mating behavioural responses.

Silencing ET^{FLP250}/dsx^{GAL4} intersecting neurons was sufficient to partially recapitulate the defects observed with fully silenced *dsx* circuitry (Rideout et al., 2010); $ET^{FLP250}/UAS>stop>TNT/dsx^{GAL4}$ mated females did not extrude their ovipositor to prevent copulation (Figure 6-9C), resulting in a significantly higher percentage of remating compared with mated controls (Figure 6-9B), and laid significantly fewer eggs in 48hr than mated controls (29.5 ± 2.2 n=30 vs. 42.2 ± 2.7 n=30 respectively). These mated females remained

highly attractive to males, demonstrated by decreased courtship latency and higher-than-usual levels of elicited courtship (Figure 6-9D,E).

If inhibiting *dsx* neural function interrupts post-mating behaviours in mated females, then activating these neurons may induce post-mating responses in virgin females. To address this, we expressed the heat-activated ion channel TrpA1 (*UAS-TrpA1*; (Hamada et al., 2008) in ET^{FLP250}/dsx^{GAL4} virgin females, and assessed the behavioural effects of transient neural activation. At the restrictive temperature, 22°C, ET^{FLP250}*/UAS>stop>TrpA1/* dsx^{GAL4} virgin females behaved indistinguishably from virgin controls (Figure 6-9F-H). At the permissive temperature, 31°C, thermal activation of these neurons resulted in reduced levels of receptivity (Figure 6-9F), and significantly higher levels of female rejection behaviours towards courting males (Figure 6-9G). Although levels of male courtship towards these females were unchanged (data not shown), a significant increase in courtship latency was observed (Figure 6-9H).

Figure 6-9 Intersecting *dsx* neurons critical for mediating post-mating behavioural responses. (A) Schematic of FLP/FRT intersectional strategy employed to subdivide *dsx* circuitry. Crossing an ET^{FLP} line with dsx^{GAL4} allows expression of the selected effectors, *UAS>stop>TNT or UAS>stop>TrpA1,* in all intersecting neurons (ET∩*dsx*) where FLP has excised the transcriptional stop cassette (>*stop*>). (B-E) Effects of silencing intersecting ET^{FLP250}/dsx^{GAL4} neurons on post-mating behaviours using *UAS>stop>TNT*. (B) Percentage remating (*P<0.01, Fisher exact test). (C) Ovipositor extrusion during courtship (**P<0.001, Kruskal-Wallis ANOVA test). (D) Male courtship latency (mean ± s.e.m., *P<0.01, Kruskal-Wallis ANOVA test). (E) Male courtship index of naïve males (**P<0.001, Kruskal-Wallis ANOVA test). Genotypes indicate mated females. Target males were wild-type. n values shown in parentheses. (F-H) Effects of artificially activating intersecting $ET^{FLP\ 250}/dsx^{GAL4}$ neurons on post-mating behaviours using *UAS>stop>TrpA*. (F) Percentage receptivity (*P<0.01, ***P<0.0001, Fisher exact test). (G) Ovipositor extrusion during courtship (***P<0.0001, Kruskal-Wallis ANOVA test). (H) Male courtship latency (*P<0.01, Kruskal-Wallis ANOVA test). Experiments were performed at the permissive and restrictive temperatures of 22°C and 31°C, respectively. Error bars indicate SEM. Genotypes indicate virgin females. Target males were wild-type. n values shown in parentheses. (Figure taken from Rezával et al., 2012).


A
dsx^GAL4
ET^FLP
dsx ∩ ET
UAS>stop>TNT
UAS>stop>TrpA1
ET^FLP250/+
UAS>stop>TNT/+ ; dsx^GAL4/+
UAS>stop>TNT/ET^FLP250 ; dsx^GAL4/+
B
Percentage remating
(31) (20) (47)
C
Ovipositor extrusion/min
(13) (13) (19)
D
Male courtship latency
(34) (28) (31)
E
Male courtship index
(34) (28) (31)
F
Percentage receptivity
22 °C
31 °C
(33) (39) (44) (43)
G
Ovipositor extrusion/min
22 °C
31 °C
(24) (20) (21) (23)
H
Male courtship latency
22 °C
31 °C
(25) (19) (22) (31)
UAS>stop>TrpA1/ ET^FLP250
UAS>stop>TrpA1/ ET^FLP250;dsx^GAL4 /+

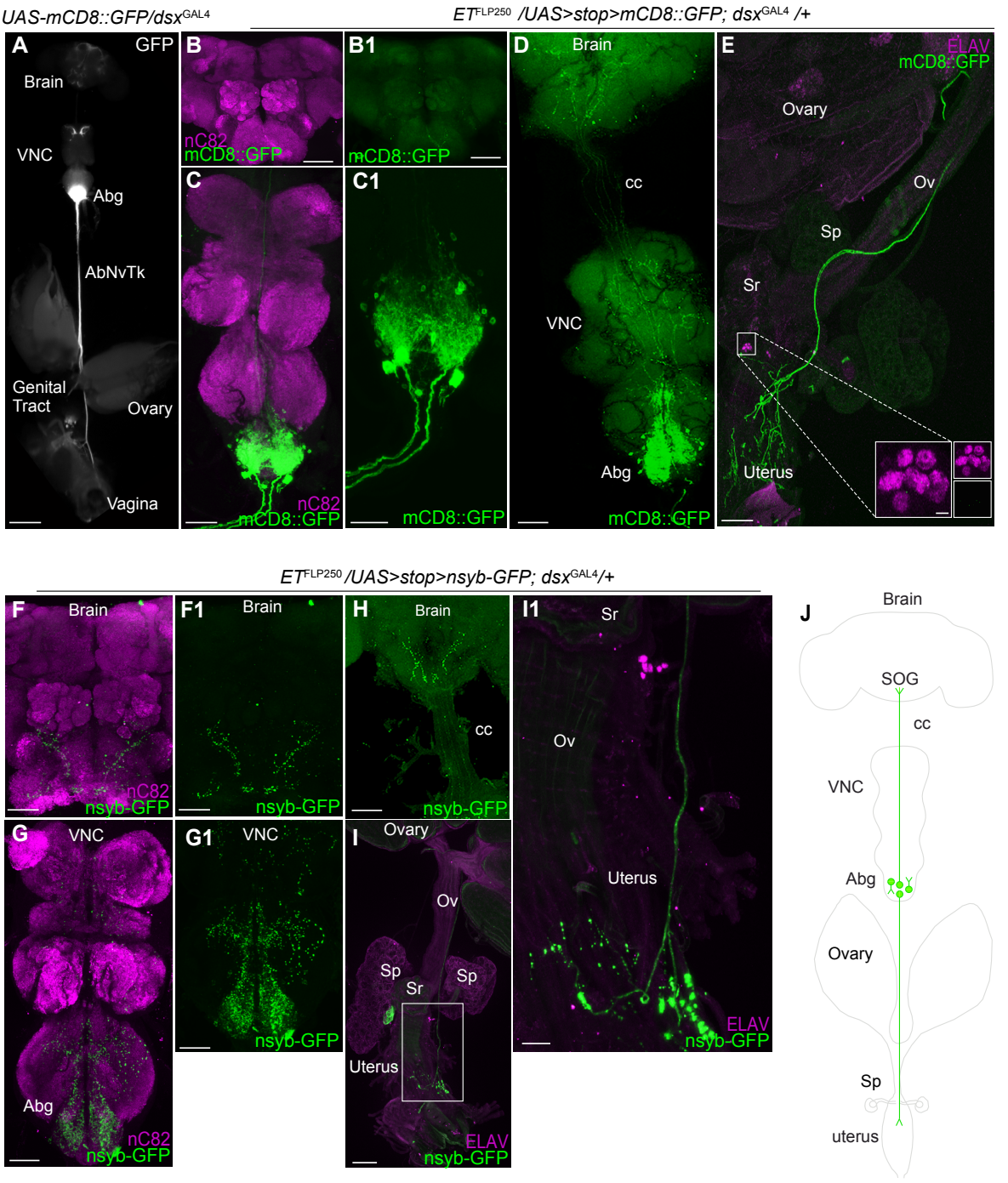


Figure 6-10 Characterization of intersected *dsx*-Abg neurons and associated projections.
(A) Epifluorescence of *dsx*^{GAL4}/*UAS-mCD8::GFP* female CNS with AbNvTk innervating the reproductive system. Scale bar = 200 µm. (B-I) Intersection of *dsx*^{GAL4}- neurons and *ET*^{FLP250} expressing (B-E) *UAS>stop>mCD8::GFP* or (F-I) *UAS>stop>nsyb-GFP* in 5 day old female CNSs and reproductive systems; (B) Female brain lacking *mCD8::GFP* expressing cell bodies, showing (B1) ascending neural projections innervating the SOG. (C) Female VNC showing ~27 *ET*$^{FLP\ 250}$/*dsx*^{GAL4} cell bodies and projections. (C1) Higher magnification of Abg (C). (D-E) Demonstration of *dsx* neural projections to (D) the brain and (E) the reproductive system. Inset in (E) higher magnification of anterior uterus depicting lack of *mCD8::GFP* expression in *dsx* sensory neurons. (F-G) Presynaptic arborisations of intersecting *dsx* neurons within the (F-FI) posterior SOG and (G-G1) VNC. (H) Cervical connection showing four ascending projections innervating the posterior SOG. (I) Presynaptic arborisations in the internal genitalia, with (I1) a higher resolution of (I) detailing terminalia ramifying on the uterus. (J) Schematic of intersected *dsx*-Abg neurons depicting (i) ascending neurons innervating the central brain, (ii) interneurons potentially conveying information to/from central circuits regulating female mating decisions and (iii) descending neurons innervating the uterus. GFP (green); neuropil counterstained with anti-nC82 (magenta); reproductive systems counterstained with anti-ELAV

(magenta). Abdominal ganglion (Abg), Abdominal nerve trunk (AbNvTk), Cervical connective (cc), Seminal receptacle (Sr), Spermathecae (Sp), Common oviduct (Ov) indicated. (A-I) Ventral views; anterior, top. (B-I) Scale bars = 50 µm. Scale bars in inset E = 10 µm. (Figure taken from Rezával et al., 2012).

6.2.6 *dsx*-Abg neurons involved in post-mating responses target the brain and reproductive system

To map the neurons responsible for this phenotype, we crossed ET^{FLP250} to the dsx^{GAL4} driver and the *UAS>stop>mCD8::GFP* reporter (Yu et al., 2010). mGFP expression was restricted to a small subset of *dsx* neurons within the Abg (27.4 ± 0.5 cells, n=30; of the ~300 Abg *dsx* neurons Figure 6-10C and C1); yet no cell bodies were detected in the majority of brain samples (13% ± 4 of them showed 1 cell stained with GFP, Figure 6-10B and B1), the reproductive system (n=18) (Figure 6-10E) and non-neural tissues (data not shown). These results show that 27 of the *dsx*-expressing Abg neurons are required for eliciting post-mating responses. Intriguingly, we identified ~four ascending *dsx*-Abg neural projections that terminate in the SOG (Figure 6-10D). Application of the presynaptic reporter *UAS>stop>nsyb-GFP* (Yu et al., 2010) in combination with ET^{FLP250} and dsx^{GAL4} revealed extensive presynaptic arborisations in the posterior SOG, where they likely form synapses (Figure 6-10F, F1 and H). These results suggest that ET^{FLP250}/*dsx* neurons in the Abg convey sensory information, such as stimuli from SP reception, to higher-order centres required for modulation of behavioural and physiological responses to mating.

We detected two descending projections from intersecting neurons in the Abg, which were found to innervate the uterus (Figure 6-10E), suggesting that these neurons may be involved in directing motor outputs to achieve specific post-mating responses, such as oviposition. *nsyb-GFP* expression confirmed presynaptic innervations of Abg-descending *dsx* neurons in the uterus (Figure 6-10I and I1). In addition, we detected a dense region of presynaptic innervations in the Abg (Figure 6-10G and G1), most likely reflecting the presence of localised *dsx* interneurons. From three-dimensional images of mCD8::GFP-labeled intersecting neurons we could determine the origin of the two descending projections to the reproductive system, and two of the four ascending projections to the brain (Figure 6-11).

Given the extensive dendritic arborizations of *ET*^{FLP250}/*dsx* neurons within the Abg, it was not possible to identify the exact origin of the two remaining ascending projections.

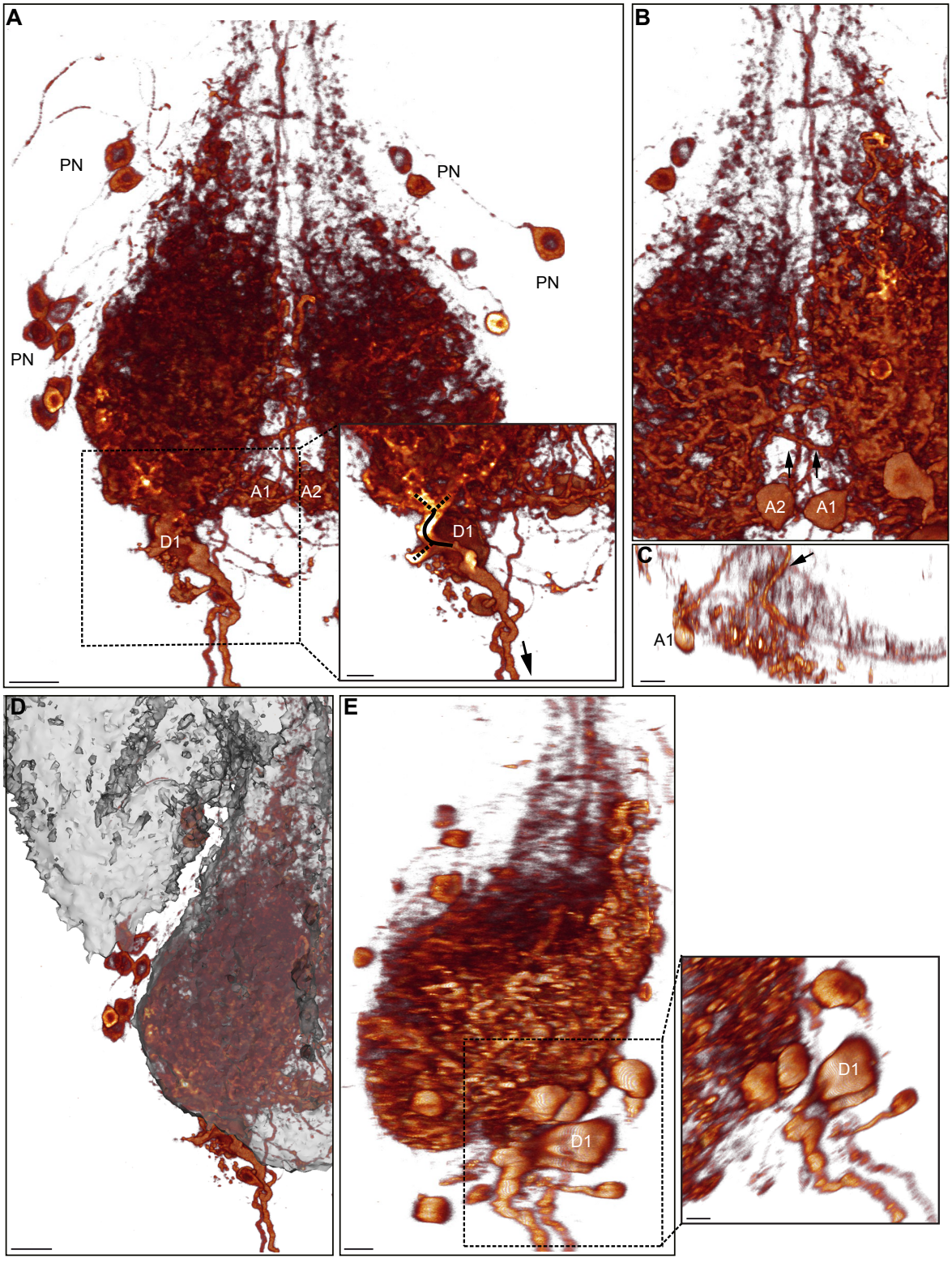


Figure 6-11 Three-dimensional images of a female Abg showing *ET*$^{FLP\ 250}$/*dsx*^{GAL4} neurons.
(A-D) Voltex rendered images of female Abgs illustrating neural topography of *ET*$^{FLP\ 250}$/*dsx*^{GAL4} intersected neurons and their associated neurites. (A) Abg (ventral view) showing *ET*$^{FLP\ 250}$/*dsx*^{GAL4} soma and associated extensive dendritic arborisations. A pair of centrally located dorsal neurons, A1 and A2, give rise to ascending projections terminating in the dorsal SOG. Additional ascending

projections are likely to originate from peripheral neurons (PN) indicated. D1 represents one of the bilaterally paired somas contributing to descending projections terminating on the uterus. A subset of confocal sections (inset of A) represents a magnified detail of Abg highlighting the D1 neuron. The D1 soma gives rise to a descending axonal projection, which ramifies on the internal genitalia (arrow), as well as extensive dendritic arborisation, formed from three branches (dashed lines) arising from a primary dendritic stem, within the Abg itself. (B) Midline of the Abg (dorsal view) showing A1 and A2 somas and their associated ascending projections (arrows) that ultimately target the brain. (C) A subset of confocal sections of the Abg (lateral view) highlights the A1 neuron (A2 out of plane of view). The A1 axon forms a characteristic dorsal loop (arrow) within in the Abg before extending to the anterior VNC. (D) Left half female Abg (ventral, coronal view) showing intersecting neurons (orange) and nc82 neuropil marker (grey). (E) Detail of left half female Abg (ventral, coronal view) highlighting descending projections of the D1 neuron. Inset in (D) is a magnified and rotated medio-lateral view of the D1 neuron and its descending axon and dendritic projections. Scale bars = 10 μm. (Figure taken from Rezával et al., 2012).

To evaluate if *dsx* intersecting neurons were sex-specific, we characterized ET^{FLP250}/*dsx* neurons in the male CNS. Whereas no neurons were found in the majority of brains stained (only 10% of brains showed a single neuron), only 4-5 *dsx* neurons (n=20) were found in the male Abg (Figure 6-12A and B). Most males show one ascending Abg neural projection running to the brain, and approximately 45% displayed two descending projections to the reproductive system (Figure 6-12 and data not shown, respectively). We also detected 1-2 cells of the male-specific *dsx*-TN1 neural cluster (Rideout et al., 2010) in the mesothoracic ganglion, which send projections that terminate in the SOG (Figure 6-12A and C). These results demonstrate clear sexual dimorphism, suggesting a specific role for female *dsx* Abg neurons in regulating sex-specific behaviours.

In summary, we have identified a *doublesex*-derived population of neurons in the Abg, which are critical for post-mating responses of *Drosophila melanogaster* females comprising (1) ascending neurons targeting the brain; (2) local interneurons; and (3) descending neurons innervating the reproductive system (see schematic Figure 6-10J). Our investigations suggest a compelling model whereby female-specific *dsx* neurons play a pivotal role in the coordinated regulation of behavioural and physiological responses following copulation; from reception of stimulatory inputs, transmission of these signals to higher-order centres for processing, to generation of the associated behavioural motor outputs.

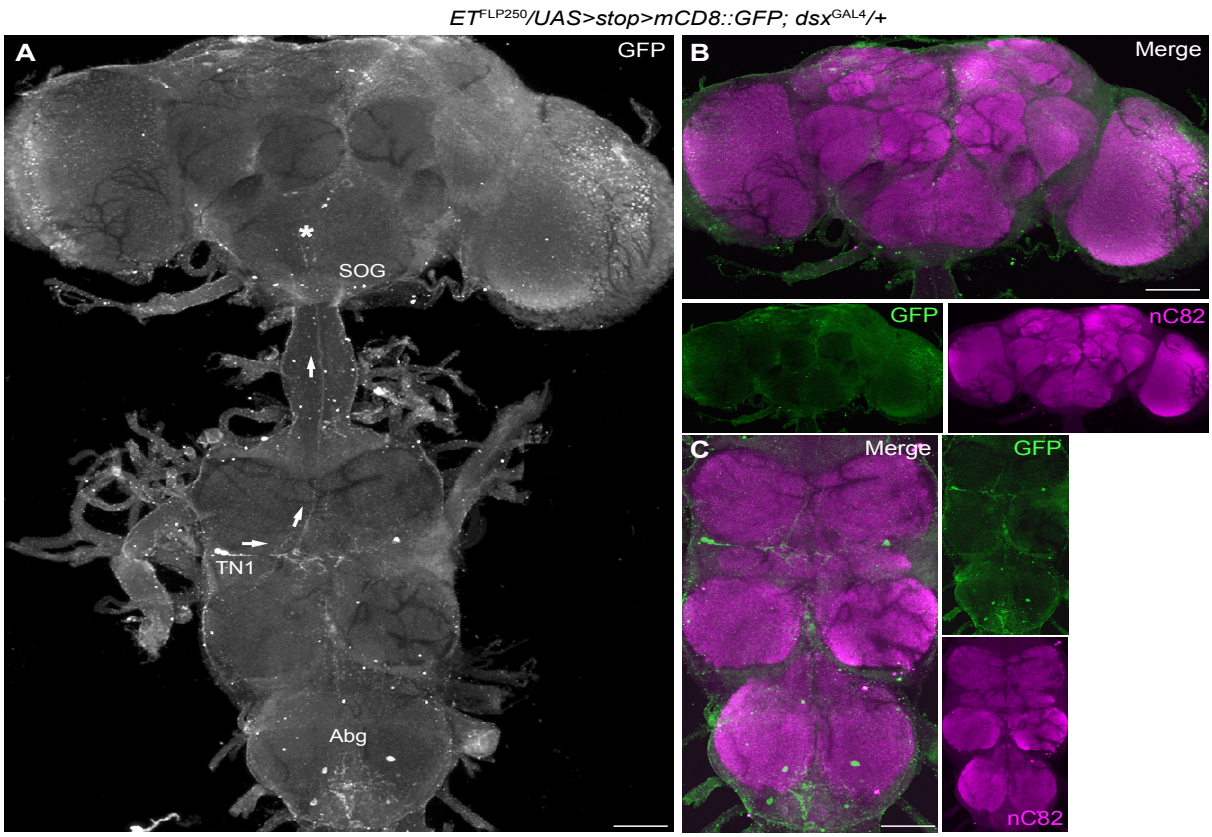


Figure 6-12 Membrane-bound GFP expression in *ET*$^{FLP\ 250}$/*dsx*^{GAL4} intersected neurons, and associated projections, in males.
(A-C) Intersection of *dsx*^{GAL4}-expressing neurons using *ET*^{FLP250} and *UAS>stop>mCD8::GFP* (green) in a 5 day old male CNS. (A) Male CNS exhibiting expression in *dsx* neurons in the VNC sending projections to innervate the posterior SOG. Note the male-specific *dsx*-TN1 neural cluster in the mesothoracic ganglion that sends projections through the cervical connective (arrows) terminating within the posterior SOG (asterisk). (B) Detail of brain from (A) demonstrating the absence of *mCD8::GFP* expressing neurons. (C) Detail of VNC from (A) exhibiting bilateral expression in TN1 neurons in the mesothoracic ganglion, in addition to 4 neurons in the Abg, with their respective projections. Neuropil counterstained with anti-nC82 (magenta). Ventral views; anterior, top. Scale bars = 50 µm. (Figure taken from Rezával et al., 2012).

6.3 Discussion

In this study we confirm the direct involvement of *dsx* neural circuitry in female post-mating responses, demonstrating that SP expression in *dsx* neurons is sufficient to induce a post-mating behavioural switch in virgin females, and that SPR expression in *dsx* neurons alone is sufficient for SP-induced post-mating behaviours. We also demonstrate *dsx* expression in most sensory neurons of the reproductive system, that not only forms a sub-population of the previously characterised *fru*$^{+}$/*ppk*$^{+}$ network, but also defines a more minimal SP-responsive neural circuit capable of inducing post-mating changes, such as reduced receptivity, increased levels of rejection, and egg-deposition, further refining the sensory circuitry

underlying the post-mating switch. These results indicate that *dsx* and *fru* shared circuitry is required for eliciting female post-mating responses.

Using an intersectional Flippase-recombinase approach to manipulate subsets of *dsx* neurons, we uncovered downstream *dsx* neural elements associated with this $dsx^{+}/fru^{+}/ppk^{+}$ uterine sensory cluster in the CNS involved in mediating post-mating responses. These *dsx* neurons in the Abg project to specific locations within the brain and the reproductive system. Our findings indicate that *dsx* circuitry not only consists of primary neurons required for sensing SP in the reproductive system, but also downstream effectors of the SP-sensory neural pathway that regulate post-copulatory behaviour of females. We propose that *dsx* neurons in the Abg act as relay neurons, transmitting SP information from the reproductive system to decision centres in the brain, and that additional *dsx* neurons in this area direct post-mating behaviours such as egg transport and oviposition.

In addition to these 'classic' post-mating behavioural responses, we also noted SP signalling to *dsx* neurons induces post-mating changes in locomotor activity between unmated and mated females. Studies have shown *Drosophila* males court immobilized females less than moving females; essentially males react to changes in female locomotion (Streisinger, 1948; Hall, 1978; Siegel and Hall, 1979; Tompkins et al., 1983), suggesting a causal link between female locomotion and increased courtship levels. It has been proposed that males are 'acoustically tuned' to signals generated by active females; stimulating increased courtship by changing the attention state of the male (Ejima and Griffith, 2008). Therefore, female mobility appears to contribute to her "sex appeal" and decreased locomotion in mated females is likely to affect the male's willingness to copulate.

6.3.1 SP-responsive sensory neurons regulate different aspects of the post-mating response

The female's nervous system must have the capacity to receive, and interpret, post-copulatory signals derived from the male seminal package to direct physiological and behavioural responses required for successful deposition of fertilised eggs. We demonstrated that two *dsx* clusters, composed of three bilateral neurons of the uterus,

comprise a more defined component of the SP-responsive sensory circuit. In addition, we have shown the majority of other *dsx* neurons originating on the internal genitalia to co-express *ppk*. As *ppk* neurons are mechanosensory (Adams et al., 1998; Grueber et al., 2003), these may be acting as uterine stretch receptors, facilitating sperm and egg transport, fertilization, and oviposition (Häsemeyer et al., 2009). Silencing neural function of *ppk* neurons appears to inhibit egg deposition, presumably by impeding egg transport along the oviducts (Yang et al., 2009). Similarly, in dsx^{GAL4} females expressing *TNT* no egg deposition is ever observed, with unfertilised eggs atrophying in the lateral oviducts (Rideout et al., 2010). In contrast, when fru^{+} neurons are silenced, deposition of successfully fertilised eggs is still observed (Yang et al., 2009), suggesting that different subsets of the $dsx^{+}/fru^{+}/ppk^{+}$ SP-responsive sensory circuit may direct distinct post-mating behavioural responses. As SP has been detected in the hemolymph of mated females (Pilpel et al., 2008), it has been suggested that SP could pass from the reproductive tract into the hemolymph to reach CNS targets (Kubli et al., 2003). The fact that neither receptivity nor oviposition was restored to control levels when *ppk-Gal80* (or *Cha-Gal80*) was expressed in dsx^{GAL4}/*UAS-mSP* flies opens the possibility that SP expression might affect additional *dsx* neurons in the CNS.

6.3.2 Co-expression of SPR and *dsx* in the female reproductive organs and potential functions in directing post-mating responses

Triggering of post-mating responses via SP reception appears to occur via a small number of neurons expressing SPR on the female reproductive tract (Häsemeyer et al., 2009; Yang et al., 2009); however, SPR is also found on surface regions of the CNS as well as in endocrine glands and other reproductive tissues (Yapici et al., 2008). Surprisingly, SPR may even be detected in the *Drosophila* male CNS where no exposure to SP would be expected, and in insects that apparently lack SP-like peptides (Yapici et al., 2009; Kim et al., 2010). SPRs are therefore potentially responsive to other ligands (Kim et al., 2010), performing functions other than those associated with post-mating responses in the diverse tissues in which SPRs are expressed.

We found extensive co-expression of *dsx*-expressing cells and SPR in the epithelium of the lower oviduct and spermathecae in females (Figure 6-4). However, mSP expression (or SPR downregulation) specifically in spermathecal secretory cells (SSC) (Schnakenberg et al., 2011) or oviduct epithelium cells (Lee et al., 2009) had no effect on receptivity or egg-laying (data not shown). In agreement with our rescue experiments using neural Gal80 drivers to intersect GAL4-responsive UAS expression in *dsx* cells, this suggests these cells are neither neural nor directly involved in SP-mediated post-mating behaviours (Figure 6-1, Figure 6-5, Figure 6-6). SPR staining in the CNS was more difficult to determine given the limitations of the antibody, while no co-localization in the brain was observed, apparent co-expression was observed between SPR and a small subset of ventral *dsx*-Abg neurons (Figure 6-4).

6.3.3 How does the female's CNS integrate information about reproductive status to switch behaviour and physiology post-copulation?

Our results indicate *dsx*-Abg neurons are required for the induction and regulation of specific components of the post-mating response. It has been shown that inhibition of neurotransmission in *apterous*-expressing Abg neurons impaired SP-mediated post-mating changes in receptivity and oviposition, emphasising the importance of these neurons in the modulation of post-mating responses (Soller et al., 2006).

The level of *dsx*-neural expression within the Abg and their associated fascicles projecting to the brain, where they form extensive presynaptic arborisations within the SOG, coupled with the effects that impairment of function in these neurons has on post-mating responses speaks to the involvement of these neurons in relaying information from the reproductive tract to the brain (Figure 6-10). That *dsx*-Abg neurons also project, and form presynaptic arborisations on the uterus, and the effects on post-mating responses when their function is impaired, again argues that these neurons play a direct role in mediating processes such as egg fertilization and oviposition. Interestingly, most *dsx* intersecting neurons are specific to females (Figure 6-10, Figure 6-12). Sex-specific behaviours can arise from either shared circuits between males and females that operate differently, and/or sex-specific circuits that

result from the presence/absence of unique circuit components in one sex *vs*. the other. Our results support the latter.

The VNC has been implicated in the modulation of post-mating responses, with an identified focus specifically involved in ovulation and transfer of eggs into the uterus for fertilization (Soller et al., 2006). Octopaminergic modulatory neurons located at the distal tip of the VNC projecting to the reproductive tract are required for triggering ovulation, possibly by regulating muscle contractions in the ovaries and oviducts (Monastirioti, 2003). Since ablation of the pars intercerebralis revealed an additional focus for egg-laying in the head (Bouletreau-Merle, 1976), and the brain appears to be required for sexual behaviours, such that decapitated virgin females neither mate nor lay eggs (Ejima et al., 2005), it seems likely that neurons in the Abg also require signals from the brain to regulate post-mating responses such as egg transport, fertilization and deposition.

6.3.4 Integrating Sensory Inputs

Higher-order circuits in the female brain must be capable of integrating sensory inputs from the olfactory, auditory, and reproductive systems to decide between the alternative actions of acceptance or rejection of the male. Early gynandromorph studies mapped a region of the dorsal brain that must be female for an animal to be receptive (Szabad and Fajszi, 1982); we have recently shown that the majority of *dsx*-neural clusters are located in this region (Rideout et al., 2010). While neurons co-expressing *dsx* and *fru* in male brains define a more restricted circuitry for determining male mating decisions, in females no overlap between dsx^{+} and fru^{+} neurons is observable in the brain (data not shown). It is also important to note that the sex-specific Fru isoform is absent in females, thus any circuits that are actively specified in the female are likely to depend on the female isoform Dsx^{F}. Most *dsx* neurons in the brain are found in the lateral protocerebrum, a region where multiple sensory inputs are thought to be integrated, and discrete motor actions selected and coordinated. Further high-resolution functional and connectivity mapping will help to define which neurons participate in specific pre- and post-mating behaviours in the female, allowing us to integrate circuit architecture with underlying cellular and synaptic properties. Future experiments will define,

what activity patterns trigger these behaviours, and what activity patterns correlate with these behaviours?

6.4 Conclusions

Our behavioural and neurogenetic analyses uncovered an essential role played by *dsx* neurons for regulating the female post-mating response. We uncovered shared circuitry between *dsx* and a subset of the previously described SP-responsive *fru*$^{+}$/*ppk*$^{+}$-expressing neurons in the reproductive system. We identified sexually dimorphic *dsx* circuitry within the abdominal ganglion (Abg) critical for mediating post-mating responses. Some of these *dsx* neurons target posterior regions of the brain while others project onto the uterus.

We propose that *dsx*-specified-circuitry is required to induce female post-mating behavioural responses; from sensing SP, to conveying this signal to higher-order circuits for processing, through to the generation of post-mating behavioural and physiological outputs.

7 Summary Discussion

7.1 Investigative summary

After considerable deliberation of the pros and cons of the different expression systems available in *Drosophila*, I selected to generate two genetically heritable transgenic tools for this study; the first tool being a novel *dsx*$^{GAL4\text{-}DBD}$ allele to exploit the ternary Split-GAL4 system (Luan et al., 2006), and the second being the novel *dsx*^{QF} allele to exploit the relatively novel Q binary system (Potter at al., 2010). The design of the GAL4-DBD and QF donor elements were based on the successful *dsx*-GAL4 donor element that was used in generating the original *dsx*^{GAL4} allele via ends-in homologous recombination (Rideout et al., 2010). These stratagems resulted in the recovery of a single *dsx*^{QF} integrant that was unable to maintain a healthy stock, and was therefore lost, and eleven *dsx*$^{GAL4\text{-}DBD}$ integrants that were recovered and verified by PCR.

In pursuing one of the *dsx*$^{GAL4\text{-}DBD}$ integrants, I validated the novel *dsx*$^{GAL4\text{-}DBD}$ allele as an accurate reporter of endogenous *dsx* gene expression; demonstrating its faithful recapitulation of *dsx* neural expression within the central nervous system (CNS) when paired with the pan neuronal hemi-driver *elav*$^{VP16\text{-}AD}$ (Luan et al., 2006). I performed a comprehensive survey of *dsx*$^{GAL4\text{-}DBD}$/ *elav*$^{VP16\text{-}AD}$ expression throughout development in the CNS of both sexes, providing a time line progression of the dynamic manner in which these neurons and neural clusters develop into the final adult expression pattern. This survey revealed significant neuroanatomical dimorphisms between males and females arising from differences in neural numbers in non-sex-specific clusters and in the presence of sex specific neurons and neural clusters. I also observed dimorphisms in the resulting neural architecture, with differences primarily exhibited in axonal density and connectivity associated with neural projections and synapses of *dsx* circuit elements. Altogether, these descriptions, in combination with comprehensive cell counts of the adult neural clusters, demonstrated the complete reiteration of previous descriptions of *dsx* expression (Lee et al., 2002; Sanders and Arbeitman, 2008; Rideout et al., 2010; Robinett et al., 2010).

To assess the extent of spatial restriction of expression offered by the intersection of the *dsx* and *elav* promoters, I compared patterns of *dsx*$^{GAL4\text{-}DBD}$/ *elav*$^{VP16\text{-}AD}$ expression to that of the

original *dsx*^{GAL4} outwith the CNS. I observed an overt lack of expression in sub-cuticular cells, oenocytes and fat body, and highly restricted patterns of expression in the reproductive system and alimentary tract. The concurrent expression *dsx*$^{GAL4\text{-}DBD}$/ *elav*$^{VP16\text{-}AD}$ in these tissues implied their neural origin, suggesting that these cells represent subsets of neurons of the peripheral nervous system (PNS).

As a tool that, for the first time, is demonstrably capable of reporting *dsx* expression in the PNS, I subsequently performed a comprehensive survey of *dsx*$^{GAL4\text{-}DBD}$/*elav*$^{VP16\text{-}AD}$-expression throughout the PNS of both sexes. I observed a restricted and dimorphic pattern of expression in neurons within the foreleg of males and females. The male-specific gustatory receptor neurons (GRNs) were observed to project to the mesothoracic gangilia (Msg), forming a male-specific contralateral pattern of projections (Possidente and Murphey, 1989; Mellert et al., 2010; Rideout et al., 2010). I also observed *dsx*$^{GAL4\text{-}DBD}$/*elav*$^{VP16\text{-}AD}$ expression within a restricted number of neurons the labellum of the mouthparts. Superficially, the number of neurons did not appear to differ between the sexes, however, their associated axonal arborisations and synapses within the suboesophageal ganigion (SOG) of the brain did appear to exhibit sexually dimorphic features; namely in the density of the axons, and the pattern of innervations. The dimorphisms in the connectivity of the *dsx*$^{GAL4\text{-}DBD}$/*elav*$^{VP16\text{-}AD}$ GRNs of the foreleg and labellum observed in this study begin to provide insight into how stimuli might undergo differential sensori-motor processing, contributing to the elicitation of sex-specific behavioural outputs.

Interestingly, I also observed expression of *dsx*$^{GAL4\text{-}DBD}$/*elav*$^{VP16\text{-}AD}$ in a subset of enteroendocrine cells of the midgut, implying that these cells require a sexual identity in their function. Though this observation is the first of its kind, this would make functional sense as nutrient requirements differ between males and mated females (Lee et al., 2013). These cells may play a key homeostatic role in modulating sex-specific nutrient preference and in modulating sex-peptide (SP) induced changes in female intestinal physiology imposed by mating (Lee et al., 2013; Cognini et al., 2011).

In a similar manner to altering female intestinal physiology, mating also induces a female post-mating behavioural switch (Kubli, 2003). Studies have shown a subset of proprioceptive neurons of the female uterus that express *fru,* sense SP post-mating, and are implicated in the regulation of female post-mating behavioural responses (Grueber et al., 2003; Grueber et al., 2007; Häsemeyer et al., 2009; Yang et al., 2009). In realising *dsx*$^{GAL4\text{-}DBD}$/*elav*$^{VP16\text{-}AD}$ expression in sensory neurons of the internal and external reproductive system of females, I, in conjunction with Dr. Carolina Rezával go on to show, that a subset of these *dsx*-expressing sensory neurons sense SP upon mating, making up part of the sensory report necessary to induce the female post-mating switch (Chapter 6; Rezával et al., 2012). When considered with the observed innervations to the internal genitalia by neurons of the Abg, it appears that the CNS may in return modulate the operation of these organs depending on the commands of decision-making neurons of the brain. Similar to females, sensory neurons of the internal and external reproductive system of males was also observed, as were innervations to the internal reproductive organs by neurons of the Abg. It is possible that sensory neurons of the reproductive system may also serve to indirectly modulate motor output specified by the Abg motoneurons, analogous to what has been demonstrated in the female.

Strikingly, motoneurons of the Abg did not only target the muscles of the reproductive systems, as innervations to sex-specific and non-sex-specific muscles of both the dorsal and ventral abdominal segment 6 (A6) were also reported. Revealing a previously uncharacterised facet of motor control specified by *dsx* circuitry. It may be postulated that appropriate motor control of these muscles may give rise to abdominal curling in the late steps of the male courtship repertoire, while in females, these neurons would serve to enable curling of her distal abdomen to deposit their eggs on food.

Finally, to assess the relative contribution of the NS to the performance of reproductive behaviours, I performed a series of behavioural assays on both male and female *dsx*$^{GAL4\text{-}DBD}$/*elav*$^{VP16\text{-}AD}$ flies. I demonstrated that the inhibition of *dsx*$^{GAL4\text{-}DBD}$/*elav*$^{VP16\text{-}AD}$ neural function in males leads to complete behavioural sterility in both males and females (Rideout et al.,

2010). Males presented with significant deficits in the early steps of courtship (orientation, following), and a complete absence of the later steps (wing extension, courtship song, and attempted copulation) of the courtship repertoire. Females appeared incapable of sampling the male's courtship display and of providing an acceptance response; even during copulation, a lack of female cooperation was evident by the continuous movement and rejections behaviours. That these females laid no eggs and remained incapable of actively rejecting further courtship evidenced by their propensity to re-mate, demonstrated that disruption of *dsx*$^{GAL4\text{-}DBD}$/*elav*$^{VP16\text{-}AD}$ neural function in females not only abrogated pre-mating behaviours, but also suppressed normal post-mating behaviours. Ultimately, these data demonstrated the fundamental necessity for *dsx* neural circuitry in the generation of both male and female reproductive behaviours.

The exhaustive interrogations carried out in Chapter 4 compellingly validated the novel *dsx*$^{GAL4\text{-}DBD}$ allele as a reporter of *dsx* expression; demonstrating that the novel pairing of *dsx*$^{GAL4\text{-}DBD}$ with the pan neuronal *elav*$^{VP16\text{-}AD}$ is capable of spatially restricting expression and genetic access to *dsx*-expressing neurons only. As such, I subsequently focused on utilising this novel allele to address the second aim of this thesis: parsing *dsx* neural circuitry into functionally distinct components.

Recent developments in thermogenetic technologies have lead to their universal use in establishing causal relationship between neurons and behaviour. Drawing on their ability to artificially activate neurons via a small temperature shift, studies have exploited thermogenetics to screen various transgenic lines for the elicitation of wild-type motor outputs, retroactively elucidating the function of the underlying neurons. To devise the stratagem that utilises thermogenetics to functionally parse *dsx* circuitry, I first sought to determine which behaviours are evoked, in both males and females, upon thermoactivation of the entire *dsx* circuitry. Hence, I drove the expression of temperature sensitive *UAS-dTrpA1* transgene under the control of *dsx*$^{GAL4\text{-}DBD}$/*elav*$^{VP16\text{-}AD}$. Shifting the temperature to the restrictive temperature of 30^{o}C resulted in the elicitation of all sub-behaviours of the courtship repertoire in males; while in females, no overt immediate behaviours were observed. To

exploit a thermogenetic approach requires the elicitation of a given behaviour upon thermoactivation; the fact that females did not display any obvious behavioural outputs restricted the efficacy of this approach to males only.

In light of these data, I subsequently focused on parsing *dsx* circuitry underlying male courtship behaviours. I employed this thermogenetic stratagem to screen a collection of ~410 enhancer trap VP16-AD lines ($ET^{VP16\text{-}AD}$), with the hope of isolating candidate lines that displayed spatially restricted clusters of *dsx*-expressing neurons. Driving the thermosensitive *UAS-dTrpA1* transgene under the control of different $dsx^{GAL4\text{-}DBD}/ET^{VP16\text{-}AD}$ combinations enabled the activation of intersected *dsx* neurons at will, whilst observing the behavioural outputs post-stimulation. Based on the fact that wing extension and abdominal curling behaviours are specified by distinct neural foci, I reasoned that the selection of lines that displayed either wing extension or abdominal curling exclusively, or that displayed overt deficits in either of these behaviours upon thermoactivation, would imply spatial restriction of *dsx* neural circuitry. Realising which neurons are expressed in these lines would correlate their activity with the elicitation of observed motor output. However, it is also important to note that correlations may also be made between neurons that appear to be absent in these lines; their absence not only suggesting their possible requirement in eliciting the behaviours that were not evoked, but also suggesting that these neurons are not necessary for the elicitation of the observed behavioural output. To this end, I retrieved 30 candidate lines that met the above-mentioned criteria.

Next, I performed neuroanatomical characterisations of nuclear GFP (nGFP) expression realised by each candidate hemidriver in combination with $dsx^{GAL4\text{-}DBD}$. Lines that displayed ectopic or overtly broad patterns of expression were omitted from subsequent investigations. Finally, a total of 6 candidate lines were found to express restricted patterns of nGFP in the CNS; of which three had elicited wing extension exclusively and three had elicited abdominal curling phenotypes upon thermoactivation. I carried out comprehensive cell counts of the neurons intersected by these lines to enable accurate comparisons to be carried out between the neurons intersected by each candidate line and the behaviours evoked by them.

Such comparisons correlated the presence of Msg clusers *dsx*-TN1 and a subset of *dsx*-TN2 in the elicitation of wing extension, and the presence of a subset of *dsx*-Abg neurons in the display of abdominal curling phenotypes. Unfortunately, large variations in the numbers and clusters of neurons in the brains of all 6 lines made it impossible to correlate their activity with either of the two behavioural outputs.

To assess the requirement of the intersected neurons in specifying distinct male courtship behaviours, each candidate hemidriver, in combination with $dsx^{GAL4\text{-}DBD}$, was used to drive the expression of the neural inhibitor, *UAS-TNT.* The behaviours of naïve males were subsequently examined in a standard courtship assay in the presence of a virgin female. The pathologies presented by these lines fell into one of two groups – i) severe disruption of both early and late steps of courtship that resulted in complete behavioural sterility – exhibited by 3 lines, and ii) deficits in the late steps of courtship with severe pathologies associated with the final stages of the courtship repertoire – also exhibited by 3 lines. Interesting, the grouping of these lines differed from those of the thermoactivation experiments.

A second round of neuroanatomical comparisons of these lines revealed a positive correlation between neural clusters in the brain, namely *dsx*-pC1, -pC2 and -pC3, and the behaviourally sterile phenotypes observed by 3 of the candidate lines. When considering candidate lines that displayed severe deficits in the final steps, two specific lines presented unique pathologies that correlated with neurons of the *dsx*-Abg. Suggesting that at least two functionally opposing clusters of neurons may exist within the *dsx*-Abg cluster: one to specify genital coupling, and a second to specify appropriate genital uncoupling post-copulation. Neuroanatomical and behavioural correlations of the final candidate line that displayed severe deficits in the late stages of courtship upon neural inhibition were inconclusive as extensive neurons were observed in both the brain and Abg.

Ultimately the results of this chapter demonstrated the success of this approach in correlating the activity of neural clusters with specific sub-behaviours of courtship. However, it is clear that the level of spatial restriction attained by these efforts were insufficient in establishing ‘cause and effect’ relationships between distinct clusters of neurons and single sub-

behaviours of the male courtship repertoire. Additional experiments that utilise these candidate lines would be essential to refine the resolution to single subsets of neurons that may then be functionally interrogated. Fortunately, the candidate lines retrieved here may be applied in diverse ways to achieve this; some of which I discuss later in this chapter.

In realising that the thermogenetic approach devised to parse *dsx* circuitry underling male behaviours was largely insufficient to perform analogous experiments in females, I, together with Dr. Carolina Rezával, devised an alternative strategy to parse *dsx* circuitry underlying female reproductive behaviours. We based this study on two interrelated findings; the observation that female post-mating responses are suppressed upon disruption of *dsx* neural function, and the observed $dsx^{GAL4\text{-}DBD}/elav^{VP16\text{-}AD}$-expression in sensory neurons of the female internal genitalia that appear topologically similar to the SP-responsive fru^{+}/ppk^{+}-expressing neurons that have previously been shown to mediate the female post-mating response. When considered together, these results implicated a role for *dsx* circuitry in specifying the female post-mating response.

We first confirmed the direct involvement of *dsx* neural circuitry in female post-mating responses, by demonstrating that SP expression in *dsx* neurons is sufficient to induce a post-mating behavioural switch in virgin females. This was further cemented by the fact that expression of sex-peptide receptor (SPR) expression in *dsx* neurons alone is also sufficient to induce SP-related post-mating behaviours. Subsequent neuroanatomical analyses revealed *dsx* expression in most sensory neurons of the reproductive system, including a sub-population of the previously characterised fru^{+}/ppk^{+} neurons located in the uterus. These data refined the sensory circuitry underlying the post-mating switch to a bilateral cluster of three $dsx^{+}/fru^{+}/ppk^{+}$ sensory neurons of the female reproductive tract. Demonstrating that *dsx* and *fru* shared circuitry is required for eliciting female post-mating responses.

Using an intersectional Flippase-recombinase approach to manipulate subsets of *dsx* neurons, we uncovered downstream *ds*x neuronal elements in the Abg, that are associated with the $dsx^{+}/fru^{+}/ppk^{+}$ uterine sensory cluster, and that appear to be involved in mediating these post-mating responses. We demonstrated that a subset of these sexually dimorphic

dsx-Abg neurons target posterior regions of the brain, while a second subset project onto the uterus. Indicating that *dsx* circuitry not only consists of primary neurons required for sensing SP in the reproductive system, but also downstream effectors of the SP-sensory neuronal pathway that regulate post-copulatory behaviour of females.

Altogether, these behavioural and neurogenetic analyses not only uncovered an essential role played by *dsx* neurons for regulating the female post-mating response, but also uncovered shared circuitry between *dsx* and a subset of the previously described SP-responsive fru^{+}/ppk^{+}-expressing neurons in the reproductive system. Future experiments that define command centres of the brain that ultimately direct the female post-mating behavioural switch, upon receipt of SP, may establish the logic by which neurons participate in specifying post-mating behaviours in the female.

7.2 Future experiments

Key to gaining further understanding about the organisation and operation of this dimorphic circuitry is continuing the process of functional mapping of both male and female circuitries. Central to this however, is refining manipulations to individual *dsx* neurons and/or neural clusters, to determine function, connectivity and the relationship each circuit element has with the surrounding neuroanatomy.

One approach using the extant $dsx^{GAL4\text{-}DBD}$ hemidriver, in conjunction with the $ET^{VP16\text{-}AD}$ lines isolated in this study, is to take advantage of an established stochastic bipartite strategy (von Philipsborn et al., 2011). By incorporating the expression of a heat-shock inducible Flippase (*hs*-FLP), FLP-mediated recombination is induced to excise the >*stop*> cassette in the *UAS*>*stop*>$dTrpA1^{myc}$ effector, ultimately restricting $dsx^{GAL4\text{-}DBD}$/$ET^{VP16\text{-}AD}$ driven expression of $dTrpA1^{myc}$ to a random subset neurons (von Philipsborn et al., 2011). The elegance of this approach comes from the fact that each unique animal can be both behaviourally and neuroanatomically characterised; using the thermosensitive dTrpA1 to render the neurons active and score for the elicitation of a given behaviour, and by using an antibody against the myc-tag to realise the neurons (and their associated projections) that are responsible for the observed behavioural output. Screenings numerous animals in this manner would allow for

correlations to be made between neurons that are repeatedly realised and the behaviour elicited by these animals. Unfortunately, that this approach entails the use of thermogenetics again limits the application of this methodology to males only.

Although thermoactivation of *dsx* neurons fails to elicit overt behaviours in females, silencing these neurons impairs both pre- and post-mating female behaviours. Illustrating that all functional interrogations of *dsx* neurons in females would require a neural silencing stratagem. Given that I systematically characterised both male and female expression patterns in all 30 $ET^{VP16\text{-}AD}$ candidate lines retrieved from the thermogenetic screen in Chapter 5, lines that reveal restricted patterns of expression in females may be used in combination with a neural silencing stratagem, to functionally dissect *dsx* circuitry underlying both pre- and post-mating behaviours. Expanding the use of these lines to study female behaviour may result in successful delineation of function of distinct subsets of *dsx*-expressing neural clusters.

Beyond this however, will be the requirement to generate novel hemidrivers that allow directed dissection of *dsx*-expressing tissues. Examples include $fru^{VP16\text{-}AD}$, to interrogate fru^{+}/dsx^{+} co-expressing neurons; neurotransmitter specific hemidrivers (e.g. octopaminergic $tbh^{VP16\text{-}AD}$ and GABAergic $Gad1^{VP16\text{-}AD}$ or $vGAT^{VP16\text{-}AD}$), to characterise neural cell types; tissue-specific drivers (*e.g.* oenocyte-specific $dsat1(PromE)^{VP16\text{-}AD}$ and fat body-specific $Lsp2^{VP16\text{-}AD}$) and chemosensory- or gustatory receptor-specific drivers (e.g. $poxn^{VP16\text{-}AD}$ and $Gr32^{VP16\text{-}AD}$) to interrogate *dsx* subtypes. Rapid generation of such lines is now possible by way of repurposing established enhancer trap or enhancer fusion lines via the convertible genetic platform that is the integrase swappable *in vivo* targeting element (InSITE; Gohl et al., 2011). This technology enables the replacement of GAL4 (or any other effector gene e.g. LexA, QF or FLP) with VP16-AD *in vivo*, without additional cloning, allowing for the preservation of the expression pattern of the original construct (Gohl et al., 2011). In the absence of such lines, novel transgenic VP16-AD drivers may need to be generated. An effective method to generate these lines would be to exploit the ribosomal-skipping mechanism of the viral T2A peptide that promotes translation of two proteins from a single

mRNA (Diao and White, 2012). This novel technology has been successful in generating novel GAL4 drivers by inserting a construct consisting of the T2A- and GAL4-coding sequences in-frame, into an exon of an endogenous gene; enabling the co-expression of both GAL4 and the endogenous gene in *Drosophila* (Diao and White, 2012). Although these lines were generated via ends-out homologous recombination, the authors are currently developing an *in vivo* system that circumvents the use of homologous recombination and enables the use of readily available MiMiC insertions (Venken, 2010) to introduce T2A-transgenes (including T2A-VP16-AD) into a coding intron of a gene of interest (Diao and White, pers. comm.).

Continuing with the use of extant transgenes, I demonstrated the successful utilisation of the dsx^{GAL4}, in combination with available enhancer-trap FLP lines (ET^{FLP}), in intersecting *dsx*-expressing neurons that mediate female post-mating behavioural responses (Chapter 6; Bohm et al., 2011). This scheme involved crossing an ET^{FLP} line with dsx^{GAL4} in the presence of a *UAS>stop>mCD8::GFP* reporter of either *UAS>stop>TNT* effectors to express membrane bound GFP or TNT in all intersecting neurons in which FLP has excised the transcriptional stop cassette (>*stop*>). By screening the novel ET^{FLP} collection (referred to as ET^{FLPX2}), these efforts may be expanded to further parse *dsx* circuitry in both males and females. As these lines contain an internal ribosome entry site (IRES) between tandem copies of FLP-encoding sequences (FLP-IRES-FLP), the FLP dosage is doubled, resulting in a higher percentage of ET^{FLPX2} lines that show unique, symmetrical and consistent expression patterns (Bohm et al., 2011).

To take advantage of the vast array of characterised GAL4 drivers and *UAS-effectors* however would require the generation of at least one of two novel transgenes: dsx^{FLP} and dsx^{LexA}. Targeted insertion of *Drosophila* codon-optimized FLP recombinase into the *dsx* locus by homologous recombination would create a dsx^{FLP} allele that drives FLP-mediated recombination specifically in *dsx* neurons. As such, preselected GAL4 drivers may be used in conjunction with the dsx^{FLP}, expressing *UAS>stop>reporters/effectors* in the intersecting cells where FLP has excised the transcriptional stop cassette (>*stop*>). In a similar manner,

targeted insertion of the coding sequence of LexA into the *dsx* locus by homologous recombination would serve to create the novel dsx^{LexA} allele that drives LexA specifically in *dsx* neurons. To achieve an intersection in expression requires the use of preselected GAL4 drivers in conjunction with the dsx^{LexA}, and the expression of both *UAS-FLP* and *LexAop>stop>reporters/effectors*. Active expression of the reporters/effectors is therefore achieved in intersecting cells where FLP has excised the transcriptional stop cassette (*>stop>*). The added bonus with this system is that it lends itself to the use of GRASP (Genetic Reconstitution Across Synaptic Partners; Feinberg et al., 2008; Gordon and Scott, 2009). This method detects potential synaptic connections based on the expression of two halves of a split-GFP on the outer membrane of distinct neuronal populations. While neither half of GFP fluoresces individually, GFP is reconstituted into a fluorescent molecule when the two cell membranes are close enough together, as in synapses. Each half of GFP is independently fused to a cell membrane targeting tag (CD4) and each portion is expressed in response to either the GAL4 or LexA transcriptional activators (*lexAop-CD4gfp11* and *UAS-CD4gfp1-10*; Gordon and Scott, 2009). By combining the dsx^{LexA} driver with extant GAL4 drivers that express in candidate post- and/or pre-synaptic partner neurons, it should be possibly to selectively label synaptic connections between candidate partners.

7.2.1 The *dsx* 'connectome'

The above-mentioned strategies present a retroactive approach to elucidate function in groups of neurons, as flies employed in these schemes must first undergo behavioural screens to assay for behavioural output(s) or deficit(s) prior to realising which neurons/tissues exhibit reporter expression. Identifying and assigning functional roles to the cells whose impairment/activation resulted in the associated behaviour. Unfortunately however, these prevalent approaches have failed to shed light on operative intricacies of a given circuit, as we have discovered little about the interpretation of sensory information, and the elements that mediate this. It is likely that sensory information from all modes of input (visual, taste, smell and hearing) converge within specific brain areas; yet, we have no knowledge of how processing centres of the CNS are capable of assigning 'weighting' effects

associated with any competing agonistic and antagonistic stimuli, to ultimately relay the correct information and elicit most appropriate behavioural outputs. The use of new technology, like optogenetics and thermogenetics (Bernstein et al. 2012) has been pivotal for the identification of command elements capable of eliciting courtship and song. It is essential however, that these methods of manipulating a defined neural circuit are complemented by other new optogenetic techniques, such as those that interrogate physiological connections between component neurons (Yao, et al. 2012). In future studies, the use of such strategies will allow the marrying of circuit architecture and underlying cellular and synaptic properties to further elucidate how neural pathways control behaviours. So what does the future hold? Pinching the logic from Olsen and Wilson's review (Olsen and Wilson 2008), "Cracking neural circuits in a tiny brain", we still need to:

- Functionally assign all *dsx*-neurons that participate in male and female reproductive behaviours (functional map)

- Establish the 'natural' response/activity pattern of these neurons during the execution of a precise behaviour (activity map)

- Determine the cellular, synaptic and circuit mechanisms underlying these neural transformations (connectivity map)

Ultimately, correlating the 'connectivity', 'functional' and 'activity' maps will provide the logic for how this, and other, dimorphic nervous systems might be coordinated with gender-appropriate physiology and sensori-motor tissues to generate sex-specific behavioural outputs. Only then may we begin to shed light on the relative values associated with each mode of sensory input, and identify compensatory mechanisms that may exist to allow for behavioural flexibility. Extrapolating models of circuit-organization to define how decisions are achieved to prioritise behavioural outputs in response to conflicting signals, and how experience may modify these behaviours, will enrich our understanding of the astonishing plasticity of nervous systems.

Appendix

Table of behaviours observed in enhancer trap VP16-AD screen.
1 denotes the presence of a given behaviour, and 0 denotes its absence.
- Candidates highlighted in blue displayed 'partial' abdominal curling phenotypes;
- Candidates highlighted in green display 'partial' behaviours in which faithful display of either wing extension or abdominal bending is observed, during which the alternative behaviour is simultaneously displayed in an unfaithful manner.

	OBSERVED BEHAVIOUR			
Stock	**Chaining**	**Wing**	**Abdominal**	**Comments**
N4A01	1	1	1	
N4A02	0	0	0	Negative control - 1st Chr
N4A03	0	0	0	Negative control - 1st Chr
N4A05	1	0	1	Partial abdominal curl
N4A06	0	0	0	Negative control - 1st Chr
N4A07	0	0	0	
N4A08	0	0	0	Negative control - 1st Chr
N4A10	1	1	1	Flicks wings
N4A11	0	0	0	Negative control - 1st Chr
N4A11B	1	1	1	
N4A16	0	0	0	Negative control - 1st Chr
N4A17A	0	0	0	Negative control - 1st Chr
N4A18	0	0	0	
N4A24	0	0	0	Negative control - 1st Chr
N4A28	0	0	0	Negative control - 1st Chr
N4A33A	1	1	1	
N4A33B	0	0	0	Negative control - 1st Chr
N4A34	1	1	1	
N4A38	0	0	0	Negative control - 1st Chr
N4A39	0	0	0	Negative control - 1st Chr
N4A41	0	0	0	Negative control - 1st Chr
N4A42	0	0	0	Negative control - 1st Chr
N4A43A	0	0	0	Negative control - 1st Chr
N4A43B	0	0	0	Negative control - 1st Chr
N4A44	0	0	0	Negative control - 1st Chr
N4A46	0	0	0	Negative control - 1st Chr
N4A47	0	0	0	Negative control - 1st Chr
N4A50	0	0	0	Negative control - 1st Chr
N4A51	0	0	1	Partial abdominal curl
N4A52	0	0	0	Negative control - 1st Chr
N4A56	0	0	0	Negative control - 1st Chr
N4A60	0	0	0	Negative control - 1st Chr
164	0	0	0	
165	1	0	1	
166A	0	0	0	
166RII	0	0	0	
166RIII	0	0	0	
167	0	0	0	
167RO	1	1	1	
167RWII	1	1	1	

168	1	1	1	
M169	1	1	1	Bilateral WE + Partail abdominal curl
170R	1	1	1	
171	1	1	1	
172II	1	1	1	
172	0	0	0	
173R	1	1	1	
174R	1	1	1	
175	0	0	0	
176	1	1	1	
177	0	0	0	
177RA	1	1	1	Partial abdominal curl
177RRII	1	1	1	
177RRIII	1	1	1	Partial abdominal curl
178R	1	0	0	
179	1	1	1	
180RII	0	0	0	
180RIII	0	0	0	
181	1	1	1	
182	1	1	1	
183	1	1	1	
184	1	1	1	Partial abdominal curl
186	0	0	0	
187	0	0	0	
189X	1	1	1	
189	1	1	1	
190	1	1	1	
191	0	0	0	
192	1	1	1	
196	1	1	1	Flicks wings
198	…	…	…	Dead stock
198R	1	1	1	
199	0	0	0	
200	0	0	0	
1	1	1	1	
2	1	1	1	Partial abdominal curl
4	0	0	0	
6	0	0	0	
7A	1	1	1	Flicks wings + partial abdominal curl
7RA	1	1	1	Flicks wings + partial abdominal curl
8	0	1	1	
10R	0	0	0	
10W	0	0	0	
12	1	1	1	
13	…	…	…	Dead stock
M18	…	0	0	Only single animal tested (unhealthy)
21	0	0	1	Partial abdominal curl
23	0	0	0	
27A	0	0	0	
27A	0	0	0	
27R	1	1	1	

28	0	0	0	
29	0	0	0	
30	1	1	1	
31	0	0	0	
32	1	1	1	Flicks wings + partial abdominal curl
34	1	1	1	
35	0	1	1	
37	1	1	1	
38	0	0	0	
39	0	0	1	Partial abdominal curl
40	0	0	0	
41	0	0	0	
42	0	1	1	Flicks wings
43	1	1	1	
44	0	0	0	
46	0	0	0	
47	0	0	1	
48	0	0	1	Partial abdominal curl
48RR	1	1	1	
48RW	1	1	1	Flicks wings + partial abdominal curl
M49	1	1	1	
49R	1	1	1	
50R	1	1	1	
50WII	1	1	1	
50WIII	1	1	1	
51	0	1	1	Flicks wings + partial abdominal curl
M52	0	0	0	
53	0	0	1	Partial abdominal curl
55	0	1	1	
57	0	0	0	
58	1	1	0	
59R	1	1	1	
60	0	0	0	
61	1	0	1	
61RA	1	0	0	
61RA	0	0	1	Partial abdominal curl
61RW	1	1	1	
62	0	0	0	
64	1	1	1	
64R	1	1	1	
65	1	1	1	
66	1	1	1	
66R	0	0	0	
68	0	0	0	
68R	0	0	0	
69	1	1	1	
70	1	1	1	
M70RA	0	0	0	
M70R	1	1	1	
71	1	1	1	
71WO	…	…	…	Dead stock

71R	0	0	0	
72	1	1	1	
72RW	1	1	1	Flicks wings
73	0	0	0	
74	0	0	0	
75	0	0	0	
75R	1	1	1	
76	0	1	1	Flicks wings + partial abdominal curl
76R	1	1	1	
77	0	0	0	
78	1	1	1	
79R	0	0	0	
79	0	1	0	
80	1	1	1	
81	0	0	1	Partial abdominal curl
82	1	1	1	
83A	0	1	1	Flicks wings + partial abdominal curl
83W	0	0	0	
84	0	1	1	
85	0	0	1	Flicks wings + partial abdominal curl
85M	0	1	1	
86	0	0	0	
87	0	0	0	
88R	1	1	1	Flicks wings
89	0	0	0	
89R	0	0	0	
90	1	1	1	
91	1	1	1	
92II	0	0	0	
92III	0	0	0	
92RA	1	1	1	
92RWII	1	1	1	
92RWIII	0	1	0	Flicks wings
94	0	0	0	
97	1	1	1	
98R	0	0	1	Partial abdominal curl
99	0	1	1	Flicks wings + partial abdominal curl
99II	0	1	1	Flicks wings + partial abdominal curl
99R	1	1	1	
100	0	0	0	
104II	0	0	0	
104	0	0	1	Partial abdominal curl
105	0	1	1	Partial abdominal curl
107	1	1	1	
109	0	0	0	
111	1	1	1	Flicks wings
112	0	1	1	Flicks wings
113	1	1	1	
114	0	1	1	Flicks wings + partial abdominal curl
115	1	1	1	
116	0	0	1	Partial abdominal curl

117	1	1	1	
117MR	0	0	0	
119	0	0	1	NB: 1st Chr???
120	1	1	1	
121	0	0	0	
126	0	0	0	
127	0	0	0	
128	0	0	0	
128R	0	0	0	
129	1	1	1	Partial abdominal curl
130	1	1	1	Partial abdominal curl NB: 1st Chr???
131	1	1	1	
134	0	0	0	
134R	1	1	1	
135	1	1	1	
136	0	0	0	
137	0	0	1	Partial abdominal curl
138	1	1	0	Group wing flicks
139	1	1	1	
140	0	0	0	
141	0	0	1	
142	0	0	0	
143	1	1	1	
144R	1	1	1	
145R	1	1	1	
145RA	0	0	0	
146R	1	1	1	
147	1	1	0	Orientation + Wing extension
148	0	0	0	
149LO	0	0	0	
149LR	1	1	1	
150	0	0	0	
150R	1	1	1	Group wing flicks + partial abdominal curl
151	0	0	1	Partial abdominal curl
152	…	…	…	Dead stock
152II	1	1	1	
152RIII	0	0	1	Partial abdominal curl
153	1	1	1	
154	0	0	0	
154RII	0	0	1	Partial abdominal curl
154RIII	1	1	1	
M154RA	1	1	1	
155	0	0	0	
155R	1	1	1	
156L	1	1	1	
156R	…	…	…	Dead stock
157	1	1	1	
158	0	0	0	
159	0	0	0	
160L	0	1	1	Flicks wings + partial abdominal curl
161	0	0	0	

161M	1	1	1	
161R	1	1	1	
162	0	0	0	
163	1	1	1	
N9A01	0	0	0	
N9A02	1	1	1	
N9A03	1	1	1	
N9A05	0	0	0	
N9A06	1	1	1	
N9A07	1	1	1	
N9A09B	0	0	1	Partial abdominal curl
N9A09C	1	1	1	
N9A10	0	0	0	
N9A11A	1	1	1	
N9A11B	0	0	0	
N9A12	1	1	1	
N9A12B	1	1	1	
N9A15	0	0	0	
N9A18	0	0	1	Partial abdominal curl
N9A21	0	0	0	
N9A22	0	0	1	Partial abdominal curl
N9A23	0	0	0	
N9A24	0	0	1	Partial abdominal curl
N9A25	0	0	1	
N9A27	1	1	1	
N9A29	0	0	1	Partial abdominal curl
N9A30	1	1	1	
N9A31B	0	0	0	
N9A36	1	1	1	
N9A37	0	0	0	
N9A38	0	0	0	
N9A39	0	0	0	
N9A40A	0	0	0	
N9A41	0	0	0	
N9A42B	1	1	1	
N9A42C	1	1	1	Extends wings in group only
N9A43	0	0	0	
N9A44A	0	0	0	
N9A45A	0	0	0	
N9A45B	1	1	1	
N9A46A	0	0	0	
N9A46B	1	1	1	
N9A47A	0	0	1	
N9A47B	1	1	1	
N9A48A	1	1	1	Flicks wings
N9A48B	…	…	…	Dead stock
N9A49	1	1	1	
N9A51C	0	0	1	Partial abdominal curl
N9A52	0	1	1	
N9A52R	0	0	0	
N9A53	0	0	0	

N9A54	1	1	1	
N9A56	0	0	0	
N9A57A	0	0	0	
N9A58	0	0	1	
N9A59	1	1	1	Flicks wings
N9A60	0	0	1	Partial abdominal curl
N9A61	0	0	1	
N9A62B	0	1	1	Flicks wings
N9A62C	1	1	1	
N9A63	0	0	0	
N9A64	1	1	1	Flicks wings + partial abdominal curl
N9A65	0	0	0	
N9A66A	0	0	0	
N9A67	0	0	0	
N9A68B	0	0	0	
N9A68C	0	0	1	
N9A69A	1	1	1	
N9A69B	0	0	0	
N9A70A	1	1	1	
N9A70B (3)	0	0	0	
N9A71A	0	0	1	Partial abdominal curl
N9A71A	0	0	1	Partial abdominal curl
N9A71B	0	0	1	Partial abdominal curl
N9A72A	1	1	1	
N9A72B	0	0	0	
N9A74B	0	1	1	
N9A74C	0	0	0	
N9A75A	1	1	1	
N9A75B	0	0	0	
N9A76B	1	1	1	
N9A77AA	1	1	1	
N9A77AB	1	1	1	
N9A77B	1	1	1	
N9A78	0	0	0	
N9A80B	0	0	0	
N9A80B	0	0	0	
N9A81A	1	1	1	
N9A81B	1	1	1	
N9A82A	0	0	0	
N9A84	1	1	1	
N9A88A	1	1	1	
N9A88B	1	1	1	
N9A89A	1	1	1	
N9A89B	0	0	1	Partial abdominal curl
N9A90A	0	0	0	
N9A90B	0	0	0	
N9A92A	0	0	0	
N9A92B	0	0	0	
N9A94B	0	0	0	
N9A96AA	…	…	…	Dead stock
N9A96AB	0	1	1	

N9A96B	0	1	1	
N9A99A	1	1	1	
N9A99B	0	0	0	
N9A100A	0	1	1	Flicks wings
N9A100B	0	0	1	Partial abdominal curl
N9B02AA	0	1	1	
N9B02AB	0	0	1	Partial abdominal curl
N9B03	0	0	0	
N9B04B	0	0	0	
N9B04C	1	1	1	
N9B05	0	0	0	
CH04	0	0	1	Partial abdominal curl
CH03	0	0	0	
BF69	0	0	1	Partial abdominal curl
BF62	0	0	1	Partial abdominal curl
BF59	0	0	1	Extreme curl
BF52	0	0	1	Partial abdominal curl
BF50	0	0	0	
BF49	0	1	1	Flicks wings + partial abdominal curl
AZ28	0	0	0	
BF41	0	0	0	
BF33S	0	0	0	
BF29	0	0	0	
BF22	0	0	0	
BF20	0	0	1	Partial abdominal curl
BF07	…	…	…	Dead cross
BF04	0	0	0	
BF01	0	1	1	Bilateral wing extension
AZ11	0	0	0	
AZ199	0	0	0	
AZ195	0	0	0	
AZ151	0	0	0	
AZ126	0	0	0	
AZ113	0	0	0	
AZ43	0	0	0	
AZ102	0	0	0	
AZ64	0	0	0	
AZ16	0	0	1	Extreme curl
AZ59	0	0	1	Partial abdominal curl
CH11	0	1	1	Bilateral wing extension
EG21	0	0	1	Partial abdominal curl
MB01	0	0	1	Extreme curl
MB13	0	0	0	
MB20	0	1	1	Slight unilateral WE + partial abdominal curl
MB23	0	0	0	
MB25S	0	0	0	
ML115	0	0	1	Partial abdominal curl
ML155	0	0	0	
ML153	0	1	1	Bilateral wing extension + partial abdominal curl
ML156	0	0	1	Extreme curl
SD01	1	1	1	

SD05S	0	0	0	
SD52	1	1	1	
VK01	0	0	0	
VK02	1	1	1	Wing extension not robust + Attempts to copulate
VK04	0	0	0	
VK29	0	1	0	Bilateral wing split (weird phenotype)
VK31	0	0	1	Partial abdominal curl
VK32	0	0	0	
VK33	0	0	1	Partial abdominal curl
VK35	0	0	0	
SD10	0	0	0	
VK361	1	1	1	
VK362	0	0	0	
AZ247	0	0	0	
AZ74	0	0	0	
VK36	0	0	0	

Bibliography

Acebes, A., Grosjean, Y., Everaerts, C., and Ferveur, J.F. (2004). Cholinergic control of synchronized seminal emissions in *Drosophila*. Curr Biol *14*, 704-710.

Adám, G., Perrimon, N., and Noselli, S. (2003). The retinoic-like juvenile hormone controls the looping of left-right asymmetric organs in *Drosophila*. Development *130*, 2397-2406.

Adams, C.M., Anderson, M.G., Motto, D.G., Price, M.P., Johnson, W.A., and Welsh, M.J. (1998). Ripped pocket and pickpocket, novel *Drosophila* DEG/ENaC subunits expressed in early development and in mechanosensory neurons. The Journal of cell biology *140*, 143-152.

Adams, E.M., and Wolfner, M.F. (2007). Seminal proteins but not sperm induce morphological changes in the *Drosophila melanogaster* female reproductive tract during sperm storage. J Insect Physiol *53*, 319-331.

Aguila, J.R., Suszko, J., Gibbs, A.G., and Hoshizaki, D.K. (2007). The role of larval fat cells in adult *Drosophila melanogaster*. J Exp Biol *210*, 956-963.

Ahmad, S.M., and Baker, B.S. (2002). Sex-specific deployment of FGF signaling in *Drosophila* recruits mesodermal cells into the male genital imaginal disc. Cell *109*, 651-661.

Ahuja, A., and Singh, R.S. (2008). Variation and evolution of male sex combs in *Drosophila*: nature of selection response and theories of genetic variation for sexual traits. Genetics *179*, 503-509.

Aigaki, T., Fleischmann, I., Chen, P.S., and Kubli, E. (1991). Ectopic expression of sex peptide alters reproductive behavior of female D. *melanogaster*. Neuron *7*, 557-563.

Aleksic, J., Lazic, R., Müller, I., Russell, S.R., and Adryan, B. (2009). Biases in *Drosophila melanogaster* protein trap screens. BMC Genomics *10*, 249.

Amrein, H., and Bray, S. (2003). Bitter-sweet solution in taste transduction. Cell *112*, 283-284.

Amrein, H., and Thorne, N. (2005). Gustatory perception and behavior in *Drosophila melanogaster*. Curr Biol *15*, R673-684.

An, W., Cho, S., Ishii, H., and Wensink, P.C. (1996). Sex-specific and non-sex-specific oligomerization domains in both of the doublesex transcription factors from *Drosophila melanogaster*. Mol Cell Biol *16*, 3106-3111.

An, X., Armstrong, J.D., Kaiser, K., and O'Dell, K.M. (2000). The effects of ectopic white and transformer expression on *Drosophila* courtship behavior. J Neurogenet *14*, 227-243,271.

Anand, A., Villella, A., Ryner, L.C., Carlo, T., Goodwin, S.F., Song, H.J., Gailey, D.A., Morales, A., Hall, J.C., Baker, B.S., et al. (2001). Molecular genetic dissection of the sex-specific and vital functions of the *Drosophila melanogaster* sex determination gene fruitless. Genetics *158*, 1569-1595.

Anholt, R.R., Lyman, R.F., and Mackay, T.F. (1996). Effects of single P-element insertions on olfactory behavior in *Drosophila melanogaster*. Genetics *143*, 293-301.

Arthur, B.I., Jallon, J.M., Caflisch, B., Choffat, Y., and Nöthiger, R. (1998). Sexual behaviour in *Drosophila* is irreversibly programmed during a critical period. Curr Biol *8*, 1187-1190.

Arbeitman, M.N., Kopp, A., Siegal, M.L., and Van Doren, M. (2010). Everything You Always Wanted to Know about Sex ... in Flies. Sexual development : genetics, molecular biology, evolution, endocrinology, embryology, and pathology of sex determination and differentiation.

Baker, B.S., Hoff, G., Kaufman, T.C., Wolfner, M.F., and Hazelrigg, T. (1991). The doublesex locus of *Drosophila melanogaster* and its flanking regions: a cytogenetic analysis. Genetics *127*, 125-138.

Baker, B.S., and Ridge, K.A. (1980). Sex and the single cell. I. On the action of major loci affecting sex determination in *Drosophila melanogaster*. Genetics *94*, 383-423.

Banghart, M., Borges, K., Isacoff, E., Trauner, D., Kramer, R,H. (2004). Light-activated ion channels for remote control of neuronal firing. Nat Neurosci *7*, 1381-1386.

Barmina, O., and Kopp, A. (2007). Sex-specific expression of a HOX gene associated with rapid morphological evolution. Dev Biol *311*, 277-286.

Barolo, S., Carver, L.A., and Posakony, J.W. (2000). GFP and beta-galactosidase transformation vectors for promoter/enhancer analysis in *Drosophila*. Biotechniques *29*, 726, 728, 730, 732.

Bellen, H.J., Tong, C., and Tsuda, H. (2010). 100 years of *Drosophila* research and its impact on vertebrate neuroscience: a history lesson for the future. Nat Rev Neurosci *11*, 514-522.

Bennet-Clark, H.C., and Ewing, A.W. (1967). Stimuli provided by Courtship of Male *Drosophila melanogaster*. Nature *215*, 669-671.

Benton, R., Vannice, K.S., Gomez-Diaz, C., and Vosshall, L.B. (2009). Variant ionotropic glutamate receptors as chemosensory receptors in *Drosophila*. Cell *136*, 149-162.

Benzer, S. (1973). Genetic dissection of behavior. Sci Am *229*, 24-37.

Bernstein, A.S., Neumann, E.K., and Hall, J.C. (1992). Temporal analysis of tone pulses within the courtship songs of 2 sibling *Drosophila* species, their interspecific hybrid, and behavioral mutants of *Drosophila melanogaster* (Diptera: Drosophilidae). J Insect Behav *5*, 15-36.

Bertram, M.J., Akerkar, G.A., Ard, R.L., Gonzalez, C., and Wolfner, M.F. (1992). Cell type-specific gene expression in the *Drosophila melanogaster* male accessory gland. Mech Dev *38*, 33-40.

Bi, X., and Rong, Y.S. (2003). Genome manipulation by homologous recombination in *Drosophila*. Brief Funct Genomic Proteomic *2*, 142-146.

Billeter, J.-C., Atallah, J., Krupp, J.J., Millar, J.G., and Levine, J.D. (2009). Specialized cells tag sexual and species identity in *Drosophila melanogaster*. Nature *461*, 987-991.

Billeter, J.-C., and Goodwin, S.F. (2004). Characterization of *Drosophila* fruitless-gal4 transgenes reveals expression in male-specific fruitless neurons and innervation of male reproductive structures. J Comp Neurol *475*, 270-287.

Billeter, J.-C., Goodwin, S.F., and O'Dell, K.M.C. (2002). Genes mediating sex-specific behaviors in *Drosophila*. Adv Genet *47*, 87-116.

Billeter, J.-C., Rideout, E.J., Dornan, A.J., and Goodwin, S.F. (2006). Control of male sexual behavior in *Drosophila* by the sex determination pathway. Curr Biol *16*, R766-776.

Billeter, J.-C., Villella, A., Allendorfer, J.B., Dornan, A.J., Richardson, M., Gailey, D.A., and Goodwin, S.F. (2006). Isoform-specific control of male neuronal differentiation and behavior in *Drosophila* by the fruitless gene. Curr Biol *16*, 1063-1076.

Bischof, J., Maeda, R.K., Hediger, M., Karch, F., and Basler, K. (2007). An optimized transgenesis system for *Drosophila* using germ-line-specific phiC31 integrases. Proceedings of the National Academy of Sciences of the United States of America *104*, 3312-3317.

Biteau, B., and Jasper, H. (2011). EGF signaling regulates the proliferation of intestinal stem cells in *Drosophila*. Development *138*, 1045-1055.

Boggs, R.T., Gregor, P., Idriss, S., Belote, J.M., and McKeown, M. (1987). Regulation of sexual differentiation in D. *melanogaster* via alternative splicing of RNA from the transformer gene. Cell *50*, 739-747.

Bohm, R.A., Welch, W.P., Goodnight, L.K., Cox, L.W., Henry, L.G., Gunter, T.C., Bao, H., and Zhang, B. (2010). A genetic mosaic approach for neural circuit mapping in *Drosophila*. Proc Natl Acad Sci USA *107*, 16378-16383.

Bownes, M. (1994). The regulation of the yolk protein genes, a family of sex differentiation genes in *Drosophila melanogaster*. Bioessays *16*, 745-752.

Brand, A. (1995). GFP in *Drosophila*. Trends Genet *11*, 324-325.

Brand, A.H., and Perrimon, N. (1993). Targeted gene expression as a means of altering cell fates and generating dominant phenotypes. Development *118*, 401-415.

Bray, S., and Amrein, H. (2003). A putative *Drosophila* pheromone receptor expressed in male-specific taste neurons is required for efficient courtship. Neuron *39*, 1019-1029.

Brent, R., and Ptashne, M. (1985). A eukaryotic transcriptional activator bearing the DNA specificity of a prokaryotic repressor. Cell *43*, 729-736.

Broughton, S.J., Kitamoto, T., and Greenspan, R.J. (2004). Excitatory and inhibitory switches for courtship in the brain of *Drosophila melanogaster*. Curr Biol *14*, 538-547.

Bullmore, E., and Sporns, O. (2009). Complex brain networks: graph theoretical analysis of structural and functional systems. Nat Rev Neurosci *10*, 186-198.

Burtis, K.C., and Baker, B.S. (1989). *Drosophila* doublesex gene controls somatic sexual differentiation by producing alternatively spliced mRNAs encoding related sex-specific polypeptides. Cell *56*, 997-1010.

Burtis, K.C., Coschigano, K.T., Baker, B.S., and Wensink, P.C. (1991). The doublesex proteins of *Drosophila melanogaster* bind directly to a sex-specific yolk protein gene enhancer. EMBO J *10*, 2577-2582.

Butler, B., Pirrotta, V., Irminger-Finger, I., and Nothiger, R. (1986). The sex-determining gene tra of *Drosophila*: molecular cloning and transformation studies. EMBO J *5*, 3607-3613.

Cabrera, G.R., Godt, D., Fang, P.-Y., Couderc, J.-L., and Laski, F.A. (2002). Expression pattern of Gal4 enhancer trap insertions into the bric à brac locus generated by P element replacement. Genesis *34*, 62-65.

Cachero, S., Ostrovsky, A.D., Yu, J.Y., Dickson, B.J., and Jefferis, G.S.X.E. (2010). Sexual Dimorphism in the Fly Brain. Current Biology *20*, 1589-1601.

Camara, N., Whitworth, C., and Van Doren, M. (2008). The creation of sexual dimorphism in the *Drosophila* soma. Curr Top Dev Biol *83*, 65-107.

Carhan, A., Allen, F., Armstrong, J.D., Hortsch, M., Goodwin, S.F., and O'Dell, K.M.C. (2005). Female receptivity phenotype of icebox mutants caused by a mutation in the L1-type cell adhesion molecule neuroglian. Genes Brain Behav *4*, 449-465.

Carreira, V.P., Mensch, J., and Fanara, J.J. (2009). Body size in *Drosophila*: genetic architecture, allometries and sexual dimorphism. Heredity *102*, 246-256.

Carvalho, G.B., Kapahi, P., Anderson, D.J., and Benzer, S. (2006). Allocrine modulation of feeding behavior by the Sex Peptide of *Drosophila*. Curr Biol *16*, 692-696.

Certel, S.J., Leung, A., Lin, C.-Y., Perez, P., Chiang, A.-S., and Kravitz, E.A. (2010). Octopamine neuromodulatory effects on a social behavior decision-making network in *Drosophila* males. PLoS ONE *5*.

Chan, Y.-B., and Kravitz, E.A. (2007). Specific subgroups of FruM neurons control sexually dimorphic patterns of aggression in *Drosophila melanogaster*. Proc Natl Acad Sci USA *104*, 19577-19582.

Chandler, D., McGuffin, M.E., Piskur, J., Yao, J., Baker, B.S., and Mattox, W. (1997). Evolutionary conservation of regulatory strategies for the sex determination factor transformer-2. Mol Cell Biol *17*, 2908-2919.

Chapman, T., Bangham, J., Vinti, G., Seifried, B., Lung, O., Wolfner, M.F., Smith, H.K., and Partridge, L. (2003). The sex peptide of *Drosophila melanogaster*: female post-mating responses analyzed by using RNA interference. Proc Natl Acad Sci U S A *100*, 9923-9928.

Chase, B.A., and Baker, B.S. (1995). A genetic analysis of intersex, a gene regulating sexual differentiation in *Drosophila melanogaster* females. Genetics *139*, 1649-1661.

Clyne, J.D., and Miesenböck, G. (2008). Sex-specific control and tuning of the pattern generator for courtship song in *Drosophila*. Cell *133*, 354-363.

Clynen, E., Ciudad, L., Bellés, X., and Piulachs, M.-D. (2011). Conservation of fruitless' role as master regulator of male courtship behaviour from cockroaches to flies. Dev Genes Evol *221*, 43-48.

Cognigni, P., Bailey, A.P., and Miguel-Aliaga, I. (2011). Enteric neurons and systemic signals couple nutritional and reproductive status with intestinal homeostasis. Cell metabolism *13*, 92-104.

Connolly, K., and Cook, R.M. (1973). Rejection responses by female *Drosophila melanogaster*: Their ontogeny, causality and effects upon the behavior of the courting male. Behavior *44*, 142-167.

Cook, R.M. (1977). Behavioral role of the sexcombs in *Drosophila melanogaster* and *Drosophila* simulans. Behav Genet *7*, 349-357.

Cook, R.M. (1979). The courtship tracking of *Drosophila melanogaster*. Biol Cybern *34*, 91-106.

Couderc, J.-L., Godt, D., Zollman, S., Chen, J., Li, M., Tiong, S., Cramton, S.E., Sahut-Barnola, I., and Laski, F.A. (2002). The bric à brac locus consists of two paralogous genes encoding BTB/POZ domain proteins and acts as a homeotic and morphogenetic regulator of imaginal development in *Drosophila*. Development *129*, 2419-2433.

Court, D.L., Sawitzke, J.A., and Thomason, L.C. (2002). Genetic engineering using homologous recombination. Annu Rev Genet *36*, 361-388.

Crickmore, M.A., and Vosshall, L.B. (2013). Opposing dopaminergic and GABAergic neurons control the duration and persistence of copulation in *Drosophila*. Cell *155*, 881-893.

Datta, S.R., Vasconcelos, M.L., Ruta, V., Luo, S., Wong, A., Demir, E., Flores, J., Balonze, K., Dickson, B.J., and Axel, R. (2008). The *Drosophila* pheromone cVA activates a sexually dimorphic neural circuit. Nature *452*, 473-477.

Dauwalder, B., Tsujimoto, S., Moss, J., and Mattox, W. (2002). The *Drosophila* takeout gene is regulated by the somatic sex-determination pathway and affects male courtship behavior. Genes Dev *16*, 2879-2892.

Davis, T., Kurihara, J., Yoshino, E., and Yamamoto, D. (2000). Genomic organisation of the neural sex determination gene fruitless (fru) in the Hawaiian species *Drosophila* silvestris and the conservation of the fru BTB protein-protein-binding domain throughout evolution. Hereditas *132*, 67-78.

de Vries, G.J., and Södersten, P. (2009). Sex differences in the brain: the relation between structure and function. Horm Behav *55*, 589-596.

DeFalco, T.J., Verney, G., Jenkins, A.B., McCaffery, J.M., Russell, S., and Van Doren, M. (2003). Sex-specific apoptosis regulates sexual dimorphism in the *Drosophila* embryonic gonad. Dev Cell *5*, 205-216.

Demir, E., and Dickson, B.J. (2005). fruitless splicing specifies male courtship behavior in *Drosophila*. Cell *121*, 785-794.

Dickson, B.J. (2008). Wired for sex: the neurobiology of *Drosophila* mating decisions. Science *322*, 904-909.

Dietzl, G., Chen, D., Schnorrer, F., Su, K.-C., Barinova, Y., Fellner, M., Gasser, B., Kinsey, K., Oppel, S., Scheiblauer, S., et al. (2007). A genome-wide transgenic RNAi library for conditional gene inactivation in *Drosophila*. Nature *448*, 151-156.

Ding, Z., Haussmann, I., Ottiger, M., and Kubli, E. (2003). Sex-peptides bind to two molecularly different targets in *Drosophila melanogaster* females. J Neurobiol *55*, 372-384.

Dornan, A.J. (2011). Structure/function analyses of neural circuitry controlling courtship behaviours in *Drosophila melanogaster*. In University of Glasgow, Volume D.Phil. (University of Glasgow).

Dornan, A.J., Gailey, D.A., and Goodwin, S.F. (2005). GAL4 enhancer trap targeting of the *Drosophila* sex determination gene fruitless. Genesis *42*, 236-246.

Duffy, J.B. (2002). GAL4 system in *Drosophila*: a fly geneticist's Swiss army knife. Genesis *34*, 1-15.

Ejima, A., Nakayama, S., and Aigaki, T. (2001). Phenotypic association of spontaneous ovulation and sexual receptivity in virgin females of *Drosophila melanogaster* mutants. Behav Genet *31*, 437-444.

Ejima, A., Smith, B.P., Lucas, C., van der Goes van Naters, W., Miller, C.J., Carlson, J.R., Levine, J.D., and Griffith, L.C. (2007). Generalization of courtship learning in *Drosophila* is mediated by cis-vaccenyl acetate. Curr Biol *17*, 599-605.

Engels, W.R. (1996). P Elements in *Drosophila* In Transposable Elements, H. Saedler and A. Gierl, eds. (Berlin: Springer-Verlag), pp. 103-123.

Erdman, S.E., and Burtis, K.C. (1993). The *Drosophila* doublesex proteins share a novel zinc finger related DNA binding domain. EMBO J *12*, 527-535.

Erdman, S.E., Chen, H.J., and Burtis, K.C. (1996). Functional and genetic characterization of the oligomerization and DNA binding properties of the *Drosophila* doublesex proteins. Genetics *144*, 1639-1652.

Ewing, A.W., and Bennet-Clark, H.C. (1968). The courtship songs of *Drosophila*. Behaviour *31*, 288-301.

Fahrbach, S.E. (2006). Structure of the mushroom bodies of the insect brain. Annu Rev Entomol *51*, 209-232.

Feinberg, E.H., Vanhoven, M.K., Bendesky, A., Wang, G., Fetter, R.D., Shen, K., and Bargmann, C.I. (2008). GFP Reconstitution Across Synaptic Partners (GRASP) defines cell contacts and synapses in living nervous systems. Neuron *57*, 353-363.

Ferveur, J.F., and Greenspan, R.J. (1998). Courtship behavior of brain mosaics in *Drosophila*. J Neurogenet *12*, 205-226.

Ferveur, J.F., Störtkuhl, K.F., Stocker, R.F., and Greenspan, R.J. (1995). Genetic feminization of brain structures and changed sexual orientation in male *Drosophila*. Science *267*, 902-905.

Fields, S., and Song, O. (1989). A novel genetic system to detect protein-protein interactions. Nature *340*, 245-246.

Fitzpatrick, M.J., Ben-Shahar, Y., Smid, H.M., Vet, L.E.M., Robinson, G.E., and Sokolowski, M.B. (2004). Candidate genes for behavioural ecology. Trends Ecol. Evol. *20*, 96-104.

Fleischmann, I., Cotton, B., Choffat, Y., Spengler, M., and Kubli, E. (2001). Mushroom bodies and post-mating behaviors of *Drosophila melanogaster* females. J Neurogenet *15*, 117-144.

Gailey, D.A., Billeter, J.-C., Liu, J.H., Bauzon, F., Allendorfer, J.B., and Goodwin, S.F. (2006). Functional conservation of the fruitless male sex-determination gene across 250 Myr of insect evolution. Mol Biol Evol *23*, 633-643.

Gailey, D.A., and Hall, J.C. (1989). Behavior and cytogenetics of fruitless in *Drosophila melanogaster*: different courtship defects caused by separate, closely linked lesions. Genetics *121*, 773-785.

Gailey, D.A., Ho, S.K., Ohshima, S., Liu, J.H., Eyassu, M., Washington, M.A., Yamamoto, D., and Davis, T. (2000). A phylogeny of the Drosophilidae using the sex-behaviour gene fruitless. Hereditas *133*, 81-83.

Gailey, D.A., Taylor, B.J., and Hall, J.C. (1991). Elements of the fruitless locus regulate development of the muscle of Lawrence, a male-specific structure in the abdomen of *Drosophila melanogaster* adults. Development *113*, 879-890.

Gao, G., McMahon, C., Chen, J., and Rong, Y.S. (2008). A powerful method combining homologous recombination and site-specific recombination for targeted mutagenesis in *Drosophila*. Proc Natl Acad Sci USA *105*, 13999-14004.

Gill, K.S. (1963). A mutation causing abnormal mating behaviour. *Drosophila* Information Service *38,* 33.

Gohl, D.M., Silies, M.A., Gao, X.J., Bhalerao, S., Luongo, F.J., Lin, C.-C., Potter, C.J., and Clandinin, T.R. (2011). A versatile in vivo system for directed dissection of gene expression patterns. Nat Methods *8*, 231-237.

Golic, K.G., and Lindquist, S. (1989). The FLP recombinase of yeast catalyzes site-specific recombination in the *Drosophila* genome. Cell *59*, 499-509.

Goodwin, S.F., Taylor, B.J., Villella, A., Foss, M., Ryner, L.C., Baker, B.S., and Hall, J.C. (2000). Aberrant splicing and altered spatial expression patterns in fruitless mutants of *Drosophila melanogaster*. Genetics *154*, 725-745.

Gordon, M.D., and Scott, K. (2009). Motor control in a *Drosophila* taste circuit. Neuron *61*, 373-384.

Greenspan, R.J., and Ferveur, J.F. (2000). Courtship in *Drosophila*. Annu Rev Genet *34*, 205-232.

Grillet, M., Dartevelle, L., and Ferveur, J.-F. (2006). A *Drosophila* male pheromone affects female sexual receptivity. Proc Biol Sci *273*, 315-323.

Grosjean, Y., Rytz, R., Farine, J.P., Abuin, L., Cortot, J., Jefferis, G.S., and Benton, R. (2011). An olfactory receptor for food-derived odours promotes male courtship in *Drosophila*. Nature *478*, 236-240.

Grueber, W.B., Ye, B., Yang, C.H., Younger, S., Borden, K., Jan, L.Y., and Jan, Y.N. (2007). Projections of *Drosophila* multidendritic neurons in the central nervous system: links with peripheral dendrite morphology. Development *134*, 55-64.

Gutierrez, E., Wiggins, D., Fielding, B., and Gould, A.P. (2007). Specialized hepatocyte-like cells regulate *Drosophila* lipid metabolism. Nature *445*, 275-280.

Hadjieconomou, D., Rotkopf, S., Alexandre, C., Bell, D.M., Dickson, B.J., and Salecker, I. (2011). Flybow: genetic multicolor cell labeling for neural circuit analysis in *Drosophila melanogaster*. Nat Methods *8*, 260-266.

Hall, J.C. (1977). Portions of the central nervous system controlling reproductive behavior in *Drosophila melanogaster*. Behav Genet *7*, 291-312.

Hall, J.C. (1979). Control of male reproductive behavior by the central nervous system of *Drosophila*: dissection of a courtship pathway by genetic mosaics. Genetics *92*, 437-457.

Hall, J.C., and Greenspan, R.J. (1979). Genetic analysis of *Drosophila* neurobiology. Annu Rev Genet *13*, 127-195.

Hamada, F.N., Rosenzweig, M., Kang, K., Pulver, S.R., Ghezzi, A., Jegla, T.J., and Garrity, P.A. (2008). An internal thermal sensor controlling temperature preference in *Drosophila*. Nature *454*, 217-220.

Hartenstein, V. (1993). Atlas of *Drosophila* Development. In The Development of *Drosophila*, M. Bate and A. Martinez-Arias, eds. (Cold Spring Harbor: Cold Spring Harbor Laboratory Press).

Häsemeyer, M., Yapici, N., Heberlein, U., and Dickson, B.J. (2009). Sensory neurons in the *Drosophila* genital tract regulate female reproductive behavior. Neuron *61*, 511-518.

Hastings, P.J., McGill, C., Shafer, B., and Strathern, J.N. (1993). Ends-in vs. ends-out recombination in yeast. Genetics *135*, 973-980.

Hasty, P., Rivera-Pérez, J., and Bradley, A. (1991). The length of homology required for gene targeting in embryonic stem cells. Mol Cell Biol *11*, 5586-5591.

Hasty, P., Rivera-Pérez, J., Chang, C., and Bradley, A. (1991). Target frequency and integration pattern for insertion and replacement vectors in embryonic stem cells. Mol Cell Biol *11*, 4509-4517.

Hausen, K., and Strausfeld, N.J. (1980). Sexually dimorphic interneuron arrangements in the fly visual system. Proc R Soc Lond B *208*, 57-71.

Hayes, S.A., Miller, J.M., and Hoshizaki, D.K. (2001). serpent, a GATA-like transcription factor gene, induces fat-cell development in *Drosophila melanogaster*. Development *128*, 1193-1200.

Heinrichs, V., Ryner, L.C., and Baker, B.S. (1998). Regulation of sex-specific selection of fruitless 5' splice sites by transformer and transformer-2. Mol Cell Biol *18*, 450-458.

Heisenberg, M. (2003). Mushroom body memoir: from maps to models. Nat Rev Neurosci *4*, 266-275.

Heisenberg, M., Heusipp, M., and Wanke, C. (1995). Structural plasticity in the *Drosophila* brain. J Neurosci *15*, 1951-1960.

Hempel, L.U., and Oliver, B. (2007). Sex-specific DoublesexM expression in subsets of *Drosophila* somatic gonad cells. BMC Dev Biol *7*, 113.

Hildreth, P.E. (1965). Fertilization in *Drosophila*. II. Time of inactivation of a gene effect. Proc Natl Acad Sci U S A *54*, 736-741.

Hoshijima, K., Inoue, K., Higuchi, I., Sakamoto, H., and Shimura, Y. (1991). Control of doublesex alternative splicing by transformer and transformer-2 in *Drosophila*. Science *252*, 833-836.

Hoshizaki, D.K., Lunz, R., Ghosh, M., and Johnson, W. (1995). Identification of fat-cell enhancer activity in *Drosophila melanogaster* using P-element enhancer traps. Genome *38*, 497-506.

Ilius, M., Wolf, R., and Heisenberg, M. (1994). The central complex of *Drosophila melanogaster* is involved in flight control: studies on mutants and mosaics of the gene ellipsoid body open. J Neurogenet *9*, 189-206.

Imai, T., Sakano, H., and Vosshall, L.B. (2010). Topographic mapping--the olfactory system. Cold Spring Harb Perspect Biol *2*, a001776.

Inagaki, H.K., Jung, Y., Hoopfer, E.D., Wong, A.M., Mishra, N., Lin, J.Y., Tsien, R.Y., Anderson, D.J. (2014). Optogenetic control of *Drosophila* using a red-shifted channelrhodopsin reveals experience-dependent influences on courtship. Nat Methods *11*, 325-332.

Ito, H., Fujitani, K., Usui, K., Shimizu-Nishikawa, K., Tanaka, S., and Yamamoto, D. (1996). Sexual orientation in *Drosophila* is altered by the satori mutation in the sex-determination gene fruitless that encodes a zinc finger protein with a BTB domain. Proceedings of the National Academy of Sciences of the United States of America *93*, 9687-9692.

Ito, K., Shinomiya, K., Ito, M., Armstrong, J.D., Boyan, G., Hartenstein, V., Harzsch, S., Heisenberg, M., Homberg, U., Jenett, A., Keshishian, H., Restifo, L.L., Rossler, W., Simpson,

J.H., Strausfeld, N.J., Strauss, R., Vosshall, L.B. (2014). A systematic nomenclature for the insect brain. Neuron *81*, 755-765.

Jallon, J.-M., Lauge, G., Orssaud, L., and Antony, C. (2008). Female pheromones in *Drosophila melanogaster* are controlled by the doublesex locus. 1-6.

Jefferis, G.S., Potter, C.J., Chan, A.M., Marin, E.C., Rohlfing, T., Maurer, C.R., Jr., and Luo, L. (2007). Comprehensive maps of *Drosophila* higher olfactory centers: spatially segregated fruit and pheromone representation. Cell *128*, 1187-1203.

Jones, W.D. (2009). The expanding reach of the GAL4/UAS system into the behavioral neurobiology of *Drosophila*. BMB Rep *42*, 705-712.

Kania, A., Salzberg, A., Bhat, M., D'Evelyn, D., He, Y., Kiss, I., and Bellen, H.J. (1995). P-element mutations affecting embryonic peripheral nervous system development in *Drosophila melanogaster*. Genetics *139*, 1663-1678.

Kawanishi, M., and Watanabe, T.K. (1980). Genetic variations of courtship song of *Drosophila melanogaster* and D. Simulans. Jap J Genet *55*, 235-240.

Kimura, K.-I. (2011). Role of cell death in the formation of sexual dimorphism in the *Drosophila* central nervous system. Dev Growth Differ *53*, 236-244.

Kimura, K.-I., Hachiya, T., Koganezawa, M., Tazawa, T., and Yamamoto, D. (2008). Fruitless and doublesex coordinate to generate male-specific neurons that can initiate courtship. Neuron *59*, 759-769.

Kimura, K.-I., Ote, M., Tazawa, T., and Yamamoto, D. (2005). Fruitless specifies sexually dimorphic neural circuitry in the *Drosophila* brain. Nature *438*, 229-233.

Kitamoto, T. (2001). Conditional modification of behavior in *Drosophila* by targeted expression of a temperature-sensitive shibire allele in defined neurons. J Neurobiol *47*, 81-92.

Kitamoto, T. (2002). Conditional disruption of synaptic transmission induces male-male courtship behavior in *Drosophila*. Proc Natl Acad Sci USA *99*, 13232-13237.

Koganezawa, M., Haba, D., Matsuo, T., and Yamamoto, D. (2010). The shaping of male courtship posture by lateralized gustatory inputs to male-specific interneurons. Curr Biol *20*, 1-8.

Kohatsu, S., Koganezawa, M., and Yamamoto, D. (2011). Female Contact Activates Male-Specific Interneurons that Trigger Stereotypic Courtship Behavior in *Drosophila*. Neuron *69*, 498-508.

Kondoh, Y., Kaneshiro, K.Y., Kimura, K.-I., and Yamamoto, D. (2003). Evolution of sexual dimorphism in the olfactory brain of Hawaiian *Drosophila*. Proc Biol Sci *270*, 1005-1013.

Kopp, A., and Duncan, I. (2002). Anteroposterior patterning in adult abdominal segments of *Drosophila*. Dev Biol *242*, 15-30.

Kopp, A., Duncan, I., Godt, D., and Carroll, S.B. (2000). Genetic control and evolution of sexually dimorphic characters in *Drosophila*. Nature *408*, 553-559.

Kramer, J.M., and Staveley, B.E. (2003). GAL4 causes developmental defects and apoptosis when expressed in the developing eye of *Drosophila melanogaster*. Genet Mol Res *2*, 43-47.

Krstic, D., Boll, W., and Noll, M. (2009). Sensory integration regulating male courtship behavior in *Drosophila*. PLoS ONE *4*, e4457.

Kubli, E. (1992). The sex-peptide. Bioessays *14*, 779-784.

Kubli, E. (2003). Sex-peptides: seminal peptides of the *Drosophila* male. Cell Mol Life Sci *60*, 1689-1704.

Kubli, E. (2008). Sexual behaviour: a receptor for sex control in *Drosophila* females. Curr Biol *18*, R210-212.

Kulkarni, S.J., and Hall, J.C. (1987). Behavioral and cytogenetic analysis of the cacophony courtship song mutant and interacting genetic variants in *Drosophila melanogaster*. Genetics *115*, 461-475.

Kuniyoshi, H., Baba, K., Ueda, R., Kondo, S., Awano, W., Juni, N., and Yamamoto, D. (2002). lingerer, a *Drosophila* gene involved in initiation and termination of copulation, encodes a set of novel cytoplasmic proteins. Genetics *162*, 1775-1789.

Kurtovic, A., Widmer, A., and Dickson, B.J. (2007). A single class of olfactory neurons mediates behavioural responses to a *Drosophila* sex pheromone. Nature *446*, 542-546.

Kvitsiani, D., and Dickson, B.J. (2006). Shared neural circuitry for female and male sexual behaviours in *Drosophila*. Curr Biol *16*, R355-356.

Kyriacou, C.P., and Hall, J.C. (1980). Circadian rhythm mutations in *Drosophila melanogaster* affect short-term fluctuations in the male's courtship song. Proc Natl Acad Sci USA *77*, 6729-6733.

Kyriacou, C.P., and Hall, J.C. (1982). The function of courtship song rhythms in *Drosophila*. Anim Behav *30*, 794-801.

Kyriacou, C.P., and Hall, J.C. (1986). Interspecific genetic control of courtship song production and reception in *Drosophila*. Science *232*, 494-497.

Lacaille, F., Hiroi, M., Twele, R., Inoshita, T., Umemoto, D., Manière, G., Marion-Poll, F., Ozaki, M., Francke, W., Cobb, M., et al. (2007). An inhibitory sex pheromone tastes bitter for *Drosophila* males. PLoS ONE *2*, e661.

Lai, S.-L., and Lee, T. (2006). Genetic mosaic with dual binary transcriptional systems in *Drosophila*. Nat Neurosci *9*, 703-709.

Lazareva, A.A., Roman, G., Mattox, W., Hardin, P.E., and Dauwalder, B. (2007). A role for the adult fat body in *Drosophila* male courtship behavior. PLoS Genet *3*, e16.

Lee, G., Foss, M., Goodwin, S.F., Carlo, T., Taylor, B.J., and Hall, J.C. (2000). Spatial, temporal, and sexually dimorphic expression patterns of the fruitless gene in the *Drosophila* central nervous system. J Neurobiol *43*, 404-426.

Lee, G., and Hall, J.C. (2001). Abnormalities of male-specific FRU protein and serotonin expression in the CNS of fruitless mutants in *Drosophila*. J Neurosci *21*, 513-526.

Lee, G., Hall, J.C., and Park, J.H. (2002). Doublesex gene expression in the central nervous system of *Drosophila melanogaster*. J Neurogenet *16*, 229-248.

Lee, G., Villella, A., Taylor, B.J., and Hall, J.C. (2001). New reproductive anomalies in fruitless-mutant *Drosophila* males: extreme lengthening of mating durations and infertility correlated with defective serotonergic innervation of reproductive organs. J Neurobiol *47*, 121-149.

Lee, H.-G., Seong, C.-S., Kim, Y.-C., Davis, R.L., and Han, K.-A. (2003). Octopamine receptor OAMB is required for ovulation in *Drosophila melanogaster*. Dev Biol *264*, 179-190.

Lee, T., and Luo, L. (1999). Mosaic analysis with a repressible cell marker for studies of gene function in neuronal morphogenesis. Neuron *22*, 451-461.

Lemaitre, B., and Miguel-Aliaga, I. (2013). The Digestive Tract of *Drosophila melanogaster*. Annu Rev Genet *47*, 377-404.

Lima, S.Q., and Miesenböck, G. (2005). Remote control of behavior through genetically targeted photostimulation of neurons. Cell *121*, 141-152.

Lin, H., Mann, K.J., Starostina, E., Kinser, R.D., and Pikielny, C.W. (2005). A *Drosophila* DEG/ENaC channel subunit is required for male response to female pheromones. Proc Natl Acad Sci U S A *102*, 12831-12836.

Liu, H., and Kubli, E. (2003). Sex-peptide is the molecular basis of the sperm effect in *Drosophila melanogaster*. Proc Natl Acad Sci USA *100*, 9929-9933.

Liu, W., and Hou, S.X. (2008). Genetic tools used for cell lineage tracing and gene manipulation in *Drosophila* germline stem cells. Methods Mol Biol *450*, 61-70.

Lu, B., LaMora, A., Sun, Y., Welsh, M.J., and Ben-Shahar, Y. (2012). ppk23-Dependent chemosensory functions contribute to courtship behavior in *Drosophila melanogaster*. PLoS Genet *8*, e1002587.

Luan, H., Peabody, N.C., Vinson, C.R., and White, B.H. (2006). Refined spatial manipulation of neuronal function by combinatorial restriction of transgene expression. Neuron *52*, 425-436.

Luo, L. (2007). Single-Neuron Labeling Using the Genetic MARCM Method. CSH Protoc *2007*, pdb.prot4789.

Ma, J., and Ptashne, M. (1987). The carboxy-terminal 30 amino acids of GAL4 are recognized by GAL80. Cell *50*, 137-142.

MacDougall, C., Harbison, D., and Bownes, M. (1995). The developmental consequences of alternate splicing in sex determination and differentiation in *Drosophila*. Dev Biol *172*, 353-376.

Mackay, T.F., Hackett, J.B., Lyman, R.F., Wayne, M.L., and Anholt, R.R. (1996). Quantitative genetic variation of odor-guided behavior in a natural population of *Drosophila melanogaster*. Genetics *144*, 727-735.

Mahr, A., and Aberle, H. (2006). The expression pattern of the *Drosophila* vesicular glutamate transporter: a marker protein for motoneurons and glutamatergic centers in the brain. Gene expression patterns : GEP *6*, 299-309.

Manning, A. (1959). The sexual isolation between *Drosophila melanogaster* and *Drosophila* simulans. Anim Behav *7*, 60-65.

Manoli, D.S., and Baker, B.S. (2004). Median bundle neurons coordinate behaviours during *Drosophila* male courtship. Nature *430*, 564-569.

Manoli, D.S., Foss, M., Villella, A., Taylor, B.J., Hall, J.C., and Baker, B.S. (2005). Male-specific fruitless specifies the neural substrates of *Drosophila* courtship behaviour. Nature *436*, 395-400.

Manoli, D.S., Meissner, G.W., and Baker, B.S. (2006). Blueprints for behavior: genetic specification of neural circuitry for innate behaviors. Trends Neurosci *29*, 444-451.

Mattox, W., Palmer, M.J., and Baker, B.S. (1990). Alternative splicing of the sex determination gene transformer-2 is sex-specific in the germ line but not in the soma. Genes Dev *4*, 789-805.

Mayer, J.R. (2006, April 3). Elements of Behavior. General Entomology ENT425, NC State University. Retreived December 3rd, 2013 from http://cals.ncsu.edu/course/ ent425/tutorial/Behavior/).

Mazzoni V, Anfora G, Virant-Doberlet M (2013) Substrate Vibrations during Courtship in Three *Drosophila* species. PLoS ONE *8(11),* e80708.

McGraw, L.A., Gibson, G., Clark, A.G., and Wolfner, M.F. (2004). Genes regulated by mating, sperm, or seminal proteins in mated female *Drosophila melanogaster*. Curr Biol *14*, 1509-1514.

McGuire SE, Le PT, Osborn AJ, Matsumoto K, Davis RL. (2003). Spatiotemporal rescue of memory dysfunction in *Drosophila*. Science *302,*1765-8.

McGuire, S.E., Roman, G., and Davis, R.L. (2004). Gene expression systems in *Drosophila*: a synthesis of time and space. Trends Genet *20*, 384-391.

McNabb, S.L., Baker, J.D., Agapite, J., Steller, H., Riddiford, L.M., and Truman, J.W. (1997). Disruption of a behavioral sequence by targeted death of peptidergic neurons in *Drosophila*. Neuron *19*, 813-823.

McRobert, S.P., and Tompkins, L. (1985). The effect of transformer, doublesex and intersex mutations on the sexual behavior of *Drosophila melanogaster*. Genetics *111*, 89-96.

McRobert, S.P., Tompkins, L., Barr, N.B., Bradner, J., Lucas, D., Rattigan, D.M., and Tannous, A.F. (2003). Mutations in raised *Drosophila melanogaster* affect experience-dependent aspects of sexual behavior in both sexes. Behav Genet *33*, 347-356.

Meinertzhagen, I.A., and Hanson, T.E. (1993). The development of the optic lob. In The development of *Drosophila melanogaster*, Volume II, M. Bate and A. Martinez-Arias, eds. (New York: Cold Spring Harbor Laboratory Press), pp. 1363-1491.

Melcher C & Pankratz MJ 2005 Candidate gustatory interneurons modulating feeding behavior in the *Drosophila* brain. PLoS Biology *3,* e305.

Mellert, D.J., Knapp, J.-M., Manoli, D.S., Meissner, G.W., and Baker, B.S. (2010). Midline crossing by gustatory receptor neuron axons is regulated by fruitless, doublesex and the Roundabout receptors. Development *137*, 323-332.

Micchelli, C.A., and Perrimon, N. (2006). Evidence that stem cells reside in the adult *Drosophila* midgut epithelium. Nature *439*, 475-479.

Miyamoto, T., and Amrein, H. (2008). Suppression of male courtship by a *Drosophila* pheromone receptor. Nat Neurosci *11*, 874-876.

Miyazaki, T., and Ito, K. (2010). Neural architecture of the primary gustatory center of *Drosophila melanogaster* visualized with GAL4 and LexA enhancer-trap systems. J Comp Neurol *518*, 4147-4181.

Moon, S.J., Lee, Y., Jiao, Y., and Montell, C. (2009). A *Drosophila* gustatory receptor essential for aversive taste and inhibiting male-to-male courtship. Curr Biol *19*, 1623-1627.

Moshitzky, P., Fleischmann, I., Chaimov, N., Saudan, P., Klauser, S., Kubli, E., and Applebaum, S.W. (1996). Sex-peptide activates juvenile hormone biosynthesis in the *Drosophila melanogaster* corpus allatum. Arch Insect Biochem Physiol *32*, 363-374.

Murphey, R.K., Possidente, D.R., Vandervorst, P., and Ghysen, A. (1989). Compartments and the topography of leg afferent projections in *Drosophila*. J Neurosci *9*, 3209-3217.

Nagoshi, R.N., and Baker, B.S. (1990). Regulation of sex-specific RNA splicing at the *Drosophila* doublesex gene: cis-acting mutations in exon sequences alter sex-specific RNA splicing patterns. Genes Dev *4*, 89-97.

Nassel, D.R. (1999). Tachykinin-related peptides in invertebrates: a review. Peptides *20*, 141-158.

Nayak, S.Y., and Singh, R.N. (1983). Sensilla on the tarsal segments and mouthparts of adult *Drosophila melanogaster* meigen (Diptera: Drosophilidae). Int. J. Insect Morphol. Embryol. *12*, 273–291.

Neckameyer, W.S., Coleman, C.M., Eadie, S., and Goodwin, S.F. (2007). Compartmentalization of neuronal and peripheral serotonin synthesis in *Drosophila melanogaster*. Genes Brain Behav *6*, 756-769.

Ng, C.S., and Kopp, A. (2008). Sex combs are important for male mating success in *Drosophila melanogaster*. Behav Genet *38*, 195-201.

O'Dell, K.M., Armstrong, J.D., Yang, M.Y., and Kaiser, K. (1995). Functional dissection of the *Drosophila* mushroom bodies by selective feminization of genetically defined subcompartments. Neuron *15*, 55-61.

Ohlstein, B., and Spradling, A. (2006). The adult *Drosophila* posterior midgut is maintained by pluripotent stem cells. Nature *439*, 470-474.

Ohlstein, B., and Spradling, A. (2007). Multipotent *Drosophila* intestinal stem cells specify daughter cell fates by differential notch signaling. Science *315*, 988-992.

Pan, Y., Meissner, G.W., and Baker, B.S. (2012). Joint control of *Drosophila* male courtship behavior by motion cues and activation of male-specific P1 neurons. Proc Natl Acad Sci U S A *109*, 10065-10070.

Pan, Y., Robinett, C.C., and Baker, B.S. (2011). Turning males on: activation of male courtship behavior in *Drosophila melanogaster*. PLoS One *6*, e21144.

Pavlou, H.J., and Goodwin, S.F. (2013). Courtship behavior in *Drosophila melanogaster*: towards a 'courtship connectome'. Curr Opin Neurobiol *23*, 76-83.

Peabody, N.C., Pohl, J.B., Diao, F., Vreede, A.P., Sandstrom, D.J., Wang, H., Zelensky, P.K., and White, B.H. (2009). Characterization of the decision network for wing expansion in *Drosophila* using targeted expression of the TRPM8 channel. J Neurosci *29*, 3343-3353.

Peixoto, A.A., Costa, R., and Hall, J.C. (2000). Molecular and behavioral analysis of sex-linked courtship song variation in a natural population of *Drosophila melanogaster*. J Neurogenet *14*, 245-256.

Peng, J., Chen, S., Büsser, S., Liu, H., Honegger, T., and Kubli, E. (2005). Gradual release of sperm bound sex-peptide controls female postmating behavior in *Drosophila*. Curr Biol *15*, 207-213.

Peng, J., Zipperlen, P., and Kubli, E. (2005). *Drosophila* sex-peptide stimulates female innate immune system after mating via the Toll and Imd pathways. Curr Biol *15*, 1690-1694.

Petersen, U.M., Kadalayil, L., Rehorn, K.P., Hoshizaki, D.K., Reuter, R., and Engström, Y. (1999). Serpent regulates *Drosophila* immunity genes in the larval fat body through an essential GATA motif. EMBO J *18*, 4013-4022.

Pfeiffer, B.D., Jenett, A., Hammonds, A.S., Ngo, T.-T.B., Misra, S., Murphy, C., Scully, A., Carlson, J.W., Wan, K.H., Laverty, T.R., et al. (2008). Tools for neuroanatomy and neurogenetics in *Drosophila*. Proc Natl Acad Sci USA *105*, 9715-9720.

Pfeiffer, B.D., Ngo, T.-T.B., Hibbard, K.L., Murphy, C., Jenett, A., Truman, J.W., and Rubin, G.M. (2010). Refinement of tools for targeted gene expression in *Drosophila*. Genetics *186*, 735-755.

Possidente, D.R., and Murphey, R.K. (1989). Genetic control of sexually dimorphic axon morphology in *Drosophila* sensory neurons. Dev Biol *132*, 448-457.

Potter, C.J., and Luo, L. (2011). Using the Q system in *Drosophila melanogaster*. Nat Protoc *6*, 1105-1120.

Potter, C.J., Tasic, B., Russler, E.V., Liang, L., and Luo, L. (2010). The Q system: a repressible binary system for transgene expression, lineage tracing, and mosaic analysis. Cell *141*, 536-548.

Pulver, S.R., Pashkovski, S.L., Hornstein, N.J., Garrity, P.A., and Griffith, L.C. (2009). Temporal dynamics of neuronal activation by Channelrhodopsin-2 and TRPA1 determine behavioral output in *Drosophila* larvae. J Neurophysiol *101*, 3075-3088.

Ram, K.R., and Wolfner, M.F. (2007). Sustained post-mating response in *Drosophila melanogaster* requires multiple seminal fluid proteins. PLoS Genet *3*, e238.

Raymond, C.S., Murphy, M.W., O'Sullivan, M.G., Bardwell, V.J., and Zarkower, D. (2000). Dmrt1, a gene related to worm and fly sexual regulators, is required for mammalian testis differentiation. Genes Dev *14*, 2587-2595.

Raymond, C.S., Shamu, C.E., Shen, M.M., Seifert, K.J., Hirsch, B., Hodgkin, J., and Zarkower, D. (1998). Evidence for evolutionary conservation of sex-determining genes. Nature *391*, 691-695.

Rein, K., Zöckler, M., Mader, M.T., Grübel, C., and Heisenberg, M. (2002). The *Drosophila* standard brain. Curr Biol *12*, 227-231.

Rezaval, C., Pavlou, H.J., Dornan, A.J., Chan, Y.B., Kravitz, E.A., and Goodwin, S.F. (2012). Neural circuitry underlying *Drosophila* female postmating behavioral responses. Curr Biol *22*, 1155-1165.

Rezával, C., Werbajh, S., and Ceriani, M.F. (2007). Neuronal death in *Drosophila* triggered by GAL4 accumulation. Eur J Neurosci *25*, 683-694.

Ribeiro, C., and Dickson, B.J. (2010). Sex Peptide Receptor and Neuronal TOR/S6K Signaling Modulate Nutrient Balancing in *Drosophila*. Curr Biol *20*, 1000-1005.

Rideout, E.J., Dornan, A.J., Neville, M.C., Eadie, S., and Goodwin, S.F. (2010). Control of sexual differentiation and behavior by the doublesex gene in *Drosophila melanogaster*. Nat Neurosci *13*, 458-466.

Ritchie, M., Townhill, R., and Hoikkala, A. (1998). Female preference for fly song: playback experiments confirm the targets of sexual selection. Anim Behav *56*, 713-717.

Ritchie, M.G., Halsey, E.J., and Gleason, J.M. (1999). *Drosophila* song as a species-specific mating signal and the behavioural importance of Kyriacou & Hall cycles in D. *melanogaster* song. Anim Behav *58*, 649-657.

Robinett, C.C., Vaughan, A.G., Knapp, J.-M., and Baker, B.S. (2010). Sex and the single cell. II. There is a time and place for sex. PLoS Biol *8*, e1000365.

Robinow, S., and White, K. (1988). The locus elav of *Drosophila melanogaster* is expressed in neurons at all developmental stages. Dev Biol *126*, 294-303.

Rong, Y.S., and Golic, K.G. (2000). Gene targeting by homologous recombination in *Drosophila*. Science *288*, 2013-2018.

Rong, Y.S., and Golic, K.G. (2001). A targeted gene knockout in *Drosophila*. Genetics *157*, 1307-1312.

Rong, Y.S., and Golic, K.G. (2003). The homologous chromosome is an effective template for the repair of mitotic DNA double-strand breaks in *Drosophila*. Genetics *165*, 1831-1842.

Rong, Y.S., Titen, S.W., Xie, H.B., Golic, M.M., Bastiani, M., Bandyopadhyay, P., Olivera, B.M., Brodsky, M., Rubin, G.M., and Golic, K.G. (2002). Targeted mutagenesis by homologous recombination in D. *melanogaster*. Genes Dev *16*, 1568-1581.

Rubin, G.M., and Spradling, A.C. (1983). Vectors for P element-mediated gene transfer in *Drosophila*. Nucleic Acids Res *11*, 6341-6351.

Rubinstein, C.D., Rivlin, P.K., and Hoy, R.R. (2010). Genetic Feminization of the Thoracic Nervous System Disrupts Courtship Song in Male *Drosophila melanogaster*. J Neurogenet.

Ruta, V., Datta, S.R., Vasconcelos, M.L., Freeland, J., Looger, L.L., and Axel, R. (2010). A dimorphic pheromone circuit in *Drosophila* from sensory input to descending output. Nature *468*, 686-690.

Ryder, E., Blows, F., Ashburner, M., Bautista-Llacer, R., Coulson, D., Drummond, J., Webster, J., Gubb, D., Gunton, N., Johnson, G., et al. (2004). The DrosDel collection: a set of P-element insertions for generating custom chromosomal aberrations in *Drosophila melanogaster*. Genetics *167*, 797-813.

Ryner, L.C., and Baker, B.S. (1991). Regulation of doublesex pre-mRNA processing occurs by 3'-splice site activation. Genes Dev *5*, 2071-2085.

Ryner, L.C., Goodwin, S.F., Castrillon, D.H., Anand, A., Villella, A., Baker, B.S., Hall, J.C., Taylor, B.J., and Wasserman, S.A. (1996). Control of male sexual behavior and sexual orientation in *Drosophila* by the fruitless gene. Cell *87*, 1079-1089.

Sadowski, I., Ma, J., Triezenberg, S., and Ptashne, M. (1988). GAL4-VP16 is an unusually potent transcriptional activator. Nature *335*, 563-564.

Salvemini, M., Polito, C., and Saccone, G. (2010). fruitless alternative splicing and sex behaviour in insects: an ancient and unforgettable love story? J Genet *89*, 287-299.

Sánchez, L., Gorfinkiel, N., and Guerrero, I. (2001). Sex determination genes control the development of the *Drosophila* genital disc, modulating the response to Hedgehog, Wingless and Decapentaplegic signals. Development *128*, 1033-1043.

Sánchez, L., and Guerrero, I. (2001). The development of the *Drosophila* genital disc. Bioessays *23*, 698-707.

Sanders, L.E., and Arbeitman, M.N. (2008). Doublesex establishes sexual dimorphism in the *Drosophila* central nervous system in an isoform-dependent manner by directing cell number. Dev Biol *320*, 378-390.

Santel, A., Winhauer, T., Blümer, N., and Renkawitz-Pohl, R. (1997). The *Drosophila* don juan (dj) gene encodes a novel sperm specific protein component characterized by an unusual domain of a repetitive amino acid motif. Mech Dev *64*, 19-30.

Scott K, Brady R, Cravchik A, Morozov P, Rzhetsky A (2001) A chemosensory gene family encoding candidate gustatory and olfactory receptors in *Drosophila*. Cell *104,* 661–673.

Shirangi, T.R., Taylor, B.J., and McKeown, M. (2006). A double-switch system regulates male courtship behavior in male and female *Drosophila melanogaster*. Nat Genet *38*, 1435-1439.

Simpson, J.H. (2009). Mapping and manipulating neural circuits in the fly brain. Adv Genet *65*, 79-143.

Singh, R.N., and Nayak, S.V. (1985). Fine structure and primary sensory projections of sensillae on the maxillary palp of *Drosophila melanogaster* Meigen (Diptera:

Drosophilidae. Int. J. Insect Morphol. Embryol. *14*, 296-301.

Siwicki, K.K., Riccio, P., Ladewski, L., Marcillac, F., Dartevelle, L., Cross, S.A., and Ferveur, J.-F. (2005). The role of cuticular pheromones in courtship conditioning of *Drosophila* males. Learn Mem *12*, 636-645.

Soller, M., Haussmann, I.U., Hollmann, M., Choffat, Y., White, K., Kubli, E., and Schäfer, M.A. (2006). Sex-peptide-regulated female sexual behavior requires a subset of ascending ventral nerve cord neurons. Curr Biol *16*, 1771-1782.

Song, H.-J., Billeter, J.-C., Reynaud, E., Carlo, T., Spana, E.P., Perrimon, N., Goodwin, S.F., Baker, B.S., and Taylor, B.J. (2002). The fruitless gene is required for the proper formation of axonal tracts in the embryonic central nervous system of *Drosophila*. Genetics *162*, 1703-1724.

Song, H.-J., and Taylor, B.J. (2003). fruitless gene is required to maintain neuronal identity in evenskipped-expressing neurons in the embryonic CNS of *Drosophila*. J Neurobiol *55*, 115-133.

Spieth, H.T. (1974). Courtship behavior in *Drosophila*. Annu Rev Entomol *19*, 385-405.

Spieth, H.T., and Ringo, J.M. (1983). Mating behavior and sexual isolation in *Drosophila*. In The Genetics and Biology of *Drosophila*, Volume 3c, M. Ashburner, H. Carson and T. J., eds. (New York: Academic Press), pp. 223–284.

Starostina, E., Liu, T., Vijayan, V., Zheng, Z., Siwicki, K.K., and Pikielny, C.W. (2012). A *Drosophila* DEG/ENaC subunit functions specifically in gustatory neurons required for male courtship behavior. J Neurosci *32*, 4665-4674.

Steinmann-Zwicky, M., Amrein, H., and Nöthiger, R. (1990). Genetic control of sex determination in *Drosophila*. Adv Genet *27*, 189-237.

Stocker, R.F. (1994). The organization of the chemosensory system in *Drosophila melanogaster*: a review. Cell Tissue Res *275*, 3-26.

Stockinger, P., Kvitsiani, D., Rotkopf, S., Tirián, L., and Dickson, B.J. (2005). Neural circuitry that governs *Drosophila* male courtship behavior. Cell *121*, 795-807.

Strausfeld, N.J. (1976). Atlas of an insect brain, (New York: Springer).

Strausfeld, N.J. (1980). Male and female visual neurones in dipterous insects. Nature *283*, 381-383.

Strausfeld, N.J. (1991). Structural organization of male-specific visual neurons in calliphorid optic lobes. J Comp Physiol A *169*, 379-393.

Strausfeld, N.J., and Meinertzhagen, I.A. (1998). The insect neuron: types, morphologies, fine structure, and relationship to the architectonics of the insect nervous system. In Microscopic anatomy of invertebrates, Volume IIB: Insecta, F.W. Harrison and M. Locke, eds. (New York: Wiley), pp. 487-538.

Struhl, G. (1982). Genes controlling segmental specification in the *Drosophila* thorax. Proc Natl Acad Sci USA *79*, 7380-7384.

Struhl, G. and Basler, K. (1993). Organizing activity of wingless protein in *Drosophila*. Cell *72(4),* 527–540

Suster, M.L., Seugnet, L., Bate, M., and Sokolowski, M.B. (2004). Refining GAL4-driven transgene expression in *Drosophila* with a GAL80 enhancer-trap. Genesis *39*, 240-245.

Sweeney, S.T., Broadie, K., Keane, J., Niemann, H., and O'Kane, C.J. (1995). Targeted expression of tetanus toxin light chain in *Drosophila* specifically eliminates synaptic transmission and causes behavioral defects. Neuron *14*, 341-351.

Szabad, J., and Fajszi, C. (1982). Control of female reproduction in *Drosophila*: genetic dissection using gynandromorphs. Genetics *100*, 61-78.

Szüts, D., and Bienz, M. (2000). LexA chimeras reveal the function of *Drosophila* Fos as a context-dependent transcriptional activator. Proceedings of the National Academy of Sciences of the United States of America *97*, 5351-5356.

Takashima, S., Adams, K.L., Ortiz, P.A., Ying, C.T., Moridzadeh, R., Younossi-Hartenstein, A., and Hartenstein, V. (2011). Development of the *Drosophila* entero-endocrine lineage and its specification by the Notch signaling pathway. Dev Biol *353*, 161-172.

Tanaka, K., Barmina, O., and Kopp, A. (2009). Distinct developmental mechanisms underlie the evolutionary diversification of *Drosophila* sex combs. Proc Natl Acad Sci USA *106*, 4764-4769.

Taylor, B.J., and Truman, J.W. (1992). Commitment of abdominal neuroblasts in *Drosophila* to a male or female fate is dependent on genes of the sex-determining hierarchy. Development *114*, 625-642.

Taylor, B.J., Villella, A., Ryner, L.C., Baker, B.S., and Hall, J.C. (1994). Behavioral and neurobiological implications of sex-determining factors in *Drosophila*. Dev Genet *15*, 275-296.

Thistle, R., Cameron, P., Ghorayshi, A., Dennison, L., and Scott, K. (2012). Contact chemoreceptors mediate male-male repulsion and male-female attraction during *Drosophila* courtship. Cell *149*, 1140-1151.

Thorne N, Chromey C, Bray S & Amrein H 2004 Taste perception and coding in *Drosophila*. Current Biology *14,* 1065–1079.

Thorne, N., Bray, S., and Amrein, H. (2005). Function and expression of the *Drosophila* gr genes in the perception of sweet, bitter and pheromone compounds. Chem Senses *30 Suppl 1*, i270-272.

Tinbergen, N. (1951). The Study of Instinct, XII Edition, (London: Oxford University Press).

Ting, C.-Y., Gu, S., Guttikonda, S., Lin, T.-Y., White, B.H., and Lee, C.-H. (2011). Focusing transgene expression in *Drosophila* by coupling Gal4 with a novel split-LexA expression system. Genetics *188*, 229-233.

Toda, H., Zhao, X., and Dickson, B.J. (2012). The *Drosophila* Female Aphrodisiac Pheromone Activates ppk23(+) Sensory Neurons to Elicit Male Courtship Behavior. Cell reports *1*, 599-607.

Tomaru, M., Matsubayashi, H., and Oguma, Y. (1885). Heterospecific interpulse intervals of courtshipsong elicit female rejection in *Drosophila* biaurarua. Anim Behav *50*, 905-915.

Tompkins, L., and Hall, J.C. (1983). Identification of Brain Sites Controlling Female Receptivity in Mosaics of DROSOPHILA MELANOGASTER. Genetics *103*, 179-195.

Tompkins, L., Siegel, R.W., Gailey, D.A., and Hall, J.C. (1983). Conditioned courtship in *Drosophila* and its mediation by association of chemical cues. Behav Genet *13*, 565-578.

Usui-Aoki, K., Ito, H., Ui-Tei, K., Takahashi, K., Lukacsovich, T., Awano, W., Nakata, H., Piao, Z.F., Nilsson, E.E., Tomida, J., et al. (2000). Formation of the male-specific muscle in female *Drosophila* by ectopic fruitless expression. Nat Cell Biol *2*, 500-506.

Venard, R., Antony, C., and Jallon, J.-M. (1989). *Drosophila* chemoreceptors. In Neurobiology of Sensory Systems, R.N. Singh and J.S. Strausfeld, eds. (New York: Plenum), pp. 377–385.

Villella, A., Ferri, S.L., Krystal, J.D., and Hall, J.C. (2005). Functional analysis of fruitless gene expression by transgenic manipulations of *Drosophila* courtship. Proc Natl Acad Sci USA *102*, 16550-16557.

Villella, A., Gailey, D.A., Berwald, B., Ohshima, S., Barnes, P.T., and Hall, J.C. (1997). Extended reproductive roles of the fruitless gene in *Drosophila melanogaster* revealed by behavioral analysis of new fru mutants. Genetics *147*, 1107-1130.

Villella, A., and Hall, J.C. (1996). Courtship anomalies caused by doublesex mutations in *Drosophila melanogaster*. Genetics *143*, 331-344.

Villella, A., and Hall, J.C. (2008). Neurogenetics of courtship and mating in *Drosophila*. Adv Genet *62*, 67-184.

Villella, A., Peyre, J.-B., Aigaki, T., and Hall, J.C. (2006). Defective transfer of seminal-fluid materials during matings of semi-fertile fruitless mutants in *Drosophila*. J Comp Physiol A Neuroethol Sens Neural Behav Physiol *192*, 1253-1269.

von Philipsborn, A.C., Liu, T., Yu, J.Y., Masser, C., Bidaye, S.S., and Dickson, B.J. (2011). Neuronal control of *Drosophila* courtship song. Neuron *69*, 509-522.

von Schilcher, F. (1976). The role of auditory stimuli in the courtship of *Drosophila melanogaster*. Anim Behav *24*, 18-26.

von Schilcher, F. (1976). The function of pulse song and sine song in the courtship of *Drosophila melanogaster*. Anim Behav *24*, 622-625.

von Schilcher, F. (1977). A mutation which changes courtship song in *Drosophila melanogaster*. Behav Genet *7*, 251-259.

von Schilcher, F., and Hall, J.C. (1979). Neural topography of courtship song in sex mosaics of *Drosophila melanogaster*. J. Comp. Physiol. *129*, 85–95.

Vosshall, L.B., Amrein, H., Morozov, P.S., Rzhetsky, A., and Axel, R. (1999). A spatial map of olfactory receptor expression in the *Drosophila* antenna. Cell *96*, 725-736.

Wang Z, Singhvi A, Kong P & Scott K 2004 Taste representations in the *Drosophila* brain. Cell *117,* 981-991.

Wang, L., and Anderson, D.J. (2010). Identification of an aggression-promoting pheromone and its receptor neurons in *Drosophila*. Nature *463*, 227-231.

Watanabe, K., Toba, G., Koganezawa, M., and Yamamoto, D. (2011). Gr39a, a highly diversified gustatory receptor in *Drosophila*, has a role in sexual behavior. Behav Genet *41*, 746-753.

Waterbury, J.A., Horabin, J.I., Bopp, D., and Schedl, P. (2000). Sex determination in the *Drosophila* germline is dictated by the sexual identity of the surrounding soma. Genetics *155*, 1741-1756.

Waterbury, J.A., Jackson, L.L., and Schedl, P. (1999). Analysis of the doublesex female protein in *Drosophila melanogaster*: role on sexual differentiation and behavior and dependence on intersex. Genetics *152*, 1653-1667.

Wheeler, D.A., Fields, W.L., and Hall, J.C. (1988). Spectral analysis of *Drosophila* courtship songs: D. *melanogaster*, D. simulans, and their interspecific hybrid. Behav Genet *18*, 675-703.

Williams, T.M., Selegue, J.E., Werner, T., Gompel, N., Kopp, A., and Carroll, S.B. (2008). The regulation and evolution of a genetic switch controlling sexually dimorphic traits in *Drosophila*. Cell *134*, 610-623.

Wolfner, M.F. (1997). Tokens of love: functions and regulation of *Drosophila* male accessory gland products. Insect Biochem Mol Biol *27*, 179-192.

Xu, T., and Rubin, G.M. (1993). Analysis of genetic mosaics in developing and adult *Drosophila* tissues. Development *117*, 1223-1237.

Yagi, R., Mayer, F., and Basler, K. (2010). Refined LexA transactivators and their use in combination with the *Drosophila* Gal4 system. Proc Natl Acad Sci USA *107*, 16166-16171.

Yang, C.-H., Rumpf, S., Xiang, Y., Gordon, M.D., Song, W., Jan, L.Y., and Jan, Y.-N. (2009). Control of the postmating behavioral switch in *Drosophila* females by internal sensory neurons. Neuron *61*, 519-526.

Yang, X.W., Model, P., and Heintz, N. (1997). Homologous recombination based modification in Escherichia coli and germline transmission in transgenic mice of a bacterial artificial chromosome. Nat Biotechnol *15*, 859-865.

Yapici, N., Kim, Y.-J., Ribeiro, C., and Dickson, B.J. (2008). A receptor that mediates the post-mating switch in *Drosophila* reproductive behaviour. Nature *451*, 33-37.

Yu, J.Y., Kanai, M.I., Demir, E., Jefferis, G.S.X.E., and Dickson, B.J. (2010). Cellular Organization of the Neural Circuit that Drives *Drosophila* Courtship Behavior. Curr Biol.

Yun, S.J., Hiraoka, Y., Nishizawa, M., Takio, K., Titani, K., Nogi, Y., and Fukasawa, T. (1991). Purification and characterization of the yeast negative regulatory protein GAL80. J Biol Chem *266*, 693-697.

Zarkower, D. (2002). Invertebrates may not be so different after all. Novartis Found Symp *244*, 115-126; discussion 126-135, 203-116, 253-117.

Zemelman, B.V., Nesnas, N., Lee, G.A., Miesenbock, G. (2003). Photochemical gating of heterologous ion channels: remote control over genetically designated populations of neurons. Proc Natl Acad Sci U S A *100*,1352-1357.

Zhang, S.D., and Odenwald, W.F. (1995). Misexpression of the white (w) gene triggers male-male courtship in *Drosophila*. Proc Natl Acad Sci U S A *92*, 5525-5529.

Zhang, W., Ge, W., and Wang, Z. (2007). A toolbox for light control of *Drosophila* behaviors through Channelrhodopsin 2-mediated photoactivation of targeted neurons. Eur J Neurosci *26*, 2405-2416.

Zhong, L., Hwang, R.Y., and Tracey, W.D. (2010). Pickpocket is a DEG/ENaC protein required for mechanical nociception in *Drosophila* larvae. Curr Biol *20*, 429-434.

Zhou, L., Schnitzler, A., Agapite, J., Schwartz, L.M., Steller, H., and Nambu, J.R. (1997). Cooperative functions of the reaper and head involution defective genes in the programmed cell death of *Drosophila* central nervous system midline cells. Proceedings of the National Academy of Sciences of the United States of America *94*, 5131-5136.

Available online at www.sciencedirect.com

SciVerse ScienceDirect

Current Opinion in Neurobiology

Courtship behavior in *Drosophila melanogaster*: towards a 'courtship connectome'

Hania J Pavlou and Stephen F Goodwin

The construction of a comprehensive structural, and importantly functional map of the network of elements and connections forming the brain represents the Holy Grail for research groups working in disparate disciplines. Although technical limitations have restricted the mapping of human and mouse 'connectomes' to the level of brain regions, a finer degree of functional resolution is attainable in the fruit fly, *Drosophila melanogaster*, due to the armamentarium of genetic tools available for this model organism. Currently, one of the most amenable approaches employed by *Drosophila* neurobiologists involves mapping neuronal circuitry underlying complex innate behaviors – courtship being a classic paradigm. We discuss recent studies aimed at identifying the cellular components of courtship neural circuits, mapping function in these circuits and defining causal relationships between neural activity and behavior.

Address
Department of Physiology, Anatomy & Genetics, University of Oxford, Oxford, OX1 3PT, UK

Corresponding author: Goodwin, Stephen F (stephen.goodwin@dpag.ox.ac.uk)

''*The ascendancy of network science has been driven by the growing realization that the behaviour of complex systems – be they societies, cells or brains – is shaped by interactions among their constituent elements*'' – (*Ed Bullmore and Olaf Sporns, 2009*) [1]

Current Opinion in Neurobiology 2013, **23**:76–83

This review comes from a themed issue on **Neurogenetics**

Edited by **Ralph Greenspan** and **Christine Petit**

For a complete overview see the Issue and the Editorial

Available online 28th September 2012

0959-4388/$ – see front matter, © 2012 Elsevier Ltd. All rights reserved.

http://dx.doi.org/10.1016/j.conb.2012.09.002

Introduction

Studies on courtship behavior have focused on two pivotal transcription factors of the *Drosophila* sex-determination hierarchy, *fruitless* (*fru*) and *doublesex* (*dsx*). These transcription factors act in concert to specify sex-specific physiology and neural circuitry [2]. Historically, how *fru* and *dsx* regulate courtship came from behavioral analyses in males and females expressing mutations at the respective loci [3]. How these genes function in specifying sexual behavior was inferred by the temporal and spatial patterns of *fru* and *dsx* expression in the nervous system, which facilitated the identification of candidate cellular components of this circuit [2].

To understand circuit organization, it is essential to functionally and neuroanatomically characterize the component parts. Silencing neurons (determining necessity), and artificially triggering the same neurons (determining sufficiency) helps ascertain causal relationships between neurons and behavior. Integrating neuroanatomical and behavioral data for each neuronal class sheds light on how information is received and interpreted, from sensory input through higher-order processing to motor outputs. While sensory neurons and motoneurons may be viewed respectively as the start and end points of this connectome, complex circuit organization arises from interneurons of the CNS that are responsible for higher order processing, and decision-making. This review will focus on studies that have defined patterns of connectivity and/or functionally mapped circuit elements underlying courtship behavior.

Courtship behavior

Drosophila males display a complex repertoire of behaviors that have evolved to achieve reproductive success. This includes following the female, tapping her with his forelegs, contacting her genitalia with his mouthparts, singing a species-specific courtship song, and bending his abdomen to copulate [3]. It is presumed that *Drosophila* females assess a courting male by 'summating' sensory cues for species type and fitness before sanctioning mating [3]. A virgin female has the ability to be unreceptive to and resist the courtship of a *Drosophila* male by exhibiting rejection behaviors, which include extruding her ovipositor, kicking, or decamping [3–6]. If she decides to accept the male, she slows down, ceases rejection behaviors and opens her vaginal plate for copulation [3]. After successful copulation, mated females become temporarily sexually unreceptive to further copulatory attempts, increasing their rate of egg-laying [7].

Circuitry underlying courtship behavior

Expression of *fruitless* and *doublesex* in sensory neurons, interneurons and motorneurons suggests that they are organized into circuit elements capable of receiving, processing and transferring information that controls sexual behavior. Indeed impinging the activity of all, or some, of these neurons have profound effects on male and

female courtship behaviors [2]. While male-specific proteins Fru^M and Dsx^M act in concert to specify male-specific circuitry [8–12], female-specific circuitry appears largely determined by the female-specific *dsx* protein, Dsx^F [12]. Given that the neuronal clusters expressing these sex-specific proteins form dimorphic neural networks directing sex-specific behavioral outputs, comparing males and females sheds light on how differing behavioral outputs may be engendered via shared circuits that operate differently and/or sex-specific circuits that result from the presence/absence of unique circuit elements.

Tools that gain genetic access to *fru* and *dsx* neurons have exploited the GAL4/UAS and LexA/lexAop binary systems, and more recently FLP recombinase has been used for genetic access to subsets of neurons [12–15,16•,17,18•,19•,20,21]. A comprehensive digital 3D atlas of *fru* neurons has been achieved using a combination of these tools in two independent approaches [19•,22,23]. Warping high-resolution tracings of individual neurons onto a common reference brain allowed the identification of neuro-anatomical dimorphisms and, by implication, differences in interconnectivity and likely pathways of neural processing [18•,19•]. Direct comparison of male vs. female *fru* neural elements confirmed three distinct modes of sexual dimorphism; (i) sex-specific neuronal clusters; (ii) differences in cell numbers within a given cluster; and (iii) sex-specific arborizations; all of which may contribute to developing neural architecture capable of eliciting sex-specific behavior(s) [11,13–17,18•,19•,24,25•,26•]. Although the connectivity between component neurons is largely hypothetical, this *fru* 'digital atlas' is serving as a neuroanatomical framework for functional studies.

Relaying sensory information

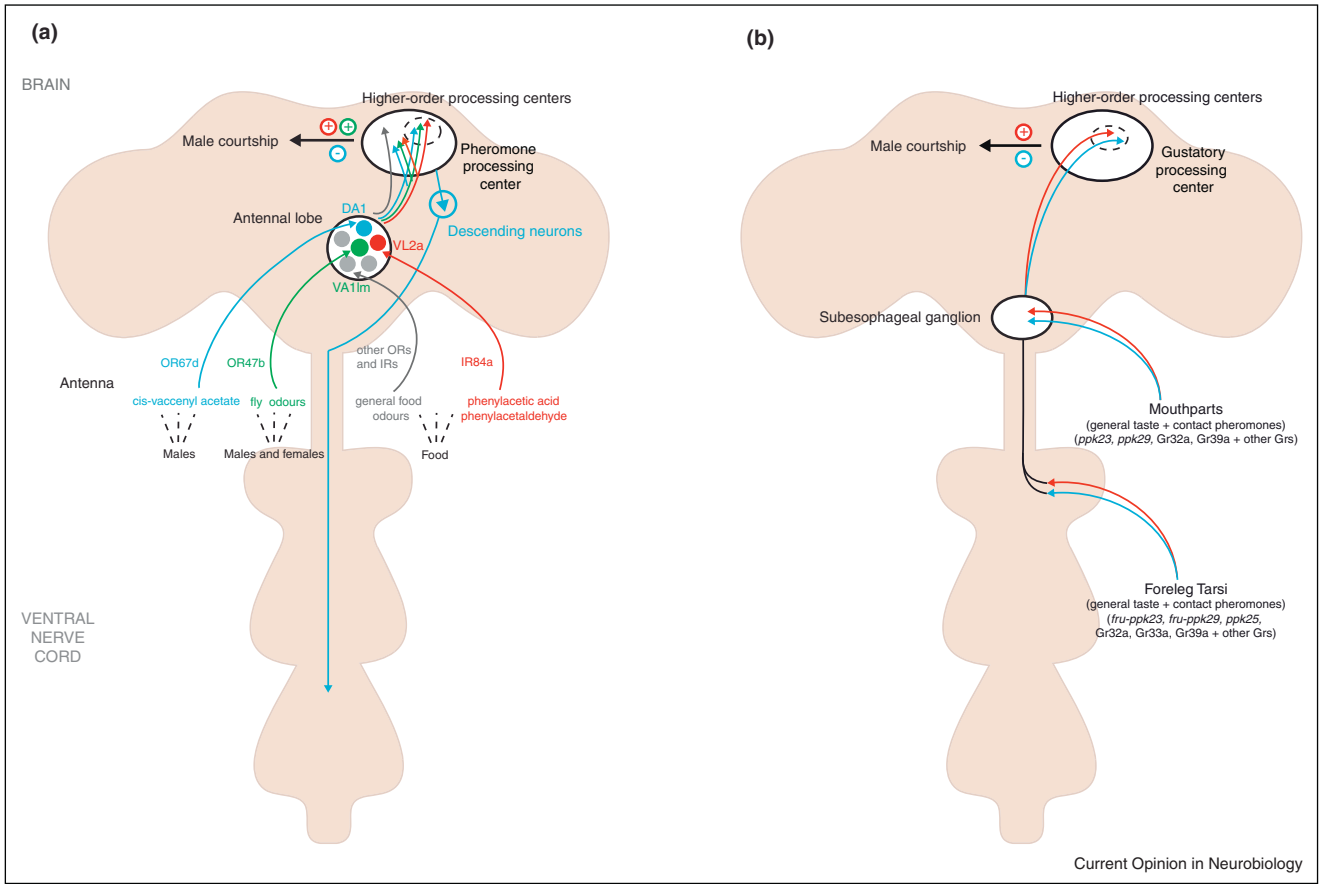
fru^{GAL4} is expressed in approximately 15% of the olfactory receptor neurons (ORNs) on the third antennal segment, which innervate olfactory trichoid sensilla [14,15]. Blocking synaptic transmission in these ORNs profoundly reduces male courtship, demonstrating their importance in detecting sex-pheromones [15]. The afferent projections of these fru^{GAL4} ORNs have been mapped to three sexually dimorphic antennal lobe glomeruli; DA1, VA1lm and VL2a, which appear to overlap with dendrites of second order fru^{GAL4} projection neurons (PNs; Figure 1A) [15,27]. A complete map of higher olfactory centers showed that pheromone-responsive PNs project to distinct compartments of the lateral horn of the protocerebrum, a region thought to be the 'sensory integration/processing center' [18•,19•,28].

To date our knowledge of the neuronal circuitry underlying the detection, processing and possible outputs of olfactory pheromones has come exclusively from studies on the male pheromone 11-*cis*-vaccenyl acetate (cVA) (Figure 1A) [24,25•,29]. cVA, sensed by Or67d ORNs in both males and females, elicits aggression amongst males [30–32], inhibits male courtship towards males and females [31,33], and promotes receptivity in females. Mapping the cVA-responsive circuit showed that it comprised as few as four physiologically connected neurons, with the fourth neuron projecting into the ventral nerve cord (VNC) and terminating in the thoracic abdominal ganglia (Abg; Figure 1A) [25•]. While some components within the circuit are male-specific others exhibit male-specific arborizations and/or synaptic connections [24,25•]. Given that dimorphic anatomical connections are particularly enriched in third order olfactory interneurons of the lateral horn [18•], these neurons may be the first elements in the olfactory pathway that respond sex-specifically to the same stimulus. In particular, dimorphic connections between DA1 PNs and higher-order olfactory neurons might explain the sex-specific behavioral responses elicited by cVA [18•,25•], though additional electrophysiology experiments are essential to determine this.

While the association between pheromones, olfaction and courtship may seem obvious, an intriguing relationship has been identified between food-olfaction and male courtship [34]. Members of a novel family of chemosensory receptors, the ionotropic glutamate receptors (Irs), localize to distinct sensory cilia of the antennae and are expressed in olfactory neurons lacking olfactory receptors (ORs) [35]. In particular, ORNs that express *Ir84a* have been shown to co-express fru^M and innervate VL2a, one of the three fru^+ sexually dimorphic glomeruli (Figure 1A) [34]. Although $Ir84a^+$ neurons are not tuned to respond to sex-specific odors, two volatile compounds normally found in *Drosophilid* food sources (phenylacetaldehyde and phenylacetic acid) were found to elicit responses in both males and females. *Ir84a* mutant males court females at diminished levels, while restoring *Ir84a* function re-establishes normal courtship levels, implicating *Ir48a* in the regulation of male courtship. Neuroanatomical analyses of second order VL2a PNs revealed distinctive intercalation with pheromonal PNs of fru^+ DA1 and VA1lm glomeruli, rather than with general food odor pathways [34] (Figure 1A). PNs from all three sexually dimorphic glomeruli target a specialized pheromone-processing region of the lateral horn, suggesting a point of integration of food and pheromonal pathways within the fru^+ 'courtship connectome'.

During the 'tapping' and 'licking' stages of courtship males are believed to assess a mate's sex and species via non-volatile pheromones, with the reception of essential information occurring largely via gustatory receptor neurons (GRN) of the foreleg (Figure 1B) [36]. Studies suggest that detection of female-enriched long-chain cuticular hydrocarbons (CHCs) stimulates male–female courtship while the detection of male-enriched CHCs

Figure 1



Proposed model for the perception and integration of sensory information in the male CNS. **(a)** Olfaction: Olfactory receptor neurons (ORNs) in the antenna detect odors and send axons to glomeruli of the antennal lobe of the brain. DA1 and VA1lm glomeruli receive pheromonal information from *Or67d*-expressing neurons (which respond to the male pheromone 11-*cis*-vaccenyl acetate, cVA) [24,31] and *Or47b*-expressing neurons (which respond to unidentified female and male-derived odors) [58,59]. While Or67d ORNs express fru, Or47b ORNs do not. Olfactory information is propagated through projection neurons to higher brain centers, such as the mushroom body and lateral horn. OR67d/DA1 neurons target fru-expressing second order neurons in a specific region of the lateral horn associated with pheromone processing. Ultimately these second order neurons form downstream fru-expressing connections (via third and fourth order neurons) that terminate in the abdominal ganglia [24,25•]. VL2a glomerulus receives information from *Ir84a*-expressing neurons, which respond to odors derived from host food/oviposition substrates [34]. VL2a projection neurons are segregated from projection neurons responding to general food odor pathways but they are anatomically interconnected with the VA1lm/DA1 pheromone pathways and target a specific area in the lateral horn involved in pheromone processing [34]. Note that only half of the male CNS is shown in the schematic. Adapted from [60]. **(b)** Gustation: In males, non-volatile pheromones are primarily detected by gustatory receptor neurons (GRNs) of the foreleg tarsi. *Gr33a* and *Gr32a* are thought to detect female-specific pheromones (acting as aphrodisiacs) and *Gr39a* is thought to detect male-specific pheromones (acting as aversive stimuli) [38,40,41]. GRNs expressing these Grs do not express fruitless. However, projections of *Gr32a*-expressing terminate in the SOG are likely to form connections with fru-expressing neurons of the ventrolateral protocerebrum that relay this signal to the higher-order lateral protocerebrum [42]. Projections of *Gr33a*-expressing and *Gr39a*-expressing GRNs remain unknown. GRNs expressing proprioceptive receptors *pickpocket-23* (*ppk23*), *ppk29* or *ppk25* co-express fruitless and have also been implicated in courtship [19•,44,45,47,48]. All three send sexually dimorphic projections to the first thoracic ganglia, of which *ppk23*-expressing and *ppk29*-expressing GRNs ascend to terminate in the SOG [19•,44,45,48]. Although downstream connections have not been described, studies have shown that gustatory information is relayed from the SOG to a distinct region of the lateral protocerebrum [16•,19•]. One population of *ppk23*-expressing GRNs respond to male-specific pheromones (to promote male–male repulsion) [44], while a second population responds to female-specific pheromones (to promote male–female courtship) [44,45]. Most aforementioned receptors are also expressed in the mouthparts; however, their specific role in these tissues has not been determined. Note that only half of the male CNS is shown in the schematic.

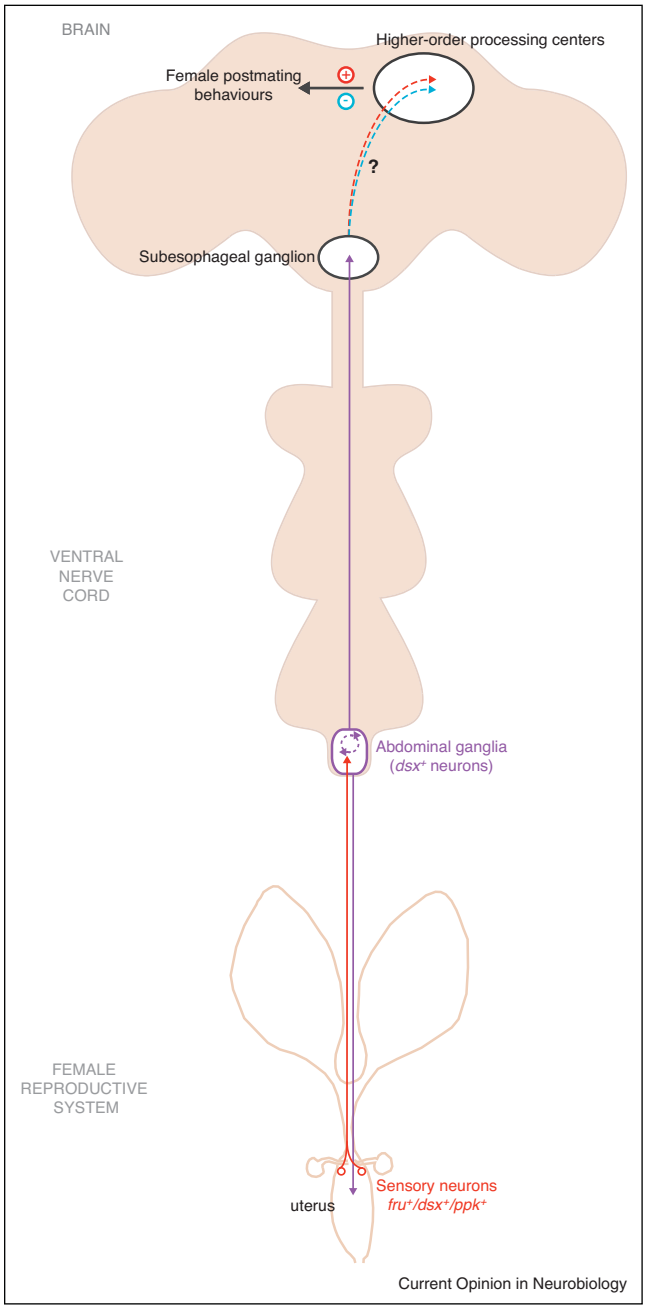
promotes male–male repulsion, preventing inappropriate male–male courtship [37]. To date, only three gustatory receptors (Gr) have been implicated in the reception of pheromones – *Gr39a* is thought to detect to female-enriched CHCs [38], while *Gr32a* and *Gr33a* may serve to detect male-enriched CHCs [39–41]. GRNs expressing each of these Grs do not express *fru*. However, axons of *Gr32a*-expressing GRNs terminate in the SOG and are likely to form connections with second-order *fru*-expressing neurons of the ventrolateral protocerebrum that relay

this signal to the higher-order lateral protocerebrum (Figure 1B) [42]. This implies that sensory neurons that do not express *fru* may be capable of relaying information to *fru*$^+$ downstream 'processing' circuitry.

Members of the degenerin/epithelial sodium channel subunit family *pickpocket-23* (*ppk23*) and *pickpocket-29* (*ppk29*) are expressed in Fru^M-positive GRNs of the foreleg tarsi [43–45]. There appears to be twice the number of *ppk23*$^+$ neurons in the male foreleg, when compared to the female [43–45], with contralateral projections within the VNC that terminate in the SOG, a sex-specific feature previously attributed to Fru^M-expressing gustatory neurons (Figure 1B) [17,46]. Males with silenced *ppk23*$^+$ neurons display reduced levels of courtship towards females and increased levels towards males, while males with silenced *ppk29*$^+$ neurons display defects in courtship towards females only [43–45]. Coupling thermogenetics with electrophysiology demonstrated that *ppk23*$^+$ neurons, which are restricted to two cells per bristle, respond to specific female pheromones [44,45]. G-CaMP imaging of *ppk23*$^+$ neurons in response to pheromonal stimulation showed that the two neurons innervating each bristle perform opposing roles forming two directly competing populations; one specifically responding to male-enriched pheromones, the second responding to female-enriched pheromones, suggesting a direct role in mediating attractive and aversive cues [44]. A third subunit, *pickpocket-25*, is expressed in sexually dimorphic *fru*$^+$ tarsal gustatory neurons that also give rise to characteristic sexually dimorphic projections within the VNC (Figure 1B). Though these neurons appear to be necessary for normal courtship initiation, specific ligands and further neuronal connections remain unknown [47,48].

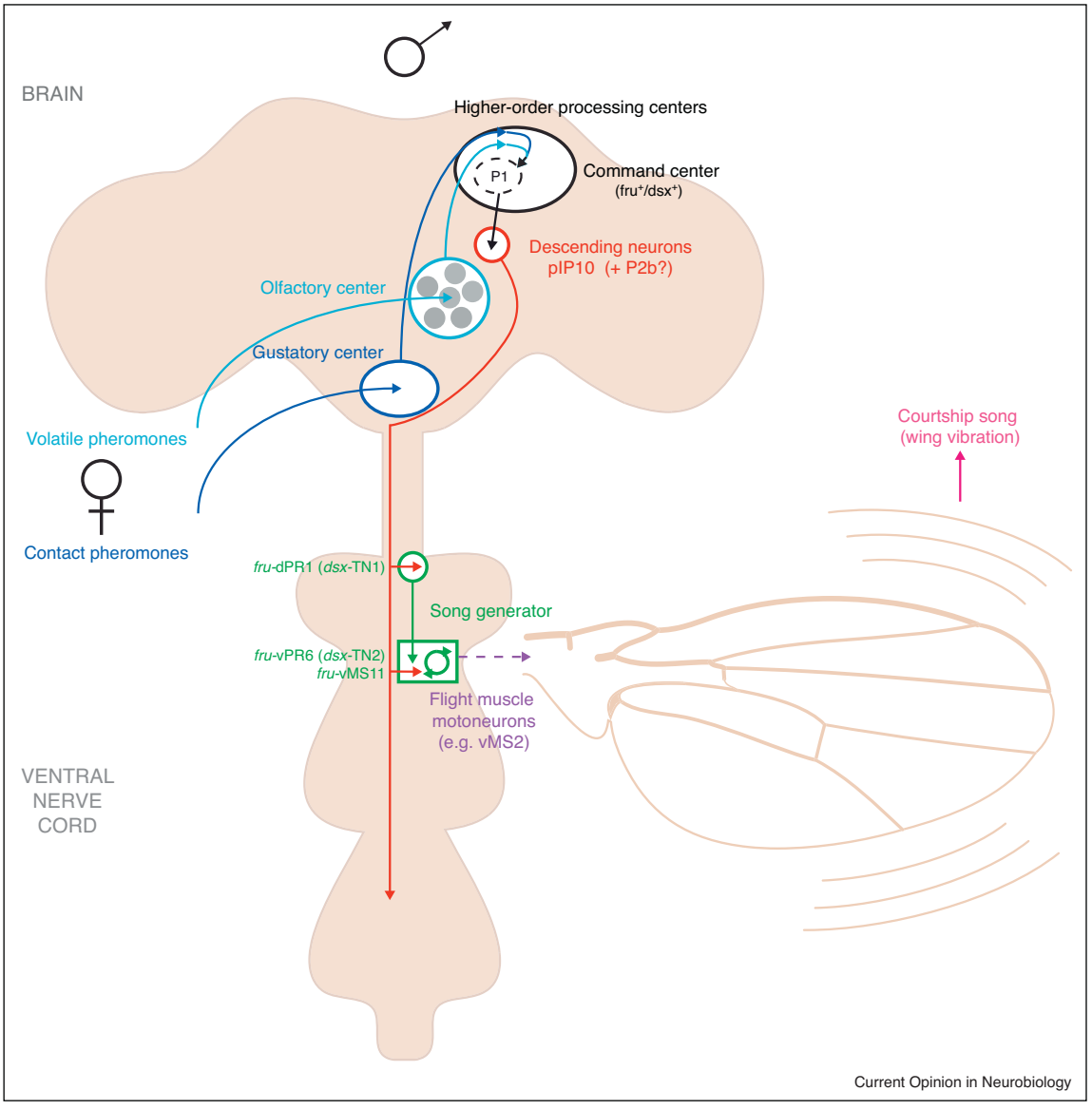
The neuronal basis of female sexual behaviors has only recently come into play with studies primarily focusing on sensory elements that modulate postmating responses (Figure 2) [21,49,50]. Postmating responses are triggered primarily by the allohormone pheromone sex peptide (SP), a small peptide synthesized in the male accessory glands that is transferred to the female during insemination [7]. A SP-responsive G protein-coupled receptor for SP-mediated postmating responses has been identified; females lacking this sex peptide receptor (SPR) remain receptive, exhibiting virgin-like behaviors, postmating [51]. Transfer of male sex peptide (SP) during copulation mediates these postmating responses by SPR activation in sensory neurons that coexpress *fru*, *dsx* and the proprioceptive neuronal marker *pickpocket* (*ppk*) in the female reproductive system [21,49,50]. In addition, a sex-specific cluster of *dsx*-expressing neurons in the Abg are required for the induction and regulation of some postmating responses [21]. This cluster consists of (1) interneurons that form synaptic arborizations within the SOG that may act downstream of sensory elements of the

Figure 2



Proposed model for the perception and integration of sex peptide (SP) sensory signals that regulate female postmating responses. SP-responsive sensory neurons expressing *fru*, *dsx* and *ppk* are localized to the uterus and project into the abdominal ganglia (Abg) and possibly into the suboesophageal ganglion (SOG) [21,49,50]. A cluster of *dsx*-expressing neurons of the Abg is required for the induction and regulation of specific postmating responses [21]. This cluster consists of (1) ascending neurons innervating the central brain, (2) descending neurons innervating the uterus and (3) local interneurons potentially (dotted line) conveying information to/from central circuits regulating female mating decisions. Higher-order central pathways may process these signals (dotted lines) to regulate female behavior; however, studies have yet to identify these processing/command elements. Note that only half of the female CNS is shown in the schematic.Adapted from [60].

Figure 3



Proposed circuitry underlying the initiation of courtship and pulse song in the male CNS. During courtship, a male extends and vibrates his wing to sing a species-specific courtship song. Five distinct fru-expressing clusters of neurons that consist of command/decision-making neurons (P1), descending interneurons (pIP10), and components of the central pattern generator (dPR1, vPR6 and vMS11) are thought to form an interconnected circuit [26•]. Thermoactivation of these neurons triggers wing extension and/or vibration in isolated males deprived of the sensory inputs that would normally induce males to sing [26•]. Thermoactivation of P1 and the descending neuron P2b independently initiate male courtship in the presence of a female. Sensing volatile and/or contact pheromones subsequently alters the activity of the P1 cluster, suggesting its capability of integrating olfactory and gustatory sensory cues when making the decision to court. Thus P1 and P2b are thought to play a key role in triggering male courtship [53••]. Although the descending cluster, P2b, is connected to P1 neurons its downstream connections within the VNC have yet to be identified. A cluster of flight muscle motoneurons, vMS2, may (dotted line) form connections with the CPG [19•]. Note that only half of the male CNS is shown in the schematic. Adapted from [61].

uterus to convey sensory information to higher-order centers, (2) neurons that form presynaptic arborizations on the uterus that may be involved in directing motor output, and (3) local interneurons that may regulate both (Figure 2).

Deciding to court

Determining causal relationships between neurons and behavior, Clyne and Miesenböck (2008) used an optogenetic strategy to activate all *fru*-expressing neurons in intact and headless flies [52]. They demonstrated the

existence of a central song pattern generator (CPG) in the mesothoracic area of the VNC in both sexes, capable of generating wing extension and courtship song in flies. However, to generate bona fide courtship song requires the expression of the male-specific isoforms of both *dsx* (Dsx^M) and *fru* (Fru^M) in the CNS, in addition to direction from male-specific higher-order 'command' neurons [9,52].

Continuing with this logic, that higher-order command neurons exist that initiate courtship behaviors, Kimura *et al.* (2008) identified a *fru*/*dsx*-expressing neuronal cluster in the dorsal posterior brain, P1, as an important neuronal element that can initiate male-type courtship behavior [11]. While restrictively thermoactivating the P1 cluster is sufficient to initiate courtship and trigger pulse song, in the presence or absence of a female [26•,53••], silencing P1 neurons in the male brain impairs song and other courtship elements [11,26•,53••]. Since P1 neurons are male-specific and are located in the lateral protocerebrum (which receives multimodal sensory input), they are ideal 'decision-making' candidates capable of integrating environmental stimuli to make the decision to court (Figure 3). A remarkable experiment demonstrated that while contact between the male tarsus and a female's abdomen provokes real-time activation of P1 neurons, the presence of cVA attenuates this response [53••], demonstrating a role for P1 neurons in integrating gustatory and olfactory information. In line with this, Pan *et al.* (2012) showed that restricted activation of P1 neurons resulted in heightened levels of following and orienting when exposed to a moving object [54]. Although visual processing appears independent of the P1 neuronal pathway, these data support the view that, by integrating multimodal sensory signals, P1 interneurons mediate the decision to initiate courtship, effectively acting as a switch for courtship initiation [26•,53••,54].

Thermoactivation of fru^+ descending interneurons, P2b and pIP10, is sufficient to initiate courtship and trigger pulse song, in the presence or absence of a female [26•,53••]. However, it has been hypothesized that these serve a downstream 'command' role, relaying information from integration/higher-processing centers to motor centers in the VNC [26•,53••]. Within the VNC, three distinct fru^+ interneuron classes are thought to be components of the CPG, as thermoactivation of these neurons did not lead to faithful recapitulation of pulse song such that (1) activation of the fru^+/dsx^+ prothoracic, dPR1, neuron elicits courtship song with a significantly longer inter-pulse interval (IPI), (2) the level of activation of the fru^+/dsx^+ mesothoracic neuronal cluster, vPR6, appears to be indirectly correlated to IPI and (3) activation of the fru^+ mesothoracic neuronal cluster, vMS11, induces wing extension without the production of song [26•]. By overlapping axonal and dendritic arborizations, von Philipsborn *et al.* (2011) described a hypothetical interconnected circuit for courtship song, linking all 5 aforementioned fru^+ neuronal classes (P1, pIP10, dPR1, vPR6 and vMS11; Figure 3) [26•]. Yu *et al.* (2011) were able to neuroanatomically map a single mesothoracic cluster, vMS2, of *fru*-expressing motoneurons innervating direct flight muscles, which could be critical for song production [19].

Conclusions

Integrating neuroanatomical data with behavioral data for each neuronal class allows us to generate hypotheses about how information may flow through the system from sensory input, through brain to motor outputs pathways. Although many of the neurons involved in courtship behavior have been identified, additional elements that mediate these signals, and the neural circuits that interpret this information still need to be identified. It is likely that sensory information from all modes of input (visual, taste, smell and hearing) converge within specific brain areas; however, we have no knowledge of how processing centers of the CNS are capable of assigning 'weighting' effects associated with any competing agonistic and antagonistic stimuli, to ultimately relay the correct information and elicit most appropriate behavioral outputs. The use of new technology, like optogenetics and thermogenetics [55] has been pivotal for the identification of command elements capable of eliciting courtship and song. These methods of manipulating a defined neural circuit through artificial stimulation complement other new optogenetic techniques, such as those that interrogate physiological connections between component neurons [56]. In future studies, the use of such strategies will allow the marrying of circuit architecture and underlying cellular and synaptic properties to further elucidate how neural pathways control behaviors. So what next? Pinching the logic from Olsen and Wilson's review [57], ''Cracking neural circuits in a tiny brain'', we still need to:

- Identify all the neurons that participate in sex-specific behaviors (functional map).
- Establish the 'natural' response/activity pattern of all neurons during presentation of a given stimulus and/or execution of a precise behavior (activity map).
- Determine the cellular, synaptic and circuit mechanisms underlying these neural transformations (connectivity map).

Ultimately, correlating the 'connectivity', 'functional' and 'activity' maps will provide the logic for how this, and other, dimorphic nervous systems might be coordinated with gender-appropriate physiology and sensorimotor tissues to generate sex-specific behavioral outputs. Only then may we begin to shed light on the relative values associated with each mode of sensory input, and identify compensatory mechanisms that may exist to allow for behavioral flexibility. Extrapolating models of circuit-organization to define how decisions are achieved

to prioritize behavioral outputs in response to conflicting signals, and how experience may modify these behaviors, will enrich our understanding of the astonishing plasticity of nervous systems.

Acknowledgements

We thank all scientists whose results are reviewed in this article. We apologize to all the investigators whose work could not be cited owing to strict space constraints. We are grateful to the Wellcome Trust and the BBSRC for funding. We thank the members of the Goodwin laboratory for helpful discussions.

References and recommended reading

Papers of particular interest, published within the period of review, have been highlighted as:

- • of special interest
- •• of outstanding interest

1. Bullmore E, Sporns O: **Complex brain networks: graph theoretical analysis of structural and functional systems**. *Nat Rev Neurosci* 2009, **10**:186-198.
2. Dauwalder B: **The roles of fruitless and doublesex in the control of male courtship**. *Int Rev Neurobiol* 2011, **99**:87-105.
3. Villella A, Hall JC: **Neurogenetics of courtship and mating in *Drosophila***. *Adv Genet* 2008, **62**:67-184.
4. Connolly K, Cook RM: **Rejection responses by female *Drosophila melanogaster*: their ontogeny, causality and effects upon the behavior of the courting male**. *Behavior* 1973, **44**:142-167.
5. Spieth HT, Ringo JM: **Mating behavior and sexual isolation in *Drosophila***. In *The Genetics and Biology of Drosophila*, vol 3c. Edited by Ashburner M, Carson HJT. Academic Press; 1983: 223-284.
6. Ejima A, Nakayama S, Aigaki T: **Phenotypic association of spontaneous ovulation and sexual receptivity in virgin females of *Drosophila melanogaster* mutants**. *Behav Genet* 2001, **31**:437-444.
7. Kubli E: **Sex-peptides: seminal peptides of the *Drosophila* male**. *Cell Mol Life Sci* 2003, **60**:1689-1704.
8. Billeter J-C, Rideout EJ, Dornan AJ, Goodwin SF: **Control of male sexual behavior in *Drosophila* by the sex determination pathway**. *Curr Biol* 2006, **16**:R766-R776.
9. Rideout EJ, Billeter J-C, Goodwin SF: **The sex-determination genes fruitless and doublesex specify a neural substrate required for courtship song**. *Curr Biol* 2007, **17**:1473-1478.
10. Sanders LE, Arbeitman MN: **Doublesex establishes sexual dimorphism in the *Drosophila* central nervous system in an isoform-dependent manner by directing cell number**. *Dev Biol* 2008, **320**:378-390.
11. Kimura K-I, Hachiya T, Koganezawa M, Tazawa T, Yamamoto D: **Fruitless and doublesex coordinate to generate male-specific neurons that can initiate courtship**. *Neuron* 2008, **59**:759-769.
12. Rideout EJ, Dornan AJ, Neville MC, Eadie S, Goodwin SF: **Control of sexual differentiation and behavior by the doublesex gene in *Drosophila melanogaster***. *Nat Neurosci* 2010, **13**:458-466.
13. Billeter J-C, Goodwin SF: **Characterization of *Drosophila* fruitless-gal4 transgenes reveals expression in male-specific fruitless neurons and innervation of male reproductive structures**. *J Comp Neurol* 2004, **475**:270-287.
14. Manoli DS, Foss M, Villella A, Taylor BJ, Hall JC, Baker BS: **Male-specific fruitless specifies the neural substrates of *Drosophila* courtship behaviour**. *Nature* 2005, **436**:395-400.
15. Stockinger P, Kvitsiani D, Rotkopf S, Tirián L, Dickson BJ: **Neural circuitry that governs *Drosophila* male courtship behavior**. *Cell* 2005, **121**:795-807.
16. • Kimura K, Ote M, Tazawa T, Yamamoto D: **Fruitless specifies sexually dimorphic neural circuitry in the *Drosophila* brain**. *Nature* 2005, **438**:229-233.

This study is the first to neuroanatomically demonstrate marked sexual dimorphism in neuron number and projection patterns of *fru*-expressing neurons. This set up the notion that sexual dimorphism develops neural architecture that is capable of eliciting sex-specific behavior.

17. Mellert DJ, Knapp J-M, Manoli DS, Meissner GW, Baker BS: **Midline crossing by gustatory receptor neuron axons is regulated by fruitless, doublesex and the Roundabout receptors**. *Development* 2010, **137**:323-332.
18. • Cachero S, Ostrovsky AD, Yu JY, Dickson BJ, Jefferis GSXE: **Sexual dimorphism in the fly brain**. *Curr Biol* 2010, **20**:1589-1601.

These comprehensive studies [18•] and [19•] generated the neuroanatomical framework that underlies many of the functional studies presented in this review.

19. • Yu JY, Kanai MI, Demir E, Jefferis GSXE, Dickson BJ: **Cellular organization of the neural circuit that drives *Drosophila* courtship behavior**. *Curr Biol* 2010, **20**:1602-1614.

These comprehensive studies [18•] and [19•] generated the neuroanatomical framework that underlies many of the functional studies presented in this review.

20. Robinett CC, Vaughan AG, Knapp J-M, Baker BS: **Sex and the single cell. II. There is a time and place for sex**. *PLoS Biol* 2010, **8**:e1000365.
21. Rezaval C, Pavlou HJ, Dornan AJ, Chan YB, Kravitz EA, Goodwin SF: **Neural circuitry underlying *Drosophila* female postmating behavioral responses**. *Curr Biol* 2012, **22**:1155-1165.
22. Lee T, Luo L: **Mosaic analysis with a repressible cell marker for studies of gene function in neuronal morphogenesis**. *Neuron* 1999, **22**:451-461.
23. Liu W, Hou SX: **Genetic tools used for cell lineage tracing and gene manipulation in *Drosophila* germline stem cells**. *Methods Mol Biol* 2008, **450**:61-70.
24. Datta SR, Vasconcelos ML, Ruta V, Luo S, Wong A, Demir E, Flores J, Balonze K, Dickson BJ, Axel R: **The *Drosophila* pheromone cVA activates a sexually dimorphic neural circuit**. *Nature* 2008, **452**:473-477.
25. • Ruta V, Datta SR, Vasconcelos ML, Freeland J, Looger LL, Axel R: **A dimorphic pheromone circuit in *Drosophila* from sensory input to descending output**. *Nature* 2010, **468**:686-690.

This study forms the basis of our understanding of processing and possible outputs of pheromone olfaction. The authors exploit an impressive array of tools including photoactivatable green fluorescent protein for neural tracing, electrophysiology, optical imaging and laser-mediated microlesioning, to functionally map the cVA responsive circuit to fourth order neurons. The revealing of overt dimorphism within the circuit validated the logic by which sensory input may be sex-specifically processed to influence sex specific behavioral outputs.

26. • von Philipsborn AC, Liu T, Yu JY, Masser C, Bidaye SS, Dickson BJ: **Neuronal control of *Drosophila* courtship song**. *Neuron* 2011, **69**:509-522.

This study employs an intersectional strategy to causally link specific aspects of courtship song with distinct *fru*-expressing neurons. Five neuronal classes were identified and functionally mapped as potentially connected functional circuit.

27. Kondoh Y, Kaneshiro KY, Kimura K-I, Yamamoto D: **Evolution of sexual dimorphism in the olfactory brain of Hawaiian *Drosophila***. *Proc Biol Sci* 2003, **270**:1005-1013.
28. Jefferis GS, Potter CJ, Chan AM, Marin EC, Rohlfing T, Maurer CR Jr, Luo L: **Comprehensive maps of *Drosophila* higher olfactory centers: spatially segregated fruit and pheromone representation**. *Cell* 2007, **128**:1187-1203.
29. Butterworth FM: **Lipids of *Drosophila*: a newly detected lipid in the male**. *Science* 1969, **163**:1356-1357.
30. Ha TS, Smith DP: **A pheromone receptor mediates 11-*cis*-vaccenyl acetate-induced responses in *Drosophila***. *J Neurosci* 2006, **26**:8727-8733.
31. Kurtovic A, Widmer A, Dickson BJ: **A single class of olfactory neurons mediates behavioural responses to a *Drosophila* sex pheromone**. *Nature* 2007, **446**:542-546.

32. Wang L, Anderson DJ: **Identification of an aggression-promoting pheromone and its receptor neurons in *Drosophila***. *Nature* 2010, **463**:227-231.

33. Ejima A, Smith BP, Lucas C, van der Goes van Naters W, Miller CJ, Carlson JR, Levine JD, Griffith LC: **Generalization of courtship learning in *Drosophila* is mediated by cis-vaccenyl acetate**. *Curr Biol* 2007, **17**:599-605.

34. Grosjean Y, Rytz R, Farine JP, Abuin L, Cortot J, Jefferis GS, Benton R: **An olfactory receptor for food-derived odours promotes male courtship in *Drosophila***. *Nature* 2011, **478**: 236-240.

35. Benton R, Vannice KS, Gomez-Diaz C, Vosshall LB: **Variant ionotropic glutamate receptors as chemosensory receptors in *Drosophila***. *Cell* 2009, **136**:149-162.

36. Spieth HT: **Courtship behavior in *Drosophila***. *Annu Rev Entomol* 1974, **19**:385-405.

37. Ferveur JF, Cobb M: In *Behavioral and Evolutionary Roles of Cuticular Hydrocarbons in Drosophila.* Edited by Bagnères AG, Blomquist GJ. Cambridge: Cambridge University Press; 2010.

38. Watanabe K, Toba G, Koganezawa M, Yamamoto D: ***Gr39a*, a highly diversified gustatory receptor in *Drosophila*, has a role in sexual behavior**. *Behav Genet* 2011, **41**:746-753.

39. Lacaille F, Hiroi M, Twele R, Inoshita T, Umemoto D, Manière G, Marion-Poll F, Ozaki M, Francke W, Cobb M *et al.*: **An inhibitory sex pheromone tastes bitter for *Drosophila* males**. *PLoS ONE* 2007, **2**:e661.

40. Miyamoto T, Amrein H: **Suppression of male courtship by a *Drosophila* pheromone receptor**. *Nat Neurosci* 2008, **11**: 874-876.

41. Moon SJ, Lee Y, Jiao Y, Montell C: **A *Drosophila* gustatory receptor essential for aversive taste and inhibiting male-to-male courtship**. *Curr Biol* 2009, **19**:1623-1627.

42. Koganezawa M, Haba D, Matsuo T, Yamamoto D: **The shaping of male courtship posture by lateralized gustatory inputs to male-specific interneurons**. *Curr Biol* 2010, **20**:1-8.

43. Lu B, LaMora A, Sun Y, Welsh MJ, Ben-Shahar Y: ***ppk23*-Dependent chemosensory functions contribute to courtship behavior in *Drosophila melanogaster***. *PLoS Genet* 2012, **8**:e1002587.

44. Thistle R, Cameron P, Ghorayshi A, Dennison L, Scott K: **Contact chemoreceptors mediate male–male repulsion and male–female attraction during *Drosophila* courtship**. *Cell* 2012, **149**:1140-1151.

45. Toda H, Zhao X, Dickson BJ: **The *Drosophila* female aphrodisiac pheromone activates *ppk23*(+) sensory neurons to elicit male courtship behavior**. *Cell Rep* 2012, **1**:599-607.

46. Possidente DR, Murphey RK: **Genetic control of sexually dimorphic axon morphology in *Drosophila* sensory neurons**. *Dev Biol* 1989, **132**:448-457.

47. Lin H, Mann KJ, Starostina E, Kinser RD, Pikielny CW: **A *Drosophila* DEG/ENaC channel subunit is required for male response to female pheromones**. *Proc Natl Acad Sci USA* 2005, **102**:12831-12836.

48. Starostina E, Liu T, Vijayan V, Zheng Z, Siwicki KK, Pikielny CW: **A *Drosophila* DEG/ENaC subunit functions specifically in gustatory neurons required for male courtship behavior**. *J Neurosci* 2012, **32**:4665-4674.

49. Häsemeyer M, Yapici N, Heberlein U, Dickson BJ: **Sensory neurons in the *Drosophila* genital tract regulate female reproductive behavior**. *Neuron* 2009, **61**:511-518.

50. Yang C-H, Rumpf S, Xiang Y, Gordon MD, Song W, Jan LY, Jan Y-N: **Control of the postmating behavioral switch in *Drosophila* females by internal sensory neurons**. *Neuron* 2009, **61**:519-526.

51. Yapici N, Kim Y-J, Ribeiro C, Dickson BJ: **A receptor that mediates the post-mating switch in *Drosophila* reproductive behaviour**. *Nature* 2008, **451**:33-37.

52. Clyne JD, Miesenböck G: **Sex-specific control and tuning of the pattern generator for courtship song in *Drosophila***. *Cell* 2008, **133**:354-363.

53. •• Kohatsu S, Koganezawa M, Yamamoto D: **Female contact activates male-specific interneurons that trigger stereotypic courtship behavior in *Drosophila***. *Neuron* 2011, **69**:498-508.
This study is a game changer. The authors use thermogenetics, genetic mosaics, and calcium imaging, in addition to developing a novel paradigm that permits imaging of neurons in a freely behaving fly. While thermoactivation of the P1 'command' cluster of the lateral protocerebrum initated courtship, the authors go one step further to demonstrate a role for P1 neurons in integrating gustatory and olfactory pheromone information, ultimately acting as a switch for courtship initiation.

54. Pan Y, Meissner GW, Baker BS: **Joint control of *Drosophila* male courtship behavior by motion cues and activation of male-specific P1 neurons**. *Proc Natl Acad Sci USA* 2012, **109**:10065-10070.

55. Bernstein JG, Garrity PA, Boyden ES: **Optogenetics and thermogenetics: technologies for controlling the activity of targeted cells within intact neural circuits**. *Curr Opin Neurobiol* 2012, **22**:61-71.

56. Yao Z, Macara AM, Lelito KR, Minosyan TY, Shafer OT: **Analysis of functional neuronal connectivity in the *Drosophila* brain**. *J Neurophysiol* 2012, **108**:684-696.

57. Olsen SR, Wilson RI: **Cracking neural circuits in a tiny brain: new approaches for understanding the neural circuitry of *Drosophila***. *Trends Neurosci* 2008, **31**:512-520.

58. van der Goes van Naters W, Carlson JR: **Receptors and neurons for fly odors in *Drosophila***. *Curr Biol* 2007, **17**:606-612.

59. Vosshall LB, Wong AM, Axel R: **An olfactory sensory map in the fly brain**. *Cell* 2000, **102**:147-159.

60. Rezaval C, Fabre CC, Goodwin SF: **Invertebrate neuroethology: food play and sex**. *Curr Biol* 2011, **21**:R960-R962.

61. Benton R: **Decision making: singin' in the brain**. *Neuron* 2011, **69**:399-401.

Current Biology 22, 1155–1165, July 10, 2012 ©2012 Elsevier Ltd All rights reserved DOI 10.1016/j.cub.2012.04.062

Article

Neural Circuitry Underlying *Drosophila* Female Postmating Behavioral Responses

Carolina Rezával,[1] Hania J. Pavlou,[1] Anthony J. Dornan,[2] Yick-Bun Chan,[3] Edward A. Kravitz,[3] and Stephen F. Goodwin[1,*]

[1]Department of Physiology, Anatomy and Genetics, University of Oxford, Sherrington Building, Parks Road, Oxford OX1 3PT, UK

[2]Institute of Molecular Cell & Systems Biology, College of Medical, Veterinary and Life Sciences, University of Glasgow, Glasgow G12 8QQ, UK

[3]Department of Neurobiology, Harvard Medical School, Boston, MA 2115, USA

Summary

Background: After mating, *Drosophila* females undergo a remarkable phenotypic switch resulting in decreased sexual receptivity and increased egg laying. Transfer of male sex peptide (SP) during copulation mediates these postmating responses via sensory neurons that coexpress the sex-determination gene *fruitless* (*fru*) and the proprioceptive neuronal marker *pickpocket* (*ppk*) in the female reproductive system. Little is known about the neuronal pathways involved in relaying SP-sensory information to central circuits and how these inputs are processed to direct female-specific changes that occur in response to mating.

Results: We demonstrate an essential role played by neurons expressing the sex-determination gene *doublesex* (*dsx*) in regulating the female postmating response. We uncovered shared circuitry between *dsx* and a subset of the previously described SP-responsive fru^+/ppk^+-expressing neurons in the reproductive system. In addition, we identified sexually dimorphic *dsx* circuitry within the abdominal ganglion (Abg) critical for mediating postmating responses. Some of these *dsx* neurons target posterior regions of the brain while others project onto the uterus.

Conclusions: We propose that *dsx*-specified circuitry is required to induce female postmating behavioral responses, from sensing SP to conveying this signal to higher-order circuits for processing and through to the generation of postmating behavioral and physiological outputs.

Introduction

In *Drosophila*, genes of the sex-determination hierarchy orchestrate the development and differentiation of sex-specific tissues, establishing sex-specific physiology and neural circuitry. *doublesex* (*dsx*) and *fruitless* (*fru*), two pivotal transcription factors of the sex determination hierarchy, establish most aspects of "maleness" and "femaleness" [1]. While *fru*/*dsx*-expressing neurons have been shown to regulate male courtship behaviors [2–5], less is known about the circuitry underlying female mating. Prior to copulation, *Drosophila* females must assess potential mates for species type and fitness before sanctioning mating [1]. An unreceptive female exhibits rejection behaviors such as kicking and ovipositor extrusion [1, 6–8]. A receptive female will facilitate copulation by slowing down, ceasing rejection behaviors, and opening her vaginal plates [1]. While virgin females are highly receptive and rapidly copulate with a suitable partner, mated females undergo a substantial change in their physiology and behavior, becoming temporarily sexually unreceptive to further copulatory attempts, while increasing oviposition [9].

These postmating responses are triggered primarily by sex peptide (SP), a small peptide synthesized in the male accessory glands and transferred to the female during insemination [9]. Females mated to SP-deficient males readily mate again [10, 11], while virgin females injected with SP are rendered unreceptive [12]. Recently, a SP-responsive G protein-coupled receptor for SP-mediated postmating responses has been identified [13]. Females lacking this sex peptide receptor (SPR) remain receptive, exhibiting virgin-like behaviors, postmating. It was shown that postmating responses could be mediated by SPR activation in a set of six to eight sensory neurons located on the reproductive tract [14, 15]. These neurons express both the sex-specific transcripts of the *fruitless* gene (fru^+), a marker for neurons likely to have sex-specific functions, and *pickpocket* (ppk^+), which is believed to encode a marker for proprioceptive neurons [14–17].

How higher-order neural circuits respond to stimuli from these receptor inputs to coordinate the change from pre- to postcopulatory states in females is unknown. As these fru^+/ppk^+ sensory neurons project to the Abg and may target the subesophageal ganglion (SOG), these regions in the central nervous system (CNS) are proposed to be involved in processing of SP-sensory information [14, 15]. The interneurons involved in transmission of this information and the specific neural loci responsible for regulation of these postmating behaviors together with their associated motor outputs remain to be determined.

Disrupting synaptic activity of dsx^{Gal4}-expressing neurons in females impairs specific courtship behaviors [4]; these virgin females are incapable of sampling the male's courtship displays and therefore incapable of providing acceptance responses. During copulation, this lack of cooperation is evident by continual female movement and rejection behaviors. Although sperm and seminal fluids are transferred, these females lay no eggs, remate, and remain incapable of suppressing further courtship, indicating that *dsx* neurons are involved in both pre- and postcopulatory female reproductive behaviors [4]. The suppression of postmating responses via disruption of *dsx* neuronal function [4] also suggested an overlap between *dsx* and the SP-responsive fru^+/ppk^+-expressing neurons in the reproductive system.

In this study we confirm the direct involvement of *dsx* neural circuitry in female postmating responses, demonstrating that SP expression in *dsx* neurons is sufficient to induce a postmating behavioral switch in virgin females. In addition, SPR expression in *dsx* neurons alone is sufficient for SP-induced postmating behaviors. We observed *dsx* expression in most sensory neurons of the reproductive system, including a subpopulation of the previously characterized fru^+/ppk^+ neurons located in the uterus, further refining the sensory

*Correspondence: stephen.goodwin@dpag.ox.ac.uk

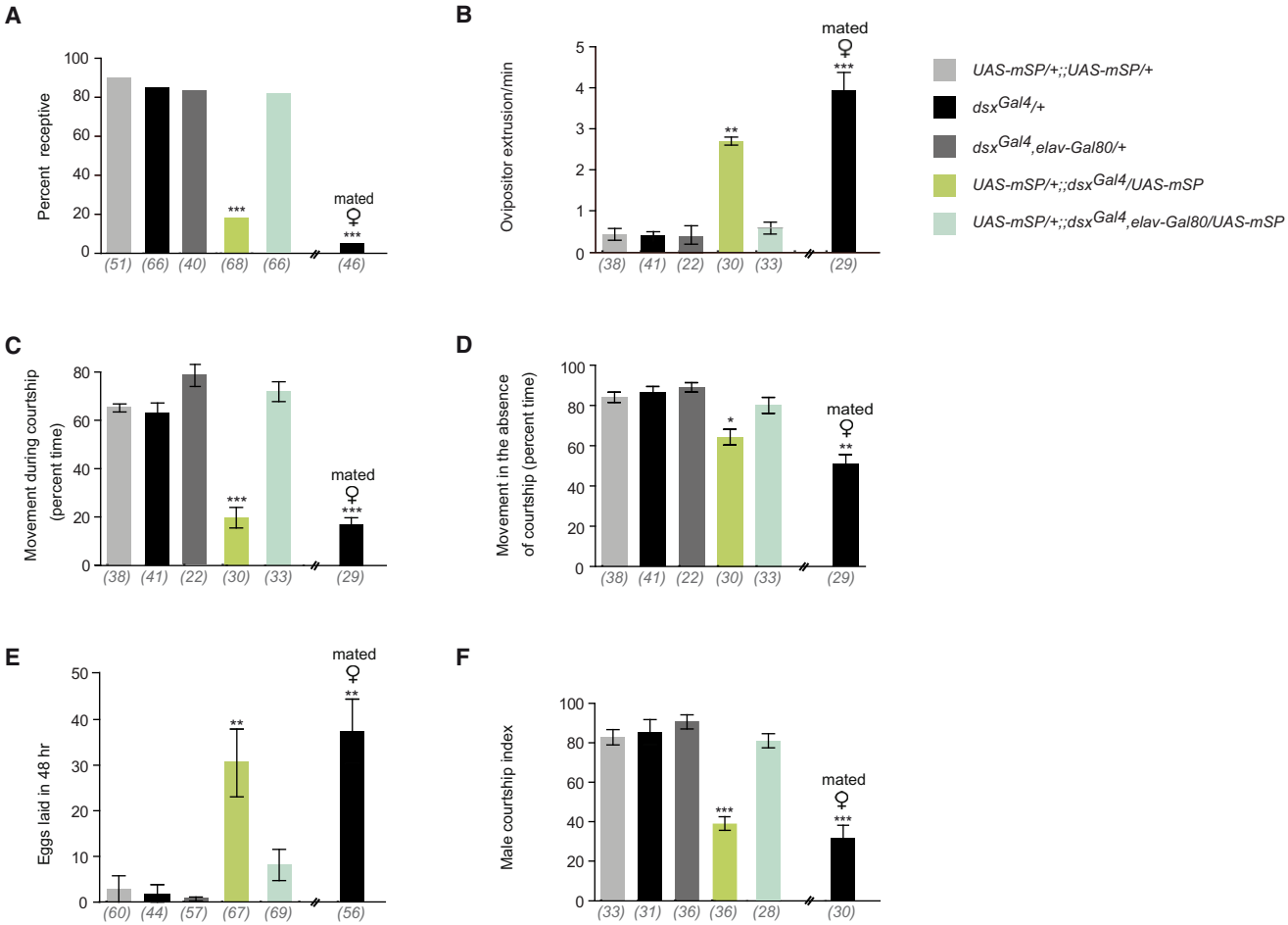


Figure 1. Behavioral Effects of mSP Expression in *dsx* Neurons in Virgin Females

(A) Percentage receptivity (***p < 0.0001, Fisher exact test).
(B) Ovipositor extrusion during courtship (**p < 0.001, ***p < 0.0001, Kruskal-Wallis ANOVA test).
(C) Percentage of time spent moving while being actively courted (***p < 0.0001, Kruskal-Wallis ANOVA test).
(D) Percentage of time spent moving in the absence of active courtship (*p < 0.05, **p < 0.001, Kruskal-Wallis ANOVA test).
(E) Egg laying (**p < 0.001, Kruskal-Wallis ANOVA test).
(F) Male courtship index of naive males (***p < 0.0001, Kruskal-Wallis ANOVA test).
Error bars indicate SEM. Genotypes indicate virgin females, unless stated otherwise. Target males were wild-type. n values shown in parentheses.

circuitry underlying the postmating switch. These results indicate that *dsx* and *fru* shared circuitry is required for eliciting female postmating responses.

Using an intersectional Flippase-recombinase approach to manipulate subsets of *dsx* neurons, we uncovered downstream *dsx* neuronal elements associated with this $dsx^{+}/fru^{+}/ppk^{+}$ uterine sensory cluster in the CNS involved in mediating postmating responses. These *dsx* neurons in the Abg project to specific locations within the brain and the reproductive system. Our findings indicate that *dsx* circuitry consists of not only primary neurons required for sensing SP in the reproductive system, but also downstream effectors of the SP-sensory neuronal pathway that regulate postcopulatory behavior of females. We propose that *dsx* neurons in the Abg act as relay neurons, transmitting SP information from the reproductive system to decision centers in the brain, and that additional *dsx* neurons in this area direct postmating behaviors such as egg transport and oviposition.

Results

Targeted Expression of Membrane-Bound SP in *doublesex*-Expressing Neurons Triggers Postmating Behaviors

Expression of a membrane-bound form of SP (mSP) in the CNS has been shown to be sufficient to induce postmating responses in virgin females and has been used to identify SP-responsive cells and tissues [15, 18]. Employing a similar strategy, we targeted expression of *UAS-mSP* to *dsx* cells under the control of dsx^{Gal4} in virgin females, allowing us to assess the role of such cells in sensing SP. These virgin females exhibited levels of receptivity comparable to mated control females (<20% copulated within 1 hr), involving levels significantly lower than those of control virgin females (>80% copulated within 1 hr) (Figure 1A). As a corollary, dsx^{Gal4}/*UAS-mSP* virgin females displayed significant levels of rejection behaviors toward courting males, as demonstrated by the increased frequency of ovipositor extrusions

(Figure 1B and [6]). We also observed an increase in oviposition in dsx^{Gal4}/*UAS-mSP* virgin females, similar to levels observed with mated controls (Figure 1E).

Studies have shown the importance of female locomotor activity for stimulating male courtship [19–21]. Consistent with this, we observed increased locomotor activity in virgin females while being courted compared with mated wild-type females (Figure 1C). Tellingly, dsx^{Gal4}/*UAS-mSP* virgin females displayed a marked decrease in locomotion while being courted (Figure 1C). It has been suggested that a female's movement could produce subtle sounds alerting males to the female's presence and initiating courtship behaviors [21]. During courtship observation periods, both dsx^{Gal4}/*UAS-mSP* virgin females and mated control females exhibited reduced levels of activity while the male was not courting, remaining static for significantly greater periods of time than control virgin females (Figure 1D). These results show that locomotion during courtship is another behavior that undergoes a dynamic change in response to the copulatory "state" of an individual female.

The male courtship index (CI) is a measure of the attractiveness of a female: naive males court virgin females persistently but display lower levels of courtship when paired with unreceptive mated females [1]. Intriguingly, wild-type naive males courted dsx^{Gal4}/*UAS-mSP* virgin females significantly less than control virgin females (<40% versus > 80%, Figure 1F). To verify that the observed decrement in male CIs was a consequence of female behavior rather than a response to potential changes in the experimental female's pheromonal profile, we repeated these experiments with decapitated (i.e., nonbehaving) dsx^{Gal4}/*UAS-mSP* virgin females. We observed that the males' CIs were indistinguishable to those displayed in the presence of wild-type virgins (Figure S1A available online). This suggests that the male's courtship behavioral outputs are undergoing dynamic modification in response to the target female's behavioral state.

We confirmed the neural etiology of the observed defects in postmating responses in dsx^{Gal4}/*UAS-mSP* virgin females by employing *elav-Gal80* [4] specifically to inhibit neuronal expression of mSP. *elav-Gal80;* dsx^{Gal4}/*UAS-mSP* virgin females were not significantly different from controls (Figures 1A–1F).

During our analyses of dsx^{Gal4}-driven nGFP expression in conjunction with *elav-Gal80* we noted repression in nonneuronal cells in the reproductive system (Figure S2B). To ensure that this repression did not impinge upon the neural etiology of the observed dsx^{Gal4}/*UAS-mSP* phenotypes, we reiterated these experiments using an alternative panneuronal repressor, *syb-Gal80* [22] (Figure S2C). dsx^{Gal4}-driven mSP expression in conjunction with *syb-Gal80* yielded behavioral results consistent with those observed using *elav-Gal80*; that is, receptivity levels were restored in dsx^{Gal4}/*UAS-mSP* coexpressing *syb-Gal80* to ~90% (n = 34), and egg laying was reduced to control levels (7.5 ± 2.4, n = 45).

These results demonstrate that expression of mSP in *dsx* neurons is sufficient to induce female postmating behaviors in virgin females, and these changes can engender complex behavioral responses in individual females as well as in potential mates.

Knocking Down SPR Function Specifically in *dsx*-Expressing Neurons Abolishes Postmating Behavioral Responses

SPR is broadly expressed in the CNS and reproductive tract ([13] and Figure S3) and is required for SP-mediated postmating behavioral responses, as females lacking SPR remain receptive, exhibiting virgin-like behaviors, even after mating or SP injection [13]. To show that dsx^{Gal4}-expressing cells respond to SP, we employed RNA interference to knock down SPR expression [13, 14] and evaluated the effects on postmating responses. While virgin dsx^{Gal4}/*UAS-SPR-IR1* females were typically receptive (data not shown), after mating they displayed no decrement in receptivity nor any increase in ovipositor extrusions compared with mated controls (~80% versus < 4% remated, respectively; Figures 2A and 2B). dsx^{Gal4}/*UAS-SPR-IR1* mated females displayed locomotor activity comparable to virgin females (Figures 2C and 2D) and significantly decreased levels of oviposition (Figure 2E). Males spent significantly more time courting dsx^{Gal4}/*UAS-SPR-IR1* mated females compared to controls (CI > 60% versus < 40%, respectively; Figure 2F). These effects were not observed when males were paired with decapitated dsx^{Gal4}/*UAS-SPR-IR1* females (Figure S1B).

We then attempted to rescue the behavioral deficits observed in SPR null mated females by restrictively expressing SPR in *dsx*-expressing cells in a SPR-deficient genetic background [*Df(1)SPR*]. Postmating responses were restored in *Df(1)SPR;UAS-SPR;*dsx^{Gal4} mated females. Rescued females exhibited significantly reduced levels of receptivity, increased ovipositor extrusion, egg laying, and decreased locomotion; they also elicited lowered levels of male courtship (Figures 3A–3F). Decapitated *Df(1)SPR;UAS-SPR;*dsx^{Gal4} mated females were found to be as attractive as decapitated mated control females to naive males (Figure S1C). We used *elav-Gal80* to confirm the neural etiology of phenotypic effects arising from impairment of SPR function in dsx^{Gal4}-expressing neurons. Expression of *elav-Gal80* in conjunction with dsx^{Gal4}/*UAS-SPR-IR1* in mated females rescued all observed behavioral deficits, including percentage of females remating and levels of egg laying (Figures 2A–2F).

These findings demonstrate the necessity and sufficiency of SPR function in *dsx* neurons to respond to, and convey, the stimulatory cues engendered by SP, resulting in the induction of postmating behavioral responses.

dsx Neurons Are Part of the fru^{+}/ppk^{+} Circuitry Involved in Sensing SP

Although SPR is detected broadly on the female reproductive tract and superficial regions of the ventral nerve cord (VNC) and brain [13], only a restricted subset of fru^{+}/ppk^{+} sensory neurons expressing SPR in the reproductive system appear necessary and sufficient for inducing SP-mediated postmating responses [14, 15].

Our behavioral observations suggest that *dsx* neurons respond directly to SP to elicit the postmating switch. To ascertain whether the fru^{+}/ppk^{+} neurons involved in modulation of postmating responses to SP signaling were also *dsx* positive, we expressed *UAS-redStinger* using dsx^{Gal4} alongside *ppk-eGFP*. The full population of *ppk* neurons associated with the female genitalia consists of two neurons on each lateral oviduct plus approximately 30 neurons organized in three bilateral clusters on the uterus (see Figure 4C; [15]). Colocalization was observed with *dsx* in most *ppk* sensory neurons; this included a pair of neurons on the lateral oviducts and the two most anterior bilateral clusters on the uterus (Figures 4A, 4C1, and 4C2). In agreement with previous characterizations, the most anterior clusters (Figure 4C1) on the uterus are bilateral clusters comprising three neurons, while the more posterior clusters (Figure 4C2) are bilateral clusters

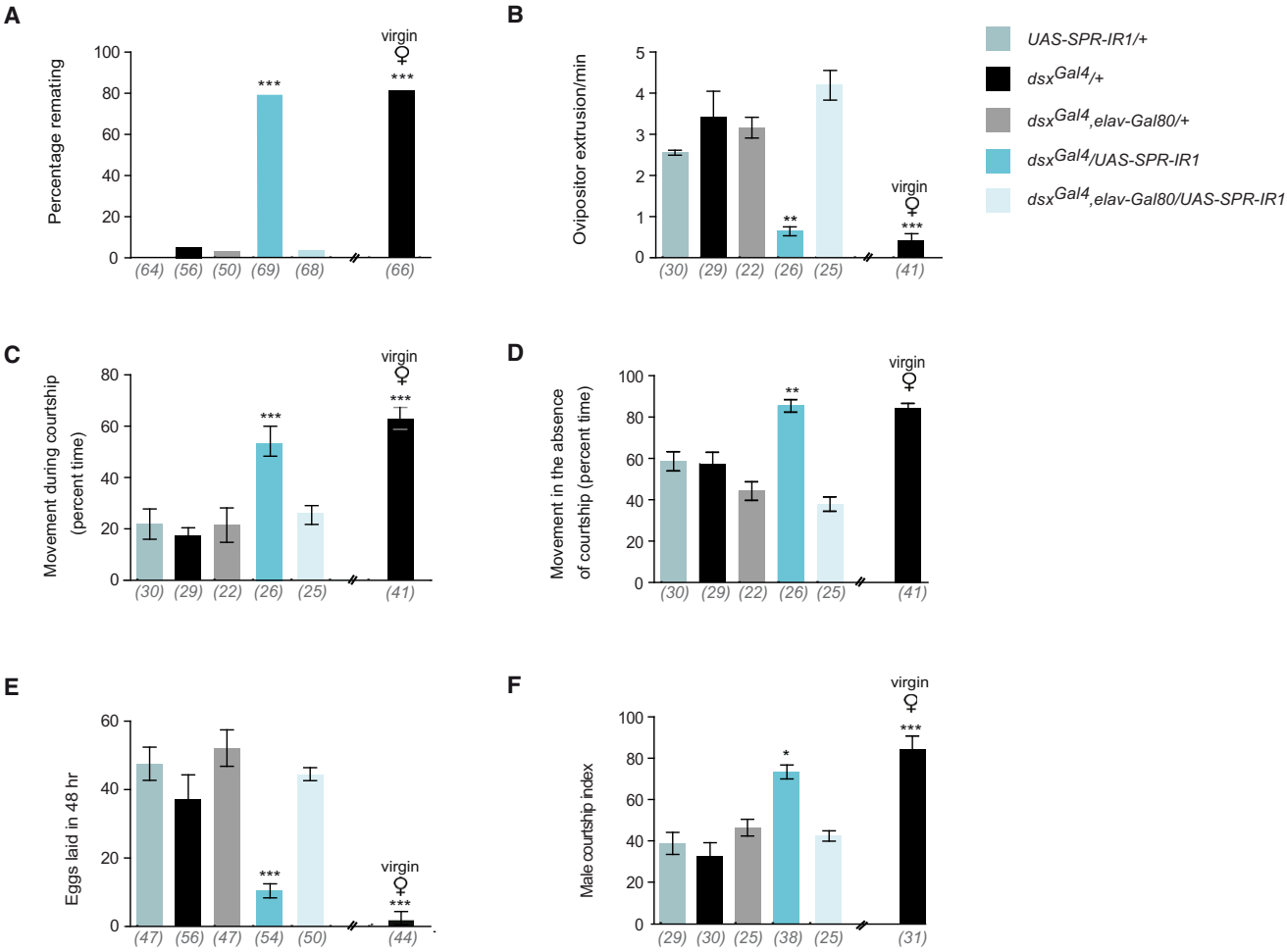


Figure 2. Knocking Down SPR Expression in *dsx* Neurons Reduces Postmating Behaviors in Mated Females

(A) Percentage remating (***p < 0.0001, Fisher exact test).

(B) Ovipositor extrusion during courtship (**p < 0.001, ***p < 0.0001, Kruskal-Wallis ANOVA test).

(C) Percentage of time spent moving while being actively courted (***p < 0.0001, Kruskal-Wallis ANOVA test).

(D) Percentage of time spent moving in the absence of active courtship (**p < 0.001, Kruskal-Wallis ANOVA test).

(E) Egg laying (***p < 0.0001, Kruskal-Wallis ANOVA test).

(F) Male courtship index of naive males (*p < 0.05, ***p < 0.0001, Kruskal-Wallis ANOVA test).

Error bars indicate SEM. Genotypes indicate mated females, unless stated otherwise. Target males were wild-type. n values shown in parentheses.

comprising seven neurons [14, 15]. Further support that dsx^{+}/ppk^{+} neurons are required for activating the postcopulatory switch was evidenced by the reduction in postmating responses observed when dsx^{Gal4} drove expression of mSP in virgin females in the presence of *ppk-Gal80* [15]; Figures 4D and 4E).

A specific subset of *ppk* neurons, one per lateral oviduct and a bilateral cluster of three neurons in the uterus, has been shown to coexpress with marker expression driven by fru^{Gal4} [14, 15]. We exploited the LexA/lexAop binary system [23] to confirm coexpression between *dsx* and *fru* using *UAS-pStingerII* (nGFP) and *lexAop-dsTomato* responsive elements in conjunction with the dsx^{Gal4} and fru^{P1LexA} drivers [24]. Coexpression was restricted to three fru^{+} neurons on each side of the uterus (Figures 4B and 4C2), with no coexpression observed on the lateral oviducts (data not shown). We have therefore refined the originally described fru^{+}/ppk^{+} SP-sensory circuit to two pivotal bilateral clusters of three $dsx^{+}/fru^{+}/ppk^{+}$ neurons.

dsx Sensory Neurons in the Female Reproductive System Appear Cholinergic

To investigate the neurochemical properties of the neurons implicated in triggering SP-mediated postcopulatory changes, we behaviorally screened neurotransmitter Gal4 lines driving mSP. Of the lines tested, only *Cha-Gal4* [25] resulted in a reduction in receptivity in virgin females, fewer than 7% of which achieved copulation in 1 hr (Table S1 and Figure S4C). Expression of *Cha-Gal4* driving nGFP in the reproductive system costained with the panneuronal marker anti-ELAV identified neurons that appear anatomically and topographically congruent with the identified *dsx* neurons—that is, two of the three neurons of the anterior bilateral cluster on the uterus (Figure 4C1), all seven neurons of the posterior bilateral cluster on the uterus (Figure 4C2), and one neuron per lateral oviduct (Figures S2A and S4A).

Consistent with these findings, *Cha-Gal80* abolished nGFP expression in all *dsx* neurons within the reproductive system (Figure S4B). Moreover, dsx^{Gal4}*/UAS-mSP* virgin females

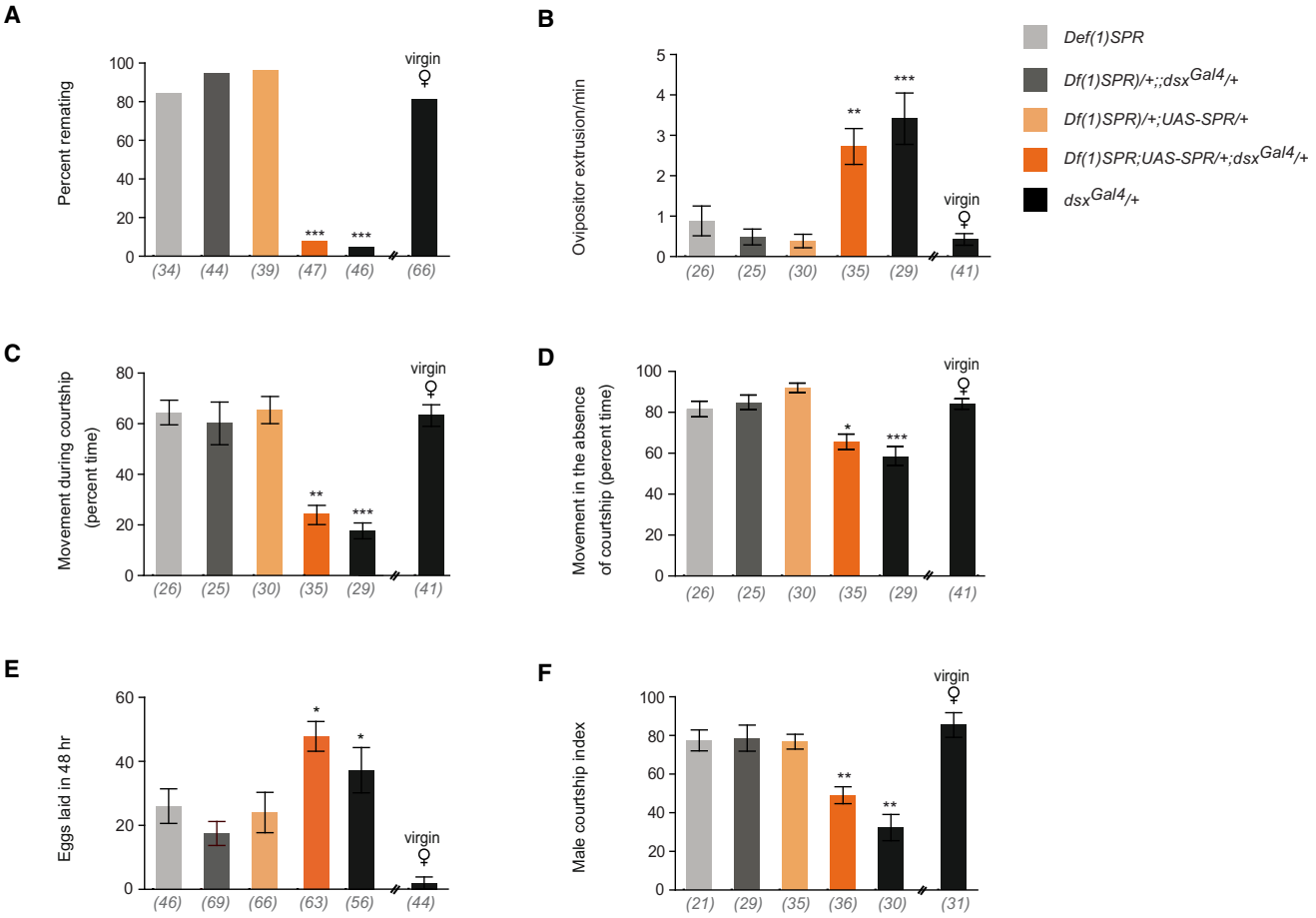


Figure 3. Expression of SPR in *dsx* Cells Alone Is Sufficient to Rescue Postmating Responses in *SPR*-Deficient Line *Df(1)SPR*

(A) Percentage remating (***p < 0.0001, Fisher exact test).
(B) Ovipositor extrusion during courtship (**p < 0.001, ***p < 0.0001, Kruskal-Wallis ANOVA test).
(C) Percentage of time spent moving while being actively courted (**p < 0.001, ***p < 0.0001, Kruskal-Wallis ANOVA test).
(D) Percentage of time spent moving in the absence of active courtship (*p < 0.05, ***p < 0.0001, Kruskal-Wallis ANOVA test).
(E) Egg laying (*p < 0.05, Kruskal-Wallis ANOVA test).
(F) Male courtship index of naive males (**p < 0.001, Kruskal-Wallis ANOVA test).
Error bars indicate SEM. Genotypes indicate mated females, unless otherwise stated. Target males were wild-type. n values shown in parentheses.

expressing *Cha-Gal80* demonstrated high levels of receptivity (~80%) and reduced levels of egg laying (Figures S4C and S4D, respectively). These results suggest that SP-responsive *dsx* neurons may be cholinergic.

Intersecting *dsx* Neurons Critical for Mediating Postmating Behavioral Responses

Although progress has been made identifying sex-peptide-responsive sensory neurons [14, 15], little is known about the downstream neural circuitry underlying postmating responses. Silencing all dsx^{Gal4} neurons impairs postmating behaviors, such that mated females failed to lay eggs, remained attractive to courting males, and remated with a second male [4]. *dsx* is expressed in ~50 neurons in the female brain and ~300 neurons in the Abg [4]. We found a subpopulation of *dsx*-Abg neurons sending two bilateral fascicles along the abdominal nerve trunks that ramify on the uterus and vaginal plates (Figure 6A), suggesting that *dsx* neurons might play a role downstream of the SP-sensory neurons in mediating postmating responses.

We implemented a FLP/FRT intersectional strategy [26] to subdivide the *dsx* circuitry into functionally defined subsets of neurons underlying postmating behaviors. This involves crossing an enhancer-trap FLP (ET^{FLP}) line with dsx^{Gal4} and a given reporter (e.g., *UAS > stop > mCD8::GFP*) or *effector (e.g., UAS > stop > TNT*) to express membrane-bound GFP or the synaptic vesicle blocker TNT in neurons in which FLP has excised the transcriptional stop cassette (> *stop* >) (Figure 5A). Screening a collection of ET^{FLP} lines specific to the nervous system by expressing *UAS > stop > TNT* in combination with dsx^{Gal4}, we identified one line (ET^{FLP250}) that showed robust impairment of postmating behavioral responses.

Silencing ET^{FLP250}/dsx^{Gal4} intersecting neurons was sufficient to partially recapitulate the defects observed with fully silenced *dsx* circuitry [4]; ET^{FLP250}/*UAS > stop > TNT*/dsx^{Gal4} mated females did not extrude their ovipositor to prevent copulation (Figure 5C), resulting in a significantly higher percentage of remating compared with mated controls (Figure 5B), and laid significantly fewer eggs in 48 hr than mated controls (29.5 ± 2.2, n = 30 versus 42.2 ± 2.7, n = 30, respectively). These mated females remained highly attractive to males, demonstrated by decreased courtship latency and higher-than-usual levels of elicited courtship (Figures 5D and 5E).

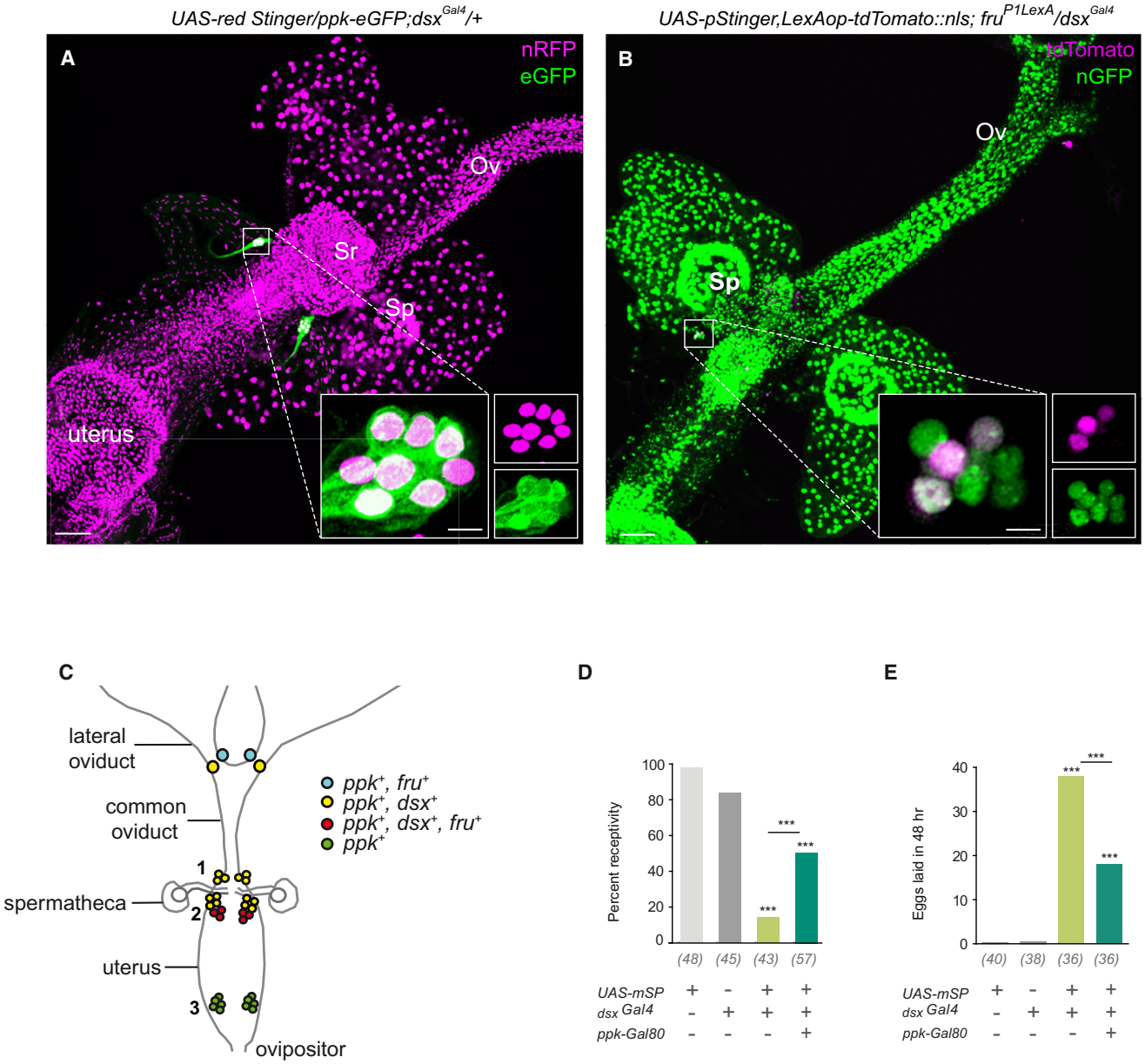


Figure 4. *dsx* Neurons Are Part of the Circuitry Involved in Sensing SP

(A) Colocalization of *ppk*- and *dsx*-expressing neurons in the female genital tract. *ppk-eGFP* was used to visualize *ppk* neurons (green), while *dsx*-expressing cells were visualized with dsx^{Gal4} and *UAS-redStinger* (nRFP; magenta). Inset in (A) shows overlap between *ppk*- and *dsx*-expressing neurons at higher optical magnification.

(B) Colocalization of *fru*- and *dsx*-expressing neurons in the female genital tract. *fru* neurons were visualized with *LexAop-tdTomato::nls* under the control of fru^{P1LexA} (tdTomato; magenta); *dsx* neurons were visualized with dsx^{Gal4} and *UAS-pStinger* (nGFP; green). Inset in (B) shows overlap between *fru*- and *dsx*-expressing neurons at higher magnification.

(A and B) Scale bars represent 50 μm and 10 μm in insets. Seminal receptacle (Sr), spermathecae (Sp), and common oviduct (Ov) are indicated.

(C) Schematic representation of the *Drosophila* female reproductive system showing different clusters of sensory neurons expressing *ppk*, *fru* and/or *dsx*. Each lateral oviduct possesses two *ppk*-expressing neurons [15], one of which is fru^+ (blue dots), while the other is dsx^+ (yellow dots). Within the uterus, the most anterior cluster (no. 1) comprises three bilateral dsx^+/ppk^+ neurons (yellow dots); the more posterior cluster (no. 2) comprises seven bilateral dsx^+/ppk^+ neurons, three of which also express *fru* (yellow and red dots respectively); while the most posterior cluster in the uterus (no. 3) appears to solely express *ppk* (green dots).

(D and E) *ppk-Gal80* expression reduces postmating behavioral responses in dsx^{Gal4}/*UAS-mSP* virgin females.

(D) Percentage receptivity (***$p < 0.0001$, Fisher exact test).

(E) Egg laying (***$p < 0.0001$, Kruskal-Wallis ANOVA test).

Error bars indicate SEM. Genotypes indicate virgin females. Target males were wild-type. n values shown in parentheses.

If inhibiting *dsx* neuronal function interrupts postmating behaviors in mated females, then activating these neurons may induce postmating responses in virgin females. To address this, we expressed the heat-activated ion channel TrpA1 (*UAS-TrpA1*; [27]) in ET^{FLP250}/dsx^{Gal4} virgin females and assessed the behavioral effects of transient neuronal

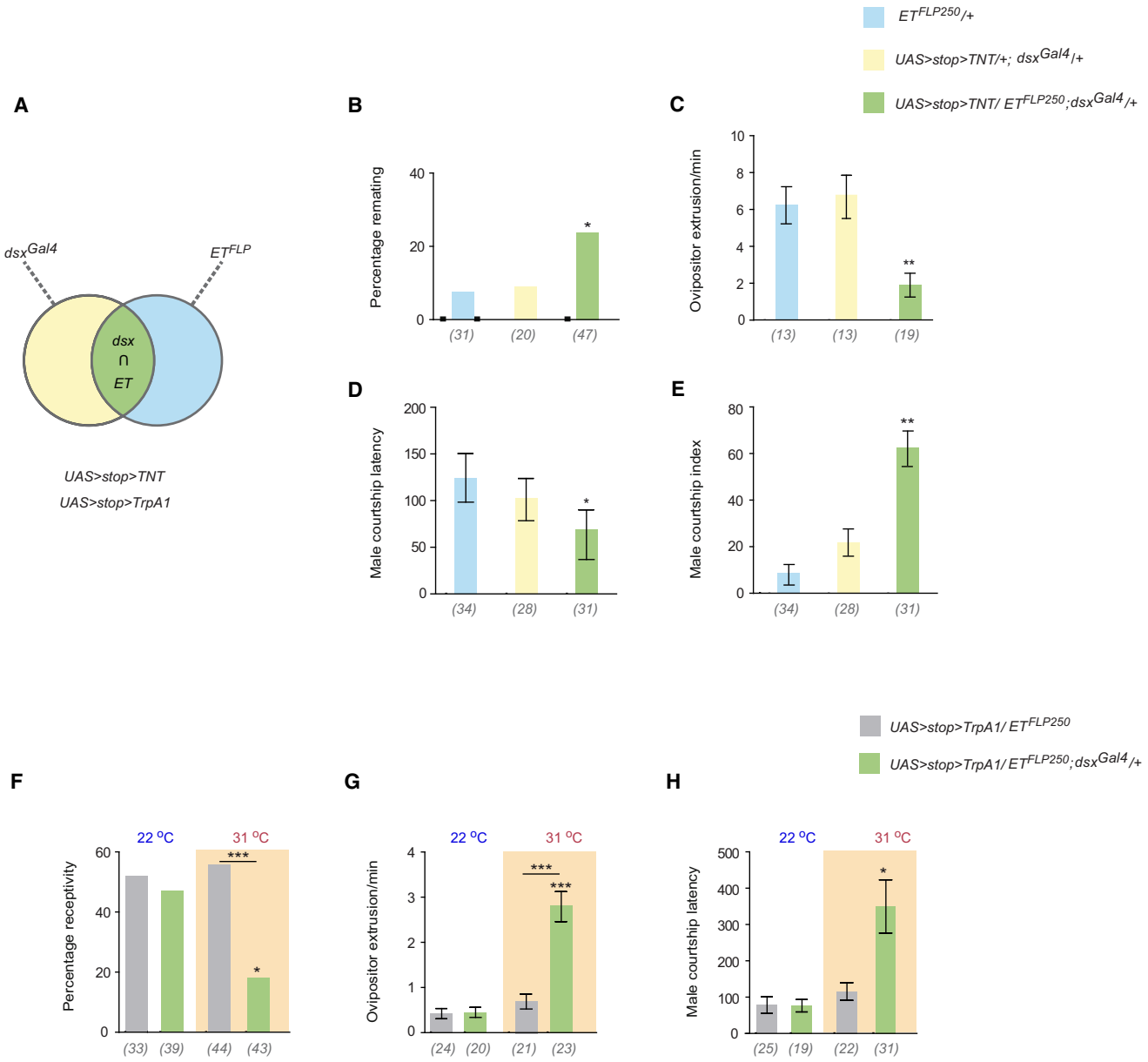


Figure 5. Intersecting *dsx* Neurons Critical for Mediating Postmating Behavioral Responses

(A) Schematic of FLP/FRT intersectional strategy employed to subdivide *dsx* circuitry. Crossing an ET^{FLP} line with dsx^{Gal4} allows expression of the selected effectors, *UAS > stop > TNT or UAS > stop > TrpA1*, in all intersecting neurons (ET∩*dsx*) where FLP has excised the transcriptional stop cassette (>*stop* >). (B–E) Effects of silencing intersecting ET^{FLP250}/dsx^{Gal4} neurons on postmating behaviors using *UAS > stop > TNT*. (B) Percentage remating (*p < 0.01, Fisher exact test). (C) Ovipositor extrusion during courtship (**p < 0.001, Kruskal-Wallis ANOVA test). (D) Male courtship latency in seconds (mean ± SEM, *p < 0.01, Kruskal-Wallis ANOVA test). (E) Male courtship index of naive males (**p < 0.001, Kruskal-Wallis ANOVA test). Genotypes indicate mated females. Target males were wild-type. n values shown in parentheses.

(F–H) Effects of artificially activating intersecting ET^{FLP250}/dsx^{Gal4} neurons on postmating behaviors using *UAS > stop > TrpA.* (F) Percentage receptivity (*p < 0.01, ***p < 0.0001, Fisher exact test). (G) Ovipositor extrusion during courtship (***p < 0.0001, Kruskal-Wallis ANOVA test). (H) Male courtship latency (*p < 0.01, Kruskal-Wallis ANOVA test). Experiments were performed at the permissive and restrictive temperatures of 22°C and 31°C, respectively. Error bars indicate SEM. Genotypes indicate virgin females. Target males were wild-type. n values shown in parentheses.

activation. At the permissive temperature, 22°C, ET^{FLP250}/*UAS > stop > TrpA1/* dsx^{Gal4} virgin females behaved indistinguishably from virgin controls (Figures 5F–5H). At the restrictive temperature, 31°C, thermal activation of these neurons resulted in reduced levels of receptivity (Figure 5F) and significantly higher levels of female rejection behaviors toward courting males (Figure 5G). Although levels of male courtship toward these females were unchanged (data not shown), a significant increase in courtship latency was observed (Figure 5H).

dsx-Abg Neurons Involved in Postmating Responses Target the Brain and Reproductive System

To map the neurons responsible for this phenotype, we crossed ET^{FLP250} to the dsx^{Gal4} driver and the *UAS > stop > mCD8::GFP* reporter [28]. mGFP expression was restricted to a small subset

of *dsx* neurons within the Abg (27.4 ± 0.5 cells, n = 30; of the ~300 Abg *dsx* neurons Figures 6C and 6C1), yet no cell bodies were detected in the majority of brain samples (13% ± 4% of them showed one cell stained with GFP, Figures 6B and 6B1), the reproductive system (n = 18) (Figure 6E), and nonneuronal tissues (data not shown). These results show that 27 of the *dsx*-expressing Abg neurons are required for eliciting postmating responses. Intriguingly, we identified approximately four ascending *dsx*-Abg neuronal projections that terminate in the SOG (Figure 6D). Application of the presynaptic reporter *UAS > stop > nsyb-GFP* [28] in combination with ET^{FLP250} and dsx^{Gal4} revealed extensive presynaptic arborizations in the posterior SOG, where they probably form synapses (Figures 6F, 6F1, and 6H). These results suggest that ET^{FLP250}/*dsx* neurons in the Abg convey sensory information, such as stimuli from SP reception, to higher-order centers required for modulation of behavioral and physiological responses to mating.

We detected two descending projections from intersecting neurons in the Abg, which were found to innervate the uterus (Figure 6E), suggesting that these neurons may be involved in directing motor outputs to achieve specific postmating responses, such as oviposition. *nsyb-GFP* expression confirmed presynaptic innervations of Abg-descending *dsx* neurons in the uterus (Figures 6I and 6I1). In addition, we detected a dense region of presynaptic innervations in the Abg (Figures 6G and 6G1), most likely reflecting the presence of localized *dsx* interneurons. From three-dimensional images of mCD8::GFP-labeled intersecting neurons, we could determine the origin of the two descending projections to the reproductive system and two of the four ascending projections to the brain (Figure S5). Given the extensive dendritic arborizations of ET^{FLP250}/*dsx* neurons within the Abg, it was not possible to identify the exact origin of the two remaining ascending projections.

To evaluate whether *dsx* intersecting neurons were sex specific, we characterized ET^{FLP250}/*dsx* neurons in the male CNS. Whereas no neurons were found in the majority of brains stained (only 10% of brains showed a single neuron), only four to five *dsx* neurons (n = 20) were found in the male Abg (Figures S6A and S6B). Most males showed one ascending Abg neuronal projection running to the brain, and approximately 45% displayed two descending projections to the reproductive system (Figure S6 and data not shown, respectively). We also detected one to two cells of the male-specific *dsx*-TN1 neuronal cluster [4] in the mesothoracic ganglion, which send projections that terminate in the SOG (Figures S6A and S6C). These results demonstrate clear sexual dimorphism, suggesting a specific role for female *dsx* Abg neurons in regulating sex-specific behaviors.

In summary, we have identified a *doublesex*-derived population of neurons in the Abg, which are critical for postmating responses of *Drosophila melanogaster* females comprising (1) ascending neurons targeting the brain; (2) local interneurons; and (3) descending neurons innervating the reproductive system (see schematic Figure 6J). Our investigations suggest a compelling model whereby female-specific *dsx* neurons play a pivotal role in the coordinated regulation of behavioral and physiological responses after copulation—from reception of stimulatory inputs and transmission of these signals to higher-order centers for processing to generation of the associated behavioral motor outputs.

Discussion

Our results show that in the female, *dsx* neurons associated with the internal genitalia not only form a component part of the previously described fru^{+}/ppk^{+} network, but in fact define a more minimal SP-responsive neural circuit capable of inducing postmating changes, such as reduced receptivity, increased levels of rejection, and egg deposition.

In addition to these "classic" postmating behavioral responses, we also noted SP signaling to *dsx* neurons induces postmating changes in locomotor activity between unmated and mated females. Studies have shown that *Drosophila* males court immobilized females less than moving females; essentially, males react to changes in female locomotion [20, 29, 30], suggesting a causal link between female locomotion and increased courtship levels. It has been proposed that males are "acoustically tuned" to signals generated by active females, stimulating increased courtship by changing the attention state of the male [21]. Therefore, female mobility appears to contribute to her "sex appeal" and decreased locomotion in mated females is likely to affect the male's willingness to copulate.

SP-Responsive Sensory Neurons Regulate Different Aspects of the Postmating Response

The female's nervous system must have the capacity to receive, and interpret, postcopulatory signals derived from the male seminal package to direct physiological and behavioral responses required for successful deposition of fertilized eggs. We demonstrated that two *dsx* clusters, composed of three bilateral neurons of the uterus, comprise a more defined component of the SP-responsive sensory circuit. In addition, we have shown the majority of other *dsx* neurons originating on the internal genitalia to coexpress *ppk*. As *ppk* neurons are mechanosensory [16, 17], these may be acting as uterine stretch receptors, facilitating sperm and egg transport, fertilization, and oviposition [14]. Silencing neural function of *ppk* neurons appears to inhibit egg deposition, presumably by impeding egg transport along the oviducts [15]. Similarly, in dsx^{Gal4} females expressing TNT no egg deposition is ever observed, with unfertilized eggs atrophying in the lateral oviducts [4]. In contrast, when fru^{+} neurons are silenced, deposition of successfully fertilized eggs is still observed [15], suggesting that different subsets of the dsx^{+}/fru^{+}/ppk^{+} SP-responsive sensory circuit may direct distinct postmating behavioral responses. As SP has been detected in the hemolymph of mated females [31], it has been suggested that this peptide could pass from the reproductive tract into the hemolymph to reach CNS targets [9]. The fact that neither receptivity nor oviposition was restored to control levels when *ppk-Gal80* (or *Cha-Gal80*) was expressed in dsx^{Gal4}/*UAS-mSP* flies opens the possibility that SP expression might affect additional *dsx* neurons in the CNS.

Coexpression of SPR and *dsx* in the Female Reproductive Organs and Potential Functions in Directing Postmating Responses

Triggering of postmating responses via SP reception appears to occur via a small number of neurons expressing SPR on the female reproductive tract [14, 15]; however, SPR is also found on surface regions of the CNS as well as in endocrine glands and other reproductive tissues [13]. Surprisingly, SPR may even be detected in the *Drosophila* male CNS, where no exposure to SP would be expected, and in insects that apparently lack SP-like peptides [13, 32]. SPRs are therefore potentially responsive to other ligands [32], performing functions other than those associated with postmating responses in the diverse tissues in which SPRs are expressed.

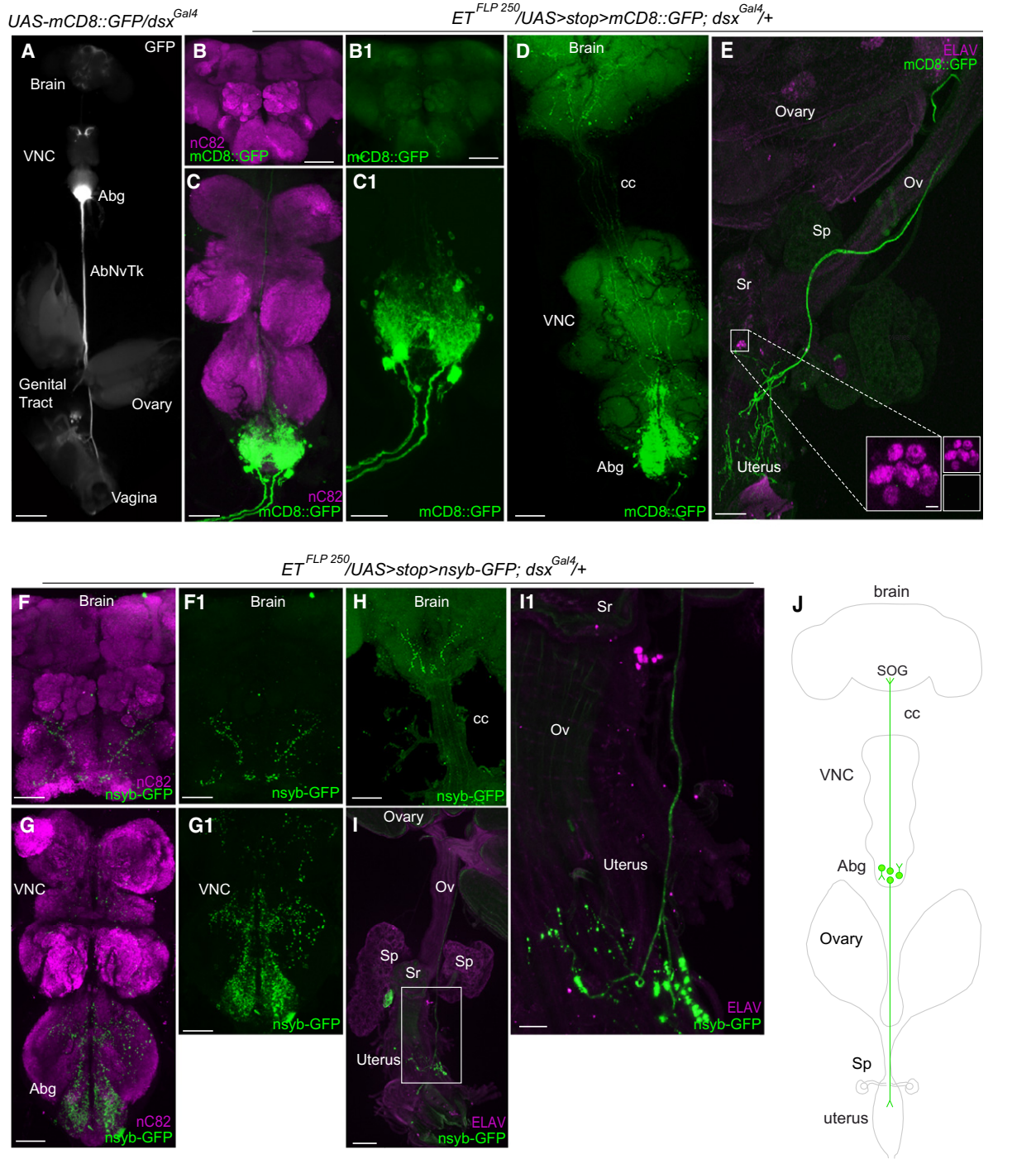


Figure 6. Characterization of Intersected *dsx*-Abg Neurons and Associated Projections

(A) Epifluorescence of dsx^{Gal4}/*UAS-mCD8::GFP* female CNS with AbNvTk innervating the reproductive system. Scale bar represents 200 μm.

(B–I) Intersection of dsx^{Gal4}– neurons and ET^{FLP250} expressing (B–E) *UAS > stop > mCD8::GFP* or (F–I) *UAS > stop > nsyb-GFP* in 5-day-old female CNSs and reproductive systems. (B) Female brain lacking *mCD8::GFP* expressing cell bodies, showing (B1) ascending neuronal projections innervating the SOG. (C) Female VNC showing ~27 $ET^{FLP\ 250}/dsx^{Gal4}$ cell bodies and projections. (C1) Higher magnification of Abg (C). (D–E) Demonstration of *dsx* neuronal projections to (D) the brain and (E) the reproductive system. Inset in (E) shows higher magnification of anterior uterus depicting lack of *mCD8::GFP* expression in *dsx* sensory neurons. (F and G) Presynaptic arborizations of intersecting *dsx* neurons within the (F and FI) posterior SOG and (G and G1) VNC. (H) Cervical connection showing four ascending projections innervating the posterior SOG. (I) Presynaptic arborizations in the internal genitalia, with (I1) a higher resolution of (I) detailing terminalia ramifying on the uterus.

(J) Schematic of intersected *dsx*-Abg neurons depicting ascending neurons innervating the central brain, interneurons potentially conveying information to/from central circuits regulating female mating decisions, and descending neurons innervating the uterus. GFP (green); neuropil counterstained with anti-nC82 (magenta); reproductive systems counterstained with anti-ELAV (magenta). Abdominal ganglion (Abg), abdominal nerve trunk (AbNvTk), cervical connective (cc), seminal receptacle (Sr), spermathecae (Sp), and common oviduct (Ov) are indicated.

(A–I) Ventral views; anterior, top. (B–I) Scale bars represent 50 μm. Scale bars in inset (E) represent 10 μm.

We found extensive coexpression of *dsx*-expressing cells and SPR in the epithelium of the lower oviduct and spermathecae in females (Figure S3). However, mSP expression (or SPR downregulation) specifically in spermathecal secretory cells (SSC) [33] or oviduct epithelium cells [34] had no effect on receptivity or egg laying (data not shown). In agreement with our rescue experiments using neuronal Gal80 drivers to intersect Gal4-responsive UAS expression in *dsx* cells, this suggests that these cells are neither neuronal nor directly involved in SP-mediated postmating behaviors (Figures 1, 2, and 3). SPR staining in the CNS was more difficult to determine given the limitations of the antibody; while no colocalization in the brain was observed, apparent coexpression was observed between SPR and a small subset of ventral *dsx*-Abg neurons (Figure S3).

How Does the Female's CNS Integrate Information about Reproductive Status to Switch Behavior and Physiology Postcopulation?

Our results indicate that *dsx*-Abg neurons are required for the induction and regulation of specific components of the postmating response. It has been shown that inhibition of neurotransmission in *apterous*-expressing Abg neurons impairs SP-mediated postmating changes in receptivity and oviposition, emphasizing the importance of these neurons in the modulation of postmating responses [35].

The level of *dsx* neuronal expression within the Abg and their associated fascicles projecting to the brain, where they form extensive presynaptic arborizations within the SOG, coupled with the effects that impairment of function in these neurons has on postmating responses, speaks to the involvement of these neurons in relaying information from the reproductive tract to the brain (Figure 6). That *dsx*-Abg neurons also project, and form presynaptic arborizations on the uterus, and that the effects on postmating responses when their function is impaired again argue that these neurons play a direct role in mediating processes such as egg fertilization and oviposition. Interestingly, most *dsx* intersecting neurons are specific to females (Figures 6 and S6). Sex-specific behaviors can arise from either shared circuits between males and females that operate differently and/or sex-specific circuits that result from the presence/absence of unique circuit components in one sex versus the other. Our results support the latter.

The VNC has been implicated in the modulation of postmating responses, with an identified focus specifically involved in ovulation and transfer of eggs into the uterus for fertilization [35]. Octopaminergic modulatory neurons located at the distal tip of the VNC projecting to the reproductive tract are required for triggering ovulation, possibly by regulating muscle contractions in the ovaries and oviducts [36, 37]. Since ablation of the pars intercerebralis revealed an additional focus for egg laying in the head [38], and the brain appears to be required for sexual behaviors, such that decapitated virgin females neither mate nor lay eggs [39], it seems likely that neurons in the Abg also require signals from the brain to regulate postmating responses such as egg transport, fertilization, and deposition.

Integrating Sensory Inputs

Higher-order circuits in the female brain must be capable of integrating sensory inputs from the olfactory, auditory, and reproductive systems to decide between the alternative actions of acceptance or rejection of the male. Early gynandromorph studies mapped a region of the dorsal brain that must be female for an animal to be receptive [40]; it has been recently shown that the majority of *dsx* neuronal clusters are located in this region [4]. While neurons coexpressing *dsx* and *fru* in male brains define a more restricted circuitry for determining male mating decisions, in females no overlap between dsx^+ and fru^+ neurons is observable in the brain (data not shown). It is also important to note that the sex-specific Fru isoform is absent in females; thus any circuits that are actively specified in the female are likely to depend on the female isoform Dsx^F. Most *dsx* neurons in the brain are found in the lateral protocerebrum, a region where multiple sensory inputs are thought to be integrated and discrete motor actions selected and coordinated. Further high-resolution functional and connectivity mapping will help to define which neurons participate in specific pre- and postmating behaviors in the female, allowing us to integrate circuit architecture with underlying cellular and synaptic properties. Future experiments will define what activity patterns trigger these behaviors and what activity patterns correlate with these behaviors.

Supplemental Information

Supplemental Information includes Supplemental Experimental Procedures, six figures, and one table and can be found with this article online at doi:10.1016/j.cub.2012.04.062.

Acknowledgments

We are grateful to Wolf Huetteroth and Scott Waddell for helping with AMIRA imaging. We also thank Bruce Baker, Barry Dickson, Wesley Grueber, Yuh Nung Jan, Julie Simpson, and Sean Sweeney for providing valuable reagents. We thank Caroline Fabre, Jeffrey Hall, Megan Neville, and Maria de la Paz Fernandez for comments on the manuscript. This work was supported by grants from the Wellcome Trust, BBSRC, and the EPA Abraham Cephalosporin Trust Fund. E.A.K. and Y.B.C. were supported by grants GM067645 and GM074675 to E.A.K.

Received: February 29, 2012
Revised: April 17, 2012
Accepted: April 23, 2012
Published online: May 31, 2012

References

1. Villella, A., and Hall, J.C. (2008). Neurogenetics of courtship and mating in Drosophila. Adv. Genet. *62*, 67–184.
2. Rideout, E.J., Billeter, J.C., and Goodwin, S.F. (2007). The sex-determination genes fruitless and doublesex specify a neural substrate required for courtship song. Curr. Biol. *17*, 1473–1478.
3. Kimura, K., Hachiya, T., Koganezawa, M., Tazawa, T., and Yamamoto, D. (2008). Fruitless and doublesex coordinate to generate male-specific neurons that can initiate courtship. Neuron *59*, 759–769.
4. Rideout, E.J., Dornan, A.J., Neville, M.C., Eadie, S., and Goodwin, S.F. (2010). Control of sexual differentiation and behavior by the doublesex gene in Drosophila melanogaster. Nat. Neurosci. *13*, 458–466.
5. von Philipsborn, A.C., Liu, T., Yu, J.Y., Masser, C., Bidaye, S.S., and Dickson, B.J. (2011). Neuronal control of Drosophila courtship song. Neuron *69*, 509–522.
6. Connolly, K., and Cook, R. (1973). Rejection responses by female Drosophila melanogaster: their ontogeny, causality and effects upon the behaviour of the courting male. Behaviour *44*, 142–166.
7. Ejima, A., Nakayama, S., and Aigaki, T. (2001). Phenotypic association of spontaneous ovulation and sexual receptivity in virgin females of Drosophila melanogaster mutants. Behav. Genet. *31*, 437–444.
8. Spieth, H.T., and Ringo, J.M. (1983). Mating behavior and sexual isolation in Drosophila. In The Genetics and Biology of Drosophila, *Volume 2c*, M. Ashburner, H.L. Carson, and J.N. Thompson, eds. (New York: Academic Press), pp. 224–284.
9. Kubli, E. (2003). Sex-peptides: seminal peptides of the Drosophila male. Cell. Mol. Life Sci. *60*, 1689–1704.

10. Liu, H., and Kubli, E. (2003). Sex-peptide is the molecular basis of the sperm effect in Drosophila melanogaster. Proc. Natl. Acad. Sci. USA *100*, 9929–9933.
11. Chapman, T., Bangham, J., Vinti, G., Seifried, B., Lung, O., Wolfner, M.F., Smith, H.K., and Partridge, L. (2003). The sex peptide of Drosophila melanogaster: female post-mating responses analyzed by using RNA interference. Proc. Natl. Acad. Sci. USA *100*, 9923–9928.
12. Chen, P.S., Stumm-Zollinger, E., Aigaki, T., Balmer, J., Bienz, M., and Böhlen, P. (1988). A male accessory gland peptide that regulates reproductive behavior of female D. melanogaster. Cell *54*, 291–298.
13. Yapici, N., Kim, Y.J., Ribeiro, C., and Dickson, B.J. (2008). A receptor that mediates the post-mating switch in Drosophila reproductive behaviour. Nature *451*, 33–37.
14. Häsemeyer, M., Yapici, N., Heberlein, U., and Dickson, B.J. (2009). Sensory neurons in the Drosophila genital tract regulate female reproductive behavior. Neuron *61*, 511–518.
15. Yang, C.H., Rumpf, S., Xiang, Y., Gordon, M.D., Song, W., Jan, L.Y., and Jan, Y.N. (2009). Control of the postmating behavioral switch in Drosophila females by internal sensory neurons. Neuron *61*, 519–526.
16. Grueber, W.B., Ye, B., Moore, A.W., Jan, L.Y., and Jan, Y.N. (2003). Dendrites of distinct classes of Drosophila sensory neurons show different capacities for homotypic repulsion. Curr. Biol. *13*, 618–626.
17. Adams, C.M., Anderson, M.G., Motto, D.G., Price, M.P., Johnson, W.A., and Welsh, M.J. (1998). Ripped pocket and pickpocket, novel Drosophila DEG/ENaC subunits expressed in early development and in mechanosensory neurons. J. Cell Biol. *140*, 143–152.
18. Nakayama, S., Kaiser, K., and Aigaki, T. (1997). Ectopic expression of sex-peptide in a variety of tissues in Drosophila females using the P [GAL4] enhancer-trap system. Mol. Gen. Genet. *254*, 449–455.
19. Tompkins, L., Gross, A.C., Hall, J.C., Gailey, D.A., and Siegel, R.W. (1982). The role of female movement in the sexual behavior of Drosophila melanogaster. Behav. Genet. *12*, 295–307.
20. Siegel, R.W., and Hall, J.C. (1979). Conditioned responses in courtship behavior of normal and mutant Drosophila. Proc. Natl. Acad. Sci. USA *76*, 3430–3434.
21. Ejima, A., and Griffith, L.C. (2008). Courtship initiation is stimulated by acoustic signals in Drosophila melanogaster. PLoS ONE *3*, e3246.
22. Rubinstein, C.D., Rivlin, P.K., and Hoy, R.R. (2010). Genetic feminization of the thoracic nervous system disrupts courtship song in male Drosophila melanogaster. J. Neurogenet. *24*, 234–245.
23. Lai, S.L., and Lee, T. (2006). Genetic mosaic with dual binary transcriptional systems in Drosophila. Nat. Neurosci. *9*, 703–709.
24. Mellert, D.J., Knapp, J.M., Manoli, D.S., Meissner, G.W., and Baker, B.S. (2010). Midline crossing by gustatory receptor neuron axons is regulated by fruitless, doublesex and the Roundabout receptors. Development *137*, 323–332.
25. Salvaterra, P.M., and Kitamoto, T. (2001). Drosophila cholinergic neurons and processes visualized with Gal4/UAS-GFP. Brain Res. Gene Expr. Patterns *1*, 73–82.
26. Bohm, R.A., Welch, W.P., Goodnight, L.K., Cox, L.W., Henry, L.G., Gunter, T.C., Bao, H., and Zhang, B. (2010). A genetic mosaic approach for neural circuit mapping in Drosophila. Proc. Natl. Acad. Sci. USA *107*, 16378–16383.
27. Hamada, F.N., Rosenzweig, M., Kang, K., Pulver, S.R., Ghezzi, A., Jegla, T.J., and Garrity, P.A. (2008). An internal thermal sensor controlling temperature preference in Drosophila. Nature *454*, 217–220.
28. Yu, J.Y., Kanai, M.I., Demir, E., Jefferis, G.S., and Dickson, B.J. (2010). Cellular organization of the neural circuit that drives Drosophila courtship behavior. Curr. Biol. *20*, 1602–1614.
29. Hall, J.C. (1978). Courtship among males due to a male-sterile mutation in Drosophila melanogaster. Behav. Genet. *8*, 125–141.
30. Streisinger, G. (1948). Experiments on sexual isolation in Drosophila. IX. Behavior of males with etherized females. Evolution *2*, 187–188.
31. Pilpel, N., Nezer, I., Applebaum, S.W., and Heifetz, Y. (2008). Mating-increases trypsin in female Drosophila hemolymph. Insect Biochem. Mol. Biol. *38*, 320–330.
32. Kim, Y.J., Bartalska, K., Audsley, N., Yamanaka, N., Yapici, N., Lee, J.Y., Kim, Y.C., Markovic, M., Isaac, E., Tanaka, Y., and Dickson, B.J. (2010). MIPs are ancestral ligands for the sex peptide receptor. Proc. Natl. Acad. Sci. USA *107*, 6520–6525.
33. Schnakenberg, S.L., Matias, W.R., and Siegal, M.L. (2011). Sperm-storage defects and live birth in Drosophila females lacking spermathecal secretory cells. PLoS Biol. *9*, e1001192.
34. Lee, H.G., Rohila, S., and Han, K.A. (2009). The octopamine receptor OAMB mediates ovulation via Ca2+/calmodulin-dependent protein kinase II in the Drosophila oviduct epithelium. PLoS ONE *4*, e4716.
35. Soller, M., Haussmann, I.U., Hollmann, M., Choffat, Y., White, K., Kubli, E., and Schäfer, M.A. (2006). Sex-peptide-regulated female sexual behavior requires a subset of ascending ventral nerve cord neurons. Curr. Biol. *16*, 1771–1782.
36. Monastirioti, M. (2003). Distinct octopamine cell population residing in the CNS abdominal ganglion controls ovulation in Drosophila melanogaster. Dev. Biol. *264*, 38–49.
37. Rodríguez-Valentín, R., López-González, I., Jorquera, R., Labarca, P., Zurita, M., and Reynaud, E. (2006). Oviduct contraction in Drosophila is modulated by a neural network that is both, octopaminergic and glutamatergic. J. Cell. Physiol. *209*, 183–198.
38. Boulétreau-Merle, J. (1976). [Destruction of the pars intercerebralis in drosophila melanogaster: effect on the fecundity and the stimulation through copulation]. J. Insect Physiol. *22*, 933–940.
39. Ejima, A., Smith, B.P., Lucas, C., Levine, J.D., and Griffith, L.C. (2005). Sequential learning of pheromonal cues modulates memory consolidation in trainer-specific associative courtship conditioning. Curr. Biol. *15*, 194–206.
40. Szabad, J., and Fajszi, C. (1982). Control of female reproduction in Drosophila: genetic dissection using gynandromorphs. Genetics *100*, 61–78.